DOCTOR OF PHILOSOPHY

Doxorubicin-induced vasotoxicity in coronary vessels

Investigating the G-protein coupled receptor mediated vasoconstriction and the effect of the MEK 1/2 inhibitor U0126

Lozahic, Caroline

Award date:
2023

Awarding institution:
Coventry University

Doxorubicin-induced vasotoxicity in coronary vessels: Investigating the G-protein coupled receptor mediated vasoconstriction and the effect of the MEK 1/2 inhibitor U0126

By

Caroline LOZAHIC

PhD

May 2023

Supervisory Team: Dr Hardip Sandhu, Prof Helen Maddock and Prof Mark Wheatley

Doxorubicin-induced vasotoxicity in coronary vessels: Investigating the G-protein coupled receptor mediated vasoconstriction and the effect of the MEK 1/2 inhibitor U0126

–

A thesis submitted in partial fulfilment of the University's requirements for the Degree of Doctor of Philosophy.

Faculty of Health and Life Sciences

Acknowledgements:

I would like to express my sincere gratitude to my Director of studies, Dr Hardip Sandhu for her continuous support and guidance during my PhD and her support and help for my moving and life in England. Thank you also for teaching me the different techniques of this project and always encouraging me. I am also extremely grateful to my two other supervisors Prof Helen Maddock and Prof Mark Wheatley for their support and guidance during my PhD. The three of them took time from their busy schedule to give me feedback over my experiments and my writing thesis.

I would also like to thanks the DTA3/Cofund Marie SKŁODOWSKA-CURIE PhD Fellowship Programme for funding my PhD. I would also express my gratitude to Prof Malcolm Walker from UCL for his collaboration and advices with the microRNA study on his ERICONC project. Besides my supervisory team, I would also like to thank my colleagues and friends in the lab for their support, teaching me some of the techniques and discussions: David Mutigwa, Sophie Russell, Choaping Np (Thanks to whom I have discovered a new passion: Climbing), Lorena Mejuto Miranda, Saffran Peck, Hoor Ayub, Romez Uddin, Adam Linekar, Josh Hurst and Jayini Thakore. Thank you all for your kindness.

Many thanks to my family who supports me throughout my PhD: my mother Pascale, father Pascal, my brother Vincent, my sister Fanny, Lanig and my cute little nephew Kenan. Thank you for your encouragements, support for all my projects and for always believing in me. I am also thankful to my friends Gaëlle and Nina for supporting me throughout my PhD and through life too. For your encouragements, your good mood during our home work-out (No grumble during work-out, right Gaëlle? ;)). I can't wait to go to our next girls' trip and travel around the world with both of you! I am grateful to have you all in my life.

Thank you,
Caroline Lozahic

Signed Declaration:

'I, Caroline Lozahic confirm that the work presented in this thesis is my own. Where information has been derived from other sources, I confirm that this has been indicated in the thesis.'

10.05.2023

Abstract:

Doxorubicin is one of the most efficient chemotherapeutic drugs used for various cancers, however, therapy with doxorubicin is associated with cardiotoxicity. The effect of doxorubicin on the vasculature remains an uncharted research area. Vascular injury can lead to an increased G-protein coupled receptor (GPCR) mediated vasoconstriction, such as through endothelin receptors subtype A (ET_A) and B (ET_B), 5-Hydroxytryptamine 1B ($5\text{-}HT_{1B}$) receptor and thromboxane prostanoid (TP) receptor. Furthermore, the expression of some GPCRs is regulated through the MEK 1/2 pathway.

This study used an organ culture model to investigate the GPCR-mediated vasocontractility in 0.5 µM doxorubicin-treated left anterior descending artery (LAD) from Sprague-Dawley rats by wire-myography. The involvement of the MEK/ERK 1/2 pathway was investigated by co-incubation with U0126 (5 µM). The following GPCR agonists were used to obtain the individual dose-response curves: ET_B agonist sarafotoxin 6c (S6c), ET_A and ET_B agonist endothelin-1 (ET-1), $5\text{-}HT_{1B}$ agonist 5-carboxamidotryptamine (5-CT), and TP agonist U46619. The specificity of each agonist was verified by the application of specific antagonists. The GPCR mRNA levels and GPCR expression and localisation on LAD arteries were investigated by Real-Time PCR and Immunohistochemistry. In addition, the circulating plasma miRNA levels in cancer patients treated with anthracycline chemotherapy including doxorubicin were studied to assess the expression pattern of circulating miRNAs, with particular focus on miRNAs associated with cardiac- and vascular- injury (collaborative project with Prof M J Walker, UCL). The miRNA expression levels in cancer patient plasma samples were investigated with TaqMan array card technology and individual RT-qPCR verification.

Application of doxorubicin altered the LAD vasoconstriction through GPCRs ET_B, $5\text{-}HT_{1B}$ and TP, and the molecular assessment revealed both transcriptional and translational mechanisms were involved. Furthermore, co-incubation with U0126 highlighted that the MEK/ERK 1/2 pathway plays a key role during the doxorubicin-altered GPCRs-mediated vasoconstriction. Analysis of the cancer patient plasma samples pre- and post- anthracycline chemotherapy revealed candidate vascular injury-associated miRNAs. Profiling of pooled plasma samples from the miRNA array study showed a significantly altered expression of 174 miRNAs as a result of anthracycline chemotherapy. From those altered miRNAs, five vascular injury associated miRNAs were selected and re-analysed on individual cancer patients samples to investigate specificity towards patients that developed cardiac dysfunction, which revealed two vascular injury associated miRNAs, miR-126 and miR-320a.

In conclusion this study shows for the first time that doxorubicin mediated its vasotoxic and cardiotoxic adverse effect on coronary vessels by targeting specific GPCRs through the MEK/ERK 1/2 pathway, and that doxorubicin-treatment of cancer patients alters key circulating vascular injury-associated miRNAs. Overall, this study has improved the understanding of doxorubicin-mediated cardiovascular adverse effects and the vascular and intracellular mechanisms involved.

Table of Contents

List of Figures:

List of Tables:

Abbreviations:

5-CT	5-Carboxamidotryptamine
5-HT	Serotonin
5-HT_{1B}	5-hydroxytryptamine receptor 1B
5-HT_{2A}	5-hydroxytryptamine receptor 2A
7TM	seven-transmembrane receptors
AC	Adenylyl cyclase
ACEi	Angiotensin converting enzyme inhibitors
AGO	Argonaute
ACM	Arrhythmogenic cardiomyopathy
AMI	Acute myocardial infarction
AP-1	Activator protein-1
ARB	Angiotensin receptors blockers
ATP	Adenosine triphosphate
BMK	big MAP kinase
BNP	B-type natriuretic peptide
BSA	Bovine serum albumin
Ca^{2+}	Calcium
CAD	Coronary artery disease
cAMP	Adenosine 3',5'-cyclic monophosphate
CD28	Cluster of Differentiation 28
cDNA	Complementary DNA
CHF	Congestive Heart Failure
CHOP	A combination that includes cyclophosphamide, doxorubicin (Adriamycin) vincristine (Oncovin) and prednisolone (a steroid)
C_{max}	Contraction obtained at the highest agonist dose
CNS	central nervous system
CO_2	Carbone dioxide
CT	Cycle threshold

CTLA-4	cytotoxic lymphocyte antigen-4
cTnI	Cardiac Troponin I
cTnT	Cardiac Troponin T
CVD	Cardiovascular Disease
DAG	Diacylglycerol
DiOHF	3',4'-dihydroxyflavonol
DMEM	Dulbecco's Modified Eagle Medium
DMSO	Dimethyl sulfoxide
DNA	Deoxyribonucleic acid
dNTPs	Deoxynucleoside triphosphates
Doxo	Doxorubicin
EC	Endothelial cells
ECG	Electrocardiogram
EDTA	Ethylene diamine tetraacetic acid
EF-1	Elongation factor 1
EMA	European Medicines Agency
E_{max}	Maximal contractile response elicited by agonist
eNOS	endothelial nitric oxide synthase
epSSG	European Paediatric Soft tissue sarcoma Study Group
ERK 1/2	Extracellular signal-regulated kinase 1 and 2
ESMO	European Society of Medical Oncology
ET-1	Endothelin-1
ET-2	Endothelin-2
ET_A	Endothelin receptors subtype A
ET_B	Endothelin receptors subtype B
FDA	Food and Drug Administration
Fe^{2+}	Ferrous ion
Fe^{3+}	Ferric ion
FEC	A combination of 5 fluorouracil, epirubicin and cyclophosphamide
GAPDH	Glyceraldehyde 3-phosphate dehydrogenase

GDP	Guanosine diphosphate
GPCR	G protein coupled receptors
GTP	Guanosine triphosphate
H_2O_2	Hydrogen peroxide
HC	Healthy control
HF	Heart Failure
$HO^{\cdot}$	Hydroxyl radicals
hrs	Hours
hs-cTnI	high sensitivity cardiac troponin I
I/R	Ischaemia/reperfusion
IA	Intercaling agent
ICI	Immune checkpoint inhibitors
IFOS	Combination of doxorubicin and ifosfamide
IHC	Immunohistochemistry
IL-9	Interleukin 9
iNOS	inducible nitric oxide synthase
IP3	Inositol trisphosphate
IVT	Idiopathic Ventricular Tachycardia
JNK	c-Jun NH2-terminal kinase
K_B	Constant of dissociation of antagonist
K_D	Constant of dissociation
KH	Krebs Henseleit buffer
LAD	Left Anterior Descending arteries
LCx	circumflex artery
LEVO	Levosimendan
LV	Left ventricle
LVEF	Left ventricular ejection fraction
MAPK	Mitogen-activated protein kinase
MCAO	Middle cerebral artery occlusion
MEK 1/2	Mitogen-activated protein kinase kinase 1/2

Mg^{2+} Magnesium

$MgCl_2$ Magnesium chloride

MI Myocardial infarction

min Minutes

miRISC MiRNA-induced silencing complex

miRNAs MicroRNAs

mM Millimole

mQ Milli-Q water (water purified with using Millipore MilliQ lab water system)

MRE MiRNA response elements

MRI Magnetic resonance imaging

mRNA Messenger RNA

NADH Nicotinamide adenine dinucleotide

NF-κB Nuclear factor-kappa B

NICE National Institute for Health and Care Excellence

nM Nano molar

NO Nitric Oxide

NOS Nitric oxide synthase

NOX NADPH Oxidases

NT-pro-BNP Natriuretic peptide tests measure levels of BNP

OC Organ culture

O2. Superoxide anion

OEA Oleylethanolamide

OH^- Hydroxide ions

$ONOO^{\cdot-}$ Peroxynitrite radicals

PAH Pulmonary arterial hypertension

PBS Phosphate-buffered saline

PBST Phosphate-buffered saline with Triton X-100

PCR Polymerase chain reaction

PD-1 Programmed cell death protein 1

PDL-1 Programmed Cell Death Ligand 1

pEC_{50} Negative logarithm of the agonist concentration that produces 50 % of the maximal contraction

PGI2 Prostanoid prostacyclin

PHT Pulmonary hypertension

PIP_2 Phosphatidylinositol 45-bisphosphate

PKA Protein Kinase A

PKC protein kinase C

pKi Negative logarithm of the molar concentration of antagonist

PKR1 Prokineticin receptor 1

PKR2 Prokineticin receptor 2

PLC Phospholipase C

PoL II Polymerase II

PROK1 Prokineticin 1

PROK2 Prokineticin 2

RNA Ribonucleic acid

RNase Ribonucleases

RNS Reactive nitrogen species

RO Reverse Osmosis water

ROI Regionof Interest

ROS Reactive oxygen species

RSV Resveratrol

RT Reverse transcriptase

RyR Ryanodine receptors

S.E.M. Standart error type

S6c Sarafotoxin 6c

SCA Septal coronary arteries

sec Secondes

SERCA Sarcoendoplasmic reticulum calcium ATPase

SHS Second-hand smoke

SMC Smooth muscle cells

SOD	Superoxide dismutases
SR	Sarcoplasmic reticulum
SST	Serum-separating tube
STEMI	ST-elevation myocardial infarction
TAD	Thoracic Aortic Disease
TKI	Tyrosine Kinase inhibitors
TE	Tris-EDTA buffer
Top2	Topoisomerase II
TP	Thromboxane prostanoid receptors
TxA2	Thomboxane A2
U46619	9,11-Dideoxy-9a,11a-methanoepoxy prostaglandin F2a
VEGF-B	Vascular endothelial growth factor B
VEGFi	Vascular endothelial growth factor inhibitors
VSMC	Vascular smooth muscle cells
WHO	World Health Organisation

Chapter 1:

1. Introduction

1.1. Cancer treatment options are improving

According to the World Health Organisation (WHO), cancer was one of the leading causes of death in 2019. In 2020, GLOBOCAN reported that worldwide 19.3 million new cancer cases emerged and that approximately 10 million cancer deaths had occurred (Sung *et al.*, 2021). Despite the increase in number of new cancer cases, the cancer survival rate has doubled in UK in the last 40 years (CancerResearchUK). This is due to the development of new treatment options and new screening tools to aid the early detection and diagnosis of cancers. The increase in cancer incidence and mortality has led to an increased use of chemotherapeutic drugs. In a population-based study, Wilson and team estimated that the number of cancer patients who will need chemotherapy will rise by 53% from 2018 to 2040 (Wilson *et al.*, 2019). Therefore, new chemotherapeutic drugs are needed to be developed and/or current chemotherapeutic drugs need to be improved to improve the outcome of cancer patients.

Different treatment options, including surgery, chemotherapy, radiotherapy and immunotherapy, are used against cancer, depending on the type of cancer, cancer development and risk factors (Sudhakar, 2009). The surgery method is the oldest oncological discipline (Wyld *et al.*, 2015) and new surgical techniques including cryosurgery were developed in the last decade to treat localised tumours, e.g. prostate cancer (Tarkowski and Rzaca, 2014). In the last decades, surgery was used in combination with new cancer treatment regimens to increase the efficiency of anti-cancer treatment, such as radiotherapy and chemotherapy. Radiotherapy is efficient to treat localised solid tumours (Schaue and McBride, 2015). Recently, technological advancement led to the development of new radiotherapy techniques including stereotactic radiotherapy, intensity-modulated radiation therapy and improved imaging systems, which are more precise and efficient. However, many tumours are insensitive to radiotherapy and the radiation doses are limited to avoid radiation-induced injury to the adjacent healthy tissue (Chen and Kuo, 2017). The other treatment option widely used is chemotherapy, which involves the administration of a combination of cytotoxic agents to treat cancers (Mehrling, 2015). Different types of chemotherapeutic drugs have been developed in the last decades and are used for the clinical intervention of cancer incidents (Chabner and Roberts, 2005, Dembic, 2020). The first chemotherapeutic drug approved by the US Food and Drug Administration (FDA) was an alkylating agent, the nitrogen mustard mustine in 1949 (Hirsch, 2006). Alkylating agents, e.g cyclophosamide, interact with deoxyribonucleic acid (DNA) through an alkyl group, leading to the formation of adducts, and thus the inhibition of DNA synthesis followed by the inhibition of ribonucleic acid (RNA) and

protein production (Colvin, 2002). Alkylating agents are mostly used to treat gynaecological oncology (Chu and Rubin, 2018). The next type of chemotherapeutic drugs approved by FDA in 1953 were the antimetabolites, e.g. methotrexate and 6-meracptopurine (Dembic, 2020). Antimetabolites family is divided in five types: folate antagonists, pyrimidine antagonists, purine antagonists, sugar-modified analogues and ribonucleotides reductase inhibitors (Sandhu and Maddock, 2014). Antimetabolites inhibit the DNA synthesis of cancer cells by altering cellular acid production and are widely used as cancer treatments for various cancers (Kumar *et al.*, 2014). The most frequently used and efficient anti-cancer drugs belong to the antibiotic anthracycline group. The first anthracycline drug approved by FDA was doxorubicin, and was isolated from *Streptomyces paucetius* bacteria in 1969 (Arcamone *et al.*, 1969). Anthracycline drug interacts with DNA and inhibits the topoisomerase II activity leading to cell apoptosis (Sandhu and Maddock, 2014). Taxoid is another class of cytotoxic drug agents, which interferes with the mitotic process in cancer cells by binding to the microtubule dimers leading to the microtubule stabilisation and thus disturbing the RNA, DNA and protein synthesis (Sandhu and Maddock, 2014). Recently, a transition from cytotoxic agents to targeted therapeutics was developed in the chemotherapy field. Tyrosine kinase inhibitors were one of the first targeted therapeutics developed with an anti-tumour activity associated with a reduced adverse effect than other conventional cytotoxic agents (Sandhu and Maddock, 2014, Dembic, 2020). There are two types of tyrosine kinase inhibitors: (i) monoclonal antibodies which inhibit the function of growth factor receptor tyrosine kinases, e.g trastuzumab, and (ii) small molecule inhibitors which target both receptor and non-receptors tyrosine kinase, e.g. imatinib (Dembic, 2020, Sandhu and Maddock, 2014). Another promising targeted anti-cancer treatment associated with limited adverse effects is immunotherapy. The aim of the immunotherapy is to rely on the host's immune system to treat cancers by stimulating the effector mechanisms of immune cells or to counteract the inhibitory and suppressive mechanisms of immune cells (Farkona *et al.*, 2016). However, this anti-cancer method is still facing challenges related to their safety and efficiency (Riley *et al.*, 2019). A recent cancer immunotherapy is the immune checkpoint inhibitors (ICI), which targets immunologic receptors on T-lymphocytes' surface to boost anti-cancer immune responses. The first ICI approved was Ipilimumab in 2011, which targets cytotoxic lymphocyte antigen-4 (CTLA-4), an immune inhibitory receptor, to treat stage 3 and 4 malignant melanoma (Shiravand *et al.*, 2022). Currently, three groups of ICI to treat various types of cancers have been approved by the FDA, including the CTLA-4 inhibitor, the programmed cell death protein-1 (PD-1) inhibitor and the programmed cell death ligand 1 (PDL-1) inhibitors (Liebl and Hofmann, 2019). Immune checkpoint receptors, such as PD-1, on T-cells' surface maintained the balance of immunity and regulated T-cells activation through their binding to specific ligand, PDL-1. CTLA-4 has a higher affinity to B7 than the CD28 receptors on T-cells surface, leading to

the inhibition of T-cells activation by blocking the CD28 signal. PD-1 on T-cells surface binds to PDL-1 expressed on tumour cells and through a negative regulation inhibit the T-cells activation. These three immune checkpoints are overexpressed in the tumour microenvironment, which supress the T-cell activity and increase the tumour resistance (Fan *et al.*, 2021). ICI blocks the IC receptors and allows the tumour-reactive T cells activation, which leads to the effective activation of anti-tumour response (Wei *et al.*, 2018).

1.2. Side-effects of cancer-therapy drugs

Although the efficiency of anti-cancer treatments improved over the last decades, the rise of the number of cancer survivors was followed by a rise of severe adverse effects. One of the main concerns of radiotherapy treatment is the risk for cancer survivors to develop secondary malignancies in the 10 – 15 years post-therapy. Furthermore, the severe adverse effects observed in cancer survivors treated with radiotherapy are cardiovascular, gastrointestinal and pulmonary adverse effects (Berkey, 2010). Although immunotherapy was developed to reduce the risk of adverse effects, the immune-related adverse events occurred in various organ systems, including cardiovascular, pulmonary, and neurologic systems (Martins *et al.*, 2019). The chemotherapeutic drugs do not only affect cancer cells, but healthy non-malignant cells as well (Thomas *et al.*, 2016). Most alkylating agents have immunosuppressive adverse effects by acutely suppressing the bone marrow. Other organs like the lungs, liver and heart can also be affected by alkylating agents, which limit the dose used during treatment (Scholar, 2007, Sandhu and Maddock, 2014). The cardiotoxic adverse effects of cyclophosphamide can lead to arrhythmia and congestive heart failure (Goldberg *et al.*, 1986, Lozahic *et al.*, 2021). The antipyrimidine 5-fluorouracil interferes with the DNA synthesis process and is used to treat various solid tumours (Sandhu and Maddock, 2014), and 1 % of patients treated with 5-fluorouracil suffer from severe adverse effects, including neurotoxicity, cardiotoxicity, encephalopathy and hyperammonemia (Thomas *et al.*, 2016). The cardiotoxicity of 5-fluorouracil can lead to different cardiovascular diseases (CVDs), including silent myocardial ischaemia, arrhythmia, and congestive heart failure in cancer patients (Sandhu and Maddock, 2014). The adverse effects of taxoids include neurotoxicity, pulmonary toxicity and gastrointestinal toxicity (Raschi *et al.*, 2010). Sunitinib is a tyrosine kinase inhibitor (TKI) and is frequently used and efficient against renal cell carcinoma (Motzer *et al.*, 2017), and can induce neurotoxicity, pulmonary toxicity, gastrointestinal toxicity, skin disorders and haematological events, including anaemia, neutropenia and thrombocytopenia as adverse effect (Hartmann *et al.*, 2009). Sunitinib is also known to induce cardiotoxicity leading to CVDs including myocardial dysfunction, hypertension and heart failure (Mahdi *et al.*, 2021). Doxorubicin from the anthracycline family is one of the most potent anti-cancer

drugs, however, the main adverse effect of doxorubicin is cardiotoxicity (Sandhu and Maddock, 2014). Doxorubicin-induced cardiotoxicity is induced through several intracellular mechanisms including mitochondrial dysfunction, reactive oxygen species (ROS) production (Gille and Nohl, 1997), oxidative stress (Minotti *et al.*, 2004), apoptosis (Kaufmann and Earnshaw, 2000), and myofibril damage (Ito *et al.*, 1990), all leading to cardiac injury in doxorubicin-treated patients (Suter and Ewer, 2013). Cardiovascular adverse effects is observed in most of the anti-cancer-drug treatment (Figure 1-1) through different characteristics and the monitoring of the cardiac function is essential before, during and post-treatment.

Figure 1-1: Cardiac adverse effects of anti-cancer drugs and monitoring techniques used in clinics. Taken from (Huang *et al.*, 2022).

1.3. Assessment of cardiac injury in the clinic

Anti-cancer therapy-induced cardiac injury can be assessed by imaging techniques and various circulating myocardial damage biomarkers. Management of the anti-cancer therapy-induced cardiotoxicity starts prior to the anti-cancer treatment with a baseline work-up and continues with a follow-up of the potential cardiac adverse effects development during and after the chemotherapy. Firstly, the baseline work-up includes the cardiac disease history of the patients, clinical examination with imaging techniques, such as left ventricular ejection fraction (LVEF) and magnetic resonance imaging (MRI), and various circulating myocardial damage biomarkers, as shown in Figure 1-1 (Curigliano *et al.*, 2012). The baseline work-up is necessary due to the risk factor of pre-existing CVD comorbidities (Jensen *et al.*, 2002). The European Society of Medical Oncology (ESMO) 2020

consensus recommends to assess the left ventricular (LV) function after a cumulative dose of anthracycline 250 mg/m^2, where m^2 is the body surface area, is reached and then after each additional 100 mg/m^2, and to periodically measure circulating biomarkers (Curigliano *et al.*, 2020). Furthermore, ESMO suggests that the assessment of cardiotoxicity post-chemotherapy is performed 6 – 12 months post-chemotherapy with cardiac biomarkers and potentially imaging techniques, and then to do a follow-up check-up every two years post-chemotherapy (Curigliano *et al.*, 2020).

The detection of early cardiac injury is commonly assessed by monitoring left ventricular ejection fraction (LVEF), using echocardiography (ECG) or cardiac magnetic resonance imaging (MRI), which are both non-invasive techniques (Thavendiranathan *et al.*, 2013, McKillop *et al.*, 1983). Doppler ECG evaluates LVEF and detects myocardial injury (McKillop *et al.*, 1983). Doppler ECG is a 2-dimensional ECG, which monitors the heart structure and function (Anavekar and Oh, 2009), however, ECG is not highly sensitive to small changes in LVEF (Oreto *et al.*, 2012). Another imaging technique used in clinics is the MRI, which is the reference standard to assess ventricular volume and function (Real *et al.*, 2023). The advantage of the cardiac MRI is the ability to offer an excellent myocardial tissue characterisation (Baxi *et al.*, 2015), which allows the early detection of cardiac injury by underlying histopathological myocardial changes (Thavendiranathan *et al.*, 2013).

The cardiotoxicity can also be assessed through circulating biomarkers of cardiac injury such as cardiac troponin I (cTnI) and B-type natriuretic peptide (BNP), or inflammatory biomarkers such as interleukins and C-reactive protein (Berezin and Berezin, 2020). In the present study, cardiac biomarkers used to assess the anti-cancer therapy-induced cardiotoxicity in cancer patients were cardiac troponin T and N-terminal proBNP (NT-pro-BNP). There are two cardiac troponin isoforms: The cTnI expressed in cardiac muscles and the cardiac troponin T (cTnT) expressed in cardiac and skeletal muscles (Wallace *et al.*, 2004). The high-sensitivity (hs-cTnI) and cTnT are the gold-standard biomarkers for the diagnostic of acute myocardial infarction (Aydin *et al.*, 2019). Myocardial damage increases the serum level of troponin, leading to the release of troponin from cardiac or skeletal muscles to blood circulation (Sandhu and Maddock, 2014). The elevation of troponin is correlated to cardiac injury severity and is monitored during CVDss, including cardiac arrhythmias, cardiomyopathies and heart failure (Chauin, 2021). The other diagnostic biomarkers for cardiac injury and heart failure widely used are brain natriuretic peptide (BNP) and *N*-terminal proBNP (NT-proBNP) (Cao *et al.*, 2019). BNP and NT-proBNP are synthesised and secreted by left ventricular myocytes as a response to mechanical stress, systemic ischaemia and hypoxia (Volpe *et al.*, 2014). The elevation of plasma BNP and NT-proBNP is also associated with arrhythmias and cardiomyopathies and is used to assess the severity of the CVD (Cao *et al.*, 2019). Recently, novel biomarkers emerged, such as the miRNAs which are described in section 1.8.

1.4. Anthracyclines

Anthracyclines are among the most potent and commonly used chemotherapeutic agents (Hutchins *et al.*, 2017). The anthracycline chemotherapy regimen is used to treat various solid tumours, such as breast cancer, leukaemia, lymphoma, melanoma and uterine cancer. The anthracycline family is composed of antineoplastic agents isolated from bacteria (Martins-Teixeira and Carvalho, 2020). The first anthracycline isolated from Gram-positive *Streptomyces paucetius* is daunorubicin, in the 1960s, followed by the discovery of doxorubicin in 1969. However, it took a further 10 years after the daunorubicin isolation to discover the anti-tumour activity of anthracyclines, i.e. daunorubicin and doxorubicin (Pinedo, 2006). Doxorubicin was the first FDA-approved anthracycline in 1974, while daunorubicin was FDA-approved in 1979 (Hande, 1998).

Among the several anthracyclines discovered over the last decades, the four most common anthracyclines are daunorubicin, doxorubicin, epirubicin and idarubicin (Table 1-1). Doxorubicin and daunorubicin are both from the first generation of anthracycline and half a century after their discovery, both are still frequently used in clinics. The structure of doxorubicin differs from the structure of daunorubicin through the side chain which contains an alcohol group, while daunorubicin's side chain contains a methyl group (Minotti *et al.*, 2004). This minor difference in structure specifies their mechanism of action. Doxorubicin is commonly used to treat acute leukaemia Hodgkins disease and non-Hodgkins lymphomas, sarcoma and various solid tumours, including breast and lung cancers, while daunorubicin is used to treat acute myeloid leukaemia and acute lymphoblastic leukaemia (Dembic, 2020, Pinedo, 2006, Minotti *et al.*, 2004).

Despite their potency, doxorubicin and daunorubicin treatments are limited by cancer resistance and cardiac adverse effects. It is known that some cancer cells develop a resistance to several anti-cancer drugs by altering the membrane transport, which is the primary mechanism against anti-cancer treatment (Chien and Moasser, 2008). Furthermore, anthracycline treatment is associated with cardiotoxicity as the main adverse effect and anthracycline-induced cardiotoxicity is exponentially dose-dependent (Raj *et al.*, 2014). The dosage of anthracycline depends on body surface area, cumulative dose and other risk factors. These risk factors are age, previous cardiac insults, and adjuvant therapy (Moudgil and Yeh, 2017). Doxorubicin and daunorubicin concentrations are limited by the cardiac adverse event, with respectively a maximum cumulative dose of 500 to 550 mg/m^2 (Robert, 1993) and 330 mg/m^2 (Pophali and Litzow, 2017). Those limitations have resulted in the development of new generations of anthracyclines.

Table 1-1: Characteristics of the different types of anthracyclines. Adapted from (Dembic, 2020, Minotti *et al.*, 2004, 2012, Pinedo, 2006, Martins-Teixeira and Carvalho, 2020)

Drug	Structure	Cancers treated	Clinical maximal cumulative dose	Year of approval by FDA
Doxorubicin	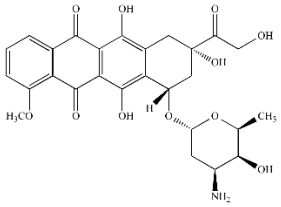	Acute leukaemia Hodgkins disease and non-Hodgkins lymphomas Sarcoma Solid tumours	500 to 550 mg/m^2 (Robert, 1993)	1974
Daunorubicin	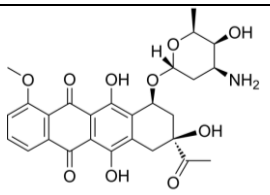	Acute myeloid leukaemia (AML) Acute lymphoblastic leukemia (ALL)	330 mg/m^2 (Pophali and Litzow, 2017)	1979
Epirubicin	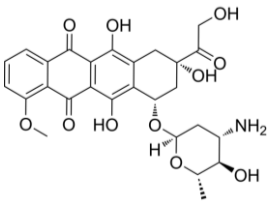	Breast cancer Gastric cancer non-Hodgkin lymphoma	900 to 1000 mg/m^2 (Robert, 1993)	1999
Idarubicin	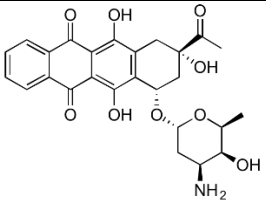	Acute myeloid leukemia (AML)	/	1990

The second generation of anthracyclines, including epirubicin and idarubicin, were developed to overcome the resistance and cardiac adverse effects of the first generation. Epirubicin, a doxorubicin analogue is approximately 30 % less cardiotoxic than doxorubicin, but is also less potent than doxorubicin (Martins-Teixeira and Carvalho, 2020). On the other hand, idarubicin shares similar activities with daunorubicin against leukaemia, but is also used to treat some solid cancer (Minotti *et al.*, 2004). The fact that these second generation of anthracyclines are less efficient than doxorubicin, underlines the necessity to uncover mechanisms involved in cancer resistance and in cardiotoxicity to obtain anti-cancer drugs with optimal potency and reduced cardiotoxicity.

1.4.1. Doxorubicin

The present study is focused on the investigation of doxorubicin-induced cardiotoxicity. Doxorubicin, also known as Adriamycin, is one of the most efficient chemotherapeutic drugs, widely used in many solid cancers. Unfortunately, it can also lead to severe cardiovascular adverse effects. Indeed, patients treated with doxorubicin have 4 % risk of developing congestive heart failure at a cumulative dose of 500 mg/m^2, and the risk increase with the dose with 36 % risk to develop congestive heart failure if the cumulative dose exceeds 600 mg/m^2 (Mitry and Edwards, 2016). Furthermore, the FDA recommends that the cumulative total lifetime dose of doxorubicin should not exceed 450 – 550 mg/m^2 of body surface area, since above this dose, the risk of congestive heart failure is largely increased (Lum *et al.*, 1985). Similarly, The National Institute for Health and Care Excellence (NICE) or British National Formulary recommends not exceeding the limit of total cumulative doses of 450 mg/m^2 (NICE). In clinical practice, the cumulative dose of doxorubicin is limited to 400 – 450 mg/m^2, but severe cardiac damages still occur at cumulative dosages substantially below this level (Rahman *et al.*, 2007). The doxorubicin-induced cardiotoxicity leads to the use of lower doses or the use of other chemotherapeutic drugs that are less efficient (Bhagat and Kleinerman, 2020).

1.4.2. Mechanism of doxorubicin during cancer-therapy

Despite many inquisitive studies, the exact doxorubicin-induced cardiotoxicity mechanism of action remains partially unknown (Minotti *et al.*, 2004). However, there are three proposed mechanisms involved: (i) intercalation of doxorubicin into DNA strands, (ii) topoisomerase II (Top2) suppression leading to DNA damage and (iii) generation of free radical species (Figure 1-2) leading to cellular apoptosis (Bhagat and Kleinerman, 2020).

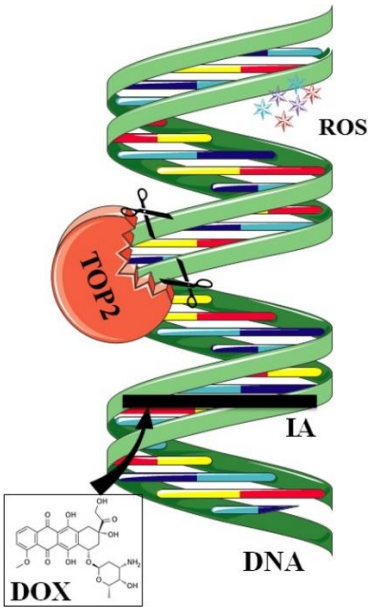

Figure 1-2: Mechanisms of action of doxorubicin in cancer cells. Taken from (Corremans *et al.*, 2019). Doxorubicin induces cancer cell death through three main mechanisms of action: the formation of a complex Top2-Dox-DNA, the intercalation of Dox into DNA strands and the generation of ROS. Top2 = Topoisomerase II, ROS = reactive oxygen species, IA = DNA intercalating agent, Dox = doxorubicin.

Doxorubicin inhibits DNA synthesis through DNA intercalation into the site containing adjacent guanine-cytosine (GC) base pairs and thus induces the formation of doxorubicin-DNA adducts (Yang *et al.*, 2014). The doxorubicin-DNA adducts can activate the DNA damage responses and thus leads to cancer cell apoptosis (Bhagat and Kleinerman, 2020). In addition to the formation of doxorubicin-DNA adducts, doxorubicin can also inhibit DNA synthesis by suppressing the Top2 activity. DNA topoisomerases are nuclear enzymes that alter the conformation of DNA helix strands during DNA replication, transcription and recombination (Bhagat and Kleinerman, 2020). Among the different types of topoisomerase, Top2 is an adenosine triphosphate (ATP)-dependent enzyme and is the main target for anthracycline anti-cancer mechanisms in the proliferative cancer cells. There are two isoforms of Top2, Top2α and Top2β. Top2α, the most common and highly expressed in proliferating cells, is involved in chromosomal segregation, while TOPIIβ is mostly prevalent in quiescent cells (Corremans *et al.*, 2019). Interestingly, Top2α is highly expressed in osteosarcoma cells and is targeted by doxorubicin during the chemotherapy treatment (Yang *et al.*, 2014). Doxorubicin binds Top2 and DNA to form a ternary complex, DOX-Top2-DNA. The stabilisation of this complex blocks DNA resealing, which induces the double-stranded DNA break, and thus resulting in the inhibition of DNA replication and the induction of cell apoptosis (Corremans *et al.*, 2019).

Another important anti-tumour mechanism of doxorubicin is the generation of free radical species leading to oxidative stress (Bhagat and Kleinerman, 2020). In the outer mitochondrial membrane, doxorubicin is reduced by the complex I to lipophilic doxorubicin deoxyaglycone. This form of doxorubicin enters into the inner membrane and competes with coenzyme Q10 as an electron acceptor (Nebigil and Desaubry, 2018). The doxorubicin form is oxidised through a one-electron reduction, such as cytochrome P450 reductase or NADH dehydrogenase, in a semiquinone radical (Corremans *et al.*, 2019). This semiquinone radical is an unstable metabolite, which releases free radicals during its conversion back to doxorubicin (Thorn *et al.*, 2011). The generated free radicals induce free radical injury to the DNA of cancer cells (Bhagat and Kleinerman, 2020). The oxidative stress, induced by intracellular ROS increases, alters cellular processes and thus leads to the generation of DNA mutations and cancer cell apoptosis (Nebigil and Desaubry, 2018). Furthermore, the increase of intracellular free radical species can also induce lipid peroxidation of the cell membrane leading to cell apoptosis (Seifried *et al.*, 2004, Pham-Huy *et al.*, 2008).

1.4.3. Mechanisms of doxorubicin-induced cardiotoxicity

Doxorubicin targets cancer cells, however non-malignant cells, including heart cells, can be affected by the cytotoxic effect of doxorubicin as well (Corremans *et al.*, 2019). Doxorubicin-mediated cardiotoxicity involves various intracellular mechanisms and factors (Thorn *et al.*, 2011). The cardiotoxicity of doxorubicin has been observed to imply different mechanisms, such as oxidative stress, calcium metabolism disorders and systemic inflammation (Podyacheva *et al.*, 2021), presented in Figure 1-3.

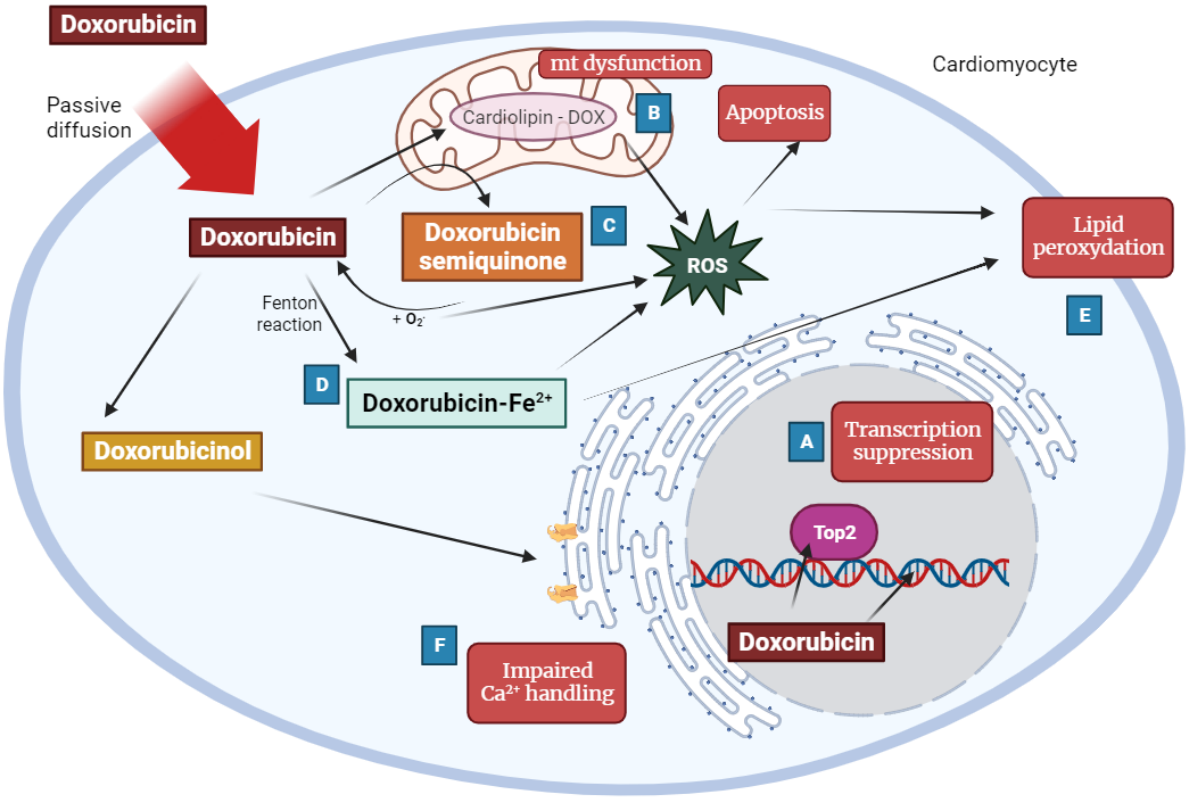

Figure 1-3: Mechanisms of cardiotoxicity induced by doxorubicin (DOX). Adapted from (Corremans *et al.*, 2019). A: Doxorubicin alters transcription through DNA intercalation and Top2 activity suppression. B: Doxorubicin accumulates in mitochondria and forms a complex with cardiolipin leading to mitochondrial dysfunction and apoptosis. C: Doxorubicin is converted in doxorubicin semiquinone through a one-electron reduction leading to ROS generation, DNA damage and cell apoptosis. D: Doxorubicin forms a complex with Fe^{2+} and generates free radical species. E: Doxorubicin induces lipid peroxidation at the cell membranes through doxorubicin-Fe^{2+} complex and ROS generation. F: Doxorubicinol is a toxic metabolite of doxorubicin, which leads to impaired Ca^{2+} handling by altering Ca^{2+}-pumps on the sarcoplasmic reticulum. Top2 = topoisomerase 2, Dox = doxorubicin, ROS = reactive oxygen species, Fe^{2+} = ferrous ion, mt = mitochondrial.

During the anti-cancer treatment, doxorubicin enters through passive diffusion and accumulates in the cardiomyocytes (Corremans *et al.*, 2019). Doxorubicin accumulates in the mitochondrial inner membrane and forms an irreversible complex with cardiolipin, leading to mitochondrial dysfunction (Octavia *et al.*, 2012). The disruption of the mitochondrial activity leads to the release of reactive oxygen species (ROS) including superoxide radical hydrogen peroxide (H_2O_2) and superoxide anion ($O_2^{\cdot-}$) (Zhou *et al.*, 2001), the production of free iron-related free radicals (Kwok and Richardson, 2003), and the formation of doxorubicinol metabolite (Olson *et al.*, 1988). Moreover, doxorubicin alters the activity of endothelial nitric oxide synthase (eNOS) and NADPH oxidase (NOX), leading to the reduction of free oxygen in superoxide free radical (Vasquez-Vivar *et al.*, 1997, Deng *et al.*, 2007). The elevation of ROS production by the mitochondrial dysfunction and altered enzymes, and the elevation of iron-

related free radicals activate the oxidative stress and lipid peroxidation, inducing cardiomyocytes apoptosis and thus leads to the cardiac dysfunction observed in patients treated with chemotherapy (Sritharan and Sivalingam, 2021).

Doxorubicin can also interfere with iron metabolism in the cardiomyocyte's cytosol (Xu *et al.*, 2005). In physiological conditions, ferric ion (Fe^{3+}) is transported from serum to the intracellular compartment by transferrin, a transporter protein. Fe^{3+}-transferrin complex is passed in the cell by endocytosis and ferric ions are reduced into ferrous ions (Fe^{2+}) by a Fenton reaction with ferrireductase (Fang *et al.*, 2023). Then, ferrous ions are, depending on intracellular iron level, either stocked in ferritin, an iron storage protein or used for the cell's vital functions and haemoprotein synthesis (Ravingerova *et al.*, 2020). During doxorubicin treatment, the release of Fe^{2+} from ferritin is disrupted, leading to disturbed cellular functions, including iron-dependant proteins (Sandhu and Maddock, 2014). Additionally, doxorubicin can bind easily to ferric ion and forms doxorubicin-Fe^{3+} complex. In presence of oxygen, this complex is reduced in doxorubicin-Fe^{2+} by reducing agents, such as NADPH (Sandhu and Maddock, 2014). The reduction promotes the generation of highly oxidative forms of ROS, ferryl and perferryl radicals and thus leads to an increase of oxidative stress and mitochondrial dysfunction (Nebigil and Desaubry, 2018). During doxorubicin-induced cardiotoxicity, the iron accumulation through the Fenton reaction induces the generation of free radical species, including hydroxide ions (OH^-) and hydroxyl radicals ($HO^{\cdot}$) leading to oxidative stress (Ravingerova *et al.*, 2020).

As in cancer cells, the doxorubicin semiquinone converts back into doxorubicin by releasing superoxide radical ($O_2^{\cdot}$), and will either be converted by superoxide dismutase (SOD) in H_2O_2 or will initiate lipid peroxidation of cardiomyocytes membranes. The lipid peroxidation induces cell membranes injury, which leads to cell apoptosis (Horenstein *et al.*, 2000). Furthermore, lipid peroxidation is also induced through the Fenton reaction, which activates lipoxygenases during the conversion of Fe^{2+} into Fe^{3+} (Wu *et al.*, 2021).

Doxorubicinol is the primary circulating metabolite of doxorubicin and is the product of the two-electron doxorubicin reduction through carbonyl reductases or aldo-keto reductases activity (Piska *et al.*, 2017). Doxorubicinol cardiac toxicity has been investigated in an isolated rabbit papillary muscles model by Olson *et al.et al.* in 1988. They measured the contractility responses and resting stress of the right ventricular papillary muscle, which was placed in a muscle bath and fixed to a force transducer and electrically stimulated to contract 30 times per minute to develop the maximal tension. Doxorubicin at a final cumulative dose of 700 µM was added to the muscle bath at 45-min intervals. The authors showed that doxorubicinol is about 30 times more efficient than doxorubicin at

reducing the contractility of isolated rabbit papillary muscles. Furthermore, they showed that the highest dose of doxorubicin (700 µM) was slightly altering the myocardial resting stress, whereas doxorubicinol at an 8-fold lower dose than doxorubicin, largely increased the myocardial resting stress, and thus depressed the diastole function (Olson *et al.*, 1988). In addition to the study of doxorubicinol toxicity in papillary muscles, Olson and team investigated the effect of doxorubicinol on ion-pump from the sarcoplasmic reticulum (SR) and they demonstrated that doxorubicin inhibits cardiac SR calcium pumps, including Ca^{2+}, Mg^{2+}, and Na^{+} /K^{+} -ATPases and thus nearly abolishes the calcium loading activity of cardiac SR leading to disturbed calcium homeostasis (Olson *et al.*, 1988, Boucek *et al.*, 1987).

The doxorubicin-induced cardiotoxicity associated with intracellular calcium overload leads to an abnormal intracellular calcium homeostasis, and thus cardiac contractile dysfunction (Shinlapawittayatorn *et al.*, 2022). The cardiac contraction is initiated by the release of calcium from the sarcoplasmic reticulum (SR) (Walweel and Laver, 2015). The doxorubicin-induced cardiotoxicity is associated with a dysregulation of receptors localised on the SR membrane and involved in the regulation of calcium homeostasis including the ryanodine receptors (RyR) (Kim *et al.*, 2006) and the sarco/endoplasmic reticulum ATPase (SERCA) (Villani *et al.*, 1980). The RyR receptors release the calcium ions from the SR to the cytosol during the muscle contraction (Fill and Copello, 2002), while the SERCA pumps transport the calcium ions from the cytosol into the SR after the muscle contraction, leading to the muscle relaxation (Bers, 2002). Treatment of isolated rat ventricular cardiomyocytes with doxorubicin (3 µM) promotes the opening of RyR, leading to the increase of intracellular diastolic calcium (Kim *et al.*, 2006). In isolated guinea pig cardiomyocytes, the doxorubicin treatment (2mg/mL) is associated with a decrease of SERCA expression, leading to a decrease in the SR calcium uptake (Villani *et al.*, 1980). However, *in vivo* models studies have showed that RyR and SERCA mRNA expression is decreased in rabbit cardiomyocytes after doxorubicin treatment during 8 weeks with a total dose of 16mg/kg (Olson *et al.*, 2005) and 20 mg/kg (Gambliel *et al.*, 2002), leading to left ventricular (LV) dysfunction (Olson *et al.*, 2005). *In vitro* models have showed that doxorubicin treatment is associated with an increase of the calcium influx into the mitochondria in rat cardiomyocytes (Doxo = 10 µM, during 18h) (Dhingra *et al.*, 2020), while the calcium loading capacity is decreased in human right atrial appendages (Doxo = 1 µM, during 90 min) (Montaigne *et al.*, 2011), leading to cardiac mitochondrial injury and thus mitochondrial dysfunction. The intracellular calcium overload is clinically associated with ischemic heart diseases, including atherosclerosis, thrombosis, and coronary spasms (Dhalla *et al.*, 2008). Furthermore, clinical studies have highlighted an increase of arterial stiffness in patients treated with anti-cancer drugs both during and after the treatment, including doxorubicin (Parr *et al.*, 2020, Mozos *et al.*, 2017, Chaosuwannakit *et al.*, 2010). Arterial

stiffness is known to be associated with CVDs, such as hypertension, stroke, and congestive heart failure (Laurent and Boutouyrie, 2020, Sutton-Tyrrell *et al.*, 2005, Chae *et al.*, 1999).

Doxorubicin-induced cardiotoxicity is also associated with an increase of the inflammatory markers. Interleukin 9 (IL-9) aggravates doxorubicin-induced cardiac injury by promoting the inflammatory response (Ye *et al.*, 2020). A recent study investigated the potential cardiotoxic effect of doxorubicin treatment (15 mg/kg) on IL-9-mediated inflammation response with *in vivo* model, C57BL/6 mice. They showed that IL-9 levels were significantly elevated in doxorubicin-treated mice and a recombinant mice IL-9 pre-treatment would aggravate the doxorubicin-induced cardiotoxicity, while an anti-IL-9 neutralizing antibody pre-treatment would alleviate the doxorubicin-induced cardiotoxicity (Ye *et al.*, 2020). Furthermore, several studies investigated the doxorubicin-induced cardiac adverse effect on vascular endothelial growth factor B (VEGF-B). VEGF-B is mainly localised in cardiomyocytes and the circulatory system, and regulates the proliferation and migration of ECs, including the coronary vessels' growth.

Doxorubicin-induced cardiotoxicity has mainly been investigated and documented on cardiomyocytes in pre-clinical studies and on cancer survivors treated with anthracyclines in clinical studies (Rawat *et al.*, 2021). Conversely, the potential vasotoxicity of doxorubicin had been poorly investigated. Some mechanisms observed in cardiomyocytes could also be involved in the cardiovascular system, such as calcium dysregulation or ROS production. Some studies demonstrated that endothelial cells were altered by doxorubicin administration (Luu *et al.*, 2018, He *et al.*, 2019, Hoffman *et al.*, 2021). Sayed-Ahmed *et al.et al.* demonstrated that ET-1 levels in plasma and cardiac nitric oxide of Sprague-Dawley rats were increased after the administration of cumulative doses of doxorubicin (from 10mg/kg to 20mg/kg) for 10 days (Sayed-Ahmed *et al.*, 2001). A clinical study with a cohort of 30 patients treated with doxorubicin observed the plasma ET-1 level to be elevated in 5 patients, and 2 of them developed clinically overt congestive heart failure. The 25 patients without an increase of the plasma ET-1 didn't develop congestive heart failure (Yamashita *et al.*, 1995). ET-1 and NO are involved in the vascular tone (Nishiyama *et al.*, 2017), their alterations by doxorubicin could induce alterations in the vasculature tone.

1.5. Anti-cancer drug, vascular toxicity and new therapeutic strategies

1.5.1. Anti-cancer drug-induced vasotoxicity

Chemotherapeutic drugs can induce vasotoxicity through "off-target" effects by targeting not only cancer cells, but also the adjacent cells from the vasculature near cancer cells. Many factors, including cardiovascular risk, genetic predispositions and pre-existing CVDs increase the risk of cancer patients

treated with chemotherapy to develop vascular issues (Hsu *et al.*, 2021). Anti-cancer drug-induced vasotoxicity is mainly induced by the alteration of endothelial function (Gao and Galis, 2021). The chemotherapy-mediated vasotoxicity leads to the development of cardiovascular issues, including hypertension, coronary artery disease, atherosclerosis and heart failure (Sandhu and Maddock, 2014, Mahdi *et al.*, 2021, Dhalla *et al.*, 2008, Volkova and Russell, 2011).

A large number of chemotherapy treatments, including anthracyclines (key cardiotoxic mechanisms of action described in section 1.4.4), lead to an excessive generation of ROS. The overproduction of ROS disrupts the intracellular functions in vascular cells, including calcium and ferric homeostasis, and alters the proteins, lipids and DNA (Hsu *et al.*, 2021). In endothelial cells (ECs), the nitric oxide synthase (NOS) catalyses the substrate L-arginine in nitric oxide (NO), which is a key mediator of vasodilation (Vallance and Hingorani, 1999). Accumulated ROS interacts with NO and induces the generation of peroxynitrite radicals ($ONOO^{-}$) and reactive nitrogen species (RNS) in ECs, which results in inflammation, apoptosis, necrosis of ECs and thus vascular injury (Lim *et al.*, 2009). Furthermore, the reduction of available NO results in the development of hypertension (Hsu *et al.*, 2021). About 80 % of cancer patients treated with TKI or VEGF inhibitors (VEGFi) develop hypertension. TKI promote the accumulation of ROS and down-regulate the nuclear factor erythroid 2-related factor 2 (Nrf2), a key regulator of antioxidant genes, while VEGFi inhibits the VEGF-induced vasodilatory and survival signalling through the NO and vasodilatory prostanoid prostacyclin (PGI_2) production in ECs. A clinical study showed that cancer patients (n = 11) treated with chemotherapeutic drugs, including doxorubicin, cisplatin, cyclophosphamide, fluorouracil, paclitaxel, bevacizumab, rituximab, and trastuzumab, had an approximatively 20 % increase in developing carotid artery stiffness compared to healthy control (n = 11) (Frye *et al.*, 2018). As described in section 1.4.4., anthracycline-induced cardiotoxicity is associated with an increase of arteries stiffness (Parr *et al.*, 2020). A clinical study investigated the potential relation of anthracycline and the development of arterial stiffness in childhood cancer survivors. The authors measured the Stiffness index β in three groups: anthracyclines-treated survivors (n = 67), other chemotherapy-treated survivors (n = 29) and healthy control (n = 72) with a 10-year follow-up (Jenei *et al.*, 2013). The β-stiffness index is a local elastic parameter used to detect arterial stiffness and thus, allows the detection of vascular injury (Rosenberg *et al.*, 2018). Jenei *et al.et al.* (2013) showed that anthracyclines induce a 3-fold increase in β-stiffness compared to healthy control and a 1.6-fold increase β-stiffness of childhood cancer survivors treated with other chemotherapy drugs. From their results, they suggested that anthracycline had an adverse effect on endothelial function and arterial stiffness (Jenei *et al.*, 2013).

Chemotherapeutic drugs can also promote the loss of density of arterioles and capillaries by altering the endothelial function leading to thrombosis and thus, microvasculature injury (Hsu *et al.*, 2021).

Doxorubicin's adverse effects on small arteries from atrial tissue had been investigated by Hader *et al.et al.* (2019). They analysed the microvascular dysfunction of small arteries on atrial appendages from children and adults cancer survivors and children and adults healthy controls. The authors showed that doxorubicin impaired the endothelial function in both groups, however, the impairment is more significant in children survivors than in adult cancer survivors. Furthermore, the authors suggest that the reduction in flow-mediated dilatation induced by doxorubicin in children cancer survivors might be involved in the delayed onset of anthracycline-induced cardiac adverse events in childhood cancer survivors compared to adults cancer survivors (Hader *et al.*, 2019). Furthermore, it has been shown that long-persistent microvascular injury can be induced without alteration of the cardiac contractile at low cumulative doses of doxorubicin regimens (0.45 mg/kg per injection and 3 injections with 2 weeks intervals) in a large-white male pigs model (Galan-Arriola *et al.*, 2022). Furthermore, chemotherapy and immunotherapy are associated with cardiac adverse effects leading to the onset of atherosclerosis (Inno *et al.*, 2021, Dhalla *et al.*, 2008). It has been shown that the risk of venous thrombosis was 16 % increased by doxorubicin treatment (Hsu *et al.*, 2021).

1.5.2. Therapeutic strategies against anti-cancer drug-induced vasotoxicity

Recent studies investigated new therapeutic strategies to protect the vascular system without altering the anti-tumour effect of anthracyclines.

The endothelin-1 (ET-1) is one of the most potent endogenous vasoconstrictive peptide in the cardiovascular system (Nishiyama *et al.*, 2017) and plasma ET-1 level is elevated in patients suffering of CVDs (Wei *et al.*, 1994). In the vascular system, ET-1 activates both endothelin receptor subtypes, ET_A and ET_B and regulates the vascular tone, through their activation (Liu *et al.*, 2003). Due to the potent vasoconstriction induced by the ET receptors, which is known to be up-regulated in CVDs (Skovsted *et al.*, 2012), it has been considered that those receptors could play a mechanistic role in anti-cancer drug-induced vasotoxicity. An elevated vasoconstriction increases the blood pressure, which can impair arteries by reducing of their elasticity, leading the decrease of the blood's flow and oxygen supply to the heart and thus, the development of heart disease (O'Rourke, 1990). A recent study investigated the efficacy of selective antagonists of either ET_A receptors alone or dual $ET_{A/B}$ receptors for preventing the sunitinib-induced hypertension. Male Wistar rats were clustered into four groups: Rats treated with vehicle, rats treated with sunitinib (14 mg/kg/day), rats treated with sunitinib and the dual $ET_{A/B}$ antagonist macitentan (30 mg/kg/day) used, and rats treated with sunitinib and either low or high doses of selective ET_A antagonist sitaxentan (30 or 100 mg/kg/day). Rats were treated for 8 days and mean arterial pressure and heart rate were measured every day.

After the 8-day treatment, the assessment of the vascular function of isolated iliac artery segments in response to the vasodilator acetylcholine and vasoconstrictors ET-1 and phenylephrine. The authors showed that both selective antagonists were alleviating the elevated sunitinib-induced blood pressure, but this increase of blood pressure was exclusively promoted by ET_A receptors. Furthermore, the dual $ET_{A/B}$ receptors antagonist increased the ET-1-mediated vasoconstriction in sunitinib-treated rat artery compared to antagonist naïve sunitinib-treated rat artery, while the presence of ET_A receptor antagonist did not alter the sunitinib-induced ET-1 mediated vasoconstriction. These results underlined the ET_A receptors involvement in sunitinib-induced vasotoxicity and that inhibiting ET_B receptors might aggravate the vascular function. Authors suggest that ET_A receptor antagonist, such as sitaxentan, might be an interesting cardioprotective agent to alleviate the onset of hypertension after sunitinib treatment (Mirabito-Colafella *et al.*, 2020).

VEGF-B is involved in coronary angiogenesis and ischaemia resistance (Hsu *et al.*, 2021). Räsänen *et al.et al.* investigated the potential cardioprotective effect of the VEGF-B gene therapy against acute and chronic doxorubicin-induced cardiotoxicity in an *in vivo* rodent model. To investigate the acute cardiotoxicity, they administrated a single dose of doxorubicin at a concentration of 15 mg/kg in C57BI6J mice (killed 20 hrs after), following the VEGF-B pre-treatment (AAV9–mVEGF-B186) or control vector, 7 days prior the doxorubicin injection. To investigate the chronic doxorubicin-induced cardiotoxicity, they administrated doxorubicin at a concentration of (6 mg/kg) every 3 days for 2 weeks, following the VEGF-B pre-treatment (AAV9–mVEGF-B186) or control vector, 7 days prior the doxorubicin injection. They showed that the VEGF-B treatment was reducing the cardiac atrophy and dysfunction induced by the doxorubicin treatment and, thus targeting the VEGF-B pathway could alleviate the doxorubicin-induced cardiotoxicity (Rasanen *et al.*, 2016). Additionally, a study in an *in vivo* rat model investigated the cardioprotective effect of resveratrol (RSV), a nonflavonoid polyphenol against doxorubicin-induced treatment. They administrated doxorubicin at a concentration of 10 mg/kg twice a week and RSV at a concentration of 50 mg/kg every day for 6 weeks in rats. They showed that doxorubicin treatment was reducing VEGF-B levels in cardiomyocytes and the pre-treatment of RSV was attenuating the VEGF-B reduction and thus alleviating the doxorubicin-induced cardiotoxicity (Tian *et al.*, 2020).

Another potential strategy to prevent anti-cancer drug-induced vasotoxicity is to target two prokineticin receptors (PKR1 and PKR2) (Hsu *et al.*, 2021). Both receptors are activated by the neuropeptides prokineticins (PROK1 and PROK2), principally released by macrophages (Nebigil, 2009) and in addition, PROK2 and PKR1 levels are altered in human patients after acute myocardial infarction (Nguyen *et al.*, 2013). Gasser *et al.et al.* investigated the involvement of PKR1 in anthracycline-induced cardiovascular toxicity. The authors showed that doxorubicin at 1 µM induced

apoptosis in cultured cardiomyocytes and in cultured ECs, as well. Furthermore, they showed that IS20, an agonist of PKR1, activated the MAPK (mitogen-activated protein kinase) signalling pathway in ECs and prevents doxorubicin-induced apoptosis. Thus, this study showed that the activation of the PKR1 signalling pathway alleviates the cardiovascular adverse effect of doxorubicin in ECs (Gasser *et al.*, 2019). The recent studies underline new strategies to treat anti-cancer drug-induced vasotoxicity and an interesting target is the GPCRs since it is already targeting by various approved drugs to treat CVDs (Santos *et al.*, 2017).

1.6. GPCR pathways involved in cardiovascular disease

1.6.1. General introduction

G-protein coupled receptors (GPCR) are the largest family of transmembrane proteins involved in the transduction of signals and central regulators of cardiovascular biology (Drake *et al.*, 2006). Approximately 30% of actual clinical pharmaceutical agents available are ligands of GPCRs (Santos *et al.*, 2017). GPCRs have a similar structure and contain a seven-transmembrane α-helical (7TM) coupled with a G protein, as shown in Figure 1-4. Ligands of GPCR can be hormones, neurotransmitters, ions and other stimuli (Rosenbaum *et al.*, 2009). According to the 7TM segments genome, GPCRs can be clustered in families with the rhodopsin family as the main family with 701 members (Kobilka, 2007). GPCRs are associated with heterotrimeric G protein ($G_{\alpha\beta\gamma}$). Extracellular ligand binds to GPCR and initiates the signal transduction pathway by provoking a conformational change in the receptor. The G protein is activated by the nucleotide exchange from guanosine diphosphate (GDP) to guanosine triphosphate (GTP), promoted by the GPCR conformational change (Massotte and Kieffer, 2005). The G-protein's α subunit binds to GTP, resulting in the dissociation of the α subunit from the β and γ subunits and thus leads to the activation of intracellular signalling proteins, depending on the α subunit type (Wettschureck and Offermanns, 2005). There are four families of G protein depending on their α subunit: G_i, G_s, $G_{12/13}$, and $G_{q/11}$ (Kamato *et al.*, 2015). As shown in Figure 1-4, the activation of G_i and G_s mediates the signalling transduction cascades that regulate the adenylyl cyclase activity, $G_{q/11}$ mediates the activation of phospholipase C (PLC) and $G_{12/13}$ activates small GTPases families (Kamato *et al.*, 2015).

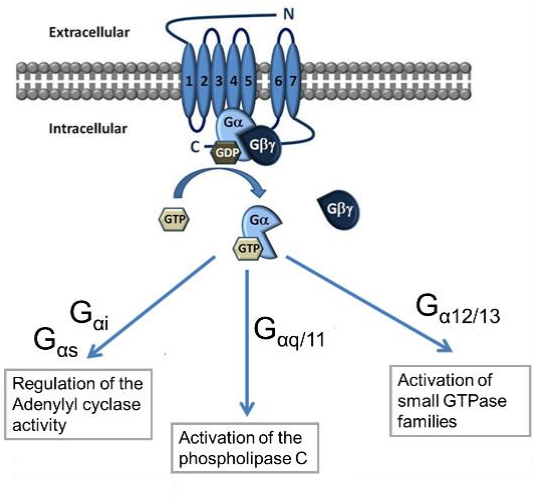

Figure 1-4: Association of the 7TM GPCRs to the four families of G protein. Figure adapted from (Kamato *et al.*, 2015)

GPCRs are widely expressed in the cardiovascular system and are already the main targets of drugs used to treat CVDs, including heart failure. GPCRs play an essential role in the function of various cardiac cells including endothelial cells and vascular smooth muscle cells (VSMCs) (Wang *et al.*, 2018).

1.6.2. Endothelin receptors

The plasma ET-1 is the main isoform localised in the cardiovascular system (Wang *et al.*, 2018) and it is established that ET-1 levels are increased in patients with chronic heart failure (Wei *et al.*, 1994). In the vascular system, ET-1 binds two types of endothelin GPCR receptors (ET_A and ET_B) (Wang *et al.*, 2018). There is two other isoforms, ET-2 and ET-3, which also play a role of vasoconstrictors. Both isoforms, ET-2 and ET-3 can also bind to the ET receptor subtypes, ET_A and ET_B However, ET_A receptors has a higher affinity for ET-1 and ET-2 than ET-3, while ET_B has the same affinity for the three isoforms (Frommer and Muller-Ladner, 2008). Moreover, ET-2 and ET-3 are less abundant in human plasma and less well characterised than ET-1 (Kowalczyk *et al.*, 2015). Recent studies suggest that ET-2 was involved in ovarian physiology (Ling *et al.*, 2013), while ET-3 is known to be more abundant in human brain (Frommer and Muller-Ladner, 2008).

Figure 1-5: ET_A and ET_B receptors signalling pathways in endothelium and smooth muscle cells leading to vasoconstriction or vasodilatation. Taken from (Enevoldsen *et al.*, 2020).

ET_A receptors are found in SMCs, while ET_B receptors are predominantly found in the endothelium, where ET_B receptors are involved in vasodilatation by NO and prostaglandin production (Liu *et al.*, 2003), but traces can be found in SMCs as well (Maguire and Davenport, 2015), as shown in Figure 1-5. However, ET_B receptors are overexpressed in SMC in presence of vascular injury and induce vasoconstriction (Johnsson *et al.*, 2008). The ET_A receptor has an affinity for ET-1 and ET-2 and is the major receptor subtype mediating vasoconstriction (Salazar *et al.*, 2007). The ET-1 binding to ET_A receptors activates the G protein of the Gq/11 and G12/13 families (Gohla *et al.*, 2000), while ET-1 binding to ET_B receptors activates the G protein of the Gi and Gq/11 families (Cramer *et al.*, 2001). In SMC, ET-1 binding to ET_A and ET_B receptors activates the Gq/11 protein, which promotes the activation of PLC. Then, PLC hydrolyses PIP_2 in DAG and IP3 leading to protein kinase C (PKC) activation and intracellular calcium accumulation (Skovsted *et al.*, 2012) (Figure 1-5). The ET-1-mediated signalling pathway induces the vasocontractile response and cell proliferation of vascular SMC (Schneider *et al.*, 2007). In the clinic, endothelin receptor specific antagonists are used to treat pulmonary arterial hypertension in patients, including bosentan (blocks both ET_A and ET_B receptors), macitentan (blocks both ET_A and ET_B receptors), and ambrisentan (blocks ET_A receptors), as shown in Figure 1-5 (Enevoldsen *et al.*, 2020).

1.6.3. Serotonin 5-HT_{1B} receptors

Serotonin was characterised for the first time in 1948 by Maurice Rapport and Irvine Page (Rapport, 1997), and in 1957 serotonin was described as a neurotransmitter (Brodie and Shore, 1957). Serotonin is a monoamine, synthetised in the central nervous system (CNS) and stored in the presynaptic neurons (Mohammad-Zadeh *et al.*, 2008). Serotonin receptors are clustered in 7 groups, from 5-HT_1 to 5-HT_7, depending of their molecular structure, signal transduction cascades and pharmacological properties (Hoyer *et al.*, 1994). The 5-hydroxytryptamine 1B (5-HT_{1B}) receptors are mostly studied in cerebral arteries (O'Quinn *et al.*, 1999, Lotfinia *et al.*, 2014), but are also found in coronary arteries along with the serotonin receptor 5-HT_{2A} (Longmore *et al.*, 2000, Maassen VanDenBrink *et al.*, 2000, Kaumann *et al.*, 1994).

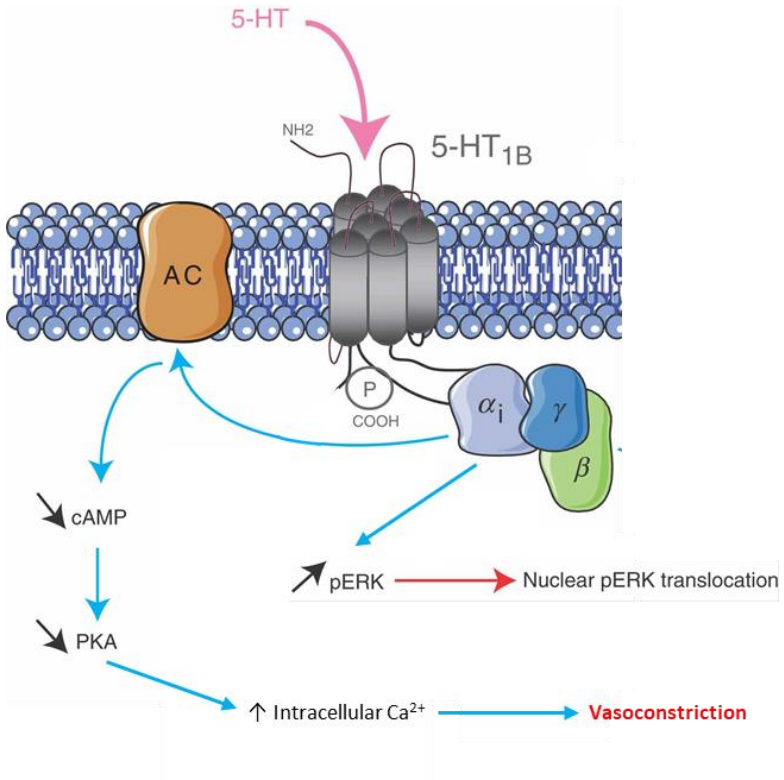

Figure 1-6: Signalling pathway of 5-HT_{1B} receptors in SMC leading to vasoconstriction. Adapted from (Masson *et al.*, 2012).

In SMC, the 5-HT_{1B} receptor is involved in vasoconstriction of the human coronary arteries, however, the serotonin vasoconstriction is predominantly induced through 5-HT_{2A} receptors (Nilsson *et al.*, 1999b). Specific binding to 5-HT_{1B} receptors activates the G-protein of Gαi subunit (Liu *et al.*, 2019). As shown in Figure 1-6, the activation of Gαi subunit associated with 5-HT_{1B} receptors inhibits the adenylyl cyclase, which reduces the cAMP formation and protein kinase A (PKA) activity leading to the

intracellular calcium release from the sarcoplasmic reticulum and vasoconstriction (Barnes and Sharp, 1999, Leenders and Sheng, 2005, Tiger *et al.*, 2018).

Previous studies with the antimigraine drug and 5-HT_{1B} agonist sumatriptan have shown that some human patients treated with sumatriptan had developed chest pain, myocardial infarction and vasospasm (Ottervanger *et al.*, 1997, Okonkwo and Ojha, 2020). It has been shown that elevated 5-HT_{1B}-mediated vasocontractile responses of cerebral and pulmonary arteries in the rat *in vitro* model were associated with several CVDs (CVD), including cerebral ischaemia (Sandhu *et al.*, 2011) and hypoxia-induced pulmonary hypertension (PHT) (Keegan *et al.*, 2001). Furthermore, the 5-HT_{1B} receptors are up-regulated in atherosclerotic rabbit coronary arteries (Ishida *et al.*, 2001).

1.6.4. Thromboxane prostanoid receptors

Thromboxane A2 (TxA2) is a potent platelet activator and vasoconstrictor (Katugampola and Davenport, 2001). Furthermore, TxA2 is the most potent agonist of the thromboxane prostanoid (TP) receptors and TxA2 binding to the TP receptors leads to vasocontractile responses (Chen, 2018).

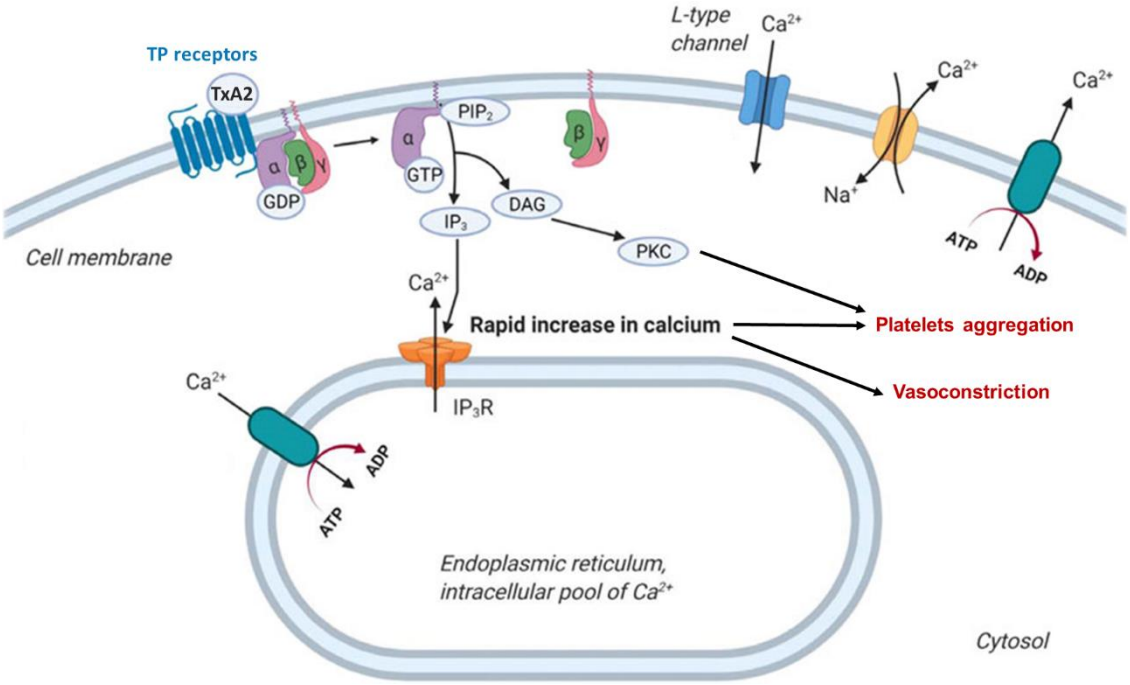

Figure 1-7: The binding of TxA2 to TP receptors activates TP signalling pathway leading to vasoconstriction. Adapted from (Trubacova *et al.*, 2022).

Elevated TxA2 levels are observed in the circulation of patients with ischemic heart disease leading to increased vasoconstriction and platelet aggregation observed during CVD (Touchberry *et al.*, 2014).

TP receptors are located in human VSMCs (Morinelli *et al.*, 1990), where TP receptors induced vasocontraction (Norel, 2007). As shown in Figure 1-7, TP receptors activate the G protein of the Gq/11 subunit, as ET_A and ET_B receptors and mediate the activation of PLC (Gao *et al.*, 2001). TP receptor mediates through this signalling pathway various cellular functions: platelet activation, vasoconstriction, EC activation and SMC proliferation (Capra *et al.*, 2014). TxA2 binding to TP receptors mediates an influx of Ca^{2+} in SMC leading to vasocontraction (Grann *et al.*, 2016). An *ex vivo* study on mesenteric arteries from hypertensive rats reported that the increased production of ROS, induced by cumulative incubation (4 min per dose) of H_2O_2 (1 – 100 µM), lead to an increase in the TxA2 production and enhanced mesenteric artery vasocontraction (Garcia-Redondo *et al.*, 2015). Pathological changes of TP pathways can lead to CVDs, like atherosclerosis, myocardial infarction and hypertension (Neri Serneri *et al.*, 1983, Katugampola and Davenport, 2001, Smyth, 2010, Martin, 1984).

1.7. Adjunct therapy as cardioprotective agents

1.7.1. Adjunct therapy currently used in clinics

Few adjuvant therapies are already clinically used as cardioprotective agents against doxorubicin-induced cardiotoxicity (Audebrand *et al.*, 2019). Antioxidants, such as vitamin C Resveratrol and Bicalein, decrease the ROS and reactive nitrogen species (RNS) levels of doxorubicin-treated patients, however, they can also decrease the anti-cancer efficiency of doxorubicin on cancer cells (Arcaro *et al.*, 2016). Dexrazoxane is an iron chelator and detoxifying agent, which reduces the topoisomerase IIβ activity. Although dexrazoxane is approved by the European Medicines Agency (EMA) and the FDA as an adjunct therapy option, dexrazoxane has been associated with an increased risk of developing myelosuppression in cancer patients (Reichardt *et al.*, 2018). Statin is an antioxidant and anti-inflammatory agent, which decreases vasodilation and platelet activity (Liao and Laufs, 2005, Oesterle *et al.*, 2017). However, studies showed that statin might also promote myopathies leading to muscle injury and diabetes (Sattar *et al.*, 2010). Some studies investigated the potential use of targeting GPCRs as preventive cardioprotective agents. The β-adrenergic receptor blockers reduced the generation of ROS, apoptosis of cardiomyocytes (Oliveira *et al.*, 2005) and have a vasodilatory effect (Mason *et al.*, 2005). However, the cardioprotective effect on chemotherapy-induced cardiotoxicity remains unclear (Avila *et al.*, 2018). Other GPCR blockers studied as potential preventive cardioprotective agents include the Angiotensin-converting enzyme inhibitors (ACEI) and angiotensin receptors blockers (ARB), as they both can preserve the left ventricular function in cancer patients treated with anthracyclines (Bosch *et al.*, 2013). Doxorubicin-induced cardiotoxicity remains an important issue

associated with cancer therapy, with no efficient and robust adjuvant therapy options available. In-depth studies of the GPCRs involvement and function during cardiotoxicity could lead to potentially identifying novel and significant adjuvant therapy options to combat cardiotoxicity as a result of doxorubicin therapy.

1.7.2. The MAPK signalling pathway

The mitogen-activated protein kinases (MAPKs) are involved during the regulation process of vascular GPCRs expression (Kacimi and Gerdes, 2003). MAPKs are serine/threonine protein kinases widely expressed in cells (Li *et al.*, 2016). There are four key MAPK signalling pathways: extracellular signal-regulated kinase (ERK), c-Jun NH2-terminal kinase (JNK), p38 isoform and big MAP kinase (BMK) (Cossa *et al.*, 2013). The ERK cascade was the first MAPK discovered and is known to get preferentially activated by shear stress or growth factor stimulation (Boulton *et al.*, 1991). The ERK 1/2 pathway is activated by various extracellular stimulants and by internal processes (Shaul and Seger, 2007) through the activation of receptor tyrosine kinase (RTK) (Sudhesh Dev *et al.*, 2021) or GPCRs (Liu *et al.*, 2019). As shown in Figure 1-8, the ERK cascade is initiated by Ras, a small G protein, which recruits and activates Raf kinases in the cytosol. Raf activates the MEK 1/2 by phosphorylation. MEK 1/2 promotes the dual phosphorylation of ERK 1/2 for ERK activation and has the role of cytoplasmic anchor protein for ERK. Activation of ERKs promotes the phosphorylation and activation of transcription factors, such as activator protein-1 (AP-1) (Whitmarsh and Davis, 1996) and nuclear factor kappa-light-chain-enhancer of activated B cells (NF-κB) (Xu *et al.*, 2008) in SMC.

The ERK cascade regulates cell proliferation, differentiation, survival and apoptosis (Shaul and Seger, 2007). In the SMC, AP-1 and NF-κB transcribe the GPCR genes in the nucleus. The GPCR mRNA is then translated in the cytosol, and afterwards exported to the cell membrane (Kacimi and Gerdes, 2003).

Figure 1-8: The MEK/ERK signalling pathway activation through RTK and GCRs. Taken from (Saab *et al.*, 2010).

Studies have investigated the MAPK signalling as a potential cardioprotective target of doxorubicin-induced cardiotoxicity. A recent study investigates the potential cardioprotective effect of a potent synthetic flavonoid with anti-oxidative properties called 3',4'-dihydroxyflavonol (DiOHF) at a concentration of 6 mg/kg (daily for 10 days from 3 days before doxorubicin treatment) in *in vivo* experiments, and 10 µM of DiOHF in the *in vitro* model administrated either 2 hrs before (preventive effect) or 2 hrs after (therapeutic effect) the doxorubicin incubation/treatment (for 24 hrs incubation in total). Doxorubicin cardiotoxicity was induced *in vivo* by doxorubicin injection (20 mg/kg by cumulative by intraperitoneal injection (i.p.)) in BALB/c mice, or by incubating H9C2 cells with 1 µM doxorubicin along with DiOHF. This study showed that DiOHF inhibits the ROS release, stabilises the mitochondrial function and reduces the apoptosis through ERK1 signalling activation leading to the suppression and reversion of doxorubicin-induced cardiotoxicity (Chang *et al.*, 2019). Another study showed that the natural fatty acid ethanolamide oleylethanolamide (OEA) could improve the ventricular remodelling and elevated cardiac function by inhibiting doxorubicin-induced apoptosis through activation of Ras/Raf-1/MEK/ERK signalling pathway using an *in vivo* rat model. They administered 3 doses of 3 mg/kg of doxorubicin by intravenous injection every other day after an overnight fasting to induce the cardiomyopathy and studied the cardioprotective effect of OEA by either (i) injecting 5 mg/kg of OEA (twice daily for 3 doses) by i.p. prior to the doxorubicin injection or

(ii) the therapeutic effect of OEA by injected 5 mg/kg of OEA (every other day for 7 days) during the 4th week after the doxorubicin treatment (Su *et al.*, 2006).

1.7.3. The MEK 1/2 inhibitor, U0126

U0126 is a small molecule MEK 1/2 inhibitor. It was synthesised in the late 1950s and discovered in 1998 as a potent inhibitor of MEK1 and MEK2 (Duncia *et al.*, 1998) (Figure 1-9). U0126 acts as a non-competitive inhibitor of MEK 1 (IC_{50} = 72nM) and MEK 2 (IC_{50} = 58nM) (Duncia *et al.*, 1998).

Figure 1-9: Structure of the 1,4-diamino-2,3-dicyano-1,4-bis[2-aminophenylthio]-butadiene (U0126)

Interestingly, U0126 showed a cardioprotective effect against ischaemia/reperfusion (I/R) by attenuating the I/R-induced apoptosis and autophagy of the myocardium in C57BL/6J mice. The I/R was induced in mice by LAD ligature for 30 min, followed by the coronary artery reperfusion to obtain an I/R model and mice were pre-treated with U0126 at 3 mg/kg (i.p.) 30 min before the I/R procedure (Wang *et al.*, 2016). A study investigated the potential cardioprotective effect of U0126 against cerebral ischaemia with an *in vivo* rat subarachnoid haemorrhage model induced by a surgical procedure. The U0126 treatment was administrated at a concentration of 0.05 mL/kg body weight of 10^{-5} M U0126 (diluted in isotonic saline plus 0.1 % dimethyl sulfoxide (DMSO)) at 6, 12 and 24 hrs post-surgery. They analysed the effect of U0126 treatment on ET_B- and 5-HT_{1B}-mediated contractile responses of cerebral arteries and quantified the expression of both receptors on the cerebral arteries. They showed that the U0126 treatment might be an interesting adjuvant therapy to treat late cerebral ischaemia by inhibiting the MEK/ERK pathway (Povlsen and Edvinsson, 2015). U0126 confers protection against cerebral vascular injury of isolated cerebral arteries, even when U0126 is administrated 6 hrs after the vascular injury (Sandhu *et al.*, 2010). Sandhu *et al.et al.* (2010) used a rat 48 hrs-incubated cerebral artery model, which mimics vascular injury mechanisms, to investigate the potential cardioprotective effect of U0126. Their data showed that U0126 optimal dose to protect the isolated cerebral arteries was 10 µM and U0126 attenuates the ET_B, 5-HT_{1B} and TP receptors elevated vasocontractile responses in 48 hrs-incubated cerebral arteries compared to fresh cerebral arteries, even when U0126 is administrated 6 hrs after the initiation of the incubation.

1.8. Detection of cardiac injury through microRNAs

MicroRNAs (miRNAs) are small non-coding single-stranded 21 – 25 nucleotide RNA compounds. In mammals, miRNAs play a key role in the regulation of specific target mRNAs and protein expression levels (O'Brien *et al.*, 2018). MicroRNA gene is transcribed from the genome by RNA polymerase II (POL II), resulting in primary miRNA, which is cleaved in precursor miRNAs by the RNase III enzymes Drosha. Precursor miRNA is transported in the cytosol with exportin 5, where it is catalysed by RNA III Dicer in miRNA/miRNA duplex. Finally, the duplex is unwinded by a helicase, resulting in mature miRNA, which is loaded into Argonaute (AGO) to form a miRNA-induced silencing complex (miRISC) (Figure 1-10) (Zhao *et al.*, 2019). MiRNA leads miRISC to specific recognition of mRNA and down-regulation of gene expression by one of these two post-translational mechanisms, translational repression and mRNA cleavage. MiRNA in miRISC binds to miRNA response elements (MREs) in the 3'-UTR of mRNA. One mRNA can be regulated by multiples miRNA and one miRNA can have several different targets (Bartel, 2004). Furthermore, miRNAs are essential in many biological processes, including angiogenesis, cellular metabolism, embryogenesis, placental development (Fu *et al.*, 2013) and pathological processes, primarily cancers, where they play the role of tumour suppressors and oncogenes (Macfarlane and Murphy, 2010).

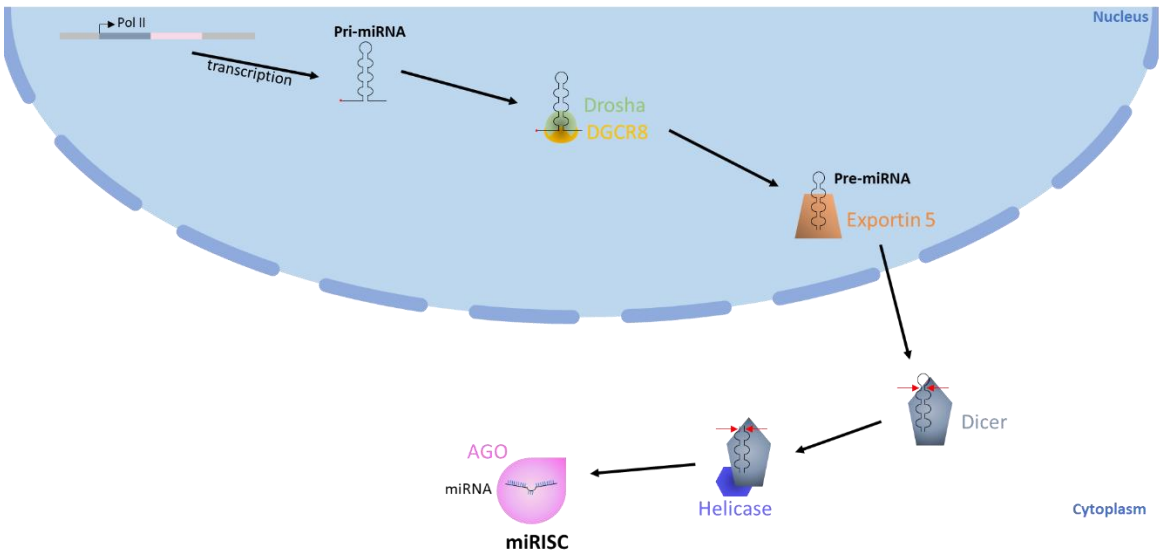

Figure 1-10: Biogenesis of miRNAs from the nucleus to the cytoplasm.

MiRNAs are attractive as biomarkers due to their tissue specificity, high sensitivity of tissue injury, high stability, early and accurate quantification leading to early detection in several disease development and as a non-invasive method (Sandhu and Maddock, 2014). Recently, it has been established that

there are different functional miRNA populations in tissues, which are involved in the reshaping of transcriptomes and the cell identity acquisition and maintenance leading to the creation of a tissue-specific localisation data for various miRNAs in mouse, rat, and human tissues (Blazie *et al.*, 2017). Furthermore, tissue-specific miRNAs, such as brain-, muscle- and liver-miRNAs, have been used as plasma biomarkers for brain, muscle and liver injuries (Laterza *et al.*, 2009). Furthermore, accurate tools were developed to quantify miRNA levels in plasma or tissues, such as the miRNA array cards. As an example, TaqMan array cards can be used to obtain a full screen of a transcriptome, identifying potential genes involved in some diseases and toxicological mechanisms (Keys *et al.*, 2010). At room temperature, miRNAs can stay stable for up to four days (Salloum-Asfar *et al.*, 2019), and their high stability in bio-fluids, including plasma, makes them a relevant biomarker tool for the early detection of diseases (Szelenberger *et al.*, 2019). Circulating miRNAs are mature miRNA localised in extracellular microenvironments, such as plasma, saliva, tears, urine, etc. (Weber *et al.*, 2010). In humans, 10 % of total miRNA can be found in plasma (Szelenberger *et al.*, 2019). There are various pathways by which miRNAs are released into bio-fluids, either through a passive mechanism, where specific cells are damaged and this leads to a leak of endogenous particles like miRNAs, or through an active mechanism, where miRNAs are released by secretion via macrovesicles, such as exosomes, or RNA-binding proteins (Zhao *et al.*, 2019). The circulating miRNA enables the non-invasive detection of disease-induced altered miRNA levels and methods to detect miRNA, such as real-time PCR using microRNA assays are easily carried out and are strong and specific methods (Dorn, 2011).

Circulating miRNAs as biomarkers have been studied in various diseases, such as cancers, heart diseases, liver diseases and neurological disorders (Szelenberger *et al.*, 2019).

Interestingly, approximately 200 miRNAs are expressed in the heart and studies underlined that some of these miRNAs were related to cardiac injury (Dorn, 2011). Recently miRNAs have been explored as potential novel biomarkers to assess cardiotoxicity at an early sub-clinical stage. The miRNAs miR-1 and miR-133 are expressed in cardiac muscle and skeletal muscle, and their expression has been extensively investigated in CVD development. Both miRNAs are involved in heart development and it has been established that the dysregulation of these miRNA expression levels in plasma leads to the development of cardiac diseases (Szelenberger *et al.*, 2019), including arrhythmia (Sandhu and Maddock, 2014), acute myocardial infarction (Wang *et al.*, 2021) and heart failure (Ghigo *et al.*, 2016, Li *et al.*, 2021).

Currently, anthracyclines-induced cardiotoxicity can be assessed by various circulating myocardial injury associated biomarkers, including measurement of circulating cTnT and BNP levels and imaging techniques, including MRI (Lipshultz *et al.*, 2012). However, many studies investigated miRNAs as

potential biomarkers for anthracycline-induced cardiotoxicity (Freres *et al.*, 2018, Leger *et al.*, 2017). In their study, Leger et al investigated circulating miRNAs expression in child and young adult (>18 years old) cancer patients treated with anthracycline. They showed miR-29b and miR-499 were up-regulated in anthracycline-treated patients. In this study, authors suggest that the acute increase of miR-29b after anthracycline treatment may underline a remodelling process in response to cardiac injury since it was shown by Luna *et al.et al.* that miR-29b is involved in the extracellular matrix (ECM) remodelling (Luna *et al.*, 2009). Furthermore, it has been shown by Wan *et al.et al.* that miR-499 has a protective role against apoptosis induced by oxidative stress after an AMI (Wan *et al.*, 2018), which is also observed after anthracycline treatment. Leger *et al.et al.* underlined the potential role of miR-29b and miR-499 as anthracycline-induced early detection biomarkers (Leger *et al.*, 2017). In another study headed by Freres *et al.et al.*, alteration of miRNA expression was observed in breast cancer patients treated with anthracycline-containing chemotherapy. The patients' age was ranging from 26 to 78 years old and patients had primary breast cancer. Each patient received neoadjuvant chemotherapy (NAC) containing epirubicin. In this study, it was demonstrated that three of the up-regulated miRNAs (miR-126-3p, 199a-3p and 423-5p) were known to be related to congestive heart failure (CHF) (Freres *et al.*, 2018). Both studies from Leger and Freres highlight the potential use of circulating miRNAs as biomarkers for anthracycline-induced cardiotoxicity. MiRNAs are also known to play a role in the angiogenesis and vascular tone through the endothelial cells function and miRNAs are associated with vascular pathological conditions by regulating the endothelial function (Fernandez-Hernando and Suarez, 2018). As an example, let-7f is a pro-angiogenic miRNA, involved in angiogenesis and endothelial function and has also been reported to be reduced in breast cancer patients with anthracycline-induced cardiotoxicity compared to non-cardiotoxic patients (Pereira *et al.*, 2020). Additionally, miR-126 is also involved in angiogenic and inflammatory processes and two studies reported that miR-126 expression was reduced in the plasma of breast cancer patients when comparing the cardiotoxicity and non-cardiotoxicity groups (Pereira *et al.*, 2020).

1.9. Summary of the current gaps about the doxorubicin-induced vasotoxicity that this thesis will fill

The doxorubicin-induced cardiotoxicity has been widely investigated over the last decades, meanwhile there is a paucity of literature on the doxorubicin-induced vasotoxicity. Most of the studies investigated the mechanisms of doxorubicin effects in the cardiomyocytes, such as the ROS overproduction and intracellular calcium overload (Corremans *et al.*, 2019). Interestingly, the activation of the GPCRs, ET_A, ET_B, $5\text{-}HT_{1B}$ and TP receptors induces an increase of the intracellular

calcium in vascular cells, leading to a vasoconstriction, however, the potential adverse effect of doxorubicin on the vascular tone of coronary arteries through the activation of these four GPCRs has not been investigated. In this study, an *in vitro* model of CVDs was designed to specifically investigate the doxorubicin-induced vasotoxicity in rat coronary arteries. The *in vitro* model of this study is the first *in vitro* model using incubated coronary arteries designed to investigate the vascular function during doxorubicin treatment with the wire-myography technique. Previous in vitro models of incubated coronary arteries were designed to mimics a vascular injury (Skovsted *et al.*, 2012), however, these models were not specific to doxorubicin-induced vascular injury. This novel *in vitro* model was used to investigate four specific GPCRs during doxorubicin-induced vasotoxicity in this thesis and, in the future, can be used to investigate other GPCRs or tested new cardioprotective agents to alleviate the doxorubicin adverse effects on the vascular tone.

In this study, the novel doxorubicin-induced vasotoxicity model was used to (i) determine if doxorubicin-induced vasotoxicity is associated with the four studied GPCRs (ET_A, ET_B, $5\text{-}HT_{1B}$ and TP receptors)-mediated vasocontractile response, (ii) identify the mechanisms involved in the doxorubicin-induced vasotoxicity leading to altered GCPR-mediated vasocontractile responses, and (iii) investigate the effect of the doxorubicin and U0126 co-treatment on altered GPCR-mediated vasocontractile response. This study will, first, allow a better understanding of the doxorubicin-induced vasotoxicity and the role of GPCRs in the doxorubicin-induced alteration of the vascular tone of rats' coronary arteries. Interestingly, there is currently no literature on the involvement of ET_A, ET_B, $5\text{-}HT_{1B}$ and TP receptors in doxorubicin-induced vasotoxicity. Secondly, the investigation will provide a better understanding of the doxorubicin effects on GPCRs production (i.e. transcription and translation) and highlight mechanisms involved in doxorubicin-induced vasotoxicity. A better understanding of the mechanisms involved in doxorubicin-induced vasotoxicity will allow the discovery of new cardioprotective agents, which could be used as adjunct therapy to improve the treatment of cardiac adverse effects of doxorubicin.

An interesting pathway to investigate as adjunct therapy is the MAPK signalling pathway, which has already been studied as cardioprotective target of doxorubicin-induced cardiotoxicity. However, the cardioprotective effects of the MEK/ERK pathway on the vascular tone altered by doxorubicin treatment has never been investigated in rat coronary arteries. Thus, in this study, the addition of U0126, the MEK 1/2 inhibitor will underline the MEK/ERK pathway involvement in doxorubicin-induced vasotoxicity and could initiate the research of adjunct treatment able to alleviate vascular adverse effects of doxorubicin in cancer patients.

The early detection of chemotherapy-induced cardiotoxicity can improve the cancer patient survival. However, the current biomarkers, as TnT and BNP, are not enough specific and image techniques are necessary to assess any potential cardiotoxicity (Curigliano *et al.*, 2012). Recently, the use of miRNA as biomarkers for cancer and CVDs has been widely investigated (Szelenberger *et al.*, 2019), however their use as biomarkers of the chemotherapy-induced vasotoxicity has been poorly investigated. In this study, plasma samples used were from cancer treated with different chemotherapy regimens containing anthracycline. Their plasma samples were collected before and after their chemotherapeutic treatment. The analysis of miRNA from the cancer patients' plasma aimed to identify potential miRNAs associated with vascular injury induced by the chemotherapy. This thesis aim to underlie a group of miRNAs associated to vascular injury and altered by the chemotherapy in cancer patients' plasma and thus participate to the discovery of novel sensitive biomarkers for an earliest diagnosis of chemotherapy-induced vasotoxicity.

1.10. Hypothesis and aims of the thesis

The aim of this thesis is, firstly, to investigate the doxorubicin-induced cardiotoxicity effects on four vascular GPCRs (ET_A, ET_B, $5\text{-}HT_{1B}$ and TP receptors), and secondly, to determine the mechanisms involved during the alteration of the GPCRs by doxorubicin-induced cardiotoxicity by investigating the effect of the MEK 1/2 specific inhibitor U0126 on GPCRs-mediated vasocontractile responses. Thirdly, the study aims to study the miRNA profile of cancer patients treated with anthracycline chemotherapy treatment regimens and underline the involvement of potential vasotoxicity-linked miRNAs (Figure 1-11).

The different objectives of this study are to:

<u>*In rat coronary vasculature:*</u>

- *The incubation of coronary arteries with doxorubicin allow the study of doxorubicin-induced vasotoxicity with a rodent in vitro model.*

  Aim: Set up an organ culture model with isolated rat left anterior descending arteries to study the cardiovascular adverse effects of doxorubicin on vascular tone.
- *The doxorubicin alters the vasocontractile response of coronary artery, through the activation of four GPCRs.*

  Aim: Determine if doxorubicin affects the ET_A, ET_B, $5\text{-}HT_{1B}$ and TP receptor-mediated vasocontraction.

- *The doxorubicin alters the GPCR-induced vasoconstriction on the transcriptional and translational levels.*

  Determine if the GPCR-induced vasocontraction observed is truly specific to the GPCR by application of specific GPCR antagonists.
- *The MEK/ERK pathway can regulate the elevated GPCR-mediated vasoconstriction induced by doxorubicin.*

  Aim: Investigate the effect of MEK 1/2 specific inhibitor U0126 on doxorubicin-induced vasotoxicity through the different studied receptors on incubated LAD arteries with vehicle or doxorubicin treatment.
- *The doxorubicin impairs the GPCR-induced vasoconstriction by altering the transcription of the studied GPCRs.*

  Aim: Determine the effect of doxorubicin on mRNA levels of the specific GPCRs
- *The doxorubicin impairs the GPCR-induced vasoconstriction by altering the translation of the studied GPCRs.*

  Aim: Study the effect of doxorubicin on GPCRs expression on LAD vessels.

In cancer patient plasma samples:

- *The chemotherapy-induced cardiotoxicity induce an alteration of specific vascular miRNA in the plasma of cancer patients.*

  Aim: Analyse the miRNA profiles of cancer patients treated with anthracycline chemotherapy regimens and find a potential correlation of cardiac events with altered vascular injury associated miRNAs.

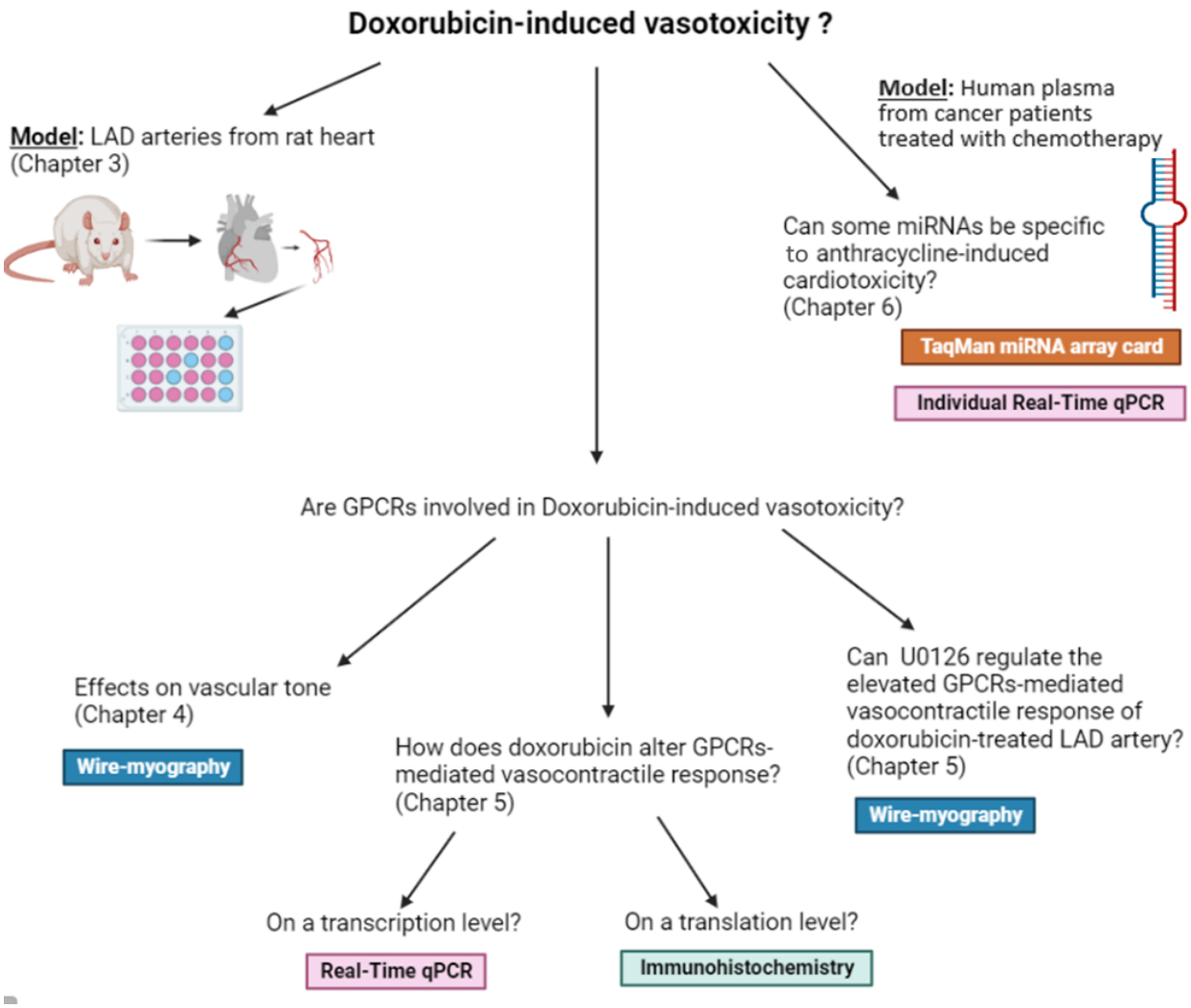

Figure 1-11: Diagram of the thesis objectives and the techniques used.

Chapter 2:

2. Materials and Methods

2.1. Animals and human samples

2.1.1. Animals and ethics

Male Sprague-Dawley rats (300 - 350g) were used during the experiments. The animals were purchased from Charles River (Margate, UK) and housed at the University of Warwick. Experiments were conducted in accordance with the Home Office Guidance on the Operation with Animals (Scientific Procedures Act 1986; The Stationary Office, London, UK) and were approved by the Ethics Committee of Coventry University. Rats were delivered to Coventry University each morning and put in a cage with standard pellet chow and free access to water and food. Rats were acclimated at least 2 hrs before the LAD isolation.

2.1.2. Human plasma samples received from external collaborators Dr Malcolm Walker and Prof Derek Yellon (UCL)

Dr Malcom Walker, Prof Derek Yellon and their team at UCL performed a clinical study to investigate the effect of remote ischaemic pre-conditioning on myocardial injury in anthracycline-treated patients. This study was approved by UCL and NHS R&D departments (REC reference: 15/LO/1116) as well as by the London – Chelsea Research Ethics Committee according to all relevant legal rules and ethics guidance, including the Data Protection Act and the Human Tissue Act. The cancer patients were adults treated with anthracycline regimen chemotherapy, who tolerate BP arm cuff inflation and were recruited in the UCL hospital's Macmillan Cancer Centre. Prior to chemotherapy infusion administration remote ischaemia conditioning (RIC) or sham procedure was processed. The RIC procedure consisted of 4 cycles of upper arm blood pressure cuff inflation to 200mm Hg for 5 min (corresponding to the ischaemia phase), followed by a cuff deflation for 5 min. The blood sample were collected before, immediately post-chemotherapy (6 to 24 hrs following the end of the treatment) and 3 months post-chemotherapy. The trial protocol is detailed in chapter 1.6.3.

2.2. Consumables and Drugs used:

2.2.1. Consumables and drugs used for rat LAD wire-myography experiments

Doxorubicin hydrochloride was purchased from Tocris Biosciences (Bristol, UK) and was dissolved in reverse osmosis (RO) water with a final stock concentration of 1 mM.

Serotonin hydrochloride, carbachol, sarafotoxin S6c, endothelin-1, 9,11-dideoxy-11α,9α-epoxymethanoprostaglandin $F_{2\alpha}$ (U46619), 5-carboxamidotryptamine maleate salt were purchased from Sigma-Aldrich (Merck KGaA, US). U46619 was dissolved in methyl acetate with a final stock concentration of 3 mM. All the other drugs were dissolved in RO water. Serotonin hydrochloride and carbachol had a final stock concentration of 10 mM. Sarafotoxin 6c and endothelin-1 had a final stock concentration of 0.1 mM. U46619 and 5-carboxamidotryptamine had a final stock concentration of 27 mM and 30 mM, respectively. The antagonists BQ788, BQ123 and Seratrodast were purchased from Tocris Biosciences (Bristol, UK). The antagonist GR55562 was purchased from Sigma-Aldrich (Merck KGaA, US). BQ788 and Seratrodast were dissolved in DMSO with a final stock concentration of 0.1 mM. BQ123 and GR55562 were dissolved in RO water with a final stock concentration of 400µM and 0.1 mM, respectively. The MEK1/2 inhibitor U0126 was purchased from EMD Millipore Corporation (Merck, US) and dissolved in Dimethylsulfoxide (DMSO) with a final stock concentration of 2mM. DMSO was purchased from Sigma-Aldrich (Merck KGaA, US). All drugs were aliquoted in suitable volumes and stored at -20 °C.

Dulbecco's Modified Eagle Medium, DMEM (1 g/L D-Glucose, 4 mM L-Glutamine, 0.11 g/L Sodium pyruvate) and Antibiotic-antimycotic (10,000 units/mL of penicillin, 10,000 µg/mL of streptomycin, and 25 µg/mL of Gibco Amphotericin B) were purchased from ThermoFisher Scientific (Massachusetts, US).

All reagents used to prepare the Krebs Henseleit (KH) buffers for the myography experiments were purchased from Fisher Bioreagents (Fisher Scientific, US).

2.2.2. Consumables used for rat or human plasma miRNA quantification

miRNeasy mini kit was purchased from Qiagen (Manchester, UK) and used for miRNA extraction from plasma samples. Chloroform (C2432), absolute ethanol, and MS2 RNA 0.8 µg/µL (10165948001) were purchased from Sigma-Aldrich (Merck KGaA, UK). Tris-EDTA (TE) buffer pH 8.0 (1 mM Tris HCl, 0.1 mM EDTA) was purchased from Invitrogen (Thermofisher, UK) and diluted in RNase-free water to obtain a final solution of 0.1 TE buffer pH 8.0.

All the following reagents were purchased from Life Technology (Thermofisher, UK). The reverse transcription was performed with TaqMan™ MicroRNA Reverse Transcription Kit (4366597) and Megaplex™ RT Primers, Human Pool A v2.1 (4399966). The pre-amplification reactions were done with TaqMan™ PreAmp Master Mix (4391128) and Megaplex™ PreAmp Primers, Human Pool A v2.1

(4399233). The qPCR reaction was performed on TaqMan™ Array Human MicroRNA A Cards v2.0 (4398965) using the TaqMan™ Universal Master Mix II, no UNG (4440049).

The reverse transcription for individual miRNA assay analysis was performed with miRNA Reverse Transcription kit from Applied Biosystems and TaqMan™ MicroRNA Assay (4427975) using the individual miRNA assays: hsa-miR-126-002228, hsa-miR-10a-000387, hsa-miR-143-002249, hsa-miR-150-000473, hsa-miR-320-002277 and endogenous control snRNA U6. The qRT-PCR for individual miRNA was performed using the individual TaqMan™ MicroRNA miRNA assays listed above (4427975) with TaqMan Universal PCR Master Mix II, no UNG (4440049).

2.2.3. Consumables used for rat LAD mRNA quantification

RNeasy Protect mini kit was purchased from Qiagen (Manchester, UK) and used to isolate mRNA from rat LAD vessels. Absolute Ethanol 100% was added to the RNeasy Protect mini kit RPE buffer purchased from Sigma-Aldrich (Merck KGaA, UK). β-Mercaptoethanol was added to the RNeasy Protect mini kit lysis RLT buffer and was purchased from Sigma-Aldrich (Merck KGaA, US). The Superscript IV™ VILO Master Mix for the reverse transcription PCR and the PowerTrack SYBR Green Master Mix for the Real-Time PCR were purchased from ThermoFisher Scientific (Massachusetts, US). Specific primers for rat GPCRs and the endogenous controls EF-1 and GAPDH were purchased from Invitrogen / ThermoFisher (Massachusetts, US) specific primers designed during previously published work (Sandhu *et al.*, 2010) and are listed in Table 2-1.

The primers were resuspended in RNAse-free water to obtain a stock concentration of 100 mM and then, diluted to obtain a work concentration of 10 mM.

Table 2-1: Primer sequences of Forward and Reverse primers for each specific gene analysed.

	GenBank ID	Forward primers	Reverse primers
Endothelin A receptor	NM_012550	ATT GCC CTC AGC GAA CAC	CAA CCA AGC AGA CGG TC
Endothelin B receptor	NM_017333	GAT ACG ACA ACT TCC GCT CCA	GTC CAC GAT GAG GAC AAT GAG
5-HT_{1B} receptor	NM_022225	TCC GGG TCT CCT GTG TAC GT	GGC GTC TGA GAC TCG CAC TT
Thromboxane A2 receptor	NM_017054	ATC TCC CAT CTT GCC ATA GTC C	CGA TGA TCC TTG GAG CCT AAA G
Elongation Factor 1	NM_175838	GCA AGC CCA TGT GTG TTG AA	TGA TGA CAC CCA CAG CAA CTG
GAPDH	NM_017008	GGC CTT CCG TGT TCC TAC C	CGG CAT GTC AGA TCC ACA AC

2.2.4. Consumables used for rat LAD immunohistochemistry

Vessels were fixed by Cellpath™ OCT Embedding Matrix from FisherScientific (Thermofisher, UK). All antibodies and normal donkey serum were purchased from Abcam (Cambridge, UK). The primary antibodies were rabbit anti-endothelin A receptor (ab178454), rabbit anti-endothelin B (ab262700), rabbit anti- serotonin 5-HT_{1B} receptor (ab13896), rabbit anti-thromboxane A2 receptor (ab233288), rabbit anti-ERK1 + ERK2 (ab17942) and mouse anti-actin (ab11003). The secondary antibodies were donkey anti-rabbit IgG H&L Alexa Fluor® 594 RED (ab150108) and donkey anti-mouse IgG Alexa Fluor® 488 GREEN (ab150073). Slides were mounted using the ProLong™ Gold Antifade Mountant purchased from Thermofisher (UK). Phosphate buffered saline (PBS, pH 7.2) was used for the dilution and washing the slides. PBS 10X and Bovine Serum Albumine (BSA) and acetone were purchased from FisherScientific (Thermofisher, UK). The Triton X-100 was purchased from Fisher Scientific (Thermofisher, UK).

2.3. Wire-myography on Left Anterior Descending arteries

2.3.1. Background of the wire-myography technique

The wire-myography technique was first introduced in 1972 by Bovan and Osher and was used to measure tension changes in small vessels (Bevan and Osher, 1972). In 1977, Mulvany and Halpern refined and developed the wire-myography technique, and their protocol is still applied in labs worldwide until this day. Their aim was to directly measure the mechanical changes in small vessel segments (Mulvany and Halpern, 1977).

The wire-myography technique is used to study vascular pharmacology by investigating the pharmacodynamics of small blood vessels (Angus and Wright, 2000). Indeed, using an *in vitro* technique allows the control of the physiological settings and nullifies the homeostatic mechanisms, such as blood flow or the autonomic nervous system central (Spiers and Padmanabhan, 2005). Moreover, pathological states like CVD can be “reproduced/mimicked” in the myograph chambers (Spiers and Padmanabhan, 2005).

The wire-myography allows mechanical measurements of rings/segments of small blood vessels. Mounted vessels are incubated in a physiological solution. Specific drugs are added to the vessel media, and these drugs interact as ligands on specific receptors expressed on the inner membrane of the vessels and this leads to altered vascular tension. Wire-myography, therefore, allows for the analysis of vascular tone through drug-receptor interaction (Angus and Wright, 2000).

For this study, rat coronary arteries were mounted on two wire-myograph setups (Multi wire myograph system - 620M, Denmark). Each wire-myograph setup had four chambers where four vessels could be studied simultaneously. All chambers have electronic heating fixed at 37 °C and are continuously gassed with 5 % CO2 and 95 % O2 (pH = 7.4).

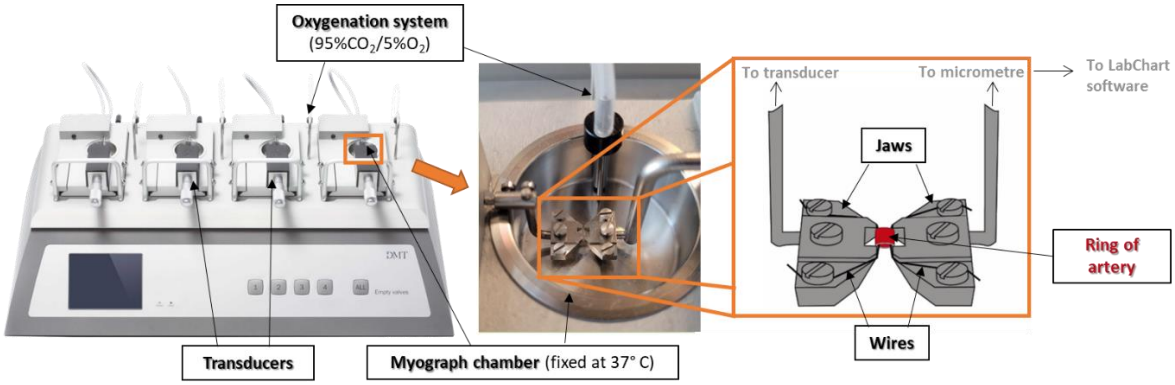

Figure 2-1: In wire-myograph systems, wires are passed through the lumen of a blood vessel and the vessel is stretched to obtain a rest tension as in physiological conditions adapted from (Wenceslau *et al.*, 2021).

In each chamber, there are two jaws: one of the jaws is attached to a force-displacement transducer, while the other jaw is connected to a micrometre. As in Figure 2-1, two wires are mounted carefully through the vessel's lumen and each wire is connected to one of the jaws in the myograph chamber. The data was recorded by the LabChart Pro 8 software (AD Instruments, UK).

2.3.2. Dissection of rat Left Anterior Descending arteries (LAD)

Rats were culled by cervical translocation and hearts were immediately removed and put in ice-cold calcium-free KH buffer (*NaCl 119 mM, $NaHCO_3$ 15 mM, KCl 4.6 mM, $NaH_2PO_4x2H_2O$ 1.2 mM, $MgCl_2x6H_2O$ 1.2 mM and glucose 5.5 mM*) gassed with 5 % CO_2 and 95 % O_2 (pH = 7.4). Heart vessels and segments were dissected using microscopy (Nikon SMZ 745T) with the left atrium facing upwards. The ice-cold gassed calcium-free KH buffer was replaced at least every 15 min. The main artery is located between the pulmonary artery and the left atrium and branches into the LAD and the LCx (Figure 2-2).

Figure 2-2: Coronary arteries in the rat heart (Buetow and Laflamme, 2018).

The myocardial tissue surrounding the LAD artery was carefully removed. Once the LAD artery was dissected free from surrounding myocardial tissue, it was cut into four segments approximately 2 mm long each, and a 40 μm diameter stainless steel wire was inserted through the lumen of each 2 mm vessel ring.

2.3.3. Acute vascular pharmacology effect of doxorubicin on rat LAD

To study the acute vascular pharmacology effect of doxorubicin, rings of LAD vessels were mounted onto the myograph immediately after dissection and immersed in a sodium KH (Na^+ KH) (*NaCl 119 mM, $NaHCO_3$ 15 mM, KCl 4.6 mM, $CaCl_2x2H_2O$ 1.5 mM, $NaH_2PO_4x2H_2O$ 1.2 mM, $MgCl_2x6H_2O$ 1.2 mM and glucose 5.5 mM*) at 37 °C and gassed with 5 % CO_2 and 95 % O_2 (pH = 7.4). The mounted vessels were given a stabilisation period of 1 hr where the Na^+ KH buffer (continuously gassed with 5 % CO_2 in O_2 at 37 °C, pH = 7.4) was changed every 15 min with a pre-tension fixed in the range of 1.16 mN/mm to 1.52 mN/mm (Ping *et al.*, 2014) after 30 minutes. Then, the direct effects of doxorubicin doses and the cumulative addition of doxorubicin on the contractile capacity were investigated. The different protocols to investigate acute vascular effects are detailed in Chapter 3, section 3.2.1.

2.3.4. Organ culture of rat LAD

The effect of doxorubicin exposure after 24 hrs or 48 hrs incubation was studied by incubating LAD rings in serum-free Dulbecco's modified Eagle's medium (*DMEM: glucose 1000 mg/L, L-glutamine 4 mM, sodium pyruvate 0.11 mg/ml*) supplemented with an antibiotic mix (*penicillin 10,000 IU/ml, streptomycin 20mg/ml*) for 24 hrs or 48 hrs at 37 °C in an incubator humidified with 5 % CO_2 and 95 % O_2 (pH = 7.4). Doxorubicin or vehicle was added to the media at the initiation of the incubation. The inhibitor of MEK 1/2, U0126 and the vehicle DMSO were also added to the media for the experiment with U0126. Details about the concentration and volume are given in the Chapter 5, section 5.2.

2.3.5. *In vitro* pharmacology to obtain dose-response curves

Vessels were mounted in Ca^{2+}free KH buffer on myograph after the 24 hrs incubation, the buffer was changed to Na^+ KH and the vessels were stabilised for 1 hr (see Figure 2-3).

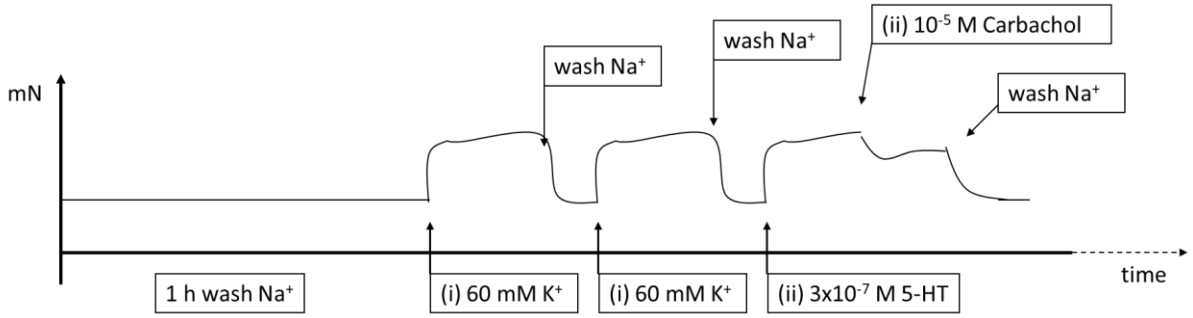

Figure 2-3: Experimental protocol to study vascular contractility and dilatory capacity of LAD vessels. Na+ = Na^+ KH, K+ = K^+ KH, 5-HT = serotonin.

A pre-tension in the range of 1.16 mN/mm to 1.52 mN/mm was applied during this stabilisation step (Ping *et al.*, 2014). After the stabilisation period, the vessels were exposed to a 60mM K^+ KH buffer to measure the maximum contraction. Vessels were washed with Na^+ KH buffer for 15 min and a second 60 mM K^+ KH buffer contraction was recorded. Vessels were washed with Na^+ KH buffer until the vascular tension came back to the baseline level. To measure vasodilatory capacity the vessels were pre-contracted with 3. 10^{-7} M serotonin (5-HT) followed by applying 10^{-5} M carbachol. Vessels were washed with Na^+ KH buffer with 15 min intervals until the vascular tension came back to the baseline level. The K^+ KH buffer maximum contraction is used as reference for the study of the GPCR agonist-mediated dose-response curves, therefore the contractile capacity, determined by the K^+ KH buffer, needs to be constant with or without added doxorubicin.

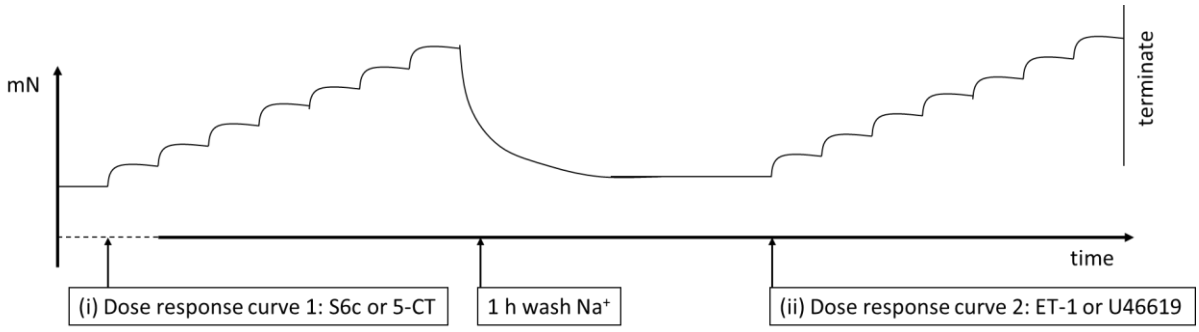

Figure 2-4: Experimental protocol to study dose-response curve of specific GPCR agonists. S6c = sarafotoxin 6c, the agonist of ET_B receptors; 5-CT = 5-carboxyamidotryptamine, the agonist of 5-HT_{1B}

receptors, ET-1 = endothelin-1, the agonist of ET_A and ET_B receptors; U46619, the agonist of TP receptors.

Once the contractile and dilatory capacity of the vessels was measured, and thus established the function and viability of the vessels, the dose-response curve was determined by applying cumulative doses of the agonists in half-log increments (Figure 2-4). The segments were either stimulated with (i) ET_B receptor agonist sarafotoxin 6c (S6c), from 10^{-14} to $10^{-7.5}$ M, followed by Na^+ KH buffer washing with 15-minute intervals until the vascular tension came back to the baseline level, where after the second dose-response curve was measured by applying ET_A and ET_B receptor agonist endothelin-1 (ET-1), from 10^{-14} to $10^{-7.5}$ M, or by stimulation with (ii) $5\text{-}HT_{1B}$ receptor agonist 5-carboxamidotryptamine (5-CT), from 10^{-12} to $10^{-5.5}$ M, followed by Na^+ KH buffer washing with 15-minute intervals until the vascular tension came back to the baseline level, where after the second dose-response curve was measured by applying thromboxane prostanoid receptor agonist U46619, from 10^{-12} to $10^{-6.5}$ M.

2.3.6. Data Analysis

All data are expressed as means ± S.E.M and n refers to the number of rats. A test of normality, named Shapiro-Wilk test, was firstly done for all the data to determine if they were normally distributed or not and then choose the most relevant statistic test for each data set. The contractile response of each vessel to the agonist was expressed as percentage of the 60mM K^+ KH buffer-induced contraction where C_{max} is the contraction at the highest dose and contractile responses were compared with Unpaired Student T-test (SPSS statistics) when there are two sets of data or Two-way ANOVA with Bonferroni's post-hoc test (GraphPad Prism 9) for multiple comparisons. The "E_{max}" values correspond to the maximal contractile response induced by agonists and are generated by the software GraphPad Prism 9. The "pEC_{50}" correspond to the negative logarithm of the agonist concentration that produces 50 % of the maximal contraction and is generated by the software GraphPad Prism 9. "E_{max}" and "pEC_{50}" are statistically analysed by either unpaired Student T-test when the data was normally distributed, or Kruskal-Wallis's test when the data wasn't normally distributed. All calculations and statistical analysis were carried out using Graph-Pad Prism 9.0 (GraphPad Software, La Jolla, USA) and SPSS Statistics version 25 (IBM). Statistical significance was determined with $p \leq 0.05$.

2.4. Quantification of mRNA from rat LAD

2.4.1. Real-Time polymerase chain reaction PCR methodology

The PCR methodology was developed by K. Mullis in 1985 (Nobel Prize awarded in 1993). The Real-Time PCR is a powerful tool to quantify nucleic acids. This technique allows for the amplification of nucleic acids sequence from a sample, even at a very low level of expression. The amplification is performed by a cyclic process which generates copies of the selected sequence of interest, which can be easily analysed by fluorescence incorporation during the copy process.

The cycles are designed in three steps at different temperatures. First, a high temperature to separate strands of cDNA. Then, the temperature is lowered to let primers, designed to flank a specific sequence, anneal to strand. Finally, a temperature is fixed around 72 °C, which is the optimum temperature for polymerase, to extend primers with dNTPs.

The quantification is done with a fluorescent reporter. SYBR green is an asymmetric cyanine dye, which has no fluorescence when it is free and becomes brightly fluorescent when it binds to DNA. The fluorescence increases with the amount of double-stranded products, as in Figure 2-5. The quantification is obtained by comparing the number of amplification cycles for the sample's response curve required to reach a threshold fluorescence level, which is the called CT value (Kubista *et al.*, 2006).

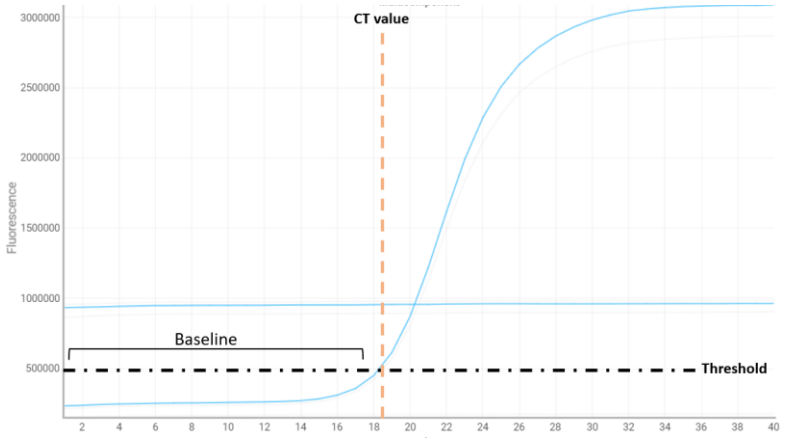

Figure 2-5: Threshold and CT values on Real-Time PCR amplification curve. The curve shows the amplification of mRNA through the different cycles of the Real-Time PCR, where the X-axis represents the number of cycles and the Y-axis represents the fluorescence emission. (Illustration realised with Biorender website)

In the present study, the real-time PCR was used to determine the mRNA expression levels for specific GPCRs and to investigate the possible differential variation of mRNA expression in the different vascular treatment groups.

2.4.2. RNA purification

Total cellular RNA was extracted from rat LAD with the RNeasy protect mini kit (Qiagen, UK), after being submerged in protect liquid at -20 °C at least overnight. LAD were lysed in the RLT buffer containing 0.01 % of β-Mercapthoethanol by homogenisation with a rotor-stator homogeniser (Ultra-Turrax T25, IKA-WERKE). Ethanol was added to the lysate to provide an appropriate binding condition. Total RNA was then fixed to the membrane of a RNeasy spin column by centrifugation, while contaminants were washed away. Following a few washes with washing the buffers RW1 and RPE, Total RNA was eluted in RNAse-free water.

Total RNA amount and purity were determined with NanoDrop™ One/OneC Microvolume UV-Vis Spectrophotometer (ThermoFisher, USA).

2.4.3. Reverse Transcription

Reverse transcription of total cellular RNA to cDNA was performed with Superscript™ IV VILO Master Mix (ThermoFisher, US) using the Eppendorf® Mastercycler® Nexus Thermal Cyclers (Merck, USA). Template RNA was mixed with SuperScript IV™ VILO Master Mix on ice. The mix was incubated (1) at 25 °C for 10 min to anneal primers. Afterwards (2) it was incubated at 50 °C for 10 min to reverse transcribe RNA, followed by incubation (3) at 85 °C for 5 min to inactivate the enzyme. The resulting cDNA product was diluted in RNAse-free water to give a final cDNA concentration of 1 ng/µL.

2.4.4. Real-Time PCR

The quantification of mRNA expression levels was determined with SYBR Green as fluorescence reporter and primers specifically designed for the four GPCRs and two endogenous control genes, EF-1 and GAPDH. The designed sequences of primers are shown in Table 2-1, in section 2.2.3.

The cDNA samples were mixed with a Superscript™ IV VILO Master Mix “yellow buffer” to visually aid during the plate loading procedure, resulting in a final concentration of 0.5 ng/µL of cDNA, which was mixed with the forward and reverse primers (500 nM), PowerTrack SYBR Green Master Mix (1X) and

RNAse-free water. Once each reaction was loaded in each well of a 96-well plate (ThermoScientific, UK), the Real-Time PCR QuantStudio 7 (QS7) was run according to the company protocol. The reaction was as follows: (1) Enzyme was activated at 95 °C for 2 min, (2) cDNA was denatured at 95°C for 15 sec, and (3) primers were annealed and extended at 60 °C for 1 min. Steps (2) and (3) were replicated for 40 cycles. This was followed by a melt curve after the real-time PCR reaction to check for nonspecific amplification. Melt curve reaction: (a) 95 °C for 15 sec, with a ramp rate of 1.6 °C/sec, (b) 60 °C for 1 min, with a ramp rate of 1.6 °C/sec, and (c) dissociation step at 95 °C for 15 sec, with a ramp rate of 0.075 °C/sec.

2.4.5. Data analysis

The mRNA data were analysed using the comparative cycle threshold (ΔCT) method (Heid *et al.*, 1996). The CT values of GAPDH and EF-1 were used as reference genes to quantify the relative amount of ET_A, ET_B, $5\text{-}HT_{1B}$ and TP receptor mRNA levels.

The relative quantification of the GPCRs mRNA compared to CT values of reference genes was determined by using the formula: $\frac{X_0}{R_0} = 2^{CT_R - CT_X}$, where X_0 is the initial amount of target mRNA, R0 is the initial amount of reference mRNA, CT_X is the CT value of the target mRNA and CT_R is the CT value of the reference mRNA (Sandhu *et al.*, 2010).

All data are expressed as means ± S.E.M and n refers to the number of rats. A shapiro-Wilk test was performed and shown that the data were not normally distributed and then a Kruskal-Wallis's test was performed for multiple comparisons. All calculations and statistical analysis were carried out using GraphPad Prism 9.0 (GraphPad Software, La Jolla, USA). Statistical significance was determined with $p \leq 0.05$.

2.5. Analysis of GPCR protein levels in rat LAD by immunohistochemistry

2.5.1. Principle of the immunohistochemistry

Immunohistochemistry (IHC) was first outlined in 1942 by Albert Coons and his team by using a fluorescent-labelled antibody applied on liver tissue sections to localise the pneumococcal antigen (Burry, 2011). The IHC method is a powerful tool to visualize and quantify the distribution and localisation of specific cellular components in cells or tissue samples (Matos *et al.*, 2010).

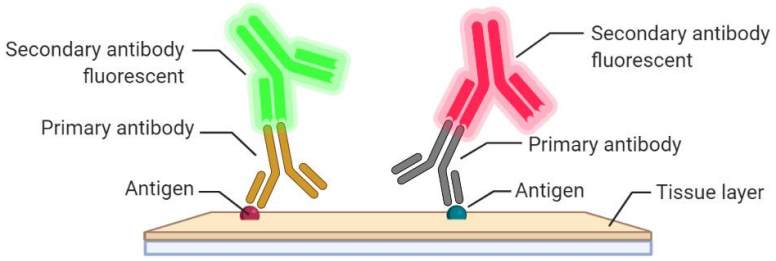

Figure 2-6: Immunohistochemistry principle (see description in text). (Illustration realised with Biorender website)

This technique has different steps: fixation, permeabilisation, blocking, primary antibodies fixation, secondary antibodies fixation, mounting and revelation.

Samples from tissue used for immunohistochemistry can be obtained by different techniques such as Cryosectioning. Sections obtained need to be fixed to slides and frozen sections are often fixed with acetone. Acetone has a span penetrability and dehydration property, which allows it to precipitate sugars and fat. Triton X-100 can also be used to permeabilise the intact membrane of cells. Serum is then used to block nonspecific targets where secondary antibodies could bind and induce false positive results. As in Figure 2-6, primary antibodies are binding the specific antigen, while fluorochrome-linked secondary antibodies then bind specifically to the primary antibodies. Finally, the visualisation of the fluorochrome, and therefore the specific antigen, by the production of visible lights at a specific wavelength with a fluorescence microscope.

2.5.2. Slide preparation and stages evolved for the reaction

Vessels were embedded in Cellpath OCT embedding matrix and frozen at -80 °C. Frozen vessels were cryosectioned into 10 µm sections, using the OTF5000 cryostat (Bright Instruments, Huntingdon, UK). Sections were adhered to Superfrost plus adhesion slides and stored at -80 °C until immunohistochemistry staining.

Thawed sections were fixed in -20 °C acetone for 10 min and rehydrated in PBS containing 0.25 % of Triton X-100 (PBST) at room temperature for 3x 5 min. The sections were blocked in PBS containing 5 % donkey serum for 1 hr at room temperature. Sections were incubated overnight at 4 °C with the primary antibodies, diluted in PBST containing 1 % Bovine Serum Albumin (BSA) and 3 % donkey serum. Sections were double immunostained with primary antibodies of one protein of interest: ET_A (1: 1000), ET_B (1: 1000), 5-HT_{1B} (1: 1000), TP (1: 500) or ERk1+ERK2 (1: 500), while the primary antibody

of actin (1: 500) was used as reference. Sections were rinsed with PBS at room temperature for 2x 15 min. Finally, sections were incubated with secondary antibodies, diluted in PBST containing 1 % Bovine Serum Albumin (BSA) and 3 % donkey serum for 1 hr at room temperature. Sections were "double-stained" with secondary antibodies for both donkey anti-rabbit IgG Alexa Fluor 488 GREEN (1: 500) and donkey anti-mouse IgG Alexa Fluor 594 RED (1: 500). Negative controls were included by omitting the primary antibodies and following the same protocol as given above. Slight green autofluorescence was observed during the negative control stains due to the internal elastic lamina and not because of the staining.

2.5.3. Interpretation and quantification

The Immunofluorescence was visualised with a confocal microscope Eclipse Ti2 (Nikon Instruments Inc. Tokyo, Japan) and photographed with an attached Nikon Orca-Flash4.0v3 camera. Images were analysed and quantified with the AR package of NIS-elements software.

The sections from the fresh vessel group were used to determine the optimal wavelength and pinhole size to compare the different incubated groups. The fluorescence intensity was measured on the entire circumference of the vessel section – called the Region of Interest (ROI) - to obtain the ROI mean intensity.

All data are expressed as means ± S.E.M and n refers to the number of rats. All data were normally distributed were analysed with Shapiro-Wilk test. Since data were normally distributed, One-way analysis of variance (ANOVA) with Fisher's post-test was performed for multiple comparisons. All calculations and statistical analysis were carried out using GraphPad Prism 9.0 (GraphPad Software, La Jolla, USA). Statistical significance was determined with $p \leq 0.05$.

2.6. Analysis of miRNA expression in human plasma samples

2.6.1. Principle of TaqMan array card

TaqMan microRNA Array cards are microfluidic cards containing 384 wells, with individual real-time qPCR reaction per well. It is a high-throughput and accurate tool for quantitative analysis of microRNA (miRNA) or mRNA. TaqMan array cards can be used to obtain a full screen of a transcriptome, identifying potential genes involved in some diseases and toxicological mechanisms (Keys *et al.*, 2010). In this project, the TaqMan Array cards are used to determine which miRNAs could be linked to the cardiotoxicity of different cardiotoxic treatments. Once key miRNAs of interest are identified with the

TaqMan array card from pooled individual group samples, individual samples are analysed with real-time qPCR targeting the key miRNAs to allow a better accuracy and reproducibility of the miRNA assay (Keys *et al.*, 2010).

2.6.2. The patient profile selected for the study

Human plasma samples were collected by Dr Malcom Walker and team (UCL: ERICONC study) as described in section 2.1.2.

Human plasma samples were collected from 19 patients: 12 men and 7 women. The median age was 53.6 (54 for the women and 51 for the men). Patients had sarcoma (n = 15), lymphoma (n = 3) or breast cancer (n = 1) and were treated with different combinations of anthracyclines, such as doxorubicin ± a Combination of doxorubicin and ifosfamide (IFOS)/Bolus/Cisplatin (n = 14), a combination of 5 fluorouracil, epirubicin and cyclophosphamide (FEC) (n = 1), a combination that includes cyclophosphamide, doxorubicin (Adriamycin) vincristine (Oncovin) and prednisolone (a steroid) (CHOP) (n = 1), an European Paediatric Soft tissue sarcoma Study Group (epSSG) (n = 1) and 2 unknown treatments. 42 % of the patients developed cardiovascular adverse effects, such as heart failure, deep vein thrombosis, thrombocytopenia, pulmonary emboli and hypertension. Plasma was collected at three different time points:

- At the beginning of the experiment, baseline group (n = 18)
- At the end of the chemotherapy, Post-Chemo group (n = 13)
- 3 months after the treatment, 3 months group (n = 13)

Due to the pandemic, some patient samples were not collected. There were 10 patients with a full set of blood samples (blood collected at all three time points), 6 patients with blood samples collected at two time points, and 3 patients with blood samples collected only at baseline time point. A total of 44 blood samples were obtained toward this study of miRNA expression.

2.6.3. Plasma collection and storage:

Plasma was collected by the UCL researchers at three different time points: at baseline, at the end of the chemotherapy and 3 months after the completion of chemotherapy. Blood samples were taken during the routine full blood count, urea and electrolytes tests of the cancer patients. The samples were collected in standard EDTA (purple top) and SST (yellow top) blood sample bottles, where the plasma was isolated and stored at -80°C within one hour of sampling. The samples were shipped to

Coventry University on dry ice using same-day delivery. At Coventry University the samples were stored at -80°C.

2.6.4. miRNA extraction of pooled human plasma samples:

Patient plasma samples were pooled together per group (i.e. baseline, end of the chemotherapy, and 3 months after chemotherapy) by pooling the same volume from each individual patient sample in that respective group.

Total miRNA from plasma samples was extracted using the miRNeasy mini kit (Qiagen). After all debris had been removed from pooled plasma samples, QIAzol from the miRNeasy mini kit containing 0.8 µg/µL MS2 RNA as spike-in was used as lysis buffer. Chloroform was added to the lysate and the aqueous phase was transferred to a new RNAse-free Eppendorf tube. Absolute ethanol was added to the lysate to provide an appropriate binding condition. Total miRNA was then fixed to the membrane of the RNeasy Mini Spin Column supplied in the miRNeasy mini kit by centrifugation, while contaminants were washed away by a few washes with the washing buffers. Total miRNA was eluted in RNAse-free water, and miRNA quality and quantity were determined with NanoDrop™ One/OneC Microvolume UV-Vis Spectrophotometer (ThermoFisher, USA).

2.6.5. TaqMan miRNA array cards: Reverse Transcription of pooled human plasma samples:

Reverse transcription of total miRNA to cDNA was performed using the TaqMan® MicroRNA Reverse Transcription kit components and the human Megaplex RT Primers (ThermoFisher, US) in Eppendorf® Mastercycler Nexus Thermal Cyclers (Merck, USA).

Extracted pooled miRNA samples were mixed with Multiscribe™ reverse transcriptase (50 U/µL), Megaplex RT primers, 10X RT buffer, RNase Inhibitor (20 U/µL), $MgCl_2$ (25 mM) and dNTPs with dTTP (100 mM) on ice and the mix was incubated for 5 min on ice. The 3 next steps were processed during 40 cycles. The mix was incubated (1) at 16 °C for 2 min to *anneal primers*. Then, it was incubated (2) at 42 °C for 1 min and incubated (3) at 50 °C for 1 sec to reverse transcribe RNA. Steps (1), (2) and (3) were repeated for 40 cycles. After the 40 cycles, the mix was incubated (4) at 85 °C for 5 min to inactivate the enzyme.

The resulting cDNA is processed directly after the reverse transcription reaction with a pre-amplification reaction before loading the cDNA on the miRNA array card.

2.6.6. TaqMan miRNA array cards: Pre-Amplification of pooled human plasma samples:

The aim of the pre-amplification reaction is to increase the quantity of the cDNA prior to running the samples on the miRNA arrays. The cDNA from pooled plasma samples were pre-amplified with a PreAmp reaction mix. Template cDNA was mixed with TaqMan® PreAmp Master Mix (2X) and Human Megaplex™ PreAmp Primers (10X) on ice. The mix was incubated at 95 °C for 10 min to activate the enzyme. Then the mix was incubated at 55 °C for 2 min to anneal the primers and at 72 °C for 2 min to extend primer on cDNA. The next 2 steps were processed during 14 cycles. The 2 steps were an incubation at 95 °C for 15 sec to denature cDNA. Followed by an incubation at 60 °C for 4 min to anneal and extend primers on cDNA. Finally, the mix was incubated at 99.9 °C for 10 min to inactivate the enzyme.

2.6.7. TaqMan miRNA array cards: Real-Time PCR reaction of pooled human plasma samples:

Human TaqMan® MicroRNA Array A cards were used to run the pooled plasma group cDNA samples. The target cDNA (pre-amplified product from plasma pools) was mixed with TaqMan® Universal PCR Master Mix No AmpErase® UNG (2X). The mix was loaded on the human TaqMan® MicroRNA Array A cards and the reaction was run on the PCR instrument QuantStudio 7 applying the 384 wells TaqMan Low-Density Array default thermal-cycling conditions. The enzyme was activated at 95 °C for 10 min. Then, the two next steps were repeated for 40 cycles. The cDNA was denatured at 95 °C for 15 sec and primers were annealed and extended at 60 °C for 1 min.

2.6.8. TaqMan miRNA array cards: Data analysis of pooled human plasma samples:

The miRNA expression cycle thresholds (C_T) are measured by the QuantStudio 7 Pro Real-Time PCR System version 1.3 (Applied Biosystems, ThermoFisher Scientific). The differential miRNA expression values were calculated using the Applied Biosystems application RQ (version 3.9) located on the online Thermo Fisher Connect cloud application by normalising the target miRNA C_T levels against the endogenous control U6 small nuclear RNA (snRNA). C_T levels higher than 35 were excluded from the analysis, due to unspecific/insignificant annealing. Analysis was carried out using the relative quantification ($\Delta\Delta C_T$) method, where the calculated RQ value is the comparison of globally normalised target miRNA against the U6 snRNA levels. The equation used was ΔRQ = 2^ (-((C_T value of target

miRNA - C_T of U6)$_{post\text{-}treatment}$ - (C_T value of target miRNA - C_T of U6)$_{baseline}$)), where C_T value is generated using the relative threshold algorithm (C_{RT}). An ΔRQ-value > 2 meant a significant increase in expression fold change, and ΔRQ-value < 0.5 meant a significant decrease in expression fold change.

2.7. Analysis of individual miRNA expression in human ERICONC plasma samples

2.7.1. MiRNA extraction of human plasma samples:

Key miRNAs associated with vascular injury (i.e. hsa-miR-126, hsa-miR-10a, hsa-miR 143, hsa-miR-150 and hsa-miR-320a) were identified from the TaqMan miRNA array cards data analysis expression of the ERICONC project human plasma (i.e. Baseline group: n = 18; Post-Chemo group: n = 13; 3 months Post-Chemo group: n = 13).

Total miRNA from plasma samples was extracted using the miRNeasy mini kit (Qiagen). QIAzol from the miRNeasy mini kit containing 0.8 µg/µL MS2 RNA was used as lysis buffer, after all debris had been removed from plasma samples. Chloroform was added to the lysate and the aqueous phase was collected in a new RNAse-free Eppendorf tube. Absolute ethanol was added to the lysate to provide an appropriate binding condition. Total miRNA was then fixed to the membrane of the RNeasy Mini Spin Column supplied in the miRNeasy mini kit by centrifugation, while contaminants were washed away by a few washes with the washing buffers. Total miRNA was eluted in RNAse-free water, and miRNA quality and quantity were determined with NanoDrop™ One/OneC Microvolume UV-Vis Spectrophotometer (ThermoFisher, USA).

2.7.2. Individual miRNA expression quantification: Reverse Transcription (human ERICONC plasma)

Reverse transcription of specific miRNAs to cDNA was performed using TaqMan® MicroRNA Reverse Transcription kit components and the specific target TaqMan miRNA assays: hsa-miR-126, hsa-miR-10a, hsa-miR 143, hsa-miR-150 and hsa-miR-320, and the U6 snRNA as housekeeping reference (ThermoFisher, US). Individual miRNA samples were mixed with Multiscribe™ reverse transcriptase (50 U/µL), RT miRNA primer assays X5, 10X RT buffer, RNase Inhibitor (20 U/µL), MgCl2 (25 mM) and dNTPs with dNTPs (100 mM) on ice. The reverse transcription reaction ran on the Eppendorf® Mastercycler Nexus Thermal Cyclers (Merck, USA) using the following setting: (1) 16 °C for 30 min to

anneal primers, (2) 42 °C for 30 min to reverse transcribe RNA, and (3) 85 °C for 5 min to inactivate the enzyme. The cDNA was diluted 1:1 with RNAse-free water after the reaction.

2.7.3. Individual miRNA expression quantification: Real-Time PCR reaction (human ERICONC plasma)

The target cDNA samples were mixed with TaqMan® Universal PCR Master Mix II no UNG and specific miRNA primer assays X20. The mix was loaded on a 96-well plate (ThermoScientific, UK). This plate was run on the real-time PCR instrument QuantStudio 7 according to the manufacturer's protocol: (1) UNG was activated at 50 °C for 2 min, (2) enzyme was activated at 95 °C for 10 min, (3) cDNA was denatured at 95 °C for 15 sec, (4) primers were annealed and extended at 60 °C for 1 min, (5) repeat step (3) and (4) for 40 cycles.

2.7.4. Individual miRNA expression quantification: Data analysis (human ERICONC plasma)

Individual miRNA expression levels were analysed using the ΔΔCt method using the U6 snRNA as endogenous control for the comparisons of the relative amount of specific miRNAs. C_T levels higher than 35 were excluded from the analysis, due to unspecific/insignificant annealing. The equation used was: $\frac{X_0}{R_0} = 2^{CT_X - CT_{RX}}$, where X_0 is the amount of target miRNA, R_0 is the amount of U6 snRNA, CT_X is the CT value of the target miRNA and CT_R is the CT value of U6 snRNA (Sandhu *et al.*, 2010). Negative control using water instead of plasma sample cDNA was included for each sample. Studied miRNAs level was expressed as values relative to the endogenous gene, U6 and normalised to baseline-collected plasma.

All data are expressed as means ± S.E.M and n refers to the number of patients. Statistical analysis was performed using Kruskal-Wallis's post-hoc test using GraphPad Prism 9.0 (GraphPad Software, La Jolla, USA). Statistical significance was determined with $p \leq 0.05$.

Chapter 3:

3. Optimisation of an organ culture model to study the doxorubicin-induced vasotoxicity on LAD arteries.

3.1. Introduction

The development of new drug testing involved the use of different models to study the pharmacological properties of the drug (Ruggeri *et al.*, 2014). First, the drugs are tested with an *in vitro* model, such as cell culture or organ culture. Then, the next step is *in vivo* experiments with animal models, where most of the potential side effects are investigated and finally, the clinical model on humans (Hughes *et al.*, 2011). One of the challenges of animal models and *in vitro* models is to make them relevant to human disease (Vandamme, 2014). For example, organ culture is an experimental model which induces phenotypic changes similar to endothelium dysfunction (Alm *et al.*, 2002) and alterations of GPCR in SMCs (Adner *et al.*, 1996, Wackenfors *et al.*, 2003). Both changes are observed in CVDs such as hypertension (Audebrand *et al.*, 2019) and heart failure (Forrester *et al.*, 2018). However, different parameters need to be set up in *in vitro* models to be an appropriate model which mimics human conditions. *In vitro* models allow the selection of the known concentration, which is an important parameter for the experiment. Drug activities, such as affinity, efficiency and potency, are concentration-dependent and a fixed concentration allows the investigation of specific drug's effects (Kenakin and ScienceDirect, 2017). The dose can be determined as therapeutic or toxic, depending on which effect is being studied, like Murata and his team, who investigated the cardiotoxic effects of the chemotherapeutic drug, doxorubicin with an *in vitro* model at therapeutic doses (0.3 and 1 µM) and a toxic dose (10 µM) (Murata *et al.*, 2001a). To study the possible toxicity of drugs, the relevant dose needs to correlate with the plasma concentration observed in patients treated with the studied drug. The exposure time to the drug is also an important parameter. Indeed, many drugs are toxic at high doses and are administrated by cumulative application of lowest doses during weeks or months.

Doxorubicin is one of the most potent chemotherapeutic drugs, widely used in many solid cancers, although it can also lead to severe cardiovascular adverse effects. The doxorubicin-induced cardiotoxicity leads to the use of lower doses or the use of other chemotherapeutic drugs that are less efficient. The cardiotoxicity of doxorubicin has been observed to imply different mechanisms, such as oxidative stress, calcium metabolism disorders and systemic inflammation (Podyacheva *et al.*, 2021). Doxorubicin accumulates in the mitochondrial inner membrane and forms an irreversible complex with cardiolipin, leading to mitochondrial dysfunction (Octavia *et al.*, 2012). The disruption of

mitochondrial activity leads to the release of reactive oxygen species (ROS) (Zhou *et al.*, 2001). Moreover, doxorubicin alters the activity of endothelial nitric oxide synthase (eNOS) and NADPH oxidase (NOX), leading to the reduction of free oxygen in superoxide free radical (Vasquez-Vivar *et al.*, 1997, Deng *et al.*, 2007). The elevation of ROS production by the mitochondrial dysfunction and altered enzymes activate the oxidative stress, inducing apoptosis of cardiomyocytes. Doxorubicin-induced cardiotoxicity is associated with an increase of intracellular calcium release from the sarcoplasmic reticulum, leading to the ROS generation and the activation of apoptotic signalling (Holmberg and Williams, 1990). Doxorubicin-induced cardiotoxicity is also associated with an increase of inflammatory markers. Ye and his team demonstrated that the interleukin 9 (IL-9), by promoting the inflammatory response, aggravates the doxorubicin-induced cardiac injury (Ye *et al.*, 2020).

Doxorubicin-induced cardiotoxicity was mainly investigated and documented on cardiomyocytes in pre-clinical and cancer patients in clinical studies (Rawat *et al.*, 2021). Conversely, the potential vasotoxicity of doxorubicin has been poorly investigated. Some mechanisms observed in cardiomyocytes could also be involved in the cardiovascular system, such as calcium dysregulation or ROS production. Some studies demonstrated that endothelial cells were altered by doxorubicin administration (Luu *et al.*, 2018, He *et al.*, 2019, Hoffman *et al.*, 2021). Sayed-Ahmed demonstrated that ET-1 levels in plasma and cardiac nitric oxide of Sprague-Dawley rats were increased after the administration of cumulative doses of doxorubicin (from 10mg/kg to 20mg/kg) for 10 days (Sayed-Ahmed *et al.*, 2001). A clinical study with a cohort of 30 patients treated with doxorubicin observed the plasma ET-1 level. Plasma ET-1 was elevated for 5 patients and 2 of them developed clinically overt congestive heart failure. The 25 patients without an increase of the plasma ET-1 didn't develop congestive heart failure (Yamashita *et al.*, 1995). ET-1 and NO are involved in the vascular tone (Nishiyama *et al.*, 2017), their alterations by doxorubicin could induce alterations in the vasculature tone.

Rodent models are widely used to investigate doxorubicin cardiomyopathy. Many *in vitro* models were created to investigate cardiovascular adverse effects on the cardiovascular system, such as the Langendorff perfusion model (Gharanei *et al.*, 2013b), cardiac cell model (Gharanei *et al.*, 2013a) or vessel model (Murata *et al.*, 2001a, Bosman *et al.*, 2021b). Gharanei used an *in vitro* Langendorff perfusion model for his experiments and determined that the optimal concentration to study cardiotoxicity was 1 µM of doxorubicin in Sprague-Dawley rat hearts (Gharanei *et al.*, 2013a, Murata *et al.*, 2001a). They used the same concentration in cell culture models of neonatal rat cardiac myocytes and HL-60 cells for 24 hrs incubation. Studies used animal artery models to investigate doxorubicin's adverse effects on vascular tone (Bosman *et al.*, 2021b, Murata *et al.*, 2001a). Murata investigated the chronic effects of doxorubicin on isolated rabbit mesenteric arteries. Rabbit

mesenteric arteries were incubated for 7 days with 0.3 µM, 1 µM or 10 µM of doxorubicin, where the two lowest doses are considered to be in the range of plasma levels observed in cancer patients treated with doxorubicin treatment (Murata *et al.*, 2001a). Bosman studied the cardiotoxic effects of doxorubicin on isolated aorta of C57BL/6J mice model. Aorta arteries were incubated for 16 hrs with a doxorubicin concentration of 1 µM to study the effects of doxorubicin on SMC contraction (Bosman *et al.*, 2021b).

Given the current findings about doxorubicin-induced cardiotoxicity, the present study aims to set up an organ culture model with isolated rat left anterior descending arteries to study the cardiovascular adverse effects of doxorubicin on vascular tone.

3.2. Material & methods

3.2.1. Acute effect of doxorubicin on fresh LAD

Rat LAD was dissected free in ice-cold Ca^{2+}-free KH buffer (pH = 7.4) and divided into rings of 2 mm, and then mounted on the myograph directly. The mounted vessels were given a stabilisation period of 1 hr where the Na^+ KH buffer (continuously gassed with 5 % CO_2 in O_2 at 37 °C, pH = 7.4) was changed every 15 min with a pre-tension fixed at 1.5 mN/mm after 30 min.

Determine if the different doses of doxorubicin modified the contractile capacity.

The LAD vessels were exposed to a 60 mM K^+ KH buffer to measure the contractile capacity (Threshold for minimum contraction set to 1 mN). The viability of the endothelium was investigated by applying K^+ KH-induced pre-contraction followed by 10^{-5} µM carbachol vasodilation. Doxorubicin (0.1 µM) was applied for 30 min, as shown in Figure 3-1. The contractile capacity and the viability of the endothelium was measured again, followed by washout with Na^+ KH buffer. The same experiment was repeated three times with different concentrations of doxorubicin (0.25, 0.5 and 1 µM).

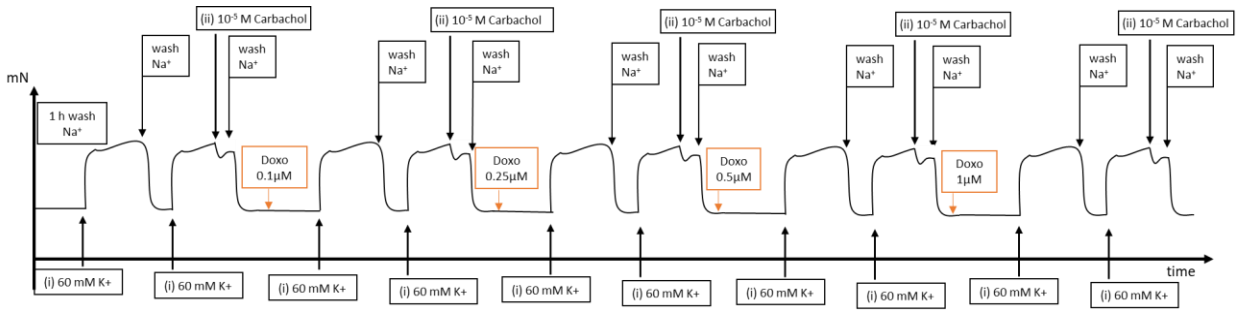

Figure 3-1: Protocol of the experiment investigating the acute effect of Doxorubicin at different concentrations on LAD vessels. Na+ = Na^+ KH, K+ = K^+ KH, Doxo = doxorubicin.

Determine if the cumulative addition of doxorubicin could impact the contractile capacity

The LAD vessels were exposed to a 60 mM K^+ KH buffer to measure the contractile capacity (threshold for minimum contraction set to 1 mN). The viability of the endothelium was investigated by applying K^+ KH-induced pre-contraction followed by 10^{-5} M carbachol vasodilation. This was followed by applying doxorubicin in a cumulative dose ranging from 0.001 µM to 10 µM (water – in increasing volumes - was applied as a vehicle/control group). There was a stabilisation period of 15 min between each dose application. Once the cumulative dose application of doxorubicin was completed, the contractile capacity and viability of the endothelium were measured again (Figure 3-2).

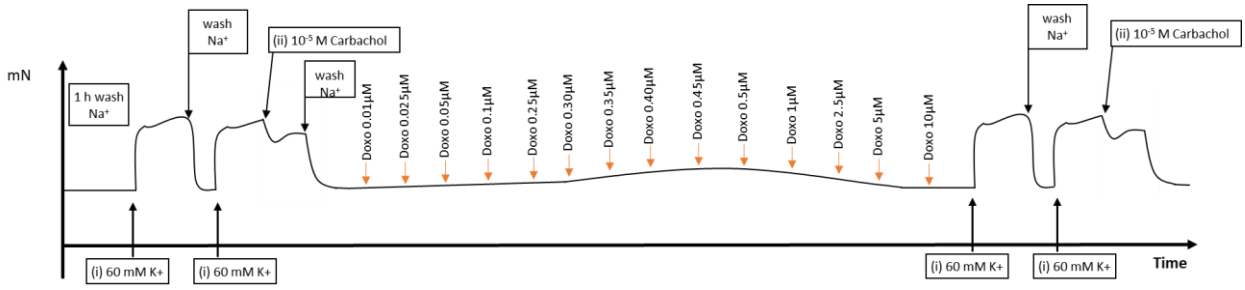

Figure 3-2: Protocol of the experiment to observe the acute effect of doxorubicin added at cumulative doses on LAD vessels. Na^+ = Na^+ KH, K+ = K^+ KH, Doxo = doxorubicin.

3.2.2. Determination of the optimal doxorubicin concentration

Rat LAD was dissected free in ice-cold Na^+ free KH (pH = 7.4) and divided into rings of 2 mm, and then incubated for 24 hrs in 1 mL of DMEM media at 37 °C and humidified with 5 % CO_2 and 95 % O_2. Doxorubicin (stock solution of 0.1 mM) was added to the media to obtain the final four doses: 0.1 µM, 0.25 µM, 0.5 µM and 1 µM. The milli-Q (mQ) water was added to the media of LAD from the vehicle group.

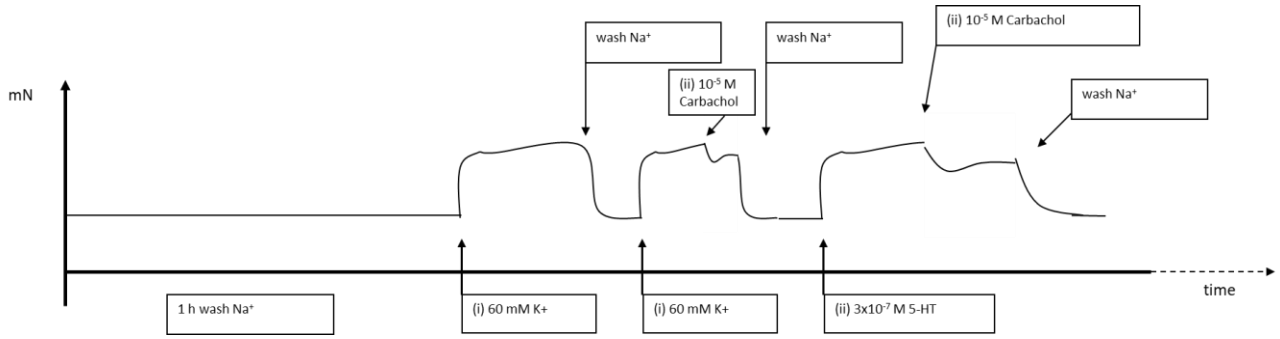

Figure 3-3: Experimental protocol to investigate optimal doxorubicin concentration. Na^+ = Na^+ KH, K+ = K^+ KH, Doxo = doxorubicin, 5-HT = serotonin.

After incubation, the LAD vessels were threaded on two 40 µM diameter stainless steel wires and mounted in Ca^{2+}-free KH buffer on the myography setup. The buffer surrounding the vessels was changed to the Na^+ KH buffer. The Na^+ KH buffer was continuously gassed with 5 % CO_2 and 95 % O_2 at 37 °C resulting in a physiological pH of 7.4. After the vessels were mounted a pre-tension in the range of 1.16 mN/mm to 1.52 mN/mm was applied (Ping *et al.*, 2014). The mounted vessels were given a stabilisation period of 1 hr where the Na^+ KH buffer was changed every 15 min, as shown in Figure 3-3. After stabilisation, the vessels were exposed to a 60 mM K^+ KH buffer to measure the contractile capacity. The threshold for minimum 60 mM KCl contraction response was set to 1 mM, and all vessels with a contractile capacity below the threshold were discarded. The viability of the endothelium was investigated by applying 3. 10^{-7} M 5-HT-induced pre-contraction followed by 10^{-5} µM carbachol vasodilation.

3.2.3. Determination of the optimal incubation time

LAD vessels were incubated in 1 mL DMEM media with 0.5 µM doxorubicin at 37 °C and humidified with 5 % CO_2 and 95 % O_2 for 24 hrs or 48 hrs to determine which incubation time was optimal. Non-incubated fresh LAD segments were included in this part of the study as well. Fresh or incubated LAD vessels were threaded on two 40 µM diameter stainless steel wires and mounted in Ca^{2+}-free KH buffer on the myography setup. The buffer surrounding the vessels was changed to the Na^+ KH buffer. The Na^+ KH buffer was continuously gassed with 5 % CO_2 in O_2 at 37 °C resulting in a physiological pH of 7.4. After the vessels were mounted, a pre-tension of 1.16-1.5 mN/mm was applied. The mounted vessels were given a stabilisation period of 1 hr where the sodium buffer was changed every 15 min, as shown in Figure 3-3. After stabilisation, the vessels were exposed to a 60 mM K^+ KH buffer to measure the contractile capacity. The threshold for minimum 60 mM KCl contraction response was set to 1 mM, and all vessels with a contractile capacity below the threshold were discarded. The viability of the endothelium was investigated by applying K^+ KH-induced pre-contraction followed by 10^{-5} µM carbachol vasodilation.

3.2.4. Real-time PCR protocol

Total cellular RNA was extracted with the RNeasy Protect liquid mini kit following the supplier's instructions. LAD arteries were removed from RNA protect reagent and homogenised in RLT buffer containing 0.01 % β-mercaptoethanol using a KIA Ultra-Turrax homogeniser (Sigma-Aldrich, USA). The samples were centrifuged for 3 min at full speed. The supernatant was mixed with 1 volume of ethanol 70 % and transferred to an RNeasy spin column placed in a 2 mL collection tube. After centrifugation

for 15 sec at room temperature (RT) at 8,000 xg, total cellular RNA was fixed on the membrane in RNeasy spin column and the flow-through was discarded. Washing buffer RW1 was added to the RNeasy spin column and samples were centrifuged for 15 sec at room temperature at 8,000 xg. The second washing buffer RPE was added to the spin column and centrifuged for 15 sec at room temperature at 8,000 xg. The last washing step was with RPE buffer and samples were centrifuged for 2 min at room temperature at 8,000 xg. RNAse-free water was added in the RNeasy spin column and samples were centrifuged for 1 min at room temperature at 8,000 xg to elute the RNA. Total RNA amount and purity were determined with NanoDrop™ One/OneC Microvolume UV-Vis Spectrophotometer (ThermoFisher, USA).

Reverse transcription of total cellular RNA to cDNA was performed with Superscript™ IV VILO Master Mix (ThermoFisher, US) in Eppendorf® Mastercycler® Nexus Thermal Cyclers (Merck, USA). Total cellular RNA was mixed with SuperScript IV™ VILO Master Mix in a 20 µL reaction volume on ice. The mix was incubated at 25 °C for 10 min to anneal primers. Afterwards, it was incubated at 50 °C for 10 min to reverse transcribe RNA. Finally, the mix was incubated at 85 °C for 5 min to inactivate the enzyme. The cDNA obtained was diluted in RNAse-free water to have a cDNA concentration of 1 ng/µL.

Real-Time PCR was performed in a Real-Time PCR instrument QuantStudio 7 (ThermoScientific, USA) with the PowerTrack SYBR Green Master Mix (1X) with cDNA (at a final concentration of 0.5 ng/µL), with the forward and reverse primers (500 nM), and with RNAse-free water to a final reaction volume of 20 µL. Negative control was added in all experiments. A yellow buffer was mixed with the cDNA to facilitate the plate loading. Elongation factor-1 (EF-1) and Glyceraldehyde 3-phosphate dehydrogenase (GAPDH) mRNA were used as endogenous control. Specific primers of ET_A and ET_B receptors, 5-HT_{1B} receptors, TP receptors, EF-1 and GAPDH were designed (Table 2-1, in 2. General Methods chapter, section 2.2.3). Primers were resuspended in RNAse-free water to obtain a stock concentration of 100 mM and then, diluted to obtain a work concentration of 10 mM. Once each reaction was loaded in each well of a 96-well plate (ThermoScientific, UK), the Real-Time PCR instruments was run according to the company protocol. First, the enzyme was activated at 95 °C for 2 min. Then, the two next steps were processed during 40 cycles. The cDNA was denatured at 95 °C for 15 sec and primers were annealed and extended at 60 °C for 1 min. A melt curve was obtained, immediately after the real-time PCR, in three steps to check for nonspecific amplification. Step 1 was at 95 °C for 15 sec, with a ramp rate of 1.6 °C/sec. Step 2 was at 60 °C for 1 min, with a ramp rate of 1.6 °C/sec. Finally, step 3, also named dissociation, was at 95 °C for 15 sec, with a ramp rate of 0.075 °C/sec.

3.2.5. Data Analysis

All data are expressed as means ± S.E.M and n refers to the number of rats. The vasocontractile response to K^+ KH was expressed in milliNewton (mN). The carbachol-mediated vasorelaxation was expressed as percentage of the 10^{-7} M 5-HT-induced contraction. To determine the acute effect of doxorubicin on vascular tension, the optimal concentration of doxorubicin, and the optimal doxorubicin incubation time, Kruskal-Wallis's tests were performed for multiple comparisons. Unpaired Student T-test was used to compare 60 mM K^+ KH contraction, endothelial viability with carbachol-mediated vasorelaxation, and the cumulative application of doxorubicin on fresh vessels. All calculations and statistical analysis were carried out using GraphPad Prism 9.0 (GraphPad Software, La Jolla, USA). Statistical significance was determined when $p < 0.05$.

3.3. Results

3.3.1. Acute effect of doxorubicin

The acute effect on 60 mM K^+ KH vasocontractile response in fresh LAD vessels was studied using four specific doses of doxorubicin (doses 0.1, 0.25, 0.5 and 1 µM) and is summed up in Figure 3-4. Control group (prior to any doxorubicin treatment) had a 60 mM K^+ KH vasocontractile response of 4.01 ± 0.28mN (n = 10), while the 0.1 µM, 0.25 µM, 0.5 µM and 1 µM doxorubicin groups, respectively, a had a 60 mM K^+ KH vasocontractile response of 3.69 ± 0.30 mN (n = 10), 3.71 ± 0.31 mN (n = 10), 3.78 ± 0.37 mN (n = 10) and 3.56 ± 0.32 mN (n = 9). All groups were compared using Kruskal-Wallis' test, and no significant difference was observed. All in all, 15 min incubation of 0.1 - 1 µM doxorubicin doesn't affect the contractile capacity of the fresh LAD vessels.

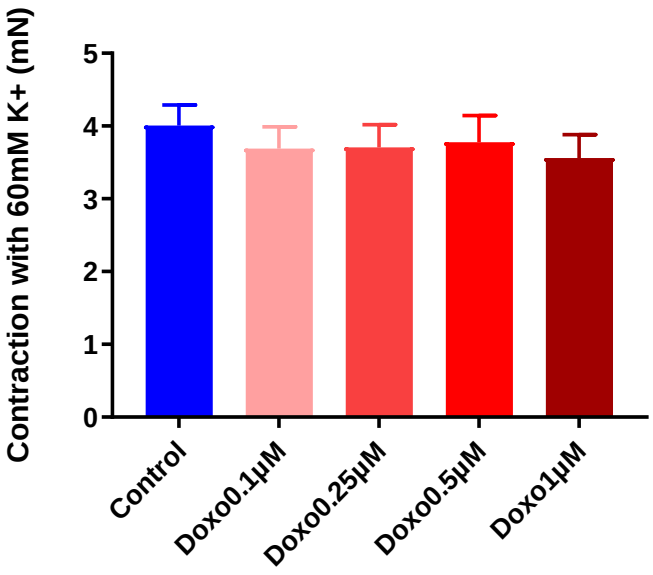

Figure 3-4: 60 mM K^+ KH vasocontractile response of LAD vessels investigated prior to and after doxorubicin treatment at various concentrations. The doxorubicin treatment (0.1 µM, 0.25 µM, 0.5 µM, and 1 µM) groups were compared to the vehicle control (prior to Doxorubicin treatment) group using Kruskal-Wallis' test (n = 9 - 10). Doxo = Doxorubicin.

The results from the cumulative application of doxorubicin (0.01 - 10 µM) to fresh LAD vessels are summarised in Figure 3-5. The cumulative application of doxorubicin seems to induce a low statistically insignificant increase in vasocontractility in concentrations 0.01 - 0.35 µM, 1 µM and 10 µM doxorubicin and a low statistically insignificant decrease in vasocontractility in concentrations 0.4 - 0.5 µM and 2.5 - 5 µM doxorubicin. A maximum increase in vasocontractility was observed at 0.01 µM and 0.05 µM doxorubicin, while a maximum decrease in vasocontractility was observed at 0.4 µM doxorubicin. All in all, the acute cumulative application of doxorubicin (0.01 - 10 µM) on fresh LAD vessels doesn't induce any change to the vascular tone (i.e. vasocontraction or vasorelaxation).

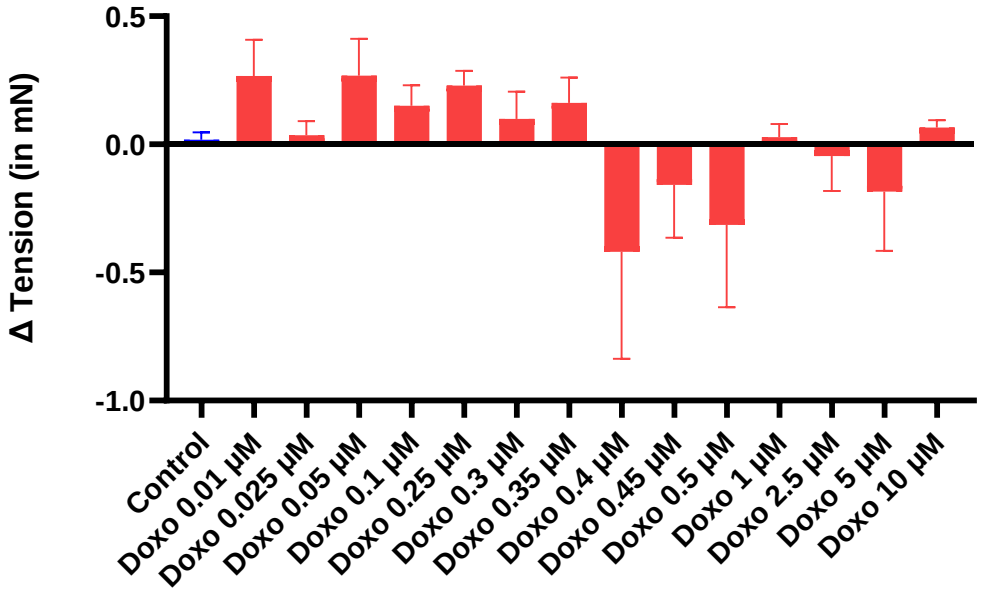

Figure 3-5: LAD vessel vascular tone (mN) after the addition of cumulative doxorubicin at a concentration range of 0.01 µM to 10 µM (n = 6). Control group is the baseline (i.e. prior to applying doxorubicin). The doxorubicin treatment (0.01 µM to 10 µM) groups were compared to the vehicle control (prior to doxorubicin treatment) group using Kruskal-Wallis' test.

The 60 mM K^+ KH vasocontractile capacity was analysed prior to (Control) and after the cumulative application of doxorubicin (0.01 - 10 µM) (After doxorubicin group) on the fresh LAD vessels. The control group had a 60 mM K^+ KH vasocontractile capacity of 2.94 ± 0.34 mN (n = 6), while the After doxorubicin group had a 60 mM K^+ KH vasocontractile capacity of 1.92 ± 0.47 mN (n = 6). There was no statistical significance between the 60 mM K^+ KH vasocontractile capacity prior to and after the cumulative application of doxorubicin (0.01-10 µM) (Figure 3-6). To summarise, the application of a single or cumulative doses of doxorubicin on fresh LAD vessels does not compromise the contractile capacity of the vessels.

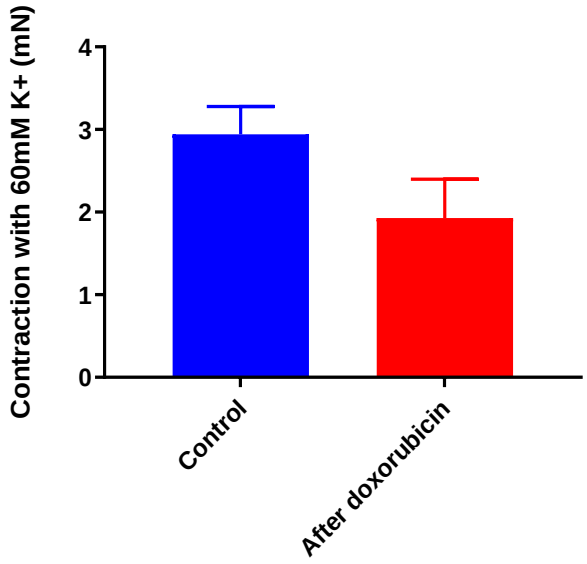

Figure 3-6: 60 mM K^+ KH vasocontractile response of LAD vessels investigated before and after the addition of cumulative doses of doxorubicin. Control group (n = 6) is the baseline (i.e. prior to applying doxorubicin). After-doxorubicin group (n = 6) is the measurement after doxorubicin application. Both groups were compared using Student T-test.

3.3.2. Determination of optimal doxorubicin concentration

LAD vessels incubated in DMEM for 24 hrs with vehicle showed an average 60 mM K^+ KH vasocontractile capacity of 2.35 ± 0.23 mN (n = 44). The presence of doxorubicin at 0.1 µM, 0.25 µM, 0.5 µM and 1 µM during the incubation induces an average 60 mM K^+ KH vasocontractile capacity of, respectively, 3.60 ± 0.31 mN (n = 12), 3.34 ± 0.40 mN (n = 16), 2.05 ± 0.21 mN (n = 32) and 0.89 ± 0.07 mN (n = 2) (figure 3-7). Vessels incubated with 0.1 µM of doxorubicin had a statistically significantly higher vasocontractile capacity compared to vehicle-incubated vessels (p-value = 0.017). Incubation with 1 µM of doxorubicin for 24 hrs was very harsh for the vessels, as only two out of five vessels survived (i.e. demonstrated a 60 mM K^+ KH vasocontractile capacity higher than 1.0 mN), and as a conclusion, 1 µM of doxorubicin is not suitable during 24 hrs of incubation as it damages the vessels and decreases the contractile capacity (p = 0.01). Vessels incubated with 0.25 µM and 0.5 µM doxorubicin had a 60 mM K+ KH vasocontractile capacity at the same level as the vehicle-incubated vessels. Therefore, 0.5 µM of doxorubicin during 24 hr-incubation was determined to be the optimal concentration of doxorubicin.

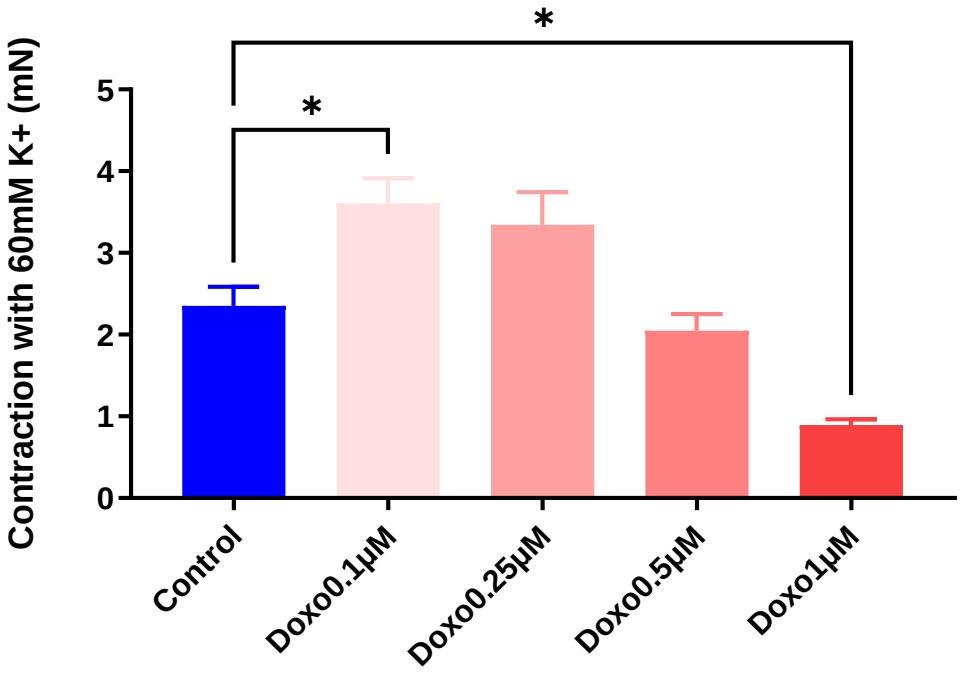

Figure 3-7: 60 mM K^+ KH vasocontractile response of LAD vessels incubated for 24 hrs with vehicle control (n = 44) or doxorubicin (Doxo) in concentrations 0.01 µM (n = 12), 0.25 µM (n = 16), 0.5 µM (n = 32), and 1 µM (n = 2). The doxorubicin groups were compared to the vehicle control group using One-Way ANOVA Kruskal-Wallis's test (* = $p < 0.05$).

The viability of the endothelium was determined by applying 3. 10^{-7} M 5-HT-induced pre-contraction followed by 10^{-5} µM carbachol vasodilation in LAD vessels incubated for fresh vessels, 24 hrs with vehicle control or 0.5 µM doxorubicin. The carbachol-mediated relaxation was expressed as a percentage of the 3. 10^{-7} M 5-HT induced vasocontraction. The vehicle control group had an average carbachol-mediated relaxation of 47 ± 4 % (n = 32), while the 0.5 µM doxorubicin group had an average carbachol-mediated relaxation of 53 ± 4 % (n = 33) (Figure 3-8), however, there was no statistically significant difference between the carbachol-mediated relaxation of vehicle control or 0.5 µM doxorubicin groups. The fresh group had an average carbachol-mediated relaxation of 80 ± 8 % (n = 6) and was significantly higher than the vehicle group 47 ± 4 % (n = 32) (p = 0.443).

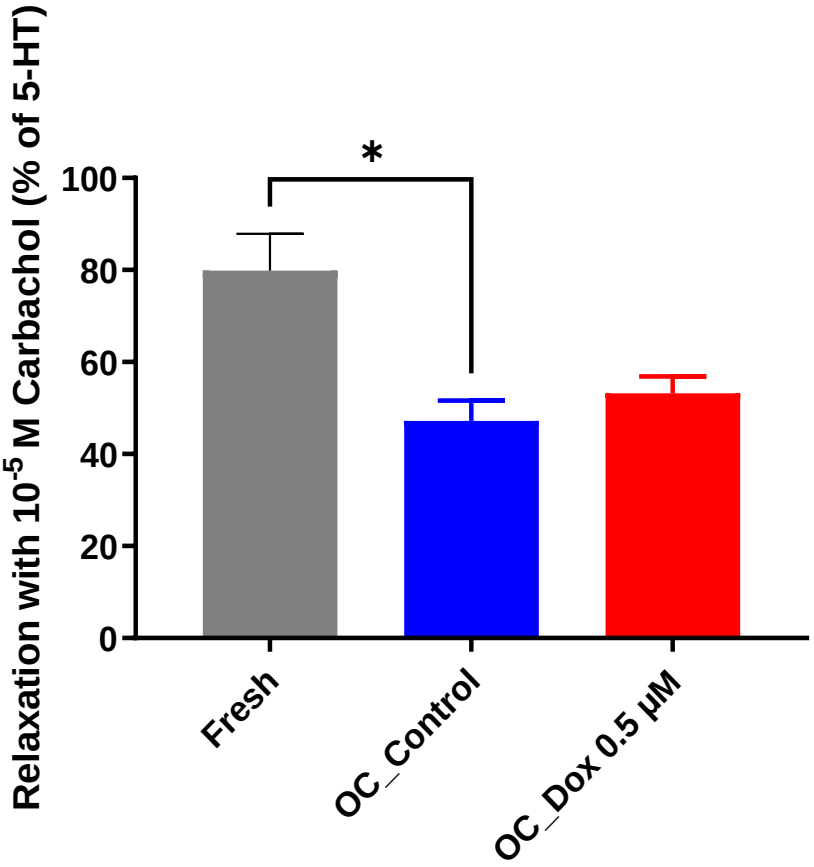

Figure 3-8: Carbachol-mediated vasorelaxation after serotonin (5-HT) pre-contraction in LAD vessels. The fresh group (n = 6) and doxorubicin group (n = 32) were compared to the vehicle control group (n = 33) using Kruskal-Wallis test. Doxo = doxorubicin, OC = organ culture.

3.3.3. Determination of optimal incubation time with 0.5 µM doxorubicin

Fresh vessels have a statistically significantly higher 60 mM K^+ KH vasocontractile capacity (2.99 ± 0.21 mN; n = 21) compared to LAD vessels incubated with vehicle for 24 hours (2.35 ± 0.23 mN; n = 23) (p = 0.034) or 48 hours 1.78 ± 0.25 mN (n = 13) (p = 0.004) (Figure 3-9).

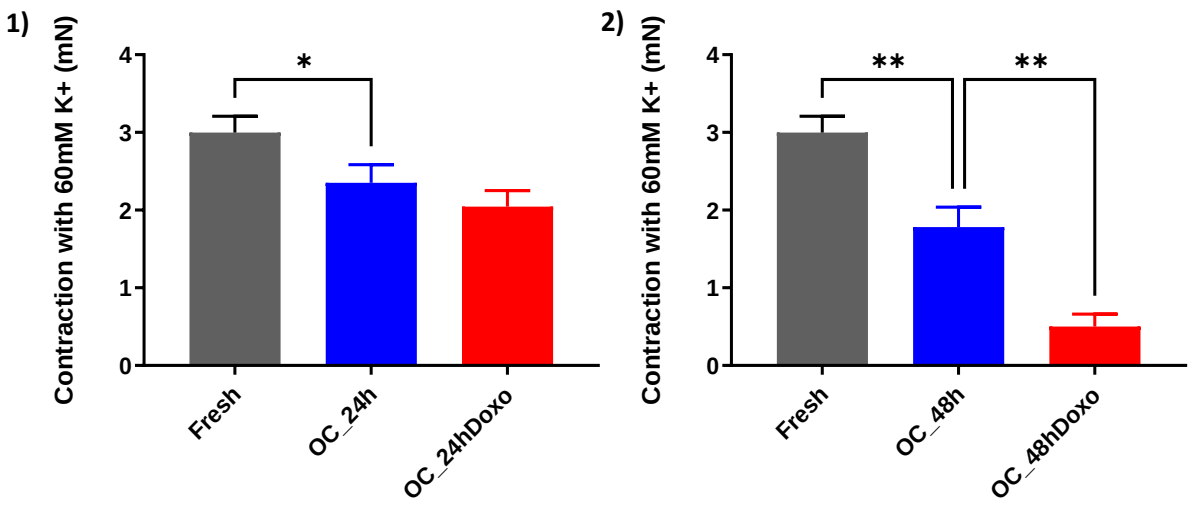

Figure 3-9: 60 mM K^+ KH vasocontractile response of LAD vessels fresh (n = 21) or incubated for 24 hrs or 48 hrs with vehicle control or 0.5 µM doxorubicin treatment. 1) 24 hrs vehicle (n = 23) or 0.5 µM doxorubicin (n = 13) incubated vessels. 2) 48 hrs vehicle (n = 13) or 0.5 µM doxorubicin (n = 10) incubated vessels. Doxo = doxorubicin, OC = organ culture. One-way ANOVA Kruskal-Wallis's test was used to analyse statistical differences (* = $p < 0.05$; ** = $p < 0.01$).

Incubation of LAD vessels with vehicle for 48 hrs does not alter the 60 mM K^+ KH vasocontractile capacity of the vehicle 48 hr-incubated LAD vessels 1.78 ± 0.25 mN (n = 13) when compared to vehicle 24 hr-incubated LAD vessels 2.35 ± 0.23 mN (n = 23).

Incubation of LAD vessels with 0.5 µM of doxorubicin for 24 hrs does not alter the 60 mM K^+ KH vasocontractile capacity of the 0.5 µM doxorubicin incubated LAD vessels 2.05 ± 0.21 mN (n = 13) when compared to vehicle incubated LAD vessels 2.35 ± 0.23 mN (n = 23). However, LAD vessels incubated for 48 hrs with 0.5 µM of doxorubicin drastically reduced the 60 mM K^+ KH vasocontractile capacity of the 48 hrs 0.5 µM doxorubicin incubated LAD vessels 0.50 ± 0.16 mN (n = 10) compared to vehicle incubated LAD vessels 1.78 ± 0.25 mN (n = 13) ($p = 0.003$).

Therefore, the time of 24 hours for the incubation of LAD rings was selected as the optimal time for the next experiments based on these results.

3.3.4. Selection of the housekeeping gene for analysis

The CT value of EF-1 and GAPDH of the 9 groups were compared to determine the most stable "housekeeping gene" to use as a reference when analysing the mRNA expression of the GPCR receptors. Statistical comparison was performed using the one-way ANOVA with Dunnett's post-hoc

test (GraphPrism 9.0 software). The CT values of GAPDH were similar for the nine groups, while some of the groups had an altered CT value for EF-1 as shown in Figure 3-10. Thus GAPDH was selected as the housekeeping gene/reference gene to investigate the mRNA expression of the studied GPCR receptors in LAD arteries.

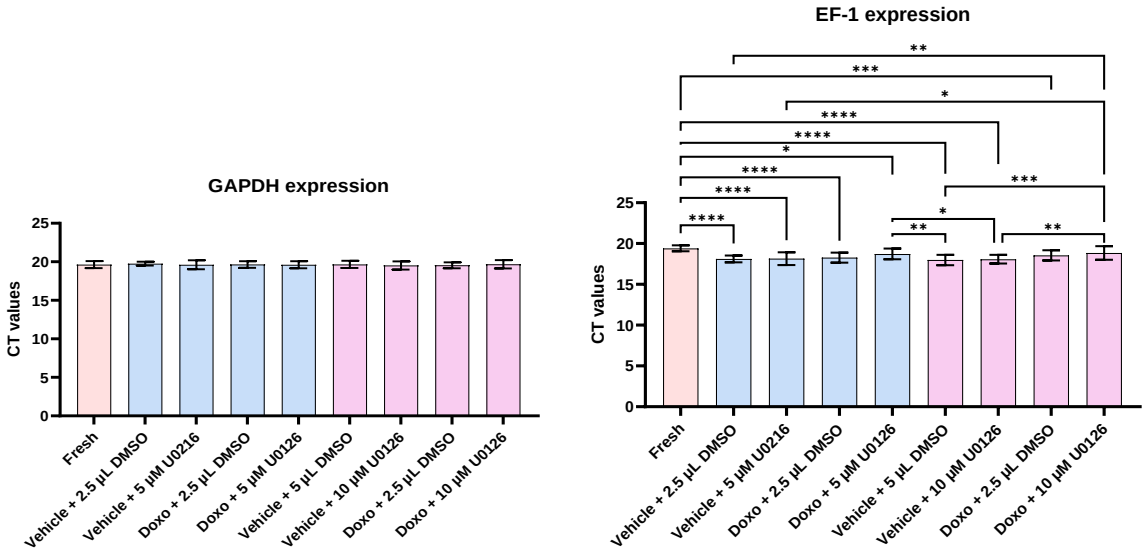

Figure 3-10: Comparison of the CT value of the housekeeping genes GAPDH and EF-1. (A) Comparison of the CT value of GAPDH. (B) Comparison of the CT value of EF-1. Multiple comparisons with one-way ANOVA and Dunnett's post-hoc test: * = $p < 0.05$, ** = $p < 0.01$, *** = $p < 0.001$, **** = $p < 0.0001$.

3.4. Discussion / Conclusion

<u>The organ culture of arteries is an interesting *in vitro* model that mimics cardiovascular diseases</u>

Organ culture of arteries is an *in vitro* model used to mimic CVD progression (Murata *et al.*, 2001a, Alm *et al.*, 2002, Skovsted *et al.*, 2012). In the present study, the incubated LAD vessels had a slight reduction of the contractile capacity when compared to the fresh vessels. Previous studies with organ culture models had shown no difference of the contractile capacity with fresh vessels (Alm *et al.*, 2002, Skovsted *et al.*, 2012, Sandhu *et al.*, 2010). Alm (2002) studied the endothelium dysfunction of isolated rat mesenteric artery branches before and after a 20 hrs incubation. They used 60 mM K^+ KH to examine the contractile capacity and observed no difference between the control group and the incubated group (Alm *et al.*, 2002). Skovsted and Sandhu investigated the GPCRs alterations on, respectively, rat LAD arteries and rat cerebral arteries for 24 hrs incubation and both observed no difference between fresh vessels and 24 hr-incubated vessels (Skovsted *et al.*, 2012, Sandhu *et al.*, 2010). However, Johansson (2008) studied the expression of rat ET_B receptors in rat LAD arteries,

where an increase of the contractile capacity was observed after 24 hrs incubation and it has been suggested that it was due to the proliferation of SMCs (Johnsson *et al.*, 2008).

In animal models, altered blood flow can provoke an acute vasoconstriction response to restore arterial shear stress to physiological homeostasis levels (Kamiya and Togawa, 1980). Circumferential stress and shear stress are two mechanical factors known to be sensitive to altered arterial pressure, as observed during some CVDs, and abnormal circumferential stress and shear stress affect remodelling factors of arteries (Wayman *et al.*, 2008). Shear stress is a mechanical factor which induces the nitric oxide (NO) release through endothelial nitric oxide synthase (eNOS) activation and regulates transcription and growth factors in endothelial cells (EC) (Noris *et al.*, 1995). In the absence of shear stress, the production of NO is altered, which leads to endothelium dysfunction (Alm *et al.*, 2002). The development of several CVDs - such as hypertension, congestive heart failure, and atherosclerosis - is mimicked during organ culture, as organ culture induces similar chronic remodelling processes as observed during these CVDs (Tai *et al.*, 2009, Ozaki and Karaki, 2002). The decrease of the contractile capacity observed in the present study could be due to the absence of shear stress and circumferential stress, leading to endothelium dysfunction. The decrease of carbachol-mediated relaxation observed on 24 hr-incubated LAD vessels, which is an indicator of endothelium dysfunction seems to correlate to the implication of previously described mechanisms in the decrease of the contractile capacity. The other models showed no decrease or conversely, an increase of the contractile capacity mimicking the chronic remodelling process observed during CVD (i.e. the proliferation of SMC). The present model showed a decrease of the contractile capacity induced by the incubation; however, the contractile capacity wasn't altered by the period of incubation (24 hrs or 48 hrs). The present model could be mimicking a severe vascular injury on LAD vessels that the remodelling process can't completely compensate to restore the contractile capacity.

In the present study, the organ culture model was used to study the doxorubicin-induced vasotoxicity and cardiotoxicity effect on coronary artery vascular tone using rat LAD arteries.

Doxorubicin treatment can be injected by a single high dose or cumulative low doses in experimental models

Doxorubicin as a chemotherapeutic drug is usually administrated by cumulative doses inferior to 360 mg of doxorubicin/m^2 during a few weeks to cancer patients (Zamorano *et al.*, 2016). Several pre-clinical studies, using animal models to investigate the doxorubicin-induced cardiotoxicity on cardiac outcomes, administrated a single high dose or cumulative low doses of doxorubicin by intraperitoneal

or intravenous injection of doxorubicin, depending on the type of toxicity observed (Podyacheva *et al.*, 2021). In *in vivo* models, acute and short-term effects of doxorubicin are mostly investigated after the injection of a single high dose of doxorubicin, whereas the chronic doxorubicin-induced cardiotoxicity is investigated by cumulative injections of lowest doses of doxorubicin during weeks or months. The doses of doxorubicin injected in animal models are equivalent to doses injected to doxorubicin-treated cancer patients (Podyacheva *et al.*, 2021). However, the concentration of doxorubicin used in *in vitro* models needs to correlate to the plasma levels, since the organ is incubated with the doxorubicin. A study by Young *et al.et al.* (1981) showed that the concentration range of 0.2 µM to 1 µM of doxorubicin applied during vessel incubation was similar to the plasma concentration of doxorubicin in doxorubicin-treated patients (Young *et al.*, 1981). Murata *et al.et al.* (2001) studied the chronic vascular toxicity of doxorubicin in rabbit mesenteric arteries and reported that, after 7 days of incubation, the optimal dose of doxorubicin was 0.3 µM (Murata *et al.*, 2001a). In another study, doxorubicin-induced cardiotoxicity and a potential adjuvant, the immunosuppressant cyclosporin A was investigated on Sprague-Dawley rat hearts using the Langendorff perfusion model and on viability studies of neonatal rat cardiac myocytes, and the optimal doxorubicin dose was 1 µM (Gharanei *et al.*, 2013b). The present study is on LAD arteries from Sprague-Dawley rats and showed that 0.5 µM was the optimal concentration of doxorubicin to investigate the doxorubicin-induced vasotoxicity on 24 hr-incubated rat LAD arteries, which is comprised in the range of the therapeutic doses of doxorubicin (Young *et al.*, 1981).

Moreover, Herman *et al.et al.* (1998) compared two genetically related Wistar Kyoto rat strains to determine the more suitable model to investigate doxorubicin-induced cardiotoxicity. They compared the cardiac adverse effects of doxorubicin on spontaneous hypertensive rats and on normotensive rats. They observed that both strains developed cardiac issues, however, the hypertensive rats were more sensitive to doxorubicin-induced cardiotoxicity. They demonstrated that rat models with more sensitive cardiovascular issues were more suitable to study the doxorubicin-induced cardiotoxicity (Herman *et al.*, 1985, Herman and Ferrans, 1998). this study's organ model is, in contrast, an *in vitro* model with a different rat strain, Sprague-Dawley. However, the organ culture of LAD arteries is mimicking the mechanisms observed in CVD, as described previously, which made it a suitable model to study the doxorubicin-induced vasotoxicity.

<u>Doxorubicin has no acute effect on the contractile capacity of LAD arteries</u>

In the present study, the acute effect of doxorubicin on contractile capacity was tested on fresh LAD vessels at four different concentrations: 0.1 µM, 0.25 µM, 0.5 µM and 1 µM after 15 min. The contractile capacity was not compromised due to doxorubicin treatment at any of the concentrations applies. Also, cumulative administration of doxorubicin on fresh LAD vessels at a concentration range of 0.01 µM to 10 µM was conducted to investigate the potential vasocontractile or vasodilatory effect of doxorubicin, however, no acute vasocontractile or vasodilatory effect was observed. This study's results are in agreement with Murata *et al.et al.* (2001), who demonstrated that doxorubicin application on fresh rabbit mesenteric arteries at a concentration range of 0.3 – 10 µM had no acute effects on smooth muscle contractility. Furthermore, they also reported that the morphology of SMCs was preserved during the doxorubicin treatment (Murata *et al.*, 2001b).

The doxorubicin-induced cardiotoxicity is concentration-dependent

Doxorubicin concentration range during 24 hrs incubation was tested by investigating the effect on the 60 mM K^+ KH vasocontractile capacity. High potassium exposure induces an increase of the extracellular potassium concentration, which modifies the potassium homeostasis leading to the depolarisation of the SMC membrane and vasoconstriction (Haddy, 1983). The 60 mM K^+ KH concentration was in agreement with previous vascular studies (Alm *et al.*, 2002, Skovsted *et al.*, 2012).

Based on Gharanei *et al.et al.* study (Gharanei *et al.*, 2013a), in this study LAD arteries were initially incubated for 24 hrs with 1 µM doxorubicin. However, this concentration of doxorubicin was too high as the contractile capacity of the vessels was almost abolished. A minimum threshold of 1 mN contractile capacity is applied in vascular contractile studies, as a contractile capacity below 1 mN represents a severely compromised nonviable vessel and is thus therefore not included in vascular studies.

A lower concentration of doxorubicin was therefore investigated. Murata *et al.et al.* (2001) used 0.3 µM and 1 µM doxorubicin during rabbit mesenteric artery incubation to investigate doxorubicin-induced vasotoxicity, and the team reported that the contractile response after 1 µM doxorubicin incubation was decreased considerable, which is in agreement with to this study's results. However, the 0.3 µM concentration of doxorubicin did not affect the contractile capacity compared to the vehicle group (Murata *et al.*, 2001a). In this study, lower concentrations of doxorubicin were tested in addition to the compromising doxorubicin concentration of 1 µM. Lower concentrations were in agreement with previous publications (Murata *et al.*, 2001a, Young *et al.*, 1981) and the following

additional lower doxorubicin concentrations were therefore investigated during 24 hrs LAD vessel incubation: 0.1 µM, 0.25 µM, and 0.5 µM. LAD vessels incubated for 24 hrs in the presence of 0.25 µM or 0.5 µM doxorubicin had a similar contractile response as vessels incubated with vehicle. The highest concentration of 0.5 µM doxorubicin that didn't compromise the LAD vessel contractile capacity was chosen as the optimal doxorubicin concentration for the present experiments. This study's results demonstrate that the optimal concentration of doxorubicin is 0.5 µM during 24 hrs incubation of rat LAD vessels to study the vasotoxic and cardiotoxic effect of doxorubicin.

The doxorubicin-induced cardiotoxicity is time-dependent

Hayward *et al.et al.* (2013) studied the doxorubicin-induced cardiotoxicity in skeletal (with isolated skeletal muscle), cardiac (with isolated perfused heart) and smooth muscle (with isolated aortic rings), after a single injection of 15 mg of doxorubicin/kg on male Sprague-Dawley rats. They studied the doxorubicin effects on day 1, day 3 and day 5 post-injection. The cardiac function was investigated by isolated heart perfusion, and aortic vascular tone was investigated by wire-myography. In vascular smooth muscle, the doxorubicin was accumulated at low doses and was retained for a longer period of time than in other tissues. Their study showed that vascular dysfunction occurs during day 1 and was sustained on day 5 (Hayward *et al.*, 2013). Murata *et al.et al.* (2001) studied the chronic effect of doxorubicin at three different concentrations - 0.3 µM, 1 µM and 10 µM - on vascular endothelium (Murata *et al.*, 2001b). Their study highlighted the long-term effect of doxorubicin on the vascular wall, which occurs during DNA damage and apoptotic changes, followed by alterations of the SMC. To determine the optimal incubation time in the present study, LAD vessels were incubated for 24 hrs and 48 hrs in an organ culture setting. The contractile capacity of LAD vessel was severely compromised in the presence of 0.5 µM doxorubicin after 48 hrs of incubation, however, 24 hrs incubation did not alter the contractile response. These results demonstrate that 24 hrs is the optimal period of incubation time to study the vasotoxic and cardiotoxic effect of 0.5 µM doxorubicin in rat LAD vessels.

Conclusion

In this chapter, the *in vitro* organ culture model of doxorubicin-induced vasotoxicity and cardiotoxicity was optimised. The data presented in this chapter showed that acute application of doxorubicin to fresh LAD vessels (from 0.01 µM to 10 µM) did not show any vasocontractile or vasodilatory effects of doxorubicin, nor did the acute application of doxorubicin (from 0.1 µM to 1 µM) to fresh LAD vessels

change the contractile or dilatory capacity of the vessels. The optimal conditions to study the vasotoxic and cardiotoxic effects of doxorubicin were narrowed down to a concentration of 0.5 μM of doxorubicin incubated for 24 hrs during organ culture settings. This optimised *in vitro* organ culture model of doxorubicin-induced vasotoxicity and cardiotoxicity will be used to study the effect of doxorubicin on GPCRs-mediated vasocontraction in the following chapters.

Chapter 4

4. The effect of doxorubicin on GPCR-mediated vasocontraction in rat coronary arteries, and the influence of GPCR specific antagonists.

Some data of this chapter are under review or published:

Peer reviewed journal:

- Submitted for publication in Archives of Toxicology (May 2023):

Title: Doxorubicin alters G-protein coupled receptor mediated vasocontraction in rat coronary arteries during an *in vitro* organ culture model.

Authors: Lozahic C., Maddock H., Wheatley M., Sandhu H.

Conferences:

- British Pharmacology Society (BPS) Pharmacology 2020 conference:

Live poster presentation: Doxorubicin-induced cardiotoxicity: Investigating the effect on G protein-coupled receptors mediated vascular tone. Miss Caroline Lozahic, Prof Helen Maddock, Dr Hardip Sandhu.

- Safety pharmacology Society (SPS):
    - 2020 SPS Virtual Meeting

Online poster presentation: Doxorubicin-induced cardiotoxicity: Investigating the effect on miRNA expression and GPCR mediated vascular tone. Caroline Lozahic, Mark Wheatley, Helen Maddock, and Hardip Sandhu.

    - 2021 Virtual Annual Meeting

Online Poster presentation: Doxorubicin-induced vasotoxicity in coronary vessels: Investigating the G-protein coupled receptor mediated vasoconstriction. Miss Caroline Lozahic, Prof Mark Wheatley, Prof Helen Maddock, and Dr Hardip Sandhu

4.1. Introduction

Clinical studies have highlighted an increase of arterial stiffness in patients treated with anticancer drugs both during and after the treatment, including doxorubicin (Parr *et al.*, 2020, Mozos *et al.*, 2017, Chaosuwannakit *et al.*, 2010). Arterial stiffness is known to be associated with CVDs, such as hypertension, stroke, and congestive heart failure (Laurent and Boutouyrie, 2020, Sutton-Tyrrell *et al.*, 2005, Chae *et al.*, 1999).

However, the doxorubicin-mediated vasotoxicity has been poorly investigated, notably on the VSMCs. A study on human coronary arteriolar function showed that chemotherapeutic treatment could induce a reduction of the endothelial function, however, the mechanisms involved were not clear (Hader *et al.*, 2019). Bosman *at al.* studied the doxorubicin-induced arterial stiffness in mouse aortic artery *in vivo* and *ex vivo* models (Bosman *et al.*, 2021a). Their team showed that doxorubicin could induce arterial stiffness even in absence of cardiac dysfunction. Moreover, the doxorubicin-mediated vasotoxicity impaired the endothelium function by reducing the endothelium-dependant vasorelaxation and enhancing the vasocontraction leading to arterial stiffness. It has been postulated that doxorubicin-induced endothelial-toxicity is caused by the accumulation of ROS in mitochondria leading to apoptosis of the endothelial cells (EC) and decrease of endothelial nitric oxide synthase (eNOS) levels, an essential enzyme for the endothelial function (He *et al.*, 2019). Doxorubicin-mediated vasotoxicity has been observed in VSMCs using different *ex vivo* models, including isolated mouse aorta (Doxo = 1 µM, during 16 hrs) (Bosman *et al.*, 2021b) and rabbit mesenteric arteries (Doxo = 0.3, 1, 10 µM, during 7 days) (Murata *et al.*, 2001a), and in an *in vivo* model: rats aorta (Doxo = 15 mg/kg during 1, 3 or 5 days) (Hayward *et al.*, 2013). These studies showed that doxorubicin (from 1 µM) was altering the vasocontractile capacity of vessels. However, the underlying specific mechanisms of action during doxorubicin-induced cardiotoxicity remain unclear. Hayward *et al.et al.* investigated the effect of doxorubicin (15 mg/kg) on cardiac (i.e. isolated heart perfusion), skeletal (i.e. isolated skeletal muscle), and smooth muscle (i.e. isolated aorta rings) function. Their studies showed that doxorubicin affected the VSMCs leading to an alteration of the vasocontractile responsiveness of rat aortic artery (Hayward *et al.*, 2013). Conflicting results have been reported regarding the doxorubicin-induced cardiotoxicity effect on VSMCs by various papers. Studies have reported that at therapeutic and toxic doses doxorubicin induces a decrease of the phenylephrine (PE)-mediated vasocontractility of vascular smooth muscle in an *ex vivo* model of isolated rat aorta (Doxo = 0.3, 1, 10 µM) (Murata *et al.*, 2001b) and a decrease of the PE-mediated vasocontractile response in an *in vivo* model of rat thoracic aorta (Doxo = 20 mg/kg) (Olukman *et al.*, 2009). Conversely, Shen *et al.et al.* observed that doxorubicin had an acute effect on the aortic vasocontractile capacity by increasing the VSMCs vasocontraction in isolated C57BL16 mouse aortic vessels during doxorubicin treatment (10 and 100

μM). The vasoconstriction was induced by the increase of Ca^{2+} release from sarcoplasmic reticulum and increase in Ca^{2+}-influx in mouse VSMCs (Shen *et al.*, 2009). The specific mechanisms involved in doxorubicin-induced vasotoxicity on VSMCs remain unclear.

The plasma ET-1 level is increased in patients with chronic heart failure (Wei *et al.*, 1994). ET-1 can bind two types of endothelin GPCR receptors (ET_A and ET_B) in the vascular system (Wang *et al.*, 2018). ET_B receptors are found in both endothelium and SMCs. In endothelial cells, ET_B receptors are involved in vasodilatation by NO and prostaglandin production, while ET_B receptors in SMC are involved in vasocontraction. ET_A receptors are found in SMCs and are mainly responsible of the VSMC vasocontraction (Maguire and Davenport, 2015). In the clinic, endothelin receptor specific antagonists are used to treat pulmonary arterial hypertension in patients, including bosentan (blocks both ET_A and ET_B receptors), macitentan (blocks both ET_A and ET_B receptors), and ambrisentan (blocks ET_A receptors) (Enevoldsen *et al.*, 2020).

The 5-hydroxytryptamine 1B (5-HT_{1B}) receptor is a serotonin GPCR receptor, and in human coronary artery SMCs 5-HT_{1B} is involved in vasoconstriction (Nilsson *et al.*, 1999b). A recent study investigated the potential cardioprotective effect of the 5-HT agonist sumatriptan against doxorubicin-induced cardiotoxicity. They administered 2.5 mg/kg of doxorubicin by intra-peritoneal injection, 3 times a week, during two weeks in rats. Sumatriptan (0.1 mg/kg) was administrated 30 min before the doxorubicin injection to investigate its potential cardioprotective properties. They demonstrated that the anti-oxidant and anti-inflammatory properties of Sumatriptan at a concentration of 0.1 mg/kg could be cardioprotective against doxorubicin-induced cardiotoxicity in rats (Sheibani *et al.*, 2021). However, Sheibani *et al.et al.* tested the cardioprotective effect of Sumatriptan at the highest concentrations of 1 and 3 mg/kg and they observed an aggravation of the doxorubicin-induced cardiotoxicity (data not shown in cited paper), while Sumatriptan at a concentration of 0.1 mg/kg showed interesting cardioprotective effects (Sheibani *et al.*, 2021). This study's results suggest a potential involvement of the serotonin receptors in doxorubicin-induced cardiotoxicity.

Thromboxane prostanoid (TP) receptor mediates platelet activation, vasoconstriction, EC activation and SMC proliferation (Capra *et al.*, 2014). Thromboxane A2 (TxA2) is the most potent agonist of the TP receptors and TxA2 binding to the TP receptors leads to vasocontractile responses (Chen, 2018). Elevated TxA2 levels are observed in the circulation of patients with ischemic heart disease leading to increased vasoconstriction and platelet aggregation observed during CVD (Touchberry *et al.*, 2014). TxA2 binding to TP receptors mediates an influx of Ca^{2+} in SMC leading to vasocontraction (Grann *et al.*, 2016). An *ex vivo* study on mesenteric arteries from hypertensive rats reported that mesenteric arteries vasoconstriction was increased by elevated TxA2 production which is promoted by the

increased production of ROS, induced by cumulative incubation (4 min per dose) of H_2O_2 (1 – 100 µM) (Garcia-Redondo *et al.*, 2015).

Due to their involvement in physiological and pathological changes of the vascular tone during CVDs and risk factor exposure, ET_A, ET_B, 5-HT_{1B} and TP receptors are interesting mediators to study during doxorubicin-mediated vasotoxicity. Specific agonists (Table 9.1 in Appendices) and antagonists (Table 9.2 in Appendices) can be used to study the vascular function of the four GPCRs mentioned above. ET_A and ET_B receptor-mediated vasoconstriction in arteries SMC, including coronary arteries SMC, can be investigated by applying ET-1 (K_D = 0.48 nM in rat cardiomyocytes) (Fareh *et al.*, 1996), while sarafotoxin 6c (S6c) ($K_D(ET_B)$ = 0.06 nM and $K_D(ET_A)$ = 1.5 µM in rat heart) (Russell and Davenport, 1996) can be used to study ET_B receptor-mediated vasoconstriction (Skovsted *et al.*, 2012). 5-carboxamidotryptamine (5-CT) is an agonist of the 5-HT_{1B} receptor, and the application of 5-CT leads to 5-HT_{1B}-mediated vasocontraction (Nilsson *et al.*, 1999b). 5-CT binds with a $pEC_{50} = 10^{-7.9}$ M to 5-HT_{1B} in the cerebral nervous system (CNS), but can also bind 5-HT_{2A} receptor found in coronary arteries with a lower affinity ($pEC_{50} = 10^{-3.5}$ M) in fibroblast-like cell isolated from the aortic thoracic smooth muscle of an embryonic rat (A7r5) (Hoyer *et al.*, 1994). 9,11-dideoxy-11α,9α-epoxymethanoprostaglandin $F_{2\alpha}$ (U46619) is an agonist of the TP receptor, and application of U46619 leads to TP-mediated vasoconstriction (Sandhu *et al.*, 2011). U46619 binds to TP receptors with an EC_{50} of 7.0 nM for the rat TP receptors in rat aorta.

The first aim of the work presented in this chapter is to determine if doxorubicin affects the ET_A, ET_B, 5-HT_{1B} and TP receptor-mediated vasocontraction. To study the involvement of these GPCRs, the vascular tone of the rat's left anterior descending (LAD) arteries in response to these GPCR agonists was studied using the *in vitro* vascular force measurement technique by wire-myography. The second aim of this chapter is to determine if the GPCR-induced vasocontraction observed is truly specific to the GPCR by application of GPCR specific antagonists. To verify the involvement of the studied specific GPCRs during doxorubicin-mediated vasotoxicity specific antagonists (ET_A specific BQ123; ET_B specific BQ788; 5-HT_{1B} specific GR55562 and TP specific Seratrodast) were used in presence of the chemotherapeutic drug or vehicle prior to GPCR agonist stimulation (Skovsted *et al.*, 2015, Maassen VanDenBrink *et al.*, 2000, Hader *et al.*, 2019, Wouters *et al.*, 1999).

4.2. Material & methods

4.2.1. Animal ethics

Male Sprague-Dawley rats (300 – 350 g) were used during the experiments. The animals were purchased from Charles River (Margate, UK) and housed at the University of Warwick. Experiments were conducted in accordance with the Home Office Guidance on the Operation with Animals (Scientific Procedures Act 1986; The Stationary Office, London, UK) and were approved by the Ethics Committee of Coventry University.

4.2.2. Materials

Doxorubicin hydrochloride was purchased from Tocris Biosciences (Bristol, UK) and was dissolved in Reverse Osmosis (RO) water with a final stock concentration of 1mM.

Serotonin hydrochloride, carbachol, sarafotoxin S6c, endothelin-1, 9,11-dideoxy-11α,9α-epoxymethanoprostaglandin $F_{2\alpha}$ (U46619), 5-carboxamidotryptamine maleate salt were purchased from Sigma-Aldrich (Merck KGaA, US). U46619 was dissolved in methyl acetate with final stock concentration of 3mM. All the other drugs were dissolved in RO water. Serotonin hydrochloride and carbachol had a final stock concentration of 10 mM. Sarafotoxin 6c and endothelin-1 had a final stock concentration of 0.1 mM. U46619 and 5-carboxamidotryptamine had a final stock concentration of 27mM and 30mM, respectively. The antagonists BQ788, BQ123 and Seratrodast were purchased from Tocris Biosciences (Bristol, UK). The antagonist GR55562 was purchased from Sigma-Aldrich (Merck KGaA, US). BQ788 and Seratrodast were dissolved in DMSO with a final stock concentration of 0.1mM. BQ123 and GR55562 were dissolved in RO water with a final stock concentration of 400µM and 0.1mM, respectively. All drugs were aliquoted in suitable volumes and stored at -20°C.

Dulbecco's Modified Eagle Medium, DMEM (1g/L D-Glucose, 4mM L-Glutamine, 0.11g/L Sodium pyruvate) and Antibiotic-antibiotic (10,000 units/mL of penicillin, 10,000 µg/mL of streptomycin, and 25 µg/mL of Gibco Amphotericin B) were purchased from ThermoFisher Scientific (Massachusetts, US). All reagents used to prepare the KH buffers for the myography experiments were purchased from Fisher Bioreagents (Fisher Scientific, US).

4.2.3. Isolated left anterior descending artery (LAD) preparation

Sprague-Dawley rats were ethically and humanely sacrificed, and LADs were rapidly dissected free, as described in chapter 2, section 2.3.2. The LAD was cut into 4 rings of approximatively 2 mm in length each and the LAD segments were divided into 2 groups. Vessels were incubated in DMEM low glucose media added either vehicle (vehicle group) or 0.5 µM doxorubicin (Doxo group) at 37 °C and humidified with 5 % CO_2 and 95 % O_2. The vessels were incubated for 24 hrs as this was determined as the optimal incubation time with 0.5 µM doxorubicin (please refer to Chapter 3 section 3.3.2).

4.2.4. Myography protocol

4.2.4.1. GPCRs dose-response protocol of LAD arteries without antagonist inhibition

Vessels were mounted in Ca^{2+}free KH buffer on the myograph after 24 hrs of incubation, and afterwards, the buffer was changed to Na^+ KH and the vessels were stabilised for 1 hr (see Figure 4-1).

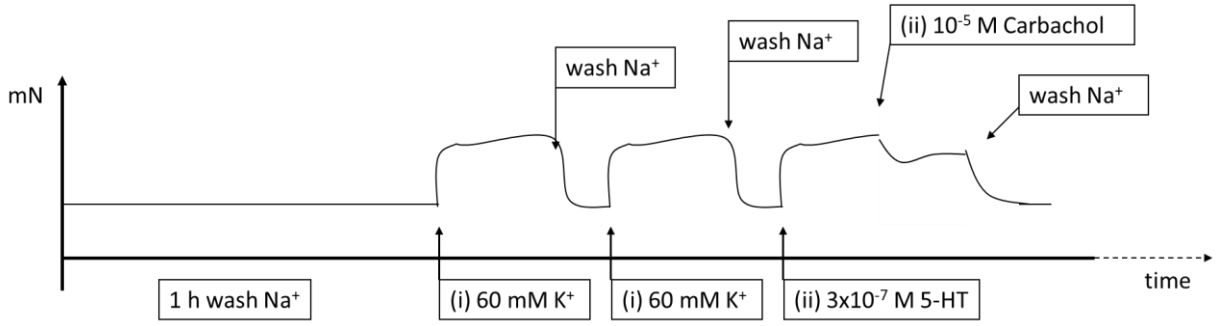

Figure 4-1: Experimental protocol to study vascular contractility and dilatory capacity of LAD vessels. Na^+ = Na^+ KH, K^+ = K^+ KH, 5-HT = serotonin.

A pre-tension in the range of 1.16mN/mm to 1.52mN/mm was applied during this stabilisation step (Ping *et al.*, 2014). After the stabilisation period, the vessels were exposed to a 60 mM K^+ KH to measure the maximum vasocontraction capacity. The K^+ KH buffer maximum vasocontraction is used as reference for the study of the GPCR agonist-mediated dose-response curves, therefore the contractile capacity, determined by K^+ KH buffer needs to be above 1 mN or else the vessels were excluded. Vessels were washed twice with Na^+ KH for 15 min and a second 60 mM K^+ KH contraction was recorded. Vessels were washed with Na^+ KH with 15 min intervals until the vascular tension came back to the baseline level (minimum 30 min). To measure the vasodilatory capacity the vessels were pre-contracted with 3. 10^{-7} M serotonin (5-HT) followed by applying 10^{-5} M carbachol. Vessels were washed with Na^+ KH with 15 min intervals until the vascular tension came back to the baseline level.

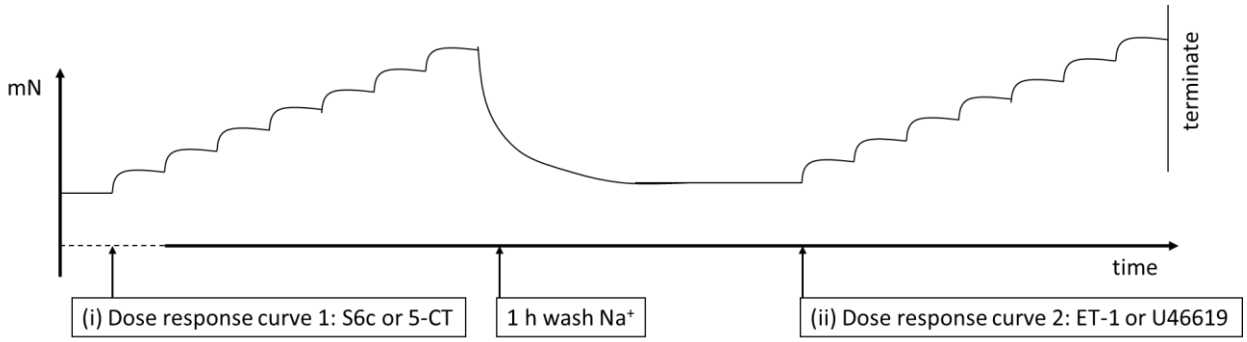

Figure 4-2: Experimental protocol to study dose-response curve of specific GPCR agonists. S6c = sarafotoxin 6c, agonist of ET_B receptors; 5-CT = 5-carboxyamidotryptamine, agonist of 5-HT_{1B} receptors, ET-1 = endothelin-1, agonist of ET_A and ET_B receptors; U46619, agonist of TP receptors

Once the vasocontractile and vasodilatory capacity of the vessels was measured - and thus established the function and viability of the vessels - the dose-response curve can be measured. As seen in Figure 4-2, cumulative doses of the specific agonists will be added, starting from the lowest dose and then increasing in half-log increments to the highest dose. The segments were either stimulated with (i) ET_B receptor agonist sarafotoxin 6c (S6c), from 10^{-14} M to $10^{-7.5}$ M, followed by Na^+ KH washing with 15 min intervals until the vascular tension reverted to the baseline level, where after the second dose-response curve was measured by applying ET_A and ET_B receptor agonist endothelin-1 (ET-1), from 10^{-14} to $10^{-7.5}$ M, or by stimulation with (ii) 5-HT_{1B} receptor agonist 5-carboxamidotryptamine (5-CT), from 10^{-12} to $10^{-5.5}$ M, followed by Na^+ KH washing with 15-minute intervals until the vascular tension reverted to the baseline level, where after the second dose-response curve was measured by applying thromboxane A2 receptor agonist U46619, from 10^{-12} to $10^{-6.5}$ M.

4.2.4.2. GPCRs dose-response protocol of LAD arteries with antagonist inhibition

Vessels were stabilized and fixed at selected pre-tension, and their contractile capacity was investigated as in the previous section 4.2.4.1.

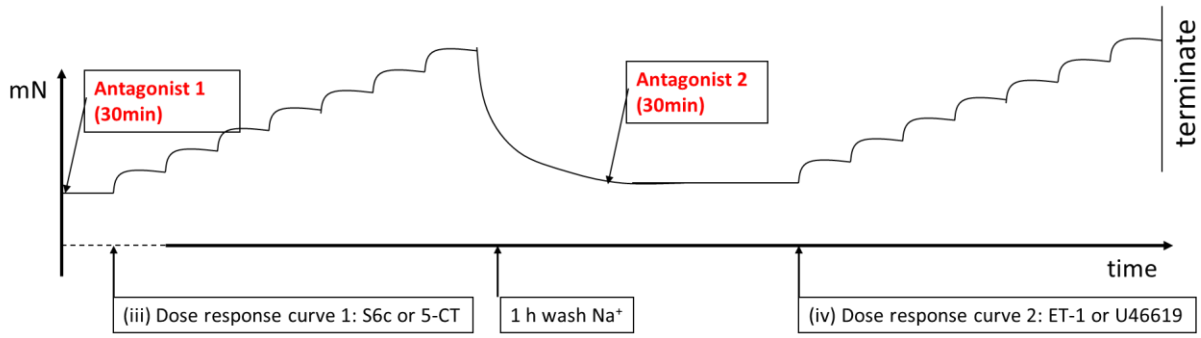

Figure 4-3: Experimental protocol to study dose-response curve of specific GPCR agonists after 30mins antagonists pre-treatment. S6c = sarafotoxin 6c, the agonist of ET_B receptors; 5-CT = 5-carboxyamidotryptamine, the agonist of $5\text{-}HT_{1B}$ receptors, ET-1 = endothelin-1, the agonist of ET_A and ET_B receptors; U46619, the agonist of TP receptors.

Once stabilised the vessels were incubated for 30 min with the antagonist, BQ788 (0.1 µM) or GR55562 (1 µM), as shown in Figure 4-3. Then, a dose-response curve was obtained, as described in previous section 4.2.4.1., by adding cumulative application of sarafotoxin 6C (10^{-14} M to $10^{-7.5}$ M) to BQ788 treated vessels or 5-carboxyamidotryptamine (10^{-12} M to $10^{-5.5}$ M) to GR55562 treated vessels. Vessels were washed in Na^+ KH for 2x 15 min, where after the vessels were incubated for 30 min with the second antagonist, BQ123 (10 µM) + BQ 788 (0.1 µM) or Seratrodast (1 µM). Finally, a second dose-response curve was obtained, as described in previous section 4.2.4.1., by adding cumulative application of endothelin-1 (10^{-14} M to $10^{-7.5}$ M) to BQ123 and BQ 788 treated vessels, or U46619 (10^{-12} M to $10^{-6.5}$ M) to Seratrodast treated vessels. The effect of BQ788 (0.1 µM) or BQ123 (10 µM) mono-administration prior to the ET-1 dose-response curve was also studied.

4.2.5. Statistical analysis

All data are expressed as mean ± SEM and n refers to the number of rats used.

Contractile responses to agonists in each vessel were expressed as percentage of the 60 mM K^+ KH-induced contraction. Student's T-test and Two-way ANOVA + Bonferroni were used as statistical tests. All statistical analyses were carried out using SPSS (T-test) or GraphPad Prism (ANOVA) software. Statistical significance was determined when $p < 0.05$.

"E_{max}" values represent the maximal contractile response elicited by the agonist and are generated by the software Graph-Pad Prism 9. C_{max} values represent the contraction obtained at the highest agonist dose and are applied when the "E_{max}" couldn't be determined due to stock concentration constrains. The "pEC_{50}" values represent the negative logarithm of the agonist concentration that produces 50 % of the maximal contractile effect and are generated with Graph-Pad Prism 9, based on the "E_{max}" value.

The calculations were carried out using Graph-Pad Prism 9 (GraphPad Software, La Jolla, USA). "E_{max}" and "pEC_{50}" values were statistically analysed with Kruskal-Wallis test, using GraphPrism software.

4.3. Results

4.3.1. Doxorubicin alters the sarafotoxin 6c (endothelin B receptor agonist) mediated vasocontraction

Vasocontractile responses to sarafotoxin 6c (ET_BR agonist)

The endothelin ET_B receptor specific agonist, sarafotoxin 6c, was used to investigate the effect of doxorubicin treatment of LAD vessels incubated for 24 hrs on ET_B receptor-mediated vasocontraction compared to vehicle-treated vessels. The dose-response curve obtained from the ET_B receptor-mediated vasocontraction was biphasic. The S6c-induced ET_B receptor-mediated vasocontraction values are given as percentage of the maximal contractile response, induced by 60 mM K^+ KH.

After 24 hrs of organ culture with 0.5 µM doxorubicin, the ET_B-mediated vasocontraction was increased in the dose range of 10^{-13} M to $10^{-10.5}$ M (Figure 4-4). The significant increase of contraction observed in the presence of 0.5 µM doxorubicin was from 13.42 ± 2.02 % (p = 0.007) at 10^{-13} M to 45.83 ± 7.30 % (p = 0.04) at $10^{-10.5}$ M compared to 4.71 ± 1.49 % at 10^{-13} M to 20.93 ± 4.93 % at $10^{-10.5}$ M in vehicle-treated vessels. 0.5 µM doxorubicin treatment did not alter the "E_{max}" of 0.5 µM doxorubicin-treated vessels ("E_{max}" = 113.30 ± 6.2 %) compared to vehicle-treated vessels ("E_{max}" = 127.0 ± 5.6 %). The ET_B receptor-mediated biphasic dose-response curve with two "pEC_{50}"-values indicates a binding and stimulation of sarafotoxin 6c to at least two ET_B subtype receptors with different affinities for sarafotoxin 6c. 0.5 µM doxorubicin treatment did not alter the "pEC_{50}" values of 0.5 µM doxorubicin treated vessels ("$pEC_{50}1$" = $10^{-12.3}$ M and "$pEC_{50}2$" = $10^{-8.7}$ M), compared to "pEC_{50}" values of vehicle treated vessels ("$pEC_{50}1$" = $10^{-12.3}$ M and "$pEC_{50}2$" = $10^{-8.9}$ M). The "E_{max}", "$pEC_{50}1$" and "$pEC_{50}2$" are shown in table 4-1.

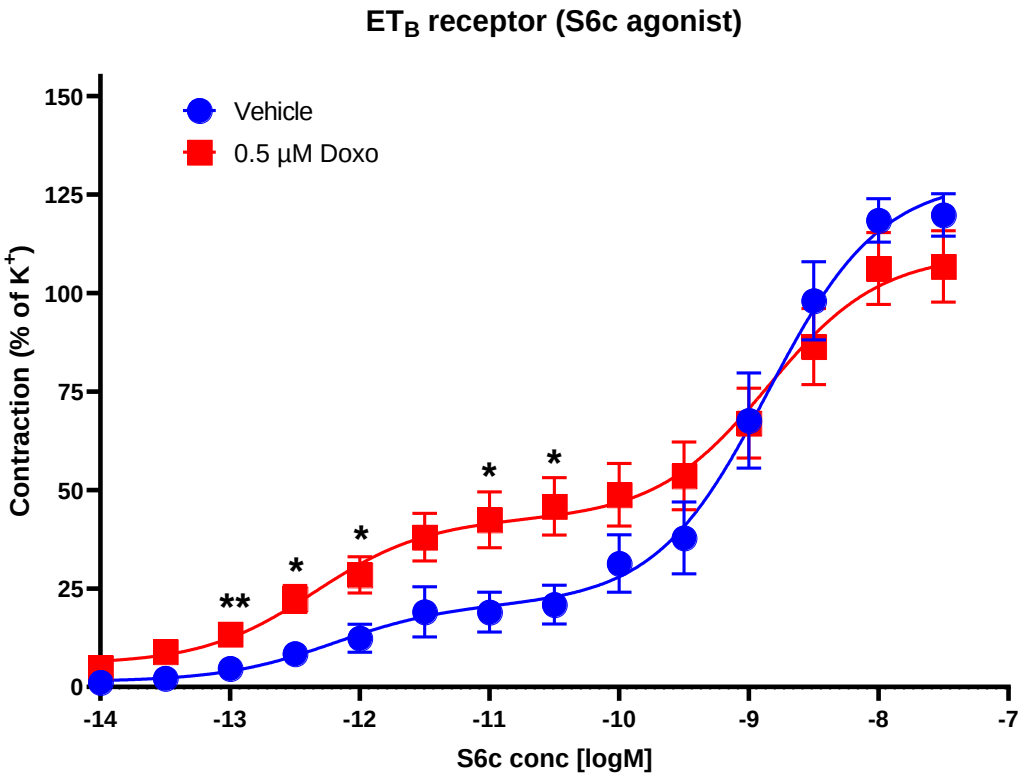

Figure 4-4: Vasocontractile response to the cumulative application of sarafotoxin 6c (S6c) (ET_B receptor agonist) normalised to 60 mM K^+ KH-induced contraction in rat LAD arteries. Doxorubicin group (n = 19; Red) was compared to Vehicle group (n = 17; Blue). Doxo = doxorubicin, S6c = Sarafotoxin 6c, K^+ = 60mM K^+ KH. Values given represent mean ± S.E.M and contractile responses were compared to vehicle group using Unpaired student T-test (* = p value < 0.05. ** = p value < 0.01).

Vasocontractile responses of sarafotoxin 6c (ET_BR agonist) in presence of BQ788 (ET_BR antagonist)

Doxorubicin and vehicle-incubated LAD arteries were exposed to an ET_B receptor specific antagonist BQ788 (0.1 µM) for 30 min, followed by cumulative application of sarafotoxin 6c to establish the ET_B receptor specificity of the sarafotoxin 6c agonist.

In 24 hrs organ-cultured vehicle arteries, the significant reduction of ET_B-mediated contraction observed after BQ788 pre-treatment of vessels was from 3.9 ± 0.4 % (p = 0.011) at 10^{-12} M to 62.9 ± 17.4 % (p = 0.030) at $10^{-8.5}$ M, compared to 12.4 ± 3.6 % at 10^{-12} M to 98.0 ± 9.9 at $10^{-8.5}$ M in vehicle-treated vessels, i.e. a difference of contraction from 8.4 % to 35.1 % at the S6c dose range 10^{-12} M to $10^{-8.5}$ M (Figure 4-5 (A)). The pre-treatment with BQ788 of vehicle vessels ("$pEC_{50}2$" = $10^{-8.42}$ M, p = 0.0136) slightly right-shifted the second phase of the biphasic curve compared to BQ788 naïve vehicle vessels ("$pEC_{50}2$" = $10^{-8.91}$ M), while the "$pEC_{50}1$" remained unaltered, as shown in Table 4-1. BQ788 pre-treatment increased the maximal ET_B-mediated contraction of BQ788 pre-treated vehicle vessels

("E_{max}" = 161.56 ± 11.95 %, p = 0.0219) compared to maximal ET_B-mediated contraction of the BQ788 naïve vehicle vessels ("E_{max}" = 127.0 ± 5.6 %)

In 24 hrs organ-cultured arteries treated with 0.5 µM doxorubicin, the ET_B-mediated contraction was reduced at almost all the S6c doses applied (Figure 4-5 (B)). The vasocontractile difference between BQ788 and BQ788 naïve vessels was significant ($p < 0.005$) at 10^{-14} M to 10^{-13} M sarafotoxin 6c application, however, the reduction of vasocontraction was less than 10 % throughout this range. At the sarafotoxin 6c concentration of $10^{-12.5}$ M to $10^{-10.5}$ M, the application of BQ788 induced a decrease of the ET_B-mediated contraction in BQ788 and doxorubicin treated vessels (from 10.0 ± 1.5 % ($p = 0.002$) at $10^{-12.5}$ M to 33.4 ± 3.1 % ($p = 0.010$) at $10^{-10.5}$ M) compared to BQ788 naïve doxorubicin-treated vessels (from 22.3 ± 3.5 % at $10^{-12.5}$ M to 45.8 ± 7.3 % at $10^{-10.5}$ M). Finally, at the sarafotoxin 6c concentration of 10^{-9} M to 10^{-8} M the ET_B-mediated contraction was reduced by 22 - 27 % in BQ788 treated vessels (from 45.0 ± 4.0 % ($p = 0.028$) at 10^{-9} M to 79.7 ± 5.7 % ($p = 0.017$) at 10^{-8} M) compared to BQ788 naïve vessels (from 66.9 ± 8.9 % at 10^{-9} M to 106.1 ± 9.1 % at 10^{-8} M). Pre-treatment with BQ788 in 0.5 µM doxorubicin-treated vessels did not alter "E_{max}" and "pEC_{50}" values compared to BQ788 naïve 0.5 µM doxorubicin vessels (Table 4-1).

(A)

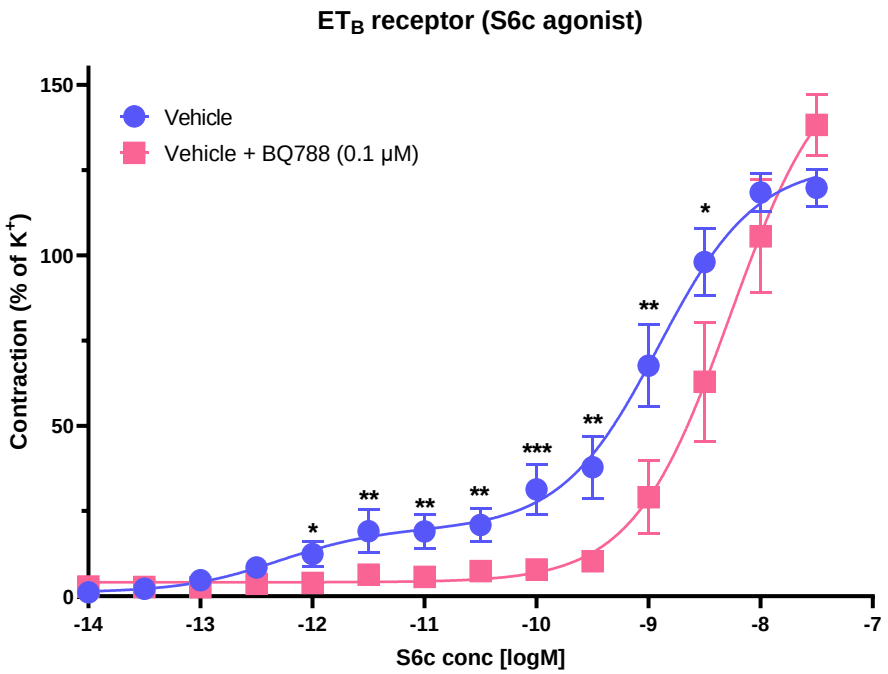

(B)

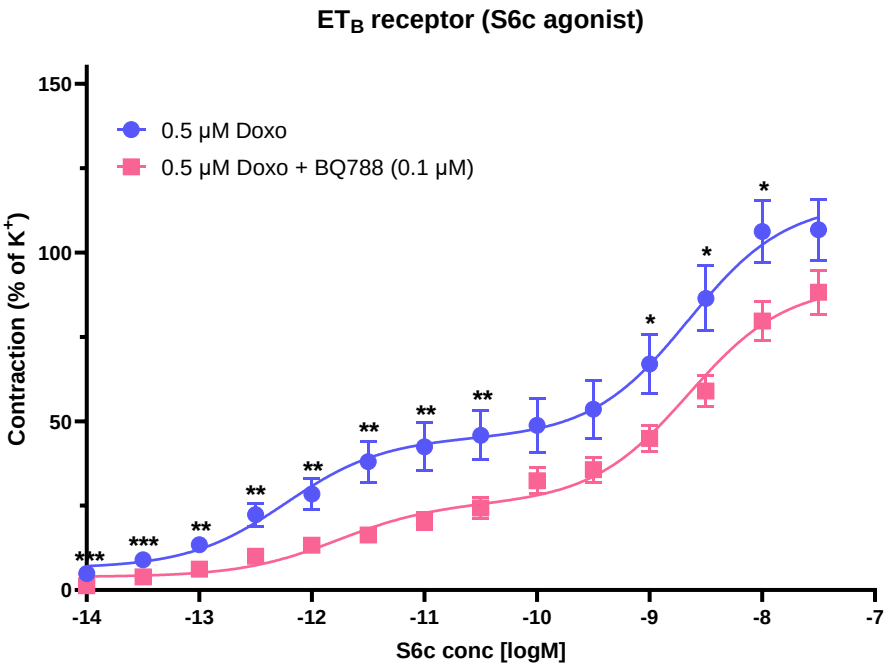

Figure 4-5: Vasocontractile response to the cumulative application of sarafotoxin 6c (ET_B receptor agonist) normalised to 60 mM K^+ KH-induced contraction in rat LAD arteries pre-treated with 30 min of 0.1 µM BQ788 (ET_B receptor antagonist). (A) Vasocontractile response to the cumulative application of sarafotoxin 6c to LAD arteries in the vehicle groups. Vehicle group (n = 17; Blue) and vehicle + 0.1 µM BQ788 (n = 8 - 9; Pink). (B) Vasocontractile response to the cumulative application of sarafotoxin 6c to LAD arteries incubated with 0.5 µM doxorubicin. Doxorubicin group (n = 18 - 19; Blue) and doxorubicin + 0.1 µM BQ788 (n = 14 - 15; Pink). Doxo = doxorubicin, S6c = Sarafotoxin 6c. Values given represent mean ± S.E.M and contractile responses were compared to vehicle group using Unpaired student T-test (* = p value < 0.05. ** = p value < 0.01. *** = p value < 0.001).

After 24 hrs of organ culture with 0.5 µM doxorubicin and 0.1 µM BQ788 pre-treatment, the ET_B-mediated vasocontraction was increased for the range of 10^{-13} M to $10^{-9.5}$ M sarafotoxin 6c compared to vehicle and 0.1 µM BQ788 pre-treatment vessels (Figure 4-6). The significant increase of contraction observed in 0.5 µM doxorubicin-treated arteries was from 10^{-13} M (6.2 ± 1.0 %, p = 0.020) to $10^{-9.5}$ M sarafotoxin 6c (35.7 ± 3.7 %, p < 0.001) and at a range of 4 % - 25 % increase compared to vehicle and 0.1 µM BQ788 pre-treatment vessels (2.7 ± 0.6 % at 10^{-13} M and 10.3 ± 1.6 % at $10^{-9.5}$ M). At the highest dose of sarafotoxin 6c applied ($10^{-7.5}$ M), the contraction was inhibited significantly in the 0.5 µM doxorubicin and 0.1 µM BQ788 pre-treatment treated vessels (88.3 ± 6.6 %, p = 0.001) compared to vehicle and 0.1 µM BQ788 pre-treatment vessels (138.2 ± 9.0 %). The BQ788 pre-treatment decrease the maximal ET_B-mediated contraction of 0.5 µM doxorubicin-treated vessels ("E_{max}" = 94.54 ± 4.4 %,

p < 0.0001) compared to the maximal ET_B-mediated contraction of 0.1 µM BQ788 pre-treatment vehicle vessels ("E_{max}" of 161.6 ± 12.0 %), while the "pEC_{50}" were not significantly altered (Table 4-1).

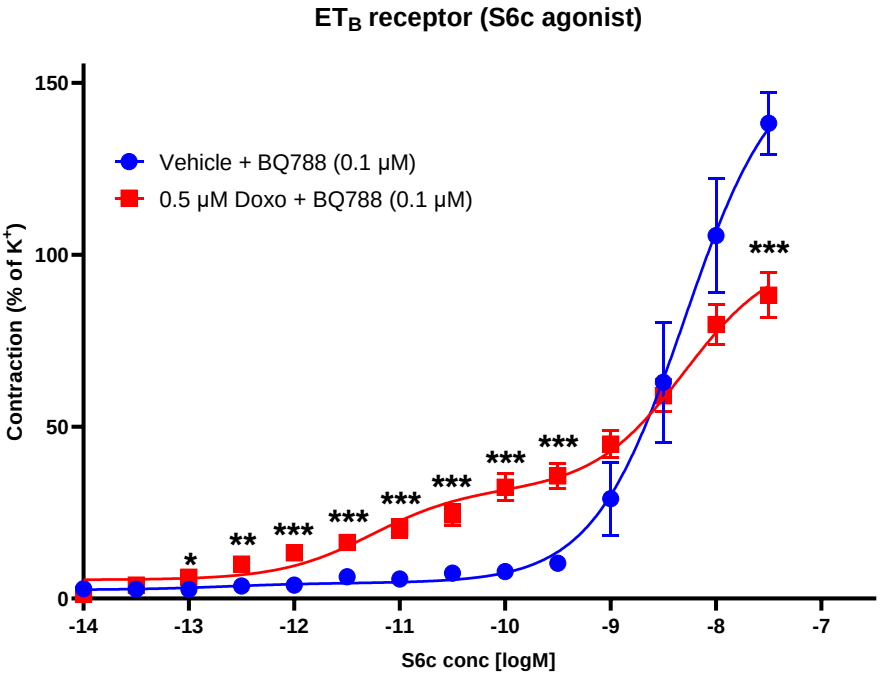

Figure 4-6: Vasocontractile response to the cumulative application of sarafotoxin 6c (ET_B receptor agonist) normalised to 60 mM K^+-induced contraction in rat LAD arteries pre-treated with 30 min of 0.1 µM BQ788 (ET_B receptor antagonist). 0.5 µM Doxorubicin + 0.1 µM BQ788 group (n = 14 - 15; Red) was compared to Vehicle + 0.1 µM BQ788 group (n = 8 - 9; Blue) using Unpaired student T-test. Doxo = doxorubicin, S6c = Sarafotoxin 6c. Values given represent mean ± S.E.M and statistical analysis: * = p value < 0.05. *** = p value < 0.001.

The data were summarised in the Figure 4-7. These results indicate that in the 24 hrs organ-cultured arteries, the observed S6c-induced vasocontraction represents ET_B specific receptor-mediated contraction. However, the pre-treatment of BQ788 seems to have highlighted a reduction of ET_B-mediated contraction at the highest dose of doxorubicin-treated arteries which was not observed without the antagonist.

Table 4-1: C_{max}, "E_{max}" and "pEC_{50}" values of BQ788 or BQ788 naïve LAD arteries incubated with vehicle or doxorubicin (0.5 µM). Values given for all agonist experiments as mean ± S.E.M. The n values represent the total amount of animals used. C_{max} is the percentage of 60 mM K^+ KH maximum contraction at S6c highest dose ($10^{-7.5}$ M), while "E_{max}" and "pEC_{50}" values were generated from fitted curves obtained by GraphPad Prism 9.

Groups	*N*	*S6c C_{max}*	*S6c "E_{max}"*	*"$pEC_{50}1$"*	*"$pEC_{50}2$"*
Vehicle	17	124.4 ± 5.4 %	127.0 ± 5.6 %	12.30 ± 0.6	8.91 ± 0.11
Vehicle + BQ788 (0.1 µM)	8-9	138.2 ± 9.0 %	161.56 ± 11.95	12.41 ± 4.70	8.26 ± 0.11
Doxorubicin (0.5 µM)	19	106.7 ± 9.1%	113.3 ± 7.0 %	12.27 ± 0.31	8.72 ± 0.20
Doxorubicin (0.5 µM) + BQ788 (0.1 µM)	14-15	88.3 ± 6.6 %	94.54 ± 4.42	11.55 ± 0.24	8.50 ± 0.11

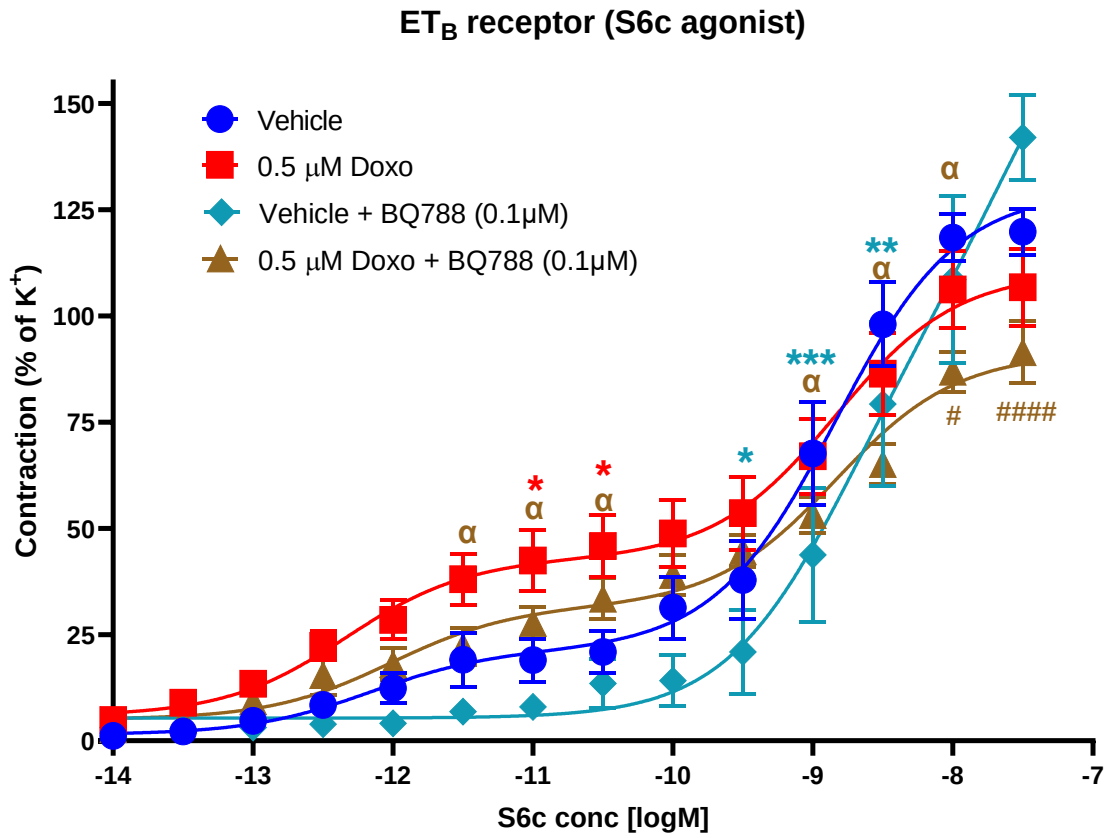

*: compared to Vehicle
α: compared to Doxorubicin
#:compared to Vehicle + BQ788

Figure 4-7: Vasocontractile response to the cumulative application of endothelin-1 (ET-1) (ET_A and ET_B receptor agonist) normalised to 60 mM K^+ KH-induced contraction in rat LAD arteries alone or pre-treated with 30 min of 0.1 µM BQ788 (ET_B receptor antagonist) and 10 µM BQ123 (ET_A receptor antagonist). Doxorubicin (n = 19; Red) and vehicle + 10 µM BQ123 + 0.1 µM BQ788 (n = 9 – 10; Green) groups were compared to Vehicle group (n = 18; Blue). Doxorubicin + 10 µM BQ123 + 0.1µM BQ788 (n = 13 - 17; Brown) was compared to doxorubicin group (n = 19; Red). Doxorubicin + 10 µM BQ123 + 0.1µM BQ788 (n = 13 - 17; Brown) was compared to vehicle + 10 µM BQ123 + 0.1 µM BQ788 (n = 9 – 10; Green). Doxo = Doxorubicin, ET-1 = Endothelin-1, K^+ = 60mM K^+ KH. Values given represent mean ± S.E.M and statistical analysis was performed with Two-way ANOVA + Bonferroni: ** = p value < 0.01. **** = p value < 0.0001. α = p value < 0.05. αααα = p value < 0.0001. # = p value < 0.05. #### = p value < 0.0001.

4.3.2. Doxorubicin does not alter the Endothelin-1 (endothelin A and B receptor agonist) mediated vasocontraction

Vasocontractile responses to endothelin-1 (ET-1) (ET_AR and ET_BR agonist)

The endothelin ET_A and ET_B receptors agonist, ET-1, was used to investigate the effect of doxorubicin on the ET_A and ET_B receptor-mediated contraction. The ET-1 dose-response curve was performed after the ET_B receptors desensitisation of LAD arteries with sarafotoxin 6c, which means some of the ET_B-mediated contraction might have been abolished and the following ET-1 mediated dose-response curve will mostly summarise the ET_A-mediated contraction (Skovsted *et al.*, 2015). The ET-1-induced contraction values are given as percentage of the maximal contractile response induced by the application of 60 mM K^+ KH.

The ET-1 dose-response curve is a monophasic curve, which seems to be in agreement with the ET_B desensitisation due to Sarafotoxin 6C pre-application argument. The ET-1-mediated vasocontraction did not alter in the vessels treated with 0.5 µM doxorubicin compared to the vehicle-treated vessels (Figure 4-7), with an "E_{max}" = 132.1 ± 23.8 % and a "pEC_{50}" = $10^{-8.35}$ M for the 0.5 µM doxorubicin incubated vessels and an "E_{max}" = 176.5 ± 5.4 % and a "pEC_{50}" = $10^{-8.22}$ M for vehicle incubated vessels, as shown in table 4-2.

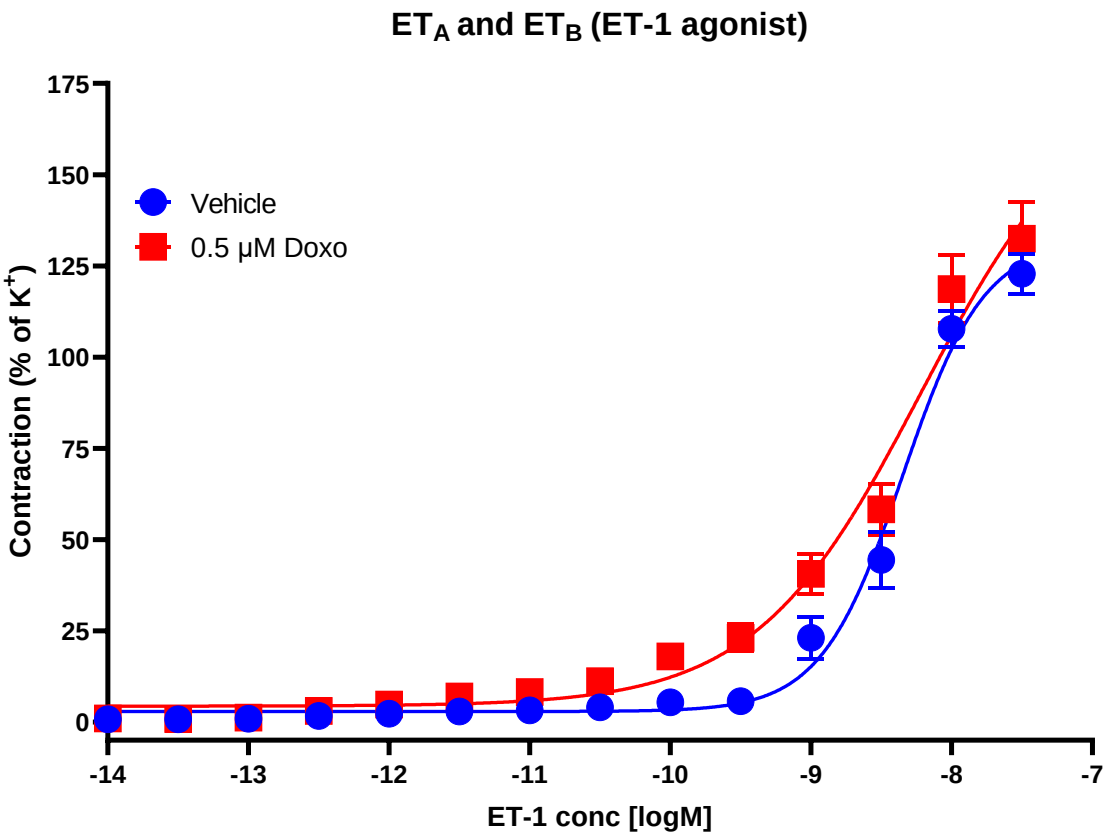

Figure 4-8: Vasocontractile response to the cumulative application of endothelin-1 (ET-1) (ET$_A$ and ET$_B$ receptor agonist) normalised to 60 mM K$^+$ KH-induced contraction in rat LAD arteries. Doxorubicin group (n = 19; Red) was compared to Vehicle group (n = 18; Blue) using Unpaired student T-test. Doxo = doxorubicin, ET-1 = endothelin-1. Values given represent mean ± S.E.M and statistical analysis: * = p value < 0.05. *** = p value < 0.001.

Vasocontractile responses of ET-1 (ET$_A$R and ET$_B$R agonist) in the presence of BQ123 (ET$_A$R antagonist) and BQ788 (ET$_B$R antagonist)

Pharmacological characterisation of ET-1 receptors ET$_A$- and ET$_B$-induced vasoconstriction in 24 hrs organ-cultured LAD arteries was investigated by the exposure of LAD arteries to ET$_A$ and ET$_B$ receptor specific antagonists. The used of both ET$_A$ and ET$_B$ receptor antagonists was performed in order to inhibit both ET-1 receptors-mediated responses since ET$_B$ desensitisation after sarafotoxin 6C application might not completely abolish the ET$_B$-mediated contraction.

LAD arteries were exposed to a mixture of the selective ET$_A$ receptor antagonist BQ123 (10 µM) and the selective ET$_B$ receptor antagonist BQ788 (0.1 µM) for 30 mins, followed by cumulative application of ET-1.

In 24 hrs organ-cultured arteries from vehicle group the ET-1 mediated contraction was reduced by 16 %, 35 % and 69 %, respectively at 10^{-9} M (7.5 ± 0.8 %, p = 0.013), $10^{-8.5}$ M (9.4 ± 1.1 %, p < 0.0001) and 10^{-8} M (39.5 ± 10.0 %, p < 0.001) of ET-1 application, in the presence of 10 µM BQ123 and 0.1 µM BQ788 mix, compared to vehicle vessels naïve from BQ123 and BQ788 pre-treatment (at 10^{-9} M: 23.1 ± 5.8 %, $10^{-8.5}$ M: 44.4 ± 7.6 % and 10^{-8} M: 107.8 ± 5.1 %) (Figure 4-8 (A)). The BQ123 and BQ788 pre-treatment did not alter the ET-mediated contraction of vehicle-treated vessels ("E_{max}" = 104.5 ± 29.1 %) compared to naïve vehicle-treated vessels ("E_{max}" = 132.1 ± 5.4 %). The pre-treatment with BQ123 and BQ788 of vehicle-treated LAD arteries results in a right-shift of the ET-1 monophasic curve compared to BQ123 and BQ788 naïve vessels with a significant decrease of "pEC_{50}" from $10^{-8.35}$ M in BQ123 and BQ788 naïve LAD arteries to $10^{-7.85}$ M (p = 0.0012) in BQ123 and BQ788 pre-treated LAD arteries (Table 4-2).

In 24 hrs organ-cultured arteries treated with 0.5 µM doxorubicin the ET-1-mediated contraction was reduced at the highest doses (10^{-9} M: 20.5 ± 3.7 %, p = 0.002 to $10^{-7.5}$ M: 46.4 ± 11.3 %, p < 0.002) in the vessels pre-treated with 10 µM BQ123 and 0.1 µM BQ788 compared to BQ123 and BQ788 naïve vessels (10^{-9} M: 40.6 ± 5.6 % to $10^{-7.5}$ M: 132.5 ± 10.2 %) (Figure 4-8 (B)). From 10^{-9} M to $10^{-7.5}$ M ET-1 application the ET-1-mediated contraction was significantly reduced with 21 %, 31 %, 88 % and 86 %, respectively at each half-log increase of ET-1 application. The pre-treatment of BQ123 and BQ788 attenuated the "E_{max}" significantly from 176.5 ± 23.8 % in the BQ123 and BQ788 naïve vessels compared to 39.8 ± 10.4 % in the vessels pre-treated with BQ123 and BQ788 (p < 0.0001). The "pEC_{50}" was increased from $10^{-8.22}$ M in the BQ123 and BQ788 naïve 0.5 µM doxorubicin vessels to $10^{-8.91}$ M (p = 0.0078) in the 0.5 µM doxorubicin pre-treated with BQ123 and BQ788 vessels (Table 4-2).

(A)

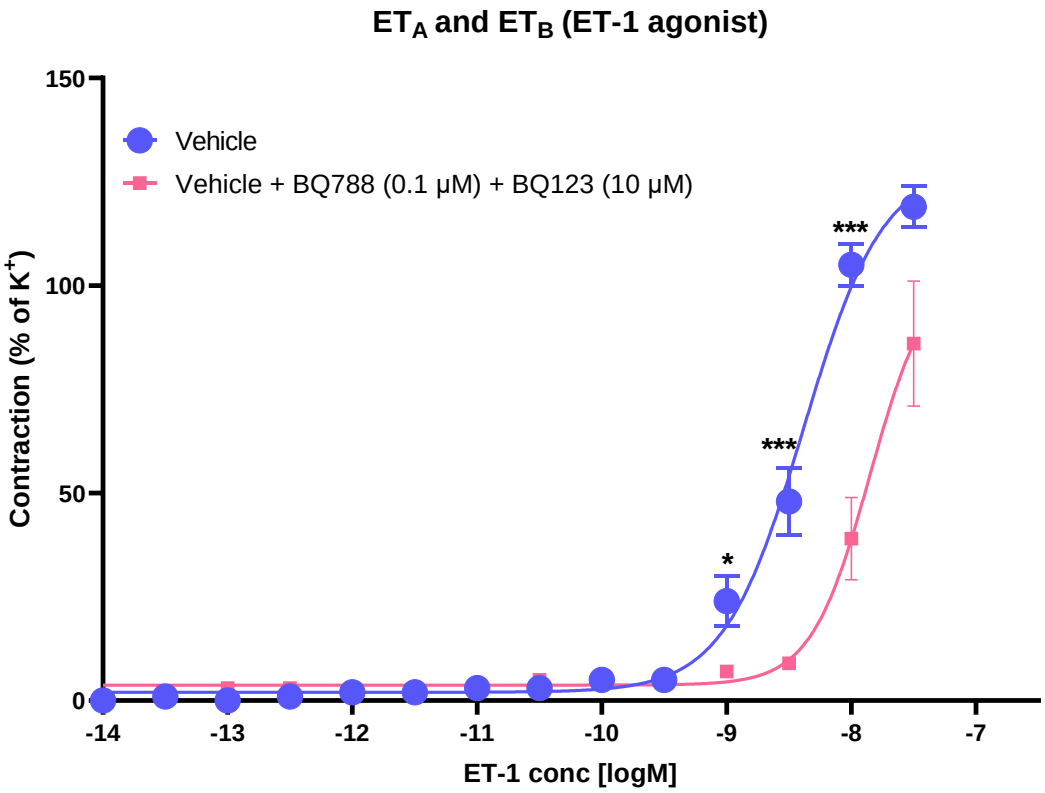
ET$_A$ and ET$_B$ (ET-1 agonist)
Vehicle
Vehicle + BQ788 (0.1 µM) + BQ123 (10 µM)
Contraction (% of K$^+$)
150
100
50
0
-14
-13
-12
-11
-10
-9
-8
-7
ET-1 conc [logM]
*
***
***

(B)

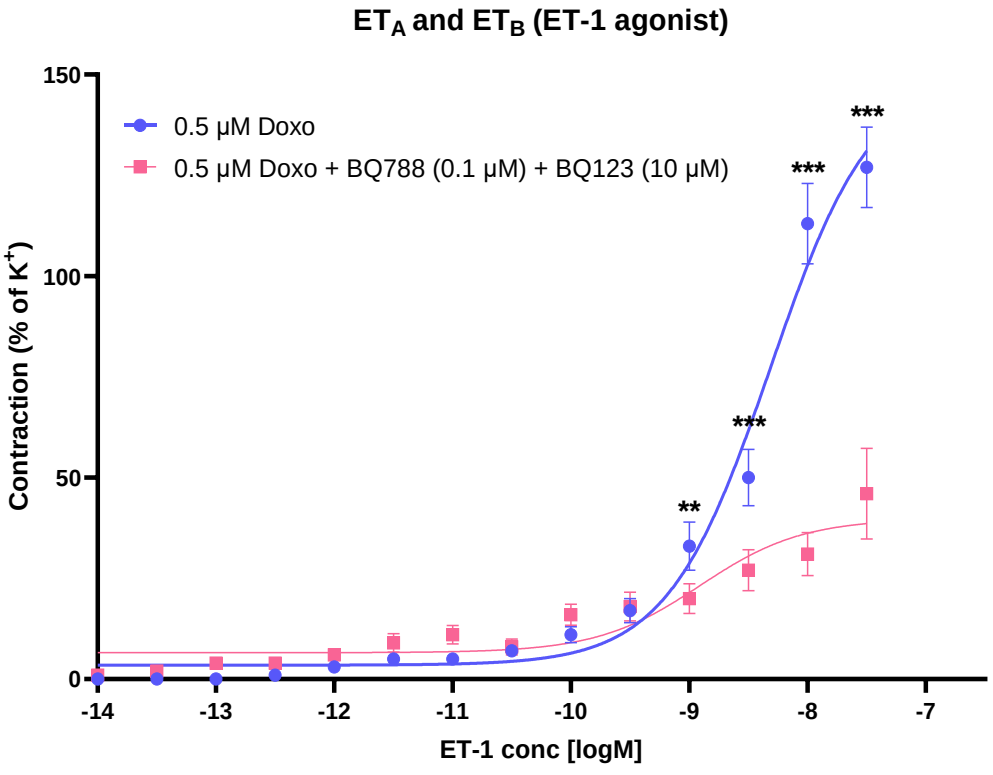
ET$_A$ and ET$_B$ (ET-1 agonist)
0.5 µM Doxo
0.5 µM Doxo + BQ788 (0.1 µM) + BQ123 (10 µM)
Contraction (% of K$^+$)
150
100
50
0
-14
-13
-12
-11
-10
-9
-8
-7
ET-1 conc [logM]
**
***
***
***

Figure 4-9: Vasocontractile response to the cumulative application of endothelin-1 (ET_A and ET_B receptor agonist) normalised to 60 mM K^+ KH-induced contraction in rat LAD arteries pre-treated with 30 mins of 0.1 µM BQ788 (ET_B receptor antagonist) and 10 µM BQ123 (ET_A receptor antagonist). (A) Contractile response to the cumulative application of ET-1 to incubated LAD artery from vehicle groups. Vehicle group (n = 18; Blue) and vehicle + 10 µM BQ123 + 0.1 µM BQ788 (n = 9 - 10; Pink). (B) Contractile response to the cumulative application of ET-1 to incubated LAD artery with 0.5 µM doxorubicin. Doxorubicin group (n = 19; Blue) and doxorubicin + 10 µM BQ123 + 0.1µM BQ788 (n = 13 - 17; Pink). Values given represent mean ± S.E.M and the comparison of both groups was statistically analysed using unpaired Student T test: *** = p value < 0.001.

After 24 hrs of organ culture with 0.5 µM doxorubicin the ET-1-mediated vasocontraction after 10 µM BQ123 + 0.1 µM BQ788 pre-treatment was increased in the ET-1 range of 10^{-10} M (16.0 ± 2.7 %, p < 0.001) to $10^{-8.5}$ M (27.0 ± 5.1 %, p = 0.001), when compared to vehicle vessels after 10 µM BQ123 + 0.1 µM BQ788 pre-treatment (10^{-10} M: 5.5 ± 0.6 % and $10^{-8.5}$ M: 9.4 ± 1.1 %) (Figure 4-9). The significant increase of contraction observed in 0.5 µM doxorubicin-treated arteries was 11 - 18 % significantly increased in the ET-1 dose range of 10^{-10} M to $10^{-8.5}$ M. However, at the highest ET-1 dose of $10^{-7.5}$ M, the vasocontraction seems to be attenuated by 40 % (Vehicle vessels: 85.9 ± 15.1 % and 0.5 µM doxorubicin-treated vessels: 46.4 ± 11.3 %), but this reduction was not significant due to the high variability observed. The 0.5 µM doxorubicin treatment attenuated the "E_{max}" significantly from 104.5 ± 29.1 % in the BQ123 and BQ788 pre-treated vehicle vessels compared to 39.8 ± 3.8 % in the 0.5 µM doxorubicin vessels pre-treated with BQ123 and BQ788 (p = 0.005). The "pEC_{50}" was increased from $10^{-7.85}$ M in the BQ123 and BQ788 pre-treated vehicle vessels to $10^{-8.91}$ M (p = 0.0013) in the 0.5 µM doxorubicin pre-treated with BQ123 and BQ788 doxorubicin vessels (Table 4-2).

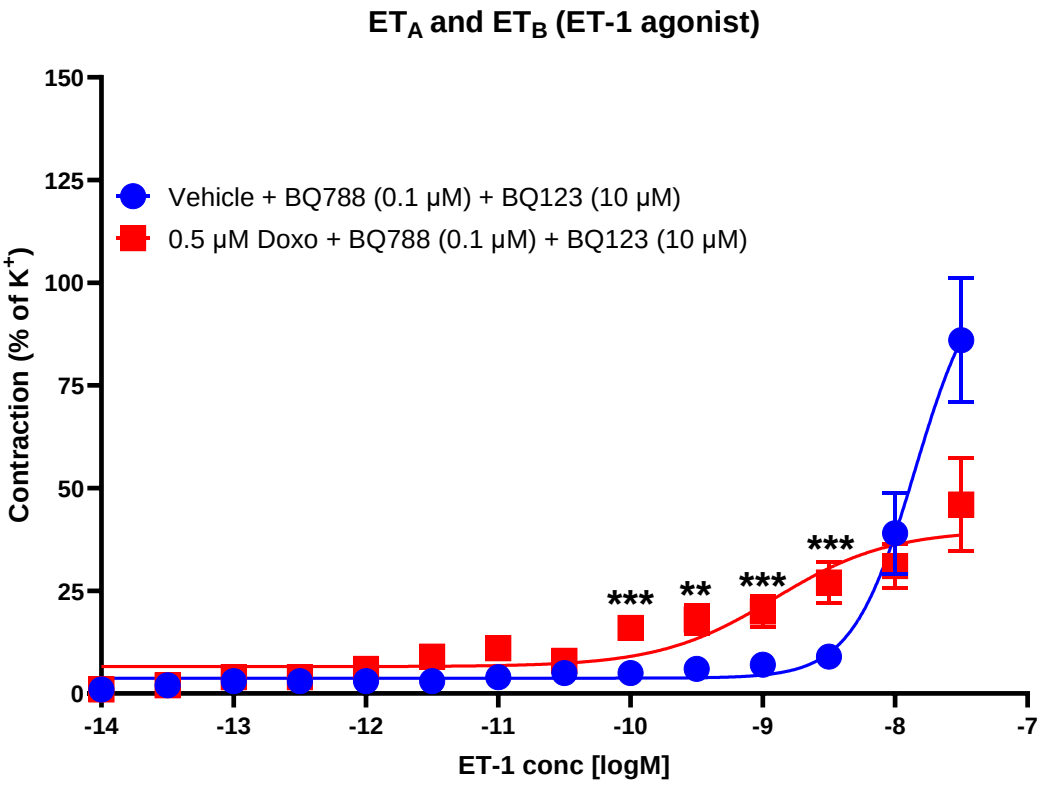

Figure 4-10: Vasocontractile response to the cumulative application of endothelin-1 (ET_A and ET_B receptor agonist) normalised to 60 mM K^+ KH-induced contraction in rat LAD arteries pre-treated with 30 mins of 0.1 µM BQ788 (ET_B receptor antagonist) and 10 µM BQ123 (ET_A receptor antagonist). Doxorubicin + 10 µM BQ123 + 0.1 µM BQ788 group (n = 13 - 17; Red) was compared to Vehicle + 10 µM BQ123 + 0.1 µM BQ788 group (n = 9 - 10; Blue) using Unpaired student T-test. Doxo = doxorubicin, ET-1 = endothelin-1. Values given represent mean ± S.E.M and statistical analysis: * = p value < 0.05. ** = p value < 0.01. *** = p value < 0.001.

Table 4-2: C_{max}, "E_{max}" and "pEC_{50}" values of BQ123 + BQ788 or BQ123 + BQ788 naive LAD arteries incubated with vehicle or doxorubicin (0.5 µM). Values given as mean ± S.E.M. The n values represent the total amount of animals used. C_{max} is the percentage of 60 mM K^+ maximum contraction at S6c highest dose ($10^{-7.5}$ M), while "E_{max}" and "pEC_{50}" values were generated from fitted curves obtained by GraphPad Prism 9.

Groups	*N*	*C_{max}*	*ET-1 "E_{max}"*	*"pEC_{50}"*
Vehicle	18	122.85 ± 5.41 %	132.06 ± 5.43	8.35 ± 0.04
Vehicle + BQ123 (10 µM) + BQ788 (0.1 µM)	9-10	85.91 ± 15.10 %	104.5 ± 29.1 %	7.85 ± 0.19
Doxorubicin (0.5 µM)	19	176.54 ± 23.81	152.8 ± 14.6 %	8.22 ± 0.20
Doxorubicin (0.5 µM) + BQ123 (10 µM) + BQ788 (0.1 µM)	13-17	31.24 ± 5.34 %	39.8 ± 3.6 %	8.91 ± 0.19

The data were summarised in the Figure 4-11. These results indicate that in the 24-hr organ-cultured LAD arteries, the observed ET-1-induced contraction represents ET-receptor-mediated contraction. However, to determine which endothelin receptor subtype is specifically involved in the contraction, the ET-1 dose-response curve needs to be performed with each antagonist separately. This will be explored in the following subsections.

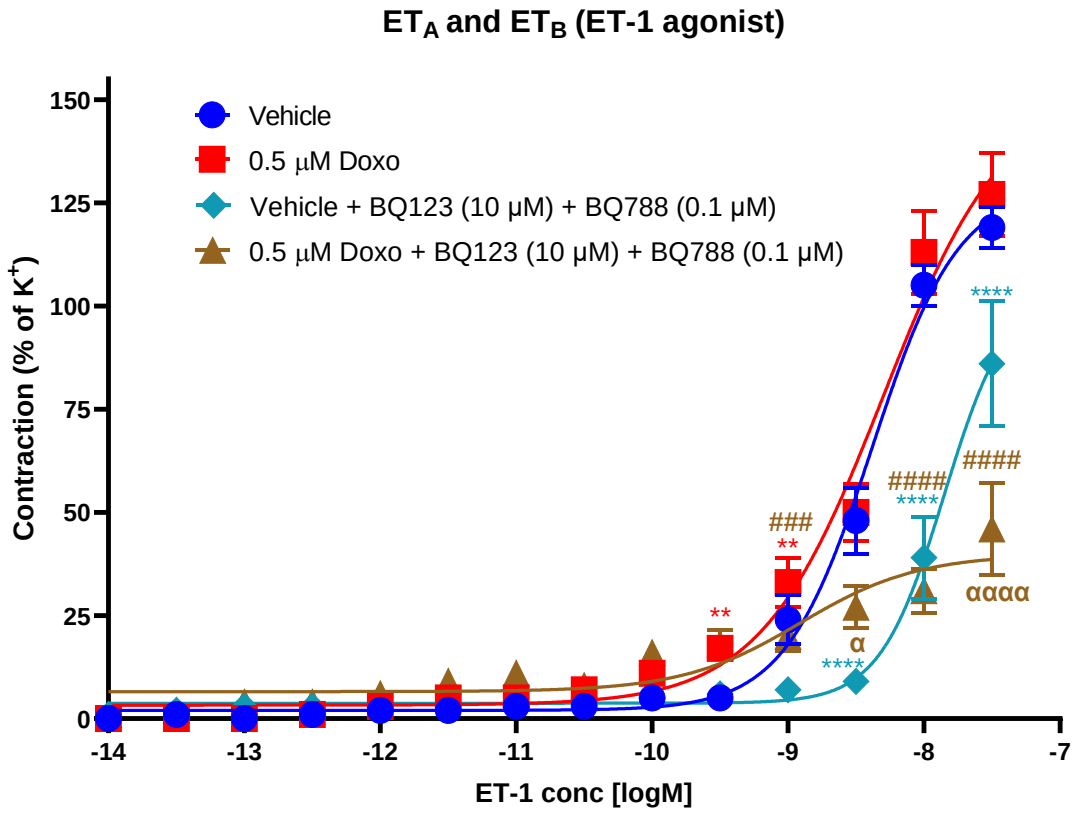

*: compared to Vehicle
α: compared to Vehicle + BQ788
#:compared to Doxorubicin

Figure 4-11: Vasocontractile response to the cumulative application of endothelin-1 (ET-1) (ET_A and ET_B receptor agonist) normalised to 60 mM K^+ KH-induced contraction in rat LAD arteries alone or pre-treated with 30 min of 0.1 µM BQ788 (ET_B receptor antagonist) and 10 µM BQ123 (ET_A receptor antagonist). Doxorubicin (n = 19; Red) and vehicle + 10 µM BQ123 + 0.1 µM BQ788 (n = 9 – 10; Green) groups were compared to Vehicle group (n = 18; Blue). Doxorubicin + 10 µM BQ123 + 0.1µM BQ788 (n = 13 - 17; Brown) was compared to doxorubicin group (n = 19; Red). Doxorubicin + 10 µM BQ123 + 0.1µM BQ788 (n = 13 - 17; Brown) was compared to vehicle + 10 µM BQ123 + 0.1 µM BQ788 (n = 9 – 10; Green). Doxo = Doxorubicin, ET-1 = Endothelin-1, K^+ = 60mM K^+ KH. Values given represent mean ± S.E.M and statistical analysis was performed with Two-way ANOVA + Bonferroni: ** = p value < 0.01. **** = p

value < 0.0001. α = p value < 0.05. αααα = p value < 0.0001. # = p value < 0.05. #### = p value < 0.0001.

Vasocontractile responses of ET-1 (ET_AR and ET_BR agonist) in the presence of BQ123 (ET_AR antagonist)

To explore which ET-1 sub-receptor type was responsible for the ET-1 mediated vasocontraction the ET_A receptors specific antagonist was applied prior to ET-1 dose-response curve of LAD arteries treated with doxorubicin and vehicle during 24 hrs exposure. LAD arteries were exposed to the ET_A receptor selective antagonist BQ123 (10 µM) for 30 mins, followed by cumulative application of ET-1.

The addition of BQ123 reduced the ET-1 dose-response curve, which may be attributed to the inhibition of ET_A receptor-mediated vasocontraction.

In the 24 hrs organ-cultured arteries from the vehicle group, the ET-1-induced contraction was significantly reduced at ET-1 doses of 10^{-9} M (21 % decrease) (2.0 ± 0.7 %, p = 0.002), $10^{-8.5}$ M (35 % decrease) (9.1 ± 3.1 %, p < 0.001), $10^{-7.5}$ M (26 % decrease) (97.4 ± 6.0 %, p = 0.018) in the BQ123 pre-treated vessels compared to BQ123 naïve vessels (10^{-9} M: 23.0 ± 5.8 %, $10^{-8.5}$ M: 44.4 ± 7.6 % and $10^{-7.5}$ M: 122.9 ± 5.4 %) (Figure 4-10 (A)). Furthermore, BQ123 pre-treatment reduced the "E_{max}" value from 132.06 ± 5.43 % in BQ123 naïve vehicle vessels to 97.0 ± 2.3 % (p = 0.0002) in BQ123 pre-treated vehicle vessels, while the "pEC_{50}" values remained unchanged (BQ123 naïve vehicle vessels: "pEC_{50}" of $10^{-8.35}$ M, BQ123 pre-treated vehicle vessels: "pEC_{50}" of $10^{-8.33}$ M) (Table 4-3).

In 24 hrs organ-cultured arteries from the 0.5 µM doxorubicin group pre-treated with BQ123, the ET-1-induced contraction was reduced (14 % decrease) at 10^{-10} M (3.5 ± 1.1 %, p = 0.001) ET-1 doses, and highly reduced (25 - 80 % decrease) at the highest ET-1 doses 10^{-9} M (15.6 ± 5.5 %, p = 0.024) to $10^{-7.5}$ M (52.6 ± 13.6 %, p < 0.001) compared to BQ123 naïve vessels (10^{-10} M: 11.2 ± 2.1 % and 10^{-9} M: 40.6 ± 5.6 % to $10^{-7.5}$ M: 132.5 ± 10.2 %) (Figure 4-10 (B)). Additionally, the pre-treatment with BQ123 reduced the "E_{max}" from 176.5 ± 23.8 % (p < 0.0001) in BQ123 naïve vessels to 61.8 ± 7.5 % in BQ123 pre-treated vessels. The "pEC_{50}" remained unaltered for the 0.5 µM doxorubicin group naïve of BQ123 pre-treatment ("pEC_{50}" = $10^{-8.22}$ M) compared to the BQ123 pre-treated vessels ("pEC_{50}" = $10^{-8.38}$ M) (Table 4-3).

Pre-treatment with BQ123 of vehicle or 0.5 µM doxorubicin treated vessels attenuates the ET-1 dose-response curve, which may be attributed to inhibition of ET_A receptor-mediated vasocontraction, and thus ET_A receptors may be essential to ET-1-induced vasocontraction of vehicle or 0.5 µM doxorubicin treated LAD arteries.

(A)

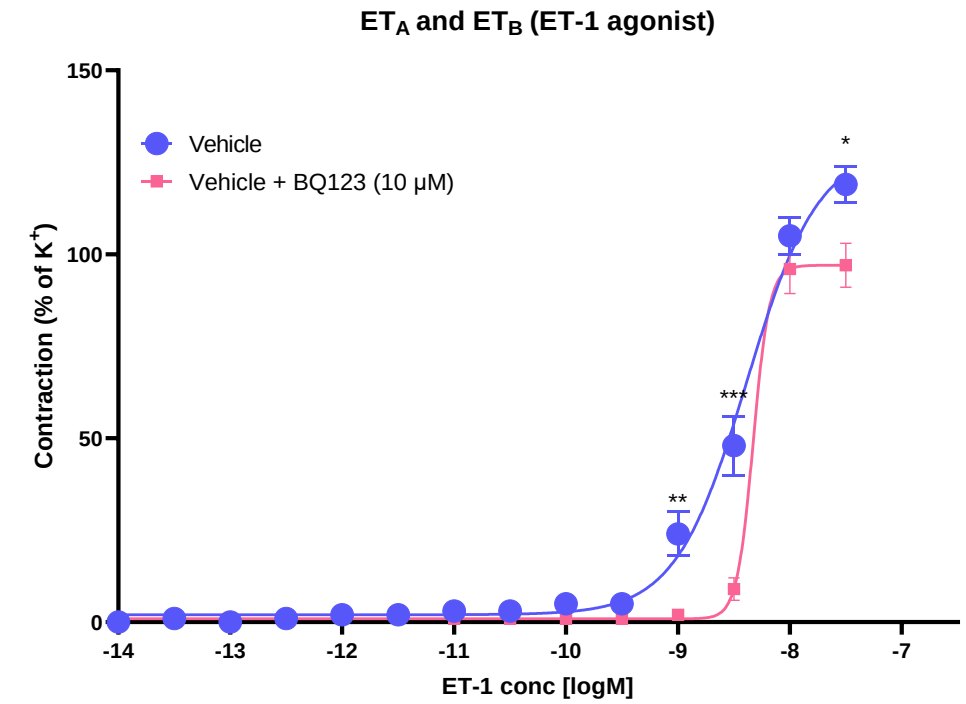

(B)

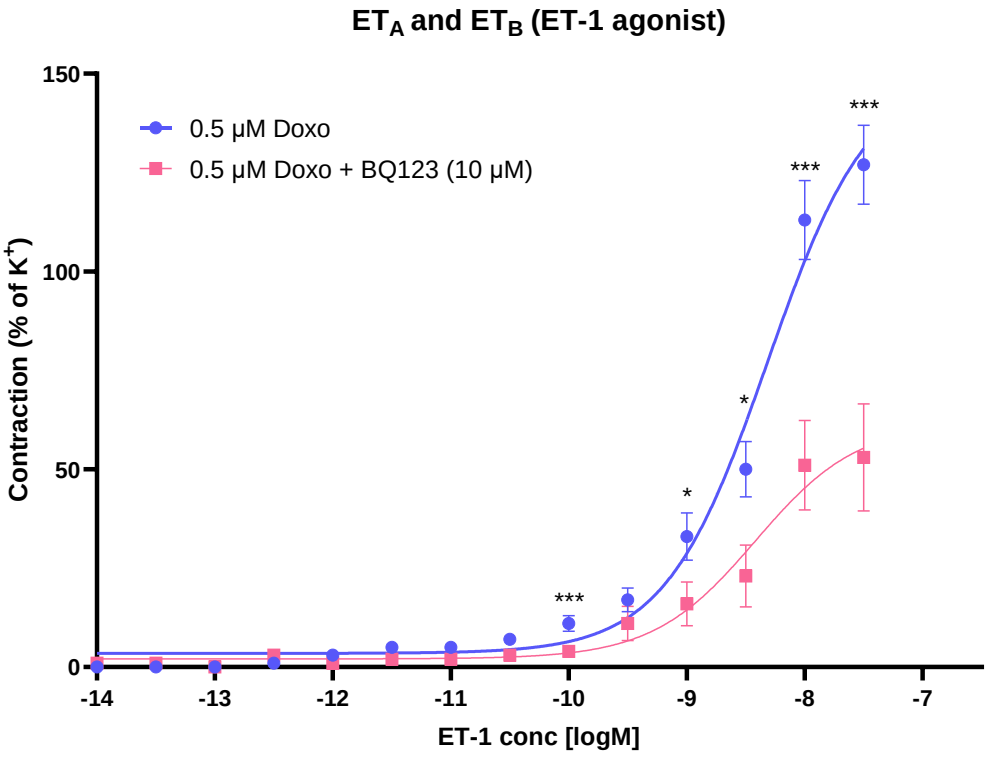

Figure 4-12: Vasocontractile response to the cumulative application of endothelin-1 (ET_A and ET_B receptor agonist) normalised to 60 mM K^+ KH-induced contraction in rat LAD arteries pre-treated with 30 min of 10 µM BQ123 (ET_A receptor antagonist). (A) Contractile response to the cumulative application of ET-1 to incubated LAD artery from vehicle groups. Vehicle group (n = 18; Blue) and

vehicle + 10 µM BQ123 (n = 6 - 7; Pink). (B) Contractile response to the cumulative application of ET-1 to incubated LAD artery with 0.5 µM doxorubicin. Doxorubicin group (n = 19; Blue) and doxorubicin + 10 µM BQ123 (n = 5 - 6; Pink). Values given represent mean ± S.E.M and the comparison of both groups was statistically analysed using unpaired Student T test: * = p value < 0.05. ** = p value < 0. 01. *** = p value < 0.001.

The 24 hrs of organ culture with 0.5 µM doxorubicin resulted in reduced ET_B-mediated vasocontraction at the highest ET-1 doses 10^{-8} M (51.1 ± 11.3 %, p = 0.014) to $10^{-7.5}$ M (52.6 ± 13.6 %, p = 0.028) in 0.5 µM doxorubicin vessels pre-treated with BQ123 compared vehicle vessels pre-treated with BQ123 at ET-1 doses 10^{-8} M (96.3 ± 6.7 %) to $10^{-7.5}$ M (97.4 ± 6.0 %) (Figure 4-11). The significant decrease of ET_B-mediated vasocontraction after pre-treatment with BQ123 was observed in 0.5 µM doxorubicin-treated arteries versus vehicle arteries at 10^{-8} M ET-1 dose (45 % reduction) and $10^{-7.5}$ M ET-1 dose (44 % reduction). 0.5 µM doxorubicin treatment reduced the "E_{max}" value from 97.0 ± 2.3 % in BQ123 pre-treated vehicle vessels to 61.8 ± 7.5 % (p = 0.0319) in BQ123 pre-treated 0.5 µM doxorubicin vessels, while the "pEC_{50}" values remained unchanged (BQ123 pre-treated vehicle vessels: "pEC_{50}" of $10^{-8.33}$ M, BQ123 pre-treated 0.5 µM doxorubicin vessels: "pEC_{50}" of $10^{-8.38}$ M) (Table 4-3).

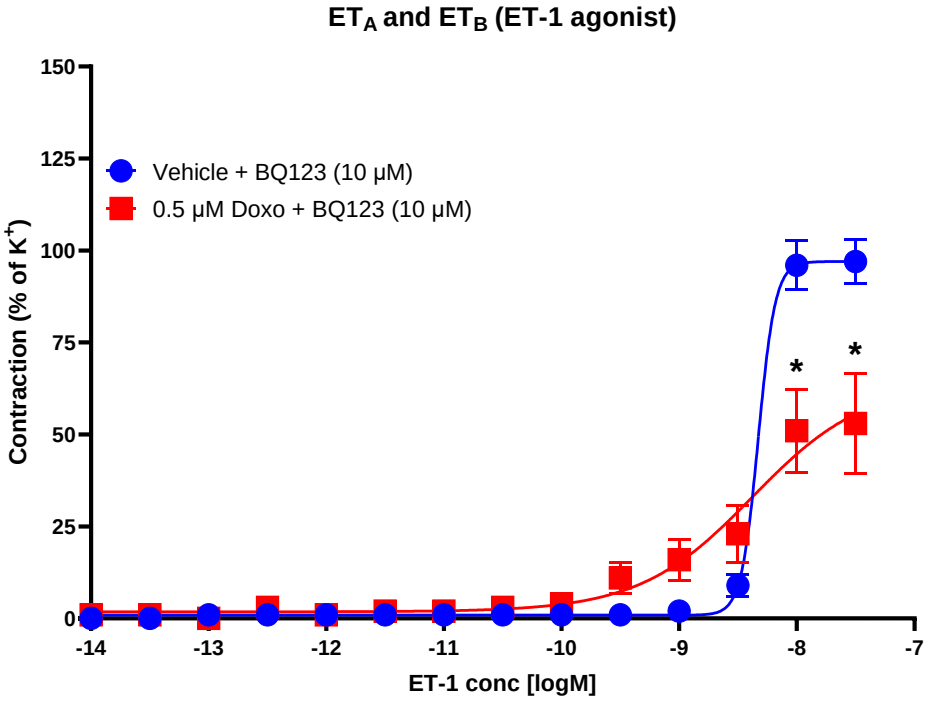

Figure 4-13: Vasocontractile response to the cumulative application of endothelin-1 (ET_A and ET_B receptor agonist) normalised to 60 mM K^+ KH-induced contraction in rat LAD arteries pre-treated with 30 mins of 10 µM BQ123 (ET_A receptor antagonist). Doxorubicin + 10 µM BQ123 group (n = 5 - 6; Red) was compared to Vehicle + 10 µM BQ123 group (n = 6 - 7; Blue), using unpaired Student T-test: * = p value < 0.05. Values given represent mean ± S.E.M.

Table 4-3: C_{max}, "Emax" and "pEC50" values of BQ123 or BQ123 naive LAD arteries incubated with vehicle or doxorubicin (0.5 µM). Values given for all agonist experiments as mean ± S.E.M. The n values represent the total amount of animals used. C_{max} is the percentage of 60 mM K^+ maximum contraction at S6c highest dose ($10^{-7.5}$ M), while "E_{max}" and "pEC_{50}" values were generated from fitted curves obtained by Graph-Pad Prism 9.

Groups	*N*	*C_{max}*	*ET-1 "E_{max}"*	*"pEC_{50}"*
Vehicle	18	122.85 ± 5.41 %	132.06 ± 5.43	8.35 ± 0.04
Vehicle + BQ123 (10 µM)	6-7	97.44 ± 5.95 %	97.01 ± 2.33 %	8.33 ± 0.08
Doxorubicin (0.5 µM)	19	132.46 ± 10.18 %	176.54 ± 23.81	8.22 ± 0.20
Doxorubicin (0.5 µM) + BQ123 (10 µM)	5-6	52.61 ± 13.55 %	61.78 ± 7.46 %	8.38 ± 0.34

The data were summarised in the Figure 4-14. These results indicate that in the 24-hrs organ-cultured arteries, the inhibition of ET_A receptor-mediated vasocontraction induced a decrease of the ET receptors-vasocontraction at the highest doses of ET-1 in the presence of 0.5 µM doxorubicin compared to vehicle group. The BQ123 pre-treatment reduces the ET-1-induced contraction in 0.5 µM doxorubicin vessels compared to vehicle vessels, while no changes were observed without BQ123 pre-treatment and thus, suggests that the ET-1-induced contraction in 0.5 µM doxorubicin-treated vessels is, mainly, mediated through ET_A receptors activation.

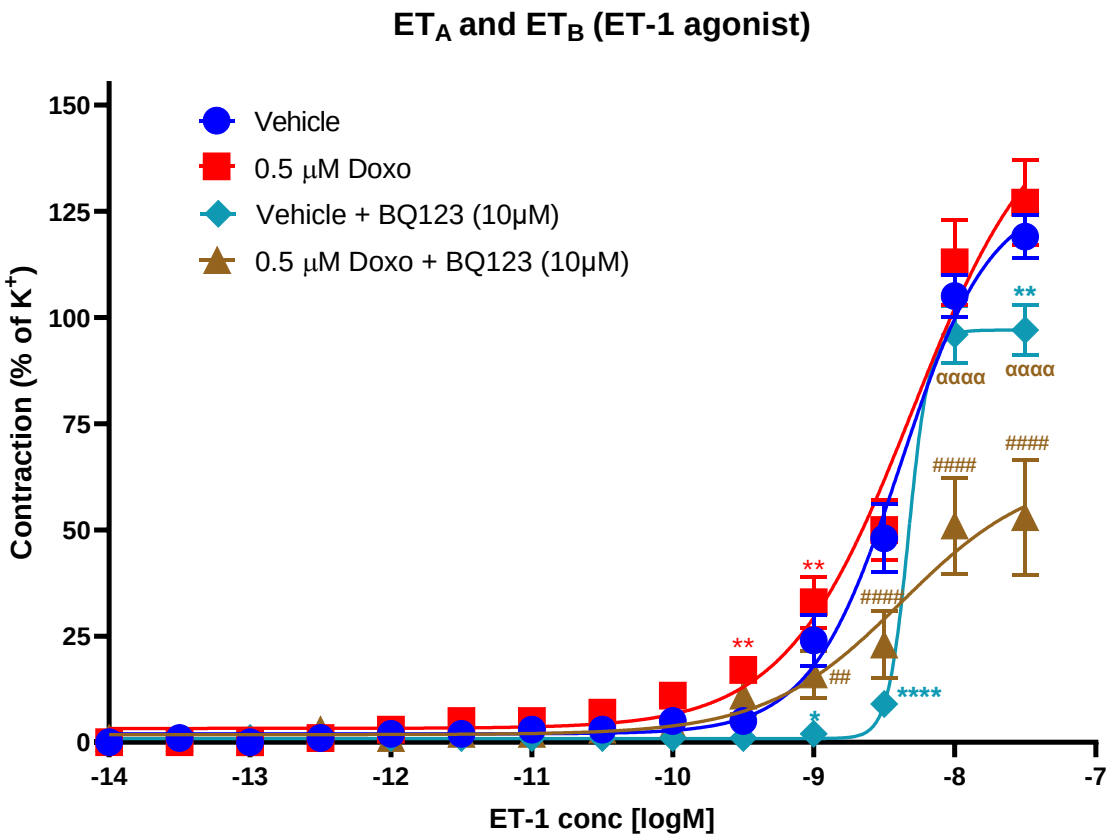

*: compared to Vehicle
α: compared to Vehicle + BQ123
#:compared to Doxorubicin

Figure 4-14: Vasocontractile response to the cumulative application of endothelin-1 (ET-1) (ET_A and ET_B receptor agonist) normalised to 60 mM K^+ KH-induced contraction in rat LAD arteries alone or pre-treated with 30 min of 10 µM BQ123 (ET_A receptor antagonist). Doxorubicin (n = 19; Red) and vehicle + 10 µM BQ123 (n = 6 - 7; Green) groups were compared to Vehicle group (n = 18; Blue). Doxorubicin + 10 µM BQ123 (n = 5 - 6; Brown) was compared to doxorubicin group (n = 19; Red). Doxorubicin + 10 µM BQ123 (n = 5 - 6; Brown) was compared to vehicle + 10 µM BQ123 (n = 6 - 7; Green). Doxo = doxorubicin, ET-1 = Endothelin-1, K^+ = 60mM K^+ KH. Values given represent mean ± S.E.M and statistical analysis was performed with Two-way ANOVA + Bonferroni: * = p value < 0.05. ** = p value < 0.01. **** = p value < 0.0001. αααα = p value < 0.0001. ## = p value < 0.01. #### = p value < 0.0001.

Vasocontractile responses of ET-1 (ET_AR and ET_BR agonist) in the presence of BQ788 (ET_BR antagonist)

To further explore which ET-1 sub-receptor type was responsible for the ET-1 mediated vasocontraction this time the ET_B receptor specific antagonist BQ788 was used. ET_B was desensitised

by application of $10^{-7.5}$ M sarafotoxin 6c and the LAD arteries were exposed to the ET_B receptor specific antagonist BQ788 (0.1 µM) for 30 min, followed by cumulative application of ET-1.

In 24 hrs incubated vehicle vessels, the ET-mediated contraction was reduced by 21 % at the ET-1 concentration of 10^{-9} M (2.5 ± 0.7 %, p = 0.002) in the vessels pre-treated with BQ788 compared to BQ788 naïve vessels (10^{-12} M: 2.3 ± 0.4 %, $10^{-9.5}$ M: 5.7 ± 1.1 % and 10^{-9} M: 23.1 ± 5.8 %), which may be attributed to the inhibition of ET_B-mediated contraction (Figure 4-12 (A)). The pre-treatment with BQ788 on LAD arteries from the vehicle group did not alter "E_{max}" or "pEC_{50}" values (Table 4-4).

In 24 hrs incubated 0.5 µM doxorubicin-treated vessels, pre-treatment with BQ788 reduced the ET-1-induced contraction with 22 % at the dose of 10^{-9} M (18.9 ± 2.9 %, p = 0.002) ET-1 when compared to BQ788 naïve vessels (40.6 ± 5.6 %) (Figure 4-12X (B)). Additionally, the pre-treatment with BQ788 did not alter the "E_{max}" and "pEC_{50}" values in BQ788 pre-treated vessels ("E_{max}" = 152.77 ± 5.60 % and "pEC_{50}" = $10^{-8.27}$ M), compared BQ788 naïve vessels ("E_{max}" = 176.54 ± 23.81 % and "pEC_{50}" = $10^{-8.22}$ M).

These results indicate that in the 24-hrs organ-cultured arteries, the inhibition of ET_B receptor-mediated vasocontraction induced a slight decrease from 10^{-12} M to 10^{-9} M in vehicle-treated vessels and at 10^{-9} M in 0.5 µM doxorubicin-treated vessels, however, the potency and maximal ET-1-induced contraction remain unchanged in vehicle- or 0.5 µM doxorubicin-treated vessels and thus may be attributed to the ET_B receptors desensitisation with S6c application.

(A)

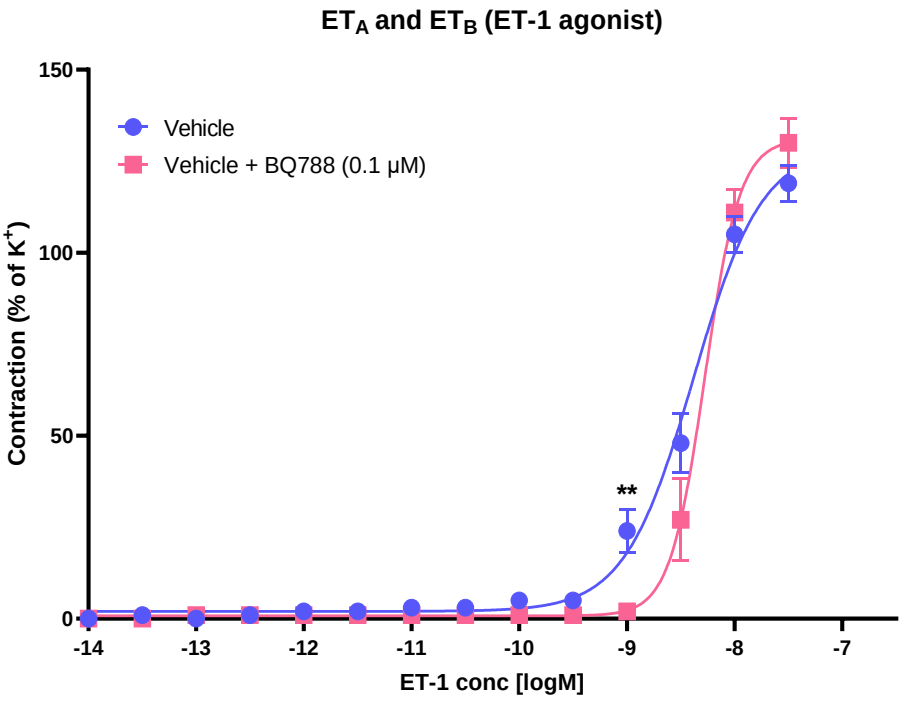

(B)

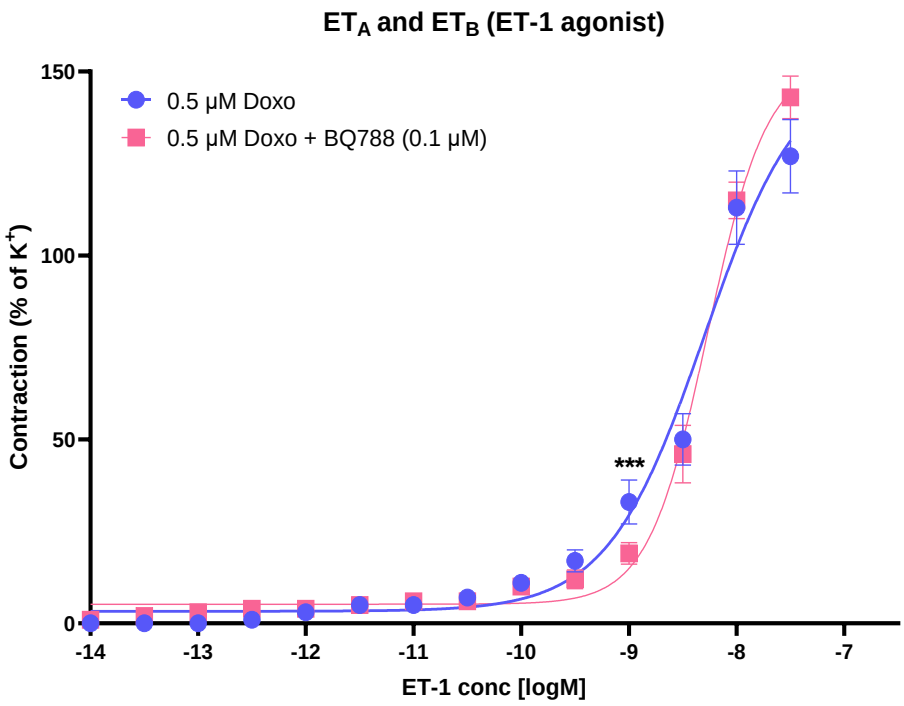

Figure 4-15: Vasocontractile response to the cumulative application of endothelin-1 (ET_A and ET_B receptor agonist) normalised to 60 mM K^+ KH-induced contraction in rat LAD arteries pre-treated with 30 mins of 0.1 µM BQ788 (ET_B receptor antagonist). (A) Contractile response to the cumulative application of ET-1 to LAD artery from vehicle groups. Vehicle group (n = 18; Blue) and vehicle + 0.1 µM BQ788 (n = 9 - 10; Pink). (B) Contractile response to the cumulative application of ET-1 to incubated LAD artery with 0.5 µM doxorubicin. Doxorubicin group (n = 19; Blue) and doxorubicin + 0.1 µM BQ788 (n = 8 - 9; Pink). Values given represent mean ± S.E.M and the comparison of both groups was statistically analysed using unpaired Student T test: * = p value < 0.05. ** = p value < 0. 01. *** = p value < 0.001.

After 24 hrs of incubation with 0.5 µM doxorubicin, the ET-1-induced vasocontraction by ET-1 application ($10^{-9.5}$ M to 10^{-9} M) was increased significantly compared to vehicle incubated vessels after 0.1 µM BQ788 pre-treatment (Figure 4-13). The increase in ET-1-induced vasocontraction observed in 0.5 µM doxorubicin-treated arteries was 11 - 17 % increase at the ET-1 doses $10^{-9.5}$ M (12.1 ± 2.6 %, p = 0.001) to 10^{-9} M (18.9 ± 2.9 %, p < 0.001) when compared to vehicle incubated vessels after BQ788 pre-treatment ($10^{-9.5}$ M: 0.7 ± 0.5 % to 10^{-9} M: 2.5 ± 0.7 %). The 0.5 µM doxorubicin treatment on BQ788 pre-treated vessels increased the "E_{max}" from 131.05 ± 4.28 % (p = 0.002) in BQ788 pre-treated vehicle vessels to 152.77 ± 5.60 % in BQ788 pre-treated 0.5 µM doxorubicin vessels, while "pEC_{50}" remained unchanged (Table 4-4).

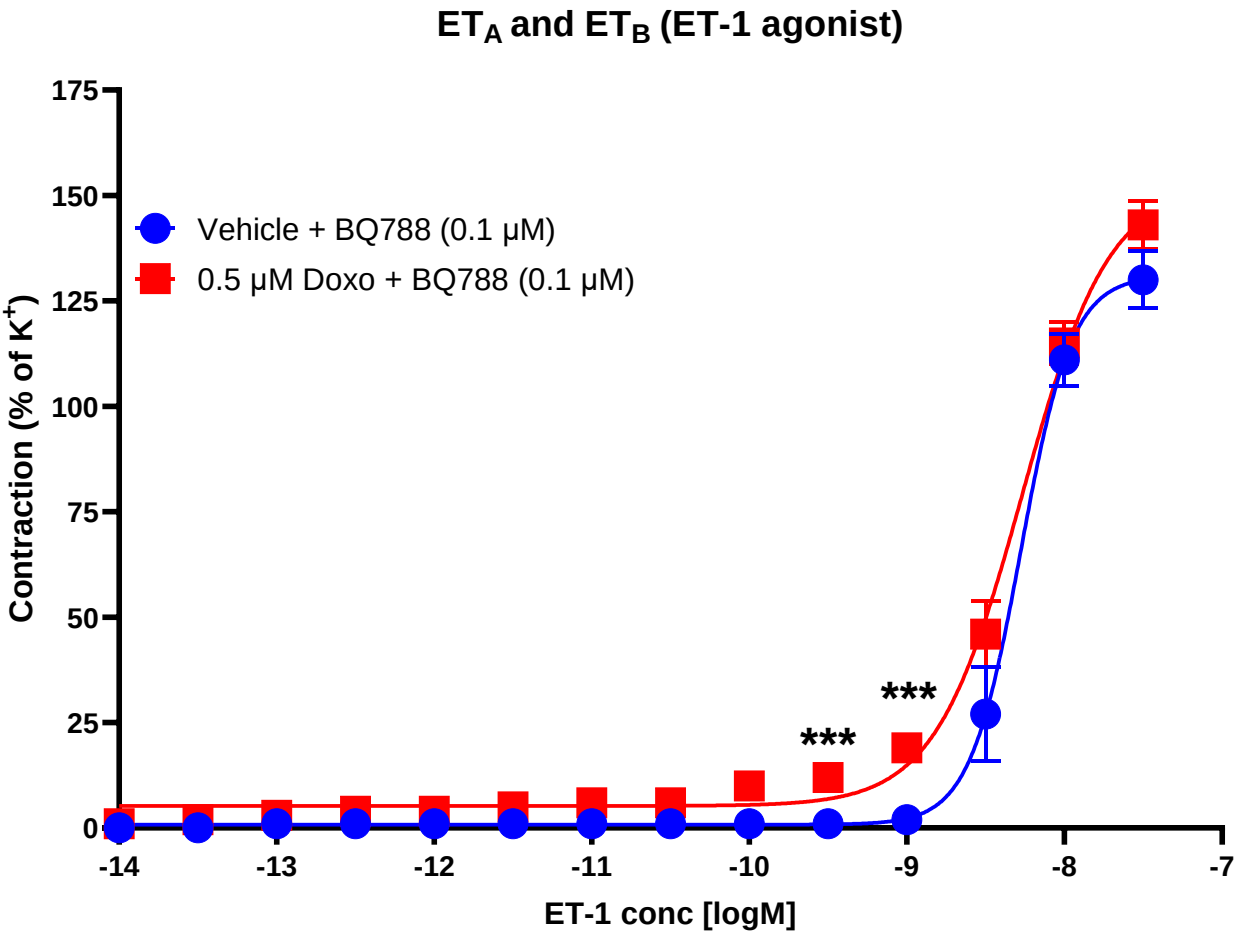

Figure 4-16: Vasocontractile response to the cumulative application of endothelin-1 (ET_A and ET_B receptor agonist) normalised to 60 mM K^+ KH-induced contraction in rat LAD arteries pre-treated with 30 mins of 0.1 µM BQ788 (ET_A receptor antagonist). Doxorubicin + 0.1 µM BQ788 group (n = 8 - 9; Red) was compared to Vehicle + 0.1 µM BQ788 group (n = 9 - 10; Blue) using Unpaired student T-test. Doxo = doxorubicin, ET-1 = endothelin-1. Values given represent mean ± S.E.M and statistical analysis: * = p value < 0.05. ** = p value < 0.01. *** = p value < 0.001.

The data were summarised in the Figure 4-17. These results indicate that in the 24-hrs incubated arteries, the inhibition of ET_B receptor-mediated vasocontraction through BQ788 induced a slight increase of the contraction at the low doses of ET-1 and a more significant increase of the maximal ET-1-induced contraction ("E_{max}" values) in presence of doxorubicin compared to vehicle group. This could indicate that after doxorubicin treatment, the ET_B receptors might reduce the ET-1-induced contraction and thus, ET_B receptors may modulate the ET_A-mediated contraction on doxorubicin-treated vessels. However, the BQ788 naïve doxorubicin vessels "E_{max}" have a high variability compared to BQ788 pre-treated 0.5 µM doxorubicin vessels, which may explain the significant increase observed

only after BQ788 pre-treatment in 0.5 µM doxorubicin vessels compared to BQ788 pre-treated vehicle vessels.

Table 4-4: C_{max}, "E_{max}" and "pEC_{50}" values of BQ788 or BQ788 naive LAD arteries incubated with vehicle or doxorubicin (0.5 µM). Values given for all agonist experiments as mean ± S.E.M. The n values represent the total amount of animals used. C_{max} is the percentage of 60 mM K^+ maximum contraction at S6c highest dose ($10^{-7.5}$ M), while "E_{max}" and "pEC_{50}" values were generated from fitted curves obtained by Graph-Pad Prism 9.

Groups	*N*	*C_{max}*	*ET-1 "E_{max}"*	*"pEC_{50}"*
Vehicle	18	122.85 ± 5.41 %	132.06 ± 5.43	8.35 ± 0.04
Vehicle + BQ788 (0.1 µM)	9-10	111.03 ± 6.24 %	131.05 ± 4.28 %	8.28 ± 0.03
Doxorubicin (0.5 µM)	19	132.46 ± 10.18 %	176.54 ± 23.81	8.22 ± 0.20
Doxorubicin (0.5 µM) + BQ788 (0.1 µM)	8-9	114.97 ± 4.97 %	152.77 ± 5.60 %	8.27 ± 0.04

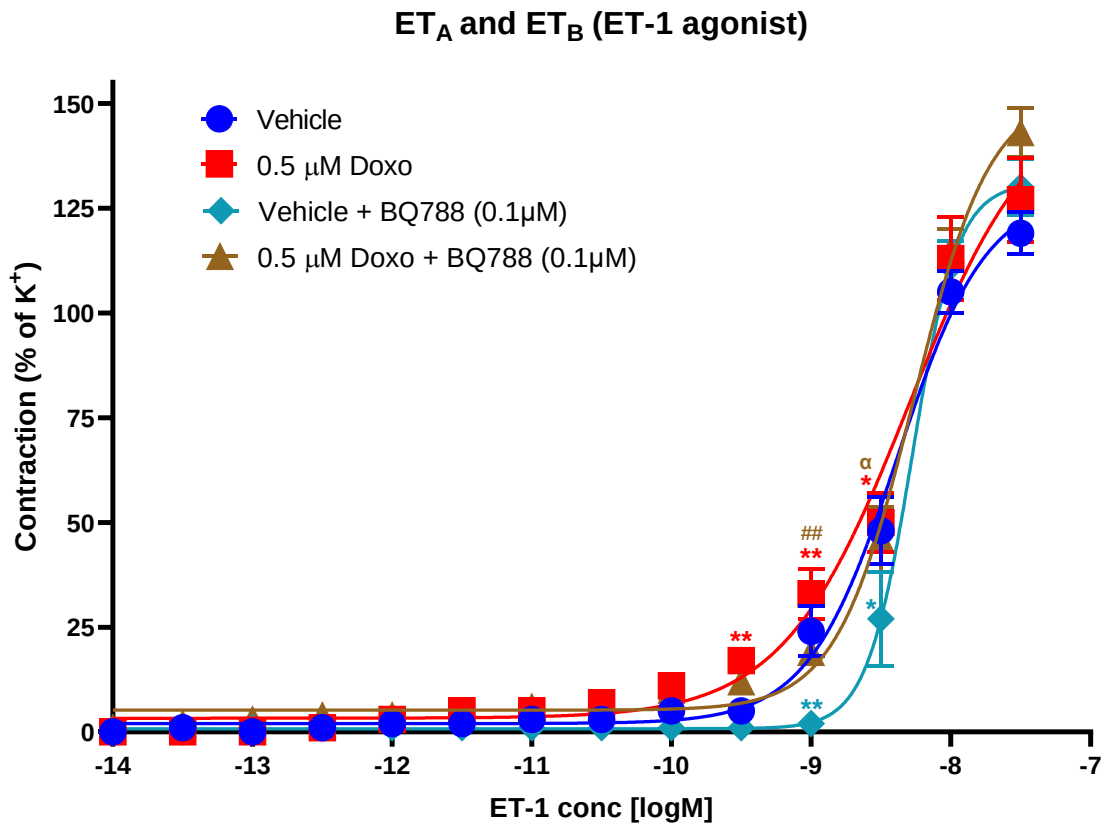

*: compared to Vehicle
α: compared to Vehicle + BQ788
#:compared to Doxorubicin

Figure 4-17: Vasocontractile response to the cumulative application of endothelin-1 (ET-1) (ET_A and ET_B receptor agonist) normalised to 60 mM K^+ KH-induced contraction in rat LAD arteries alone or pre-treated with 30 min of 0.1 µM BQ788 (ET_B receptor antagonist). Doxorubicin (n = 19; Red) and vehicle + 0.1 µM BQ788 (n = 9 - 10; Green) groups were compared to Vehicle group (n = 18; Blue). Doxorubicin + 0.1 µM BQ788 (n = 8 - 9; Brown) was compared to doxorubicin group (n = 19; Red). Doxorubicin + 0.1 µM BQ788 (n = 8 - 9; Brown) was compared to vehicle + 0.1 µM BQ788 (n = 9 - 10; Green). Doxo = doxorubicin, ET-1 = Endothelin-1, K^+ = 60 mM K^+ KH. Values given represent mean ± S.E.M and statistical analysis was performed with Two-way ANOVA + Bonferroni: * = p value < 0.05. ** = p value < 0.01. α = p value < 0.05. ## = p value < 0.01.

In summary, ET_B desensitisation by applying $10^{-7.5}$ M Sarafotoxin 6c highly reduced the ET_B-mediated contraction ("E_{max}" and "pEC_{50}" were not altered), however, it was not completely abolished (the first phase of ET-1 dose-response curve was decreased after BQ788 pre-treatment in vehicle vessels). The first phase of a biphasic ET-1 dose-response curve will be dependent on the ET_B-mediated vasocontraction, followed by the ET_A-mediated vasocontraction during the second phase, which indicates that ET_A receptor has a lower affinity to ET-1 than ET_B receptor. Additionally, the inhibition of ET_B receptors seems to increase the ET-1-mediated contraction at the middle phase of the curve in the presence of doxorubicin, whereas conversely, the inhibition of ET_A receptors leads to the decrease of ET-1-mediated contraction at the last phase of the ET-1 dose-response curve.

4.3.3. Doxorubicin alters the 5-carboxamidotryptamine (serotonin 1B receptor agonist) mediated vasocontraction

Vasocontractile responses to 5-carboxamidotryptamine ($5\text{-}HT_{1B}$ agonist)

The serotonin $5\text{-}HT_{1B}$ receptor specific agonist 5-carboxamidotryptamine (5-CT) was applied to the incubated LAD vessels to investigate the effect of doxorubicin on $5\text{-}HT_{1B}$ receptor-mediated vasocontraction. The dose-response curve obtained by applying 5-CT resulted in a biphasic $5\text{-}HT_{1B}$ receptor-mediated vasocontraction curve for the 0.5 µM doxorubicin-treated vessels. The $5\text{-}HT_{1B}$-induced vasocontraction values are given as percentage of the maximal contractile response, induced by 60 mM K^+ KH.

After 24 hrs of organ culture with 0.5 µM doxorubicin, the $5\text{-}HT_{1B}$-mediated vasocontraction was increased for at the 5-CT concentration range of 10^{-9} M to 10^{-6} M compared to vehicle incubated vessels (Figure 4-14). The increase of $5\text{-}HT_{1B}$-mediated vasocontraction starts slowly (< 7 %) at 10^{-9} M (5.0 ± 1.0 %, p = 0.002) to 10^{-8} M 5-CT (10.0 ± 3.0 %, p < 0.001) and progressively increase (12 - 28 %)

from $10^{-7.5}$ M (15.0 ± 3.0 %, p < 0.001) to 10^{-6} M 5-CT (35.0 ± 6.0 %, p < 0.001) in 0.5 µM doxorubicin-treated vessels when compared to vehicle incubated vessels (at 10^{-9} M: 2.0 ± 0.0 % to 10^{-8} M: 3.0 ± 1.0 % and at $10^{-7.5}$ M: 3.0 ± 1.0 % to 10^{-6} M: 7.0 ± 1.0 %). The 5-CT dose-response curve of both groups did not reach the final plateau at the highest dose due to stock constraints, and therefore final "E_{max}" and "pEC_{50}" values could not be obtained. However, the vasocontraction obtained at the highest dose is mentioned as C_{max} and was observed to be 34.0 ± 8.0 % for the vehicle incubated vessels and 69.0 ± 9.0 % for 0.5 µM doxorubicin-treated vessels, in spite of these quite distinct C_{max} values, statistical significance at $10^{-5.5}$ M 5-CT was not obtained due to high variation (Table 4-5).

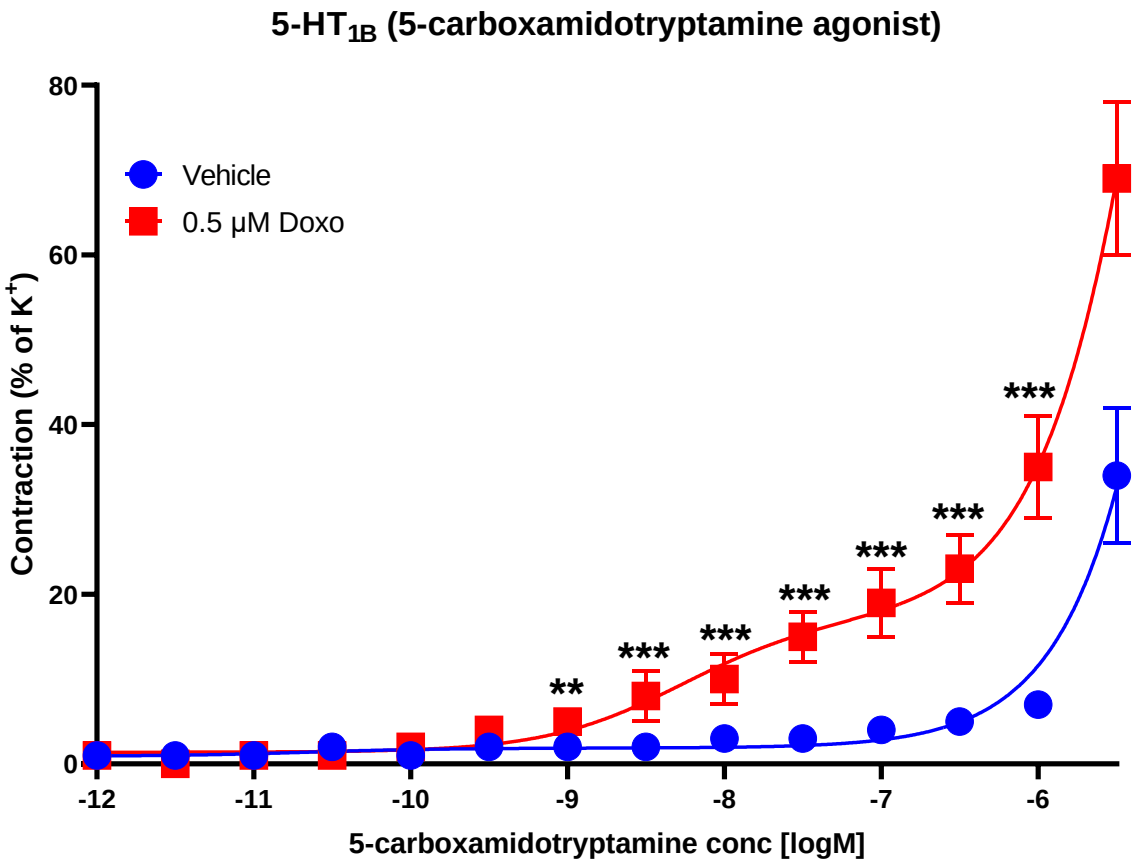

Figure 4-18: Vasocontractile response to the cumulative application of 5-carboxamidotryptamine (5-CT) (5-HT_{1B} receptor agonist) normalised to 60 mM K^+ KH-induced contraction in rat LAD arteries. Doxorubicin group (n = 13; Red) was compared to Vehicle group (n = 16; Blue) using unpaired Student T-test: ** = p value < 0.01. *** = p value < 0.001. Doxo = doxorubicin, 5-CT = 5-Carboxamidotryptamine. Values given represent mean ± S.E.M.

These results showed that the 5-CT dose response obtained after 0.5 µM doxorubicin incubation was biphasic, while the dose-response curve after vehicle incubation seems to be monophasic, but the absence of "E_{max}" does not allow the confirmation of a monophasic curve.

Vasocontractile responses of 5-CT (5-HT_{1B} agonist) in presence of GR55562 (5-HT_{1B} antagonist)

0.5 µM doxorubicin and vehicle incubated LAD arteries were exposed to a 5-HT_{1B} receptor specific antagonist GR55562 (1 µM) for 30 min, followed by cumulative application of 5-CT to establish the 5-HT_{1B} receptor specificity of the 5-CT agonist.

In 24 hrs organ-cultured arteries incubated with vehicle, the 5-HT_{1B}-mediated contraction was significantly reduced by 23 % at $10^{-5.5}$ M 5-CT (C_{max} = 11.0 ± 2.0 %, p = 0.009) after GR55562 pre-treatment, compared to GR55562 naïve vessels (C_{max} = 34.0 ± 8.0 %) (Figure 4-15 (A)).

In the doxorubicin incubated vessels, the 5-HT_{1B}-mediated contraction was also significantly reduced at 5-CT concentration ranging from $10^{-7.5}$ M to 10^{-6} M after GR55562 pre-treatment, compared to GR55562 naïve vessels (Figure 4-15 (B)). The GR55562 mediated decrease (by 8 %, 11 %, 12 % and 17 %) the 5-CT vasocontraction at 5-CT concentrations of $10^{-7.5}$ M (7.0 ± 2.5 %, p = 0.036), 10^{-7} M (8.0 ± 2.9 %, p = 0.040), $10^{-6.5}$ M (11.0 ± 3.4 %, p = 0.037), 10^{-6} M (18.0 ± 5.5 %, p = 0.029), when compared to GR55562 naïve vessels ($10^{-7.5}$ M: 15.0 ± 3.0 %, 10^{-7} M: 19.0 ± 4.0 %, $10^{-6.5}$ M: 23.0 ± 4.0 %, 10^{-6} M: 35.0 ± 6.0 %).

(A)

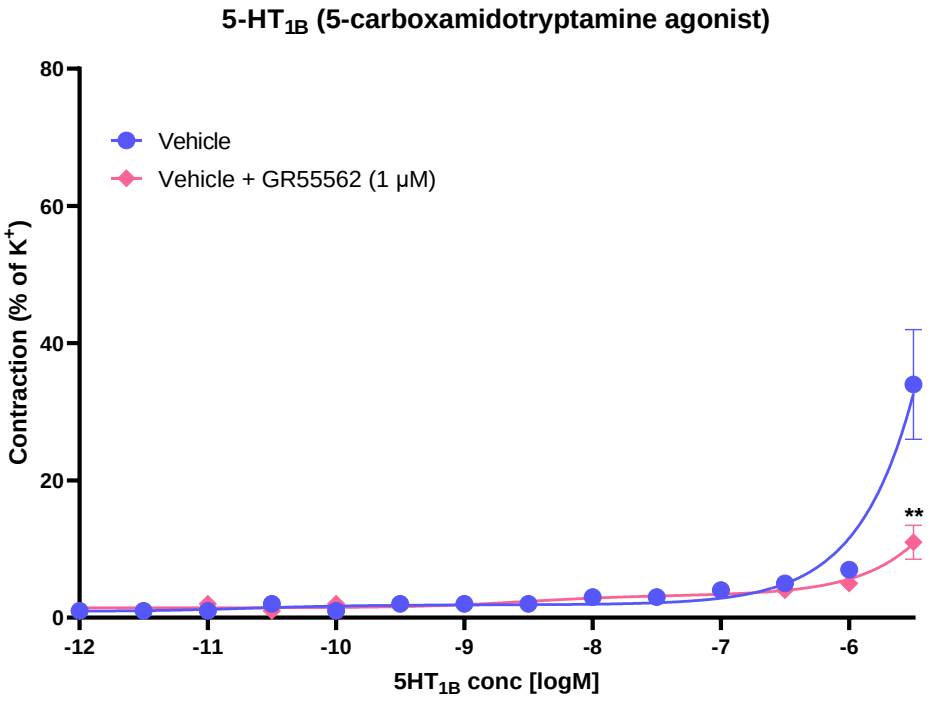

(B)

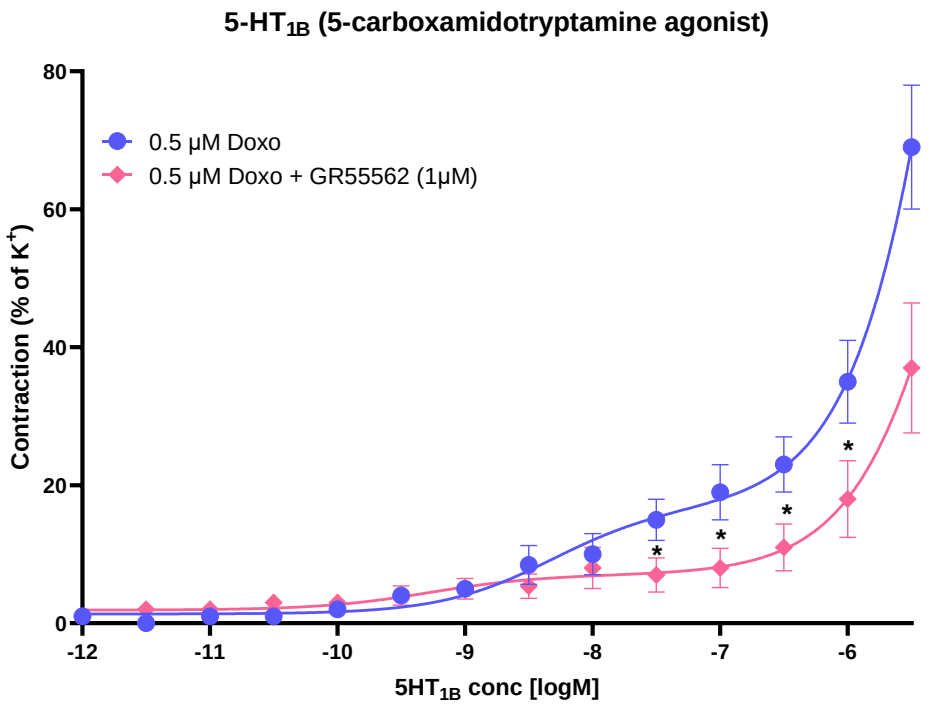

Figure 4-19: Vasocontractile response to the cumulative application of 5-CT (5-HT_{1B} receptor agonist) normalised to 60 mM K^+ KH-induced contraction in rat LAD arteries pre-treated with 30 mins of 1 µM GR55562 (5-HT_{1B} receptor antagonist). (A) Vasocontractile response to the cumulative application of 5-CT to LAD arteries in the vehicle groups. Vehicle group (n = 16; Blue) and vehicle + 1 µM GR55562 (n = 13 - 14; Pink). (B) Vasocontractile response to the cumulative application of 5-CT to LAD arteries incubated with 0.5 µM doxorubicin. Doxorubicin group (n = 13; Blue) and doxorubicin + 1 µM GR55562 (n = 9 - 10; Pink). Doxo = doxorubicin, 5-CT = 5-Carboxamidotryptamine. Values given represent mean ± S.E.M and the comparison of both groups was statistically analysed using unpaired Student T test: * = p value < 0.05. ** = p value < 0.01.

After 24 hrs of organ culture with 0.5 µM doxorubicin the 5-HT_{1B}-mediated vasocontraction after GR55562 pre-treatment was increased in the 5-CT concentration range of 10^{-8} M to $10^{-5.5}$ M when compared to vehicle-treated vessels also receiving GR55562 pre-treatment (Figure 4-16). The increase in vasocontraction observed in the 0.5 µM doxorubicin-treated arteries was slight (< 7 %) at 10^{-8} M (8.0 ± 3.0 %, p = 0.050) to $10^{-6.5}$ M (11.0 ± 3.4 %, p = 0.037) 5-CT and higher (26 %) at 10^{-6} M (18.0 ± 5.5 %, p = 0.009) and $10^{-5.5}$ M 5-CT (37.0 ± 9.4 %, p = 0.003), when compared to vehicle-treated vessels after GR55562 pre-treatment (10^{-8} M (3.0 ± 0.7 %) to $10^{-6.5}$ M (4.0 ± 0.6 %) and 10^{-6} M (5.0 ± 1.0 %) and $10^{-5.5}$ M (11.0 ± 2.5 %)) (Table 4-5). The increase in 5-HT_{1B}-mediated vasocontraction after 0.5 µM doxorubicin compared to vehicle-treated vessels was similar in GR55562 pre-treated and GR55562 naïve vessels.

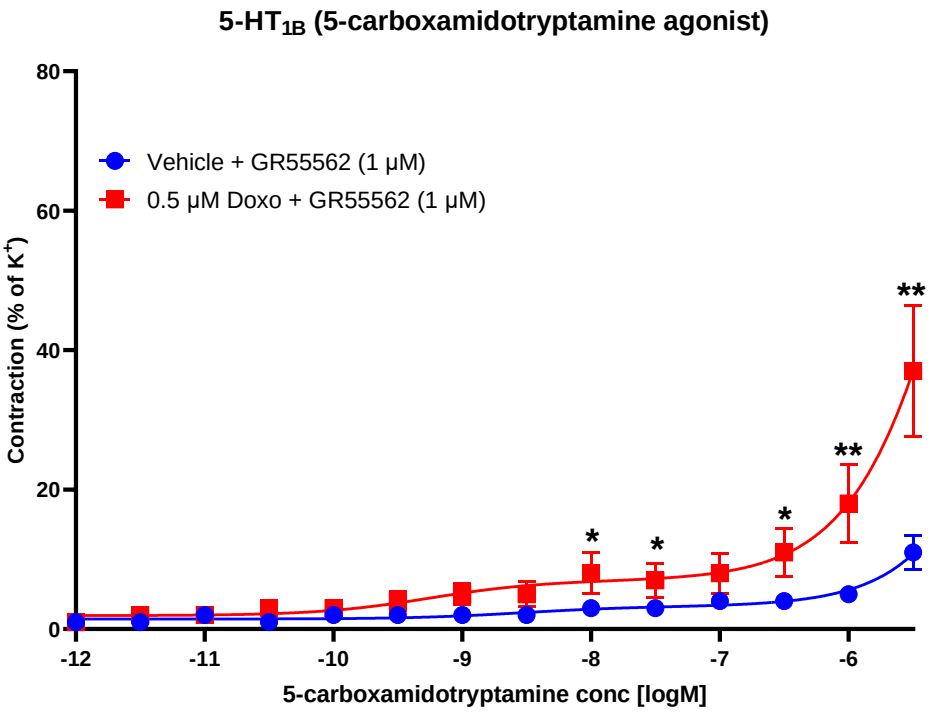

Figure 4-20: Vasocontractile response to the cumulative application of 5-CT (5-HT_{1B} receptor agonist) normalised to 60 mM K^+ KH-induced contraction in rat LAD arteries pre-treated with 30 mins of 1 µM GR55562 (5-HT_{1B} receptor antagonist). Vasocontractile response to the cumulative application of 5-CT to LAD arteries in the doxorubicin group pre-treated with 1 µM GR55562 (n = 9 - 10; Red) compared to Vehicle group pre-treated with 1 µM GR55562 group (n = 13 - 14; Blue) using unpaired Student T-test: * = p value < 0.05. ** = p value < 0.01. *** = p value < 0.001. Doxo = doxorubicin, 5-CT = 5-Carboxamidotryptamine. Values given represent mean ± S.E.M.

Table 4-5: C_{max} values of GR55562 or GR55562 naïve LAD arteries incubated with vehicle or doxorubicin (0.5 µM). C_{max} = the contraction obtained at the highest agonist dose and is applied when the "E_{max}" couldn't be determined due to stock concentration constrains. Values given as mean ± S.E.M. The n values represent the total amount of animals used. GR55562 pre-treated vessels were compared to GR55562 naïve vessels, using unpaired Student T-test:

Groups	*N*	*C_{max}*
Vehicle	16	34.0 ± 8.0 %
Vehicle + GR55562 (1 µM)	13-14	11.0 ± 2.0 %
Doxorubicin (0.5 µM)	13	69.0 ± 9.0 %
Doxorubicin (0.5 µM) + GR55562 (1 µM)	9-10	37.0 ± 9.4 %

The data were summarised in the Figure 4-21. These results indicate that the increase of the 5-CT-induced contraction observed in 0.5 µM doxorubicin-incubated vessels compared to vehicle-incubated vessels, was specific to the 5-HT_{1B} receptors activation. Furthermore, 0.5 µM doxorubicin

treatment seems to induce a biphasic 5-HT_{1B}-mediated contraction of 0.5 µM doxorubicin incubated vessels, while the 5-HT_{1B}-mediated contraction of vehicle-incubated vessels was a monophasic contraction.

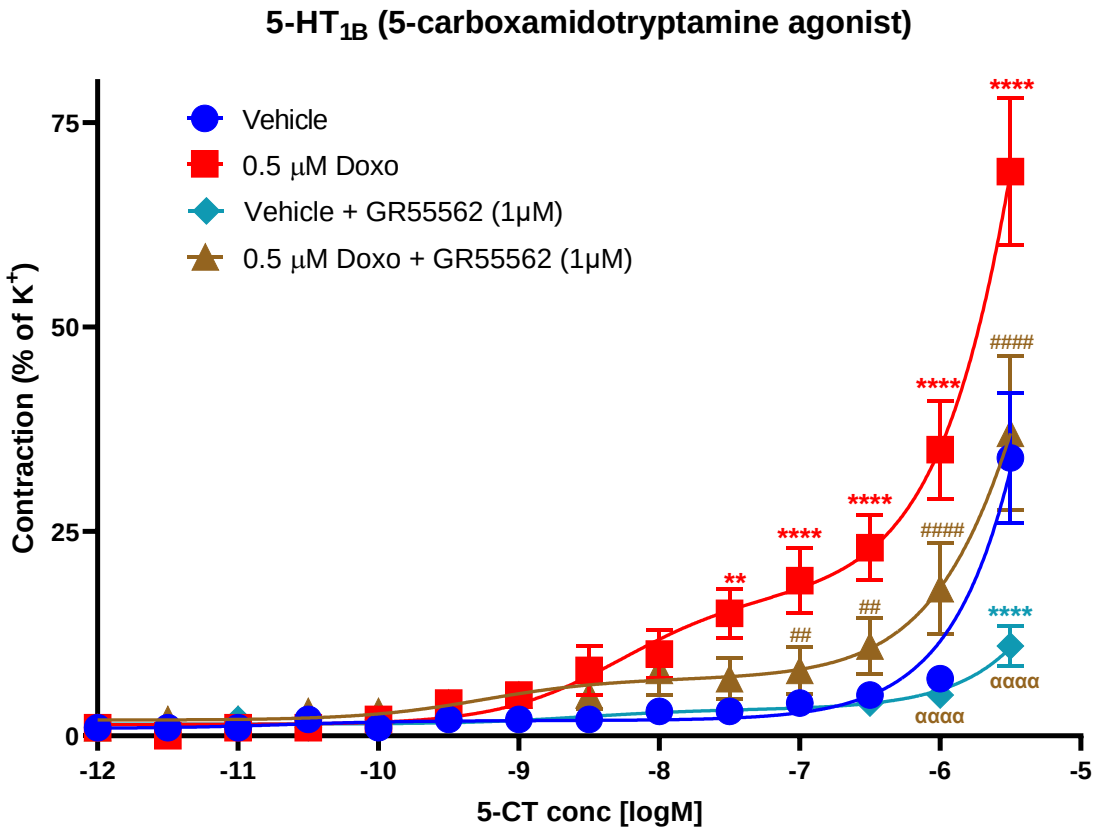

Figure 4-21: Vasocontractile response to the cumulative application of 5-carboxamidotryptamine (5-CT) (5-HT_{1B} receptor agonist) normalised to 60 mM K^+ KH-induced contraction in rat LAD arteries alone or pre-treated with 30 min of 1 µM GR55562 (5-HT_{1B} receptor antagonist). Doxorubicin (n = 13; Red) and vehicle + 1 µM GR55562 (n = 13 - 14; Green) groups were compared to Vehicle group (n = 16; Blue). Doxorubicin + 1 µM GR55562 (n = 9 - 10; Brown) was compared to doxorubicin group (n = 19; Red). Doxorubicin + 1 µM GR55562 (n = 9 - 10; Brown) was compared to vehicle + 1 µM GR55562 (n = 13 - 14; Green). Doxo = doxorubicin, 5-CT = 5-Carboxamidotryptamine, K^+ = 60 mM K^+ KH. Values given represent mean ± S.E.M and statistical analysis was performed with Two-way ANOVA + Bonferroni: ** = p value < 0.01. **** = p value < 0.0001. αααα = p value < 0.0001. ## = p value < 0.01. #### = p value < 0.0001.

4.3.4. Doxorubicin alters the U46619 (thromboxane A2 receptor agonist) mediated vasocontraction

Vasocontractile responses to U46619 (Thromboxane A2 agonist)

The Thromboxane prostanoid A2 (TP) receptor specific agonist U46619 was applied to incubated vessels to investigate the effect of doxorubicin on TP receptor-mediated vasocontraction. The TP-induced vasocontraction values are given as percentage of the maximal contractile response, induced by 60 mM K^+ KH.

After 24 hrs of incubation with 0.5 µM doxorubicin, the TP-mediated vasocontraction was increased at U46619 concentrations of 10^{-8} M to $10^{-7.5}$ M compared to vehicle treated vessel (Figure 4-17). The TP-mediated vasocontraction of 0.5 µM doxorubicin treated vessels was significantly increased by 17 % at 10^{-8} M U46619 (21.0 ± 3.0 %, p = 0.001) and 36 % at $10^{-7.5}$ M U46619 (47.0 ± 6.0 %, p = 0.007), when compared to vehicle treated vessels at 10^{-8} M (4.0 ± 1.0 %) and at $10^{-7.5}$ M (10.0 ± 3.0 %). The maximal TP-mediated vasocontraction of 0.5 µM doxorubicin-treated vessels ("E_{max}" = 111.7 ± 8.7 %, p = 0.0013) was increased compared to the maximal TP-mediated contraction observed in vehicle treated vessels ("E_{max}" = 80.6 ± 5.1 %). Furthermore, the 0.5 µM doxorubicin incubation right-shifted the U46619 dose response curve of 0.5 µM doxorubicin-treated vessels ("pEC_{50}" = $10^{-7.40}$ M, p = 0.0009) compared to vehicle-treated vessels ("pEC_{50}" = $10^{-7.09}$ M) (Table 4-6).

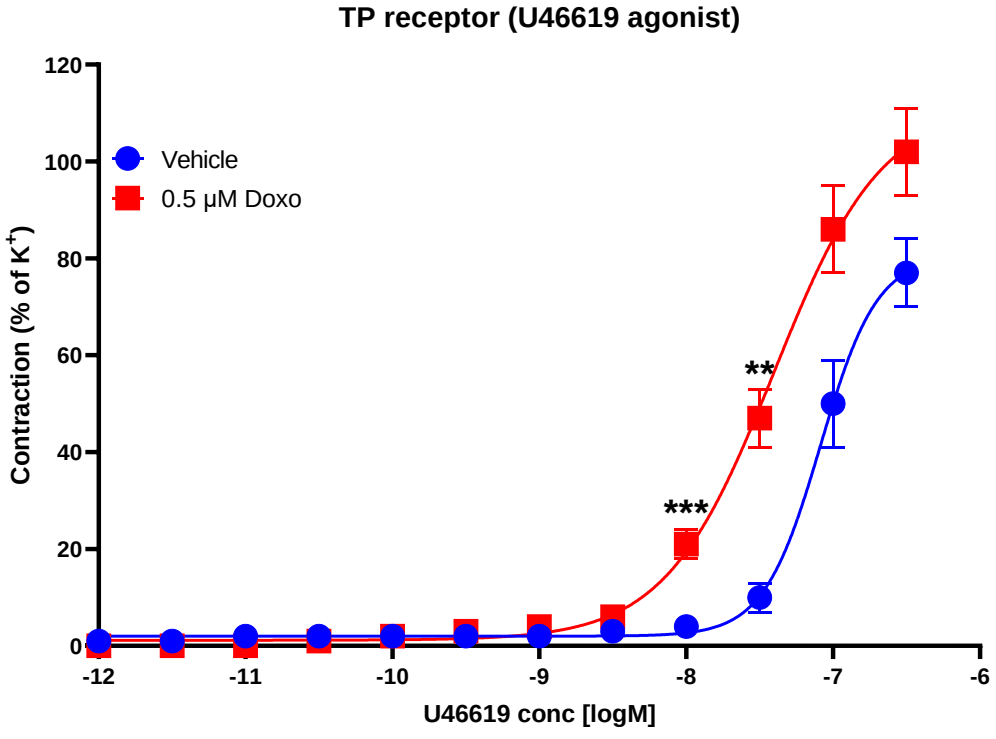

Figure 4-22: Vasocontractile response to the cumulative application of U46619 (TP receptor agonist) normalised to 60 mM K^+ KH-induced contraction in rat LAD arteries. Doxorubicin group (n = 14; Red) was compared to Vehicle group (n = 15; Blue) using Unpaired Student T-test: *** = p value < 0.001. Doxo = doxorubicin. Values given represent mean ± S.E.M.

Vasocontractile responses of U46619 (TP agonist) in the presence of Seratrodast (TP antagonist)

Doxorubicin and vehicle incubated LAD arteries were exposed to a TP receptor specific antagonist Seratrodast (1 µM) for 30 mins, followed by cumulative application of U46619 to establish the TP specificity of the U46619 agonist. After incubation with 1 µM Seratrodast, the U46619 dose-response curve of both 0.5 µM doxorubicin and vehicle treated vessels did not reach the final plateau at the highest dose due to stock constraints, however, the maximal vasocontraction at $10^{-6.5}$ M U46619 was called C_{max} and used for comparison between the groups.

In 24 hrs vehicle incubated vessels, the TP-mediated contraction was reduced significantly at the highest doses of U46619 in the presence of Seratrodast compared to Seratrodast naïve vehicle vessels (Figure 4-18 (A)). The U46619 dose-response curve of Seratrodast pre-treated vehicle incubated vessels did not reach the final plateau at the highest dose due to stock constraints, however, the TP-mediated vasocontraction was reduced with 44 % decrease at 10^{-7} M U46619 (6.0 ± 1.0 %) and 47 % decrease at $10^{-6.5}$ M U46619 (C_{max} = 29.8 ± 11.2 %) in the Seratrodast pre-treated vehicle vessels compared with the Seratrodast naïve vehicle vessels with a TP-mediated vasocontraction of 50.0 ± 9.0 % ($p < 0.001$) at 10^{-7} M and a C_{max} of 77.2 ± 7.2 % ($p < 0.001$). The "pEC_{50}" value of Seratrodast pre-treated vehicle vessels was not obtained due to the absence of maximal U46619-induced vasocontraction ("E_{max}").

In 24 hrs 0.5 µM doxorubicin incubated vessels, the TP-mediated contraction was reduced in Seratrodast pre-treated vessels compared with the Seratrodast naïve vessels from U46619 concentrations of 10^{-8} M and $10^{-6.5}$ M (Figure 4-18 (B)). The Seratrodast pre-treatment significantly decreased the TP-mediated vasocontraction in the 0.5 µM doxorubicin-treated vessels at U46619 concentrations from 10^{-8} M to $10^{-6.5}$ M ($p < 0.001$), compared to the Seratrodast naïve 0.5 µM doxorubicin treated vessels (Figure 4-18 (B)). The reduction of vasocontraction in 0.5 µM doxorubicin-treated vessels pre-treated with Seratrodast observed was a 16 % decrease at 10^{-8} M (5.0 ± 1.9 %), a 36 % decrease at $10^{-7.5}$ M (11.0 ± 3.9 %), a 62 % decrease at 10^{-7} M (24.0 ± 7.4 %) and a 54 % decrease $10^{-6.5}$ M U46619 (C_{max} = 48.3 ± 13.1 %) compared to doxorubicin-treated vessels (10^{-8} M: 21.0 ± 3.0 % to $10^{-7.5}$ M: 47.0 ± 6.0 %; 10^{-7} M: 86.0 ± 9.0 % and $10^{-6.5}$ M (C_{max} = 102.2 ± 9.3 %)). The increase in TP-

mediated vasocontraction after 0.5 µM doxorubicin compared to vehicle-treated vessels was similar in Seratrodast pre-treated and Seratrodast naïve vessels.

(A)

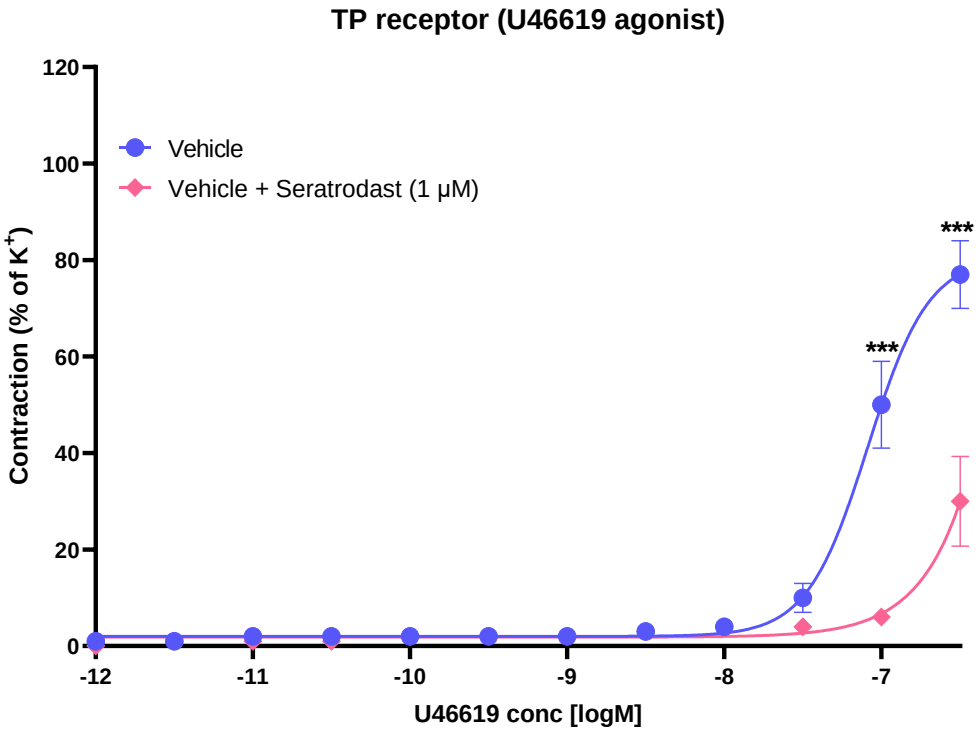

(B)

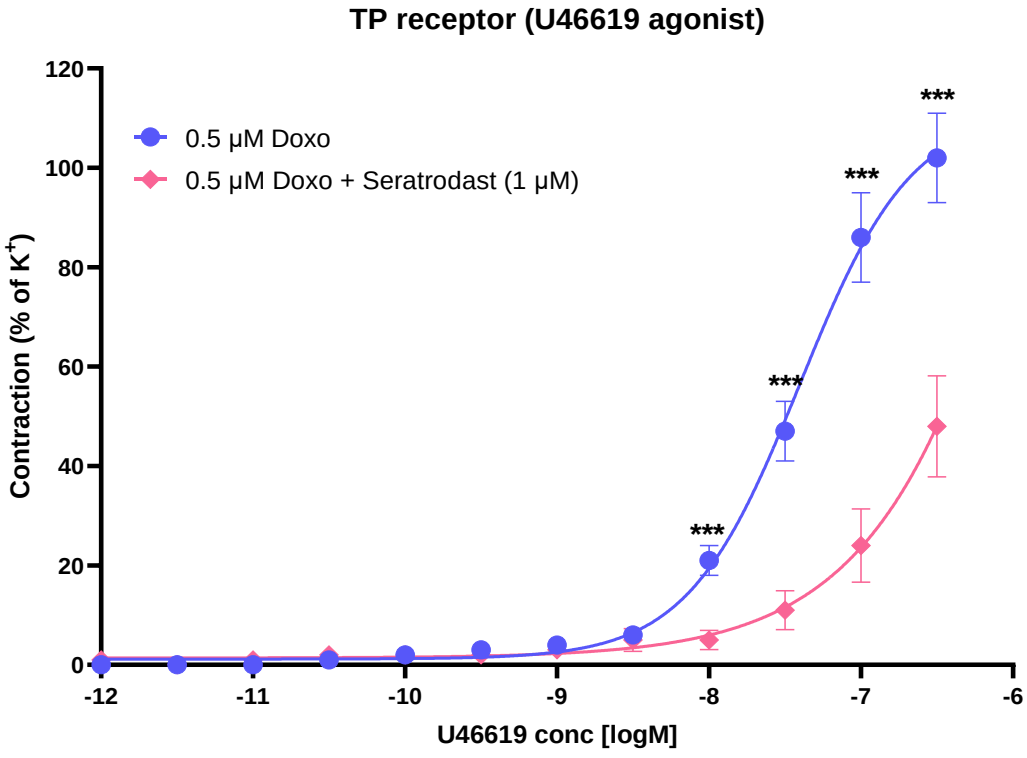

Figure 4-23: Vasocontractile response to the cumulative application of U46619 (TP receptor agonist) normalised to 60 mM K^+ KH-induced contraction in rat LAD arteries pre-treated with 30 mins of 1 µM Seratrodast (TP receptor agonist). (A) Vasocontractile response to the cumulative application of U46619 to LAD artery from vehicle groups. Vehicle group (n = 15; Blue) and vehicle + 1 µM Seratrodast (n = 12 - 13; Pink). (B) Vasocontractile response to the cumulative application of U46619 to incubated LAD artery with 0.5 µM doxorubicin. Doxorubicin group (n = 14; Blue) and doxorubicin + 1 µM Seratrodast (n = 9 - 10; Pink). Doxo = doxorubicin. Values given represent mean ± S.E.M and the comparison of both groups was statistically analysed using unpaired Student T test: *** = p value < 0.001.

After 24 hrs of incubation with 0.5 µM doxorubicin or vehicle and Seratrodast pre-treatment of both vessel groups, the TP-mediated vasocontraction was significantly increased in the 0.5 µM doxorubicin treated vessels by 7 % at U46619 concentrations $10^{-7.5}$ M (11.0 ± 3.9 %) and by 18 % at 10^{-7} M (24.0 ± 7.4 %), compared to the vehicle-treated vessels at $10^{-7.5}$ M (4.0 ± 0.5 %, p = 0.030) and 10^{-7} M (6.0 ± 1.2 %, p = 0.003) (Figure 4-19). The U46619 dose-response curve of both 0.5 µM doxorubicin and vehicle incubated vessels, after 1 µM Seratrodast pre-treatment, did not reach the final plateau at the highest dose due to stock constrains, however, the maximal vasocontraction C_{max} (at $10^{-6.5}$ M) in Seratrodast pre-treated 0.5 µM doxorubicin vessels (C_{max} = 48.3 ± 13.1 %) seems to be increased compared to C_{max} in Seratrodast pre-treated vehicle vessels (C_{max} = 29.8 ± 11.2 %), but this rise was not significant due to the high variability observed (Table 4-6).

The increase in TP-mediated vasocontraction after 0.5 µM doxorubicin compared to vehicle-treated vessels was similar in Seratrodast pre-treated and Seratrodast naïve vessels.

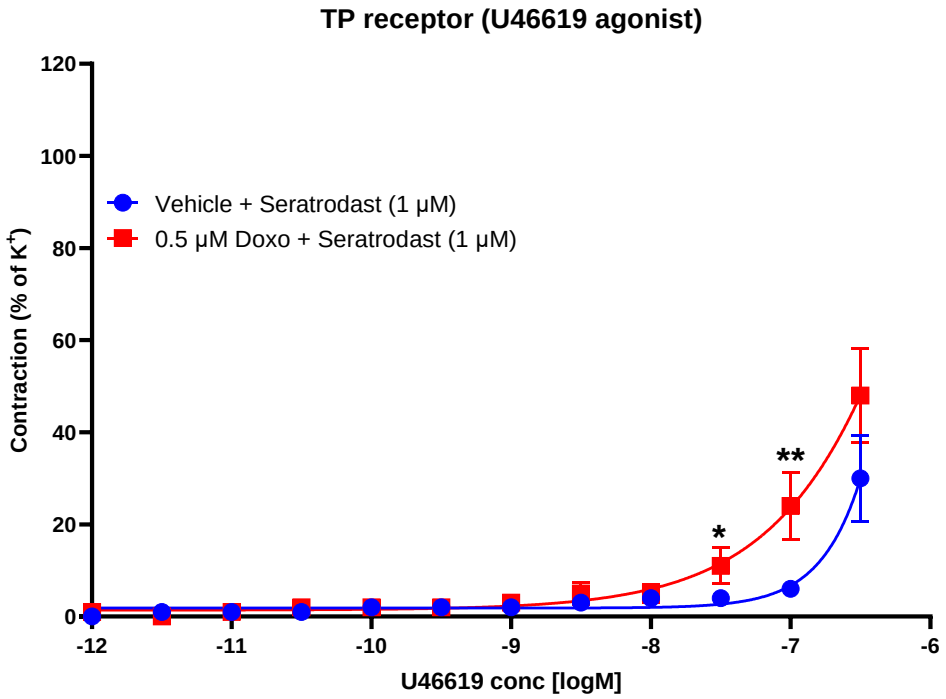

Figure 4-24: Vasocontractile response to the cumulative application of U46619 (TP receptor agonist) normalised to 60 mM K^+ KH-induced contraction in rat LAD arteries pre-treated with 30 mins of 1 µM Seratrodast (TP receptor antagonist). Vasocontractile response to the cumulative application of U46619 to LAD arteries in the doxorubicin group pre-treated with 1 µM Seratrodast (n = 9 - 10; Red) was compared to Vehicle pre-treated with 1 µM Seratrodast group (n = 12 - 13; Blue) using unpaired Student T-test: *** = p value < 0.001. Values given represent mean ± S.E.M.

The data were summarised in the Figure 4-215 These results indicate that in the 24-hr organ-cultured arteries, the observed U46619-induced contraction represents TP receptor-mediated specific vasocontraction.

Table 4-6: C_{max}, "E_{max}" and "pEC_{50}" values of Seratrodast or Seratrodast naïve LAD arteries incubated with vehicle or doxorubicin (0.5 µM). C_{max} is the percentage of 60 mM K^+ maximum contraction at S6c highest dose ($10^{-7.5}$ M), while "E_{max}" and "pEC_{50}" values were generated from fitted curves obtained by Graph-Pad Prism 9.

Groups	*N*	*C_{max}*	*"E_{max}"*	*"pEC_{50}"*
Vehicle	15	77.2 ± 7.2 %	80.6 ± 5.1 %	7.09 ± 0.05
Vehicle + Seratrodast (1 µM)	12 - 13	29.8 ± 11.1 %	/	/
Doxorubicin (0.5 µM)	14	102.2 ± 9.3 %	111.7 ± 8.2 %	7.40 ± 0.09
Doxorubicin (0.5 µM) + Seratrodast (1 µM)	9 - 10	48.3 ± 13.1 %	/	/

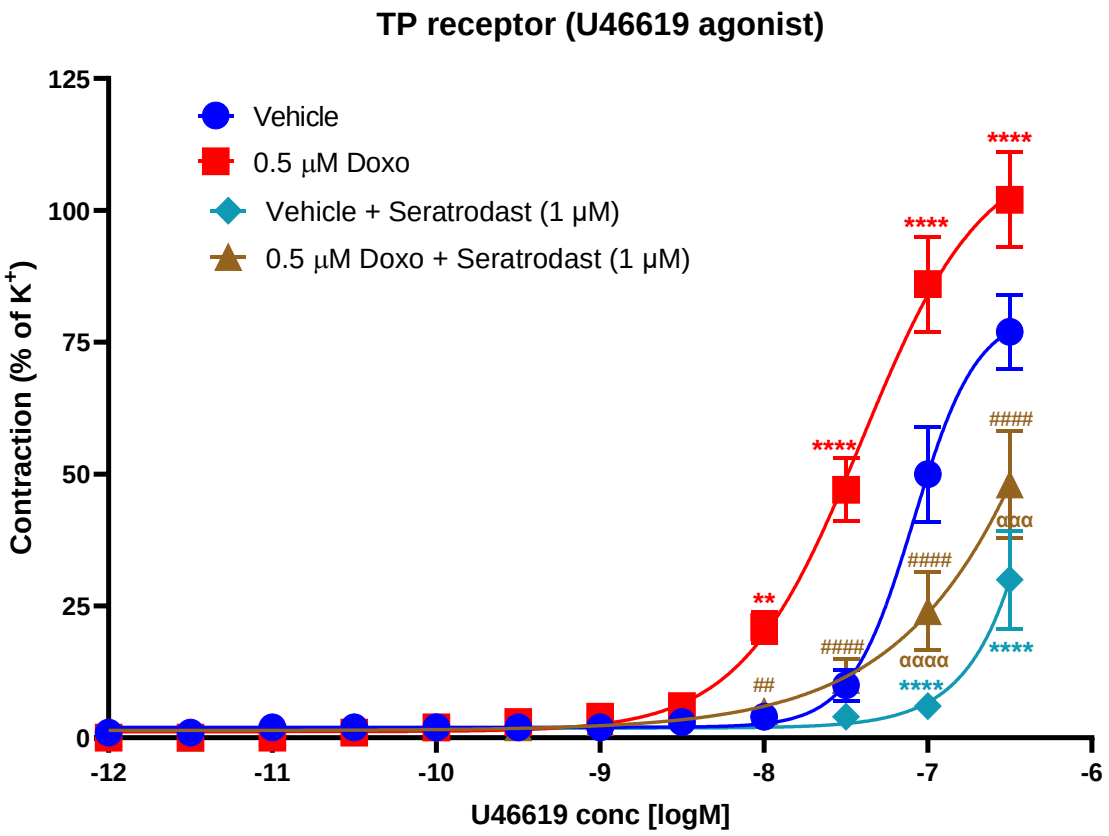

*: compared to Vehicle
α: compared to Doxorubicin
#:compared to Vehicle + BQ788

Figure 4-25: Vasocontractile response to the cumulative application of U46619 (TP receptor agonist) normalised to 60 mM K^+ KH-induced contraction in rat LAD arteries alone or pre-treated with 30 min of 1 µM Seratrodast (TP receptor antagonist). Doxorubicin (n = 13; Red) and vehicle + 1 µM Seratrodast (n = 12 - 13; Green) groups were compared to Vehicle group (n = 16; Blue). Doxorubicin + 1 µM Seratrodast (n = 9 - 10; Brown) was compared to doxorubicin group (n = 19; Red). Doxorubicin + 1 µM Seratrodast (n = 9 - 10; Brown) was compared to vehicle + 1 µM GR55562 (n = 13 - 14; Green). Doxo = doxorubicin, 5-CT = 5-Carboxamidotryptamine, K^+ = 60 mM K^+ KH. Values given represent mean ± S.E.M and statistical analysis was performed with Two-way ANOVA + Bonferroni: ** = p value < 0.01. **** = p value < 0.0001. ααα = p value < 0.001. αααα = p value < 0.0001. ## = p value < 0.01. #### = p value < 0.0001.

4.4. Discussion / Conclusion

The doxorubicin treatment seems to have an effect on the vascular tone of the rat coronary arteries, through specific GPCRs, namely ET_A, ET_B, 5-HT_{1B} and TP receptors. The application of GPCR specific

antagonists BQ123, BQ788, GR55562 and Seratrodast confirms the vascular tone effect observed through the application of the GPCR specific agonist. For a better reading of the discussion, the dose-response curves of each receptor (in the presence of both agonist and antagonist) have been grouped in the same graphs in Figures 4-7, 4-11, 4-14, 4-17, 4-21 and 4-25.

4.4.1. ET_B receptors-mediated contraction is enhanced by doxorubicin treatment

The endothelin B receptors have 2 subtypes in the cardiovascular system. ET_B receptors are located in both endothelial cells and VSMCs; however, the two subtypes have an opposite effect on vascular tone. In the endothelial cells, the ET_B receptors induce vasodilation, through the NO and prostacyclin synthesis (Liu *et al.*, 2003), while the ET_B receptors signalling pathway in VSMC results in a vasocontraction, via phospholipase C (PLC), diacylglycerol / inositol trisphosphate (DAG/IP3) pathway activation (Skovsted *et al.*, 2012). Under normal physiological conditions, ET_B receptors are largely expressed in ECs and induce vasodilatation (Hirata *et al.*, 1993), while ET_B receptors are poorly expressed in VSMCs and thus can't induce significant vasoconstriction (Hirata *et al.*, 1993). However, in the presence of vascular injury, the ET_B receptors in the SMC are up-regulated (Johnsson *et al.*, 2008), and an ET_B-mediated vasoconstriction is observed (Skovsted *et al.*, 2012), due to the up-regulation of ET_B mRNA (Eskesen and Edvinsson, 2006) and subsequent rise in ET_B receptors in the VSMC membrane.

The present study's results have shown a strong S6c-induced vasoconstriction of 24-hr organ-cultured LAD arteries incubated with vehicle or 0.5 µM doxorubicin (Figure 4-7), which is similar to Skovsted (2017) findings, which used a different technique to induce CVD with rat LAD arteries model. Skovsted *et al.et al.* used organ-cultured rat LAD arteries as model to study the up-regulation of ET_B receptors related to CVDs, as it was performed in this study. However, the group induced ischaemia by occluding the LAD arteries through ligating for 30 min, followed by reperfusion to mimic the remodelling processes of CVD, while a 24 hrs organ culture with doxorubicin to mimic the CVD remodelling processes was used in this study. After the I/R, the LAD arteries were dissected free and divided into two groups (upstream or downstream the ligature) and mounted on wire-myograph to measure the S6c dose-response curve. Their data showed that the ET_B-mediated contraction was increased in ischemic LAD segments downstream of the ligature compared to the non-ischemic LAD segments, which had a negligible S6c-induced contraction (Skovsted *et al.*, 2017).

Furthermore, it was shown that the doxorubicin treatment (0.5 µM) seems to induce a further increase of the ET_B-mediated contraction from 10^{-13} M to $10^{-10.5}$ M compared to vehicle-incubated LAD arteries (Figure 4-7), which could underline a potential doxorubicin-induced vasotoxicity. However, the "E_{max}" and "pEC_{50}" values of the vehicle and doxorubicin treated LAD vessels remained unchanged.

It has been established that the constant dissociation (K_D) of S6c for ET_B receptors (0.06 ± 0.02 nM) is 59,400-fold higher than the K_D for ET_A receptors (3.50 ± 0.26 µM) in rat left ventricle, meaning the S6c-induced vasoconstriction is predominantly mediated through ET_B receptors signalling pathways (Russell and Davenport, 1996). Previous studies have shown that sarafotoxin 6c application produces a monophasic curve. Eskesen and her team compared the sarafotoxin 6c-induced vasoconstriction of overnight organ-cultured LAD arteries to fresh LAD arteries from rats and showed that the organ culture of LAD arteries leads to an increase of sarafotoxin 6c-induced vasoconstriction of LAD arteries. However, both fresh and organ-cultured LAD arteries produced monophasic S6c-induced dose-response curve after cumulative application of sarafotoxin 6c ranging from 10^{-12} M to $10^{-7.5}$ M (Eskesen and Edvinsson, 2006). Furthermore, Johnsson and her team also investigated the sarafotoxin 6c dose-response curves of fresh or 24 hrs-incubated rat LAD arteries with cumulative application of sarafotoxin 6c ranging from 10^{-12} M to $10^{-6.5}$ M. Their data showed that the sarafotoxin 6c dose-response curves were monophasic and the cultured-LAD arteries had a strong ET_B-mediated vasoconstriction while fresh LAD arteries had negligible ET_B-mediated vasoconstriction (Johnsson *et al.*, 2008). Based on both previous studies, Skovsted examined the early time course and potential mechanisms involved in the enhanced ET_B-mediated response to sarafotoxin 6c of cultured LAD arteries and septal coronary arteries (SCA). The LAD and SCA arteries were incubated for 1½ hrs, 4 hrs, 7 hrs or 24 hrs and mounted on a wire-myograph to perform sarafotoxin 6c dose-response curve with concentrations ranging from 10^{-12} M to $10^{-7.5}$ M. Their data showed that the up-regulation of ET_B-mediated vasoconstriction was strong after 7 hrs incubation and that the sarafotoxin 6c dose response curves were monophasic at all of the included incubation time intervals (Skovsted *et al.*, 2012).

In contrast to the three studies mentioned above using the same model (i.e. organ-cultured rat LAD arteries), cumulative application of sarafotoxin 6c with concentrations ranging from 10^{-14} M to $10^{-7.5}$ M resulted in biphasic curves in the present study. Here it was shown that the sarafotoxin 6c application to vehicle-incubated LAD arteries reach a first plateau from $10^{-11.5}$ M to $10^{-10.5}$ M, as shown in Figure 4-7. One explanation to this monophasic versus biphasic curve phenomenon could be explained with the initial start dose of sarafotoxin 6c, as the sarafotoxin 6c application starts from 10^{-14} M, while the other studies start the application at 10^{-12} M. The higher concentration of sarafotoxin 6c application in the other studies could have resulted in omitting the first plateau, as this plateau is only reached at a lower sarafotoxin 6c dose level.

In the present results, the presence of a sarafotoxin 6c biphasic curve shows the implication of two different ET_B subtype receptors. The first hypothesis (i) is that at the first phase of the sarafotoxin 6c dose-response curve, both ET_B subtypes have antagonistic effects and these ET_B subtypes' competition leads to the low vasocontraction depending on both ET_B subtypes' affinity. For clarification, the ET_B

subtype from EC will be called ET_{B1} and the ET_B subtype from SMC will be called ET_{B2}. The binding of sarafotoxin 6c to ET_{B2} receptors induces a vasocontraction while the binding of sarafotoxin 6c to ET_{B1} receptors induces a vasorelaxation. The interaction between these 2 subtypes with opposite vasocontractile response effects could explain the low vasocontraction at the first phase of the sarafotoxin 6c biphasic curve. The LAD arteries included in this study have an average of 50% of the endothelium left after 24 hrs of organ culture and subsequently getting mounted on the wire-myography (Figure 3-8 in chapter 3, section 3.3.2). The lack of ECs means there are fewer ET_{B1} receptors functional to induce vasorelaxation. Moreover, studies have highlighted the up-regulation of ET_{B2} during vascular injury. Miasiro *et al.et al.* investigated the sarafotoxin 6c biphasic curved in the fresh isolated guinea-pig ileum with different agonists (sarafotoxin 6c and IRL1620) and antagonists (BQ123, PD145065, RES-701-1 and Apamin) obtained by recording the isometric responses through a Narco Biosystem force transducer. They observed a relaxation followed by a contraction of the vessels when they applied cumulative doses of sarafotoxin 6c and the use of antagonists confirm it was due to two distinct ET_B receptors (Miasiro *et al.*, 1999). This paper could illustrate the activation of ET_{B1} at low doses and the activation of ET_{B2} at higher doses. The up-regulation of ET_{B2} and/or the down-regulation of ET_{B1} could explain the vasoconstriction at both phases of the biphasic sarafotoxin 6c dose-response curve, which would show primarily ET_{B2}-mediated contraction. However, further studies are needed to investigate if this hypothesis is true.

Additionally, upon pre-treatment with the ET_B receptor antagonist BQ788, a decrease of the vasocontraction was observed in all of the studied LAD arteries (Figure 4-7). This study's data showed the BQ788 pre-treatment of both vehicle- and doxorubicin-treated LAD arteries (Figure 4-7) resulted in a significant reduction ($p = 0.0002$) of the maximal ET_B-mediated contraction in doxorubicin-incubated LAD arteries (97 %) compared to vehicle-incubated LAD arteries (154 %). However, it was shown that in vessels incubated with doxorubicin, the BQ788 induces a decrease at the highest doses of sarafotoxin 6c, while the contraction is recovered in vehicle-incubated vessels. Moreover, the doxorubicin-incubated vessels still induce an increased vasocontraction after BQ788 pre-treatment during the first phase but induce a decrease in vasocontraction at the highest doses of sarafotoxin 6c. The mechanisms involved in this switch remain undefined, however, some hypotheses were suggested.

The doxorubicin treatment could (i) modify the structure of the binding site on the ET_B receptors leading to an increase of the binding of antagonist BQ788 to the ET_B receptors or a decrease of the agonist sarafotoxin 6c affinity to the ET_B receptors and thus may explain the reduction of the maximal ET_B-mediated vasoconstriction observed in BQ788 pre-treated doxorubicin LAD arteries, compared to BQ788 pre-treated vehicle LAD arteries. The doxorubicin treatment combined with the 30 min

antagonist pre-treatment, followed by the cumulative application of sarafotoxin 6c could (ii) desensitise the ET_B receptors and thus decrease the number of ET_B receptors available for the sarafotoxin 6c binding, leading to the down-regulation of the S6c-induced contraction.

Furthermore, in vehicle-treated LAD arteries, the BQ788 pre-treatment failed to inhibit the ET_B-mediated vasocontraction at high S6c concentration (Figure 4-7). It is known that ET_B receptors are rapidly desensitised by phosphorylation through the G protein-coupled receptor kinase type 2 upon stimulation by the agonist S6c and then internalised from the VSMC membrane at high S6c doses (Russell and Davenport, 1996, Gregan *et al.*, 2004) and thus BQ788 might simply not be able to adequately compete with S6c and bind to ET_B receptors at high S6c doses and elicits its antagonistic effect.

As shown previously, the organ culture of rat LAD arteries induces a significant up-regulation of ET_B receptors in SMC (Skovsted *et al.*, 2017). Doxorubicin is known to interact with DNA (Rawat *et al.*, 2021) and could (iii) potentially have a toxic effect during the ET_B receptors transcription leading to a modification of the ET_B receptors' properties.

The results observed in this chapter showed that ET_B-mediated contraction is altered by doxorubicin treatment, however, the mechanisms associated with ET_B-mediated vasocontraction observed during the first phase of biphasic S6c dose-response curve of rat LAD arteries are unclear and need more investigation.

4.4.2. Doxorubicin-induced cardiotoxicity is not associated with altered ET_A-mediated vasocontractile response, however, BQ123 highlights a potential alteration of ET_A receptors.

ET-1 is the ligand of ET_A and ET_B receptors. ET_A receptors are expressed in the SMCs and are mainly responsible for the vasoconstriction (Yanagisawa *et al.*, 1988) and blood pressure (Donato *et al.*, 2014) in normal physiological conditions. However, in pathological conditions, ET_A and ET_B are both involved in vasoconstriction (Skovsted *et al.*, 2015).

The present results showed that the doxorubicin treatment (0.5 µM) has no effect on the contractile response of endothelin receptors when applying the endothelin-1 agonist (Figure 4-11). The ET-1 dose-response curve was performed after an ET_B receptors desensitisation by applying $10^{-7.5}$ M dose of Sarafotoxin 6c.

The addition of ET_B receptor antagonist BQ788 prior to the ET-1 dose-response curve illustrated a slight reduction of the contraction of LAD arteries from vehicle group (Figure 4-17). These findings demonstrate that ET_B-mediated contraction was nearly abolished by applying $10^{-7.5}$ M dose of Sarafotoxin 6c, and that the ET_B-mediated contraction was observed during the first phase of ET-1 dose-response curve. The addition of the ET_A receptor antagonist BQ123 prior to the ET-1 dose-response curve confirmed that ET_A-mediated contraction was observed at the higher doses of ET-1 application (Figure 4-14).

Based on this study's results with the addition of either ET_A selective antagonist BQ123 or ET_B selective antagonist BQ788, it is evident that the ET-1 dose-response curve performed without antagonist corresponds mainly to the ET_A-mediated vasocontractile response, which means doxorubicin treatment has no effect on ET_A-mediated vasocontractile response. This study's findings are in agreement with Skovsted *et al.et al.* (2017) findings, which showed that ET_A-mediated vasocontractile response is not altered in their *in vitro* model mimicking cerebral ischaemia (as described in section 4.4.4).

Interestingly in the present results, BQ123 pre-treatment showed that the ET_A-mediated contraction was significantly reduced in the presence of doxorubicin incubation, from 150.5 % in BQ123-incubated vehicle LAD arteries to 61.8 % in BQ123-incubated doxorubicin LAD arteries (Figure 4-14). Therefore, BQ123 pre-treatment might have highlighted a potential doxorubicin-induced alteration of the ET_A receptors. Furthermore, the addition of both ET_A and ET_B receptors antagonists BQ123 and BQ788 simultaneously identified a stronger decrease of the last phase of the ET-1-dose-response curve compared to the application of individual antagonist (BQ123 or BQ788) (Figure 4-11), while there is no decrease observed with only BQ788 (Figure 4-17). Based on these results, the inhibition of both ET_A and ET_B receptors induced a higher decrease than ET_A receptors inhibition alone.

4.4.3. 5-HT_{1B} receptors-mediated contraction is enhanced by doxorubicin treatment

The 5-HT_{1B} receptors have been mostly studied in cerebral arteries, where their activation is involved during many disorders, such as migraine (O'Quinn *et al.*, 1999) or memory (Lotfinia *et al.*, 2014). However, 5-HT_{1B} and 5-HT_2 are two serotonin receptor subtypes involved in serotonin response in coronary arteries (Longmore *et al.*, 2000, Maassen VanDenBrink *et al.*, 2000, Kaumann *et al.*, 1994). Studies on the anti-migraine drug and 5-HT_{1B} agonist sumatriptan have demonstrated that patients treated with sumatriptan can develop chest pain, myocardial infarction, and vasospasm (Ottervanger *et al.*, 1997, Okonkwo and Ojha, 2020).

The present study showed that the 5-carboxamidotryptamine dose-response curve performed after doxorubicin treatment resulted in a biphasic dose-response curve, which highlights the potential implication of two different serotonin subtype receptors during the 5-CT-mediated contraction. The current finding is consistent with Hansen-Schwartz *et al.et al.* (2003) findings, which showed that the agonist 5-CT has a high affinity to 5-HT_{1B} with a pEC_{50} of 7.7 in rat cerebral arteries and a low affinity to 5-HT_{2A} with a pEC_{50} of 5.1 in rat cerebral arteries (Hansen-Schwartz *et al.*, 2003).

The 5-HT_{1B} selective antagonist GR55562 with a pK_B of 6.4 for the 5-HT_{1B} receptors in cerebral arteries was used to verify that the present results were specific to the 5-HT_{1B} receptor activation (Hansen-Schwartz *et al.*, 2003), prior to the assessment of 5-CT-mediated vasocontractile response. Addition of 5-HT_{1B} receptor specific antagonist GR55562 demonstrated that the observed 5-CT mediated contractile alteration in doxorubicin-treated coronary arteries was due to the 5-HT_{1B} receptors with a significant decrease of the C_{max} from 34 % in vehicle-treated LAD arteries to 11 % in GR55562-treated vehicle LAD arteries ($p = 0.009$) (Figure 4-21) and decrease the biphasic dose-response curve observed after doxorubicin treatment at the concentrations from $10^{-7.5}$ M 5-CT to 10^{-6} M 5-CT in doxorubicin-treated LAD arteries ($p < 0.05$) compared to GR55562-treated doxorubicin LAD arteries (Figure 4-21).

Based on the present results, it has been suggested that the affinity of 5-CT binding to 5-HT_{1B} receptors is increased after doxorubicin treatment compared to vehicle in LAD coronary arteries (Figure 4-21). Binding of 5-CT ligand to the 5-HT_{1B} receptors inhibits the adenylyl cyclase, which reduces the cAMP formation and PKA activity leading to the intracellular calcium release from the sarcoplasmic reticulum and thus finally vasoconstriction (Barnes and Sharp, 1999, Leenders and Sheng, 2005, Tiger *et al.*, 2018). However, due to stock limitations, the lack of "E_{max}" values for the vehicle group makes it difficult to determine if the 5-HT_{1B}-mediated contraction is increased by doxorubicin treatment.

To the best of our knowledge, there are no studies on the involvement of doxorubicin-induced vasotoxicity mediated through the 5-HT_{1B} receptors in either human or animal coronary arteries. However, in support of the present study's findings, previous studies have demonstrated that doxorubicin-induced cardiotoxicity can decrease cAMP formation. cAMP is a second messenger transducing the action of several GPCRs, including 5-HT_{1B} receptors (Gerlo *et al.*, 2011) and 5-HT_{1B} receptors activation induces the reduction of cAMP levels, which leads to the release of intracellular calcium and thus a contraction (Albert and Tiberi, 2001). Calderone *et al.et al.* (1991) studied the doxorubicin-induced changes on rabbit left and right ventricular tissues, where cumulative doses of 0.75 mg/kg of doxorubicin were administrated three times a week for 11 weeks to induce doxorubicin-induced cardiomyopathy. Their data showed that the adenylyl cyclase activity and generation were reduced in the cardiomyocytes, which suggests that the decrease of adenylyl cyclase could contribute

to the decrease of myocardial contractility in their heart failure model (Calderone *et al.*, 1991). Furthermore, in another study, Efentakis *et al.et al.* (2020) investigated the potential cardioprotective effect of an inotropic vasodilator Levosimendan (LEVO) on murine cardiomyocytes after a doxorubicin sub-chronic cardiotoxicity (Efentakis *et al.*, 2020). Their data showed that LEVO can be cardioprotective by inhibiting PDE-3, which induces the activation of the cAMP/PKA pathway and leads to abrogate the intracellular calcium release. Interestingly, the present results showed indirectly that by increasing the 5-HT_{1B}-mediated vasocontractile response, doxorubicin could lead to a decrease of the cAMP formation (Figure 1-6 in chapter 1, section 1.6.3), as observed in the previously described studies investigating doxorubicin-induced cardiotoxicity.

Thus, these previous studies seem to be in indirect agreement with this study, as doxorubicin treatment increases the 5-HT_{1B}-mediated vasocontractile responses in isolated coronary arteries and targeting the 5-HT_{1B} pathways could be a potential adjuvant therapy for cancer patients. Doxorubicin-induced cardiotoxicity involves a complex set of mechanisms involved, and the effect through 5-HT_{1B} receptors could be one of the mechanisms of action that the vasotoxicity is developing. However, the exact mechanism of action involved in the doxorubicin-induced vasotoxicity through 5-HT_{1B} receptors remains unclear and needs to be highlighted by molecular studies.

4.4.4. Thromboxane A2 receptors-mediated contraction is enhanced by doxorubicin treatment

This study's findings showed the effect of doxorubicin treatment on coronary artery's vascular tone, through the involvement of TP receptors. The agonist U46619 dose-response curve showed a significant left-shift of the curve, from $10^{-7.09}$ M in vehicle-treated LAD arteries to $10^{-7.40}$ M in doxorubicin-treated LAD arteries ($p = 0.0009$), and significant elevation of the maximal TP-mediated contraction after 0.5 µM doxorubicin incubation, from 80.6 % in vehicle-treated LAD arteries to 11.7 % vehicle-treated LAD arteries ($p = 0.0013$) (Figure 4-25), suggesting an elevation of the TP receptors potency and contractile response to the agonist U46619. Interestingly, it was shown that the pre-treatment of Seratrodast confirms the role of TP receptors in the observed increase of vasocontraction of doxorubicin-treated LAD arteries (Figure 4-25).

Thromboxane A2 is a potent platelet activator and vasoconstrictor (Katugampola and Davenport, 2001). In SMCs, thromboxane A2 ligand binds to TP receptors leading to PLC activation. PLC hydrolyses PIP_2 in DAG and IP3 leading to PKC activation and intracellular calcium accumulation. This pathway induces a strong vasoconstriction and platelet activation, which alter platelets shape, aggregation and secretion (Chen, 2018). Pathological changes of the TP signalling pathways can lead to CVDs, like

atherosclerosis, myocardial infarction and hypertension (Neri Serneri *et al.*, 1983, Katugampola and Davenport, 2001, Smyth, 2010, Martin, 1984).

The functional effect of doxorubicin treatment on TP receptor-mediated vasocontraction has not been investigated prior, however, a recent study reported that doxorubicin-induced cardiotoxicity involves thrombus formation. An *in vivo* model using 10-week-old C57BL/6 mice was used to investigate thrombus formation. Doxorubicin was administrated at a concentration of 5 mg/kg/week to the mice for 4 weeks and the platelet activity was analysed. It was shown that chronic treatment of doxorubicin enhanced platelet activity, leading to thrombus and vascular injury (Lv *et al.*, 2020). Conversely, studies on isolated platelets from human blood samples (collected from 18 – 25 years old patients) showed that treatment with 5 – 100 µM doxorubicin had no direct effect on the platelet activity (Kim *et al.*, 2009, Kim *et al.*, 2011). The aggregation and procoagulant activity of platelets are two main factors of thrombosis and both are enhanced by the intracellular calcium release and a prolongated increase of pro-coagulation (Heemskerk *et al.*, 2002). In this study, it has been shown that TP-mediated contraction of doxorubicin-treated LAD vessels was elevated compared to vehicle-treated LAD vessels and the elevated TP-mediated vasocontraction might be induced by (i) an increase of TP receptors affinity to U46619, highlighted through the increase of the "pEC_{50}"-value in LAD vessels treated with doxorubicin, (ii) an increase in TP receptors translation or (iii) a TP-mediated contractile hyper-responsiveness (i.e. increase of "E_{max}"), leading to the increase of intracellular calcium and PKC activity, via PLC activation. The vasoconstrictor and platelet activation properties of TP receptors underlined the potential involvement of TP receptors in doxorubicin-induced vasotoxicity. The factors involved in the increase of TP-mediated contraction remain undefined and molecular studies are needed, however, this study's findings and previous studies underline the potential benefits that an adjuvant therapy targeting the TP receptor pathway could have on cancer patients.

4.4.5. Conclusion

From this study's novel findings, it is evident that doxorubicin induces vasotoxicity by increasing the contraction of three of the studied GPCRs, ET_B, $5\text{-}HT_{1B}$ and TP receptors. The addition of the GPCR specific antagonist confirmed the specific involvement of each GPCR receptor and suggest a potential doxorubicin-induced alteration of ET_A receptors.

The molecular mechanisms involved in vasotoxicity remain undefined for these GPCRs. The mRNA expression and receptors density of the GPCRs could underline some of the mechanisms involved in the doxorubicin-induced vasotoxicity and further studies were conducted to investigate the cellular and molecular mechanisms involved in doxorubicin-induced cardiotoxicity which will be discussed in

the next chapter. Furthermore, these GPCRs are involved in smooth muscle differentiation via MAPK pathways (Liu *et al.*, 2019, Skovsted *et al.*, 2017, Bolla *et al.*, 2002). Further studies were conducted to investigate the attenuation of the elevated GPCR-mediated vasoconstriction associated with the doxorubicin-induced vasotoxicity by inhibiting the MEK/ERK pathway with a MEK 1/2 inhibitor U0126 which will be discussed in the next chapter.

Chapter 5:

5. Effect of a MERK 1/2 inhibitor (U0126) on doxorubicin-induced vasotoxicity.

Some data of this chapter are under review or published:

Peer reviewed journal:

- Submitted for publication in British journal of Pharmacology (June 2023):

Title: Involvement of MEK/ERK pathway during G-protein coupled receptor mediated doxorubicin induced vasotoxicity in rat coronary arteries

Authors: Lozahic C., Maddock H., Wheatley M., Sandhu H.

Conferences:

- British Pharmacology Society (BPS) Pharmacology 2022 conference in Liverpool:

Poster presentation: Doxorubicin-induced vasotoxicity in coronary vessels: Investigating the G-protein-coupled receptor mediated vasoconstriction and the effect of an MEK 1/2 inhibitor U0126. Miss Caroline Lozahic, Prof Helen Maddock, Dr Hardip Sandhu.

- BSCR Autumn meeting 2022: Cardiac remodelling – Basic mechanisms to clinical management, Belfast:

Poster presentation: Doxorubicin-induced vasotoxicity in coronary vessels: Investigating the G-protein-coupled receptor mediated vasoconstriction and the effect of an MEK 1/2 inhibitor U0126. Caroline Lozahic, Mark Wheatley, Helen Maddock and Hardip Sandhu

- CSELS conference, June 2022, Coventry:

Poster presentation: Doxorubicin-induced vasotoxicity in coronary vessels: Investigating the G protein coupled receptor mediated vasoconstriction and the effect of an MEK 1/2 inhibitor U0126. Caroline Lozahic, Mark Wheatley, Helen Maddock and Hardip Sandhu.

PGR seminar:

Oral presentation (2022), Coventry: G-protein coupled receptor (GPCR) involvement during anthracycline-induced cardiotoxicity and potential pathways involved.

5.1. Introduction

In recent years, research into cancer therapy has taken significant steps towards more effective, precise and less invasive cancer treatment options. New and innovative cancer therapy options include antimicrobial peptides (de la Fuente-Nunez *et al.*, 2017) and immunotherapy (Paz-Ares *et al.*, 2018). Despite the recent advancements, chemotherapy drugs remain the most efficient cancer treatments to treat various cancer types. However, chemotherapy drugs are associated with cardiotoxicity, which is defined as cardiac toxicity as a direct effect of chemotherapy. Understanding the mechanism of action of cancer drugs can potentially lead to improvement in cancer drug development and management of adverse effects by implementing adjunct therapy (Anand *et al.*, 2022, Lozahic *et al.*, 2021).

Anthracyclines are among the most potent and commonly used chemotherapeutic agents (Hutchins *et al.*, 2017). Anthracycline chemotherapy regimen is used alone or in combination with other cancer treatments to treat various solid tumours, such as breast cancer, lymphoma or sarcoma, and haematological malignancies (Volkova and Russell, 2011). Anthracycline drugs target cancer cells and non-malignant cells by inducing apoptosis through different mechanisms of action, such as DNA intercalation and topoisomerase II enzyme inhibition (Minotti *et al.*, 2004). Unfortunately, cancer patients treated with anthracyclines are at risk of developing cardiac-related adverse effects, including arrhythmia (Buza *et al.*, 2017) and heart failure (Kamphuis *et al.*, 2020).

Doxorubicin is one of the anthracycline drugs commonly used in solid cancer. Unfortunately, doxorubicin is associated with severe cardiac adverse effects. Doxorubicin-induced cardiotoxicity involves various intracellular mechanisms including mitochondrial dysfunction, reactive oxygen species production (Gille and Nohl, 1997) leading to oxidative stress (Minotti *et al.*, 2004), apoptosis (Kaufmann and Earnshaw, 2000), and myofibril damage (Ito *et al.*, 1990). The efficacy of doxorubicin in treating cancer is limited by cumulative dose-dependent cardiotoxicity (Lefrak *et al.*, 1973). Doxorubicin-induced cardiotoxicity can occur acutely after therapy (i.e. within the first weeks of administration). The acute cardiotoxicity effects of doxorubicin range from loss of myocardial contractility (Raj *et al.*, 2014) to impaired left ventricular ejection fraction (Pinedo, 2006). Doxorubicin-induced cardiotoxicity can also occur long-term. Early chronic cardiotoxic adverse effects from doxorubicin occur during the first year, such as the development of dilated cardiomyopathy (Raj *et al.*, 2014). Cardiotoxicity from doxorubicin treatment can also occur many years down the line, where the accumulation of previous cardiac dysfunction leads to the development of a weakened heart and thinning the left ventricular (LV) wall, leading to a reduction of the systolic function (Sandhu and Maddock, 2014).

The doxorubicin treatment can induce cardiovascular damage via several mechanisms, including oxidative stress, calcium homeostasis dysregulation, iron-related free radicals and systemic inflammation (Podyacheva *et al.*, 2021) (Olson *et al.*, 1988). The doxorubicin accumulates in the mitochondrial inner membrane and disrupts the mitochondrial activity, leading to mitochondria dysfunction (Octavia *et al.*, 2012) and thus overproduction of reactive oxygen species (ROS) production (Zhou *et al.*, 2001). Furthermore, doxorubicin alters the endothelial nitric oxide synthase (eNOS) and NADPH oxidase (NOX) activities and thus leads to the reduction of free oxygen in superoxide free radical (Vasquez-Vivar *et al.*, 1997, Deng *et al.*, 2007). The overproduction of ROS associated with the doxorubicin-induced cardiotoxicity coupled to the iron-related free radicals overload lead to oxidative stress, lipid peroxidation and cells apoptosis, and thus into the cardiac dysfunction observed in patients treated with chemotherapy (Sritharan and Sivalingam, 2021). The ROS generation and apoptotic signalling activation are also induced by the increase of intracellular calcium release from the sarcoplasmic reticulum during doxorubicin-mediated cardiotoxicity (Holmberg and Williams, 1990). Intracellular calcium overload is clinically associated with ischaemic heart diseases, including atherosclerosis, thrombosis, and coronary spasms (Dhalla *et al.*, 2008). Furthermore, clinical studies have highlighted an increase of arterial stiffness in patients treated with anticancer drugs both during and after the treatment, including doxorubicin (Parr *et al.*, 2020, Mozos *et al.*, 2017, Chaosuwannakit *et al.*, 2010). Doxorubicin-induced cardiotoxicity is also associated with an increase of the inflammatory markers. Interleukin 9 (IL-9) aggravates doxorubicin-induced cardiac injury by promoting the inflammatory response (Ye *et al.*, 2020).

The G-protein coupled receptors (GPCRs) are interesting targets to alleviate doxorubicin-induced cardiotoxicity. GPCRs are the largest and most important families of transmembrane proteins (Rosenbaum *et al.*, 2009) and are well-known to be key vasotension regulators in CVDs, such as hypertension and heart failure (Forrester *et al.*, 2018, Audebrand *et al.*, 2019). GPCRs located in SMC membranes play the role of mechanoreceptors (Chen *et al.*, 2020) and stimulation of these GPCRs can lead to vasocontraction (Audebrand *et al.*, 2019). The study in the previous chapter investigated the effects of doxorubicin on vascular function through GPCR-mediated vasoconstriction in the coronary LAD artery. Doxorubicin was associated with an altered vascular function of coronary arteries through the vasoconstriction mediated by endothelin ET_A and ET_B, serotonin 5-HT_{1B} and thromboxane prostanoid TP GPCR receptors. However, the intracellular pathways leading to the doxorubicin-induced dysfunction of the vascular tone of coronary vessels are yet to be investigated and identified. ET-1 activates the two endothelin GPCR receptor subtypes: ET_A receptor and ET_B receptor, in the cardiovascular system (Wang *et al.*, 2018). ET_A receptors are located in SMCs and are mainly responsible for VSMC vasoconstriction (Bacon and Davenport, 1996), while ET_B receptors are located

predominantly in EC, where ET_B receptors are responsible for vasodilatation (Tykocki *et al.*, 2009). Furthermore, ET_B receptors located in SMCs are involved in vasocontraction (Haynes *et al.*, 1995). Similarly, both ET_A and ET_B receptors, located in rodent SMCs, induced VSMC vasocontraction, while ET_B receptors, located predominantly in ECs, are responsible of vasodilatation. The ET-1 binding to ET_A receptors activates the G protein of the Gq/11 and G12/13 proteins (Gohla *et al.*, 2000), while ET-1 binding to ET_B receptors activates the G protein of the Gi and Gq/11 proteins (Cramer *et al.*, 2001), leading to contractile response and cell proliferation of VSMCs (Schneider *et al.*, 2007). The activation of these G proteins activates ERK 1/2 pathways, involved in VSMC proliferation, mainly through ET_A receptors (Chen *et al.*, 2009). In SMCs the serotonin GPCR receptor 5-hydroxytryptamine 1B (5-HT_{1B}) receptor is involved in vasoconstriction of human coronary arteries (Nilsson *et al.*, 1999b). Furthermore, the 5-HT_{1B} receptors are up-regulated in atherosclerotic rabbit coronary arteries (Ishida *et al.*, 2001). Specific binding to 5-HT_{1B} receptors activates the G protein of the Gαi/o subunit leading to the selective phosphorylation of ERK 1/2 (Liu *et al.*, 2019). Thromboxane prostanoid (TP) GPCR receptor mediates platelet activation, vasoconstriction, EC activation and SMC proliferation (Capra *et al.*, 2014, Chen, 2018). TP receptors are localised in human VSMC (Morinelli *et al.*, 1990), where TP receptors induced vasocontraction (Norel, 2007). Similarly, the TP receptor activation in rodent SMC leads to vasoconstriction of aortic vessels (Rolin *et al.*, 2007). TP receptors activate the G protein of the Gq/11 subunit leading to the ERK activation through a PKC-regulated mechanism (Gao *et al.*, 2001).

Some studies investigated the potential use of targeting GPCRs as preventive cardioprotective agents. The β-adrenergic receptor blockers reduced the generation of ROS, apoptosis of cardiomyocytes (Oliveira *et al.*, 2005) and have vasodilatory effects (Mason *et al.*, 2005). Other GPCR blockers studied as potential preventive cardioprotective agents include Angiotensin-converting enzyme inhibitors (ACEI) and angiotensin receptor blockers (ARB) (Bosch *et al.*, 2013). Doxorubicin-induced cardiotoxicity remains an important issue associated with cancer therapy, with no efficient and robust adjuvant therapy options available. In-depth studies of the GPCRs' involvement and function during cardiotoxicity could lead to potentially identifying novel and significant adjuvant therapy options to combat cardiotoxicity as a result of doxorubicin therapy. Interestingly, Yu *et al.et al.* (2021) showed that sorafenib (3 mg/L), a VEGF-targeting agent, was promoting vasoconstriction through the up-regulation of ET_B-mediated vasocontractile response and ET_B receptor expression in 24 hrs-incubated rat mesenteric arteries and 10 μM U0126 alleviated the elevated ET_B vasoconstriction (Yu *et al.*, 2021), which highlight the potential cardioprotective effect of U0126 against doxorubicin-induced cardiotoxicity.

The mitogen-activated protein kinases (MAPKs) are involved during the regulation process of vascular GPCRs expression (Kacimi and Gerdes, 2003). The ERK cascade, one of the key MAPK signalling pathways, was the first MAPK discovered and is known to get preferentially activated by shear stress or growth factor stimulation (Boulton *et al.*, 1991). The ERK 1/2 pathway is activated by various extracellular stimulation and by internal processes (Shaul and Seger, 2007) through the activation of receptor tyrosine kinase (RTK) (Sudhesh Dev *et al.*, 2021) or GPCRs (Liu *et al.*, 2019). The ERK cascade is initiated by Ras, a small G protein, which recruits and activates Raf kinases in the cytosol. Raf activates the MEK 1/2 by phosphorylation. MEK 1/2 promotes the dual phosphorylation of ERK 1/2 for ERK activation and has the role of cytoplasmic anchor protein for ERK. Activation of ERKs promotes the phosphorylation and activation of transcription factors, such as activator protein-1 (AP-1) (Whitmarsh and Davis, 1996) and nuclear factor kappa-light-chain-enhancer of activated B cells (NF-κB) (Xu *et al.*, 2008) in SMC. The ERK cascade regulates cell proliferation, differentiation, survival and apoptosis (Shaul and Seger, 2007). In the SMC, AP-1 and NF-κB transcribe the GPCR genes in the nucleus. The GPCR mRNA is then translated in the cytosol and afterwards exported to the cell membrane (Kacimi and Gerdes, 2003).

Studies have investigated the MAPK signalling as a potential cardioprotective target of doxorubicin-induced cardiotoxicity. A recent study investigates the potential cardioprotective effect of a potent synthetic flavonoid with anti-oxidative properties called 3',4'-dihydroxyflavonol (DiOHF) at a concentration of 6 mg/kg (daily for 10 days from 3 days before doxorubicin treatment) in *in vivo* experiments, and 10 µM of DiOHF in the *in vitro* model administrated either 2 hrs before (preventive effect) or 2 hrs after (therapeutic effect) the doxorubicin incubation/treatment (for 24 hrs incubation in total). Doxorubicin cardiotoxicity was induced *in vivo* by doxorubicin injection (20 mg/kg by cumulative intraperitoneal injection (i.p.)) to BALB/c mice, or by incubating H9C2 cells with 1 µM doxorubicin along with DiOHF. This study showed that DiOHF inhibits the ROS release, stabilises the mitochondrial function and reduces the apoptosis through ERK1 signalling activation leading to the suppression and reversion of doxorubicin-induced cardiotoxicity (Chang *et al.*, 2019). Another study showed that the natural fatty acid ethanolamide oleylethanolamide (OEA) could improve ventricular remodelling and elevated cardiac function by inhibiting doxorubicin-induced apoptosis through activation of Ras/Raf-1/MEK/ERK signalling pathway using an *in vivo* rat model. They administered 3 doses of 3 mg/kg of doxorubicin by intravenous injection (i.v.) every other day after an overnight fasting to induce the cardiomyopathy and studied the cardioprotective effect of OEA by either (i) injecting 5 mg/kg of OEA (twice daily for 3 doses) by i.p. prior to the doxorubicin injection or (ii) the therapeutic effect of OEA by injected 5 mg/kg of OEA (every other day for 7 days) during the 4th week after the doxorubicin treatment (Su *et al.*, 2006).

U0126 is a small molecule MEK 1/2 inhibitor. U0126 acts as a non-competitive inhibitor of MEK 1 (IC_{50} = 72nM) and MEK 2 (IC_{50} = 58nM) (Duncia *et al.*, 1998). Interestingly, U0126 shows a cardioprotective effect against I/R by attenuating the I/R-induced apoptosis and autophagy myocardium in C57BL/6J mice (Wang *et al.*, 2016). A study investigated the potential cardioprotective effect of U0126 against cerebral ischaemia with an *in vivo* rat subarachnoid haemorrhage model induced by a surgical procedure and showed that the U0126 treatment might be an interesting adjuvant therapy to treat the late cerebral ischaemia by inhibition of the MEK/ERK pathway (Povlsen and Edvinsson, 2015). U0126 confers protection against cerebral vascular injury of isolated cerebral arteries, even when U0126 was administrated 6 hrs after the vascular injury (Sandhu *et al.*, 2010). Sandhu *et al.et al.* (2010) used rat 48 hrs-incubated cerebral arteries model, which mimics vascular injury mechanisms, to investigate the potential cardioprotective effect of U0126. Their data showed that U0126's optimal dose to protect the isolated cerebral arteries was 10 μM and U0126 attenuates the ET_B, 5-HT_{1B} and TP receptors elevated vasocontractile responses in 48 hrs-incubated cerebral arteries compared to fresh cerebral arteries, even when U0126 is administrated 6 hrs after the initiation of the incubation.

Aims of the study in this chapter:

Doxorubicin-induced cardiotoxicity will be investigated in LAD arteries, co-administered with the MEK 1/2 inhibitor U0126 to understand the role of MEK/ERK 1/2 involvement during the doxorubicin-induced vascular dysfunction effect on the endothelin ET_A and ET_B, serotonin 5-HT_{1B} and thromboxane prostanoid TP GPCR receptors.

The functional, phenotypic, and genotypic changes on LAD arteries were investigated in vehicle and doxorubicin LAD arteries with or without U0126.

The aims of the current study were to investigate:

(1) The effect of U0126 on doxorubicin-induced vasotoxicity through the different studied receptors on incubated LAD arteries with vehicle or doxorubicin treatment.
(2) The effect of doxorubicin on mRNA levels of the specific GPCRs
(3) The effects of doxorubicin on GPCRs expression on LAD vessels.

5.2. Materials and methods

5.2.1. Animal ethics

Male Sprague-Dawley rats (300 - 350g) were used during the experiments. The animals were purchased from Charles River (Margate, UK) and housed at the University of Warwick. Experiments were conducted in accordance with the Home Office Guidance on the Operation with Animals (Scientific Procedures Act 1986; The Stationary Office, London, UK) and were approved by the Ethics Committee of Coventry University.

5.2.2. Materials

Doxorubicin hydrochloride was purchased from Tocris Biosciences (Bristol, UK) and was dissolved in Reverse Osmosis (RO) water with a final stock concentration of 1 mM.

Serotonin hydrochloride, carbachol, sarafotoxin S6c, endothelin-1, 9,11-dideoxy-11α,9α-epoxymethanoprostaglandin $F_{2\alpha}$ (U46619), 5-carboxamidotryptamine maleate salt were purchased from Sigma-Aldrich (Merck KGaA, US). U46619 was dissolved in methyl acetate with a final stock concentration of 3 mM. All the other drugs were dissolved in RO water. Serotonin hydrochloride and carbachol had a final stock concentration of 10 mM. Sarafotoxin 6c and endothelin-1 had a final stock concentration of 0.1 mM. U46619 and 5-carboxamidotryptamine had a final stock concentration of 27 mM and 30 mM, respectively. The MEK 1/2 inhibitor U0126 was purchased from EMD Millipore Corporation (Merck, US) and dissolved in Dimethylsulfoxide (DMSO) with a final stock concentration of 2 mM. DMSO was purchased from Sigma-Aldrich (Merck KGaA, US). All drugs were aliquoted in suitable volumes and stored at -20 °C.

Dulbecco's Modified Eagle Medium, DMEM (1 g/L D-Glucose, 4mM L-Glutamine, 0.11 g/L Sodium pyruvate) and Antibiotic-antibiotic (10,000 units/mL of penicillin, 10,000 µg/mL of streptomycin, and 25 µg/mL of Gibco Amphotericin B) were purchased from ThermoFisher Scientific (Massachusetts, US). All reagents used to prepare the KH buffers for the myography experiments were purchased from Fisher Bioreagents (Fisher Scientific, US).

5.2.3. Isolated left anterior descending artery (LAD) preparation

Adult male Sprague-Dawley rats were ethically and humanely sacrificed, and LADs were rapidly dissected free, as described in section 2.3.2. The LAD was cut in 4 rings of approximatively 2 mm in length each (for myography) or in approximatively 4 mm (for PCR and immunohistochemistry). The rings were divided into eight groups and incubated in DMEM low glucose media at 37 °C and

humidified with 5 % CO_2 and 95 % O_2 for 24 hrs. The experiment was first conducted with the addition of 10 µM of U0126 or 0.5 % of DMSO in media and divided into four groups:

- Vehicle group (containing 0.5 % of DMSO)
- 10 µM U0126 group (containing 0.5 % of DMSO)
- 0.5 µM doxorubicin group (containing 0.5 % of DMSO)
- 0.5 µM of doxorubicin and 10 µM of U0126 group (containing 0.5 % of DMSO)

Afterwards, the experiment was optimised by the addition of 5 µM of U0126 or 0.25 % of DMSO, and the following groups were included:

- Vehicle group (containing 0.25 % of DMSO)
- 5 µM U0126 group (containing 0.25 % of DMSO)
- 0.5 µM doxorubicin group (containing 0.25 % of DMSO)
- 0.5 µM of doxorubicin and 5 µM of U0126 group (containing 0.25 % of DMSO)

Please note that the vehicle group in this chapter refers to DMEM added DMSO (either 0.25 % or 0.50 %), contrary to DMEM treated with water as in the previous chapter.

After 24 hrs of incubation, the vessels used for Real-Time PCR were submerged in 200 µL RNA protect reagent and stored in -20 °C freezer. Vessels for immunohistochemistry were fixed in Cellpath™ OCT Embedding Matrix (Thermofisher, USA) and stored in -80 °C freezer.

5.2.4. Myography protocol

Vessels were mounted in Ca^{2+} free KH buffer on the myograph after 24 hrs of incubation, and afterwards, the buffer was changed to Na^+ KH and the vessels were stabilised for 1 hr (see figure 5-1).

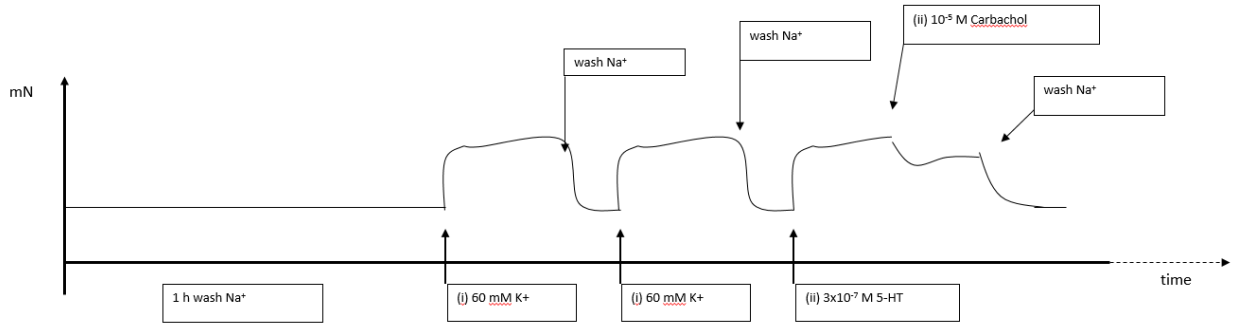

Figure 5-1: Experimental protocol to study vascular contractility and dilatory capacity of LAD vessels. Na+ = Na^+ KH, K+ = K^+ KH, 5-HT = serotonin.

A pre-tension in the range of 1.16mN/mm to 1.52mN/mm was applied during this stabilisation step (Ping *et al.*, 2014). After the stabilisation period, the vessels were exposed to a 60 mM K^+ KH to

measure the maximum vasocontraction and vessels with a K^+ KH vasocontractile response below 1 mN were excluded. Vessels were washed twice with Na^+ KH for 15 min and a second 60 mM K^+ KH contraction was recorded and used as reference for the study of the GPCR agonist mediated dose-response curves). Vessels were washed with Na^+ KH with 15 min intervals until the vascular tension came back to the baseline level (minimum 30 min). To measure vasodilatory capacity the vessels were pre-contracted with 3. 10^{-7} M serotonin (5-HT) followed by applying 10^{-5} M carbachol. Vessels were washed with Na^+ KH with 15 min intervals until the vascular tension came back to the baseline level.

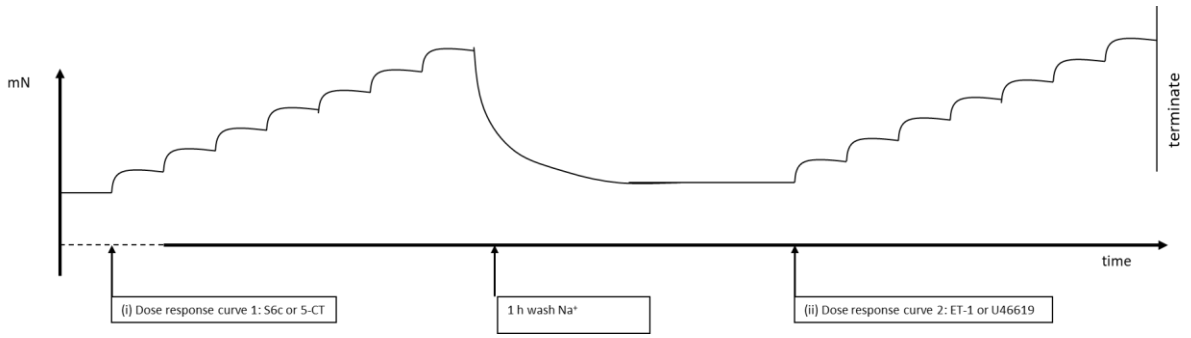

Figure 5-2: Experimental protocol to study dose-response curve of specific GPCR agonists. S6c = sarafotoxin 6c, the agonist of ET_B receptors; 5-CT = 5-carboxyamidotryptamine, the agonist of 5-HT_{1B} receptors, ET-1 = endothelin-1, the agonist of ET_A and ET_B receptors; U46619, the agonist of TP receptors

Once the contractile and dilatory capacity of the vessels was measured - and thus established the function and viability of the vessels - the dose-response curve can be measured. As seen in Figure 5-2, cumulative doses of the specific agonists will be added, starting from the lowest dose and then increased in half-log increments to the highest dose. The segments were either stimulated with (i) ET_B receptor agonist sarafotoxin 6c (S6c), from 10^{-14} M to $10^{-7.5}$ M, followed by Na^+ KH washing with 15-min intervals until the vascular tension reverted to the baseline level, where after the second dose-response curve was measured by applying ET_A and ET_B receptor agonist endothelin-1 (ET-1), from 10^{-14} M to $10^{-7.5}$ M, or by stimulation with (ii) 5-HT_{1B} receptor agonist 5-carboxamidotryptamine (5-CT), from 10^{-12} M to $10^{-5.5}$ M, followed by Na^+ KH washing with 15 min intervals until the vascular tension reverted to the baseline level, where after the second dose-response curve was measured by applying thromboxane A2 receptor agonist U46619, from 10^{-12} M to $10^{-6.5}$ M.

5.2.5. Real time PCR protocol

Total cellular RNA was extracted with the RNeasy protect liquid mini kit following the supplier's instructions. LAD arteries were removed from RNA protect reagent and homogenised in RLT buffer containing 0.01 % β-mercaptoethanol using a KIA Ultra-Turrax homogeniser (Sigma-Aldrich, USA). The samples were centrifuged for 3 min at full speed. The supernatant was mixed with 1 volume of ethanol 70 % and transferred to an RNeasy spin column placed in a 2 mL collection tube. After centrifugation for 15 sec at room temperature (RT) at 8,000 xg, total cellular RNA was fixed on the membrane in RNeasy spin column and the flow-through was discarded. Washing buffer RW1 was added to the RNeasy spin column and samples were centrifuged for 15 sec at room temperature at 8,000 xg. The second washing buffer RPE was added to the spin column and centrifuged for 15 sec at room temperature at 8,000 xg. The last washing step was with RPE buffer and samples were centrifuged for 2 min at room temperature at 8,000 xg. RNAse-free water was added in the RNeasy spin column and samples were centrifuged for 1 min at room temperature at 8,000 xg to elute the RNA. Total RNA amount and purity were determined with NanoDrop™ One/OneC Microvolume UV-Vis Spectrophotometer (ThermoFisher, USA).

Reverse transcription of total cellular RNA to cDNA was performed with Superscript™ IV VILO Master Mix (ThermoFisher, US) in Eppendorf® Mastercycler® Nexus Thermal Cyclers (Merck, USA). Total cellular RNA was mixed with SuperScript IV™ VILO Master Mix in a 20 µL reaction volume on ice. The mix was incubated at 25 °C for 10 min to anneal primers. Afterwards, it was incubated at 50 °C for 10 min to reverse transcribe RNA. Finally, the mix was incubated at 85 °C for 5 min to inactivate the enzyme. The cDNA obtained was diluted in RNAse-free water to have a cDNA concentration of 1 ng/µL.

Real-Time PCR was performed in a Real-Time PCR instrument QuantStudio 7 (ThermoScientific, USA) with the PowerTrack SYBR Green Master Mix (1X) with cDNA (at a final concentration of 0.5 ng/µL), with the forward and reverse primers (500 nM), and with RNAse-free water to a final reaction volume of 20 µL. Negative control was added in all experiments. A yellow buffer was mixed with the cDNA to facilitate the plate loading. Glyceraldehyde 3-phosphate dehydrogenase (GAPDH) mRNA was used as endogenous control. Specific primers of ET_A and ET_B receptors, 5-HT_{1B} receptors, TP receptors, EF-1 and GAPDH were designed (Table 2-1, in 2. General Methods chapter, section 2.2.3). Primers were resuspended in RNAse-free water to obtain a stock concentration of 100 mM and then, diluted to obtain a work concentration of 10 mM. Once each reaction was loaded in each well of a 96-well plate (ThermoScientific, UK), the Real-Time PCR instrument was run according to the company protocol. First, the enzyme was activated at 95 °C for 2 min. Then, the two next steps were processed during 40 cycles. The cDNA was denatured at 95 °C for 15 sec and primers were annealed and extended at 60 °C for 1 min. A melt curve was obtained, immediately after the real-time PCR, in three steps to check for

nonspecific amplification. Step 1 was at 95 °C for 15 sec, with a ramp rate of 1.6 °C/sec. Step 2 was at 60 °C for 1 min, with a ramp rate of 1.6 °C/sec. Finally, step 3, also named dissociation, was at 95 °C for 15 sec, with a ramp rate of 0.075 °C/sec.

5.2.6. Immunohistochemistry protocol

Frozen arteries were cryosectioned in 10 µm sections using the cryostat OTF5000 (Bright instruments, Huntingdon, UK). Sections were collected onto superfrost plus adhesion slides and stored at - 80 °C until immunohistochemistry staining. Thawed sections were fixed in – 20 °C Acetone for 20 min, dried for 5 min at room temperature (RT) and rehydrated in PBS containing 0.25 % of Triton X-100 (PBST) at room temperature for 3 x 5 min. Then, the sections were blocked in PBS containing 5 % donkey serum for 1 hr at room temperature. Sections were incubated overnight at 4 °C with primary antibodies, diluted in PBST containing 1 % Bovine Serum Albumin (BSA) and 3 % donkey serum. Sections were double immunostained with primary antibodies of one protein of interest: ET_A (1: 1000), ET_B (1: 1000), 5-HT_{1B} (1: 1000), TP (1: 500) or pERk (1: 500) and with primary antibodies of actin (1: 500) used as reference. Sections were rinsed with PBS at room temperature for 2 x 15 min. Finally, sections were incubated with secondary antibodies, diluted in PBST containing 1 % Bovine Serum Albumin (BSA) and 3 % donkey serum for 1 hr at room temperature. Sections were double immunostaining with both secondary antibodies: donkey anti-rabbit IgG Alexa Fluor 488 GREEN (1: 500) and donkey anti-mouse IgG Alexa Fluor 594 RED (1: 500). Negative controls were identified by omitting the primary antibodies and following the same protocol. Please note that autofluorescence was observed due to the internal elastic lamina and not because of any unspecific staining.

The Immunofluorescence was visualised with a confocal microscope Eclipse Ti2 (Nikon Instruments Inc.; Tokyo, Japan) and photographed with an attached Nikon Orca-Flash4.0v3 camera. Images were analysed and quantified with the AR package of NIS-elements software. The wavelengths and pinhole size were fixed with Fresh group's sections and used on the other groups. The fluorescence intensity was measured on the entire circumference of the vessel section, named the ROI (Region of Interest) to obtain the ROI mean intensity.

5.2.7. Statistical analysis

All data are expressed as mean ± S.E.M. and n refers to the number of animals used.

Contractile responses to agonists in each vessel were expressed as percentage of the K^+ KH-induced contraction. Vasocontractile responses were analysed with two-way analysis of variance (ANOVA) with Bonferroni's post-hoc test. "E_{max}" values represent the maximal contractile response elicited by

the agonist and are generated by the software Graph-Pad Prism 9. C_{max} values represent the contraction obtained at the highest agonist dose and are applied when the "E_{max}" couldn't be determined due to stock concentration constraints. The "pEC_{50}" values represent the negative logarithm of the agonist concentration that produces 50 % of the maximal contractile effect and are generated with Graph-Pad Prism 9, based on "E_{max}" value. The calculations were carried out using Graph-Pad Prism 9 (GraphPad Software, La Jolla, USA). "E_{max}" and "pEC_{50}" values were statistically analysed with Kruskal-Wallis test, using GraphPrism software.

The mRNA data were analysed using the comparative cycle threshold (ΔCT) method (Hansen-Schwartz *et al.*, 2002). The CT values of GAPDH was used as reference gene to quantify the relative amount of ET_A, ET_B, 5-HT_{1B} and TP receptors mRNA. The relative quantification of the GPCRs mRNA compared to CT values of reference genes was obtained by using the formula: $\frac{X_0}{R_0} = 2^{CT_X - CT_{RX}}$, where X_0 is the initial amount of target mRNA, R0 is the initial amount of reference mRNA, CT_X is the CT value of the target mRNA and CT_R is the CT value of the reference mRNA (Sandhu *et al.*, 2010). The mRNA expression was analysed with Kruskal-Wallis's test for multiples comparisons and protein expression was analysed with one-way analysis of variance (ANOVA) with Fisher's post-test used for multiples comparisons.

5.3. Results

5.3.1. Endothelin ET_B receptor

5.3.1.1. Wire-myography: ET_B receptors-mediated contraction

The endothelin ET_B receptor specific agonist sarafotoxin 6c was used to investigate the effect of doxorubicin on ET_B receptor-mediated contraction in the presence or absence of the MEK 1/2 inhibitor U0126. The dose-response curves obtained by the ET_B receptor-mediated contraction were monophasic after treatment with 0.25 % DMSO vehicle and 5 µM U0126, as shown in Figure 5-3, while they were biphasic in the previous chapter in the absence of 0.25 % DMSO and 5 µM U0126 incubation, as shown in Figure 9-1. The S6c-induced contraction values are given as percentage of the maximal contractile response induced by 60 mM K^+ KH buffer. The "E_{max}" and "pEC_{50}" values are given in Table 5-1. The difference of contraction between the groups and the p values are given in Table 9-3 in Appendices.

5.3.1.1.1. ET_B-mediated contraction in 0.5 µM of doxorubicin with and without 5 µM of U0126 (containing 0.25 % of DMSO)

- *The effect of 0.5 µM doxorubicin treatment on ET_B-mediated contraction in 24-hr-incubated LAD vessels (containing 0.25 % DMSO):*

The ET_B-mediated contraction was reduced at the three highest concentrations of S6c: a reduction of 50 % for $10^{-8.5}$ M (62.70 ± 12.10 %, $p < 0.0001$) and $10^{-7.5}$ M (C_{max} = 86.09 ± 12.97 %, $p < 0.0001$) and 60 % reduction for 10^{-8} M (80.25 ± 12.88 %, $p < 0.0001$) on 0.5 µM doxorubicin vessels (n = 8 - 9), when compared to vehicle vessels (n = 7 - 8; 112.81 ± 10.52 % at $10^{-8.5}$ M, 135.75 ± 7.85 % at $10^{-7.5}$ M (C_{max}) and 140.15 ± 10.31 % at 10^{-8} M), as observed in Figure 5-3. The 0.5 µM doxorubicin incubation induced a reduction of the ET_B-mediated contraction of 0.5 µM doxorubicin-treated LAD arteries ("E_{max}" = 93.3 ± 7.2 %, $p < 0.0001$), when compared to vehicle LAD arteries ("E_{max}" = 151.5 ± 7.1 %). The "pEC_{50}" value of S6c-induced contraction of 0.5 µM doxorubicin-treated LAD vessels ("pEC_{50}" = $10^{-8.69}$ M) was not altered compared to the vehicle-treated LAD vessels ("pEC_{50}" = $10^{-8.73}$ M).

- *The effect of 5 µM U0126 treatment on ET_B-mediated contraction in 24-hr-incubated LAD vessels (containing 0.25 % DMSO):*

The incubation of 5 µM U0126 of vehicle-treated LAD vessels did not alter the ET_B-mediated contraction of 5 µM U0126-incubated vehicle LAD vessels (n = 8 - 9) when compared to U0126 naïve vehicle-treated LAD vessels (n = 7 - 8), as observed in Figure 5-3. The "E_{max}" and "pEC_{50}" values of 5 µM U0126-incubated vehicle LAD vessels ("E_{max}" = 151.17 ± 9.14 %, "pEC_{50}" = $10^{-8.73}$ M) were not altered, when compared to U0126 naïve vehicle-treated LAD vessels ("E_{max}" = 151. 54 ± 7.11 %, "pEC_{50}" = $10^{-8.87}$ M), as shown in Table 5-1.

- *The effect of 0.5 µM doxorubicin treatment on ET_B-mediated contraction in the presence of 5 µM U0126 in 24-hr-incubated LAD vessels (containing 0.25 % DMSO):*

The ET_B-mediated contraction was reduced at the three highest concentrations of S6c: a reduction of 52 % for $10^{-8.5}$M (61.2 ± 9.7 %, $p < 0.0001$), of 72 % for 10^{-8}M (68.2 ± 9.2 %, $p < 0.0001$) and of 65 % at $10^{-7.5}$M (C_{max} = 70.6 ± 8.7 %, $p < 0.0001$) on doxorubicin-treated LAD vessels (n = 8 - 9), when compared to vehicle-treated LAD vessels (n = 7 - 8; $10^{-8.5}$ M: 112.81 ± 10.52 %, 10^{-8} M: 140.15 ± 10.31 % and $10^{-7.5}$ M (C_{max}): 135.75 ± 7.85 %), as observed in Figure 5-3. The 5 µM U0126 incubation induced a reduction of the ET_B-mediated contraction of 0.5 µM doxorubicin-treated LAD vessels ("E_{max}" = 75.25 ± 4.77 %, $p < 0.0001$), when compared to U0126 naïve vehicle-treated LAD vessels ("E_{max}" = 151. 54 ± 7.11 %), while the "pEC_{50}" values were not altered (Table 5-1).

The incubation with 5 µM U0126 did not alter the ET_B-mediated contraction of 0.5 µM doxorubicin-treated LAD vessels (n = 8 - 9) when compared to U0126 naïve 0.5 µM doxorubicin-treated LAD vessels (n = 8 - 9). The inhibition effect of U0126 showed a tendency towards lowering the maximal ET_B-mediated contraction of 0.5 µM doxorubicin-treated LAD vessels ("E_{max}" = 75.25 ± 4.77 %), compared to U0126 naïve 0.5 µM doxorubicin-treated LAD vessels ("E_{max}" = 93.28 ± 7.22 %), but the reduction is not statistically significant. The "pEC_{50}" of 0.5 µM doxorubicin-treated LAD vessels was unaltered by the 5 µM U0126 incubation (Table 5-1).

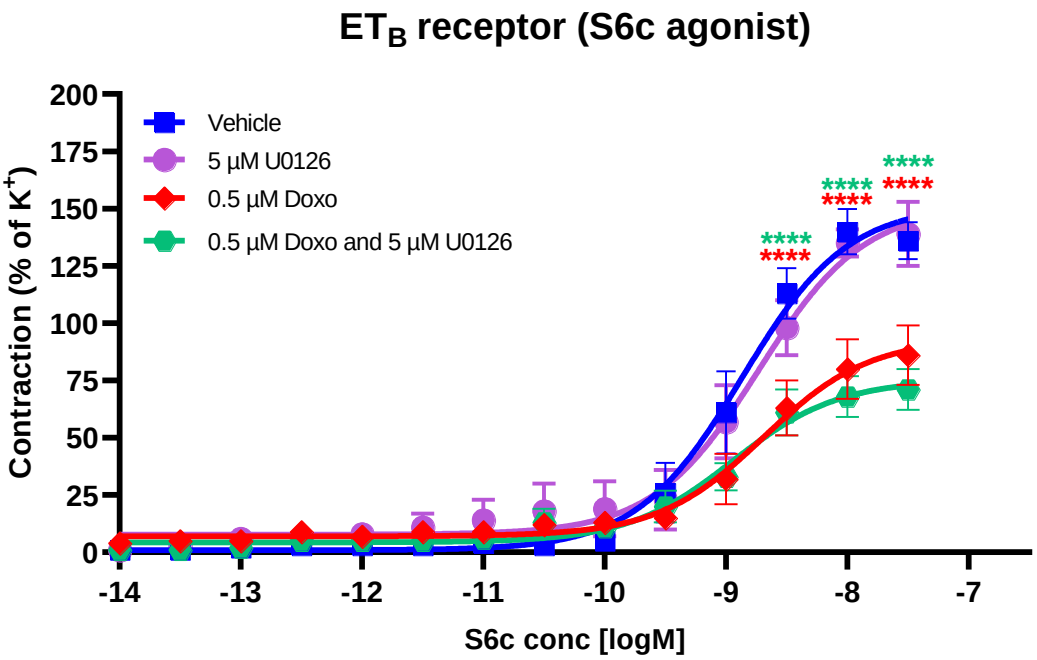

Figure 5-3: Vasocontractile response to the cumulative application of sarafotoxin 6c (S6c) (ET_B receptor agonist) normalised to 60 mM K^+ KH-induced vasocontraction in rat LAD arteries, after 0.25 % DMSO or 5 µM U0126 incubation. Vehicle group (containing 0.25 % DMSO; n = 7 - 8), 0.5 µM Doxorubicin group (containing 0.25 % DMSO; n = 8 - 9), 0.5 µM doxorubicin and 5 µM U0126 (n = 8 - 9) and 5 µM U0126 group (n = 8 - 9). S6c = sarafotoxin 6c, Doxo = doxorubicin, DMSO = Dimethyl sulfoxide. Contractile responses were compared to vehicle group using Two-way ANOVA and Bonferroni's test (**** = $p < 0.0001$) and compared to doxorubicin group using one-way ANOVA and Bonferroni's test.

Table 5-2: C_{max}, "E_{max}" and "pEC_{50}" values of vehicle or 0.5 µM doxorubicin incubated LAD arteries with DMSO or MEK 1/2 inhibitor U0126: 0.25 % DMSO and 5 µM U0126 incubation. Values given for all agonist experiments and as mean ± S.E.M. N values represent the total amount of animals used. The "E_{max}" and "pEC_{50}" values of the different groups are compared to the vehicle-treated LAD vessels (with 0.25 % DMSO) with ANOVA and Dunnett's post-hoc test, while C_{max} is compared using two-way ANOVA with Bonferroni's post-hoc test: ** = $p < 0.01$, *** = $p < 0.001$.

Groups	*N*	*S6c C_{max}*	*S6c "E_{max}"*	*"pEC_{50}"*
Vehicle	7-8	135.75 ± 7.85 %	151. 54 ± 7.11 %	8.87 ± 0.09
0.5 µM Doxorubicin	8-9	86.09 ± 12.97 % ****	93.28 ± 7.22 % ***	8.69 ± 0.15
0.5 µM Doxorubicin and 5 µM U0126	8-9	70.62 ± 8.71 % ****	75.25 ± 4.77 % ***	8.94 ± 0.13
5 µM U0126	8-9	139.08 ± 13.95 %	151.17 ± 9.14 %	8.73 ± 0.11

5.3.1.1.2. ET_B-mediated contraction in 0.5 µM of doxorubicin with and without 10 µM of U0126 (containing 0.5 % of DMSO)

- *The effect of 0.5 µM doxorubicin treatment on ET_B-mediated contraction in 24-hr-incubated LAD vessels (containing 0.5 % DMSO):*

ET_B-mediated vasocontraction of 0.5 µM doxorubicin-treated LAD vessels (n = 10 – 11) was significantly elevated (29 – 32 % increase) from $10^{-11.5}$ M (34.77 ± 5.55 %, p = 0.0287) to 10^{-11} M (38.57 ± 5.88 %, p = 0.016) when compared to vehicle-treated LAD vessels (n = 7 – 8; $10^{-11.5}$ M: 5.56 ± 2.14 % %, 10^{-11} M: 7.42 ± 2.80 %). Conversely, the ET_B-mediated contraction of 0.5 µM doxorubicin-treated LAD vessels (n = 10 - 11) was reduced at the three highest concentrations of S6c: a reduction of 59 % at $10^{-8.5}$ M (85.65 ± 8.52 %, p < 0.0001), 66 % at 10^{-8} M (103.72 ± 8.31 %, p < 0.0001) and 67 % at $10^{-7.5}$ M (C_{max} = 104.49 ± 8.15 %, p < 0.0001), when compared to vehicle-treated LAD vessels (n = 7 - 8; $10^{-8.5}$ M: 144.94 ± 11.83 %, 10^{-8} M: 169.79 ± 7.98 % and $10^{-7.5}$ M (C_{max}): 170.69 ± 7.82 %) (Figure 5-3). The 0.5 µM doxorubicin incubation induced a reduction of the ET_B-mediated contraction of doxorubicin-treated LAD vessels ("E_{max}" = 108.5 ± 5.4 %, p < 0.0001) when compared to vehicle-treated LAD vessels ("E_{max}" = 180.2 ± 5.8 %). The "pEC_{50}" values of S6c-induced contraction of 0.5 µM doxorubicin-treated LAD vessels were not altered, compared to vehicle-treated LAD vessels (Table 5-2).

- *The effect of 10 µM U0126 treatment on ET_B-mediated contraction in 24-hr-incubated LAD vessels (containing 0.5 % DMSO):*

The 10 µM U0126 incubation of vehicle-treated LAD vessels decreased the ET_B-mediated contraction of 10 µM U0126-incubated vehicle LAD vessels (n = 7 - 8) by 41 % at $10^{-9.5}$ M (14.04 ± 3.46 %, p = 0.0012) and 44 % at 10^{-9} M (49.95 ± 10.40 %, p = 0.0003) when compared to LAD vessels with vehicle and 0.5 % DMSO (n = 7 - 8; $10^{-9.5}$ M: 55.49 ± 17.72 % and 10^{-9} M: 93.89 ± 18.47 %). The 10 µM U0126 incubation of vehicle-treated LAD vessels slightly right-shifted the second phase of the biphasic curve from a "$pEC_{50}2$" of $10^{-8.63}$ M (p = 0.0007) for the 10 µM U0126-incubated vehicle LAD vessels to a "$pEC_{50}2$" of $10^{-9.06}$ M for the U0126 naïve vehicle-treated LAD vessels. However, the 10 µM U0126 incubation did not alter the maximal ET_B-mediated contraction with a mean "E_{max}" of 189.6 ± 5.8 % for

10 µM U0126-incubated vehicle LAD vessels and a mean "E_{max}" of 180.2 ± 5.8 % for U0126 naïve vehicle-treated LAD vessels.

- *The effect of 0.5 µM doxorubicin treatment on ET_B-mediated contraction in the presence of 10 µM U0126 in 24-hr-incubated LAD vessels (containing 0.5 % DMSO):*

The 10 µM U0126 incubation reduced the ET_B-mediated vasocontraction of 0.5 µM doxorubicin-treated LAD vessels (n = 7 - 8) by 38 % to 124 % decrease from S6c $10^{-9.5}$ M (16.52 ± 4.49 %, p = 0.0016) to $10^{-7.5}$ M (C_{max} = 47.32 ± 15.19 %, p < 0.0001), when compared to U0126 naïve vehicle-treated LAD vessels (n = 10 - 11) from $10^{-9.5}$ M (55.49 ± 17.72 %) to $10^{-7.5}$ M (C_{max} = 170.69 ± 7.82 %), as shown in Figure 5-3. The 10 µM U0126 incubation of 0.5 µM doxorubicin-treated LAD vessels induced a reduction of the maximal ET_B-mediated contraction of 10 µM U0126-incubated doxorubicin LAD vessels ("E_{max}" = 53.0 ± 7.9 %, p < 0.0001) when compared to vehicle-treated LAD vessels ("E_{max}" = 180.2 ± 5.8 %). The two "pEC_{50}" values of 10 µM U0126-incubated doxorubicin LAD vessels were not altered compared to U0126 naïve vehicle-treated LAD vessels.

Furthermore, the 10 µM U0126 incubation of 0.5 µM doxorubicin-treated LAD vessels (n = 10 - 11) reduced the ET_B-mediated contraction by 29 % to 57 % at 10^{-11} M (10.20 ± 2.19 %, p = 0.0246) and from 10^{-10} M (41.78 ± 5.98 %, p < 0.05) to $10^{-7.5}$ M (C_{max} = 47.32 ± 15.19 %, p = 0.001), when compared to U0126 naïve 0.5 µM doxorubicin LAD vessels (n = 10 - 11) at 10^{-11} M (38.57 ± 5.88 %) and from 10^{-10} M (41.78 ± 5.98 %) to $10^{-7.5}$ M (C_{max} = 104.49 ± 8.15 %). The 10 µM U0126 incubation induced a reduction of the maximal ET_B-mediated contraction of 10 µM U0126-incubated 0.5 µM doxorubicin LAD vessels ("E_{max}" = 53.0 ± 7.9 %, p < 0.0001) when compared to U0126 naïve 0.5 µM doxorubicin-treated LAD vessels ("E_{max}" = 108.5 ± 5.4 %). The two "pEC_{50}" values of 10 µM U0126-incubated 0.5 µM doxorubicin LAD vessels were not altered compared to U0126 naïve 0.5 µM doxorubicin-treated LAD vessels.

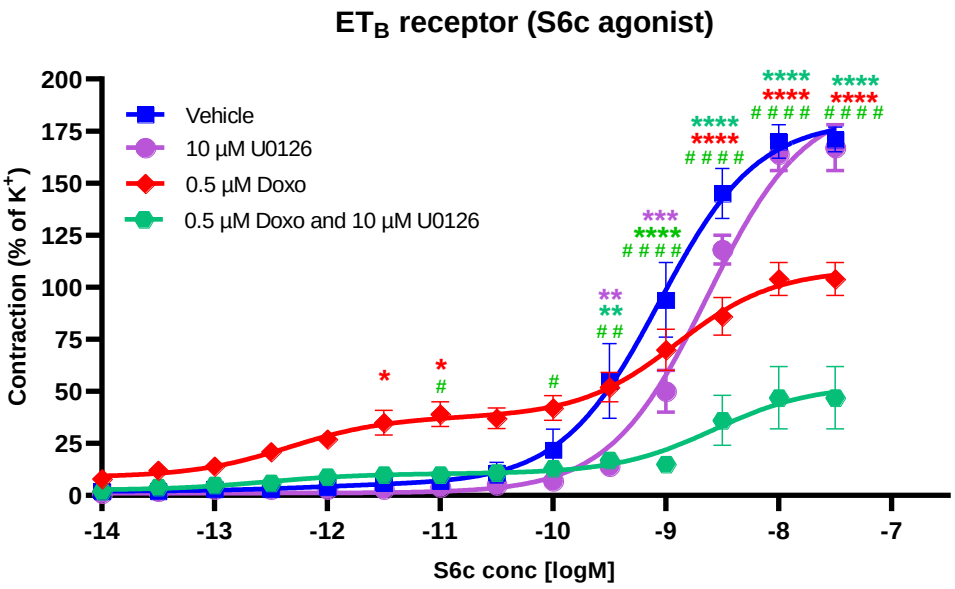

Figure 5-4: Vasocontractile response to the cumulative application of sarafotoxin 6c (S6c) (ET_B receptor agonist) normalised to 60 mM K^+ KH-induced contraction in rat LAD arteries, after 0.5 % DMSO or 10 µM U0126 incubation. Vehicle group (0.5 % DMSO; n = 7 - 8); 0.5 µM doxorubicin group (0.5 % DMSO; n = 10 - 11), 0.5 µM Doxorubicin and 10 µM U0126 (n = 7 - 8); 10 µM U0126 (n = 7 - 8). S6c = sarafotoxin 6c, DMSO = Dimethyl sulfoxide. Contractile responses compared to Vehicle group using two-way ANOVA and Bonferroni's test (* = p < 0.05, ** = p < 0.01, *** = p < 0.001, **** = p < 0.0001) and compared to 0.5 µM doxorubicin group using two-way ANOVA and Bonferroni's test: **#** = p < 0.05, **##** = p <0.01 and **####** = p < 0.0001.

Table 5-2: C_{max}, "E_{max}" and "pEC_{50}" values of vehicle or doxorubicin incubated LAD arteries with DMSO or MEK 1/2 inhibitor U0126: 0.5 % DMSO and 10 µM U0126 incubation. Values given for all agonist experiments and as mean ± S.E.M. N values represent the total amount of animals used. The "E_{max}" and "pEC_{50}" values of the different groups are compared to the vehicle-treated LAD vessels (with 0.25 % DMSO) with ANOVA and Dunnett's post-hoc test: *** = p < 0.001. The 10 µM U0126-incubated doxorubicin LAD vessels were compared to U0126 naïve doxorubicin-treated LAD vessels (with 0.5 % DMSO) with ANOVA and Dunnett's post-hoc test: ### = p < 0.001, while C_{max} is compared using two-way ANOVA with Bonferroni's post-hoc test: ** = p < 0.01, *** = p < 0.001.

Groups	*N*	*S6c C_{max}*	*S6c "E_{max}"*	*"$pEC_{50}1$"*	*"$pEC_{50}2$"*
Vehicle	7-8	170.69 ± 7.82 %	180.2 ± 5.8 %	12.25 ± 5.02	9.06 ± 0.09
0.5 µM Doxorubicin	10-11	104.49 ± 8.15 % ***	108.5 ± 5.4 % ***	12.34 ± 0.37	8.9 ± 0.16
0.5 µM Doxorubicin and 10 µM U0126	7-8	47.32 ± 15.19 % ***, ###	53.0 ± 7.9 % ***, ###	12.55 ± 1.54	8.57 ± 0.33
10 µM U0126	7-8	167.19 ± 10.65 %	189.6 ± 5.8 %	/	8.63 ± 0.05 ***

5.3.1.2. Real-Time PCR: quantification of ET_B receptor mRNA levels

Gene expression of the endothelin ET_B receptors was investigated in rat LAD arteries by Real-Time PCR. Negative controls were included for each studied gene. Endothelin ET_B receptors mRNA level was expressed as values relative to the endogenous gene, GAPDH and normalised to vehicle-incubated LAD vessels. Both figures, 5-5 (A) and 5-5 (B) showed the same tendency towards reduction or increase of ET_B receptors mRNA between the different groups, however, the significant difference was observed only in vessels after 24-hrs incubation containing 0.5 % DMSO or 10 µM U0126, as shown in figure 5-5 (B).

Figure 5-5 (A) showed the mRNA levels on LAD vessels incubated with 0.25 % DMSO or 5 µM U0126. The 5 µM U0126 treatment does not alter the ET_B receptors mRNA level of vehicle-treated LAD vessels (1.536 ± 0.265; n = 10) and 0.5 µM doxorubicin-treated LAD vessels (0.859 ± 0.165; n = 9) compared to U0126 naïve vehicle-treated LAD vessels (1.00 ± 0.150; n = 10) and U0126 naïve 0.5 µM doxorubicin-treated LAD vessels (0.708 ± 0.220; n = 9).

Figure 5-5 (B) showed the mRNA levels on LAD vessels incubated with 0.5 % DMSO or 10 µM U0126. Endothelin ET_B receptors mRNA level was down-regulated significantly from vehicle-treated LAD vessels (1.00 ± 0.163; n = 10) to 0.5 µM doxorubicin-treated LAD vessels (0.459 ± 0.123, p = 0.006; n = 10) and 10 µM U0126-treated doxorubicin LAD vessels (0.547 ± 0.087, p = 0.041; n = 10). 10 µM U0126-treated 0.5 µM doxorubicin LAD vessels (0.547 ± 0.087; n = 10) showed a tendency towards a reduction of ET_B receptors mRNA, compared to vehicle-treated LAD vessels (1.00 ± 0.163; n = 10), but there is no statistical difference.

(A) (B)

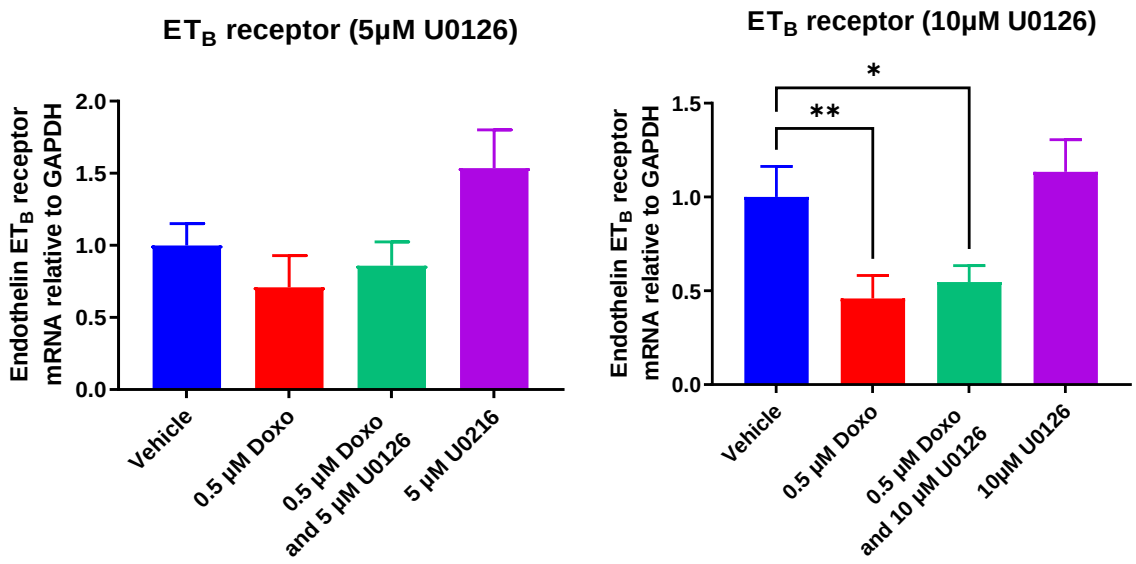

Figure 5-5: Real-Time PCR of ET_B receptors in LAD arteries with DMSO (Vehicle or Doxorubicin) or U0126 (Vehicle + U0126 or Doxorubicin + U0126). (A) Comparison of ET_B receptors mRNA levels on LAD arteries from Vehicle group (containing 0.25 % DMSO; n = 10), 0.5 µM doxorubicin group (containing 0.5 µM doxorubicin and 0.25 % DMSO; n = 9), 0.5 µM doxorubicin + 5 µM U0126 group (containing 0.5 µM doxorubicin and 5 µM U0126; n = 9) and 5 µM U0126 (containing 5 µM U0126; n = 10). **(B)** Comparison of ET_B receptors mRNA levels on LAD arteries from Vehicle group (containing 0.5 % DMSO; n = 10), 0.5 µM doxorubicin group (containing 0.5 µM doxorubicin and 0.5 % DMSO; n = 10), 0.5 µM doxorubicin + 10 µM U0126 group (containing 0.5 µM doxorubicin and 10 µM U0126; n = 10) and 10 µM U0126 (containing 10 µM U0126; n = 10). Doxo = doxorubicin, ET_B = endothelin B. Data are expressed as mean ± S.E.M. values relative to GAPDH mRNA levels (n = 10) and normalised to vehicle group. The groups were compared by multiple comparisons using one-way ANOVA Kruskal-Wallis' test (* = $p < 0.05$, ** = $p < 0.01$).

5.3.1.3. Immunohistochemistry: Quantification of ET_B receptor levels

The quantification of ET_B receptors expression on LAD vessels was obtained by measuring the ROI mean intensity and the intensity was normalised to 24 hrs vehicle-incubated LAD vessels from vehicle group.

Figure 5-6 (A) showed both vehicle-treated LAD vessels and doxorubicin-treated LAD vessels incubated with either 0.25 % of DMSO or 5 µM of U0126. The 5 µM U0126 incubation of vehicle-treated LAD vessels (1.150 ± 0.060; n = 4) showed an increase of ET_B receptors expression on LAD vessels when compared to the U0126 naïve vehicle-treated LAD vessels (1.00 ± 0.040, p = 0.048; n = 4). No significant difference was observed between the other groups. The 5 µM U0126 incubation of 0.5 µM doxorubicin-treated LAD vessels (1.00 ± 0.0277; n = 4) did not alter the ET_B receptors expression on LAD vessels, compared to U0126 naïve 0.5 µM doxorubicin-treated LAD vessels (1.035 ± 0.058; n = 4).

Figure 5-6 (B) showed the quantification of both vehicle-treated LAD vessels and 0.5 µM doxorubicin-treated LAD vessels incubated with either 0.5 % DMSO or 10 µM U0126. No statistical difference was observed between the different groups. The 10 µM U0126 incubation of vehicle-treated LAD vessels (1.117 ± 0.064; n = 4) did not alter the ET_B receptors expression compared to the U0126 naïve vehicle-treated LAD vessels (1.00 ± 0.088; n = 4). Similarly, 10 µM U0126 incubation of 0.5 µM doxorubicin-treated LAD vessels (1.016 ± 0.051; n = 4) did not alter the ET_B receptors expression compared to the U0126 naïve 0.5 µM doxorubicin-treated LAD vessels (1.098 ± 0.184; n = 4).

(A)

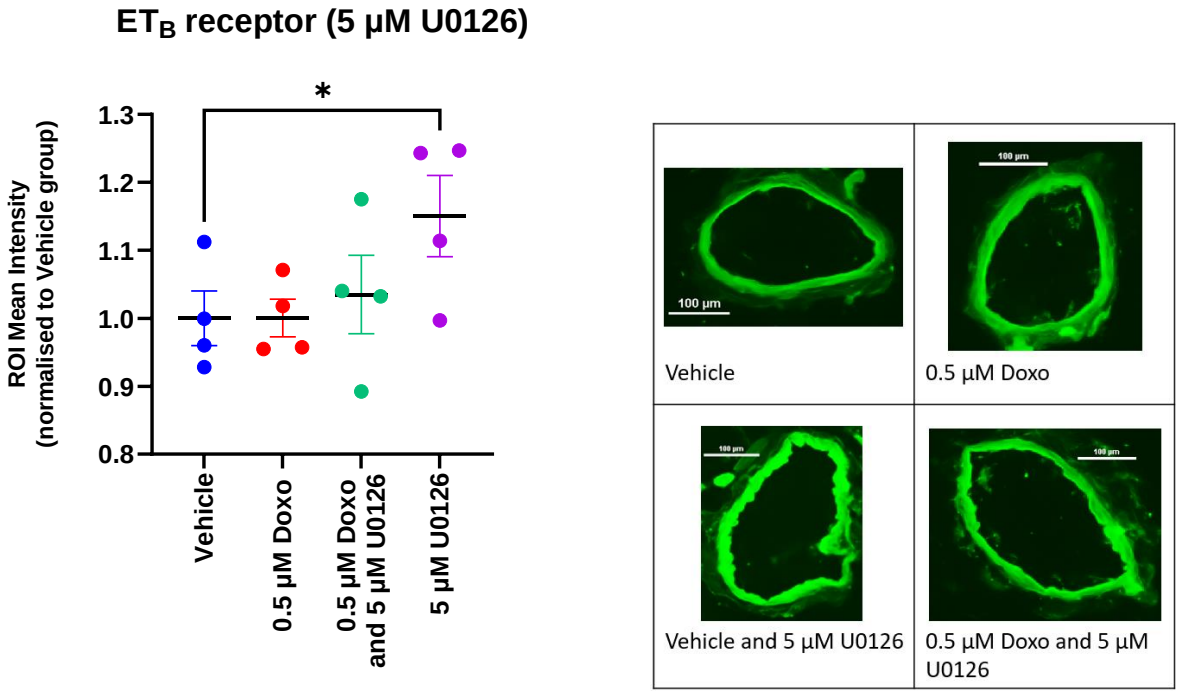

(B)

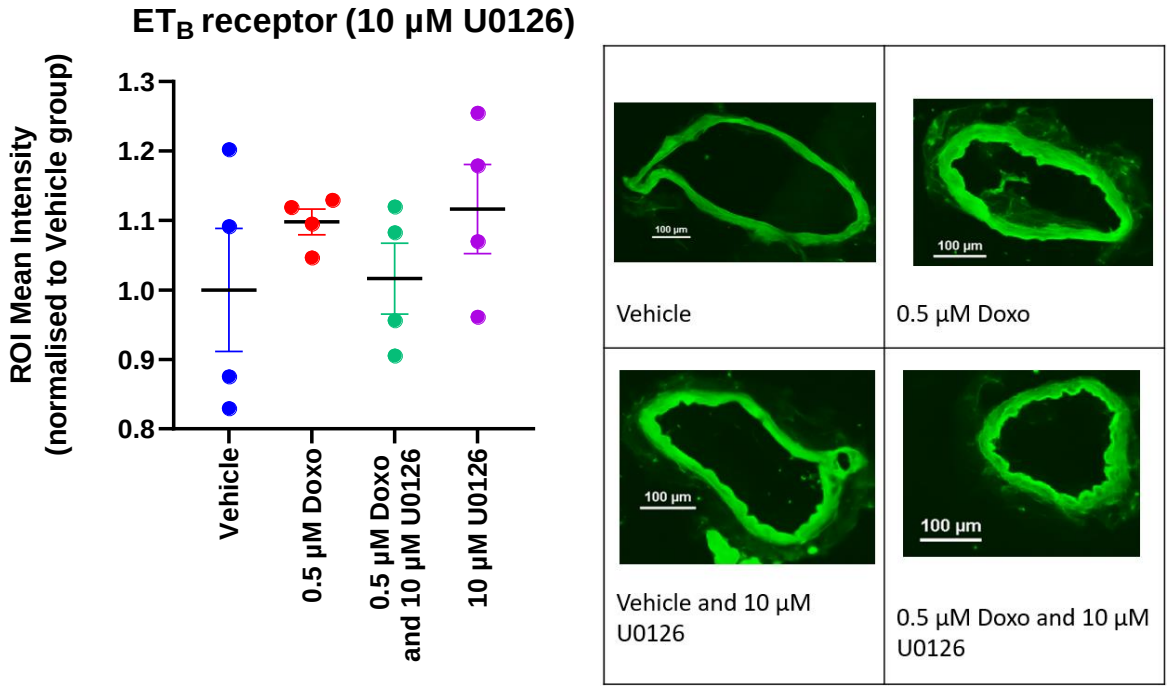

Figure 5-6: Quantification of the endothelin ET$_B$ receptors expression in LAD arteries by immunofluorescence. (A) Comparison of ET$_B$ receptors expression on LAD arteries from Vehicle group (containing 0.25 % DMSO; n = 4), 0.5 µM doxorubicin group (containing 0.5 µM doxorubicin and 0.25 % DMSO; n = 4), 0.5 µM doxorubicin + 5 µM U0126 group (containing 0.5 µM doxorubicin and 5 µM

U0126; n = 4) and 5 µM U0126 (containing 5 µM U0126; n = 4). **(B)** Comparison of ET_B receptors expression on LAD arteries from Vehicle group (containing 0.5 % DMSO; n = 4), 0.5 µM doxorubicin group (containing 0.5 µM doxorubicin and 0.5 % DMSO; n = 4), 0.5 µM doxorubicin + 10 µM U0126 group (containing 0.5 µM doxorubicin and 10 µM U0126; n = 4) and 10 µM U0126 (containing 10 µM U0126; n = 4). Doxo = doxorubicin, ET_B = endothelin B, ROI = region of interest. The groups were compared by multiple comparisons using one-way ANOVA and Fisher's test (* = $p < 0.05$).

5.3.2. Endothelin A receptor

5.3.2.1. Wire-myography: ET_A receptors-mediated contraction

The endothelin ET_A and ET_B receptors specific agonist, endothelin-1 (ET-1), was used to investigate the effect of doxorubicin on ET_A and ET_B receptor-mediated vasocontraction after DMSO or MEK 1/2 inhibitor U0126 incubation. However, in this study, the dose-response curve was performed after an ET_B receptors desensitisation of LAD arteries with sarafotoxin 6c (10^{-14} M to $10^{-7.5}$ M). So, the ET_B-mediated vasocontraction is nearly abolished and the ET-1 dose-response curve shows ET_A-mediated vasocontraction (Skovsted *et al.*, 2015). The ET-1-induced contraction values are given as percentage of the maximal contractile response, induced by K^+ KH. "E_{max}" and "pEC_{50}" values are given in Table 5-3 and 5-4. The different vasocontraction values of each group and the p values are given in the Tables 9-5 and 9-6 in Appendices.

5.3.2.1.1. ET_A and ET_B-mediated contraction in 0.5 µM of doxorubicin with and without 5 µM of U0126 (containing 0.25 % of DMSO)

- *The effect of 0.5 µM doxorubicin treatment on ET_A and ET_B-mediated contraction in 24-hr-incubated LAD vessels (containing 0.25 % DMSO):*

The 0.5 µM doxorubicin treatment induced a vasocontraction (30 % increase) at $10^{-8.5}$ M (41.18 ± 8.87 %, p = 0.0001) of 0.5 µM doxorubicin-treated LAD vessels (n = 10 - 11) when compared to vehicle-treated LAD vessels (n = 9 – 10) at $10^{-8.5}$ M: 10.88 ± 5.75 % (Figure 5-7). The 0.5 µM doxorubicin incubation did not alter the maximal ET-1-induced vasocontraction of 0.5 µM doxorubicin-treated LAD vessels ("E_{max}" = 151.64 ± 6.68 %) when compared to vehicle-treated LAD vessels ("E_{max}" = 137.48 ± 4.53 %). The "pEC_{50}" of 0.5 µM doxorubicin-treated LAD vessels ("pEC_{50}" = $10^{-8.29}$ M) was not altered compared to the pEC5 0 of vehicle-treated LAD vessels ("pEC_{50}" = $10^{-8.19}$ M) (Table 5-3).

- *The effect of 5 µM U0126 treatment on ET_A and ET_B -mediated contraction in 24-hr-incubated LAD vessels (containing 0.25 % DMSO):*

The incubation of 5 µM U0126 of vehicle-treated LAD vessels reduced by 29 % and 21 %, the ET-1-mediated contraction of 5 µM U0126-incubated vehicle LAD vessels (n = 9 - 10) at 10^{-8} M (85.00 ± 10.02 %, p = 0.0006) and $10^{-7.5}$ M (C_{max} = 115.69 ± 12.00 %, p = 0.0298), when compared to U0126 naïve vehicle-treated LAD vessels (n = 9 - 10) at 10^{-8} M (113.70 ± 11.25 %) and $10^{-7.5}$ M (C_{max} = 136.60 ± 12.41 %) (Figure 5-7). The 5 µM U0126 incubation reduced the maximal ET-1-induced vasocontraction of vehicle-treated LAD vessels ("E_{max}" = 118.14 ± 4.82 %, p = 0.0245), when compared to U0126 naïve vehicle-treated LAD vessels ("E_{max}" = 137.48 ± 4.53 %). The "pEC_{50}" value of 5 µM U0126-incubated vehicle LAD vessels was not altered compared to U0126 naïve vehicle-treated LAD vessels, as shown in Table 5-3.

- *The effect of 0.5 µM doxorubicin treatment on ET_A and ET_B -mediated contraction in the presence of 5 µM U0126 in 24-hr-incubated LAD vessels (containing 0.25 % DMSO):*

The ET-1-mediated contraction of 0.5 µM doxorubicin-treated LAD vessels, after 5 µM U0126 incubation (n = 10 - 11), was reduced by 35 % at ET-1 10^{-8} M (78.66 ± 11.24 %, p < 0.0001) and by 33 % at ET-1 $10^{-7.5}$ M (C_{max} = 104.38 ± 14.17 %, p < 0.0001) when compared to U0126 naïve vehicle-treated vessels (n = 9 - 10) at 10^{-8} M (113.70 ± 11.25 %) and $10^{-7.5}$ M (C_{max} = 136.60 ± 12.41 %)(Figure 5-7). The inhibition effect of 5 µM U0126 on 0.5 µM doxorubicin-treated LAD vessels reduced the maximal ET-1 -induced contraction of 5 µM U0126-incubated 0.5 µM doxorubicin LAD vessels ("E_{max}" = 105.76 ± 5.69 %, p = 0.0001) when compared to U0126 naïve vehicle-treated LAD vessels ("E_{max}" = 137.48 ± 4.53), while the "pEC_{50}" values of ET-1-induced contraction of 5 µM U0126-incubated 0.5 µM doxorubicin LAD vessels was not altered when compared to U0126 naïve vehicle-treated vessels.

Furthermore, the incubation with 5 µM U0126 of 0.5 µM doxorubicin-treated LAD vessels significantly decreased (by 28 % to 43 %) the ET-1-induced contraction of 5 µM U0126-incubated 0.5 µM doxorubicin LAD vessels (n = 10 - 11), at $10^{-8.5}$ M (13.29 ± 3.42 %, p = 0.0003), 10^{-8} M (78.66 ± 11.24 %, p < 0.0001) and $10^{-7.5}$ M (104.38 ± 14.17 %, p < 0.0001), when compared to U0126 naïve 0.5 µM doxorubicin-treated LAD vessels from $10^{-8.5}$ M (41.18 ± 8.87 %), 10^{-8} M (121.62 ± 9.13 %) and $10^{-7.5}$ M (147.18 ± 12.90 %). ET-1 induced vasocontraction values and p-values are detailed in Table 9-5 in Appendices. The inhibition effect of 5 µM U0126 on 0.5 µM doxorubicin-treated LAD vessels did not alter the maximal ET-1-induced vasocontraction ("E_{max}"= 105.76 ± 5.69 %) compared to U0126 naïve 0.5 µM doxorubicin-treated LAD vessels ("E_{max}"= 151.64 ± 6.68 %). The "pEC_{50}" value of ET-1-induced contraction of 5 µM U0126–incubated 0.5 µM doxorubicin LAD vessels was not altered, compared to U0126 naïve 0.5 µM doxorubicin-treated LAD vessels (Table 5-3).

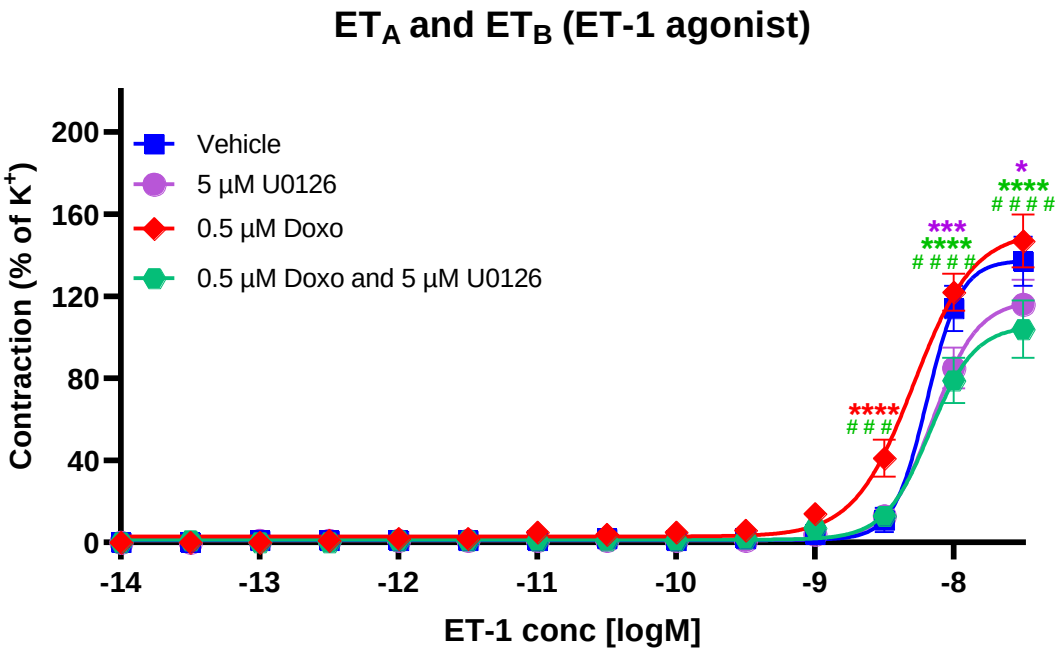

Figure 5-7: Vasocontractile response to the cumulative application of endothelin-1 (ET-1) (ET_A and ET_B receptor agonist) normalised to 60 mM K^+ KH-induced contraction in rat LAD arteries, after 0.25 % DMSO or 5 µM U0126 incubation. Vehicle group (containing 0.25 % DMSO; n = 9 - 10), 0.5 µM Doxorubicin group (containing 0.25 % DMSO; n = 10 - 11), 0.5 µM doxorubicin and 5 µM U0126 (n = 10 - 11) and 5 µM U0126 (n = 9 - 10). ET-1 = Endothelin-1, DMSO = Dimethyl sulfoxide. Vasocontractile responses were compared to vehicle group using two-way ANOVA and Bonferroni's test (* = $p < 0.05$, *** = $p < 0.001$ and **** = $p < 0.0001$) and compared to doxorubicin group using two-way ANOVA and Bonferroni's test (## = $p < 0.01$, #### = $p < 0.0001$).

Table 5-3: C_{max}, "E_{max}" and "pEC_{50}" values of vehicle or doxorubicin incubated LAD arteries with DMSO or MEK 1/2 inhibitor U0126: 0.25 % DMSO and 5 µM U0126 incubation. Values given for all Endothelin-1 experiments and as mean ± S.E.M. N values represent the total amount of animals used. The different groups are compared to the vehicle-treated LAD vessels (containing 0.25 % DMSO) with ANOVA and Dunnett's post-hoc test: * = $p < 0.05$, *** = $p < 0.001$. The 10 µM U0126-incubated doxorubicin LAD vessels were compared to U0126 naïve doxorubicin-treated LAD vessels (containing 0.5 % DMSO) with ANOVA and Dunnett's post-hoc test: ### = $p < 0.001$.

Groups	*N*	*C_{max}*	*ET-1 "E_{max}"*	*"pEC_{50}"*
Vehicle	9-10	136.60 ± 12.41 %	137.48 ± 4.53 %	8.19 ± 0.03
0.5 µM Doxorubicin	10-11	147.18 ±12.90 %	151.64 ± 6.68 %	8.29 ± 0.04
0.5 µM Doxorubicin and 5 µM U0126	10-11	104.38 ± 14.17 % ****, ####	105.76 ± 5.69 % ***	8.17 ± 0.04
5 µM U0126	9-10	115.69 ± 12.00 % *	118.14 ± 4.82 % *	8.15 ± 0.03

5.3.2.1.2. ET_A and ET_B-mediated contraction in 0.5 µM of doxorubicin with and without 10 µM of U0126 (containing 0.5 % of DMSO)

- The effect of 0.5 µM doxorubicin treatment on ET_A and ET_B -mediated contraction in 24-hr-incubated LAD vessels (containing 0.5 % DMSO):

The ET-mediated vasocontraction of 0.5 µM doxorubicin-treated LAD vessels (n = 8 - 10) was reduced by 44 % and 32 % at 10^{-8} M ET-1 (115.66 ± 10.66 %, $p < 0.0001$) and at $10^{-7.5}$ M (C_{max} = 140.23 ± 12.73 %, p = 0.0028) when compared to vehicle-treated LAD vessels (n = 7 - 8) at 10^{-8} M ET-1 (159.91 ± 7.93 %) and $10^{-7.5}$ M ET-1 (C_{max} = 172.46 ± 5.64 %) (Figure 5-8). The 0.5 µM doxorubicin incubation did not alter the maximal ET-1-induced contraction and the receptor's affinity to ET-1 of 0.5 µM doxorubicin-treated LAD vessels ("E_{max}" = 174.3 ± 25.9 %, "pEC_{50}" = $10^{-8.17}$ M) when compared to vehicle-treated LAD vessels ("E_{max}" = 184.1 ± 11.0 %, "pEC_{50}" = $10^{-8.38}$ M) (Table 5-4).

- *The effect of 10 µM U0126 treatment on ET_A and ET_B -mediated contraction in 24-hr-incubated LAD vessels (containing 0.5 % DMSO):*

The 10 µM U0126 incubation of vehicle-treated LAD vessels (n = 7 - 8) decreased the ET-1-induced vasocontraction by 28 % at 10^{-9} M (4.78 ± 0.71 %, p = 0.016), 43 % at $10^{-8.5}$ M (17.75 ± 5.08 %, $p < 0.0001$) and 32 % at $10^{-7.5}$ M (C_{max} = 204.04 ± 14.61 %, p = 0.0097) when compared to vehicle-treated LAD vessels (respectively, 32.99 ± 15.42 %, 61.12 ± 20.17 % and 172.46 ± 5.64 %) (Figure 5-8). The 10 µM U0126 incubation of vehicle-treated LAD vessels slightly right-shifted the ET-1 dose-response curve from a "pEC_{50}" of $10^{-8.38}$ M, p = 0.0047 for the U0126 naïve vehicle-treated LAD vessels to a "pEC_{50}" of $10^{-8.16}$ M for 10 µM U0126-incubated vehicle LAD vessels. However, the 10 µM U0126 incubation did not alter the maximal ET-1-induced vasocontraction of vehicle-treated LAD vessels, with a mean "E_{max}" of 205.8 ± 5.74 % for 10 µM U0126-incubated vehicle LAD vessels compared to a mean "E_{max}" of 184.1 ± 11.0 % for the U0126 naïve vehicle-treated LAD.

- *The effect of 0.5 µM doxorubicin treatment on ET_A and ET_B -mediated contraction in the presence of 10 µM U0126 in 24-hr-incubated LAD vessels (containing 0.5 % DMSO):*

The ET-1-induced contraction was reduced at $10^{-8.5}$ M ET-1 (11.29 ± 2.62 %, $p < 0.0001$) (by 50 %), 10^{-8} M (57.61 ± 11.04 %, $p < 0.0001$) (by 102 %) and $10^{-7.5}$ M (86.00 ± 10.39 %, $p < 0.0001$) (by 86 %), on 10 µM U0126-incubated 0.5 µM doxorubicin LAD vessels (n = 8 - 9), when compared to U0126 naïve vehicle-treated LAD vessels ($10^{-8.5}$ M: 61.12 ± 20.17 %, 10^{-8} M: 159.91 ± 7.93 % and $10^{-7.5}$ M: 172.46 ± 5.64 %) (Figure 5-8). The 10 µM U0126 incubation of 0.5 µM doxorubicin-treated LAD vessels highly reduced the maximal ET-1-induced vasocontraction ("E_{max}" = 89.4 ± 5.82 %, $p< 0.0001$) compared to

U0126 naïve vehicle-treated LAD vessels ("E_{max}" = 184.1 ± 11.0 %). Furthermore, the 10 µM U0126 incubation of 0.5 µM doxorubicin-treated LAD vessels slightly right-shifted the ET-1 dose-response curve from a "pEC_{50}" of $10^{-8.38}$ M (p = 0.0019) for U0126 naïve vehicle-treated LAD vessels to a "pEC_{50}" of $10^{-8.10}$ M for 10 µM U0126-incubated doxorubicin LAD vessels.

Furthermore, the 10 µM U0126 incubation of 0.5 µM doxorubicin-treated LAD vessels reduced (by 22 % to 54 %) the ET-1-induced vasocontraction from 10^{-9} M (10.70 ± 2.64 %, p = 0.0488) to $10^{-7.5}$ M (86.00 ± 10.39 %, p < 0.0001) when compared to U0126 naïve 0.5 µM doxorubicin-treated LAD vessels (from 10^{-9} M: 33.24 ± 6.92 % to $10^{-7.5}$ M: 140.23 ± 12.73 %). The 10 µM U0126 incubation did not alter the ET-1-induced vasocontraction of 0.5 µM doxorubicin-treated LAD vessels ("E_{max}" = 89.4 ± 5.82 %, p = 0.0102) when compared to U0126 naïve 0.5 µM doxorubicin-treated LAD vessels ("E_{max}" = 174.3 ± 25.9 %), while the "pEC_{50}" remain unchanged (Table 5-4).

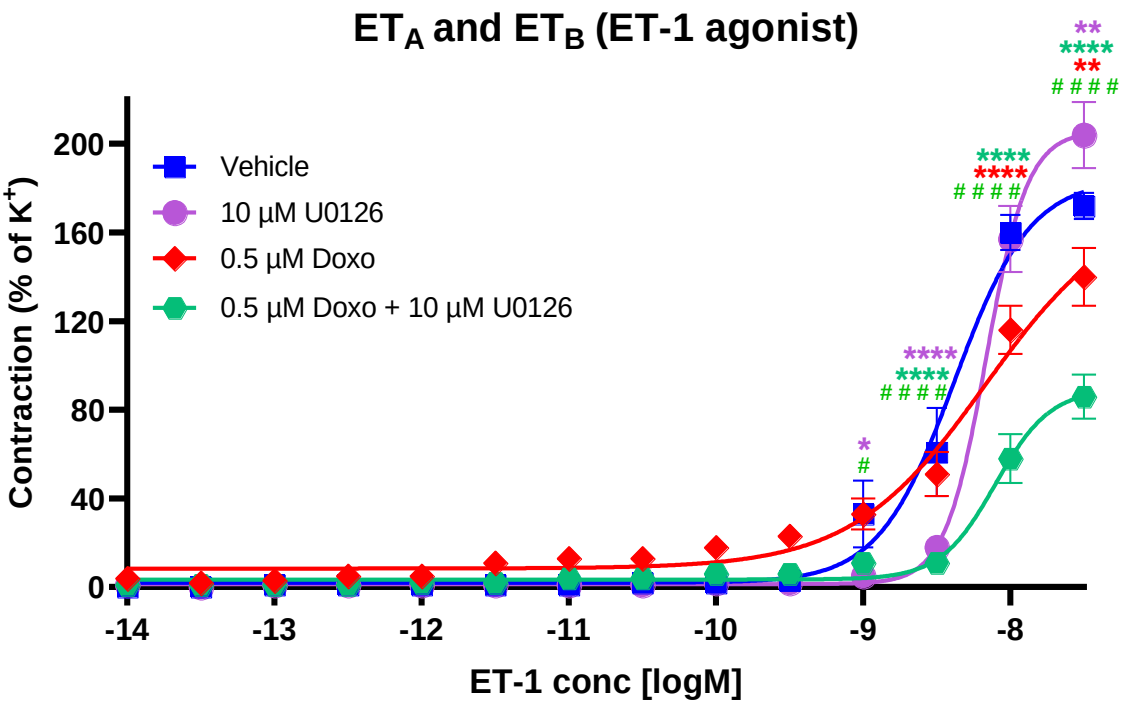

Figure 5-8: Vasocontractile response to the cumulative application of endothelin-1 (ET-1) (ET_A and ET_B receptor agonist) normalised to 60 mM K^+ KH-induced contraction in rat LAD arteries, after 0.5 % DMSO or 10 µM U0126 incubation. Vehicle group (0.5 % DMSO; n = 7 - 8); 0.5 µM doxorubicin group (0.5 % DMSO; n = 8 - 10), 0.5 µM doxorubicin and 10 µM U0126 (n = 8 - 9); 10 µM U0126 (n = 7 - 8). ET-1 = Endothelin-1, Dimethyl sulfoxide. Vasocontractile responses compared to vehicle group using two-way ANOVA and Bonferroni's test (* = p < 0.05, ** = p < 0.01, *** = p < 0.001 and **** = p < 0.0001) and compared to 0.5 µM doxorubicin group using two-way ANOVA and Bonferroni's test (# = p < 0.05 and #### = p < 0.0001).

Table 5-4: C_{max}, "E_{max}" and "pEC_{50}" values of vehicle or doxorubicin incubated LAD arteries with DMSO or MEK 1/2 inhibitor U0126: 0.5 % DMSO and 10 µM U0126 incubation. Values given for all Endothelin-1 experiments and as mean ± S.E.M. N values represent the total amount of animals used. The "E_{max}" and "pEC_{50}" values of the different groups are compared to the vehicle-treated LAD vessels (containing 0.25 % DMSO) with ANOVA and Dunnett's post-hoc test: ** = p < 0.01, *** = p < 0.001 and **** = p < 0.0001. The 10 µM U0126-incubated 0.5 µM doxorubicin LAD vessels were compared to U0126 naïve doxorubicin-treated LAD vessels (containing 0.5 % DMSO) with ANOVA and Dunnett's post-hoc test: # = p < 0.05 and #### = p < 0.0001, while C_{max} is compared using two-way ANOVA with Bonferroni's post-hoc test: ** = p < 0.01, **** or #### = p < 0.0001 .

Groups	*N*	*ET-1 C_{max}*	*ET-1 "E_{max}"*	*"pEC_{50}"*
Vehicle	7-8	172.46 ± 5.64 %	184.1 ± 11.0 %	8.38 ± 0.06
0.5 µM Doxorubicin	8-10	140.23 ± 12.73 % **	174.3 ± 25.9 %	8.17 ± 0.18
0.5 µM Doxorubicin and 10 µM U0126	8-9	86.00 ± 10.39 % ****, ####	89.4 ± 5.82 % ***, #	8.10 ± 0.05 **
10 µM U0126	7-8	204.04 ± 14.61 % **	205.8 ± 5.74 %	8.16 ± 0.02 **

5.3.2.2. Real-Time PCR: quantification of ET_A receptor mRNA levels

Gene expression of the endothelin ET_A receptors was investigated in rat LAD arteries by Real-Time PCR. Negative controls were included for each studied gene. Endothelin ET_A receptors mRNA level was expressed as values relative to GAPDH and normalised to vehicle-treated LAD vessels.

Figure 5-9 (A) showed the mRNA levels of both vehicle-treated LAD vessels and 0.5 µM doxorubicin-treated vessels after the incubation with either 0.25 % DMSO or 5 µM U0126. The 0.5 µM doxorubicin treatment reduced the ET_A receptors mRNA level of the 0.5 µM doxorubicin-treated LAD vessels (0.540 ± 0.144; n = 9) when compared to the vehicle-treated LAD vessels (1.00 ± 0.148, p = 0.033; n = 10). Similarly, 5 µM U0126 incubation reduced the ET_A receptors mRNA level of the 0.5 µM doxorubicin-treated LAD vessels (0.289 ± 0.060; n = 9) when compared to the U0126 naïve vehicle-treated LAD vessels (1.00 ± 0.148, p = 0.001; n = 10). The 5 µM U0126 incubation of 0.5 µM doxorubicin-treated LAD vessels did not alter the ET_A receptors mRNA level of 5 µM U0126-treated 0.5 µM doxorubicin LAD vessels (0.289 ± 0.060; n = 9) when compared to the U0126 naïve 0.5 µM doxorubicin-treated LAD vessels (0.540 ± 0.144; n = 9). The 5 µM U0126 incubation of vehicle-treated LAD vessels did not alter

the ET_A receptors mRNA level of 5 µM U0126-treated vehicle LAD vessels (1.009 ± 0.124; n = 10) when compared to the U0126 naïve vehicle LAD vessels (1.00 ± 0.148; n = 10).

Figure 5-9 (B) showed the mRNA levels of both vehicle-treated LAD vessels and 0.5 µM doxorubicin-treated vessels after the incubation with either 0.5 % DMSO or 10 µM U0126. The mRNA level of ET_A receptors in each group of treated LAD vessels showed a similar tendency as the treated LAD vessel groups from Figure 5-9 (A) but with a higher significance. The 0.5 µM doxorubicin treatment induced a down-regulation of the ET_A receptors mRNA level of the 0.5 µM doxorubicin-treated LAD vessels (0.287 ± 0.749, p = 0.0008; n = 10) when compared to the vehicle-treated LAD vessels (1.00 ± 0.232; n = 10). The 10 µM U0126 incubation of 0.5 µM doxorubicin-treated LAD vessels induced a reduction of the ET_A receptors mRNA level in the 10 µM U0126-treated 0.5 µM doxorubicin LAD vessels (0.206 ± 0.039; n = 10) when compared to the vehicle-treated LAD vessels 1.00 ± 0.232 (n = 10) (p < 0.0001). The 10 µM U0126 incubation of vehicle-treated LAD vessels (0.816 ± 0.131; n = 10) did not alter the ET_A receptors mRNA level when compared to U0126 naïve vehicle LAD vessels (1.00 ± 0.232; n = 10). The 10 µM U0126 incubation of 0.5 µM doxorubicin-treated LAD vessels (0.206 ± 0.039; n = 10) did not alter the ET_A receptors mRNA level when compared to U0126 naïve 0.5 µM doxorubicin-treated LAD vessels (0.287 ± 0.749; n = 10).

(A) (B)

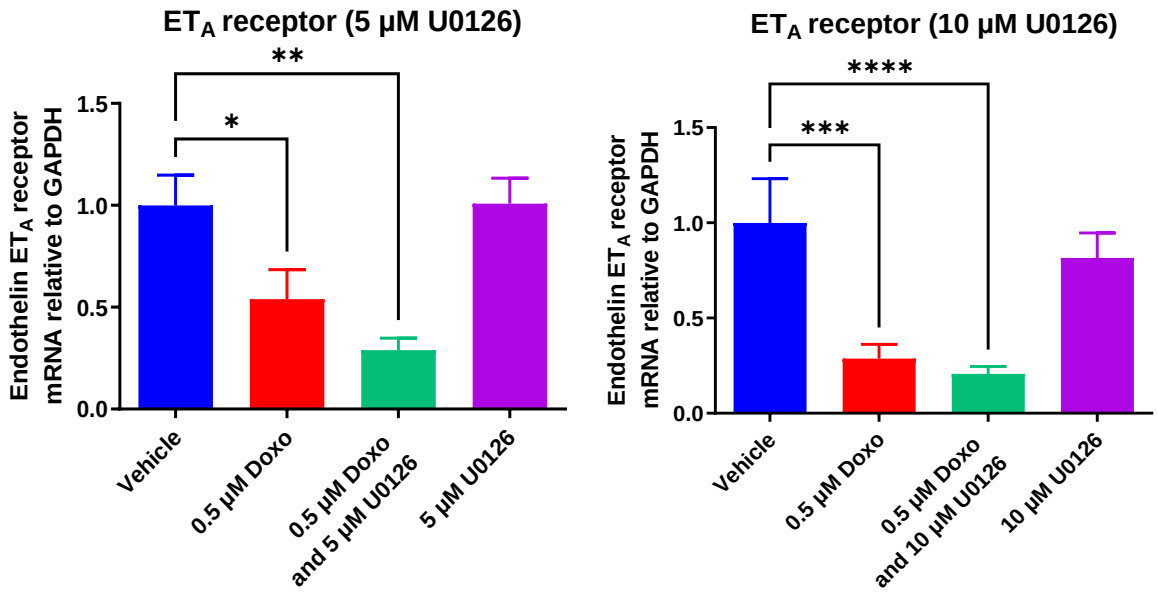

Figure 5-9: Real-Time PCR of ET_A receptors in LAD arteries with DMSO (Vehicle or Doxorubicin) or U0126 (Vehicle + U0126 or Doxorubicin + U0126). (A) Comparison of ET_A receptors mRNA levels on LAD arteries from Vehicle group (containing 0.25 % DMSO; n = 10), 0.5 µM doxorubicin group (containing 0.5 µM doxorubicin and 0.25 % DMSO; n = 9), 0.5 µM doxorubicin and 5 µM U0126 group (n = 9) and 5 µM U0126 (n = 10). **(B)** Comparison of ET_A receptors mRNA levels on LAD arteries from

Vehicle group (containing 0.5 % DMSO; n = 10), 0.5 µM doxorubicin group (containing 0.5 µM doxorubicin and 0.5 % DMSO; n = 10), 0.5 µM doxorubicin and 10 µM U0126 group (n = 10) and 10 µM U0126 (n = 10). Doxo = doxorubicin, ET_A = endothelin A. Data are expressed as mean ± S.E.M. values relative to GAPDH mRNA levels (n = 10) and normalised to vehicle group. The groups were compared by multiple comparisons using one-way ANOVA Kruskal-Wallis' test (* = $p < 0.05$, ** = $p < 0.01$, *** = $p < 0.001$, **** = $p < 0.0001$).

5.3.2.3. Immunohistochemistry: Quantification of ET_A receptor levels

The quantification of ET_A receptors was obtained by measuring the ROI mean intensity and the intensity was normalised to LAD vessels from vehicle group. The ET_A receptors expression on LAD vessels from most of the groups was widely spread.

Figure 5-10 (A) showed the ET_A receptors expression of both vehicle-treated LAD vessels and 0.5 µM doxorubicin-treated vessels after the incubation with either 0.25 % DMSO or 5 µM U0126. No statistical difference was observed between the different groups. The 5 µM U0126 incubation of vehicle-treated LAD vessels (1.055 ± 0.023; n = 4) did not alter the ET_A receptors expression compared to the U0126 naïve vehicle-treated LAD vessels (1.00 ± 0.033; n = 4). Similarly, the 5 µM U0126 incubation of 0.5 µM doxorubicin-treated LAD vessels (0.949 ± 0.066; n = 4) did not alter the ET_A receptors expression compared to the U0126 naïve 0.5 µM doxorubicin-treated LAD vessels (0.992 ± 0.040; n = 4).

Figure 5-10 (B) showed the ET_A receptors expression of both vehicle-treated LAD vessels and 0.5 µM doxorubicin-treated vessels after the incubation with either 0.5 % DMSO or 10 µM U0126. No statistical difference was observed between the different groups. Likely, the 10 µM U0126 incubation of vehicle-treated LAD vessels (0.947 ± 0.044; n = 4) did not alter the ET_A receptors expression compared to the U0126 naïve vehicle-treated LAD vessels (1.00 ± 0.047; n = 4). The 10 µM U0126 incubation of 0.5 µM doxorubicin-treated LAD vessels (1.015 ± 0.033; n = 4) did not alter the ET_A receptors expression compared to the U0126 naïve 0.5 µM doxorubicin-treated LAD vessels (1.016 ± 0.064; n = 4).

(A)

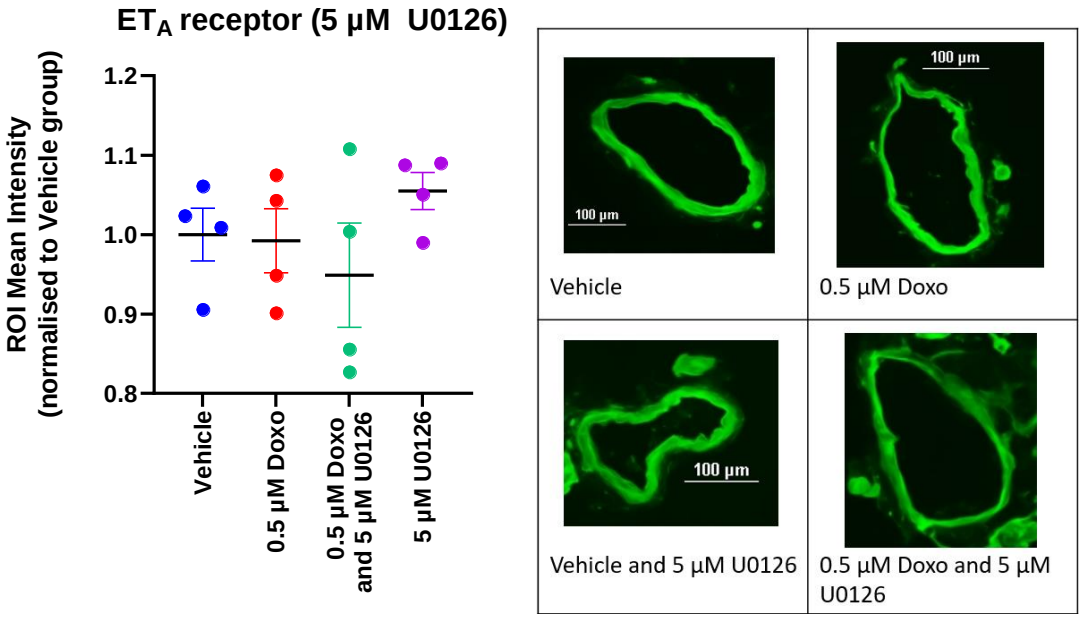

(B)

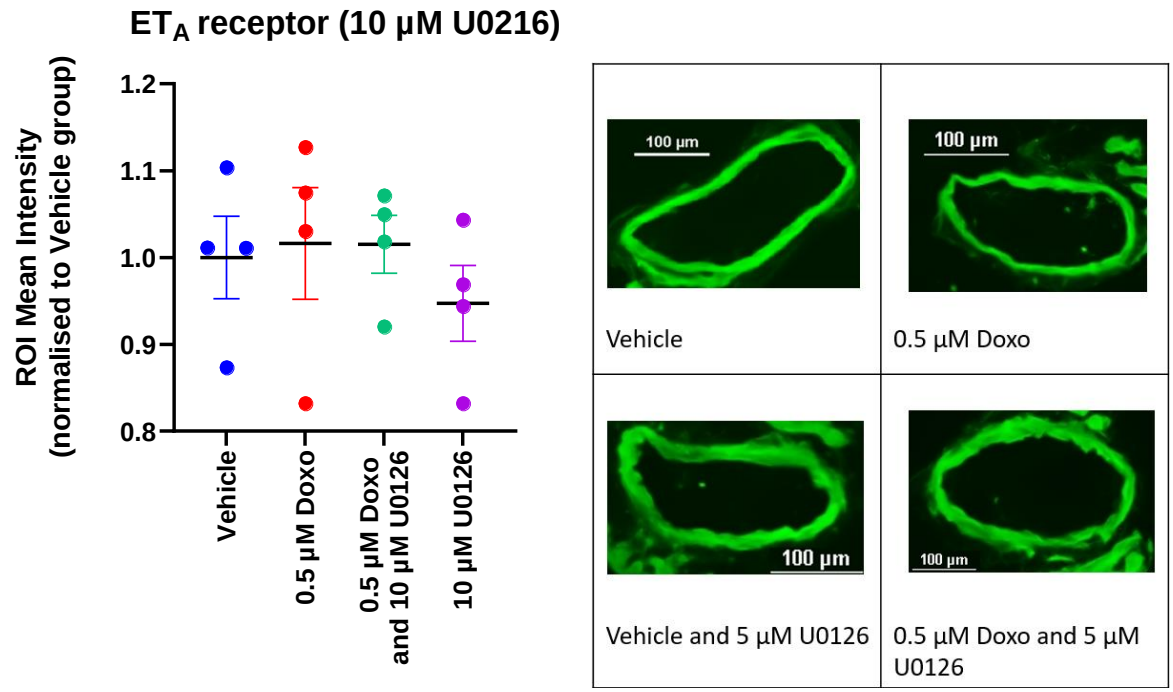

Figure 5-10: Quantification of the endothelin ET$_A$ receptors expression in LAD arteries by immunofluorescence. (A) Comparison of ET$_A$ receptors expression on LAD arteries from Vehicle group (containing 0.25 % DMSO; n = 4), 0.5 µM doxorubicin group (containing 0.25 % DMSO; n = 4), 0.5 µM doxorubicin and 5 µM U0126 group (n = 4) and 5 µM U0126 (n = 4). **(B)** Comparison of ET$_A$ receptors expression on LAD arteries from Vehicle group (containing 0.5 % DMSO; n = 4), 0.5 µM doxorubicin group (0.5 % DMSO; n = 4), 0.5 µM doxorubicin + 10 µM U0126 group (n = 4) and 10 µM U0126 (n = 3). Doxo = doxorubicin, ET$_A$ = endothelin A, ROI = region of interest. The groups were compared by multiple comparisons using one-way ANOVA and Fisher's test (* = $p < 0.05$, ** = $p < 0.01$).

5.3.3. 5-hydroxytryptamine receptor 1B

5.3.3.1. Wire-myography: 5-HT_{1B} receptors-mediated contraction

The serotonin 5-HT_{1B} receptor specific agonist, 5-CT, was used to investigate the effect of doxorubicin on 5-HT_{1B} receptor-mediated contraction with DMSO or MEK 1/2 inhibitor, U0126. The dose-response curve obtained by the 5-HT_{1B} receptor-mediated contraction was a biphasic curve, as shown in Figures 5-11 and 5-12. The 5-HT_{1B}-mediated contraction values are given as percentage of the maximal contractile response, induced by K^+ KH. The 5-CT dose-response curve of LAD vessels did not reach the final plateau at the highest dose due to stock constraints, and therefore final "E_{max}" and "pEC_{50}" values could not be obtained. However, the contraction obtained at the highest dose is mentioned as C_{max} and are given in Table 5-5 and 5-6. The difference of vasocontraction between the groups and the p values are given in Tables 9-7 and 9-8 in Appendices.

5.3.3.1.1. 5-HT_{1B}-mediated contraction in 0.5 µM of doxorubicin with and without 5 µM of U0126 (containing 0.25 % of DMSO)

- *The effect of 0.5 µM doxorubicin treatment on 5-HT_{1B}-mediated contraction in 24-hr-incubated LAD vessels (containing 0.25 % DMSO):*

The 0.5 µM doxorubicin treatment induced an elevation (12 % - 49 % increase) of 5-HT_{1B}-mediated vasocontraction of 0.5 µM doxorubicin-treated LAD vessels (n = 14 - 16) from 10^{-8} M 5-CT (13.47 ± 3.43 %, p = 0.0458) to 10^{-6} M 5-CT (46.69 ± 7.23 %, p < 0.0001) when compared to vehicle-treated LAD vessels (n = 11 - 12) from 10^{-8} M 5-CT (2.30 ± 0.45 %) to 10^{-6} M 5-CT (8.26 ± 2.11 %) (Figure 5-11). The 0.5 µM doxorubicin treatment increased the C_{max} value from 25.54 ± 7.18 % for vehicle-treated LAD vessels to 74.93 ± 7.82 % (p < 0.0001) for 0.5 µM doxorubicin-treated LAD vessels. The 5-CT dose-response of 0.5 µM doxorubicin-treated LAD vessels was biphasic due to the activation of 2 different serotonin receptors, while the 5-CT dose-response of vehicle-treated LAD vessels was monophasic.

- *The effect of 5 µM U0126 treatment on 5-HT_{1B}-mediated contraction in 24-hr-incubated LAD vessels (containing 0.25 % DMSO):*

The incubation of 5 µM U0126 of vehicle-treated LAD vessels did not alter the 5-HT_{1B}-mediated vasocontraction of 5 µM U0126-incubated vehicle LAD vessels (n = 10 - 11) when compared to U0126 naïve vehicle-treated LAD vessels (n = 11 - 12) (Figure 5-11). The mean C_{max} of 5 µM U0126-incubated vehicle LAD vessels was 25.82 ± 7.46 % and the mean C_{max} of U0126 naïve vehicle-treated LAD vessels was 25.54 ± 7.18 %.

- *The effect of 0.5 µM doxorubicin treatment on 5-HT_{1B}-mediated contraction in the presence of 5 µM U0126 in 24-hr-incubated LAD vessels (containing 0.25 % DMSO):*

The 5-HT_{1B}-mediated vasocontraction of 5 µM U0126-incubated 0.5 µM doxorubicin vessels (n = 14 - 16) was not altered when compared to vehicle-treated vessels (Figure 5-11). The 5 µM U0126 incubation of 0.5 µM doxorubicin-treated LAD vessels, showed a tendency to slightly left-shift the 5-CT dose-response curve when compared to U0126 naïve vehicle-treated LAD vessels, but the absence of "pEC50" value did not allow the confirmation of the potential variation of 5-HT_{1B} receptor affinity.

Furthermore, the 5 µM U0126 incubation of 0.5 µM doxorubicin-treated LAD vessels reduced (22 % and 38 % decrease) the 5-HT_{1B}-mediated vasocontraction at 10^{-6} M 5-CT (24.73 ± 7.46 %, $p < 0.0001$) and $10^{-5.5}$ M (C_{max} = 36.88 ± 9.33 %, $p < 0.0001$), compared to U0126 naïve 0.5 µM doxorubicin-treated LAD vessels at 10^{-6} M 5-CT (46.69 ± 7.23 %) and $10^{-5.5}$ M (C_{max} = 74.93 ± 7.82 %) (Figure 5-11). The 5 µM U0126 incubation of 0.5 µM doxorubicin-treated LAD vessels might have slightly right-shifted the 5-CT dose-response curve when compared to 0.5 µM doxorubicin-treated LAD vessels, but the absence of "pEC_{50}" values did not allow the confirmation of the potential reduction of 5-HT_{1B} receptor affinity.

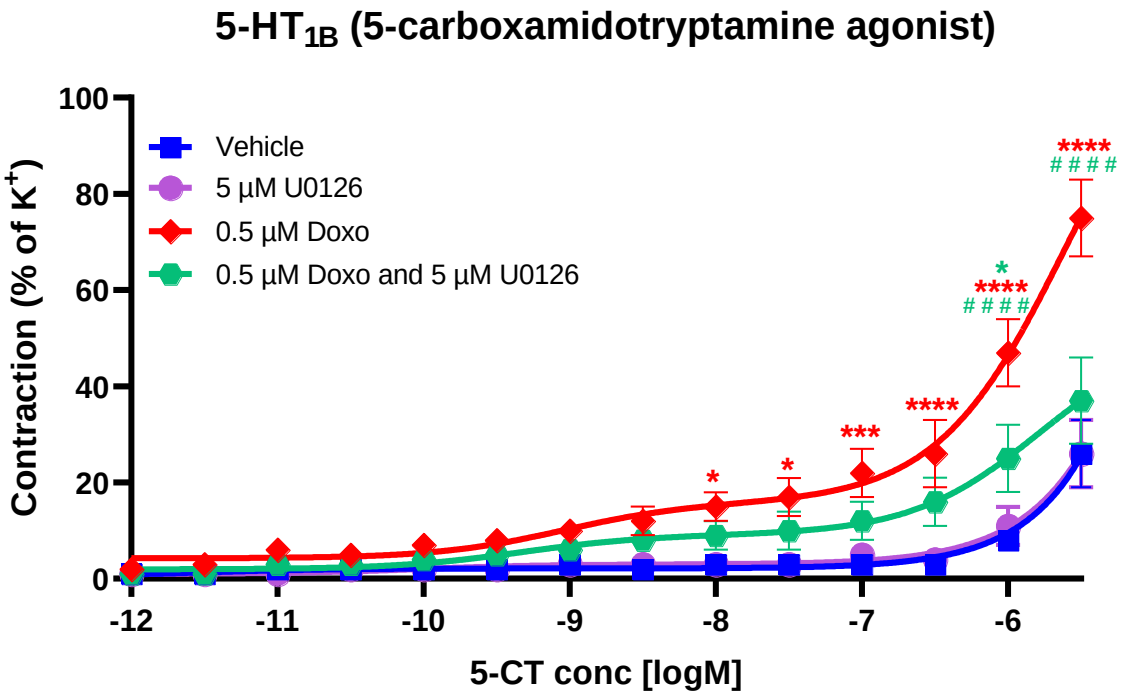

Figure 5-11: Vasocontractile response to the cumulative application of 5-carboxamidotryptamine (5-CT) (5-HT_{1B} receptor agonist) normalised to 60 mM K^+ KH-induced contraction in rat LAD arteries, after 0.25 % DMSO or 5 µM U0126 incubation. Vehicle group (containing 0.25 % DMSO; n = 11 - 12), 0.5 µM doxorubicin group (containing 0.25 % DMSO; n = 14 - 16), 0.5 µM doxorubicin and 5 µM U0126 (n = 9) and 5 µM U0126 (n = 10 - 11). 5-CT = 5-carboxamidotryptamine, DMSO = Dimethyl sulfoxide. Contractile responses compared to vehicle group using two-way ANOVA and Bonferroni's test (* = p

< 0.05, *** = p < 0.001) and compared to 0.5 µM doxorubicin group using two-way ANOVA and Bonferroni's test (### = p < 0.001).

Table 5-5: The C_{max} values of vehicle or doxorubicin incubated LAD arteries with DMSO or MEK 1/2 inhibitor U0126: 0.25 % DMSO and 5 µM U0126. C_{max} = the contraction obtained at the highest agonist dose and is applied when the "E_{max}" couldn't be determined due to stock concentration constraints; Values given for 5-CT experiments and as mean ± S.E.M. N values represent the total amount of animals used C_{max} values of the different groups were compared to the vehicle-treated LAD vessels with two-way ANOVA and Bonferroni's post-hoc test: *** = p < 0.001. C_{max} value of the 5 µM U0126-incubated 0.5 µM doxorubicin LAD vessels was compared to the 0.5 µM doxorubicin-treated LAD vessels with ANOVA and Bonferroni's post-hoc test: #### = p < 0.0001.

Groups	*N*	C_{max}
Vehicle	11-12	25.54 ± 7.18 %
0.5 µM Doxorubicin	14-16	74.93 ± 7.82 % ****, ####
0.5 µM Doxorubicin and 5 µM U0126	9	36.88 ± 9.33 %
5 µM U0126	10-11	25.82 ± 7.46 %

5.3.3.1.2. 5-HT_{1B}-mediated contraction in 0.5 µM of doxorubicin with and without 10 µM of U0126 (containing 0.5 % of DMSO)

- *The effect of 0.5 µM doxorubicin treatment on 5-HT_{1B}-mediated contraction in 24-hr-incubated LAD vessels (containing 0.5 % DMSO):*

The 0.5 µM doxorubicin treatment induced an increase of 5-HT_{1B}-mediated contraction (by 12 % to 32 %) of 0.5 µM doxorubicin-treated LAD vessels (n = 9 - 10) from the concentrations of $10^{-7.5}$ M 5-CT (16.10 ± 3.76 %, p = 0.0325) to 10^{-6} M (39.85 ± 7.60 %, p < 0.0001), compared to vehicle-treated LAD vessels (n = 8 - 9) from the concentrations of $10^{-7.5}$ M 5-CT (2.31 ± 0.41 %) to 10^{-6} M (7.82 ± 2.91 %) (Figure 5-12). The 0.5 µM doxorubicin treatment significantly increased the 5-HT_{1B}-mediated contraction of 0.5 µM doxorubicin-treated LAD vessels (C_{max} = 65.58 ± 8.13 %, p < 0.0001) compared to vehicle-treated LAD vessels (C_{max} = 43.53 ± 14.60 %).

- *The effect of 10 µM U0126 treatment on 5-HT_{1B}-mediated contraction in 24-hr-incubated LAD vessels (containing 0.5 % DMSO):*

The 10 µM U0126 incubation of vehicle-treated LAD vessels decreased the 5-HT_{1B}-mediated contraction of 10 µM U0126-incubated vehicle LAD vessels (n = 8 - 9) by 37 % at the concentration of $10^{-5.5}$ M, with a mean C_{max} of 6.99 ± 0.71 % ($p < 0.0001$), compared to vehicle-treated LAD vessels (n = 8 - 9) with a mean C_{max} of 43.53 ± 14.60 % (Figure 5-12).

- *The effect of 0.5 µM doxorubicin treatment on 5-HT_{1B}-mediated contraction in the presence of 10 µM U0126 in 24-hr-incubated LAD vessels (containing 0.5 % DMSO):*

The 10 µM U0126 incubation of 0.5 µM doxorubicin-treated LAD vessels (n = 7 - 8) significantly decreased by 22 % the 5-HT_{1B}-mediated contraction with a C_{max} of 22.30 ± 5.60 % ($p < 0.0001$), when compared to U0126 naïve vehicle-treated LAD vessels with a C_{max} of 43.53 ± 14.60 % (n = 9 - 10) (Figure 5-12).

The 10 µM U0126 incubation of 0.5 µM doxorubicin-treated LAD vessels reduced (13 % to 44 % decrease) the 5-HT_{1B}-mediated contraction of 10 µM U0126-incubated 0.5 µM doxorubicin LAD vessels at 10^{-7} M (5.75 ± 2.58 %, $p = 0.0457$) and from 10^{-6} M (12.39 ± 3.93 %, $p < 0.0001$) to $10^{-5.5}$ M (C_{max} = 22.30 ± 5.60 %, $p < 0.0001$), when compared to 0.5 µM doxorubicin-treated LAD vessels at 10^{-7} M (18.75 ± 4.59 %) and from 10^{-6} M (39.85 ± 7.60 %) to $10^{-5.5}$ M (C_{max} = 65.58 ± 8.13 %) (Figure 5-12).

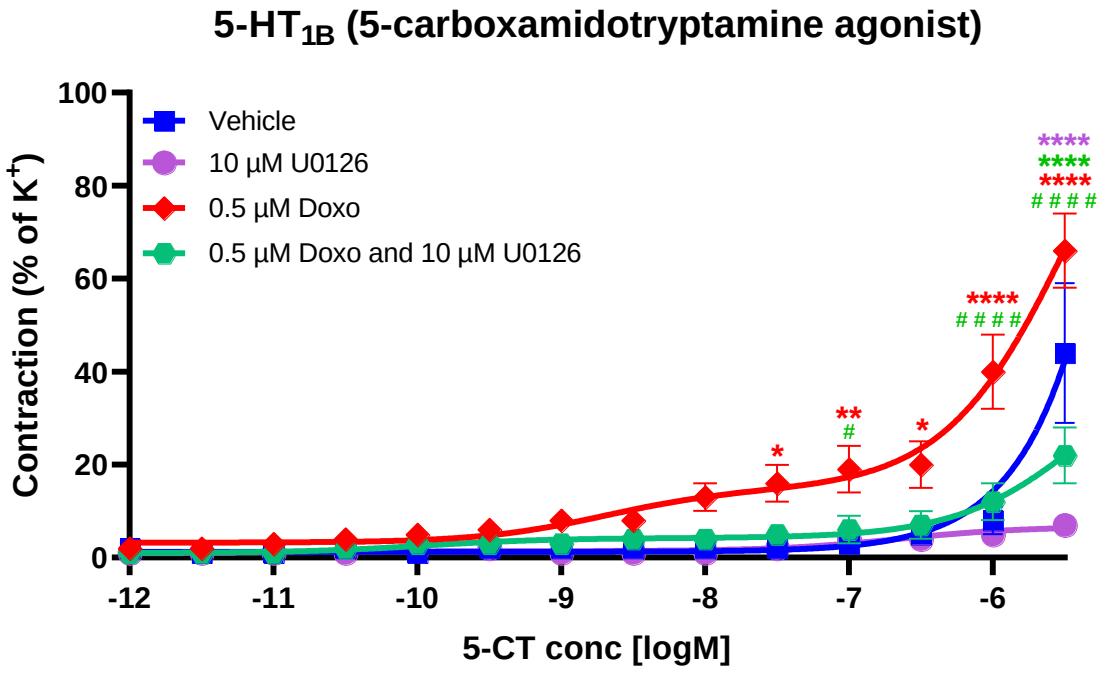

Figure 5-12: Vasocontractile response to the cumulative application of 5-carboxamidotryptamine (5-CT) (5-HT_{1B} receptor agonist) normalised to 60 mM K^+ KH-induced contraction in rat LAD arteries, after 0.5 % DMSO or 10 µM U0126 incubation. Vehicle group (containing 0.5 % DMSO; n = 8 - 9), 0.5 µM doxorubicin group (containing 0.5 % DMSO; n = 9 - 10), 0.5 µM doxorubicin and 10 µM U0126 (n = 7 - 8) and 10 µM U0126 (n = 8 - 9). 5-CT = 5-carboxamidotryptamine, DMSO = Dimethyl sulfoxide.

Contractile responses compared to vehicle group using two-way ANOVA and Bonferroni's test (* = p < 0.05, ** = p < 0.01, **** = p < 0.0001) and compared to 0.5 µM doxorubicin group using on-way ANOVA and Bonferroni's test (# = p < 0.05, #### = p < 0.0001).

Table 5-6: C_{max} values of vehicle or doxorubicin incubated LAD arteries with DMSO or MEK 1/2 inhibitor U0126: 0.5 % DMSO and 10 µM U0126 incubation. C_{max} = the contraction obtained at the highest agonist dose and is applied when the "E_{max}" couldn't be determined due to stock concentration constrains; Values given for 5-CT experiments and as mean ± S.E.M. N values represent the total amount of animals used. C_{max} values of the different groups were compared to the vehicle-treated LAD vessels with Two-way ANOVA and Bonferroni's post-hoc test: * = p < 0.05. C_{max} value of the 10 µM U0126-incubated doxorubicin LAD vessels was compared to the 0.5 µM doxorubicin-treated LAD vessels with Two-way ANOVA and Bonferroni's post-hoc test: ## = p < 0.01.

Groups	*N*	C_{max}
Vehicle	8-9	43.5 ± 14.6 %
0.5 µM Doxorubicin	9-10	65.6 ± 8.1 % ****
0.5 µM Doxorubicin and 10 µM U0126	7-8	22.3 ± 5.6 % ****, ####
10 µM U0126	8-9	7.0 ± 0.7 % ****

5.3.3.2. Real-Time PCR: quantification of 5-HT_{1B} receptor mRNA levels

Gene expression of the endothelin 5-HT_{1B} receptors was investigated in LAD arteries by Real-Time PCR. Negative controls were included for each receptor. Serotonin 5-HT_{1B} receptors mRNA expression was expressed as values relative to GAPDH and normalised to vehicle-treated LAD vessels. Both figures 5-13 (A) and 5-13 (B) showed the same tendency towards reduction or increase of 5-HT_{1B} receptors mRNA between the different groups, however, a significant difference is observed only after 0.5 % DMSO or 10 µM U0126 incubation, as shown in figure 5-13 (B).

Figure 5-13 (A) showed the mRNA levels of the 0.25 % DMSO or 5 µM U0126 incubation of vehicle-treated or 0.5 µM doxorubicin-treated LAD vessels. The 0.5 µM doxorubicin-treated LAD vessels (1.203 ± 0.093; n = 9) showed a tendency towards an up-regulation of 5-HT_{1B} receptors mRNA, compared to vehicle-treated LAD vessels (1.00 ± 0.094; n = 10), but there is no statistical difference. The 5 µM U0126 incubation of vehicle-treated LAD vessels (1.108 ± 0.090; n = 10) did not alter the 5-HT_{1B} receptor mRNA level compared to U0126 naïve vehicle-treated LAD vessels (1.00 ± 0.094; n = 10). The 5 µM incubation of 0.5 µM doxorubicin-treated LAD vessels (1.150 ± 0.080; n = 9) did not alter the 5-

HT_{1B} receptors mRNA level compared to U0126 naïve 0.5 µM doxorubicin-treated LAD vessels (1.203 ± 0.093; n = 9).

Figure 5-13 (B) showed the mRNA levels of the 0.5 % DMSO or 10 µM U0126 incubation of vehicle-treated or 0.5 µM doxorubicin-treated LAD vessels. The 5-HT_{1B} receptors mRNA level was up-regulated significantly from vehicle-treated LAD vessels (1.00 ± 0.085; n = 10) to 0.5 µM doxorubicin-treated LAD vessels (1.267 ± 0.077, p = 0.041; n = 10). The 10 µM U0126 incubation of 0.5 µM doxorubicin-treated LAD vessels (1.108 ± 0.076; n = 10) showed a tendency towards a down-regulation of 5-HT_{1B} receptor mRNA, compared to U0126 naïve 0.5 µM doxorubicin-treated LAD vessels (1.267 ± 0.077; n = 10), but there is no statistical difference. The 10 µM U0126 incubation of vehicle-treated LAD vessels (0.986 ± 0.041; n = 10) did not alter the 5-HT_{1B} receptors mRNA level compared to U0126 naïve vehicle-treated LAD vessels (1.00 ± 0.085; n = 10).

(A) (B)

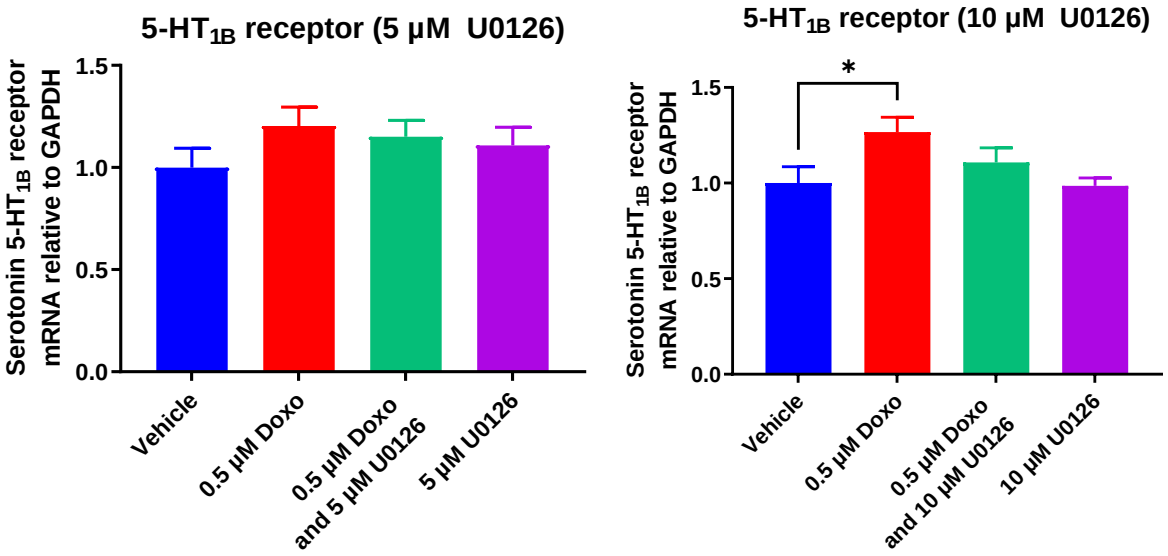

Figure 5-13: Real-Time PCR of 5-HT_{1B} receptors in LAD arteries with DMSO (Vehicle or Doxorubicin) or U0126 (Vehicle + U0126 or Doxorubicin + U0126). (A) Comparison of 5-HT_{1B} receptor mRNA levels on LAD arteries from Vehicle group (containing 0.25 % DMSO; n = 10), 0.5 µM doxorubicin group (containing 0.5 µM doxorubicin and 0.25 % DMSO; n = 9), 0.5 µM doxorubicin and 5 µM U0126 group (n = 9) and 5 µM U0126 (n = 10). **(B)** Comparison of 5-HT_{1B} receptors mRNA levels on LAD arteries from Vehicle group (containing 0.5 % DMSO; n = 10), 0.5 µM doxorubicin group (containing 0.5 µM doxorubicin and 0.5 % DMSO; n = 10), 0.5 µM doxorubicin and 10 µM U0126 group (n = 10) and 10 µM U0126 (n = 10). Data are expressed as mean ± S.E.M. values relative to GAPDH mRNA levels (n = 10) and normalised to vehicle group. Doxo = doxorubicin, 5-HT1B = 5-hydroxytryptamine 1B. The groups were compared by multiple comparisons using one-way ANOVA Kruskal-Wallis' test (* = p < 0.05).

5.3.3.3. Immunohistochemistry: Quantification of 5-HT$_{1B}$ receptor levels

The quantification of serotonin 5-HT$_{1B}$ receptors was obtained by measuring the ROI mean intensity and the intensity was normalised to vehicle-treated LAD vessels average.

Figure 5-14 (A) showed the 5-HT$_{1B}$ receptors expression of both vehicle-treated LAD vessels and 0.5 µM doxorubicin-treated vessels after the incubation with either 0.25 % DMSO or 5 µM U0126. The 5-HT$_{1B}$ receptors expressions on LAD vessels of the four groups are widely spread. No statistical difference was observed between the different groups. The 5 µM U0126 incubation of vehicle-treated LAD vessels (0.987 ± 0.019; n = 4) did not alter the 5-HT$_{1B}$ receptors expression compared to the U0126 naïve vehicle-treated LAD vessels (1.00 ± 0.010; n = 4). Likewise, the 5 µM U0126 incubation of 0.5 µM doxorubicin-treated LAD vessels (0.993 ± 0.017; n = 4) did not alter the 5-HT$_{1B}$ receptor expression compared to the U0126 naïve 0.5 µM doxorubicin-treated LAD vessels (0.982 ± 0.024; n = 4).

Figure 5-14 (B) showed the 5-HT$_{1B}$ receptors expression of both vehicle-treated LAD vessels and 0.5 µM doxorubicin-treated vessels after the incubation with either 0.5 % DMSO or 10 µM U0126. The 0.5 µM doxorubicin treatment of LAD vessels increased the 5-HT$_{1B}$ receptors expression of the 0.5 µM doxorubicin-treated LAD vessels (1.023 ± 0.006; n = 4) when compared to the vehicle-treated LAD vessels (1.00 ± 0.009, p = 0.038; n = 4). The 10 µM U0126 incubation of vehicle-treated LAD vessels (1.009 ± 0.007; n = 3) did not alter the 5-HT$_{1B}$ receptors expression compared to the U0126 naïve vehicle-treated LAD vessels (1.00 ± 0.009; n = 4). The 10 µM U0126 incubation of 0.5 µM doxorubicin-treated LAD vessels (0.996 ± 0.005; n = 4) did not alter the 5-HT$_{1B}$ receptors expression compared to the U0126 naïve 0.5 µM doxorubicin-treated LAD vessels (1.023 ± 0.006; n = 4).

(A)

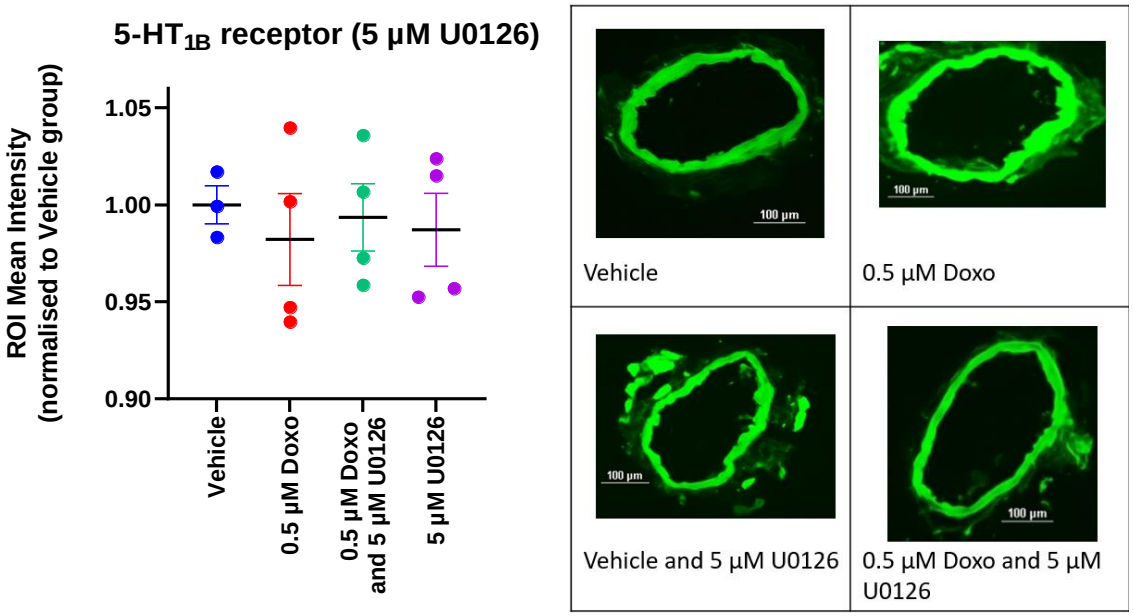

(B)

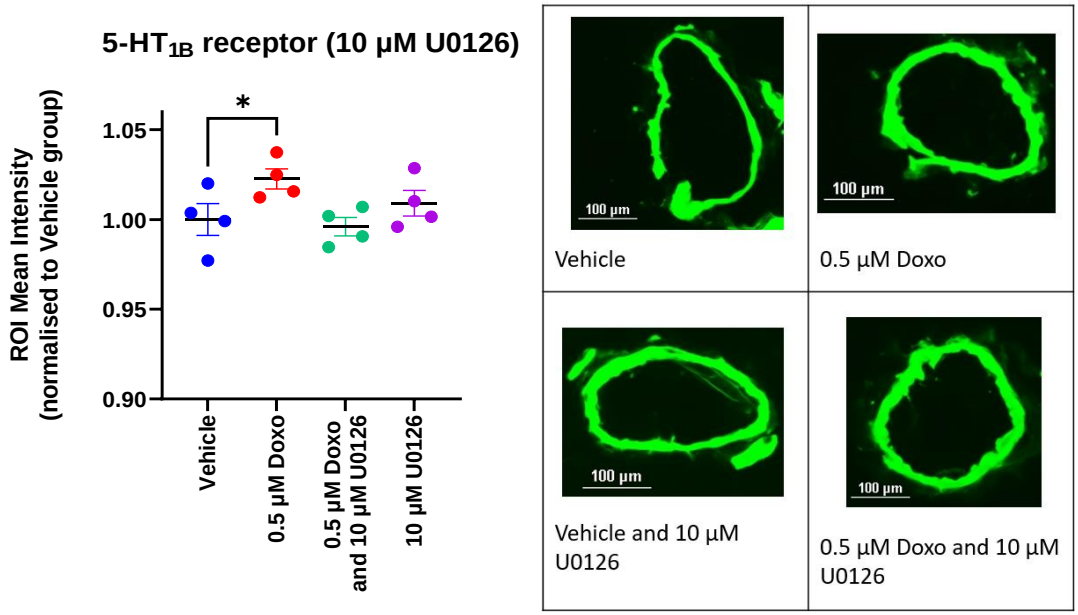

Figure 5-14: Quantification of the 5-HT$_{1B}$ receptor expression in LAD arteries by immunofluorescence. (A) Comparison of 5-HT$_{1B}$ receptor expression on LAD arteries from Vehicle group (containing 0.25 % DMSO; n = 4), 0.5 µM doxorubicin group (containing 0.5 µM doxorubicin and 0.25 % DMSO; n = 4), 0.5 µM doxorubicin and 5 µM U0126 group (n = 4) and 5 µM U0126 (n = 4). **(B)** Comparison of 5-HT$_{1B}$ receptors expression on LAD arteries from Vehicle group (containing 0.5 % DMSO; n = 4), 0.5 µM doxorubicin group (containing 0.5 µM doxorubicin and 0.5 % DMSO; n = 4), 0.5 µM doxorubicin and 10 µM U0126 group (n = 4) and 10 µM U0126 (n = 3). Doxo = doxorubicin, 5-HT$_{1B}$ = 5-hydroxytryptamine 1B, ROI = region of interest. The groups were compared by multiple comparisons using one-way ANOVA and Fisher's test (* = $p < 0.05$).

5.3.4. Thromboxane prostanoid (TP) receptor

5.3.4.1. Wire-myography: Thromboxane prostanoid TP receptors-mediated vasocontraction

The thromboxane prostanoid (TP) receptor specific agonist, U46619, was used to investigate the effect of doxorubicin on TP receptor-mediated vasocontraction after 24-hr-incubation with DMSO or MEK 1/2 inhibitor, U0126. The TP-induced vasocontraction values are given as percentage of the maximal contractile response, induced by K^+ KH. "E_{max}" and "pEC_{50}" values of are given in Tables 5-7 and 5-8. The difference of vasocontraction between the groups and the p values are given in Tables 9-9 and 9-10 in Appendices.

5.3.4.1.1. TP receptor-mediated contraction in 0.5 µM of doxorubicin with and without 5 µM of U0126 (containing 0.25 % of DMSO)

- *The effect of 0.5 µM doxorubicin treatment on TP receptor-mediated contraction in 24-hr-incubated LAD vessels (containing 0.25 % DMSO):*

As shown in Figure 5-15, TP-mediated vasocontraction of 0.5 µM doxorubicin-treated LAD vessels was increased (by 21 % to 47 %) from 10^{-8} M (24.79 ± 6.21 %, p = 0.0265) to $10^{-6.5}$ M (C_{max} = 106.69 ± 5.98 %, p = 0.0032), when compared to vehicle-treated LAD vessels from 10^{-8} M (4.26 ± 0.93 %) to $10^{-6.5}$ M (C_{max} = 81.09 ± 14.83 %) (Table 9-9 in Appendices). The 0.5 µM doxorubicin incubation significantly increased the TP-mediated contraction of 0.5 µM doxorubicin-treated LAD vessels ("E_{max}" = 116.4 ± 8.1 %, p = 0.0168), when compared to vehicle-treated LAD vessels ("E_{max}" = 83.3 ± 7.4 %). Furthermore, the 0.5 µM doxorubicin treatment induced a left-shift of the U46619 dose-response curve of 0.5 µM doxorubicin-treated LAD vessels ("pEC_{50}"=$10^{-7.46}$ M, p = 0.0008) compared to vehicle-treated LAD vessels ("pEC_{50}"= $10^{-7.07}$ M).

- *The effect of 5 µM U0126 treatment on TP receptor-mediated contraction in 24-hr-incubated LAD vessels (containing 0.25 % DMSO):*

The incubation of 5 µM U0126 on vehicle-treated LAD vessels did not alter the TP-mediated contraction of 5 µM U0126-incubated vehicle LAD vessels (n = 13 - 15), when compared to vehicle-treated LAD vessels (Figure 5-15). Furthermore, the 5 µM U0126 incubation of 0.5 µM doxorubicin LAD vessels did not alter the maximal TP-mediated contraction and the TP receptor's affinity of 5 µM U0126-incubated vehicle LAD vessels ("E_{max}" = 90.5 ± 16.7 %, "pEC_{50}" = $10^{-7.06}$), when compared to U0126 naïve vehicle-treated LAD vessels ("E_{max}" = 83.3 ± 7.4 %, "pEC_{50}" = $10^{-7.07}$ M).

- *The effect of 0.5 µM doxorubicin treatment on TP receptor-mediated contraction in the presence of 5 µM U0126 in 24-hr-incubated LAD vessels (containing 0.25 % DMSO):*

The TP-mediated vasocontraction increased (27 % increase) at $10^{-7.5}$ M (34.07 ± 11.36 %, p = 0.007) in 5 µM U012-incubated 0.5 µM doxorubicin vessels when compared to U0126 naïve vehicle-treated vessels at $10^{-7.5}$ M (7.44 ± 2.20 %) (Figure 5-15). The inhibition effect of 5 µM U0126 on 0.5 µM doxorubicin-treated LAD vessels did not alter the "E_{max}" and "pEC_{50}" values of 5 µM U0126-incubated 0.5 µM doxorubicin LAD vessels ("E_{max}"= 78.5 ± 13.7 %, "pEC_{50}" = $10^{-7.36}$ M) when compared to U0126 naïve vehicle-treated LAD vessels ("E_{max}"= 83.3 ± 7.4 %, "pEC_{50}" = $10^{-7.07}$ M).

Furthermore, the 5 µM U0126 incubation of 0.5 µM doxorubicin-treated LAD vessels slightly decreased (by 34 %) the TP-mediated vasocontraction of 5 µM U0126-incubated 0.5 µM doxorubicin LAD vessels at 10^{-7} M (56.92 ± 15.12 %, p < 0.0001) and $10^{-6.5}$ M (73.03 ± 13.74 %, p = 0.0001) when compared to U0126 naïve 0.5 µM doxorubicin-treated LAD vessels at 10^{-8} M (24.79 ± 6.21 %) and 10^{-}

$^{6.5}$ M (106.69 ± 5.98 %) (Figure 5-15). The inhibition effect of 5 µM U0126 on 0.5 µM doxorubicin-treated LAD vessels did not alter the maximal TP-mediated vasocontraction and the TP receptor's affinity (to U46619) of 5 µM U0126-incubated 0.5 µM doxorubicin LAD vessels ("E_{max}" = 78.5 ± 13.7 %, "pEC_{50}" = $10^{-7.36}$ M) when compared to U0126 naïve 0.5 µM doxorubicin-treated LAD vessels ("E_{max}" = 83.3 ± 7.4 %, "pEC_{50}" = $10^{-7.07}$ M).

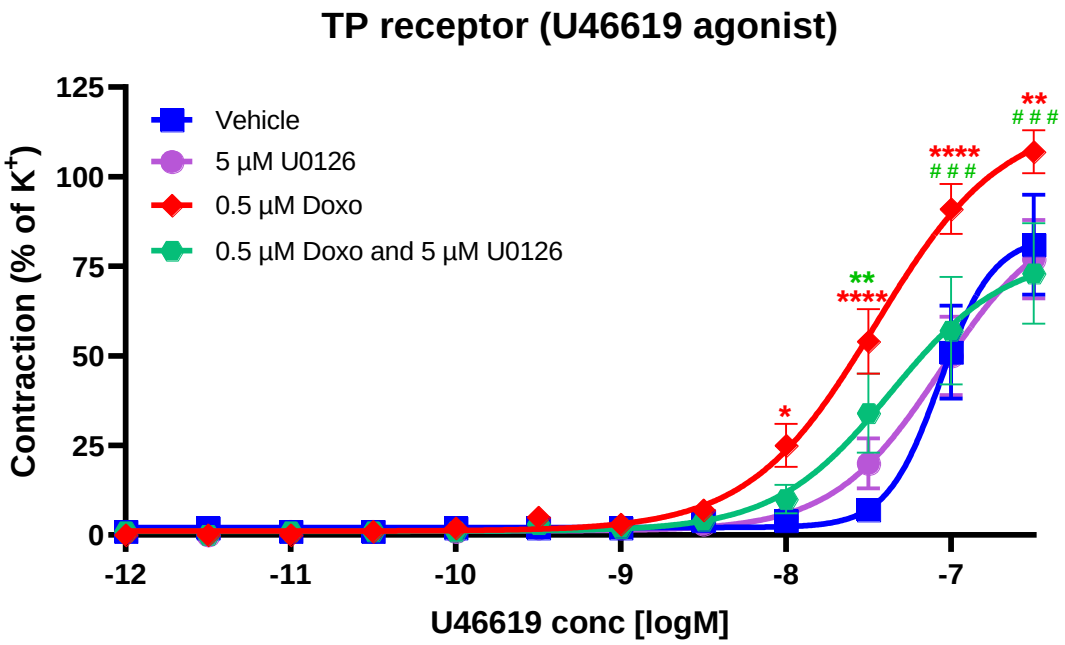

Figure 5-15: Vasocontractile response to the cumulative application of 9,11-dideoxy-11α,9α-epoxymethanoprostaglandin $F_{2α}$ (U46619) (TP receptor agonist) normalised to 60 mM K^+ KH-induced contraction in rat LAD arteries, after 0.25 % DMSO or 5 µM U0126 incubation. Vehicle group (containing 0.25 % DMSO; n = 12 - 13), 0.5 µM doxorubicin group (containing 0.25 % DMSO; n = 13 - 15), 0.5 µM doxorubicin and 5 µM U0126 (n = 9 - 10) and 5 µM U0126 (n = 13 - 15). U46619 = agonist of thromboxane prostanoid receptors, DMSO = Dimethyl sulfoxide. Vasocontractile responses compared to vehicle group using two-way ANOVA and Bonferroni's test (* = $p < 0.05$, ** = $p < 0.01$, **** = $p < 0.0001$) and compared to 0.5 µM doxorubicin group using two-way ANOVA and Bonferroni's test (### = $p < 0.001$).

Table 5-7: C_{max}, "E_{max}" and "pEC_{50}" values of vehicle or doxorubicin incubated LAD arteries with DMSO or MEK 1/2 inhibitor U0126: 0.25 % DMSO and 5 µM U0126 incubation. Values given for all Endothelin-1 experiments and as mean ± S.E.M. N values represent the total amount of animals used. The "E_{max}" and "pEC_{50}" values of the different groups are compared to the vehicle-treated LAD vessels (containing 0.25 % DMSO) with ANOVA and Dunnett's post-hoc test: * = $p < 0.05$, *** = $p < 0.001$. The 10 µM U0126-incubated 0.5 µM doxorubicin LAD vessels were compared to U0126 naïve doxorubicin-treated LAD vessels (containing 0.5 % DMSO) with ANOVA and Dunnett's post-hoc test: $^{\#}$ = $p < 0.05$

and $^{\#\#\#\#}$ = p < 0.0001, while C_{max} is compared using two-way ANOVA with Bonferroni's post-hoc test: ** = p < 0.01.

Groups	*N*	*C_{max}*	*"E_{max}"*	*"pEC_{50}"*
Vehicle	12-13	81.09 ± 14.83 %	83.3 ± 7.4 %	7.07 ± 0.06
0.5 µM Doxorubicin	13-15	106.69 ± 5.98 % **	116.4 ± 8.1 % *	7.46 ± 0.08 ***
0.5 µM Doxorubicin and 5 µM U0126	9-10	73.03 ± 13.74 %	78.5 ± 13.7 %	7.36 ± 0.19
5 µM U0126	13-15	77.38 ± 11.04 %	90.5 ± 16.7 %	7.06 ± 0.17

5.3.4.1.2. TP receptor-mediated contraction in 0.5 µM of doxorubicin with and without 10 µM of U0126 (containing 0.5 % of DMSO)

- *The effect of 0.5 µM doxorubicin treatment on TP receptor-mediated contraction in 24-hr-incubated LAD vessels (containing 0.5 % DMSO):*

The 0.5 µM doxorubicin treatment induced a significant increase (29 % increase) of TP-mediated vasocontraction from $10^{-7.5}$ M (47.47 ± 6.34 %, p = 0.0005) to 10^{-7} M U46619 (97.24 ± 5.91 %, p = 0.0004), in 0.5 µM doxorubicin-treated LAD vessels (n = 10 - 11) when compared to vehicle-treated LAD vessels from $10^{-7.5}$ M (17.73 ± 10.63 %) to 10^{-7} M U46619 (68.08 ± 18.70 %) (Figure 5-16). The 0.5 µM doxorubicin incubation seems to induce an increase of the maximal TP-mediated vasocontraction from "E_{max}" = 104.5 ± 10.5 % for the vehicle-treated LAD vessels to "E_{max}" = 122.7 ± 5.6 % for the 0.5 µM doxorubicin-treated LAD vessels, but the statistical significance of "E_{max}" values was not obtained due to high variation. However, the 0.5 µM doxorubicin treatment increased the TP receptor affinity to U46619 with a "pEC_{50}" of $10^{-7.37}$ M (p = 0.0427) for the 0.5 µM doxorubicin-treated LAD vessels, compared to the "pEC_{50}" of $10^{-7.13}$ M for the vehicle-treated LAD vessels.

- *The effect of 10 µM U0126 treatment on TP receptor-mediated contraction in 24-hr-incubated LAD vessels (containing 0.5 % DMSO):*

The U46619 dose-response curve of 10 µM U0126-incubated vehicle LAD vessels did not reach the final plateau at the highest dose due to stock constraints, and therefore final "E_{max}" and "pEC_{50}" values could not be obtained. However, the vasocontraction obtained at the highest dose ($10^{-6.5}$ M) is mentioned as C_{max}. The 10 µM U0126 incubation of vehicle-treated LAD vessels reduced the TP-mediated vasocontraction of 10 µM U0126-incubated vehicle LAD vessels (n = 7 - 8) by 51 % at 10^{-7} M (17.19 ± 4.34 %, p < 0.0001) and 44 % at $10^{-6.5}$ M (55.21 ± 16.43 %, p < 0.0001), when compared to U0126 naïve vehicle-treated LAD vessels at 10^{-7} M (68.08 ± 18.70 %) and $10^{-6.5}$ M (99.10 ± 11.81 %) (Figure 5-16).

- *The effect of 0.5 µM doxorubicin treatment on TP receptor-mediated contraction in the presence of 10 µM U0126 in 24-hr-incubated LAD vessels (containing 0.5 % DMSO):*

The TP-mediated contraction was reduced (24 % and 42 % decrease) at, respectively, 10^{-7} M (43.83 ± 8.65 %, p = 0.0071) and $10^{-6.5}$ M (C_{max} = 56.57 ± 9.71 %, p < 0.0001), on 0.5 µM doxorubicin vessels with 10 µM U0126 (n = 10 - 11) when compared to U0126 naïve vehicle-treated vessels at 10^{-7} M (68.08 ± 18.70 %) and $10^{-6.5}$ M (C_{max} = 99.10 ± 11.81 %) (Figure 5-16). The inhibition effect of 10 µM U0126 on 0.5 µM doxorubicin-treated LAD vessels reduced the maximal TP-mediated vasocontraction of 10 µM U0126-incubated 0.5 µM doxorubicin LAD vessels ("E_{max}"= 62.3 ± 9.4 %, p = 0.0182) when compared to U0126 naïve vehicle-treated LAD vessels ("E_{max}"= 122.7 ± 5.6 %), while the "pEC_{50}" remain unchanged (Table 5-8).

The 10 µM U0126 incubation of 0.5 µM doxorubicin-treated LAD vessels significantly reduced (23 %, 53 % and 57 % decrease) the TP-mediated contraction of 0.5 µM doxorubicin LAD vessels with 10 µM U0126 at $10^{-7.5}$ M U46619 (23.78 ± 5.30 %, p = 0.0051), at 10^{-7} M U46619 (43.83 ± 8.65 %, p < 0.0001) and $10^{-6.5}$ M U46619 (56.57 ± 9.71 %, p < 0.0001) when compared to 10 µM U0126 naïve 0.5 µM doxorubicin-treated LAD vessels at $10^{-7.5}$ M U46619 (17.73 ± 10.63 %), at 10^{-7} M U46619 (68.08 ± 18.70 %) and $10^{-6.5}$ M U46619 (99.10 ± 11.81 %) (Figure 5-16). The inhibition effect of 10 µM U0126 on 0.5 µM doxorubicin-treated LAD vessels significantly reduced the maximal TP-mediated contraction of 10 µM U0126-incubated 0.5 µM doxorubicin LAD vessels ("E_{max}"= 62.3 ± 9.4 %, p < 0.0001), when compared to U0126 naïve 0.5 µM doxorubicin-treated LAD vessels ("E_{max}"= 122.7 ± 5.6 %), while the "pEC_{50}" values remain unaltered (Table 5-8).

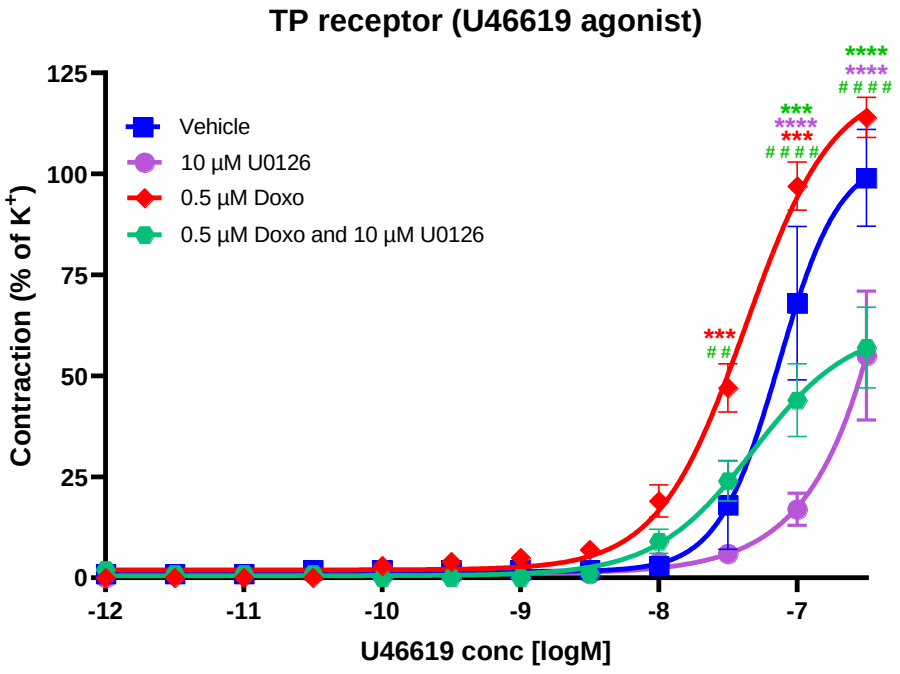

Figure 5-16: Vasocontractile response to the cumulative application of 9,11-dideoxy-11α,9α-epoxymethanoprostaglandin $F_{2\alpha}$ (U46619) (TP receptor agonist) normalised to 60 mM K^+ KH-induced contraction in rat LAD arteries, after 0.5 % DMSO or 10 µM U0126 incubation. Vehicle group (containing 0.5 % DMSO; n = 8 - 9), 0.5 µM doxorubicin group (containing 0.5 % DMSO; n = 10 - 11), 0.5 µM doxorubicin and 10 µM U0126 (n = 9 - 10) and 10 µM U0126 (n = 7 - 8). U46619 = agonist of thromboxane prostanoid receptor, DMSO = Dimethyl sulfoxide. Vasocontractile responses compared to vehicle group using two-way ANOVA and Bonferroni's test (*=p<0.05, **=p<0.01, ***=p<0.005) and compared to0.5 µM doxorubicin group using two-way ANOVA and Bonferroni's test (# = p < 0.05, ## = p < 0.01, ### = p < 0.001).

Table 5-8: The C_{max}, "E_{max}" and "pEC_{50}" values of vehicle or doxorubicin incubated LAD arteries with DMSO or MEK 1/2 inhibitor U0126: 0.5 % DMSO and 10 µM U0126 incubation. C_{max} = the contraction obtained at the highest agonist dose and is applied when the "E_{max}" couldn't be determined due to stock concentration constraints; Values given for U46619 experiments and as mean ± S.E.M. N values represent the total amount of animals used. The "E_{max}" and "pEC_{50}" values of the different groups are compared to the vehicle-treated LAD vessels (containing 0.25 % DMSO) with ANOVA and Dunnett's post-hoc test: * = p < 0.05, **** = p < 0.0001. The 10 µM U0126-incubated 0.5 µM doxorubicin LAD vessels were compared to U0126 naïve doxorubicin-treated LAD vessels (containing 0.5 % DMSO) with ANOVA and Dunnett's post-hoc test: $^{\#}$ = p < 0.05 and $^{\#\#\#\#}$ = p < 0.0001, while C_{max} is compared using two-way ANOVA with Bonferroni's post-hoc test: * = p < 0.05, $^{\#\#\#}$ = p < 0.001 and **** or $^{\#\#\#\#}$ = p < 0.0001.

Groups	*N*	*C_{max}*	*"E_{max}"*	*"pEC_{50}"*
Vehicle	8-9	99.10 ± 11.81 %	104.5 ± 10.5 %	7.13 ± 0.08
0.5 µM Doxorubicin	10-11	113.67 ± 5.45 %	122.7 ± 5.6 %	7.37 ± 0.05 *
0.5 µM Doxorubicin and 10 µM U0126	9-10	56.57 ± 9.71 % ****, $^{\#\#\#\#}$	62.3 ± 9.4 %*, $^{\#\#\#}$	7.32 ± 0.16
10 µM U0126	7-8	55.21 ± 16.43 % ****	/	/

5.3.4.2. Real-Time PCR: quantification of TP receptor mRNA levels

Gene expression of the endothelin TP receptors was investigated in rat LAD arteries by Real-Time PCR. Negative controls were included for each receptor. TP receptors mRNA expression was expressed as values relative to GAPDH and normalised to vehicle-treated LAD vessels. Both figures 5-17 (A) and 5-17 (B) showed the same tendency towards increase or reduction of TP receptors mRNA between the different groups.

Figure 5-17 (A) showed the mRNA levels on vehicle-treated LAD vessels or 0.5 µM doxorubicin-treated LAD vessels after the incubation with either 0.25 % DMSO or 5 µM U0126. The 0.5 µM doxorubicin treatment of LAD vessels (1.065 ± 0.077; n = 9) did not alter the TP receptors mRNA level compared

to vehicle-treated LAD vessels (1.00 ± 0.105; n = 10). The 5 µM U0126 of vehicle-treated LAD vessels (1.005 ± 0.086; n = 10) did not alter the TP receptor mRNA level compared to U0126 naïve vehicle-treated LAD vessels (1.00 ± 0.105; n = 10). The 5 µM incubation of 0.5 µM doxorubicin-treated LAD vessels (1.131 ± 0.057; n = 9) did not alter the TP receptor mRNA level compared to U0126 naïve 0.5 µM doxorubicin-treated LAD vessels (1.065 ± 0.077; n = 9).

Figure 5-17 (B) showed the mRNA levels on vehicle-treated LAD vessels or 0.5 µM doxorubicin-treated LAD vessels after the incubation with either 0.5 % DMSO or 10 µM U0126. The 0.5 µM doxorubicin treatment of LAD vessels (1.153 ± 0.094; n = 10) showed a tendency towards an increase of TP receptor mRNA level, compared to vehicle-treated LAD vessels (1.00 ± 0.084; n = 10), but there is no statistical difference. The 10 µM U0126 incubation of vehicle-treated LAD vessels (0.992 ± 0.069; n = 10) did not alter the TP receptor mRNA level compared to U0126 naïve vehicle-treated LAD vessels (1.00 ± 0.084; n = 10). The 10 µM U0126 incubation of 0.5 µM doxorubicin-treated LAD vessels (1.083 ± 0.066; n = 10) did not alter the TP receptor mRNA level compared to U0126 naïve 0.5 µM doxorubicin-treated LAD vessels (1.153 ± 0.094; n = 10).

(A) (B)

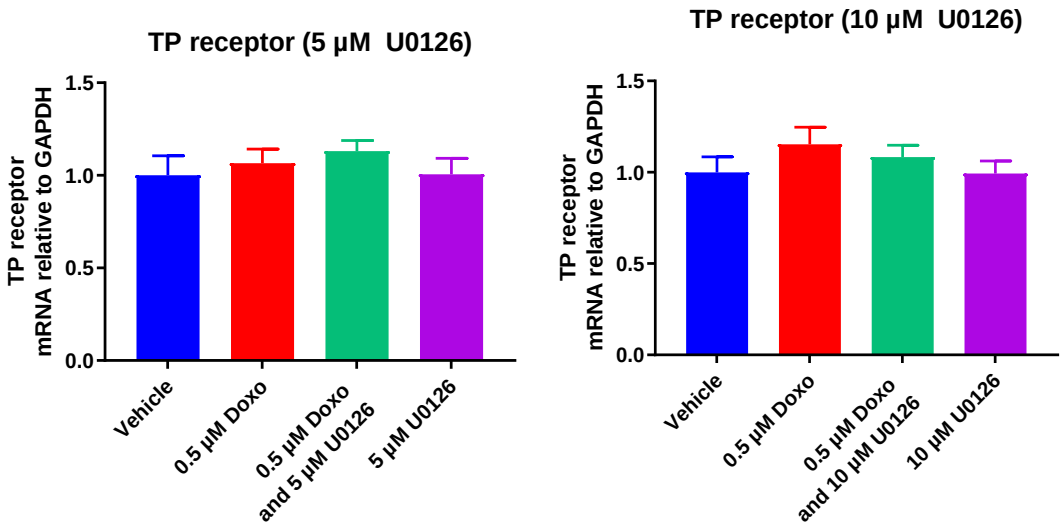

Figure 5-17: Real-Time PCR of TP receptors in LAD arteries with DMSO (Vehicle or Doxorubicin) or U0126 (Vehicle + U0126 or Doxorubicin + U0126). (A) Comparison of TP receptor mRNA levels on LAD arteries from Vehicle group (containing 0.25 % DMSO; n = 10), 0.5 µM doxorubicin group (containing 0.5 µM doxorubicin and 0.25 % DMSO; n = 9), 0.5 µM doxorubicin and 5 µM U0126 group (n = 9) and 5 µM U0126 (containing 5 µM U0126; n = 10). **(B)** Comparison of TP receptor mRNA levels on LAD arteries from Vehicle group (containing 0.5 % DMSO; n = 10), 0.5 µM doxorubicin group (with 0.5 µM doxorubicin and 0.5 % DMSO; n = 10), 0.5 µM doxorubicin and 10 µM U0126 group (n = 10) and 10 µM U0126 (n = 10). Data are expressed as mean ± S.E.M. values relative to GAPDH mRNA levels (n = 10) and normalised to vehicle group. Doxo = doxorubicin, TP = thromboxane prostanoid. The groups were compared by multiple comparisons using one-way ANOVA Kruskal-Wallis' test.

5.3.4.3. Immunohistochemistry: Quantification of TP receptor levels

The quantification of TP receptors was obtained by measuring the ROI mean intensity and the intensity was normalised to vehicle-treated LAD vessels average.

Figure 5-18 (A) showed the TP receptors expression of both vehicle-treated LAD vessels and 0.5 µM doxorubicin-treated vessels after the incubation with either 0.25 % DMSO or 5 µM U0126. The 5 µM U0126 incubation of vehicle-treated LAD vessels (1.159 ± 0.054; n = 4) induced an increase of TP receptor expression when compared to the U0126 naïve vehicle-treated LAD vessels (1.00 ± 0.027, p = 0.0395; n = 4). No significant difference was observed between the other groups. The TP receptors expression on 0.5 µM doxorubicin-treated LAD vessels was 1.094 ± 0.066 (n = 4) and after the 5 µM U0126 incubation, the TP receptor expression on 0.5 µM doxorubicin-treated LAD vessels was 1.147 ± 0.038 (n = 4).

Figure 5-18 (B) showed the TP receptor expression of both vehicle-treated LAD vessels and 0.5 µM doxorubicin-treated vessels after the incubation with either 0.5 % DMSO or 10 µM U0126. No statistical difference was observed between the different groups. The 10 µM U0126 incubation of vehicle-treated LAD vessels (0.964 ± 0.065; n = 3) did not alter the TP receptors expression compared to the U0126 naïve vehicle-treated LAD vessels (1.00 ± 0.018; n = 4). The 10 µM U0126 incubation of 0.5 µM doxorubicin-treated LAD vessels (0.982 ± 0.017; n = 4) did not alter the TP receptor expression compared to the U0126 naïve 0.5 µM doxorubicin-treated LAD vessels (0.839 ± 0.116; n = 4).

(A)

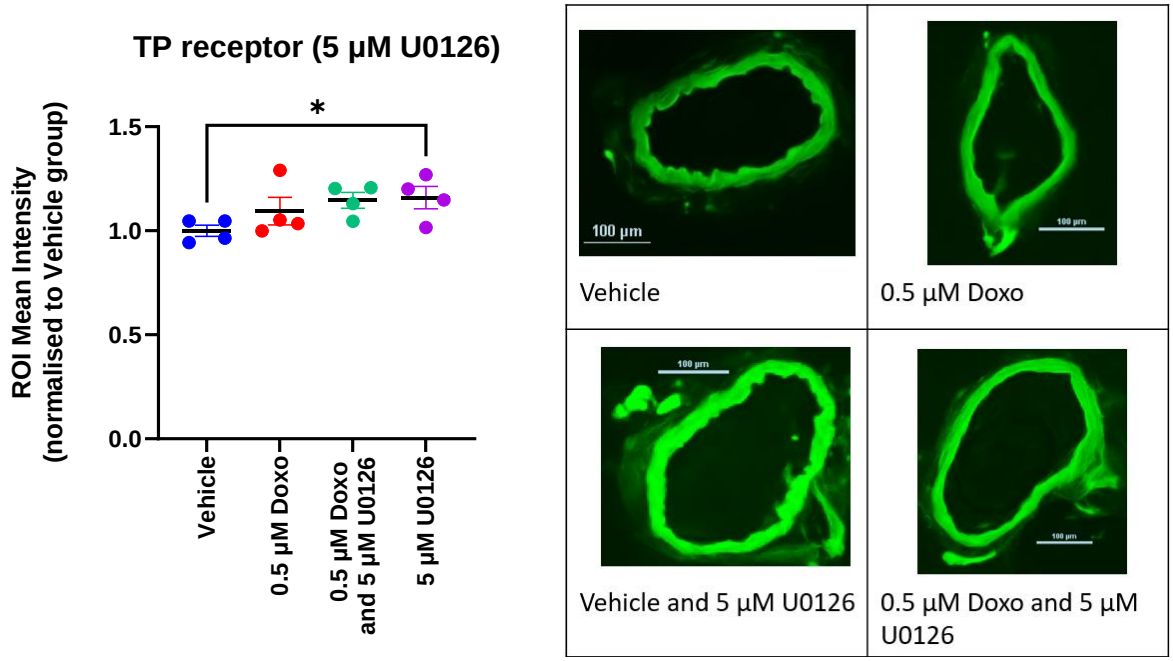

(B)

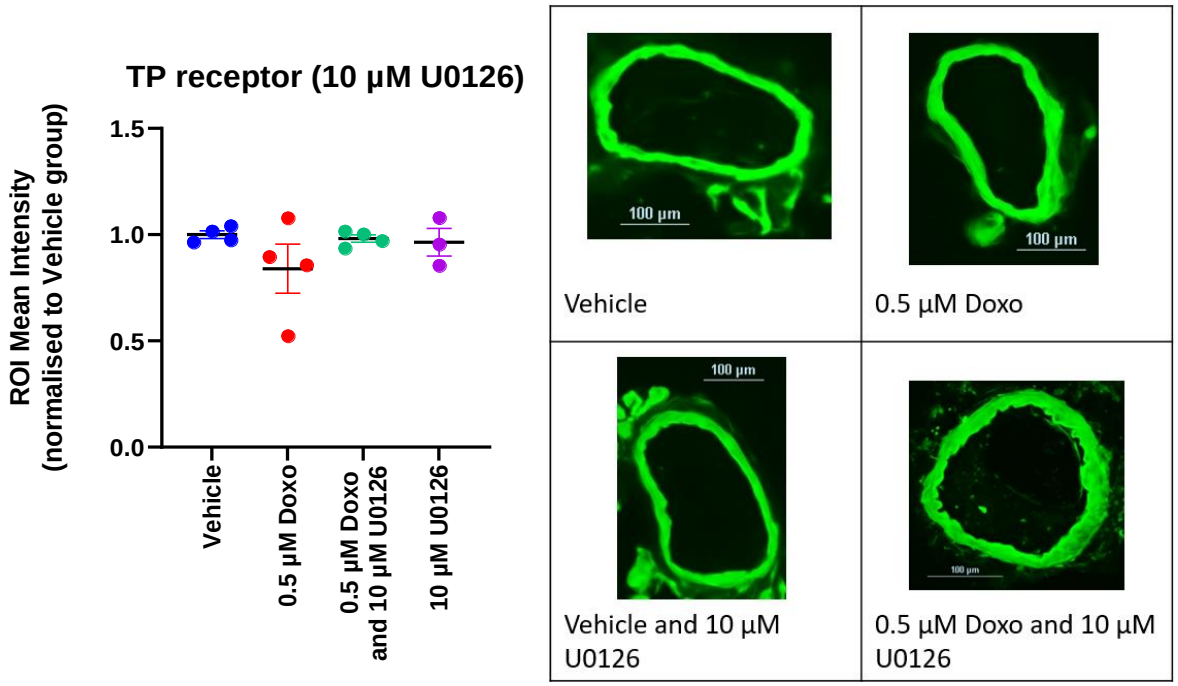

Figure 5-18: Quantification of the TP receptors expression in LAD arteries by immunofluorescence. (A) Comparison of TP receptors expression on LAD arteries from Vehicle group (containing 0.25 % DMSO; n = 4), 0.5 µM doxorubicin group (containing 0.5 µM doxorubicin and 0.25 % DMSO; n = 4), 0.5 µM doxorubicin and 5 µM U0126 group (n = 4) and 5 µM U0126 (n = 4). **(B)** Comparison of TP receptor expression on LAD arteries from Vehicle group (containing 0.5 % DMSO; n = 4), 0.5 µM doxorubicin group (containing 0.5 µM doxorubicin and 0.5 % DMSO; n = 4), 0.5 µM doxorubicin and 10 µM U0126 group (n = 4) and 10 µM U0126 (n = 3). Doxo = doxorubicin, TP = thromboxane prostanoid, ROI = region of interest. The groups were compared by multiple comparisons using one-way ANOVA and Fisher's test (* = $p < 0.05$).

5.3.5. pERK quantification in LAD arteries:

The efficiency of the MEK 1/2 inhibitor U0126 used in this study can be tested by the quantification of pERK expression by the use of the immunohistochemistry technique. The quantification was obtained by measuring the ROI mean intensity and the intensity was normalised to vehicle group (i.e. vehicle = 1).

Figure 5-19 (A) showed the studied groups with 0.25 % of DMSO or 5 µM of U0126. Incubation of LAD vessels with 0.5 µM doxorubicin did not alter the pERK expression of the 0.5 µM doxorubicin-treated LAD vessels 1.025 ± 0.015 (n = 4) when compared to the vehicle-treated LAD vessels 1.00 ± 0.023 (n = 4). LAD vessels incubated in DMEM with vehicle and 5 µM U0126 (0.901 ± 0.053; n = 4) and with doxorubicin and 5 µM U0126 (0.889 ± 0.0428; n = 4) showed a tendency towards a reduction of pERK expression compared to vehicle LAD vessels 1.00 ± 0.023 (n = 4), but there was no statistical difference. The incubation with 5 µM U0126 of doxorubicin-treated LAD arteries 0.889 ± 0.0428 (n = 4) induced a

significant reduction of pERK expression compared to 0.5 µM doxorubicin-treated LAD vessels 1.025 ± 0.015 (p = 0.0228; n = 4). pERK expression of vehicle-treated LADs vessels incubated with 5 µM U0126 0.901 ± 0.053 (n = 4) was significantly decreased, compared to 0.5 µM doxorubicin-incubated LAD vessels 1.025 ± 0.015 (p = 0.0433; n = 4).

Figure 5-19 (B) showed the quantification of the studied groups with 0.5 % of DMSO or 10 µM of U0126. Incubation of LAD vessels with 0.5 µM doxorubicin did not alter the pERK expression of the 0.5 µM doxorubicin-treated LAD vessels 1.002 ± 0.025 (n = 4) when compared to the vehicle-treated LAD vessels 1.00 ± 0.065 (n = 4). LAD vessels incubated in DMEM with vehicle and 5 µM U0126 (0.781 ± 0.035; n = 3) and with doxorubicin and 5 µM U0126 (0.795 ± 0.033; n = 4) showed a reduction of pERK expression compared to vehicle-treated LAD vessels 1.00 ± 0.065 (respectively, p = 0.003 and p = 0.005; n = 4). The LAD vessels incubated in DMEM with vehicle and 5 µM U0126 (0.781 ± 0.035; n = 3) and with doxorubicin and 5 µM U0126 (0.795 ± 0.033; n = 4) showed a reduction of pERK expression compared to 0.5 µM doxorubicin-treated LAD vessels (1.002 ± 0.025; n = 4) (respectively, p = 0.003 and p = 0.005).

(A)

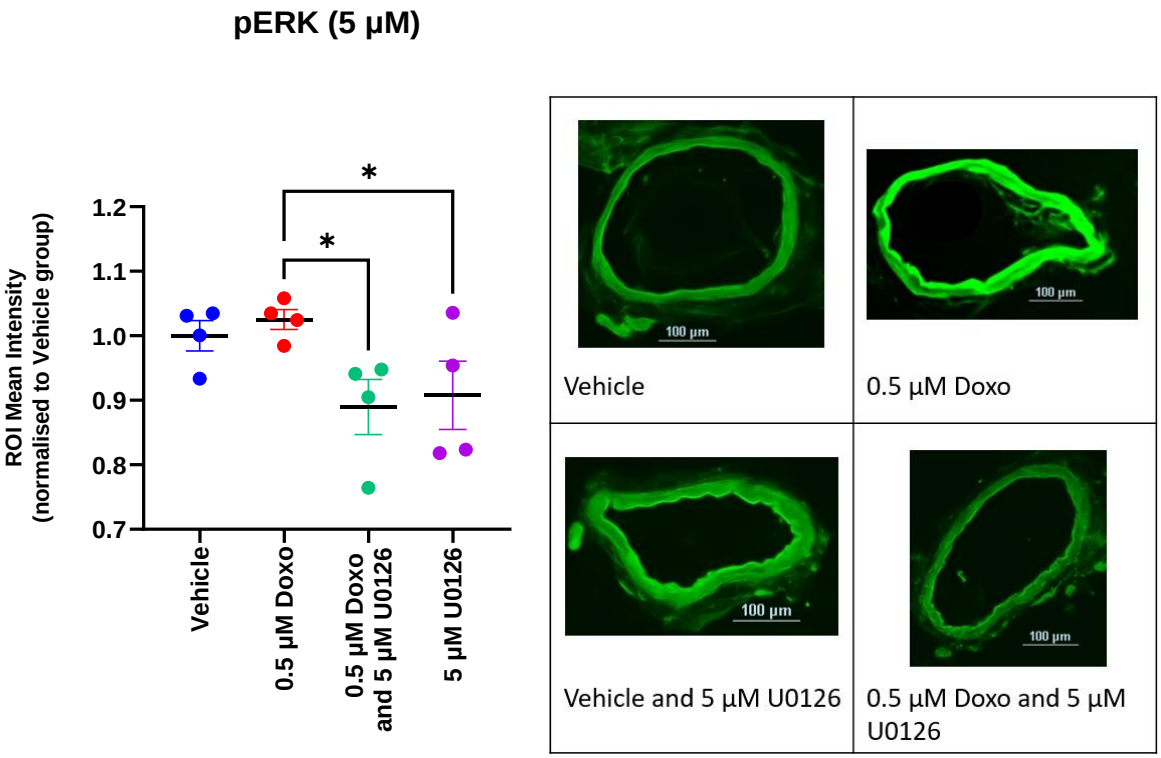

(B)

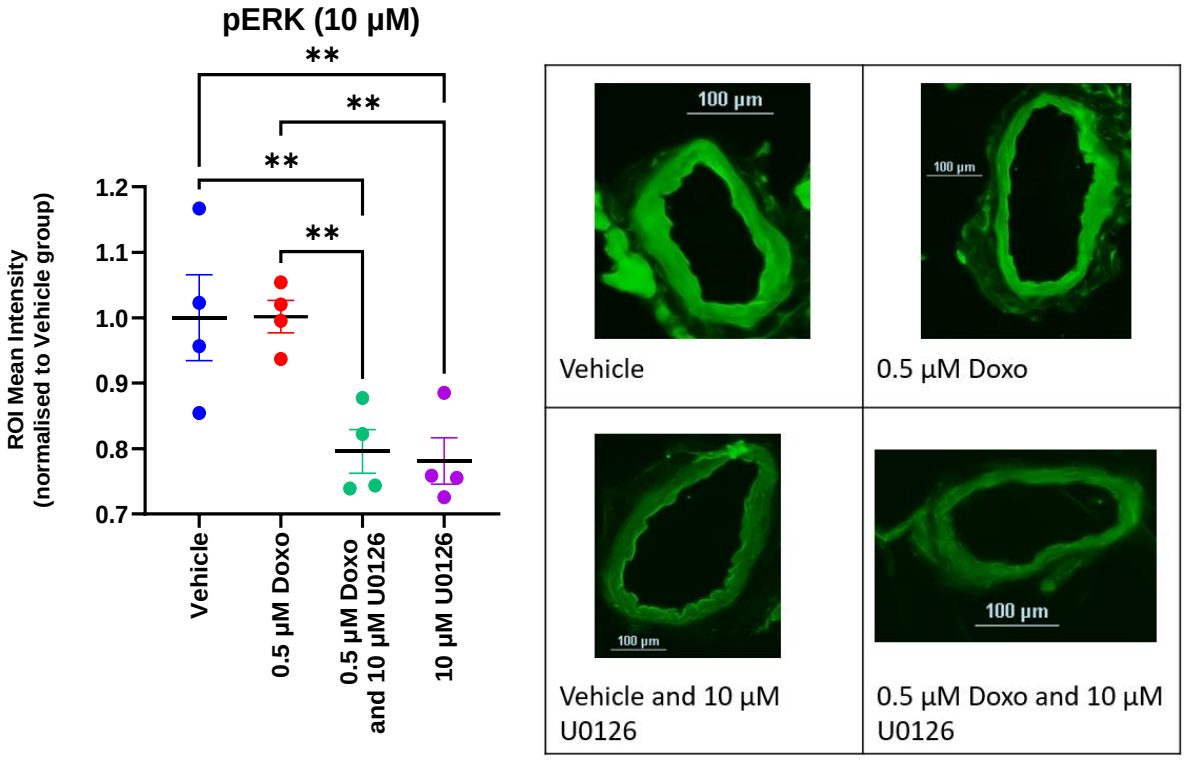

Figure 5-19: Quantification of the pERK expression in LAD arteries by immunofluorescence. (A) Comparison of pERK expression on LAD arteries from Vehicle group (containing 0.25 % DMSO; n = 4), 0.5 µM doxorubicin group (containing 0.5 µM doxorubicin and 0.25 % DMSO; n = 4), 0.5 µM doxorubicin and 5 µM U0126 group (n = 4) and 5 µM U0126 (n = 4). (B) Comparison of pERK on LAD arteries from Vehicle group (containing 0.5 % DMSO; n = 4), 0.5 µM doxorubicin group (containing 0.5 µM doxorubicin and 0.5 % DMSO; n = 4), 0.5 µM doxorubicin and 10 µM U0126 group (n = 4) and 10 µM U0126 (n = 3). The groups were compared by multiple comparisons using one-way ANOVA and Fisher's test (* = $p < 0.05$, ** = $p < 0.01$)

5.4. Discussion

5.4.1. Summary of the main findings of this chapter:

The adverse vascular effects of doxorubicin treatment were investigated on the four studied GPCRs after DMSO (U0126 solvent) incubation of vehicle or doxorubicin-treated LAD arteries during 24 hrs, while the cardioprotective effect of U0126 was investigated on the four studied GPCRs after U0126 incubation of vehicle or doxorubicin-treated LAD arteries during 24 hrs. The U0126 was initially set up at a concentration of 10 µM, but the 5-HT_{1B} and TP-mediated contractions were too highly reduced in the vehicle LAD arteries. The U0126 was, then, set up at a concentration of 5 µM. Both concentrations were studied on vehicle and doxorubicin LAD arteries with incubation in 0.25 % DMSO or 5 µM and 0.5 % DMSO or 10 µM.

The present results of this chapter demonstrate that the 0.5 µM doxorubicin treatment alters the ET_B, 5-HT_{1B} and TP–mediated vasocontractile responses of LAD vessels. Furthermore, the MEK 1/2 inhibitor U0126 confers cardioprotection by alleviating the elevated ET_B, 5-HT_{1B} and TP vasocontractile responses observed in LAD vessels after doxorubicin treatment.

It was shown that 5-HT_{1B}-mediated vasocontractile response was significantly increased by the doxorubicin incubation (Figures 5-11 and 5-12). The elevated 5-HT_{1B}-mediated vasocontractile response is related to the significant elevation of 5-HT_{1B} receptors mRNA level (Figure 5-13) and 5-HT_{1B} receptors expression (Figure 5-14) in doxorubicin-treated LAD vessels. The U0126 pre-treatment at both concentrations 5 µM and 10 µM, attenuates the elevated 5-HT_{1B} mRNA level and 5-HT_{1B} receptors expression of LAD vessels leading to the reduction of the elevated 5-HT_{1B}-mediated vasocontractile response of doxorubicin-treated LAD vessels.

Similarly, TP receptors function was altered by the doxorubicin treatment of LAD vessels. The TP-mediated vasocontractile response of LAD vessels was significantly increased after doxorubicin treatment (Figures 5-15 and 5-16). However, the doxorubicin treatment did not alter the TP mRNA level and TP receptors expression on the LAD vessels. U0126 pre-treatment at both concentrations 5 µM and 10 µM confers a protection against doxorubicin-induced cardiotoxicity by attenuating the elevated TP-mediated vasocontractile response of doxorubicin-treated LAD vessels without altering the TP mRNA level (Fig 5-17) and TP receptors expression (Figure 5-18) on LAD vessels.

The 10 µM U0126 pre-treatment excessively reduces the 5-HT_{1B} and TP-mediated vasocontractile responses of doxorubicin-treated LAD vessels compared to the vehicle-treated LAD vessels, while the 5 µM U0126 alleviates the 5-HT_{1B} and TP-mediated vasocontractile responses of doxorubicin-treated LAD vessels until a recover of the vasocontractile response observed in vehicle-treated LAD vessels.

Interestingly, the doxorubicin treatment significantly reduced the ET_A mRNA level (Figure 5-9) without altering the ET_A receptor expression (Figure 5-10) and the ET_A-mediated vasocontractile responses (Figures 5-7 and 5-8). The U0126 pre-treatment significantly reduced the ET_A-mediated vasocontractile response and the ET_A receptor mRNA level of doxorubicin-treated LAD vessels while U0126 pre-treatment did not alter the ET_A receptor expression on doxorubicin-treated LAD vessels.

Doxorubicin treatment induced an increase of the ET_B-mediated vasocontractile response, followed by a decrease of the ET_B-mediated vasocontractile response (Figures 5-3 and 5-4). Furthermore, the ET_B receptor mRNA level was significantly decreased in LAD vessels after doxorubicin treatment which is consistent with the depressed ET_B-mediated vasocontractile response. The U0126 pre-treatment

reduced the ET_B-mediated vasocontractile responses and the ET_B receptors mRNA level of U0126 plus doxorubicin-treated LAD vessels compared to U0126 naïve vehicle-treated LAD vessels.

5.4.2. The MEK 1/2 inhibitor U0126 was diluted in DMSO

To investigate the cardioprotective effect of 10 µM U0126, the naïve vehicle-treated LAD vessels and naïve U0126 doxorubicin-treated LAD vessels were incubated with 0.5 % of DMSO as control group. Furthermore, the U0126 was also investigated at a lower dose of 5 µM and the LAD vessels used as control groups were incubated with 0.25 % of DMSO. The DMSO is frequently used in pharmacology and toxicology studies to facilitate drug deliveries and no toxic effects were observed at doses ≤ 0.5 % (Sangweni *et al.*, 2021) and thus, the percentage of DMSO used in the present experiment did not exceed 0.5 % of DMSO to minimise the potential negative effect of DMSO on LAD arteries.

The experiments with 10 µM or 5 µM U0126 were done separately and both experiments followed the same trend for the ET_A, TP and 5-HT_{1B} receptors but, the significance differs between both experiments for some results.

Indeed, the maximal 5-HT_{1B}-mediated vasocontraction was significantly increased in doxorubicin plus 0.25 % DMSO-incubated LAD arteries compared to vehicle plus 0.25 % DMSO-incubated LAD arteries, while the maximal 5-HT_{1B}-mediated vasocontraction was increased but it was not significant in doxorubicin plus 0.5 % DMSO-incubated LAD arteries compared to vehicle plus 0.5 % DMSO-incubated LAD arteries. Interestingly, The n number of LAD arteries incubated 0.25 % DMSO was ranging from 12 to 16 LAD arteries, while the n number of LAD arteries incubated 0.5 % DMSO was ranging from 8 to 10 LAD arteries and thus might explain the absence of significance observed in groups of LAD arteries incubated with 0.5 % DMSO. Similarly, the same difference was observed with TP receptors, where the maximal TP-mediated vasocontractile response was significantly up-regulated in doxorubicin plus 0.25 % DMSO LAD arteries (n = 13 - 15), compared to vehicle plus 0.25 % DMSO LAD arteries (n = 12 -13), while the maximal TP-mediated vasocontractile response was up-regulated but not significantly in doxorubicin plus 0.5 % DMSO LAD arteries (n = 10 - 11), compared to vehicle plus 0.5 % DMSO LAD arteries (n = 8 - 9).

The DMSO incubation might have a potential influence on the ET_B-mediated vasocontractile response of LAD vessels. The enhanced ET_B-mediated contraction of doxorubicin-treated vessels during the first phase of the dose-response curve is observed only with 0.5 % DMSO, while a weak contraction was observed with 0.25 % DMSO but was not significant.

A few reasons could explain the difference observed: (i) the concentration of DMSO could influence the LAD arteries' vascular tone or (ii) the number of rats used in this chapter study which is lower than in the previous chapter could explain the reduction of significance.

Indeed, the incubation of both vehicle and doxorubicin LAD arteries with 0.25 % DMSO tend towards an increase of ET_B-mediated contraction, but the results in this study were not significant. The number of rats used in the study per group was around 7 – 9, while in the previous chapter, it was 17 – 19.

The lowest n number could be the reason of the absence of some difference between doxorubicin and vehicle LAD arteries observed in the previous studies. Furthermore, the dose-response curves observed in doxorubicin-treated LAD arteries incubated with 0.5 % DMSO (n = 10 - 11) are similar to the results of the previous chapter. The absence of significance for the enhanced ET_B-mediated contraction in the experiment with 0.25 % of DMSO might be attributable to the too-high variability of contraction due to the lowest number of LAD arteries per group.

5.4.3. The MEK 1/2 inhibitor U0126 reduced the pERK expression on rat LAD arteries, while doxorubicin treatment did not alter the pERK expression.

The MEK/ERK signalling pathway is activated by RTK or GPCRs (Sudhesh Dev *et al.*, 2021, Liu *et al.*, 2019). ERK pathway is initiated by Ras, a small G protein, which recruits and activates Raf kinases in the cytosol. Raf phosphorylates MEK 1/2, which has as only substrate, ERK 1/2. MEK 1/2 promotes the dual phosphorylation of ERK 1/2 for ERK activation leading to the activation of AP-1 (Whitmarsh and Davis, 1996) and NF-κB (Xu *et al.*, 2008) in SMC. The inhibition of MEK leads to a reduction of the expression of pERK (Ong *et al.*, 2015).

In this study, the cardioprotective potential of MAPK was tested by inhibiting MEK 1/2 with the specific inhibitor, U0126. The present findings confirm the efficiency of U0126 with the significant reduction of pERK expression in vehicle and doxorubicin-treated LAD arteries after U0126 pre-treatment at both concentrations, 5 µM and 10 µM (Figure 5-19). This study's results are consistent with Sandhu *et al.et al.* (2010), which showed that U0126 at 10 µM attenuates the pERK expression in isolated cerebral arteries (Sandhu *et al.*, 2010). It was shown that the inhibition effect of U0126 was still effective at the concentration of 5 µM, which will be interesting for the experiment with 5-HT_{1B} and TP receptors.

Additionally, the present results showed that the 0.5 µM doxorubicin treatment did not alter the pERK expression on LAD vessels. Other studies showed a different outcome, but this may be because they used a different *in vitro* model. Choi *et al.et al.* (2008) demonstrate that the effects of doxorubicin on

pERK expression were dose-dependent, and doxorubicin treatment (0.01-1 μM) increased pERK expression in Human HCC cell lines (HepG2, Hep3B) (Choi *et al.*, 2008). Additionally, another study showed that pERK expression was also increased in rat neonatal cardiomyocytes by doxorubicin treatment at a concentration of 1 μM. This increase promoted p53 upstream leading to apoptosis and the MEK 1/2 inhibitor U0126 (Liu *et al.*, 2008). Both studies were working with cell cultures of rat neonatal cardiomyocytes and human HCC cells, while in the present study rat LAD arteries were used and thus may explain the different effects of doxorubicin treatment on pERK. Additionally, the doxorubicin concentration was at 1 μM, which is twice this study's concentration (0.5 μM) and thus may also explain the pERK elevated expression after doxorubicin treatment because doxorubicin-induced cardiotoxicity is dose-dependent.

Furthermore, a study with a tumour-bearing mouse model showed that the MEK/ERK signalling pathway can induce doxorubicin-induced drug resistance and tumour growth (Christowitz *et al.*, 2019). Other studies suggested that blocking the MEK/ERK signalling pathways could reduce the resistance and increase the doxorubicin efficiency against cancer cells (Chen *et al.*, 2015, Shukla *et al.*, 2010). Those studies combined with the present results suggest that the inhibition of the MEK/ERK signalling pathway could increase the doxorubicin efficiency against cancer cells and decrease the risk to develop cardiac issues after the doxorubicin treatment.

5.4.4. The ET_B-mediated vasocontractile response is altered by doxorubicin treatment on transcriptional and potentially post-translational levels and MEK 1/2 inhibitor U0126 alters the depressed doxorubicin-induced ET_B-mediated contraction.

The ET-1 is involved in many CVDs, including hypertension (Stauffer *et al.*, 2008), coronary vasospasm (Toyo-oka *et al.*, 1991), atherosclerosis (Fan *et al.*, 2000) and myocardial infarction (Kolettis, 2014). Previous studies have shown ET_B receptors up-regulation on VSMC occurs as a result of CVD in different *in vitro* models, including rat cerebral and coronary arteries (Sandhu *et al.*, 2010, Skovsted *et al.*, 2012), and human cerebral arteries (Ansar *et al.*, 2013) and *in vivo* model as dog coronary arteries (Teerlink *et al.*, 1994).

This study showed that ET_B-mediated vasocontractile response is increased on the first phase of the biphasic curve of doxorubicin-treated LAD arteries from $10^{-12.5}$ M ET-1 to $10^{-9.5}$ M ET-1 (Figure 5-4). This chapter's finding is consistent with the results from the previous chapter (Chapter 4, section 4.4.1), and Skovsted (2012) and Sandhu (2010) findings, which showed the up-regulation of ET_B-

mediated vasocontraction after vascular injury of isolated cerebral arteries (Sandhu *et al.*, 2010) and of isolated LAD and SCA arteries (Skovsted *et al.*, 2012).

Skovsted used an ex-vivo model with rat LAD arteries fresh or incubated for a period of ½ hr, 4 hrs, 7 hrs and 24 hrs and ET_B receptors expression and ET_B-mediated vasocontraction (with S6c and ET-1 agonists) were analysed. Their data showed an increase of ET_B receptors expression leading to the up-regulation of the ET_B-mediated vasocontraction of incubated- LAD and SCA arteries, compared to fresh arteries (Skovsted *et al.*, 2012). Furthermore, Sandhu used fresh or 48-hrs-incubated cerebral arteries to study the potential cardioprotective effect of MEK/ERK pathway inhibitors (U0126, PD98059, SL327, or AG126) against the up-regulation of vascular GPCR observed during cerebral ischaemia and stroke. Their data showed the up-regulation of the ET_B receptors mRNA level and ET_B-mediated vasocontractile responses of cerebral arteries after 48 hrs incubation, compared to the fresh cerebral arteries (Sandhu *et al.*, 2010).

However, the present results showed that the maximal ET_B-mediated vasocontractile response was alleviated by the doxorubicin treatment (0.5 µM) from 151.5 % in vehicle-treated LAD arteries to 93.3 % in doxorubicin-treated LAD arteries in Figure 5-3 and from 180.2 % in vehicle-treated LAD arteries to 108.5 % in doxorubicin-treated LAD arteries in Figure 5-4. Furthermore, the present study's findings showed that the depressed ET_B-mediated vasocontractile response is related to a reduction of the ET_B receptor transcription, with the decrease of the ET_B receptor mRNA level from 1.00 ± 0.148 in vehicle-treated LAD arteries to 0.540 ± 0.1440.289 ± 0.060 ($p = 0.033$) in doxorubicin-treated LAD arteries, in Figure 5-5 (A) and from 1.00 ± 0.232 in vehicle-treated LAD arteries to 0.287 ± 0.749 ($p = 0.0008$) in doxorubicin-treated LAD arteries, in Figure 5-5 (B). The depressed ET_B-mediated vasocontractile response observed in this study's results is opposite to Sandhu and Skovsted's findings. However, the cardiotoxic effect of doxorubicin was observed on the ET_B receptors, while Skovsted and Sandhu were comparing the cardiotoxic effect induced by their organ culture model mimicking CVD to fresh arteries.

The present study investigated the transcriptional and translational changes observed in this study's CVD model, the 24 hrs-cultured LAD arteries compared to fresh arteries (Figure 9-2 in Appendices). It was shown that ET_B receptor mRNA levels are highly increased in 24-hrs-cultured LAD arteries compared to fresh isolated vessels (shown in appendices), which correlates to Sandhu and Skovsted's findings.

In the previous chapter (Chapter 4, section 4.4.1), the S6c biphasic curve observed could be due to the duality of action of both ET_B receptor subtypes in EC and SMC on vascular tone. In the present study, the biphasic curve is observed on 0.5 µM doxorubicin-treated LAD arteries, but it is not observed on

vehicle-treated LAD arteries, which suggests that the doxorubicin treatment could alter the ET_B-mediated vasocontractile response through two distinct pathways.

This study's results suggest that doxorubicin treatment initially induces an elevation of the ET_B-mediated vasocontraction, followed by a depressed ET_B-mediated vasocontractile response. The initial increased ET_B-mediated vasocontractile response might be induced by doxorubicin treatment on post-translational levels or the alteration of ET_B-activated proteins, as described for the TP receptors (section 5.4.6). The ET_B receptor induces vasoconstriction through its association to Gq/11 proteins (Cramer *et al.*, 2001), leading to PLC activation, which hydrolyses PIP2 in IP3 and DAG, promoting intracellular calcium release and PKC activation (Rosendorff, 1997). Furthermore, this study showed that the followed depressed ET_B-mediated vasocontractile response is induced by doxorubicin treatment on a transcriptional level.

However, doxorubicin-induced depressed ET_B vasocontractile response might be cardiotoxic for LAD arteries. Indeed, studies showed that the decrease of ET_B receptor expression during vascular remodelling could have a negative effect on the vessels. *In vivo* study on endogenous ET_B receptor–knockout (KO) mice investigated the involvement of ET-1-ET_B system in vascular remodelling after injury. They induced the vascular remodelling by ligating the carotid artery and used ET receptors antagonists, the ET_A receptors specific antagonist, TA-0201 (0.5 mg/kg/day) and the ET_B receptors specific antagonist, A-192621 (30 mg/kg/day), to study the involvement of the receptor in the vascular remodelling. They demonstrated that a loss of ET_B receptor–mediated NO release in KO mice leads to a decrease of the NO release and to pathological aggravation of the vascular injury. Furthermore, they suggest that the loss of ET_B receptor–mediated apoptosis of VSMCs may contribute to the aggravation of the vascular injury in KO mice (Murakoshi *et al.*, 2002). It was supported by another study which showed that abnormal vascular remodelling was observed in endothelial NO synthase–deficient mice after vascular ligation (external carotid artery ligation) and that the eNOS absence was increasing the VSMCs proliferation and thus leads to the increase of the vessel wall thickness (Rudic *et al.*, 1998). Thus, the present results demonstrate that doxorubicin has a potential vasotoxic effect through vascular function and ET_B receptor transcription on rat coronary arteries.

Interestingly, dual actions of doxorubicin treatment on ET_B receptors in LAD arteries seem to play opposite roles. The initial ET_B-induced vasoconstriction (ranging from S6c $10^{-11.5}$ M to 10^{-11} M) observed after doxorubicin treatment might be associated with cardiotoxicity. However, the depressed maximal vasocontractile response of ET_B observed after doxorubicin treatment (Figure 5-4) has an opposite effect by decreasing the ET_B transcription, which has been elevated by the organ

culture mimicking CVD (Figure 9-8) and thus doxorubicin alleviates elevated ET_B-mediated vasoconstriction leading to a decrease of the ET_B-induced cardiotoxicity.

Furthermore, in the present study's results, no decrease of the ET_B receptor expression was observed following the transcriptional attenuation, which might be because the mRNA level and the ET_B expression on LAD arteries were analysed at the same time, 24 hrs after the organ culture initiation and thus, more time might be needed to observe ET_B receptor expression alteration on LAD arteries.

The main aim of this chapter was to investigate the potential cardioprotective effect of the MEK 1/2 inhibitor U0126 on doxorubicin-induced cardiotoxicity. It is known that ET_B receptors are regulated by the MEK/ERK pathway (Chen *et al.*, 2009). Furthermore, there is evidence that MEK/ERK inhibition alleviates the ET_B elevated vasocontractile response in isolated rat cerebral arteries (*in vitro*) after DSP exposure (Sandhu *et al.*, 2010) and in isolated human cerebral arteries (*in vitro*) after organ culture mimicking cerebral ischaemia (Ansar *et al.*, 2013).

In this study, results showed that U0126 pre-treatment at both concentrations 5 µM and 10 µM alleviates the doxorubicin-incubated initial elevated ET_B-mediated vasocontractile response and the depressed maximal ET_B-mediated vasocontractile response (Figures 5-3 and 5-4). This study's findings are consistent with Sandhu and Skovsted's findings, which show that U0126 treatment attenuates ET_B-mediated vasoconstriction in isolated rat cerebral arteries (Sandhu *et al.*, 2010) and rat coronary arteries (Skovsted *et al.*, 2012).

Furthermore, it was shown that U0126 pre-treatment did not alter ET_B receptor transcription and translation, which suggests U0126 may alter the ET_B vasocontractile response on a post-translational level or by regulating an ET_B-activated protein. Skovsted *et al.et al.* (2012) showed that the strong up-regulation observed in coronary arteries after 24 hrs incubation was alleviated by U0126 treatment (10 µM) on a translational level, while this study's results suggest U0126 treatment alleviates doxorubicin-induced ET_B vasoconstriction on a post-translational level or by regulating ET_B-activated protein. Doxorubicin might have a different pathway to induce cardiotoxicity, which explains the difference with Skovsted's findings.

The ET_B-mediated vasoconstriction is negligible in fresh coronary arteries, while ET_B-mediated vasocontractile response is strongly increased in 24 hrs-incubated coronary arteries, which is a model mimicking CVD. In the present study, the U0126 pre-treatment alleviates the depressed ET_B-mediated maximal vasocontractile response in doxorubicin-treated arteries from 93.2 % in doxorubicin-treated LAD arteries to 75.25 % in 5 µM U0126-incubated doxorubicin LAD arteries (Figure 5-3) and from 108.5 % in doxorubicin-treated LAD arteries to 53.0 % in 10 µM U0126-incubated doxorubicin LAD arteries

(Figure 5-4). Since it was shown that doxorubicin treatment already attenuates the ET_B-mediated maximal vasocontractile response, the U0126 treatment aggravates the depressed ET_B-mediated maximal vasocontractile response. However, according to Skovsted's data, ET_B-mediated maximal vasocontractile response should be negligible in normal conditions and thus, the doxorubicin and U0126 co-incubation could confer protection against abnormal elevated ET_B vasoconstriction due to the up-regulation of ET_B receptors in SMC observed during cardiotoxicity (Skovsted *et al.*, 2012).

Interestingly, the absence of ET_B receptors transcriptional and translational changes after U0126 treatment while the ET_B-mediated vasoconstriction is reduced, is consistent with the hypothesis of this study: that doxorubicin treatment alters the ET_B-activated protein.

5.4.5. The ET_A receptors transcription is reduced by 0.5 µM doxorubicin incubation on LAD arteries, whereas the vasocontractile response, through ET_A receptors, remains unchanged and MEK 1/2 inhibitor U0126 alters ET_A-mediated vasocontractile response induced by doxorubicin treatment.

The ET-1 is involved in many CVDs, including hypertension, atherosclerosis, and congestive heart failure, and ET_A receptors blockade had already been investigated as cardioprotective therapy (Nasser and El-Mas, 2014).

As in the previous chapter, the ET-1 dose-response curves were performed after ET_B receptors desensitisation, which nearly abolish ET_B-mediated contraction leading to an ET_A-mediated monophasic curve. The present study showed that doxorubicin-induced cardiotoxicity was not altering the ET_A-mediated vasocontractile response with unchanged pharmacological parameters, "E_{max}" and "pEC_{50}", however, at some doses of ET-1, an increased ET_A-mediated contraction in doxorubicin-treated LAD arteries was observed compared to vehicle-treated LAD arteries (Figures 5-7 and 5-8). These results are consistent with the previous chapter's results (Chapter 4, section 4.4.2).

This study's results showed that ET_A receptor transcription is down-regulated by doxorubicin treatment (0.5 µM), with the attenuation of ET_A receptor mRNA level from 1.00 ± 0.148 in vehicle-treated LAD arteries to 0.540 ± 0.144 ($p = 0.033$) in doxorubicin-treated LAD arteries in Figure 5-9 (A) and 1.00 ± 0.232 in vehicle-treated LAD arteries to 0.287 ± 0.749 ($p = 0.0008$) in doxorubicin-treated LAD arteries in Figure 5-9 (B). However, this study's data showed that ET_A-mediated vasocontractile response remains unchanged although ET_A receptor transcription is reduced. The present results are consistent with the Chapter 4 results (Chapter 4, section 4.4.2), which showed that the doxorubicin

and BQ123 (ET_A receptors specific antagonist) co-incubation induced a reduction of the ET_A-mediated contractile response, compared to LAD arteries incubated with only BQ123. It was shown that 0.5 µM doxorubicin treatment could induce either a reduction of ET_A receptors expression (a reduction of the transcription or translation) coupled with an elevated vasocontractile response or, by the opposition, the ET_A receptors expression was unchanged and coupled to a reduced vasocontractile response.

Thus, the absence of the maximal ET_A-mediated contractile response alteration coupled with the reduction of ET_A receptors mRNA level suggests that doxorubicin treatment might induce post-translational changes of ET_A receptors, associated with a reduction of ET_A receptors transcription.

Therefore, the doxorubicin-induced cardiotoxicity may interfere with ET_A receptors through two distinct mechanisms: (i) a reduction of the ET_A transcription and (ii) a post-translational change or alteration of ET_A-activated protein. Both mechanisms were observed with ET_B receptors, however, it seems the mechanism involved in ET_A-mediated vasoconstriction has a stronger effect than in ET_B-mediated vasoconstriction, which compensates for the reduction of ET_A transcription.

This study's model mimics the development of cardiovascular dysfunction at the LAD artery level. The doxorubicin treatment reduces the ET_A receptors transcription of doxorubicin-treated LAD arteries, compared to vehicle-treated LAD arteries, while the organ culture did not alter the ET_A receptors mRNA level (Figure 9-1 in Appendices). Furthermore, the ET_A receptors expression on LAD arteries and ET_A receptors mRNA level were both analysed after 24 hrs incubation and thus might be too early to observe ET_A receptors expression changed, due to the reduction of ET_A receptors mRNA level, which is another possible explanation of the observed alteration of ET_A receptors.

This study's findings showed that doxorubicin reduces both endothelin receptor transcription in coronary arteries and may induce an ET_A hyper-responsiveness potentially through post-translational changes or alteration of ET_A-activated protein.

Interestingly, several studies on animal and human models investigated ET_A antagonists to confer cardioprotection against endothelin receptor-mediated cardiotoxicity. Animal studies showed that ET_A receptors antagonists BQ123 and BMS 182874 attenuate respectively, the development of hypoxic pulmonary hypertension in Sprague Dawley rats (Bonvallet *et al.*, 1994) and prevent the vascular remodelling in the aorta and mesenteric arteries of aldosterone-infused Sprague Dawley rats (Park and Schiffrin, 2001). However, in a study with the ET_A receptors blockade LU 135252 injected *in vivo* on stroke-prone spontaneously hypertensive rat, although the cardiac hemodynamics were improved, the inhibition of ET_A receptors worsened the cardiac remodelling, by increasing the dilatation of left ventricle and not preventing the cardiac hypertrophy (Xia *et al.*, 2006). Furthermore, human studies

were also performed to elucidate the potential of ET_A receptor blockade as cardioprotective therapy. Sitaxsentan is a selective ET_A receptors blockade used to treat pulmonary arterial hypertension (PAH). A 1-year prospective study was performed on PAH patients in an international multicentre trial. It was demonstrated that 1 year after the treatment, the sitaxsentan treatment reduces the risks to develop worsened clinical outcomes and reduces the mortality rate (Benza *et al.*, 2008). However, as in the animal model, harmful effects were observed in patients with chronic heart failure. Indeed, a clinical study with 642 chronic heart failure patients investigate the darusentan (at 10, 25, 50, 100 or 300 mg daily for 24 weeks) long-term effect on left-ventricular remodelling. The patients with chronic heart remodelling were receiving an angiotensin-converting-enzyme inhibitor, beta blocker, or aldosterone antagonist, additionally to the ET_A receptors blockade. They showed that the heart failure was worsened in 11 % patients and the cardiac remodelling was not improved by the ET_A receptors blockade (Anand *et al.*, 2004).

These different studies with ET_A receptors blockade showed that the inhibition of ET_A receptors can be beneficial in hypertension (Gao *et al.*, 2021, Raichlin *et al.*, 2008), however, it can become deleterious when combined to heart failure (Nasser and El-Mas, 2014), which highlight the need of new therapeutic targets to regulate elevated ET-mediated vasoconstriction like MAPK pathway.

This study investigated the potential cardioprotective effect of the MEK 1/2 inhibitor U0126 on doxorubicin-induced cardiotoxicity. It is known that ET_A receptors are regulated by the MEK/ERK pathway (Chen *et al.*, 2009). Furthermore, there is evidence that MEK/ERK inhibition alleviates the ET_A elevated vasocontractile response in isolated rat cerebral arteries after induced cerebral ischaemia (Henriksson *et al.*, 2007) and in isolated human cerebral arteries (*in vitro*) after organ culture mimicking cerebral ischaemia (Cao *et al.*, 2016).

In the present results, it was shown that U0126 treatment alleviates the ET_A-mediated vasocontractile response from 151.6 % in doxorubicin-treated LAD arteries to 105.8 % in 5 µM U0126-incubated doxorubicin LAD arteries (Figure 5-7) and from 174.3 % in doxorubicin-treated LAD arteries to 89.4 % in 10 µM U0126-incubated doxorubicin LAD arteries (Figure 5-8). This study's results are consistent with Cao's findings, which showed that U0126 treatment alleviates the second-hand smoke (SHS)-exposure-induced elevated ET_A-mediated vasocontractile response in cerebral arteries (Cao *et al.*, 2016).

Cao *et al.et al.* (2016) investigated the effect of cigarette smoke on ET receptors in cerebral arteries by exposing rats to SHS for 12 weeks or 8 weeks, followed by 4 weeks of U0126 (5 mg/kg or 15 mg/kg) injection, twice a day. Their data showed that SHS exposure was inducing an abnormal increase of ET_A-mediated vasocontractile response, ET_A mRNA level and ET_A receptor expression on cerebral arteries

and the U0126 treatment alleviates the ET_A-mediated vasocontractile response by reducing ET_A receptor mRNA level and ET_A receptors expression in cerebral arteries. Furthermore, Henriksson *et al.et al.* (2007) investigated the cardioprotective effect of U0126 when U0126 (100 mg/kg) is injected in rats during transient middle cerebral artery occlusion (MCAO), which mimics cerebral ischaemia. Their data showed that 24 hrs after the MCAO procedure and U0126 injection, the MCAO-induced elevated ET_A-mediated vasocontractile response was attenuated and the brain damages were decreased, which highlights the cardioprotective effect of U0126 against cardiotoxicity (Henriksson *et al.*, 2007).

Although this study showed that U0126 treatment alleviates the ET_A vasocontractile response as observed in the two papers, the present results showed that the U0126 treatment did not interfere on transcriptional and translational levels, which is different from Cao's findings. However, the different outcomes can be explained by the different cardiotoxic agents used in experiments, doxorubicin-induced cardiotoxicity does not involve the same mechanisms as SHS-exposure-induced cardiotoxicity. Furthermore, the present results showed that the U0126 treatment has not effect on ET_A-mediated vasocontractile response in U0126-incubated vehicle LAD arteries, while it significantly decreases the ET_A-mediated vasocontractile response in U0126-incubated doxorubicin LAD arteries. However, although doxorubicin treatment significantly decreases the ET_A receptor mRNA level, the U0126 treatment does not decrease the ET_A receptor mRNA level in U0126-induced doxorubicin LAD arteries (0.206 ± 0.039), compared to doxorubicin-treated LAD arteries (0.287 ± 0.749), as shown in Figure 5-9 (B). Thus, the depressed ET_A-mediated vasocontractile response observed after U0126 pre-treatment suggests that U0126 alleviates the hyper-responsiveness mediates by doxorubicin on post-translational levels and highlights the depressed ET_A-mediated vasocontractile response induced by the doxorubicin-induced reduction of the ET_A receptor transcription.

Therefore, this study showed that doxorubicin-induced cardiotoxicity is associated with a decrease of ET_A receptor transcription and ET_A-mediated hyper-responsiveness potentially induces by post-translational change or ET_A-activated protein. Furthermore, U0126 treatment confers protection against the doxorubicin-induced ET_A hyper-responsiveness, however, it also highlights the depressed ET_A transcription which leads to a depressed ET_A vasocontractile response. The depressed ET_A vasocontractile response might be cardioprotective by reducing vasoconstriction induced by both ET receptor subtypes, since the CVD model increased the ET_B transcription in SMC.

5.4.1. The MEK 1/2 inhibitor U0126 confers protection against the elevated 5-HT_{1B}-mediated vasocontractile response induced by doxorubicin treatment on transcriptional and translational levels.

The 5-HT_{1B} receptors are mostly studied in cerebral arteries (O'Quinn *et al.*, 1999, Lotfinia *et al.*, 2014), but are also localised in coronary arteries with another serotonin receptor, 5-HT_{2A} (Longmore *et al.*, 2000, Maassen VanDenBrink *et al.*, 2000, Kaumann *et al.*, 1994). The activation of 5-HT_{1B} receptors inhibits the adenylyl cyclase, which reduces the cAMP formation and PKA activity leading to the intracellular calcium release from the sarcoplasmic reticulum and vasoconstriction (Barnes and Sharp, 1999, Leenders and Sheng, 2005, Tiger *et al.*, 2018). Previous studies with sumatriptan, an antimigraine drug and 5-HT_{1B} agonist, have shown that some human patients treated with sumatriptan had developed chest pain, myocardial infarction and vasospasm (Ottervanger *et al.*, 1997, Okonkwo and Ojha, 2020). It is well established that the elevation of the 5-HT_{1B}-mediated vasocontractile responses of cerebral and pulmonary arteries in a rat *in vitro* model has been implicated in several CVDs (CVD), including cerebral ischaemia (Sandhu *et al.*, 2011)and hypoxia-induced pulmonary hypertension (PHT) (Keegan *et al.*, 2001).

In the present results, it was shown that doxorubicin-induced cardiotoxicity was associated with the 5-HT_{1B} elevated vasocontractile response of rats' LAD arteries (Figures 5-11 and 5-12) with an increase of the C_{max} from 25.5 % in vehicle-treated LAD arteries to 74.9 % in doxorubicin-treated LAD arteries. Additionally, the 5-CT dose-response curve of doxorubicin LAD arteries seems to be left-shifted, when compared to vehicle LAD arteries, illustrating the increase of 5-CT potency for 5-HT_{1B} by the doxorubicin-induced cardiotoxicity. To our knowledge, this is the first study to show that doxorubicin-induced cardiotoxicity is associated with 5-HT_{1B}-mediated vasoconstriction in the rat LAD arteries. However, Sheibani *et al.et al.* (2021) have shown that Sumatriptan at a concentration of up to 1 mg/kg was aggravating the doxorubicin-induced cardiotoxicity (2.5 mg/kg) in rats (Sheibani *et al.*, 2021) which is consistent with this study's results.

To establish the doxorubicin adverse effects leading to the 5-HT_{1B} elevated vasocontractile response, the potential transcriptional and translational changes of 5-HT_{1B} receptors in LAD vessels were investigated during doxorubicin treatment. Interestingly, this study demonstrated that the 5-HT_{1B} receptor level was increased from 1.00 ± 0.085 in vehicle-treated LAD arteries to 1.267 ± 0.077 ($p = 0.041$) in doxorubicin-treated LAD arteries (Figure 5-14). Furthermore, the 5-HT_{1B} receptor elevated mRNA level was consistent with the 5-HT_{1B} receptor elevated expression from 1.00 ± 0.009 in vehicle-treated LAD arteries to 1.023 ± 0.006 ($p = 0.038$) in doxorubicin-treated LAD arteries (Figure 5-13).

The 5-HT_{1B} receptors have been further investigated in pulmonary arteries since it has been established that in human pulmonary circulation, the vasoconstriction of small and large pulmonary arteries was mediated by 5-HT_{1B} receptors (Morecroft *et al.*, 1999). In contrast, in animal models as non-hypoxic rats, the pulmonary vasoconstriction to 5-HT is predominantly mediated by the 5-HT_{2A} receptor, while in the chronic hypoxic pulmonary hypertensive rat (CHPHT), the 5-HT_{1B} mRNA level is increased (MacLean *et al.*, 1996). However, in the CHPHT, which have a marked right ventricular hypertrophy (markers of pulmonary hypertension) after exposure to hypoxia, the vasoconstriction is the result of both 5-HT_{1B} and 5-HT_{2A} receptors activation and 5-HT_{1B} mRNA level is increased (Hunter *et al.*, 1974). This study's findings on the 5-HT_{1B} receptors' role in the doxorubicin-induced cardiotoxicity are similar to the findings of Keegan *et al.et al.* (2001), which showed the development of hypoxia-induced PHT in Wistar rats is associated with elevated 5-HT_{1B}–mediated vasocontractile response coupled to elevated 5-HT_{1B} receptor mRNA level. To investigate the role of 5-HT_{1B} in the development of hypoxia-induced PHT, the rodents were placed in a hypobaric chamber (550 mbar) for 14 days to induce the hypoxia and rats were either treated with a 5-HT_{1B} receptors selective antagonist GR127935 (3 mg/kg/day) or H_2O alone, while mice were either wild-type or 5-HT_{1B} knockout. Interestingly, their data suggest that 5-HT_{1B} receptors are involved in the pulmonary vascular remodelling and thus elevated 5-HT_{1B} vasocontractile response is potentially one of the mechanisms of the hypoxia-induced PHT (Keegan *et al.*, 2001). Furthermore, the 5-HT_{1B} receptors implication in cerebral ischaemia has been shown in Sandhu *et al.et al.* paper (2011), using *in vitro* model mimicking cerebral ischaemia, similar to the present *in vitro* model. They have incubated isolated cerebral arteries in the same condition as this study's model (for 24 hrs, at 37 °C, in humidified 5 % CO_2 and 95 % O_2 in DMEM supplemented with an antibiotics mix). Their data showed 5-HT_{1B} receptor mRNA level and 5-HT_{1B}-mediated vasocontractile response were increased in pathological cardiovascular conditions (Sandhu *et al.*, 2011). This study's findings associated with these two papers show the implication of 5-HT_{1B} receptors from different rat vessels (coronary, pulmonary and cerebral) in the cardiotoxicity and highlight the necessity to regulate the 5-HT_{1B} enhanced vasocontractile response.

Thus, in the present study, it was established that doxorubicin-treated LAD arteries vasoconstriction involves the 5-HT_{1B} receptors by increasing their transcription leading to the elevation of 5-HT_{1B} receptors expression on LAD vessels and thus enhancing the 5-HT_{1B}-mediated vasocontractile response. Additionally, as mentioned in the previous chapter (chapter 4, section 4.4.3), several studies showed that doxorubicin-induced cardiotoxicity was associated with a decrease of adenylyl cyclase (AC) activity (Calderone *et al.*, 1991) and cAMP formation (Efentakis *et al.*, 2020), which are both involved in 5-HT_{1B}-mediated vasoconstriction. Therefore, the present findings on 5-HT_{1B} receptors are

correlated to the studies showing that doxorubicin treatment is associated with a down-regulation of AC and cAMP.

The main aim of this chapter was to investigate the potential cardioprotective effect of the MEK 1/2 inhibitor U0126 on doxorubicin-induced cardiotoxicity. There is evidence that MEK/ERK inhibition alleviates the 5-HT_{1B} elevated vasocontractile response in isolated cerebral arteries (*in vitro*) after cerebral ischaemia (Sandhu *et al.*, 2010) and in rat cerebral arteries (*in vivo*) after subarachnoid haemorrhage (SAH) (Beg *et al.*, 2006). The U0126, a MEK 1/2 inhibitor is known to have antioxidant properties by reducing the ROS level in isolated PC12 cells (Ong *et al.*, 2015). U0126 as cardioprotective treatment has been investigated with *in vitro* and *in vivo* rodent models and Povlsen *et al.et al.* (2015) were in the process to perform a clinical trial with U0126 as adjuvant therapy against late cerebral ischaemia (Povlsen and Edvinsson, 2015).

In this study, results showed that the U0126 pre-treatment confers cardioprotection by alleviating the 5-HT_{1B} receptor mRNA level in doxorubicin-treated LAD arteries from 1.267 ± 0.077 to 1.108 ± 0.076 in 10 µM U0126-incubated doxorubicin LAD arteries which is not significant but the 5-HT_{1B} receptor mRNA level attenuation allows the recovery of the 5-HT_{1B} receptor mRNA level observed in U0126 naïve vehicle-treated LAD arteries (1.00 ± 0.085) (Figure 5-13). The 5-HT_{1B} receptor mRNA level attenuation by 10 µM U0126 leads to the attenuation of 5-HT1B receptors expression and thus the alleviation of the 5-HT_{1B}-mediated vasocontraction of LAD arteries. U0126 was shown to be cardioprotective at a concentration of 10 µM where it attenuates the 5-HT_{1B}-mediated C_{max} from 65.6 % for U0126 naïve doxorubicin-treated LAD arteries to 22.3 % for 10 µM U0126-incubated doxorubicin LAD arteries but it is not significant (Figure 5-12). Interestingly, this study's findings are in agreement with Beg *et al.et al.* (2006) and Sandhu *et al.et al.* (2010) findings. Beg *et al.et al.* showed that a treatment with an ERK 1/2 inhibitor SB386023-b given before and after the SAH procedure was abolishing the 5-HT_{1B} up-regulation in rat SAH cerebral arteries, which highlights the cardioprotective effect of MEK/ERK pathway by regulating 5-HT_{1B}-mediated vasocontractile response (Beg *et al.*, 2006). Furthermore, this study's results are consistent with Sandhu *et al.et al.* (2010) findings, which showed that U0126 at 10 µM alleviated the 5-HT_{1B} elevated vasocontractile response in rat 48 hrs-cultured cerebral arteries which, they speculated was associated with increased translation. Their data showed that 5-HT_{1B}-mediated vasocontractile response and 5-HT_{1B} receptor expression were attenuated by the 10 µM U0126 treatment, while the 5-HT_{1B} receptor mRNA level remain unchanged in cerebral arteries. However, this study's data showed that after the 10 µM U0126 treatment the elevated 5-HT_{1B} receptor mRNA level observed after doxorubicin treatment was abolished, which suggests that the U0126 treatment confers cardioprotection by down-regulating the 5-HT_{1B} receptor transcription which leads to attenuating the 5-HT_{1B} receptor expression on LAD arteries and thus alleviating 5-HT_{1B}

elevated vasocontractile response of doxorubicin-treated LAD arteries. The different outcomes of the present findings and Sandhu *et al.et al.* findings may be attributable to the different settings, which are the incubation period (48 hrs in Sandhu's paper and 24 hrs for the present experiment), the arteries used (cerebral arteries in Sandhu's paper and coronary arteries for the present experiment) and the studied CVD (Cerebral ischaemia in Sandhu's paper and doxorubicin-induced cardiotoxicity for the present experiment).

The present study showed that 10 µM U0126 treatment was alleviating the 5-HT_{1B} receptor transcription leading to the attenuation of the elevated 5-HT_{1B}-mediated vasocontractile response and thus suggests that 10 µM U0126 treatment is an interesting cardioprotective agent against doxorubicin-induced cardiotoxicity. However, this study's data showed that the U0126 pre-treatment at a concentration of 10 µM has a potentially negative effect on vehicle-treated LAD arteries by reducing the 5-HT_{1B} C_{max} from 43.5 % for the U0126 naïve vehicle-treated LAD arteries to 7.0 % for the 10 µM U0126 vehicle-treated arteries (Figure 5-12). The U0126 pre-treatment at a concentration of 5 µM was tested to reduce the risk of U0126 negative effects and it attenuates the 5-HT_{1B} receptor mRNA level from 1.203 ± 0.093 (doxorubicin-treated LAD arteries) to 1.150 ± 0.080 (5 µM U0126-incubated doxorubicin LAD arteries) and the attenuation allows the recovery of the 5-HT_{1B} receptor mRNA level observed in vehicle-treated LAD arteries (1.00 ± 0.09). The regulation of the 5-HT_{1B} receptor transcription leads to the significant reduction of 5-HT_{1B}-mediated vasocontraction of doxorubicin-treated LAD arteries from a C_{max} of 74.9 % (doxorubicin-treated LAD arteries) to a C_{max} of 36.9 % (5 µM U0126-incubated doxorubicin LAD arteries) until the recovery of the 5-HT_{1B}-mediated vasocontraction observed in vehicle-treated LAD arteries (C_{max} = 25.5 %) but the attenuation was not significant compared to U0126 naïve doxorubicin-treated LAD arteries.

Thus, it was demonstrated that the U0126 treatment confers protection against doxorubicin-induced cardiotoxicity by down-regulating the 5-HT_{1B} receptor transcription and the U0126 optimal concentration to regulate 5-HT_{1B}-mediated vasocontractile response is the 5 µM concentration.

5.4.2. The MEK 1/2 inhibitor U0126 confers protection against the elevated TP-mediated vasocontractile response induced by doxorubicin treatment potentially on a post-translational level.

Thromboxane A2 is a potent platelet activator and vasoconstrictor (Katugampola and Davenport, 2001). In SMCs, thromboxane A2 binds to TP receptors leading to phospholipase C (PLC) activation.

PLC hydrolyses PIP2 in DAG and IP3 leading to PKC activation and intracellular calcium accumulation. This pathway induces vasoconstriction and platelet activation, which alter the platelets' shape, aggregation and secretion. Pathological changes in TP receptor pathways can lead to CVDs, like atherosclerosis, myocardial infarction and hypertension (Neri Serneri *et al.*, 1983, Katugampola and Davenport, 2001, Smyth, 2010, Martin, 1984).

In the results, it was shown that doxorubicin-induced cardiotoxicity was associated with an abnormal elevation of the TP-mediated vasocontractile response. Doxorubicin treatment (at 0.5 µM) was shown to increase the maximal TP-mediated vasocontractile response from 83.3 % in vehicle-treated LAD arteries to 116.4 % in doxorubicin-treated arteries and the TP receptor potency for the agonist U46619 with a "pEC_{50}" value from $10^{-7.07}$ M in vehicle-treated LAD arteries to $10^{-7.46}$ M in doxorubicin-treated LAD arteries (Figure 5-15). As mentioned in the previous chapter, it has been shown that chronic treatment of doxorubicin enhanced the platelet activity, leading to thrombus and vascular injury (Lv *et al.*, 2020), however this elevation of platelet activity is not induced by the platelets (Kim *et al.*, 2009, Kim *et al.*, 2011), which suggest that the elevation of the platelet activity might be caused by a vascular signalling pathway induced by other cells, such as the activation of TP receptors on SMCs. This study's findings are consistent with the elevation of platelet activity since TP receptor activation is known to induce vasoconstriction and also activate the platelets (Smyth, 2010).

To underline the molecular mechanisms involved in the doxorubicin-induced TP receptor elevated vasocontractile response, the transcriptional and translational changes of TP receptors in rat incubated-LAD arteries were investigated during doxorubicin treatment (0.5 µM). The present data showed that the doxorubicin treatment did not alter the TP receptor mRNA level or the TP receptors expression on rat incubated-LAD arteries. In this study's results, it was shown that doxorubicin-induced cardiotoxicity does not interfere on transcriptional and translational levels, which leads to the hypothesis that doxorubicin may interfere on a post-translational level or on other proteins in the TP receptor signalling pathway. In contrast, Zhang's findings (2008) showed that the lipid-soluble cigarette smoking particles (DSP), which can be associated with CVD, including atherosclerosis and coronary arteries disease (Ezzati *et al.*, 2005) was up-regulating the TP-mediated vasocontractile response in 24 hrs-incubated superior mesenteric arteries on translational level (Zhang *et al.*, 2008). However, they observed the abnormal TP receptor vasocontractility during CVD, using superior mesenteric arteries, while LAD arteries were used and the cardiotoxicity was induced through a different cardiotoxic agent DSP and thus may explain that TP vasoconstriction-associated cardiotoxicity involves mechanisms on translational level, while this study's results showed that doxorubicin interferes on a post-translational level.

Interestingly, Sikarwar *et al.et al.* (2014) showed that the Gαq protein associated with the TP receptor of pulmonary arteries was altered on a post-translational level in hypoxic pulmonary hypertension (Sikarwar *et al.*, 2014), which is similar to this study's hypothesis that doxorubicin treatment may induce cardiotoxicity on a post-translational level. They exposed new piglets to hypoxia for 72 hrs to provoke hypoxic pulmonary hypertension (HPH) and used the pulmonary arteries to investigate the potential post-translational change of Gαq involved in HPH. The association of TP receptors to the G protein of Gq/11 subunit leads to vasoconstriction (Mederos y Schnitzler *et al.*, 2008). Sikarwar *et al.et al.* data showed that hypoxia increases the palmitoylation of Gαq, which facilitates the association of TP receptor and Gαq and thus leads to elevated TP-mediated vasocontractile response. Palmitoylation is one of the post-translational mechanisms and is known to regulate the membrane receptor interactions (Linder and Deschenes, 2007) leading to an elevation of the trafficking and coupling of GPCRs to their specific G protein (Edgerton *et al.*, 1994). This study's data showed that the affinity of the TP receptor for his specific agonist U46619 was increased after doxorubicin treatment, which could be due to an increase of the GPCRs trafficking and coupling by post-translational changes, leading to the observed TP receptor hyper-responsiveness, as in Sikarwar's paper (Sikarwar *et al.*, 2014).

This study's results could also suggest that the elevated TP-mediated vasocontractile response of doxorubicin-treated LAD arteries is because doxorubicin treatment interferes with other proteins leading to the intracellular calcium release: PLC, PIP2, IP3 or DAG. Interestingly, this study's hypothesis is consistent with Min's findings, which investigated the effect of doxorubicin on the protein kinase C-δ (PKCδ) and the potential regulation through JNK. They worked with mouse lymphocytic leukaemia L1210 cells and showed that doxorubicin was up-regulating the PKCδ gene expression via c-jun and ATF2 transcription factors activation from the JNK signalling pathway (Min *et al.*, 2008). The PKCδ is involved to the apoptosis pathway (Reyland, 2007), however, this paper showed that PKC gene expression is a potential target of doxorubicin-induced cardiotoxicity.

Thus, in this study it was suggested that doxorubicin-induced cardiotoxicity is associated with either TP receptor abnormal post-translational change or the alteration of TP-activated proteins, leading to the elevated vasocontractile response observed on doxorubicin-treated LAD arteries, when compared to vehicle-treated LAD arteries.

The main aim of this chapter was to investigate the potential cardioprotective effect of the MEK 1/2 inhibitor U0126 on doxorubicin-induced cardiotoxicity. It is known that TP receptors are regulated by the MEK/ERK pathway (Morinelli *et al.*, 1994). Furthermore, there is evidence that MEK/ERK inhibition alleviates the TP elevated vasocontractile response in isolated rat cerebral arteries (*in vitro*) after DSP

exposure (Sandhu *et al.*, 2010) and in isolated human cerebral arteries (*in vitro*) after organ culture mimicking cerebral ischaemia (Ansar *et al.*, 2013).

In this study, it was shown that MEK 1/2 inhibitor U0126 (5 µM) alleviates the doxorubicin-induced TP receptor elevated vasocontractile response from 116.4 % in doxorubicin-treated LAD arteries to 78.5 % in 5 µM U0126-incubated doxorubicin LAD arteries, which is not significant but the TP receptor vasocontractile response attenuation allows the recovery of the TP receptor vasocontractile response observed in U0126 naïve vehicle-treated LAD arteries (83.3 %) (Figure 5-15). Interestingly, this study's findings are consistent with Sandhu's (2010) and Ansar's (2013) findings.

Sandhu *et al.et al.* (2010) showed that the 10 µM U0126 treatment, even added 6 hrs after the beginning of the organ culture, down-regulated the TP elevated vasocontractile response in 48 hrs-cultured cerebral arteries compared to fresh cerebral arteries without altering the transcription and translation, which suggest U0126 confers protection against CVD on a post-translational level since their organ culture model was mimicking cerebral ischaemia (Sandhu *et al.*, 2010). Furthermore, Ansar *et al.et al.* (2013) investigated the MAPK signalling pathway influence on the cerebrovascular receptor, including TP receptors, in isolated human cerebral arteries. Their data showed that the TP-mediated vasocontractile response observed in 48 hrs-incubated human cerebral arteries was increased compared to fresh human cerebral arteries, while the TP receptor expression on human cerebral arteries remained unchanged. Interestingly, they also showed that the U0126 treatment at 5 µM was down-regulating the elevated TP-mediated vasocontractile response until the recovery of TP-mediated vasocontractile response observed in fresh human cerebral arteries without altering the TP receptor expressions (Ansar *et al.*, 2013), which highlight the potential of U0126 to confer protection in human arteries by down-regulating TP receptor vasoconstriction in CVD model. Sandhu and Ansar's results are consistent with the present results, as it was shown that U0126-induced attenuation of TP vasocontractile response was not on transcriptional (Fig 5-17) or translational levels (Fig 5-18).

Interestingly, the absence of transcriptional and translational changes is consistent with this study's hypothesis that doxorubicin-induced TP elevated vasocontractile responses might be induced by the alteration of another protein from the TP receptor signalling pathway, for example, the Gq protein as observed in Sikarwar paper (Sikarwar *et al.*, 2014) or the PKC as observed in Min paper (Min *et al.*, 2008).

Furthermore, in the present study, the U0126 pre-treatment at a concentration of 10 µM was tested, however, the TP-mediated vasocontractile response observed after 10 µM U0126 pre-treatment was significantly attenuated compared to the U0126 naïve vehicle-treated LAD arteries, from 99.1 % in vehicle-treated LAD vessels to 55.2 % in 10 µM U0126-incubated vehicle LAD arteries and 56.6 % in 10

μM U0126-incubated doxorubicin LAD arteries. It was established that the U0126 optimal concentration to regulate the doxorubicin-induced TP elevated vasocontractile response was 5 μM.

Interestingly, it was shown that TP receptors expression on rat LAD arteries was significantly up-regulated from 1.00 ± 0.027 U0126 naïve vehicle-treated LAD vessels to 1.159 ± 0.054 ($p = 0.0395$) on vehicle plus 5 μM U0126-treated LAD vessels (Figure 5-18 (A)). The present finding is consistent with Zhang *et al.et al.* (2009) findings, which have developed an organ culture model with rat mesenteric arteries to investigate the receptor changes from vascular SMCs in CVD. They investigated the thromboxane A2 receptors changes and the inhibitor effect of U0126 on the receptors and showed that the organ culture of mesenteric arteries leads to a depressed TP-mediated contraction caused by the transcriptional down-regulation of the receptor's expression. Additionally, they demonstrated that the down-regulation was induced through the MEK/ERK signal pathway and the U0126 incubation can reverse the depressed TP-mediated vasocontraction induced by the transcriptional down-regulation of the receptor (Zhang *et al.*, 2009). In this study, the organ culture of rat LAD arteries induced a transcriptional down-regulation of TP receptors (Figure 9-4 in Appendices), which is consistent with Zhang's findings. Furthermore, the down-regulation of TP receptors expression was also observed on cultured-LAD arteries, but only after the 0.25 % DMSO incubation.

Although the up-regulation of TP receptors on 5 μM U0126 plus vehicle-treated LAD arteries correlates with the results of Zhang's study, the present results showed no effect of U0126 (5 or 10 μM) on TP receptors transcription in LAD arteries. The different effects of the U0126 pre-treatment on TP receptors of vehicle and doxorubicin-treated LAD arteries suggest that doxorubicin-induced vasotoxicity promotes the elevated TP-mediated contractile response through post-translational changes or an altered protein involved in the pathway from TP receptors to intracellular the calcium release leading to the LAD arteries vasocontraction.

Thus, this study's results showed that MEK 1/2 inhibitor U0126 confers protection against doxorubicin-induced cardiotoxicity by alleviating the TP-mediating vasocontractile response on post-translational level or through the regulation of either PLC, PIP2, PKC.

5.5. Conclusion

From this chapter novel cellular and molecular analysis of doxorubicin-induced vasotoxicity, it is clear that doxorubicin alters the four studied GPCRs on different intracellular levels. This study's results showed that the 5-HT_{1B} receptor is altered on transcriptional and translational levels, leading to elevated 5-HT_{1B} vasocontractile response. U0126 alleviates doxorubicin-induced 5-HT_{1B}

vasoconstriction by reversing the increased 5-HT_{1B} transcription and translation. Furthermore, it was shown that doxorubicin increases the TP-mediated vasocontractile response via post-translational change or TP-activated protein (Gq/11, PLC, PIP2, Dag, IP3 and PKC) alteration. U0126 alleviates elevated TP vasoconstriction induced by doxorubicin potentially on a post-translational level or TP-activated protein. This study's results showed that doxorubicin decreases the transcription of both endothelin subtypes. Furthermore, it was shown that doxorubicin might induce an ET_A hyper-responsiveness and an initial elevated ET_B vasocontractile response through post-translational change or ET_A/ET_B-activated protein. U0126 alleviates ET_A hyper-responsiveness induced by doxorubicin on a post-translational level, which leads to a depressed ET_A vasocontractile response. Similarly, U0126 alleviates ET_B vasocontractile response induced by doxorubicin on a post-translational level, which leads to a depressed ET_B vasocontractile response. Therefore, the decrease of both ET receptor vasocontractile responses by U0126 might reverse the organ culture-induced elevated ET_B transcription in SMC. Thus, U0126 offers a promising remedy to attenuate the doxorubicin-induced cardiotoxicity. More studies are needed to underline the potential post-translational changes associated with the doxorubicin-induced vasotoxicity or the potential altered proteins involved in vasoconstriction and MEK/ERK signalling pathway to confirm if U0126 can be an efficient adjuvant therapy to chemotherapy-induced cardiotoxicity. Furthermore, other MAPK signalling pathways, such as JNK or p38, or inhibitor pathways might also be considered as relevant adjuvant therapy and could be studied.

Currently, the potential doxorubicin-induced cardiotoxicity cannot be efficiently predicted in cancer patients. Recently, a new biomarker was investigated to detect CVD, the miRNA. The next chapter will investigate the potential role of cardiovascular specific miRNA as biomarkers in the plasma of cancer patients treated with anthracyclines.

Chapter 6

6. The expression pattern of circulating miRNAs in cancer patients treated with anthracycline

Some data of this chapter are under review or published:

Peer reviewed journal:

- Submitted for publication in International Journal of Molecular Sciences (June 2023):

Title: miRNA expression profile of cancer patients treated with anthracycline.

Authors: Lozahic C., Mutigwa D., Macklin A., Mallouppas M, Maddock H., Walker M.J., Sandhu H.,

Conferences:

- BSCR Autumn meeting 2022: Cardiac remodelling – Basic mechanisms to clinical management, Belfast:

Poster presentation: Cardiac Injury miRNA Profile in Cancer Patients Treated with doxorubicin. David Mutigwa, Michael Mallouppas, Robin Chung, Caroline Lozahic, Helen Maddock,

J. Malcolm Walker, Derek Yellon and Hardip Sandhu

6.1. Introduction

6.1.1. Doxorubicin-induced cardiotoxicity

Anthracyclines are known to be one of the most efficient and commonly used families of chemotherapeutic drugs (Anand *et al.*, 2022). Anthracyclines are used especially in solid cancers, such as sarcoma, lymphoma, and breast cancer (Volkova and Russell, 2011). Cancer was the leading cause of death in 2019 worldwide according to estimates of World Health Organisation (WHO), and this increase in cancer incidents has led to an increase of chemotherapy demand (Sung *et al.*, 2021). Indeed, the rise of patients who need chemotherapy is estimated to be 53 % from 2018 to 2040 according to a population-based study (Wilson *et al.*, 2019). However, anthracyclines are associated with cardiac adverse effects and can range from mild to severe issues, such as hypertension (Suter and Ewer, 2013), loss of myocardial contraction (Raj *et al.*, 2014), arrhythmias (Buza *et al.*, 2017), coronary artery disease (Volkova and Russell, 2011) and heart failure (Kamphuis *et al.*, 2020).

Doxorubicin is one of the anthracycline drugs commonly used to treat solid cancers. The doxorubicin-induced cardiotoxicity involves various intracellular mechanisms, including mitochondrial dysfunction, reactive oxygen species production (Gille and Nohl, 1997) leading to oxidative stress (Minotti *et al.*, 2004), apoptosis (Kaufmann and Earnshaw, 2000), and myofibril damage (Ito *et al.*, 1990). Doxorubicin-induced cardiotoxicity is also associated with intracellular calcium overload leading to abnormal intracellular calcium homeostasis, and thus cardiac contractile dysfunction (Shinlapawittayatorn *et al.*, 2022). Furthermore, intracellular calcium overload is clinically associated with ischemic heart disease development, including atherosclerosis, thrombosis, and coronary spasms (Dhalla *et al.*, 2008). Clinical studies have highlighted an increase of arterial stiffness in patients treated with anticancer drugs both during and after the treatment, including doxorubicin (Parr *et al.*, 2020, Mozos *et al.*, 2017, Chaosuwannakit *et al.*, 2010). Furthermore, arterial stiffness is known to be associated with CVDs, such as hypertension, stroke, and congestive heart failure (Laurent and Boutouyrie, 2020, Sutton-Tyrrell *et al.*, 2005, Chae *et al.*, 1999).

6.1.2. Clinical biomarkers of cardiotoxicity

Clinicians assess anthracycline-induced cardiotoxicity with various circulating myocardial damage biomarkers and imaging techniques. Cardiac issues can be monitored through the assessment of relevant circulating biomarkers levels (Lipshultz *et al.*, 2012). The high-sensitivity (hs-cTnI) and cTnT are the gold-standard biomarkers for the diagnostic of acute myocardial infarction (Aydin *et al.*, 2019). The elevation of troponin is correlated to cardiac injury severity and is monitored during CVDs, including cardiac arrhythmias, cardiomyopathies and heart failure (Chauin, 2021). The other

diagnostic biomarkers for cardiac injury and heart failure widely used are brain natriuretic peptide (BNP) and *N*-terminal proBNP (NT-proBNP) (Cao *et al.*, 2019). BNP and NT-proBNP are synthesised and secreted by left ventricular myocytes as a response to mechanical stress, systemic ischaemia and hypoxia (Volpe *et al.*, 2014). The elevation of plasma BNP and NT-proBNP is also associated with arrhythmias and cardiomyopathies and is used to assess the severity of CVD (Cao *et al.*, 2019). Cardiac injury can also be monitored by non-invasive techniques, including Doppler electrocardiography (ECG) and magnetic resonance imaging. Cardiac imaging techniques evaluate the left ventricular ejection fraction (LVEF) and detect myocardial injury (McKillop *et al.*, 1983). The management of anthracycline-induced cardiotoxicity start before the anthracyclines treatment with a baseline work-up. This cardiac baseline work-up consists in reducing the cardiotoxic risk by evaluating the cardiac disease history, doing clinical examination with imaging techniques and various circulating myocardial damage biomarkers. A follow-up of the potential cardiac adverse effects development is essential during and after the chemotherapy (Curigliano *et al.*, 2012).

Over the past years, microRNAs (miRNAs) have been explored as potential novel biomarkers to assess cardiotoxicity. miRNAs are small non-coding single-stranded RNA compounds 21 – 25 nucleotides in length (Szelenberger *et al.*, 2019). Intracellularly in mammals, miRNAs play key roles in the regulation of mRNA and protein levels. Mature miRNAs can also be found in the extracellular microenvironment, such as the plasma, saliva, tears and urine, and are specified as circulating miRNAs (Weber *et al.*, 2010). The circulating miRNAs in plasma represent 10 % of the total human miRNAs (Szelenberger *et al.*, 2019). The miRNAs are released into bio-fluids through either the passive or the active way. The passive way occurs when cells are injured, and miRNAs are released as endogenous particles. The active way involves miRNAs being released by secretion via macrovesicles (i.e. exosomes) or via binding to RNA-binding proteins, such as HDL or AGO2 (Zhao *et al.*, 2019). The endogenous miRNAs are highly stable and can stay at room temperature for up to four days (Salloum-Asfar *et al.*, 2019).

6.1.3. The ERICONC study

Prof Malcolm Walker, Prof Derek Yellon and their team at UCL compared the effect of remote ischaemic pre-conditioning on myocardial injury in a single-center double-blinded randomised placebo-controlled study during the "Effect of Remote Ischaemic Conditioning in ONCology" (ERICONC) project (Chung *et al.*, 2016). Their project was reviewed and approved with a favourable opinion from the United Kingdom National Research Ethics Service (NRES) (London-Chelsea Committee NRES REC reference: 15/LO/1116). The ERICONC study protocol is registered on the public trials database clinicaltrials.gov NCT 02471885 (Chung *et al.*, 2016). They hypothesised that the sub-clinical myocardial injury as a result of anthracyclines chemotherapy would be reduced by remote ischaemic pre-conditioning, using a blood pressure (BP) cuff. Cancer patients were adults with

capacity, aged 21.9 – 72.9 years old, treated with anthracycline regimen chemotherapy, who tolerate BP arm cuff inflation and were recruited in the UCL hospital's Macmillan Cancer Centre. Cardiac injury implications in cancer patients were assessed before chemotherapy with ECG and baseline blood tests, with biomarkers including TnT, NT-proBNP and miRNAs. Patients were excluded if they had a myocardial infarction in the 4 previous weeks of chemotherapy or if they had a defined cardiac diagnosis which may alter the cardiac injury biomarker results. The patient profiles are presented in Table 6-1. There were 19 patients included in the ERICONC study, with 37 % females and a median age of 53.6 years old (average = 49.6 years old). Three types of cancers were observed: fifteen patients had sarcoma, three had lymphoma and one had breast cancer. Patients were treated with different chemotherapy regimens presented in Table 6-1. Prior to chemotherapy infusion administration remote ischaemia conditioning (RIC) or sham procedure was processed (Table 6-1). The RIC procedure consisted of 4 cycles of upper arm blood pressure cuff inflation to 200mm Hg for 5 min (corresponding to the ischaemia phase), followed by a cuff deflation for 5 min. A total of eight patients developed cardiac issues post-chemotherapy, including five RIC-treated patients and three sham patients. The cardiac issues observed during this project were arrhythmia, postural hypotension, fast atrial fibrillation, left arm deep vein thrombosis, Thrombocytopenia and hypokalaemia, pulmonary emboli portal vein thrombosis and heart failure. Potential cardiac injury development was monitored through ECG and blood sample assessment immediately post-chemotherapy (6 to 24 hrs following the end of the treatment) and 3 months post-chemotherapy.

Due to the onset of the COVID-19 pandemic, the number of patients in ERICONC project was lower than planned. According to the conclusion from the PhD thesis by Dr Michael Mallouppas (UCL), the TnT level was elevated post-chemotherapy, however, no changes were observed when he compared the TnT level of RIC patients to sham patients. Furthermore, the NT-proBNP level was elevated 3 months post-chemotherapy compared to the NT-proBNP level pre-chemotherapy, while no changes were observed when he compared the NT-proBNP level of RIC patients to sham patients. The LV function of all patients measured by LVEF was not altered from the baseline to 3 months post-chemotherapy (Mallouppas *et al.*, 2023).

Table 6-1: Representation of the ERICONC patient profile

ID	Gender	Age	Arm (RIC=1, Sham=2)	Cancer	Chemotherapy treatment		TnT (ng / L)			BNP (ng / L)		Cardiac events	Other clinical events
					Regimen	dose mg/m2	Baseline	PC	3M PC	Baseline	3M PC		
R01	Male	56.2	2	Sarcoma	DOX / CISPLATIN	450 (75 * 6)	9			49	49	Asymptomatic non sustained VT / Arrhythmia (VT)	Aneamia requiring Transfusion
R02	Female	72.9	2	Lymphoma	R CHOP	250 (50 * 4 + 25 * 2)	6	17	12	107	181	Postural hypotension	Lower Resiratory Infection with neutropenia
R03	Female	68.5	1	Lymphoma	CHOP	300 (50 * 6)	4	27	29	164	515	Fast Atrial Fibrillation	Dizziness with DOXORUBIN infusion - rate slowed slowed, Non Neutropenic Fever, Readmitted post STC with CMV colitis. Complicated by BK virus infection, sepsis, ARDS, fast AF and AKI requiring ITU support
R04	Male	69.5	1	Sarcoma	DOXORUBICIN	450 (75 * 6)	9	68	22	49	74		Disease Progression
R05	Male	35.9	2	Sarcoma	DOX 75 IFOS 9G	240 (60 * 4)	11	15	11	49	74		Wound Infection (Leg) - requiring hospital admission 3 weeks ABX and Vac dressing
R06	Female	67.6	1	Sarcoma	DOX IFOS	262 (75 - 75 -56 -56)	5	15	11		132	L arm deep vein thrombosis	Neutropenic Sepsis, Febrile Neutropenia
R07	Male	63.8	1	Sarcoma	DOXORUBICIN	225 (75 * 3)	12	22	21	49	1168		Progression of Disease (chemotherapy changed), Leg Celulitis
R08	Female	29.2	2	Breast	FEC PC	300 (100 * 3)	3	6	16	69	70		
R09	Male	42.1	1	Sarcoma	DOX IFOS	225 (75 * 3)	5	7	8	49	49		Neutropenic Sepsis
R10	Female	56.5	1	Sarcoma	DOXORUBICIN	150 (75 * 2)			19		776		Progression of Disease (cancer), Pyrexia (unknown cause), Constiptaion /Abdominal pain - Confrimed on CT - complication of Chemo.
R11	Male	45.3	2	Sarcoma	DOX / CISPLATIN	428 (75 * 2 + 64 * 2 + 75 * 2)	7	17	17	58	49	Thrombocytopenia, Hypokalaemia	Neutropenic sepsis due to profound myelosuppresion and mucositis, Anemaia requiring transfusion
R12	Male	34.6	2	Sarcoma	DOX 75 IFOS 9G	300 (75 * 4)	4		30	49	53	Pulmonary emboli	UTI (Back pain x1 week admission to local hospital), Progression of disease- bone mets, liver and inderterminent lung changes suspicious of mets - found from PET CT and MRI
R13	Male	44.9	1	Sarcoma	DOX 75 IFOS 9G	450 (75 * 6)	7	13		76	101		Aneamia 67g/L Requiring transfusion
R15	Male	21.9	1	Sarcoma	EpSSG (IVADOx 4 IVA 5-6)	240 (60 * 4)			6	67	230	Portal vein thrombosis	Mucositis & Neutropenia - Admission locally, Non Neutropenic Fever, Neutropenic Fever / Tooth Abcess
R16	Male	67.4	1	Sarcoma	Dox 75 Bolus	75 (1 dose)	25			503			
R17	Male	26.6	1	Sarcoma	DOXORUBICIN 75	450 (75 * 6)	4	42		49	49		Febrile Neutropenia - requiring inpatient admission
R19	Female	62.6	1	Sarcoma	DOX IFOS	270 (75 * 2 + 60 * 2)	6		27	59	190		Progression of Disease found on MRI - (L maxillary sarcoma). "The left maxillary sarcoma has continued to grow in spite of treatment - the largest increase in size involves the pre-antral component of the tumour".
R20	Male	53.6	2	Sarcoma	DOX 75 Bolus	225 (75 * 3)	6	12	11	82	108	Heart failure	disease progression - chemo stopped, disease progression
R21	Female	23.7	1	Lymphoma	ABVD	50 (25 * 2)	3			49			Abdominal Pain post fetility preservation - overnight admission Thought to be caused by hyper ovarian stimulation / bleed post egg extraction..

6.2. Methods

6.2.1. Ethics for the Human plasma samples received from external collaborator Prof Malcolm Walker (UCL)

The ERICONC study was approved by UCL and NHS R&D departments (London-Chelsea Committee NRES REC reference: 15/LO/1116) as well as by the Research Ethics Committee according to all relevant legal rules and ethics guidance, including the Data Protection Act and the Human Tissue Act. The external collaborators collected plasma at different time-points: at baseline, at the end of the chemotherapy, and 3 months after chemotherapy completion. Blood samples were taken during the routine full blood count, urea and electrolytes tests of the cancer patients. The samples were collected in standard EDTA (purple top) and SST (yellow top) blood sample bottles and the plasma was isolated and stored at -80°C within one hour of sampling. The samples were shipped to Coventry University on dry-ice using same-day delivery. At Coventry University the samples were stored at -80°C.

6.2.2. Patient profile of the ERICONC miRNA study

Human plasma samples were collected from 19 patients: 12 men and 7 women. The median age was 53.6 years (54 years for women and 51 years for men). Patients had sarcoma (n = 15), lymphoma (n = 3) or breast cancer (n = 1) and were treated with different combinations of anthracyclines, such as doxorubicin ± IFOS/Bolus/Cisplatin (n = 14), FEC (n = 1), CHOP (n = 1), epSSG (n = 1) and 2 unknown treatments. A total of 42 % of the patients developed cardiovascular adverse effects, i.e. Asymptomatic non-sustained VT (R01), Postural hypotension (R02), Fast Atrial Fibrillation (R03), L arm deep vein thrombosis (R06), Hypokalaemia and thrombopenia (R11), Pulmonary emboli (R12), Portal vein thrombosis (R15) and Heart failure (R20). Plasma was collected at three different time points:

- At the beginning of the experiment, baseline group (n = 18)
- At the end of the chemotherapy, Post-Chemo group (n = 13)
- 3 months after the treatment, 3 months group (n = 13)

Due to the COVID-19 pandemic, some patient samples were not collected. There were 10 patients with a full set of blood samples (blood collected at all three time points), 6 patients with blood samples collected at two time points, and 3 patients with blood samples collected only at baseline time point. A total of 44 blood samples from the ERICONC study were obtained from UCL toward this study of miRNA expression at Coventry University.

6.2.3. Materials: Consumables used for the ERICONC patients plasma sample miRNA assessment

The miRNeasy mini kit was purchased from Qiagen (Manchester, UK) and used for miRNA extraction from plasma samples. Chloroform (C2432), absolute ethanol, and MS2 RNA 0.8µg/µL (10165948001) were purchased from Sigma-Aldrich (Merck KGaA, UK). TE buffer pH8.0 (1mM Tris HCl, 0.1mM EDTA) was purchased from Invitrogen (Thermofisher, UK) and diluted in RNase-free water to obtain a final solution of 0.1 TE buffer pH8.0.

All the following reagents were purchased from Life Technology (Thermofisher, UK): TaqMan™ MicroRNA Reverse Transcription Kit (4366597) and Megaplex™ RT Primers, Human Pool A v2.1 (4399966), TaqMan™ PreAmp Master Mix (4391128) and Megaplex™ PreAmp Primers, Human Pool A v2.1 (4399233), TaqMan™ Array Human MicroRNA A Cards v2.0 (4398965) and TaqMan™ Universal Master Mix II, no UNG (4440049), miRNA Reverse Transcription kit from Applied Biosystems (4366597), TaqMan™ MicroRNA Assay (4427975), the individual miRNA assays (4427975): hsa-miR-126-002228, hsa-miR-10a-000387, hsa-miR-143-002249, hsa-miR-150-000473, hsa-miR-320-002277 and endogenous control snRNA U6.

6.2.4. Methods: Human miRNA array cards protocol

6.2.4.1. MiRNA extraction of pooled human plasma samples

Patient plasma samples were pooled together per group (i.e. baseline, end of the chemotherapy, and 3 months after chemotherapy) by adding the same volume from each individual patient sample in that respective group.

Total miRNA from plasma samples was extracted using the miRNeasy mini kit (Qiagen). After all debris had been removed from pooled plasma samples, QIAzol from the miRNeasy mini kit containing 0.8 µg/µL MS2 RNA as spike-in was used as lysis buffer. Chloroform was added to the lysate and the aqueous phase was transferred to a new RNAse-free Eppendorf tube. Absolute ethanol was added to the lysate to provide an appropriate binding condition. Total miRNA was then fixed to the membrane of the RNeasy Mini Spin Column supplied in the miRNeasy mini kit by centrifugation, while contaminants were washed away by washing with the washing buffers supplied in the kit. Total miRNA was eluted in RNAse-free water, and miRNA quality and quantity were determined with NanoDrop™ One/OneC Microvolume UV-Vis Spectrophotometer (ThermoFisher, USA). The extracted miRNA samples are stored at -80 °C until further analysis.

6.2.4.2. Reverse transcription of pooled human plasma samples

Reverse transcription of total miRNA to cDNA was performed using the TaqMan® MicroRNA reverse Transcription kit components and the Human Megaplex RT Primers (ThermoFisher, US) in Eppendorf® Mastercycler Nexus Thermal Cyclers (Merck, USA).

Extracted pooled miRNA samples were mixed with Multiscribe™ reverse transcriptase (50 U/µL), Megaplex RT primers, 10X RT buffer, RNase Inhibitor (20 U/µL), $MgCl_2$ (25 mM) and dNTPs with dTTP (100mM) on ice and the mix was incubated for 5 min on ice. The three next steps were processed during 40 cycles. The mix was incubated (1) at 16 °C for 2 min to *anneal primers*. Then, it was incubated (2) at 42 °C for 1 min and incubated (3) at 50 °C for 1 sec to reverse transcribe RNA. Steps (1), (2) and (3) were repeated for 40 cycles. After the 40 cycles, the mix was incubated (4) at 85 °C for 5 min to inactivate the enzyme.

The resulting cDNA was processed directly after the reverse transcription reaction with a pre-amplification reaction before loading the cDNA on the miRNA array card.

6.2.4.3. Pre-Amplification of pooled human plasma samples

The aim of the pre-amplification reaction is to increase the quantity of the cDNA prior to running the samples on the miRNA arrays. The cDNA from pooled plasma samples were pre-amplified with a PreAmp reaction mix. Template cDNA was mixed with TaqMan® PreAmp Master Mix (2X) and Human Megaplex™ PreAmp Primers (10X) on ice. The mix was incubated at 95 °C for 10 min to activate the enzyme. Then the mix was incubated at 55 °C for 2 min to anneal the primers and at 72 °C for 2 min to extend the primer on cDNA. The next two steps were processed during 14 cycles. The two steps were an incubation at 95 °C for 15 sec to denature cDNA. Followed by incubation at 60 °C for 4 min to anneal and extend primers on cDNA. Finally, the mix was incubated at 99.9 °C for 10 min to inactivate the enzyme.

6.2.4.4. TaqMan miRNA human array card protocol using pooled human plasma samples

Human TaqMan® MicroRNA Array A cards (version 2.0) were used to run the pooled plasma group cDNA samples. The target cDNA (pre-amplified product from plasma pools) was mixed with TaqMan® Universal PCR Master Mix No AmpErase® UNG (2X). The mix was loaded on the human TaqMan® MicroRNA Array A cards and the reaction was run on the PCR instrument QuantStudio 7 applying the 384 well TaqMan Low-Density Array default thermal-cycling conditions. The enzyme was activated at

95 °C for 10 min. Then, the two next steps were repeated for 40 cycles. The cDNA was denatured at 95 °C for 15 sec and primers were annealed and extended at 60 °C for 1 min.

6.2.4.5. Data analysis of TaqMan miRNA array card analysis

The miRNA expression cycle thresholds (C_T) are measured by the QuantStudio 7 Pro Real-Time PCR System version 1.3 (Applied biosystems, ThermoFisher Scientific). The differential miRNA expression values were calculated using the Applied Biosystems application RQ (version 3.9) located on the online Thermo Fisher Connect cloud application by normalising the target miRNA C_T levels against the endogenous control U6 small nuclear RNA (snRNA). C_T levels higher than 40 were excluded from the analysis, due to unspecific/insignificant annealing. Analysis was carried out using the relative quantification ($\Delta\Delta C_T$) method, where the calculated RQ value is the comparison of globally normalised target miRNA against the U6 snRNA levels. The equation used was $\Delta RQ = 2^{\wedge} (-((C_T \text{ value of target miRNA} - C_T \text{ of U6})_{\text{post-treatment}} - (C_T \text{ value of target miRNA} - C_T \text{ of U6})_{\text{baseline}}))$, where C_T value is generated using the relative threshold algorithm (C_{RT}). An ΔRQ-value > 2 meant a significant increase in expression fold change, and ΔRQ-value < 0.5 meant a significant decrease in expression fold change.

6.2.5. Methods: Individual miRNA expression protocol

6.2.5.1. miRNA extraction of individual human plasma samples

Key miRNAs associated with vascular injury (i.e. hsa-miR-126, hsa-miR-10a, hsa-miR 143, hsa-miR-150 and hsa-miR-320a) were identified from the TaqMan miRNA array cards data analysis expression of the ERICONC project human plasma samples (i.e. Baseline group: n = 18; Post-Chemo group: n = 13; 3 months Post-Chemo group: n = 13). Individual patient plasma samples were extracted using the miRNeasy mini kit (Qiagen) using the same protocol as mentioned in section "6.2.1.1. miRNA extraction of pooled human plasma samples".

6.2.5.2. Reverse transcription of individual human plasma samples

Reverse transcription of specific miRNAs to cDNA was performed using TaqMan® MicroRNA reverse Transcription kit components and the specific target TaqMan miRNA assays: hsa-miR-126, hsa-miR-10a, hsa-miR 143, hsa-miR-150 and hsa-miR-320, and the U6 snRNA as housekeeping reference (ThermoFisher, US). Individual miRNA samples were mixed with Multiscribe™ reverse transcriptase (50 U/µL), RT miRNA primer assays (x5), 10x RT buffer, RNase Inhibitor (20 U/µL), MgCl2 (25 mM) and

dNTPs with dNTPs (100 mM) on ice. The reverse transcription reaction run on the Eppendorf® Mastercycler Nexus Thermal Cyclers (Merck, USA) using the following setting: (1) 16 °C for 30 min to anneal primers, (2) 42 °C for 30 min to reverse transcribe RNA, and (3) 85 °C for 5 min to inactivate the enzyme. The cDNA was diluted 1:1 with RNAse-free water after the reaction.

6.2.5.3. Individual key miRNA expression quantification by Real-Time PCR of individual human plasma samples

The target cDNA samples were mixed with TaqMan® Universal PCR Master Mix II no UNG and specific miRNA primer assays (x20). The mix was loaded on a 96-well plate (ThermoScientific, UK). This plate was run on the real-time PCR instrument QuantStudio 7 according to the manufacturer's protocol: (1) UNG was activated at 50 °C for 2 min, (2) enzyme was activated at 95 °C for 10 min, (3) cDNA was denatured at 95 °C for 15 sec, (4) primers were annealed and extended at 60 °C for 1 min, (5) repeat step (3) and (4) for 40 cycles.

6.2.5.4. Data analysis of individual key miRNA expression levels from individual human plasma samples

Individual miRNA expression levels were analysed using the ΔΔCt method using the U6 snRNA as endogenous control for the comparisons of the relative amount of specific miRNAs. The equation used was: $\frac{X_0}{R_0} = 2^{CT_X - CT_{RX}}$, where X_0 is the amount of target miRNA, R_0 is the amount of U6 snRNA, CT_X is the CT value of the target miRNA and CT_R is the CT value of U6 snRNA. C_T levels higher than 40 were excluded from the analysis, due to unspecific/insignificant annealing. Negative control using water instead of plasma sample cDNA was included for each sample. The miRNA level was expressed as values relative to the endogenous gene, U6 and normalised to baseline-collected plasma.

All data are expressed as means ± S.E.M and n refers to the number of patients. Statistical analysis was performed using One-Way ANOVA with Dunnett's post-hoc test using Graph-Pad Prism 9.0 (GraphPad Software, La Jolla, USA). Statistical significance was determined with $p \leq 0.05$.

6.3. Results

6.3.1. miRNA assessment of pooled plasma samples of the ERICONC study with the TaqMan Human miRNA array cards A

The effect of anthracycline chemotherapy was observed at three different time points (i.e. baseline, post-chemotherapy and 3 months post-chemotherapy) on circulating miRNA levels in cancer patients. The heatmap in Figure 6-1 showed the down-regulation (in blue, RQ < 0.5) or up-regulation (in red, RQ > 2.0) of miRNAs expression levels in pooled cancer patients plasma samples at time points post-chemotherapy and 3 months post-chemotherapy compared to baseline. From this miRNA array analysis, five key miRNAs associated with cardiac- and vascular-injury were identified based on a literature search (i.e. hsa-miR-10a, hsa-miR-126, hsa-miR-143, hsa-miR-150 and hsa-miR-320a).

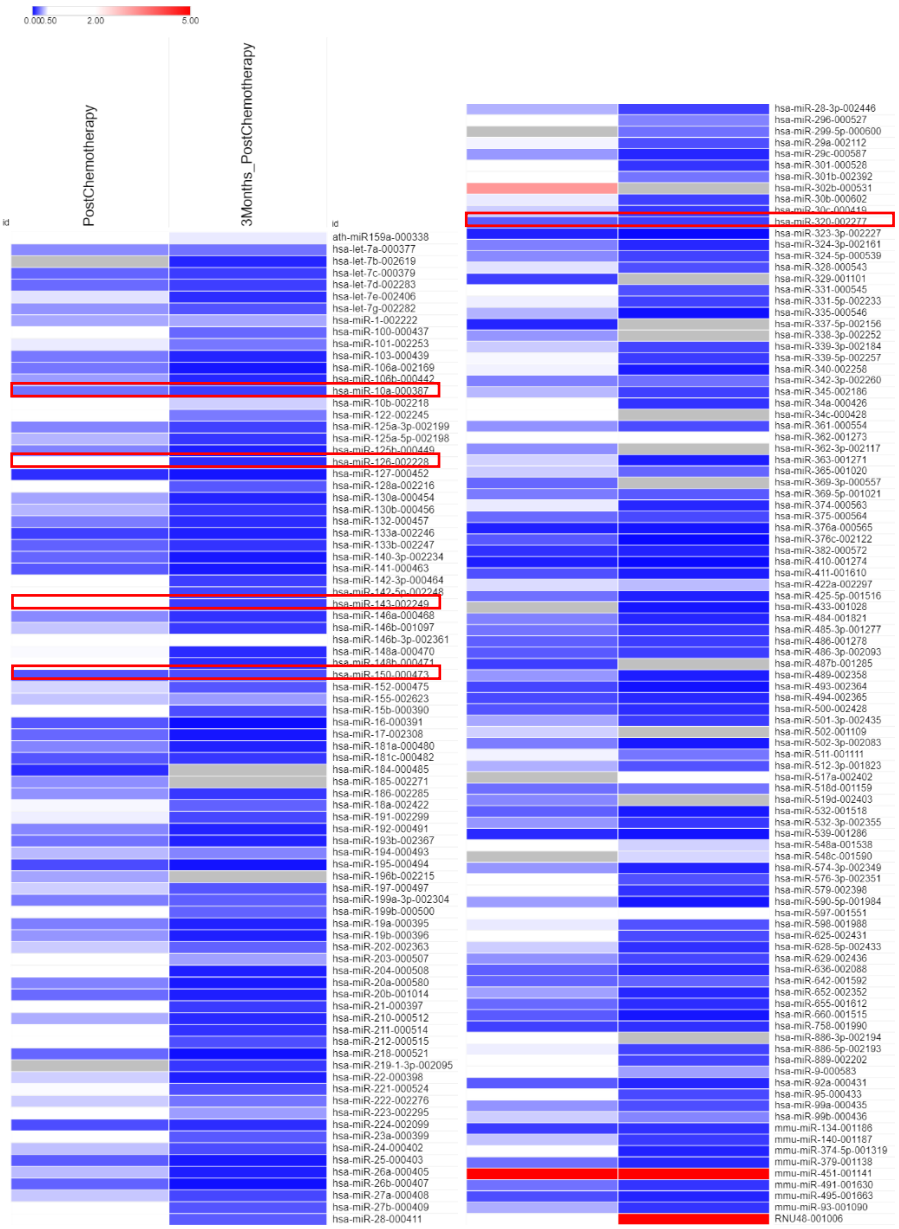

Figure 6-1: Heatmap of the miRNA expression in pooled plasma samples from the ERICONC study at the time points post-chemotherapy and three months post-chemotherapy compared to baseline. miRNA expression was determined by quantitative Real-Time PCR using TaqMan Human Array Cards A on QuantStudio 7. Data was internally normalised to U6 as endogenous gene and analysed using RQ app on the ThermoFisher Cloud supplication. The RQ value of miRNAs in plasma of cancer patients at the baseline was set up to 1 and RQ values of miRNAs from both post-chemotherapy and three months post-chemotherapy time points were normalised to baseline's RQ value. RQ values < 0.5 specify a significantly down-regulated target (Blue), while RQ > 2.0 specify a significantly up-regulated target (Red). The absence of RQ value was shown in grey, while the non-significant RQ values were in white.

The miR-10a expression at the end of chemotherapy was 4-fold reduced (RQ = 0.224) compared to baseline, while the miR-10a expression at three-month post-chemotherapy was 8-fold reduced (RQ = 0.122) compared to baseline (Figure 6-2 (A)). The miR-126 expression in pooled patients' plasma samples was not altered after the time point immediately after chemotherapy (RQ = 0.546) compared to the baseline, however, the miR-126 expression was 11-fold reduced at three months following the chemotherapy (RQ = 0.087) compared to baseline (Figure 6-2 (B)). Similarly, the miR-143 expression in pooled plasma samples was not altered straight after chemotherapy (RQ = 0.987) compared to baseline, while three months following the chemotherapy the miR-143 expression was 9-fold reduced (RQ = 0.116) compared to baseline (Figure 6-2 (C)). The miR-150 expression at the post-chemotherapy time point was 6-fold reduced (RQ = 0.162) compared to baseline, and the level of miR-150 expression stayed reduced at three-month post-chemotherapy, as it was 7-fold reduced (RQ = 0.149) compared to baseline (Figure 6-2 (D)). The miR-320a expression at the time point post-chemotherapy was 6-fold reduced (RQ = 0.181) compared to baseline, and at three-month post-chemotherapy the miR-320a expression was 8-fold reduced (RQ = 0.124) compared to baseline (Figure 6-2 (E)).

(A)

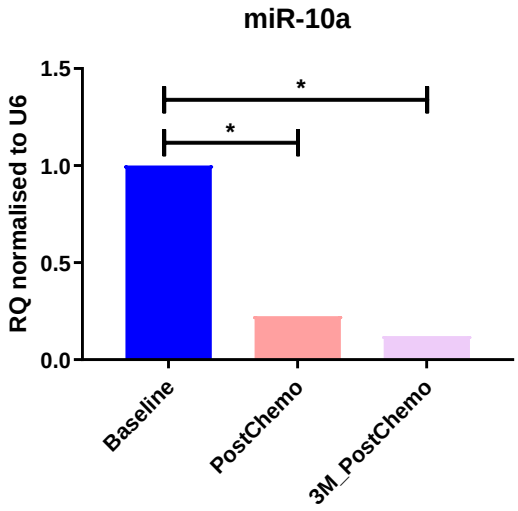
miR-10a
RQ normalised to U6
1.5
1.0
0.5
0.0
*
*
Baseline
PostChemo
3M_PostChemo

(B)

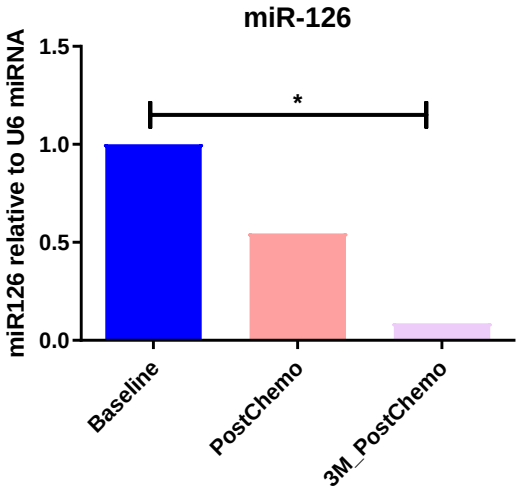
miR-126
miR126 relative to U6 miRNA
1.5
1.0
0.5
0.0
*
Baseline
PostChemo
3M_PostChemo

(C)

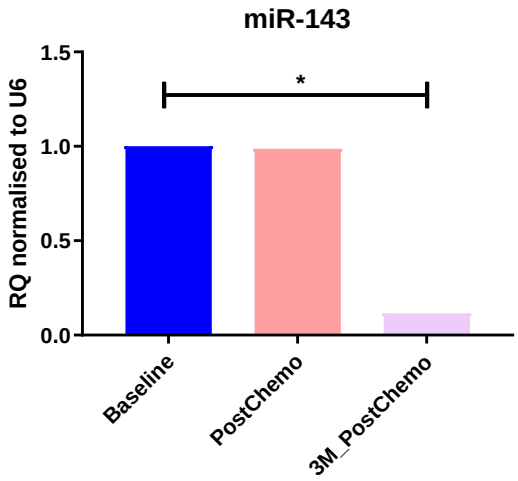
miR-143
RQ normalised to U6
1.5
1.0
0.5
0.0
*
Baseline
PostChemo
3M_PostChemo

(D)

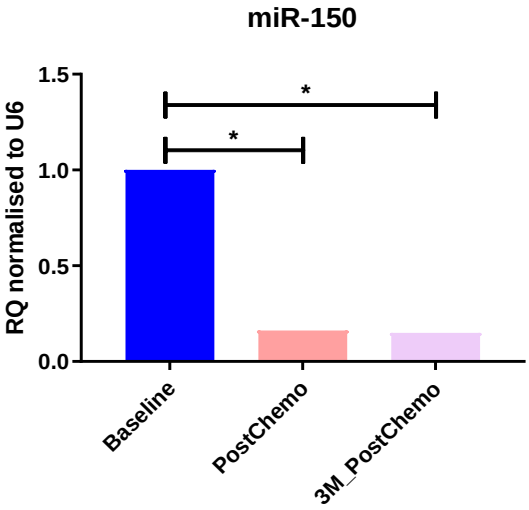
miR-150
RQ normalised to U6
1.5
1.0
0.5
0.0
*
*
Baseline
PostChemo
3M_PostChemo

(E)

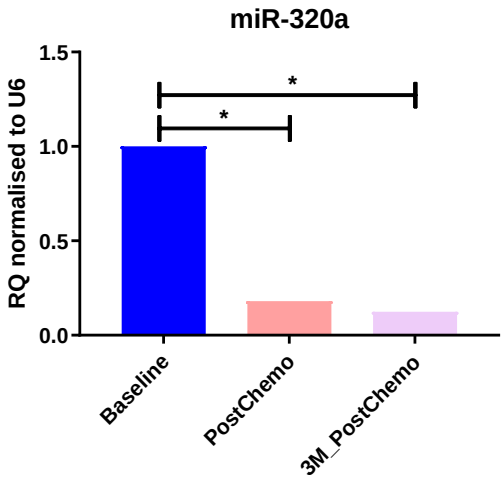
miR-320a
RQ normalised to U6
1.5
1.0
0.5
0.0
*
*
Baseline
PostChemo
3M_PostChemo

Figure 6-2: Quantification of miR-10a, miR-126, miR-143, miR-150 and miR-320a expression levels in pooled human plasma samples from the ERICONC study using the TaqMan Human miRNA array card A derived RQ values. Comparison of miRNA levels in pooled human plasma samples at different time points: Baseline, post-chemotherapy and three months post-chemotherapy. Baseline = Plasma was collected at the beginning of the treatment, PostChemo = plasma was collected at the end of the chemotherapy and 3M_PostChemo = plasma was collected three months post-chemotherapy. Data are expressed as RQ values relative to U6 snRNA, an endogenous internal control and normalised to baseline group. RQ values < 0.5 specify a significantly down-regulated target, while RQ > 2.0 specify a significantly up-regulated target.

6.3.2. Analysis of individual key miRNA expression profiles in individual human plasma samples from the ERICONC study

6.3.2.1. Quantification of miR-10a level in individual human plasma samples

The expression of miR-10a was investigated in individual human plasma samples by Real-Time PCR. Figure 6-3 shows the miR-10a levels in individual human plasma samples. The miR-10a plasma levels were not altered at the end of the chemotherapy (0.67 ± 0.20) and three months post-chemotherapy (1.01 ± 0.20), when compared to the miR-10a plasma level at baseline (1.0 ± 0.21).

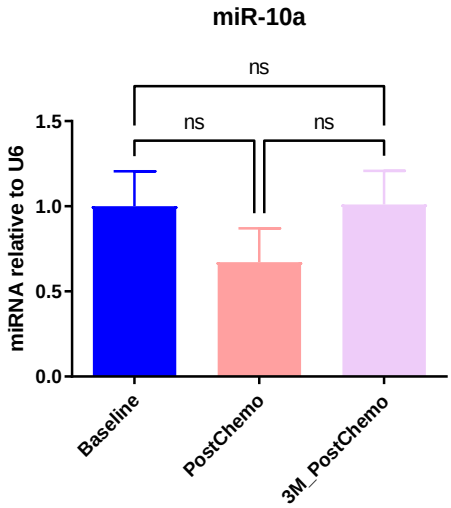

Figure 6-3: Real-time PCR of miR-10a in individual human plasma samples. Comparison of miR-10a levels in human plasma samples from Baseline group (n = 18), PostChemo (n = 13), 3M_PostChemo (n = 13). Baseline = Plasma was collected at the beginning of the treatment, PostChemo = plasma was collected at the end of the chemotherapy and 3M_PostChemo = plasma was collected three months post-chemotherapy. Data are expressed as mean ± S.E.M. values relative to U6 snRNA levels (n = 13 - 18) and normalised to baseline group. The groups were compared by multiple comparisons using one-way ANOVA Kruskal-Wallis' test.

To investigate if the miRNA alteration was specific to patients experiencing cardiovascular issues, the plasma samples were divided into two groups: the patients who developed cardiac issues and the patient who did not develop cardiac issues.

Figure 6-4 (A) shows the miR-10a levels in plasma from patients with cardiac issues, while Figure 6-4 (B) shows the miR-10a levels in plasma from patients without cardiac issues. The miR-10a plasma levels were not altered at the end of the chemotherapy (0.66 ± 0.47) and three months post-chemotherapy (1.63 ± 0.44) compared to the miR-10a level at baseline (1.00 ± 0.28) in patients with cardiac issues (Figure 6-4 (A)). Similarly, the miR-10a plasma levels were not altered at the end of the chemotherapy (0.64 ± 0.20) and three months post-chemotherapy (0.75 ± 0.23) compared to miR-10a at baseline (1.00 ± 0.25) in patients without cardiac issues (Figure 6-4 (B)).

(A) (B)

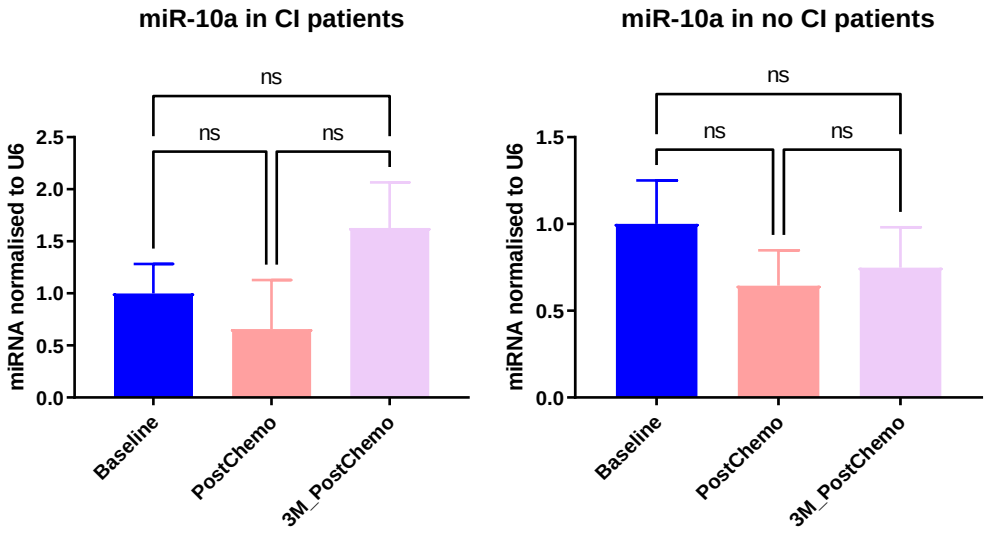

Figure 6-4: Real-time PCR of miR-10a in individual human plasma samples with or without cardiac issues (CI). (A) Comparison of miR-10a levels in plasma samples of anthracycline-treated patients with cardiac issues from Baseline group (n = 8), PostChemo (n = 5), 3M_PostChemo (n = 7). (B) Comparison of miR-10a levels in plasma samples of anthracycline-treated patients without cardiac issues from Baseline group (n = 10), PostChemo (n = 8), 3M_PostChemo (n = 6). Baseline = Plasma was collected at the beginning of the treatment, PostChemo = plasma was collected at the end of the chemotherapy and 3M_PostChemo = plasma was collected three months post-chemotherapy, CI = cardiac issues. Data are expressed as mean ± S.E.M. values relative to U6 snRNA levels (n = 13 - 18) and normalised to baseline group. The groups were compared by multiple comparisons using one-way ANOVA Kruskal-Wallis' test.

The miR-10a expression level was investigated in the individual patient samples from patients that were experiencing cardiac issues after anthracycline chemotherapy (Figure 6-5). The miR-10a level

was reduced at the end of the chemotherapy for patients R03, R11, R12 and R15, while it was increased in patient R02, compared to the miR-10a level at baseline.

The expression pattern of miR-10a level three months post-chemotherapy compared to baseline varied for each patient, and it was reduced in patients R01 and R20, while it was increased in patients R02, R06, R11 and R12. The expression pattern of miR-10a in patient R03 three months post-chemotherapy did not alter compared to baseline.

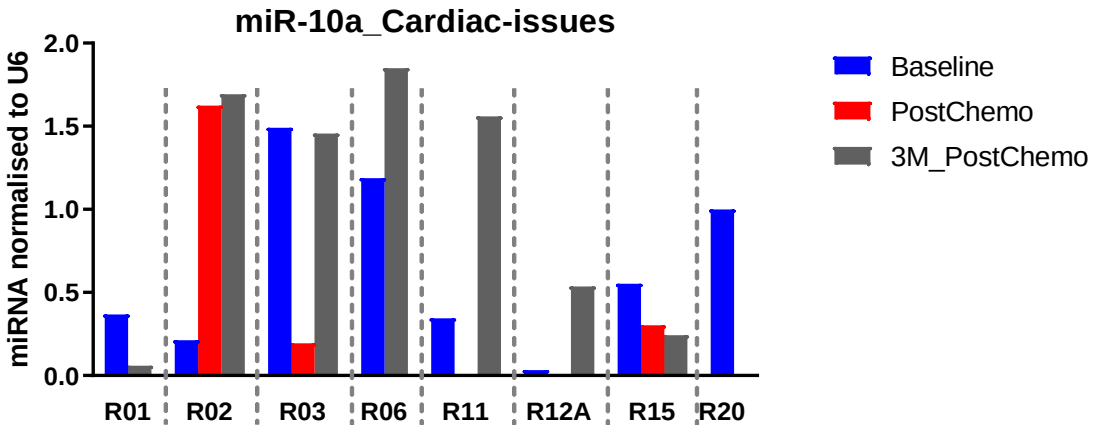

Figure 6-5: miR-10a levels Post-chemotherapy for each individual patient with cardiac issues. Baseline = Plasma was collected at the beginning of the treatment, PostChemo = plasma was collected at the end of the chemotherapy and 3M_PostChemo = plasma was collected three months post-chemotherapy. Post-chemotherapy expression of miR-10a was compared to baseline.

6.3.2.2. Quantification of miR-126 level in human plasma

The expression of miR-126 was investigated in individual human plasma samples by Real-Time PCR.

Figure 6-6 shows the miR-126 levels in individual human plasma samples. The miR-126 level in patients' plasma samples was decreased at the end of the chemotherapy (0.82 ± 0.52, p = 0.014) compared to the miR-126 level in patients' plasma at the baseline (1.00 ± 0.25). The miR-126 level in patients' plasma samples, three months post-chemotherapy (0.74 ± 0.17) was not altered when compared to the miR-126 plasma level at baseline (1.00 ± 0.25). The miR-126 level in patients' plasma samples was not altered from the end of the chemotherapy (0.82 ± 0.52) to three months post-chemotherapy (0.74 ± 0.17).

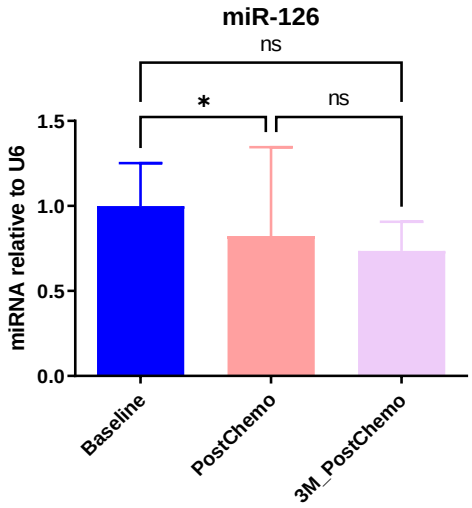

Figure 6-6: Real-time PCR of miR-126 in individual human plasma samples. Comparison of miR-126 levels in human plasma samples from Baseline group (n = 18), PostChemo (n = 13), 3M_PostChemo (n = 13). Baseline = Plasma was collected at the beginning of the treatment, PostChemo = plasma was collected at the end of the chemotherapy and 3M_PostChemo = plasma was collected three months post-chemotherapy. Data are expressed as mean ± S.E.M. values relative to U6 snRNA levels (n = 13 – 18) and normalised to baseline group. The groups were compared by multiple comparisons using one-way ANOVA Kruskal-Wallis' test (* = $p < 0.05$).

To investigate if the miRNA alteration was specific to patients experiencing cardiovascular issues, the plasma samples were divided into two groups: the patients who developed cardiac issues after the chemotherapy and the patients who did not develop cardiac issues.

Figure 6-7 (A) shows the miR-126 levels in plasma from patients with cardiac issues, while Figure 6-7 (B) shows the miR-126 levels in plasma from patients without cardiac issues. The miR-126 level in the plasma of patients with cardiac issues was reduced at the end of the chemotherapy (0.18 ± 0.12, $p = 0.035$) compared to the miR-126 level observed at baseline (1.00 ± 0.38). Additionally, the miR-126 level in plasma samples of patients with cardiac issues observed three months post-chemotherapy (0.79 ± 0.17) was not altered compared to the miR-126 level at baseline (1.00 ± 0.38). However, the miR-126 level in plasma of patients with cardiac issues observed three months post-chemotherapy (0.79 ± 0.17, $p = 0.029$) was up-regulated compared to the miR-126 level immediately at the end of the chemotherapy (0.18 ± 0.12), as shown in Figure 6-7 (A). The miR-126 levels in the plasma of patients without cardiac issues were not altered at the end of the chemotherapy (1.07 ± 0.71) and 3 months post-chemotherapy (0.74 ± 0.30) compared to baseline (1.00 ± 0.34), in Figure 6-7 (B)). Additionally, the miR-126 level in plasma samples of patients without cardiac issues was not altered

from the end of chemotherapy (1.07 ± 0.34) to three months following the chemotherapy (0.74 ± 0.30).

(A) (B)

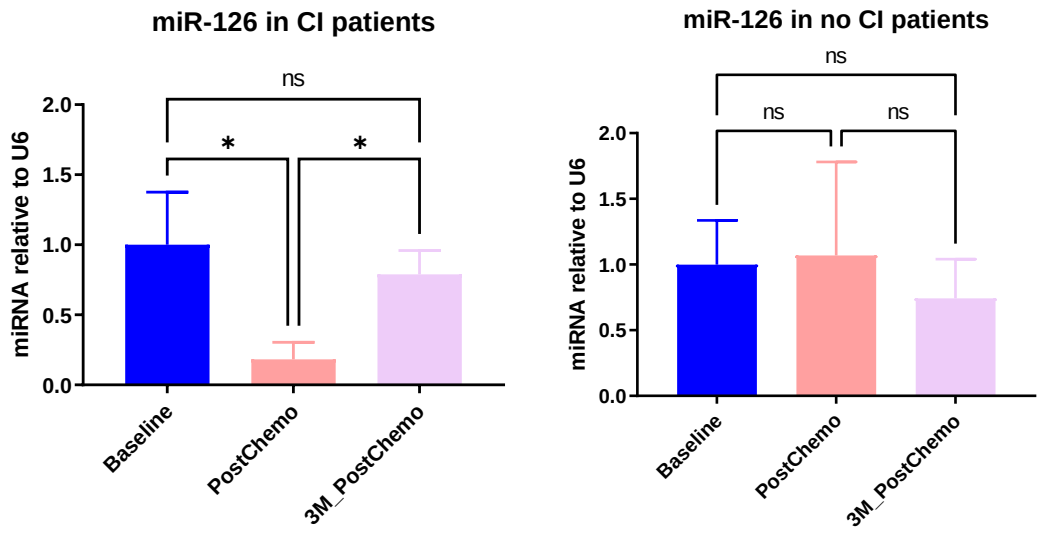

Figure 6-7: Real-time PCR of miR-126 in individual human plasma samples with or without cardiac issues (CI). (A) Comparison of miR-126 levels in plasma samples of anthracycline-treated patients with cardiac issues from Baseline group (n = 8), PostChemo (n = 5), 3M_PostChemo (n = 7). (B) Comparison of miR-126 levels in plasma samples of anthracycline-treated patients without cardiac issues from Baseline group (n = 10), PostChemo (n = 8), 3M_PostChemo (n = 6). Baseline = Plasma was collected at the beginning of the treatment, PostChemo = plasma was collected at the end of the chemotherapy and 3M_PostChemo = plasma was collected three months post-chemotherapy, CI = cardiac issues. Data are expressed as mean ± S.E.M. values relative to U6 snRNA levels (n = 13 – 18) and normalised to baseline group. The groups were compared by multiple comparisons using one-way ANOVA Kruskal-Wallis' test (* = $p < 0.05$).

The miR-126 expression level was investigated in the individual patient samples from patients that were experiencing cardiac issues after anthracycline chemotherapy (Figure 6-8). The miR-126 level at the end of the chemotherapy followed the same trend in all patients (R02, R03, R11, R12 and R15) which was a reduction. The expression pattern of miR-126 level three months post-chemotherapy compared to baseline varied for each patient, as it was reduced in the patients' plasma samples R01, R03 and R15, while it was increased in patients' plasma samples R02, R06, R11 and R12.

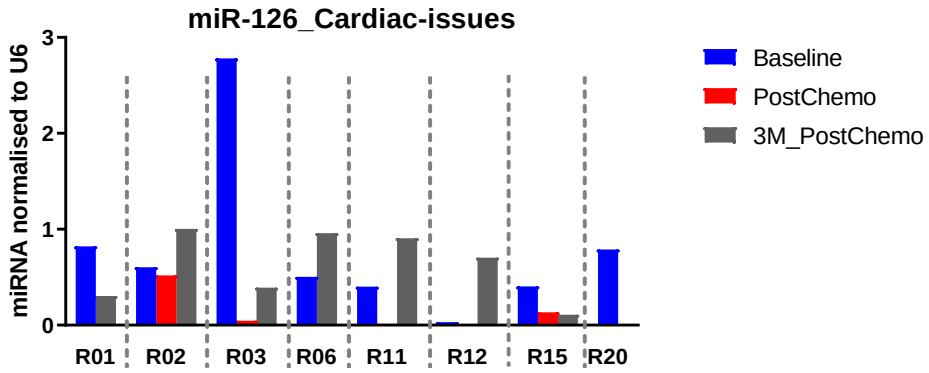

Figure 6-8: miR-126 levels Post-chemotherapy for each individual patient with cardiac issues. Baseline = Plasma was collected at the beginning of the treatment, PostChemo = plasma was collected at the end of the chemotherapy and 3M_PostChemo = plasma was collected three months post-chemotherapy. Post-chemotherapy expression of miR-126 was compared to baseline.

6.3.2.3. Quantification of miR-143 level in human plasma

The expression of miRNA 143 was investigated in individual human plasma samples by Real-Time PCR.

Figure 6-9 shows the miR-143 levels in individual human plasma samples. The miR-143 plasma levels were not altered at the end of the chemotherapy (0.87 ± 0.34) and three months post-chemotherapy (0.61 ± 0.13) compared to the miR-143 plasma level at baseline (1.00 ± 0.25).

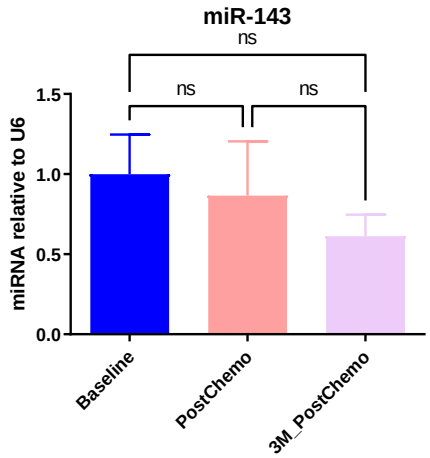

Figure 6-9: Real-time PCR of miR-143 in individual human plasma samples. Comparison of miR-143 levels in human plasma from Baseline group (n = 18), PostChemo (n = 13), 3M_PostChemo (n = 13). Baseline = Plasma was collected at the beginning of the treatment, PostChemo = plasma was collected at the end of the chemotherapy and 3M_PostChemo = plasma was collected three months post-chemotherapy. Data are expressed as mean ± S.E.M. values relative to U6 snRNA levels (n = 13 – 18) and normalised to baseline group. The groups were compared by multiple comparisons using one-way ANOVA Kruskal-Wallis' test.

To investigate if miRNA alteration was specific to patients experiencing cardiovascular issues, the plasma samples were divided into two groups: the patients who developed cardiac issues and the patient who did not develop cardiac issues.

Figure 6-10 (A) shows the miR-143 levels in plasma from patients with cardiac issues, while Figure 6-10 (B) shows the miR-143 levels in plasma from patients without cardiac issues. The miR-143 levels in the plasma of patients with cardiac issues were not altered at the end of the chemotherapy (0.40 ± 0.20) and three months post-chemotherapy (1.10 ± 0.25) compared to the miR-143 level at baseline (1.00 ± 0.40), in Figure 6-10 (A). Additionally, the miR-143 level in the plasma of patients with cardiac issues was increased from the end of the chemotherapy (0.40 ± 0.20; p = 0.047) to three months following the chemotherapy (1.10 ± 0.25). The miR-143 levels in plasma from patients without cardiac issues were not altered at the end of the chemotherapy (0.93 ± 0.37) and three months post-chemotherapy (0.47 ± 0.19) compared to the miR-143 plasma level at baseline (1.00 ± 0.28), in Figure 6-10 (B). Additionally, the miR-143 level in patients without cardiac issues was not altered from the end of chemotherapy (0.93 ± 0.37) to three months following the chemotherapy (0.47 ± 0.19).

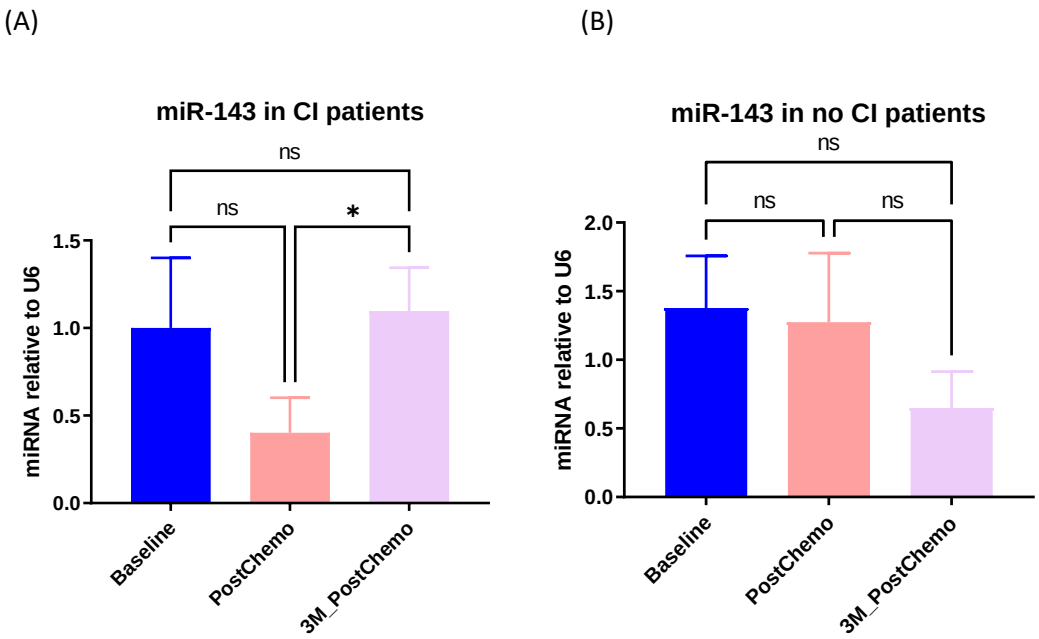

Figure 6-10: Real-time PCR of miR-143 in individual human plasma samples with or without cardiac issues (CI). (A) Comparison of miR-143 levels in plasma samples of anthracycline-treated patients with cardiac issues from Baseline group (n = 8), PostChemo (n = 5), 3M_PostChemo (n = 7). (B) Comparison of miR-143 levels in plasma samples of anthracycline-treated patients without cardiac issues from Baseline group (n = 10), PostChemo (n = 8), 3M_PostChemo (n = 6). Baseline = Plasma was collected at the beginning of the treatment, PostChemo = plasma was collected at the end of the chemotherapy and 3M_PostChemo = plasma was collected three months post-chemotherapy, CI = cardiac issues. Data are expressed as mean ± S.E.M. values relative to U6 snRNA levels (n = 13 – 18) and normalised

to baseline group. The groups were compared by multiple comparisons using one-way ANOVA Kruskal-Wallis' test (* = $p < 0.05$).

The miR-143 expression level was investigated in the individual patient samples from patients that were experiencing cardiac issues after anthracycline chemotherapy (Figure 6-11). The miR-143 level was reduced at the end of the chemotherapy for patients R03, R11 and R12 while it was increased in patients R02 and R15 compared to the miR-143 level at baseline. The expression pattern of miR-143 level three months post-chemotherapy compared to baseline varied for each patient, and it was reduced for patients R01 and R03. The expression pattern of miR-143 was increased in patients R02, R06, R11 and R12 while the expression pattern of miR-143 in patient R15 did not vary at three months following chemotherapy compared to baseline.

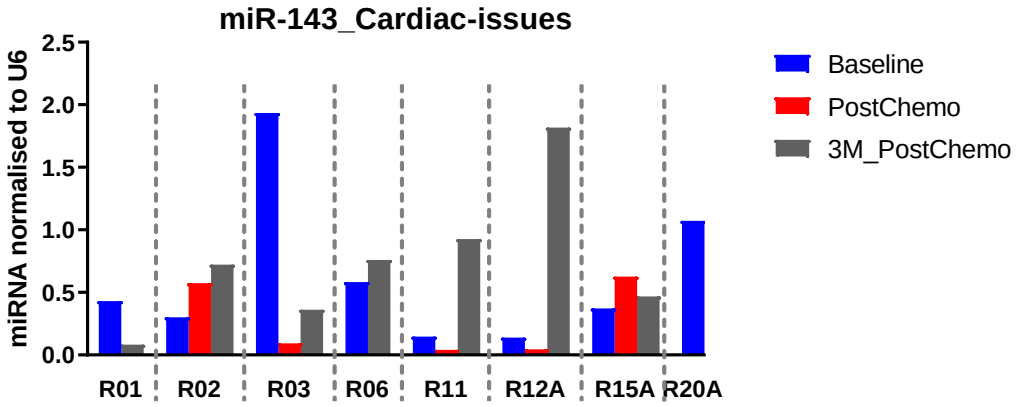

Figure 6-11: miR-143 levels Post-chemotherapy for each individual patient with cardiac issues. Baseline = Plasma was collected at the beginning of the treatment, PostChemo = plasma was collected at the end of the chemotherapy and 3M_PostChemo = plasma was collected three months post-chemotherapy. Post-chemotherapy expression of miR-143 was compared to baseline.

6.3.2.4. Quantification of miR-150 level in human plasma

The expression of miRNA 150 was investigated in individual human plasma samples by Real-Time PCR. Figure 6-12 shows the miR-150 levels in individual human plasma samples. The miR-150 level in patients' plasma samples was significantly reduced at the end of the chemotherapy (0.21 ± 0.05, $p < 0.0001$) compared to the miR-150 level in patients plasma's samples at baseline(1.00 ± 0.18). The miR-150 level in patients' plasma samples was not altered three months post-chemotherapy (0.54 ± 0.08) compared to the miR-150 plasma samples level at baseline (1.00 ± 0.18). Furthermore, the miR-150 level in patients' plasma samples was increased from the end of the chemotherapy (0.21 ± 0.05; $p = 0.007$) to three months post-chemotherapy (0.54 ± 0.08).

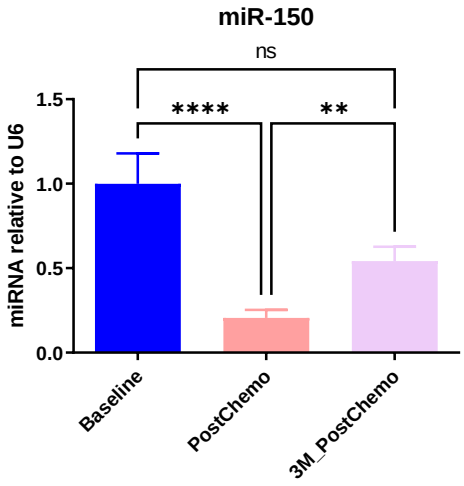

Figure 6-12: Real-time PCR of miR-150 in individual human plasma samples. Comparison of miR-150 levels in individual human plasma samples from Baseline group (n = 18), PostChemo (n = 13), 3M_PostChemo (n = 13). Baseline = Plasma was collected at the beginning of the treatment, PostChemo = plasma was collected at the end of the chemotherapy and 3M_PostChemo = plasma was collected three months post-chemotherapy. Data are expressed as mean ± S.E.M. values relative to U6 snRNA levels (n = 13 – 18) and normalised to baseline group. The groups were compared by multiple comparisons using one-way ANOVA Kruskal-Wallis' test (** = $p < 0.01$, **** = $p < 0.0001$).

To investigate if the miRNA alteration was specific to patients experiencing cardiovascular issues, the plasma samples were divided into two groups: the patients who developed cardiac issues after the chemotherapy and the patients who did not develop cardiac issues.

Figure 6-13 (A) shows the miR-150 levels in plasma from patients with cardiac issues, while Figure 6-13 (B) shows the miR-150 levels in plasma from patients without cardiac issues. The miR-150 level in the plasma of patients with cardiac issues was significantly reduced at the end of the chemotherapy (0.13 ± 0.05, p = 0.0003) compared to the miR-150 level at baseline (1.00 ± 0.31). Additionally, the miR-150 level in plasma of patients with cardiac issues observed three months post-chemotherapy (0.63 ± 0.13) was not altered compared to the miR-150 level at baseline (1.00 ± 0.31). However, the miR-150 level in plasma of patients with cardiac issues observed three months post-chemotherapy (0.63 ± 0.13, p = 0.017) was increased compared to the miR-150 level immediately at the end of the chemotherapy (0.13 ± 0.05), as shown in Figure 6-13 (A).

The miR-150 level in the plasma of patients without cardiac issues was also reduced at the end of the chemotherapy (0.26 ± 0.07; p = 0.0007) and three months post-chemotherapy (0.42 ± 0.06; p = 0.047), when compared to the miR-150 plasma level at baseline (1.00 ± 0.22), in Figure 6-13 (B). However, the

miR-150 level in patients without cardiac issues was not altered from the end of chemotherapy (0.26 ± 0.07) to three months following the chemotherapy (0.42 ± 0.06).

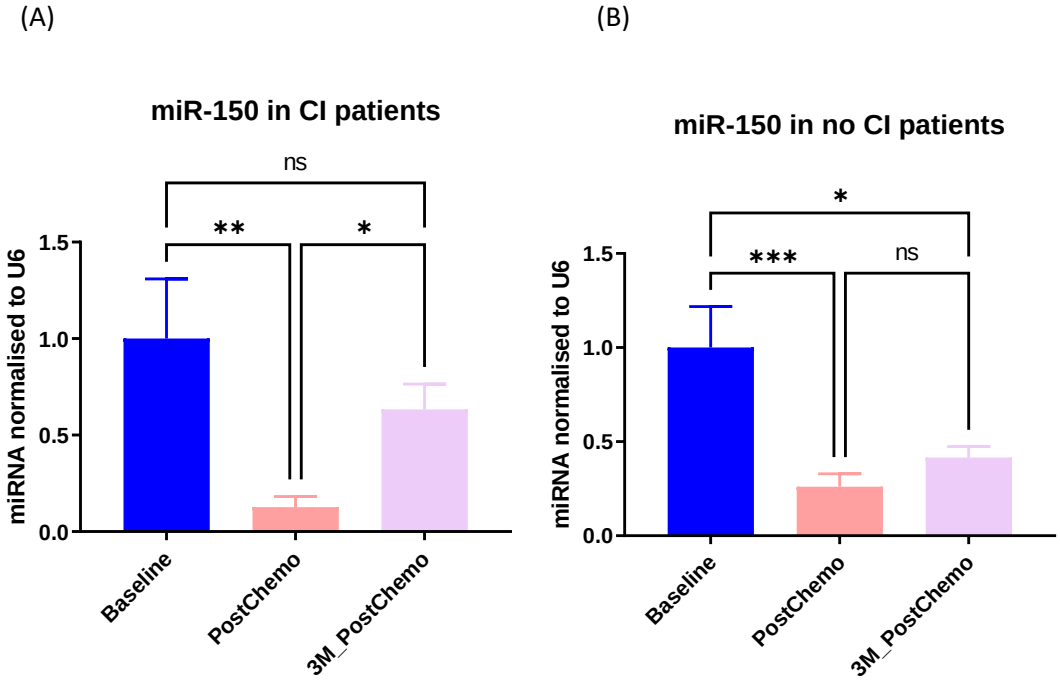

Figure 6-13: Real-time PCR of miR-150 in individual human plasma samples with or without cardiac issues (CI). (A) Comparison of miR-150 levels in plasma samples of anthracycline-treated patients with cardiac issues from Baseline group (n = 8), PostChemo (n = 5), 3M_PostChemo (n = 7). (B) Comparison of miR-150 levels in plasma samples of anthracycline-treated patients without cardiac issues from Baseline group (n = 10), PostChemo (n = 8), 3M_PostChemo (n = 6). Baseline = Plasma was collected at the beginning of the treatment, PostChemo = plasma was collected at the end of the chemotherapy and 3M_PostChemo = plasma was collected three months post-chemotherapy, CI = cardiac issues. Data are expressed as mean ± S.E.M. values relative to U6 snRNA levels (n = 13 – 18) and normalised to baseline group. The groups were compared by multiple comparisons using one-way ANOVA Kruskal-Wallis' test (* = $p < 0.05$, ** = $p < 0.01$, *** = $p < 0.001$).

The miR-150 expression level was investigated in the individual patient samples from patients that were experiencing cardiac issues after anthracycline chemotherapy (Figure 6-14). The miR-150 level at the end of the chemotherapy followed the same trend in five patients (i.e. R02, R03, R11, R12 and R15) which was a reduction. The expression pattern of miR-150 level in plasma samples at three months post-chemotherapy varied for each patient, and it was reduced in patients R01, R03 and R15, while it was increased in patients R06 and R12, and unchanged in patients R02 and R11 compared to miR-150 level in plasma samples at baseline.

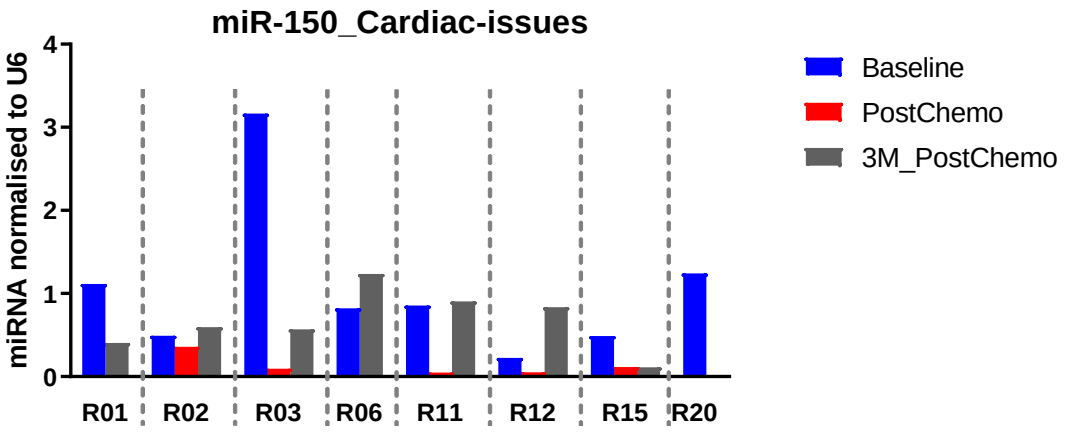

Figure 6-14: miR-150 levels Post-chemotherapy for each individual patient with cardiac issues. Baseline = Plasma was collected at the beginning of the treatment, PostChemo = plasma was collected at the end of the chemotherapy and 3M_PostChemo = plasma was collected three months post-chemotherapy. Post-chemotherapy expression of miR-150 was compared to baseline.

6.3.2.5. Quantification of miR-320a level in human plasma

The expression of miRNA-320a was investigated in individual human plasma samples by Real-Time PCR. Figure 6-15 shows the miR-320a levels in individual human plasma samples. The miR-320a level in patients' plasma samples was reduced at the end of the chemotherapy (0.61 ± 0.25; p = 0.039) compared to the miR-320a level in patients plasma samples at baseline (1.00 ± 0.23). The miR-320a level in patients' plasma at three months post-chemotherapy (0.48 ± 0.08) was not altered when compared to the miR-320a plasma level at baseline (1.00 ± 0.25). The miR-320a expression levels in patients' plasma samples were not altered from the end of the chemotherapy (0.61 ± 0.25) to three months post-chemotherapy (0.48 ± 0.08).

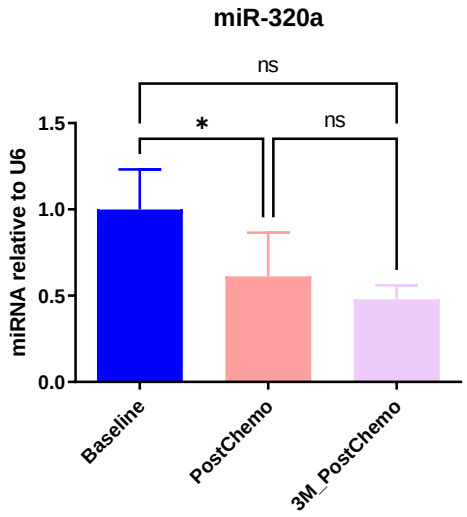

Figure 6-15: Real-time PCR of miR-320a in individual human plasma samples. Comparison of miR-320a levels in individual human plasma samples from Baseline group (n = 18), PostChemo (n = 13), 3M_PostChemo (n = 13). Baseline = Plasma was collected at the beginning of the treatment, PostChemo = plasma was collected at the end of the chemotherapy and 3M_PostChemo = plasma was collected three months post-chemotherapy. Data are expressed as mean ± S.E.M. values relative to U6 snRNA levels (n = 13 – 18) and normalised to baseline group. The groups were compared by multiple comparisons using one-way ANOVA Kruskal-Wallis' test (* = $p < 0.05$).

To investigate if the miRNA alteration was specific to patients experiencing cardiovascular issues, the plasma samples were divided into two groups: the patients who developed cardiac issues after the chemotherapy and the patients who did not develop cardiac issues.

Figure 6-16 (A) shows the miR-320a levels in plasma from patients with cardiac issues, while Figure 6-16 (B) shows the miR-320a levels in plasma from patients without cardiac issues. The miR-320a level in plasma samples of patients with cardiac issues at the end of the chemotherapy was reduced (0.25 ± 0.17, $p = 0.038$) compared to the miR-320a level at baseline (1.00 ± 0.40). Additionally, the miR-320a level in plasma of patients with cardiac issues observed three months post-chemotherapy (0.48 ± 0.13) was not altered compared to the miR-320a level at baseline (1.00 ± 0.40) or at three months post-chemotherapy (0.48 ± 0.13), as shown in Figure 6-16 (A).

The miR-320a level in the plasma of patients without cardiac issues was not altered at the end of the chemotherapy (0.85 ± 0.39) and three months post-chemotherapy (0.47 ± 0.11), when compared to the miR-320a plasma level at baseline (1.00 ± 0.29), in Figure 6-16 (B). Additionally, the miR-320a level in patients without cardiac issues was not altered from the end of chemotherapy (0.85 ± 0.39) to three months following the chemotherapy (0.47 ± 0.11).

(A) (B)

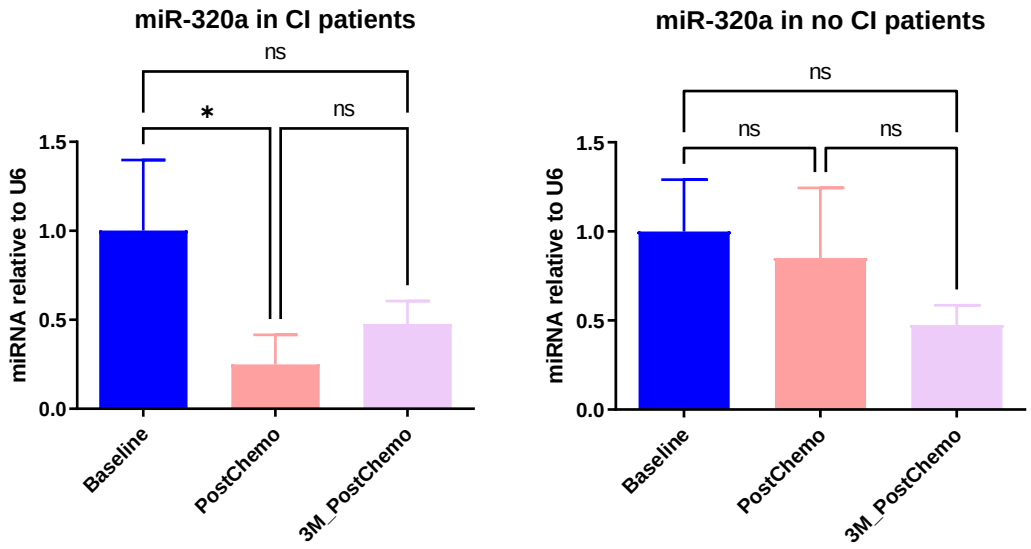

Figure 6-16: Real-time PCR of miR-320a in individual human plasma samples with or without cardiac issues (CI). (A) Comparison of miR-320a levels in plasma samples of anthracycline-treated patients with cardiac issues from Baseline group (n = 8), PostChemo (n = 5), 3M_PostChemo (n = 7). (B) Comparison of miR-320a levels in plasma samples of anthracycline-treated patients without cardiac issues from Baseline group (n = 10), PostChemo (n = 8), 3M_PostChemo (n = 6). Baseline = Plasma was collected at the beginning of the treatment, PostChemo = plasma was collected at the end of the chemotherapy and 3M_PostChemo = plasma was collected three months post-chemotherapy, CI = cardiac issues. Data are expressed as mean ± S.E.M. values relative to U6 snRNA levels (n = 13 – 18) and normalised to baseline group. The groups were compared by multiple comparisons using one-way ANOVA Kruskal-Wallis' test (* = $p < 0.05$).

The miR-320a expression level was investigated in the individual patient samples from patients that were experiencing cardiac issues after anthracycline chemotherapy (*Figure 6-17*). The miR-320a level at the end of the chemotherapy followed the same trend in all patients (R02, R03, R11, R12 and R15) which was a reduction. The expression pattern of the miR-320a level at three months post-chemotherapy compared to baseline varied for each patient, and it was reduced in patients R01, R02 and R15, while it was increased in patients R06, R11 and R12, and unchanged for patients R03 compared to miR-320a level in plasma at baseline.

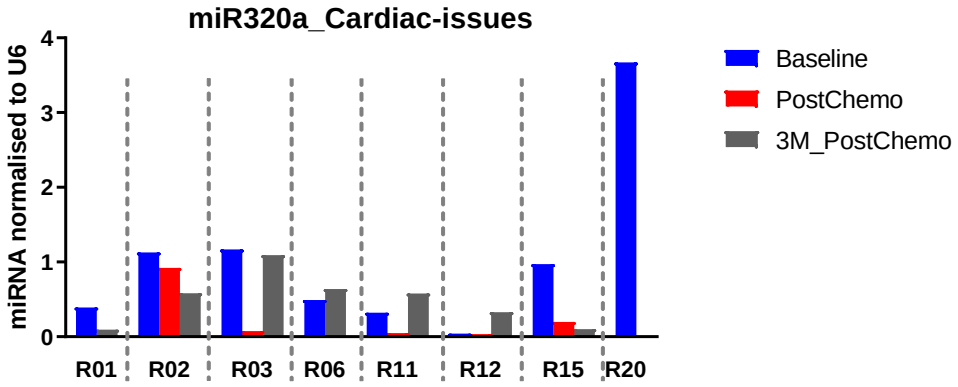

Figure 6-17: MiR-320a levels Post-chemotherapy for each individual patient with cardiac issues. Baseline = Plasma was collected at the beginning of the treatment, PostChemo = plasma was collected at the end of the chemotherapy and 3M_PostChemo = plasma was collected three months post-chemotherapy. Post-chemotherapy expression of miR-320a was compared to baseline.

6.4. Discussion

After pooling the plasma samples from the anthracycline-treated sarcoma patients into three groups at different time points (i.e. baseline, post-chemotherapy and 3 months post-chemotherapy), a miRNA screening analysis using the TaqMan Human miRNA array card A was performed to determine which vascular injury associated miRNAs were potentially altered by the chemotherapy and thus needed further investigation on the individual patient sample level. Analysis revealed that five miRNAs had previously been associated with vasotoxicity according to the literature, namely endothelial miRNAs miR-10a and miR-126 (McDonald *et al.*, 2012), miR-143 involved in hypertension (Kontaraki *et al.*, 2014), angiogenic miR-320a (Yin *et al.*, 2016), and hypertrophy related miR-150 (van Rooij *et al.*, 2006).

During the 3 months follow-up period for the ERICON study, ten patients did not develop cardiac issues, while eight patients develop cardiac issues with a variety of severity, ranging from hypokalaemia and thrombopenia, postural hypotension, asymptomatic non-sustained ventricular tachycardia, fast atrial fibrillation, pulmonary emboli, left arm deep vein thrombosis, portal vein thrombosis to heart failure. The expression pattern of the five miRNAs of interest (i.e. miR-10a, miR-126, miR-143, miR-150 and miR-320a) was investigated for each individual patient displaying cardiac issues at each time point (Figure 6-18).

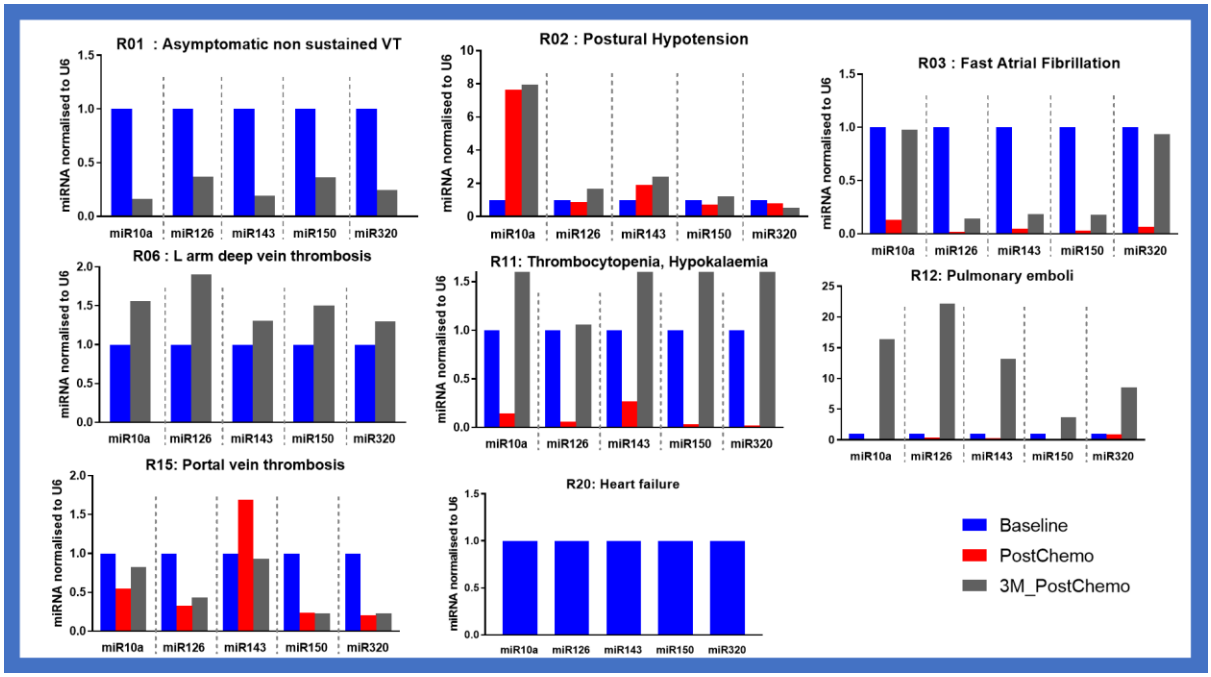

Figure 6-18: Summary of the expression pattern of miRNAs miR-10a, miR-126, miR-143, miR-150 and miR-320a in each individual anthracycline-treated sarcoma patient with cardiac issues. Samples were taken at three time points: baseline, post-chemotherapy and 3 months post-chemotherapy. PostChemo samples were not measured in patients R01, R06, and R20, while 3 months follow-up PostChemo sample was not measured in patient R20.

6.4.1. Array assays versus individual assays analysis

As shown in Table 6-2, the results from the miRNA array cards and the individual assays are similar, however, some miRNA level expressions differ depending of the technique. The difference of both techniques can be attributable to a few reasons: Firstly, the experiment with TaqMan array card has a pre-amplification step, following the reverse transcription step, while the experiment with individual assays does not have this pre-amplification step. The pre-amplification step increases the cDNA concentration of the sample, which facilitates the miRNA detection Real-Time PCR quantification (Sekovanic *et al.*, 2021). In this study, interestingly two miRNAs, miR-10a and miR-143 did not show any alteration post-chemotherapy (both time point) compared to the baseline during the experiment with individual Real-Time qPCR and had both mean Ct values above 33 at the three time points, while their mean Ct values during the experiment with array card were below 30 (Table 6-3). The elevated Ct values indicate a low concentration of miRNA in the sample and thus a lower sensitivity, which reduces the reliability of the detection.

Table 6-2: Summary of the miRNAs level alteration in pooled cancer patient plasma samples from the ERICONC study analyses with TaqMan miRNA array cards and individual plasma samples. CI = cardiac issues

miRNAs	TaqMan miRNA array card		Individual assays		
	Patients' samples pooled		All patients	Non-CI patients	CI patients
	Compared to baseline (n = 1)		Compared to baseline (n = 18)		
	Post-chemo	3 months Post-chemo	Post-chemo	Post-chemo	Post-chemo
	(n = 1)	(n = 1)	(n = 13)	(n = 8)	(n = 5)
miR-10a	↓	↓	-	-	-
miR-126	-	↓	↓	-	↓
miR-143	-	↓	-	-	-
miR-150	↓	↓	↓	↓	↓
miR-320a	↓	↓	↓	-	↓

Table 6-3: Average of Ct values at the three different time points (i.e. baseline, Post-chemotherapy and 3 month post-chemotherapy) of miRNA TaqMan array cards versus average Ct values of individual samples. Post-chemo = Post-chemotherapy, Ct = cycle threshold

	miRNA array cards _ Ct values			Individual assays _ Ct values		
miRNA	**Baseline**	**Post-Chemo**	**3M_Post-Chemo**	**Baseline**	**Post-Chemo**	**3M_Post-Chemo**
hsa-miR-10a	28.744	29.373	29.804	34.558	34.170	34.469
hsa-miR-126	19.487	18.827	21.03	23.694	23.853	23.901
hsa-miR-143	28.382	26.869	29.504	34.113	33.369	34.556
hsa-miR-150	18.841	19.933	19.602	27.011	27.649	27.727
hsa-miR-320a	29.134	30.07	30.164	27.197	26.855	27.888

Secondly, to investigate if the five key miRNAs mentioned above were associated with post-chemotherapy cardiac events, the 19 patients were clustered into two groups depending of the clinical events that occurred post-chemotherapy and some patients had their plasma samples collected only at one or two different time points. By splitting the patients into patients with cardiac events group and the patients without cardiac events, the n number of the study was also split, respectively, in n = 5 and n = 8, leading to an higher variability of the three time points and thus a reduction of the sensitivity. Thirdly, the experiment with individual assays was repeated for each plasma sample, which increased the risk of human error while handling compared to the experiment with array card where the patients' plasma samples were pooled in three groups (i.e. baseline, post-chemotherapy and 3-month post-chemotherapy). Human error while handling can also cause an increase of the variability at different time points. Therefore, in the present study, the results obtained with the array card analysis are more relevant than individual assays and the discussion will focus on the TaqMan miRNA

array card assays results, however, the individual assays underlined interesting variation for some miRNAs expression (i.e. MiR-126, miR-320a and miR-150) and complete the array assay analysis.

6.4.2. Circulating levels of miR-10a

In this study, miR-10a expression is 4-fold reduced post-chemotherapy and 8-fold reduced three months post-chemotherapy compared to miR-10a expression at the baseline in pooled patient plasma samples analysed with TaqMan miRNA array cards (Figure 6-2 (A)). The miR-10a is an anti-inflammatory miRNA and the down-regulation of miR-10a is associated with inflamed ECs (McDonald *et al.*, 2012). MiR-10a was the first mechano-miRNA identified in *in vivo* endothelium, where miR-10a are involved in the regulation of endothelial dysfunction (Kumar *et al.*, 2014). MiR-10a is known to be associated with several diseases, including rheumatoid arthritis, atherosclerosis, and cancer (Das and Rao, 2022). The involvement of miR-10a has been highly investigated in oncological diseases, including gastrointestinal cancer, AML, breast cancer, etc., due to the key role of miR-10a in the regulation of cell proliferation and differentiation (Gao *et al.*, 2023). Furthermore, circulating miR-10a expression level is down-regulated in CVDs, such as atherosclerosis (Fang *et al.*, 2010) and miR-10a plays a role in the development of atherosclerosis by altering the endothelial function (Kumar *et al.*, 2014).

Interestingly, Fang *et al.et al.* (2010) investigated the implication of miR-10a in athero-susceptible endothelium in swine arterial tissues *in vivo* and cultured human aortic endothelial cells (HAEC) *in vitro*. The authors report that miR-10a level was decreased in the athero-susceptible regions of the inner aortic arch and aorto-renal branches compared to the other regions in adult pigs and that miR-10a down-regulation might contribute to the endothelial pro-inflammatory NF-κB activation (Fang *et al.*, 2010). Furthermore, Luo *et al.et al.* (2016) showed that plasma miR-10a levels were lower in CAD patients and were negatively associated with CAD severity. In their study, the authors investigated the miR-10a levels in 80 patients who had a diagnostic coronary angiography for chest pain evaluation, and among those patients, 60 patients were diagnosed with CAD, while the 20 other patients were not diagnosed with CAD and described as control patients. Furthermore, the CAD severity was not the same among the CAD patients with 29 stable angina pectoris (SAP) patients, 17 unstable angina pectoris or non-STEMI (UAP/NSTEMI) patients and 14 ST-elevation myocardial infarction (STEMI) patients. The authors report that miR-10a was lower in CAD patients and that miR-10a levels in the plasma of the STEMI patients were also decreased compared to miR-10a levels in the plasma of SAP and UAP/NSTEMI patients, which underlines the potential use of miR-10a as a non-invasive biomarker to predict CAD and indicate the severity of CAD (Luo *et al.*, 2016). Both studies (Fang's paper and Luo's paper) underlined the cross-link of vascular diseases and miR-10a expression down-regulation in human aortic endothelial cells and human plasma samples. The present study is in agreement with

their findings, suggesting that the reduction of circulating miR-10a expression might be related to vascular injury.

Furthermore, Desai *et al.et al.* investigate the miRNAs involved in doxorubicin-induced chronic cardiotoxicity. $B6C3F_1$ mice were exposed to cumulative doses of doxorubicin or saline solution for 2, 3, 4, 6 or 8 consecutive weeks with a doxorubicin concentration of 3 mg/kg administrated weekly by intravenous. Blood samples were collected 1 week following the last dose to mimic the early-onset cardiotoxicity observed in cancer patients. The authors reported that myocardial damage, determined with cardiac biomarkers (i.e. cTnT and cTnI) and cardiac pathology, occurs 1-week post-treatment with the doxorubicin total cumulative dose of 12 mg/kg or above. At the total cumulative dose of 9 mg/kg of doxorubicin, circulating miRNAs with altered expression compared to miRNAs in saline solution-exposed mice plasma samples were considered early doxorubicin-sensitive miRNAs. Interestingly, miR-10a expression is 2.2-fold reduced in 9 mg/kg doxorubicin-exposed mice plasma samples compared to miR-10a expression in saline solution-exposed mice plasma samples (Desai *et al.*, 2022). This study is consistent with the present results, where miR-10a expression is reduced in human plasma post-chemotherapy. Therefore, this study combined to those three papers suggests that miR-10a might be related to the anti-cancer treatment and/or be associated with vascular injury.

6.4.3. Circulating levels of miR-126

The array analysis of the present study showed that miR-126 expression was not immediately decreased, but the reduction (11-fold) of miR-126 expression is reported three months post-chemotherapy baseline in pooled patient plasma samples analysed with TaqMan miRNA array cards (Figure 6-2 (B)). Furthermore, the experiment with individual Real-Time qPCR analysis showed that the miR-126 expression was reduced by 6-fold post-chemotherapy in the plasma sample of cancer patients who developed post-chemotherapy cardiac events and miR126 expression was recovered at 3 months post-chemotherapy (Figure 6-7 (A)).

It is well established that miR-126 is highly expressed in the cardiovascular system (Romaine *et al.*, 2015), where miR-126 is involved in angiogenesis and vascular integrity maintenance (Wang *et al.*, 2008). In physiological conditions, miR-126 is one of the main endothelial-enriched miRNAs and mediates angiogenesis by inhibiting the intracellular inhibitors of VEGF signalling pathways and thus enhancing VEGF pro-angiogenic activity and vessels formation (Selven *et al.*, 2021). The involvement of miR-126 in the diagnosis, prognosis and tumorigenesis and therapy of lung cancer has been largely investigated (Chen *et al.*, 2021). MiR-126 expression level is altered in various cancers, including liver (Di Martino *et al.*, 2018), lung (Wang *et al.*, 2015b), colon cancer (Selven *et al.*, 2021) and melanoma

(Caporali *et al.*, 2019). Furthermore, several studies showed that depressed miR-126 expression is associated with cardiac injury (Khanaghaei *et al.*, 2016). The miR-126 expression level alteration has been investigated in various CVDs including atherosclerosis (Kin *et al.*, 2012), coronary artery disease (Wang *et al.*, 2017) and heart failure (Seronde *et al.*, 2015), where the miR-126 expression level was decreased in patients who developed CVDs.

In agreement with this study's findings, Wang *et al.et al.* showed that miR-126 was down-regulated in coronary artery disease (CAD) patients. They investigated miR-126 level by RT-qPCR and placental growth factor (PLGF) level, a member of the VEGF family by ELISA in plasma of 24 healthy control (HC) patients and 60 CAD patients, including 22 patients with acute myocardial infarction (AMI) and 38 patients with angina pectoris (AP). Their data showed that plasma miR-126 expression is decreased in CAD patients and that the depressed miR-126 level was associated with the severity of the CAD, which indicates that miR-126 is not only interesting as CAD biomarker but also as a marker to follow the CAD progression. Furthermore, they showed that miR-126 expression is associated with plasma PLGF levels, which underlines a potential mechanism of miR-126 in CAD (Wang *et al.*, 2017). Furthermore, miR-126 is highly expressed in endothelial cells (EC) and is the most abundant miRNA found during EC differentiation, where miR-126 is involved in endothelial repair (Fish *et al.*, 2008). Kin *et al.et al.* (2012) investigated the impaired miRNA in tissue and plasma from atherosclerotic abdominal aortic aneurysm (AAA) patients. Tissue samples were full-thickness aortic wall samples from 13 AAA patients and 7 patients without atherosclerotic changes, as control aorta. Interestingly, their data showed that miR-126 is significantly up-regulated in AAA tissues compared to control tissues, while plasma miR-126 level was inversely correlated in AAA plasma compared to control plasma. Thus, miR-126 expression is reduced in plasma during atherosclerosis (Kin *et al.*, 2012), which is consistent with this study's results. Impairment of circulating miR-126 has also been associated with heart failure. Seronde *et al.et al.* (2015) showed that in a cohort of 236 acute heart failure (AHF) patients, lower expression of miR-126 and miR423-5p was observed in patients who were readmitted in the year following the admission, which suggests miR-126 decreased expression during AHF might be a predictor of the AHF severity (Seronde *et al.*, 2015). In agreement with Seronde *et al.et al.* findings, Yamada *et al.et al.* (2021) showed that in a large-scale cohort in Japan (JACC study), low plasma levels of miR-126 is associated with the increased of premature death compared to medium plasma levels of miR-126 (Yamada *et al.*, 2021).

Furthermore, a systemic-review underlined the miR-126 down-regulation in the plasma of cancer patients during Epirubicin/cyclophosphamide followed by docetaxel (EC-D) neoadjuvant chemotherapy-induced cardiotoxicity (Pereira *et al.*, 2020). In the studies used in the systematic review, Zhu *et al.et al.* (2018) showed that both angiogenic miRNAs miRlet-7f and miR-126 were two

interesting predictive non-invasive biomarkers of cardiotoxicity in triple-negative breast cancer patients, who are treated with EC-D neoadjuvant chemotherapy (Zhu *et al.*, 2018), while Qin *et al.et al.* (2018) showed that the plasma miR-126 down-regulation was negatively correlated with cTnI expression in EC-D-induced cardiotoxicity patients (Qin *et al.*, 2018). Therefore, previous studies highlight the reduction of circulating miR-126 expression in several CVDs, including CAD (Wang *et al.*, 2017), atherosclerosis (Kin *et al.*, 2012) and acute heart failure (Seronde *et al.*, 2015) and are in agreement with the present project's results, suggesting that the reduction of circulating miR-126 expression reported in patients who developed cardiac injury post-chemotherapy might be associated with vasotoxicity. Furthermore, both studies involving drug-induced cardiotoxicity (Zhu *et al.*, 2018, Qin *et al.*, 2018) are in agreement with the present results, which suggest that plasma miR-126 may be down-regulated by the chemotherapy-induced cardiotoxicity.

6.4.4. Circulating levels of miR-143

The miR-143 expression was not altered immediately post-chemotherapy, however, 3 months later, miR-143 was 9-fold reduced in the plasma of chemotherapy-treated patients (Figure 6-2 (C)).

MiR-143 forms a cluster with miR145 which is involved in VSCM differentiation (Rangrez *et al.*, 2011). The miR cluster 143/145, which comprises miR-143 and miR-145, plays a role in several cellular functions, including vascular muscle cell proliferation and differentiation (Das and Pillai, 2015). It is well established that miR cluster 143/145 targets various genes involved in tumorigenesis and are considered tumour suppressors (Das and Pillai, 2015). Furthermore, miR cluster 143/145 expression is altered by several CVDs, including hypertension, atherosclerosis, and coronary arteries disease (Zhao *et al.*, 2015).

Kontaraki *et al.et al.* investigated the expression levels of miRNAs known to play a role in hypertension and analyses their expression levels in peripheral blood mononuclear cells (PBMCs) in hypertensive patients. For this study, 60 patients suffering of essential hypertension and 29 healthy patients were recruited. The authors showed that the miR-143 expression level in PBMCs of hypertensive patients was 9-fold reduced compared to miR-143 in PBMCs of healthy patients. The authors were able to associate the miR-143 lower expression levels to a cardiac parameter used to diagnose hypertension: 24-hrs ambulatory blood pressure monitoring (ABPM) parameter. Pulse pressure was monitored in hypertensive patients and they were able to associate the depressed miR-143 expression level to the measured 24 hrs-pulse pressure. Kontaraki suggests that miR-143 might be a marker of cardiovascular events and be involved in the organ injury reported in hypertensive patients (Kontaraki *et al.*, 2014).

Furthermore, Liu *et al.et al.* investigate the miR143 and miR145 expression levels in the plasma of patients suffering of carotid artery plaques. They collected blood samples from 55 patients with carotid artery plaques and 45 patients without carotid artery plaques. The authors found that circulating miR-143 and miR-145 expression levels were down-regulated in patients with carotid artery plaques compared to healthy patients (Liu *et al.*, 2017).

Therefore, the depressed miR-143 expression level post-chemotherapy might be associated with vascular injury.

6.4.5. Circulating levels of miR-150

Plasma miR-150 expression is 6-fold reduced post-chemotherapy and 7-fold reduced 3 months post-chemotherapy compared to the miR-150 expression at the baseline, in cancer patients treated with chemotherapy (Figure 6-2 (D)). Furthermore, according to individual assays, in patients with cardiac issues, the 8-fold decrease observed immediately after chemotherapy compared to baseline was followed by a significant 5-fold increase of plasma miR-150 level observed 3 months post-chemotherapy compared to post-chemotherapy, which leads to the recovery of the plasma miR-150 level observed before the chemotherapy (Figure 6-13 (A)). Meanwhile, in the patients without cardiac issues, the 4-fold decrease observed immediately after chemotherapy was also observed 3 months post-chemotherapy with a 2-fold decrease compared to the baseline (Figure 6-13 (B)).

MiR-150 is a hematopoietic cell-specific miRNA, which is preferentially expressed in mature B-cells and T-cells (Vasilatou *et al.*, 2010). MiR-150 is associated with various haematological malignancies including pancreatic, colorectal, oesophageal cancers and solid tumours including gastric, breast, lung and liver cancers (Wang *et al.*, 2015a). Furthermore, miR-150 has been associated with cardiac hypertrophy in a rodent model (van Rooij *et al.*, 2006) and has been suggested as a prognosis biomarker of severe AMI (Devaux *et al.*, 2013). Interestingly, a study investigated in a rodent model, the association of miR-150 and doxorubicin-induced cardiotoxicity (Desai *et al.*, 2014).

The implication of miR-150 expression in cardiac hypertrophy has been investigated on two established mice models of cardiac hypertrophy by van Rooij *et al.et al.* (2006). Their first model was obtained by thoracic artic banding, which lead to an overload on the heart and thus cardiac hypertrophy, while their second model was transgenic mice expressing Calcineurin A in the heart, which leads to cardiac hypertrophy. The authors report that miR-150 expression was down-regulated in the heart tissue of both models, where the cardiac hypertrophy was determined by transthoracic echocardiography and hematoxylin and eosin staining (van Rooij *et al.*, 2006).

Devaux *et al.et al.* investigated the use of 4 miRNAs: miR16, miR27a, miR-101 and miR-150 to predict LV dysfunction after AMI in a cohort of 150 AMI patients. The LV dysfunction was determined by echocardiography and an increase in the markers of myocyte necrosis (CK and TnI) above the normal range. Furthermore, they evaluated the LV contractility by the LV wall motion index score (WMIS), where a WMIS > 1.2 is associated with impaired LV contractility and WMIS ≤ 1.2 is associated with preserved LV contractility. To predict the impaired LV dysfunction after AMI in patients, they studied the miRNA levels and Nt-proBNP level in the plasma. Their data showed that miR-150 and miR-101 levels were down-regulated, while miR-16 and miR-27a were up-regulated in the plasma of patients suffering of impaired LV dysfunction. Furthermore, the authors report that the Nt-proBNP analysis combined to miRNAs analysis was a more predictive model to detect impaired LV dysfunction than the Nt-proBNP analysis alone, which underlines the potential of these miRNAs to improve the prognostic of LV remodelling following AMI (Devaux *et al.*, 2013). In this study, a decreased of the miR-150 expression in the plasma of patients suffering of cardiac issues was reported, however, the depressed miR-150 expression was also reported in the plasma of patients who did not develop any cardiac issues.

Interestingly, Desai *et al.et al.* (2014) used a cardiotoxicity mouse model to investigate the miRNAs involved in doxorubicin-induced cardiac injury and they showed that miR-150 was down-regulated in doxorubicin-treated mice. The authors treated mice weekly with cumulative doxorubicin doses (6, 8, 12, 18 or 24 mg/kg) or sterile saline and the cardiotoxicity was evaluated by the measurement of plasma cTnT levels and observation of the cardiac lesions with a microscope. The authors report that miR-150 expression down-regulation in doxorubicin-treated mice compared to control mice was observed from the doxorubicin dose of 12 mg/kg, while the plasma cTnT level alteration was detected from the doxorubicin of 18 mg/kg and the cardiac lesions were observed from doxorubicin dose of 24 mg/kg, which showed that miR-150 expression was down-regulated before the doxorubicin-induced cardiac injury and earlier than the plasma cTnT biomarker (Desai *et al.*, 2014). These findings are different from the present findings that suggest doxorubicin induced a down-regulation of miR-150 expression in both patients with and without cardiac injury.

Furthermore, radiotherapy can also lead to a decrease of the miR-150 levels in plasma, as shown by Dinh *et al.et al.* (2016). The authors report that the plasma miR-150 expression was significantly down-regulated in five non-small cell lung cancer patients treated with thoracic radiation therapy, which showed that miR-150 might be a potential biomarker to study radiotherapy toxicity (Dinh *et al.*, 2016). Their findings are consistent with the present findings, where the cancer patients were treated with different regimens of chemotherapy and their plasma miR-150 expression was down-regulated.

Thus, this study's results suggest that plasma miR-150 down-regulation is observed in cancer patients treated with chemotherapy, however, the down-regulation might not be selective to the chemotherapy-induced cardiotoxicity. However, more studies are needed to determine if depressed miR-150 expression is either associated with vascular injury or tumour suppression.

6.4.6. Circulating levels of miR-320a

The miR-320a expression was 6-fold reduced post-chemotherapy and 8-fold reduced 3 months post-chemotherapy compared to baseline in chemotherapy-treated patients plasma samples, according to the array assays (Figure 6-2 (E)). Furthermore, the plasma miR-320a expression was 4-fold reduced immediately post-chemotherapy compared to baseline in patients with cardiac injury (Figure 6-16 (A)), while miR-320a expression remains unaltered post-chemotherapy compared to baseline in patients without cardiac injury (Figure 6-16 (B)).

MiR-320a is a tumour-suppressive miRNA and is dysregulated in various cancers, including pancreatic, colorectal, breast cancers and osteosarcoma (Khandelwal *et al.*, 2021). However, miR-320a was first associated with I/R-induced cardiac injury, which underlines the key role of miR-320a in CVDs (Ren *et al.*, 2009). It has been well established that circulating miR-320a is associated with several heart diseases, including arrhythmogenic cardiomyopathy (Sommariva *et al.*, 2017), Thoracic Aortic Dissection (Zou *et al.*, 2017) and STEMI (Jakob *et al.*, 2017, Galeano-Otero *et al.*, 2020). Furthermore, miR-320a can be associated with drug-induced cardiotoxicity, e.g. doxorubicin-induced cardiotoxicity where miR320a expression level is decreased in a rodent model (Yin *et al.*, 2016).

The present study is in agreement with Sommariva *et al.et al.* (2017) findings, which showed that miR-320a expression is reduced in patients with arrhythmogenic cardiomyopathy (ACM) compared to healthy control (HC) patients and Idiopathic Ventricular Tachycardia (IVT) patients, which a benign condition (Sommariva *et al.*, 2017). ACM is an acquired progressive heart disease which is characterised by substantial ventricular arrhythmias and alteration of ventricular systolic function (Calore *et al.*, 2015, Corrado *et al.*, 2017). Following a screening expression of 377 miRNAs from three ACM patients and three HC patients, which showed 121 miRNAs potentially involved in ACM from 110 male patients (53 HC patients, 36 ACM patients and 21 IVT patients), Sommariva analysed these 121 miRNAs by RT-qPCR and discovered that only miR-320a expression was significantly decreased in plasma of ACM patients compared to both HC and IVT patients, which means miR-320a might be an interesting non-invasive biomarker to detect early ACM. Furthermore, their data showed that miR-320a level in plasma was a better tool to discriminate ACM to IVT than other clinical parameters, including BNP levels and LVEF, which is currently a challenging task (Sommariva *et al.*, 2017).

Furthermore, Zou *et al.et al.* (2017) showed that miR-320a expression is inhibited by hsa-circRNA-101238 increased level in human TAD tissues from six types A TAD patients, compared to thoracic aortic tissues from six healthy control donors (without aortic diseases). Their data showed that hsa-circRNA-101238 up-regulation in human TAD tissues might act as a miRNA sponge leading to the inhibition of miR-320a and thus increasing the Matrix Metalloproteinase 9 (MMP-9) mRNA expression, which is an mRNA associated with TAD, however, their study needs to be confirmed with a largest cohort (Zou *et al.*, 2017). Interestingly, MMP-9 is studied as a potential biomarker for cardiac remodelling in clinical and animal studies (Halade *et al.*, 2013). Additionally, MMP-9 is known to be implicated in atherosclerosis and plaque rupture, mechanisms of acute coronary syndrome (ACS) and thus increased MMP-9 expression is a potential diagnostic biomarker in ACS (Konstantino *et al.*, 2009). MMP-9 overexpression observed in B lymphocytes during multiple sclerosis (MS) is inhibited by miR-320a (Aung *et al.*, 2015), which suggests that miR-320a down-regulation could lead to an overexpression of MMP-9 leading to cardiovascular events and thus these studies about MMP-9 support this study's finding that miR-320a is associated with cardiovascular events.

In contrast, studies on STEMI showed that miR-320a expression was up-regulated in STEMI patients, compared to control patients (Jakob *et al.*, 2017, Galeano-Otero *et al.*, 2020). Galeano-Otero *et al.et al.* (2020) showed that the miR-320a was significantly expressed in human serum during ischaemia-induced failing myocardium (Galeano-Otero *et al.*, 2020), whereas the present study used plasma samples. However, Jakob *et al.et al.* (2017) showed plasma miR-320a up-regulation was associated with cardiovascular events in STEMI patients (Jakob *et al.*, 2017). According to these studies and the present results, the impairment of miR-320a might be dependent of the type of CVD.

Yin *et al.et al.* (2016) investigated the miR-320a expression and mechanisms involved in doxorubicin-induced cardiotoxicity. Their data showed that circulating miR-320a was down-regulated in anthracycline-treated patients, which is consistent with this study's findings. However, miR-320a expression was up-regulated in the heart of doxorubicin-treated mice (Intra-peritoneal injection of 25 mg/kg doxorubicin), which is inversely correlated to their levels in human plasma. Furthermore, their data showed that miR-320a is associated with doxorubicin-induced cardiotoxicity by disturbing the vascular homeostasis through the decrease of ventricular growth factor A (VEGF-A) expression in mice hearts (Yin *et al.*, 2016).

Therefore, this study postulates that the decrease of plasma miR-320a level in patients with cardiac issues observed immediately after the chemotherapy may be associated with anthracycline-induced cardiotoxicity in this study, which means miR-320a might be an interesting candidate as anthracycline-induced cardiotoxicity non-invasive biomarkers.

6.5. Conclusion

In this study's novel findings, the five vascular miRNAs (i.e. miR-10a, miR-126, miR-143, miR-150 and miR-320a) expression levels were reduced post-chemotherapy. Several studies reported the cross-link of the depressed miRNAs expression level to CVDs. Furthermore, a few studies have investigated these five miRNAs expression level after anti-cancer treatment. According to this study, the key miRNAs are miR-126 and miR-320a, which were reduced post-chemotherapy after analysis with array assays, but both were significantly reduced in chemotherapy-treated patients who developed cardiac events, as well. However, more studies are needed, with a larger cohort of chemotherapy-treated patients and to have a better understanding of the mechanisms involved in this miRNAs alteration during CVDs.

Chapter 7

7. GENERAL DISCUSSION

7.1. Discussion

This thesis focused on the alteration of GPCRs-mediated vascular tone by the anti-cancer treatment doxorubicin and the MEK 1/2 inhibitor U0126, after 24-hr organ culture of LAD arteries, which mimics the doxorubicin-induced cardiotoxicity. Furthermore, this thesis focused principally on the GPCRs signalling pathway and mechanisms in VSMCs, where the four studied GPCRs are mainly involved in vasoconstriction.

Resume of the key findings

This study has shown that:

- Doxorubicin-induced cardiotoxicity can be studied with an organ-cultured model. Doxorubicin effect can be investigated in LAD arteries at a concentration of 0.5 µM with a 24 hrs incubation in DMEM supplemented with antibiotics at 37 °C with a mixture of 5 % CO_2 and 95 % O_2.
- This study showed that doxorubicin treatment alters the vascular tone of LAD arteries by altering the vasocontractile responses mediated by ET_B, 5-HT_{1B} and TP GPCR receptors:
    - The doxorubicin incubation of LAD arteries leads to an increase of the vasoconstriction during the first phase of the stimulation representing a high affinity of the agonist to the receptor, followed by a decrease of the ET_B-mediated vasocontractile responses during the second phase of the stimulation representing a lower affinity of the agonist to the receptor. The depressed ET_B-mediated vasocontractile response is correlated with the decrease of ET_B mRNA level during doxorubicin treatment, however, the increased ET_B-mediated vasocontractile response observed in the first phase of the curve might be due to post-translational changes. The co-incubation of doxorubicin and U0126 leads to a decrease of the ET_B-mediated vasocontractile response without altering the transcription and translation expression levels of ET_B mRNA or receptors.
    - Doxorubicin incubation down-regulates the transcription of ET_A receptors in LAD arteries. However, the maximal vasocontractile response "E_{max}" through ET_A receptor-mediated vasocontraction is not altered. The absence of alteration on ET_A-mediated vascular tone, although the ET_A miRNA is reduced, may be attributable to either (i) the fact that a longer time is needed to observe a change of the ET_A receptors expression on LAD arteries and on ET_A-mediated vascular tone or (ii) that a potential

doxorubicin-induced post-translational change of ET_A receptors increase the ET_A receptors affinity to G protein leading to higher vasoconstriction which compensates the reduction of ETA receptors transcription. Similarly to ET_B receptors, co-incubation of doxorubicin and U0126 leads to a decrease of the ET_A-mediated vasocontractile response without altering the transcription and translation expression levels of ET_A mRNA or receptors.

- Doxorubicin leads to an increase of the 5-HT_{1B}-mediated vasocontractile responses through the increase of 5-HT_{1B} transcription and translation levels. The co-incubation of doxorubicin with U0126 alleviates the elevation of 5-HT_{1B}-mediated vasocontractile response by reducing 5-HT_{1B} mRNA level and 5-HT_{1B} receptor expression in LAD arteries.
- Doxorubicin alters the TP receptor activity by increasing the TP-mediated vasocontractile response without altering the TP receptor transcription or translation expression levels of TP mRNA or receptors. These findings suggest that doxorubicin-induced vasotoxicity alters the TP-mediated vasocontractile response on a post-translational level or alters other proteins involved in the TP receptors signalling pathway. Interestingly, elevated TP-mediated vasocontractile response is alleviated by the co-incubation of LAD arteries with doxorubicin and U0126.

- TaqMan miRNA array analysis of human cancer patients treated with anthracyclines during the ERICONC study in collaboration with Prof Walker (UCL) showed that the expression levels of five vascular injury-associated miRNAs (i.e. miR-10a, miR-126, miR-143, miR-150 and miR-320a) were reduced after chemotherapy treatment compared to baseline.
    - The two vascular injury-associated miRNAs miR-320a and miR-126 were down-regulated in the circulation of cancer patients suffering from cardiac issues as a result of the cardiotoxic adverse effect from the chemotherapy compared to cancer patients who did not develop cardiac issues. These interesting findings suggest that miR-320a and miR-126 are potentially involved in chemotherapy-induced cardiac- and vascular-injury, and could potentially be explored as novel biomarkers of therapy-induced vascular injury associated.

7.1.1. The doxorubicin-induced vasotoxicity *in vitro* model: Organ culture

Previous studies have already used organ culture to mimic CVD (CVD) progression in various arteries (Alm *et al.*, 2002, Murata *et al.*, 2001b, Skovsted *et al.*, 2012). However, the doxorubicin-induced vasotoxicity on rat LAD arteries has never been investigated prior to this PhD project. In this study, the

in vitro CVD organ culture model was optimised to investigate specifically doxorubicin-induced vasotoxicity.

There is an absence of shear- and circumferential- stress in the *in vitro* organ cultured arteries model. The absence of shear- and circumferential- stress are two mechanical factors involved in physiological homeostasis regulation. In physiological conditions, shear stress is known to induce NO release through eNOS activation and regulate transcription and growth factors in EC (Noris *et al.*, 1995). During *in vitro* organ culture of arteries, the absence of shear- and circumferential- stress alters the NO release leading to endothelium dysfunction (Alm *et al.*, 2002). Furthermore, CVDs such as hypertension or HF have already been investigated with the *in vitro* organ cultured artery model, as it mimics the CVD chronic remodelling processes (Ozaki and Karaki, 2002, Tai *et al.*, 2009).

To study the potential alteration of GPCRs-mediated vasocontractile responses by doxorubicin of the LAD arteries, it was necessary to assess the contractile capacity of LAD arteries and confirm that arteries from each group had a similar contractile capacity, thus the experiment's results are specific to GPCRs-mediated vasocontractile response. Furthermore, the contractile capacity was used as reference for the study of the GPCR agonist-mediated dose-response curves. In this study, the contractile capacity of the LAD arteries was investigated by switching the Na^+ KH buffer to 60 mM K^+ KH buffer in the wire-myograph bath. The high concentration of K^+ KH buffer leads to the depolarisation of the SMC membrane and induces a strong vasocontraction of the artery (maximum vasocontractile capacity) (Haddy, 1983). The decrease of K^+ KH-induced vasocontraction of organ culture incubated LAD arteries compared to fresh LAD arteries in this study mimics a severe vascular injury of LAD arteries that is not fully compensated by the remodelling processes (Ozaki and Karaki, 2002, Tai *et al.*, 2009). Furthermore, the viability of the endothelium tested by carbachol administration following 5-HT pre-contraction of this study's LAD arteries was reduced.

Young *et al.et al.* showed that plasma concentration of doxorubicin was estimated to reach 1 µM immediately post-treatment and sustained at approximately 0.2 µM throughout the doxorubicin treatment in doxorubicin-treated patients (Young *et al.*, 1981). Previous studies on doxorubicin-induced cardiotoxicity applied various doxorubicin concentrations ranging from 0.3 µM for incubated rabbit mesenteric arteries (Murata *et al.*, 2001a) to 1 µM in isolated rat heart (Gharanei *et al.*, 2013b). During this study, the optimal concentration of doxorubicin was investigated and ranged from 0.1 µM to 1 µM applied to organ-cultured LAD arteries. It was determined that the highest doxorubicin concentration that didn't alter the contractile capacity of rat LAD arteries was 0.5 µM, while 1 µM of doxorubicin application was very toxic and decreased the contractile capacity of LAD arteries considerably, leading to detrimental damage of the LAD arteries. As for the doxorubicin incubation

period time, the range differs depending of the study-, organ-, species- or artery- type investigated during previous studies. In this study incubation times 24 hrs and 48 hrs were investigated. The contractile capacity of LAD arteries incubated with 0.5 µM doxorubicin was severely compromised after 48 hrs incubation, while the contractile capacity was not altered by the 24 hrs incubation with 0.5 µM doxorubicin. The 24 hrs incubation period determined during this study is consistent and in agreement with the findings of Hayward *et al.et al.*, which showed that vascular injury occurs during the first 24 hrs of the doxorubicin exposure (*in vivo* injection of 15 mg of doxorubicin/kg) in rat aortic rings (Hayward *et al.*, 2013).

Furthermore, this experiment showed that doxorubicin treatment has no acute vasocontractile or vasodilatory effect on fresh LAD arteries. This is in agreement with and supported by the findings of Murata *et al.et al.*, which showed that doxorubicin treatment ranging from 0.3 µM to 10 µM had no acute effect on the smooth muscle contractility of isolated doxorubicin incubated rabbit mesenteric arteries (Murata *et al.*, 2001b).

Therefore, the optimised *in vitro* doxorubicin-induced vasotoxicity organ culture model in this study applied 0.5 µM doxorubicin during the incubation period of 24 hrs to mimic severe vascular injury on LAD arteries and investigate the effect of doxorubicin on GPCRs-mediated vasocontractile responses on rat LAD arteries during these doxorubicin incubation specifications.

7.1.2. Doxorubicin and GPCRs-mediated vasocontractile response

This project investigated the SMC-mediated vasocontractile responses of LAD arteries mediated by endothelin ET_A and ET_B receptors, serotonin 5-HT_{1B} receptors and thromboxane TP receptors of LAD arteries incubated for 24 hrs with 0.5 µM doxorubicin. To the best of our knowledge, this is the first study to investigate the doxorubicin-induced vasotoxicity through GPCR specific signalling pathways exploring the involvement of ET_A, ET_B, 5-HT_{1B} and TP receptors.

In the present study, the potential cardioprotective effect of MEK 1/2 specific inhibitor U0126 was also investigated. It is known that U0126 at 10 µM attenuates the pERK expression during organ culture of isolated cerebral arteries (Sandhu *et al.*, 2010).

7.1.2.1. The effect of doxorubicin on the endothelin ET_B receptor:

It is well established that ET_B-mediated vasocontractile response in animal *in vitro* models mimics the CVDs remodelling processes (Eskesen and Edvinsson, 2006, Johnsson *et al.*, 2008). Interestingly, the

present study showed a strong ET_B-mediated vasocontraction with a biphasic dose-response curve after 24 hrs incubation with either vehicle or 0.5 uM doxorubicin, while S6c dose-response curves of previous studies are monophasic (Eskesen and Edvinsson, 2006, Johnsson *et al.*, 2008, Skovsted *et al.*, 2017). In this study, the presence of an S6c biphasic curve underlines the implication of two different ET_B subtype receptors. Different hypotheses have been suggested in this discussion: the first hypothesis is that at the first phase of the S6c dose-response curve, both SMC and EC ET_B subtypes elicit their vascular responses depending of the ET_B subtype affinity, as ET_B in SMC induce vasocontractile and ET_B in EC induces vasodilatory effects, and the combined stimulation of these SMC and EC ET_B subtypes leads to the low vasocontraction. Interestingly, Miasiro *et al.et al.* investigated the S6c biphasic curved in the fresh isolated guinea-pig ileum and they observed a relaxation followed by a contraction of the vessels when they applied cumulative doses of S6c and the use of antagonists confirmed it was due to two distinct ET_B receptors located on EC and SMC, respectively (Miasiro *et al.*, 1999). The up-regulation of ET_B in SMC and/or the down-regulation of ET_B in EC could explain the second phase of the S6c dose-response curve, which would show only SMC-specific ET_B-mediated contraction. However, further studies are needed to investigate if this hypothesis is true.

Furthermore, this study showed that ET_B-mediated vasocontractile response is increased on the first phase of the biphasic curve of doxorubicin-treated LAD arteries from $10^{-12.5}$ M ET-1 to $10^{-9.5}$ M ET-1, and this is similar to Skovsted (2012) and Sandhu (2010) findings, which showed the up-regulation of ET_B-mediated vasocontraction after vascular injury of isolated cerebral arteries (Sandhu *et al.*, 2010) and of isolated LAD and septal coronary arteries (Skovsted *et al.*, 2012). However, it has been shown that the maximal ET_B-mediated vasocontractile response of coronary arteries is alleviated by the 0.5 µM doxorubicin treatment and the depressed ET_B-mediated vasocontractile response is related to a reduction of the ET_B receptor transcription. Therefore, this study suggests that doxorubicin treatment initially induces an elevation of the ET_B-mediated vasocontraction, followed by a depressed ET_B-mediated vasocontractile response. The initial increased ET_B-mediated vasocontractile response might be induced by doxorubicin treatment on either post-translational levels or the alteration of ET_B-activated proteins. In the SMC, the ET_B receptor induces vasoconstriction through its association with Gq/11 proteins (Cramer *et al.*, 2001), leading to PLC activation, which hydrolyses PIP2 in IP3 and DAG promoting intracellular calcium release and PKC activation (Rosendorff, 1997). Furthermore, this study shows that the following depressed ET_B-mediated vasocontractile response is induced by doxorubicin treatment on a transcriptional level.

The present study showed that MEK 1/2 specific inhibitor U0126 pre-treatment at both concentrations of 5 µM and 10 µM alleviates the doxorubicin-incubated initial elevated ET_B-mediated vasocontractile response and that the attenuated maximal ET_B-mediated vasocontractile response when U0126 is co-

administered with doxorubicin is meditated without altering the ET_B receptor transcription or translation. This suggests that U0126 may alter the ET_B vasocontractile response in the presence of doxorubicin on a post-translational level or by regulating an ET_B-activated protein. In agreement, other studies have shown that U0126 treatment attenuates ET_B-mediated vasoconstriction during organ culture incubation which mimics cerebral ischaemia conditions in *in vitro* experiments with isolated rat cerebral arteries (Sandhu *et al.*, 2010) and *in vitro* experiments with rat coronary arteries (Skovsted *et al.*, 2012). The optimal U0126 concentration to attenuate the doxorubicin-increased ET_B-mediated vasocontraction is 5 µM because 10 µM U0126 excessively reduces the second phase of ET_B-mediated vasoconstriction in vehicle-treated LAD arteries, which may lead to a loss of vasocontractility of LAD arteries.

7.1.2.2. The effect of doxorubicin on the endothelin ET_A receptors:

This study showed that the 0.5 µM doxorubicin treatment during 24 hrs of incubation of LAD segments did not affect the contractile response of endothelin receptors when applying the ET-1 agonist. The ET-1 dose-response curves were performed after ET_B receptors desensitisation with S6c, which nearly abolished the ET_B-mediated contraction leading to a monophasic curve. The addition of ET_A selective antagonist BQ123 and ET_B selective antagonist BQ788 showed that the ET-1 dose-response curve performed without antagonist pre-application corresponded to the ET_A-mediated vasocontractile response. Thus, doxorubicin did not alter the ET_A-mediated vasocontractile response and the pharmacological parameters, "E_{max}" and "pEC_{50}", did not change. However, at some doses of ET-1, the ET_A-mediated contraction in doxorubicin-treated LAD arteries was increased compared to vehicle-treated LAD arteries. In agreement, Skovsted *et al.et al.* (2017) showed that ET_A-mediated vasocontractile response was not altered during the *in vitro* model mimicking I/Rby LAD occlusion and they compared LAD segments from downstream the ligature to the LAD segments from upstream the ligature (Skovsted *et al.*, 2017). Furthermore, during this study the ET_A receptor transcription is down-regulated by 0.5 µM doxorubicin treatment, however, the ET_A receptor expression on SMC of LAD arteries is not altered. This might be explained by the fact that both ET_A receptor mRNA levels and receptor expression were analysed after 24 hrs of incubation, and thus it might be too early to observe any change in the ET_A receptors expression. Another explanation could be that this study demonstrated that although ET_A receptor mRNA level is reduced by doxorubicin treatment, maximal ET_A-mediated contractile response remains unaltered, suggesting that doxorubicin treatment might induce a post-translational change of ET_A receptors or alteration of an ET_A-activated protein, associated with a reduction of ET_A receptors transcription. Interestingly, several studies on animal and human models investigated ET_A antagonists to confer cardioprotection against endothelin receptor-

mediated cardiotoxicity. Most of these studies used ET_A receptor antagonist, such as darusentan, ambrisentan and atrasentan to alleviate the elevated ET-1-mediated vasocontractile response, induced by the elevation of ET_B receptors expression in SMC during hypertension by blocking ET_A receptors vasocontractile response (Gao *et al.*, 2021, Raichlin *et al.*, 2008). However, it was shown that ET_A receptors blockade can induce deleterious effects when combined to heart failure (Nasser and El-Mas, 2014), which underlines the need of new therapeutic targets to regulate elevated ET-mediated vasoconstriction such as the MEK 1/2 pathway inhibitor U0126.

This project showed that MEK 1/2 specific inhibitor U0126 treatment reduces the doxorubicin-induced ET_A vasocontractile response compared to vehicle-treated LAD arteries. Interestingly, the U0126 treatment does not alter the ET_A receptors transcription in doxorubicin-treated LAD arteries, while the ET_A-mediated vasocontractile response is decreased, compared to U0126 naïve doxorubicin-treated LAD arteries. This decrease of vasocontractile response observed only with doxorubicin and U0126 co-treatment supports the hypothesis which suggests that a post-translational change or an alteration of one of the ET_A-activated proteins is induced by doxorubicin treatment. Both U0126 doses altered the ET_A-mediated vasocontractile response however the depressed ET_A vasocontractile response could act as a compensatory mechanism, as selective ET_A antagonists in pulmonary arteries hypertension patients (Benza *et al.*, 2008), by reducing vasoconstriction induces by both ET receptors subtype, since the CVD model increased the ET_B transcription in SMC. The optimal U0126 concentration to attenuate the doxorubicin-increased ET_A-mediated vasoconstriction is 5 µM, because the treatment 10 µM U0126 decreased the vasoconstriction in vehicle-treated LAD arteries compared to U0126 naïve vehicle-treated LAD arteries, while 5 µM U0126 has no effects on vehicle-treated LAD arteries.

7.1.2.3. The effect of doxorubicin on the serotonin 5-HT_{1B} receptor:

The current study showed that the 5-CT mediated dose-response curve resulted in a biphasic dose-response curve after doxorubicin treatment. This suggests the implication of two different serotonin subtype receptors during 5-CT-mediated vasocontraction. These findings are consistent with Hansen-Schwartz *et al.et al.* findings, which underlined the implication of 5-HT_{1B} receptors with a high 5-CT affinity (pEC_{50} = 7.7 in rat cerebral arteries) and 5-HT_{2A} receptors with a low 5-CT affinity (pEC_{50} = 5.1 in rat cerebral arteries) (Hansen-Schwartz *et al.*, 2003). Although 5-HT_{1B} receptors are mostly studied in SMC of cerebral arteries (Lotfinia *et al.*, 2014, O'Quinn *et al.*, 1999), they are also localised in the SMC of the coronary arteries where they are involved in the vasocontraction along with 5-HT_{2A} receptors (Kaumann *et al.*, 1994). It has been demonstrated that patients treated with 5-HT_{1B} specific agonist sumatriptan, an antimigraine drug, can develop chest pain, myocardial infarction, and

vasospasm (Ottervanger *et al.*, 1997, Okonkwo and Ojha, 2020). This study's findings showed that doxorubicin treatment enhances the 5-HT_{1B}-mediated vasocontractile response through increased 5-HT_{1B} receptor transcription levels, leading to the elevation of 5-HT_{1B} receptors expression in SMC of LAD arteries as well. Some studies have demonstrated that doxorubicin-induced cardiotoxicity was associated with a decrease of adenylyl cyclase (AC) activity (Calderone *et al.*, 1991) and cAMP formation (Efentakis *et al.*, 2020), which are both involved in the pathway of 5-HT_{1B}-mediated vasoconstriction. Indeed, 5-HT_{1B} receptor activation leads to the inhibition of the adenylyl cyclase, which reduces the second messenger cAMP formation and PKA activity inducing intracellular calcium release from the sarcoplasmic reticulum and thus the vasoconstriction (Barnes and Sharp, 1999, Leenders and Sheng, 2005, Tiger *et al.*, 2018).

In previous studies, it has been shown that the MEK/ERK 1/2 inhibition with U0126 alleviates the 5-HT_{1B} elevated vasocontractile response in *in vitro* experiments with isolated cerebral arteries compared to fresh cerebral arteries to mimic the vascular effects of post-cerebral ischaemia (Sandhu *et al.*, 2010) and in *in vivo* experiments with rat cerebral arteries after subarachnoid haemorrhage (SAH) (Beg *et al.*, 2006). The current study showed that 5 µM and 10 µM U0126 treatment attenuated the doxorubicin-induced increase in 5-HT_{1B} receptor-mediated vasocontraction on the transcriptional level in coronary arteries, and thus mediated vascular protection during doxorubicin treatment. The optimal U0126 concentration to attenuate the doxorubicin-increased 5-HT_{1B}-mediated vasocontraction is 5 µM, because the 10 µM U0126 excessively reduces the 5-HT_{1B}-mediated vasoconstriction of doxorubicin-treated LAD arteries compared to vehicle-treated LAD arteries, while the 5 µM U0126 alleviates the 5-HT_{1B}–mediated vasoconstriction of doxorubicin-treated LAD arteries until a recover of the vasocontractile response observed in vehicle-treated LAD vessels

7.1.2.4. The effect of doxorubicin on the thromboxane TP receptor:

In this study, it was shown that doxorubicin treatment induced an increase of the TP-mediated vasocontractile response. However, the TP receptor transcription and translation levels were not altered suggesting that doxorubicin-induced increase in TP-mediated vasocontraction is associated with post-translational mechanisms where there is either a TP receptor abnormal post-translational change or there is an alteration of the TP-activated proteins. Although the functional effect of doxorubicin treatment on TP receptors-mediated vasocontraction has not been investigated prior, Lv *et al.et al.* showed that chronic doxorubicin-induced cardiotoxicity enhances platelet activity leading to thrombus and vascular injury in 10-week-old C57BL/6 mice after 4 weeks of doxorubicin injection at a concentration of 5 mg/kg/week (Lv *et al.*, 2020). In SMC, thromboxane A2 binds to TP receptors

leading to phospholipase C (PLC) activation. PLC hydrolyses PIP2 in DAG and IP3 leading to PKC activation and intracellular calcium accumulation. This pathway induces vasoconstriction and platelet activation, which alter the platelets' shape, aggregation and secretion. Pathological changes of TP receptor pathways can lead to CVDs, like atherosclerosis, myocardial infarction and hypertension (Neri Serneri *et al.*, 1983, Katugampola and Davenport, 2001, Smyth, 2010, Martin, 1984).

Interestingly, Sikarwar *et al.et al.* (2014) showed that the Gαq protein associated with the TP receptor of pulmonary arteries was altered on a post-translational level in hypoxic pulmonary hypertension (Sikarwar *et al.*, 2014), which is consistent with this study's hypothesis that doxorubicin treatment may induce increased TP-mediated vasocontraction on either post-translational level or through alteration of the TP-activated proteins. The study by Sikarwar *et al.et al.* used an *in vivo* model of hypoxic pulmonary hypertension (HPH) in HEK293T cells stably expressing TPα to investigate the potential post-translational change of Gαq involved in HTH and showed that hypoxia increases the palmitoylation of Gαq, which facilitates the association of TP receptor and Gαq and thus leading to elevated TP-mediated vasocontractile response. This study's results showed that the affinity of TP receptor for the TP receptor specific agonist U46619 was increased after doxorubicin treatment, which could be due to an increase of the GPCRs trafficking and coupling by post-translational changes, leading to the observed TP receptor hyper-responsiveness in agreement with Sikarwar's study (Sikarwar *et al.*, 2014).

The present study demonstrated that 5 µM and 10 µM MEK 1/2 inhibitor U0126 treatment attenuated the doxorubicin-induced increase in TP receptor-mediated vasocontraction on a post-translational level or through the regulation of TP-activated proteins. Interestingly, mono-incubation with 5 µM MEK 1/2 inhibitor U0126 increased the TP receptor protein levels compared to vehicle-incubated LAD vessels, however, the TP receptor-mediated vasocontraction through U46619 was unaltered in vehicle and U0126 mono-incubated LAD vessels. Previous studies have identified that MEK/ERK 1/2 inhibition alleviates the TP elevated vasocontractile response in *in vitro* experiments with isolated rat cerebral arteries exposed to cigarette smoking particle risk factors (Sandhu *et al.*, 2010), and in *in vitro* experiments with isolated human cerebral arteries after organ culture incubation which mimics cerebral ischaemia conditions (Ansar *et al.*, 2013), which is in agreement with the findings from this study. Previous studies have shown that 10 µM U0126 treatment added 6 hrs following the initial incubation alleviates the elevated TP-mediated vasocontractile response of 48 hrs-incubated rat cerebral arteries without transcription and translation changes (Sandhu *et al.*, 2010) and 5 µM U0126 treatment alleviates the vasocontractile response observed in fresh human cerebral arteries without altering the TP receptor expressions (Ansar *et al.*, 2013), which underline that U0126 confers vascular protection in rodent and human arteries by alleviating the TP receptor vasoconstriction in CVD

models. The optimal U0126 concentration to attenuate the doxorubicin-increased TP-mediated vasocontraction is 5 µM, because, as for 5-HT_{1B} receptors, the 10 µM U0126 excessively reduces the TP-mediated vasoconstriction of doxorubicin-treated LAD arteries compared to vehicle-treated LAD arteries, while the 5 µM U0126 alleviates the TP–mediated vasoconstriction of doxorubicin-treated LAD arteries until the recovery of the vasocontractile response observed in vehicle-treated LAD arteries.

7.1.3. Expression of vascular injury associated circulating miRNAs in cancer patients treated with anthracycline:

In addition to the rat vascular studies with the cardiotoxic chemotherapy drug doxorubicin, this study also investigated the expression of circulating miRNAs in pooled samples of cancer patients treated with anthracycline chemotherapy using the TaqMan miRNA Array card technology, with follow-on emphasis on vascular injury associated miRNA expression in individual samples of cancer patients. The TaqMan miRNA Array card is a high-throughput and accurate tool for quantitative analysis of differential miRNA expression from samples using real-time qPCR technology. The array versus individual miRNA results were similar, but not completely identical, and this can be attributable to (i) the pre-amplification step during the experiment with TaqMan miRNA Array card, which increases the sensitivity of qPCR analysis compared to the individual real-time qPCR without pre-amplification step (Sekovanic *et al.*, 2021). Furthermore, there is also (ii) the low number of patients in this study, in particular when patients are clustered in two groups depending of the development of cardiac events, or (iii) the risk of human error in handling during the individual assays and both can lead to an high variability of miRNA expression levels. In previous studies, the miRNAs miR-10a, miR-126, miR-143, miR-150 and miR-320a have been associated with vascular diseases (Luo *et al.*, 2016, Fish *et al.*, 2008, Zhao *et al.*, 2015, Devaux *et al.*, 2013, Sommariva *et al.*, 2017) and in this study, all five miRNAs were significantly reduced when analysed using the TaqMan miRNA Array technology on pooled patients samples at 3 months post-chemotherapy compared to baseline, whereas the expression of miR-10a, miR-150 and miR-320a was reduced at post-chemotherapy compared to baseline as well. However, in individually assessed cancer patients' samples only miR-126, miR-150 and miR-320a expression levels were decreased in post-chemotherapy compared to baseline in cancer patients suffering from cardiovascular complications, whereas at time point 3 months post-chemotherapy the expression of miR-126, miR-150 and miR-320a had returned to baseline. Only the expression of miR-150 was decreased at both post-chemotherapy and 3 months post-chemotherapy compared to baseline in patients without cardiovascular complications.

In the present study, the circulating miR-10a was significantly reduced in pooled plasma samples of cancer patients at both post-chemotherapy and 3 months post-chemotherapy time points compared to baseline when analysed with the TaqMan miRNA Array card. Studies have shown that circulating miR-10a levels are reduced in CVDs, such as coronary artery disease (Luo *et al.*, 2016) or atherosclerotic disease (Fang *et al.*, 2010, Kuo *et al.*, 2021). The reduction of circulating miR-10a at both post-chemotherapy time points in cancer patients underlines a potential involvement of miR-10a in chemotherapy-induced cardiotoxicity.

A decrease in circulating miR-126 level has been associated with CVDs including atherosclerosis (Kin *et al.*, 2012), coronary artery disease (Wang *et al.*, 2017) and heart failure (Seronde *et al.*, 2015). Furthermore, it was shown that miR-126 is down-regulated in the plasma samples of cancer patients during Epirubicin/cyclophosphamide chemotherapy followed by docetaxel neoadjuvant chemotherapy-induced cardiotoxicity (Pereira *et al.*, 2020), highlighting the potential involvement of circulating miR-126 in drug-induced vasotoxicity. The current study underlined the reduced circulating miR-126 levels in cancer patients 3 months post-chemotherapy compared to baseline according to the miRNA array card study and in cancer patients with cardiovascular complications at time point post-chemotherapy compared to baseline according to the individual miRNA study.

The circulating miR-143 levels were reduced only at the time point 3 months post-chemotherapy compared to baseline according to the miRNA array card analysis. Reduced levels of circulating miR-143 have been associated with hypertension in patients (Kontaraki *et al.*, 2014), which is in agreement with the findings of this study.

Previous studies have shown that circulating miR-150 levels are reduced in AMI patients (Devaux *et al.*, 2013) or during cardiac hypertrophy (van Rooij *et al.*, 2006). In animals, a study using a mice model to assess doxorubicin-induced cardiotoxicity on the miR-150 expression levels showed that a reduction in circulating miR-150 level was observed at low doses of doxorubicin, whereas cTnT levels remained unaltered in the mice. This study suggested that miR-150 might be an interesting target to identify early diagnosis of doxorubicin-induced cardiotoxicity (Desai *et al.*, 2014). In agreement with Desai *et al.et al.*, the current work showed a decrease of circulating miR-150 at both post-chemotherapy and 3 months post-chemotherapy compared to the baseline level of pooled plasma from cancer patients according to the miRNA array card analysis. However, the individually assessed miR-150 results showed that patients with and without cardiovascular complications had a decrease in the circulating miR-150 levels post-chemotherapy compared to baseline, while cancer patients developing cardiac issues had a recovery of their miR-150 level 3 months post-chemotherapy where the miR-150 levels went back to baseline.

Circulating miR-320a expression levels have been associated with several heart diseases including arrhythmogenic cardiomyopathy (Sommariva *et al.*, 2017), thoracic aortic dissection (Zou *et al.*, 2017) and STEMI(Jakob *et al.*, 2017, Galeano-Otero *et al.*, 2020). In the present study, the miR-320a expression level in pooled cancer patient plasma samples was reduced post-chemotherapy and 3 months post-chemotherapy compared to baseline. Furthermore, analysis of miR-320a expression in individual samples highlights that decrease of circulating miR-320a level at post-chemotherapy compared to baseline in cancer patients who developed cardiac issues, as well as in patients with and without cardiovascular complications. At time point 3 months post-chemotherapy the expression level of miR-320a went back to baseline. This finding is consistent with a study that showed a reduction of miR-320a in human plasma after anthracyclines treatment (Yin *et al.*, 2016).

7.2. Study Limitations / Further suggestions

In the current study, the MEK 1/2 inhibitor U0126 was diluted in DMSO, which is known to induce toxic effects at higher doses. DMSO is frequently used in pharmacology and toxicology studies to facilitate drug delivery and no toxic effects have been reported at doses ≤ 0.5 % (Sangweni *et al.*, 2021). The percentage of DMSO used during this study did not exceed 0.5 % in order to minimise the potential negative toxic effect of DMSO on LAD arteries. Although DMSO concentration has no adverse effects in this *in vitro* model, the use of U0126 dissolved in DMSO may be unfavourable to explore further in potential *in vivo* studies. However, some studies have already used DMSO to dissolve U0126 in rat *in vivo* models, such as the Povlsen *et al.et al.* (2015) study, which diluted U0126 in an isotonic saline solution plus 0.1 % DMSO (Povlsen and Edvinsson, 2015). Interestingly, in another study, Christensen *et al.et al.* (2019) replaced DMSO with cremophor EL to dilute U0126, as they reasoned that cremophor EL is already used as vehicle in clinical trials and is a synthetic non-ionic surfactant and is therefore a more suitable dissolvent. Furthermore, this study showed that U0126 treatment effects were similar with either DMSO or cremophor EL dilutions (Christensen *et al.*, 2019).

Studies with similar GPCR functional vascular experiment layouts have investigated the receptor expression using the western blot technique (Skovsted *et al.*, 2015, Zhang *et al.*, 2008). In the current study, the receptor expression in SMC of LAD arteries was investigated by immunohistochemistry using a performant confocal microscope Eclipse Ti2 (Nikon Instruments Inc. Tokyo, Japan) with the AR package of NIS-elements software to quantify the fluorescence intensity. Using the immunohistochemistry technique in this study allowed for the quantification and localisation of the specific GPCRs in the SMC of the LAD arteries. However to complete the findings it could be interesting to also quantify the expression of the receptor using the western blot technique.

In the present study, doxorubicin-induced cardiotoxicity was investigated only on GPCR-mediated vasoconstriction. It has been shown by clinical studies that arterial stiffness is increased in patients treated with anticancer drugs, both during and after the chemotherapy treatment, including doxorubicin (Parr *et al.*, 2020, Mozos *et al.*, 2017, Chaosuwannakit *et al.*, 2010). In future investigations, it could be interesting to assess the doxorubicin-induced cardiotoxicity effect on the GPCR-mediated vasodilatory response as well, such as β-adrenoreceptors in SMC, which induce the artery relaxation through Gs activation and cAMP formation (Itoh *et al.*, 1982) or angiotensin II type 2 in human RCs from coronary micro-arteries, which activate B2 receptors and NO release (Batenburg *et al.*, 2004).

The current project focused on four specific GPCRs – endothelin ET_A/ET_B receptors, serotonin 5-HT_{1B} receptors and TP receptors – to investigate the doxorubicin-induced vasotoxicity. In further studies, the serotonin 5-HT_{2A} receptor would have been an interesting choice, as the serotonin 5-HT_{2A} receptor is involved in the vascular tone of coronary arteries (Kaumann *et al.*, 1994). The study of 5-HT_{2A} receptors would allow a better understanding of the doxorubicin-induced vasotoxicity effects on the post-translational level pathways since 5-HT_{2A} activation leads to the activation of the same signalling pathway through the activation of PLC - and thus the intracellular calcium release mediated vasocontraction - as observed during ET_A, ET_B and TP receptors activation and signalling (Nagatomo *et al.*, 2004).

In the miRNA study, the number of cancer patients treated with chemotherapy was low compared to other studies, which used a cohort of patients to investigate the miRNAs expression level during CVD development. However, since plasma samples are pooled prior to application on the TaqMan miRNA Array cards it increases the miRNA detection and specificity of the results. Furthermore, this study aimed to underline miRNAs related to chemotherapy-induced vascular injury in patients samples split up depending of the development of cardiovascular complications, which unfortunately reduced the number of cancer patients further. Further studies with a larger cohort of patients included are necessary to determine if the circulating vascular injury-associated miRNAs identified in this study could be used as early biomarkers of chemotherapy-induced cardiac- and vascular- injury in circulating cancer patient samples.

7.3. Conclusion

This novel study demonstrated that doxorubicin treatment in an *in vitro* organ culture setting of rat LAD arteries altered the ET_A, ET_B, 5-HT_{1B} and TP-mediated vasocontractile response through intracellular mechanisms. Doxorubicin treatment reduced the transcriptional levels of both endothelin receptors, while it increases the transcriptional level of serotonin 5-HT_{1B} receptors, while the 5-HT_{1B} receptor levels were also increased by doxorubicin treatment. This study suggests that the alteration of the vascular tone through ET_A, ET_B or TP receptors might be induced by intracellular transcriptional or post-translational modifications. To the best of our knowledge, this is the first study to show that doxorubicin-induced vasotoxicity is associated with altered ET_B-, 5-HT_{1B}- and TP-mediated vasocontractile responses. Furthermore, this study also demonstrated that the MEK/ERK 1/2 pathway might be interesting to target to attenuate the doxorubicin-meditated vasocontractile response. (Figure 7-1).

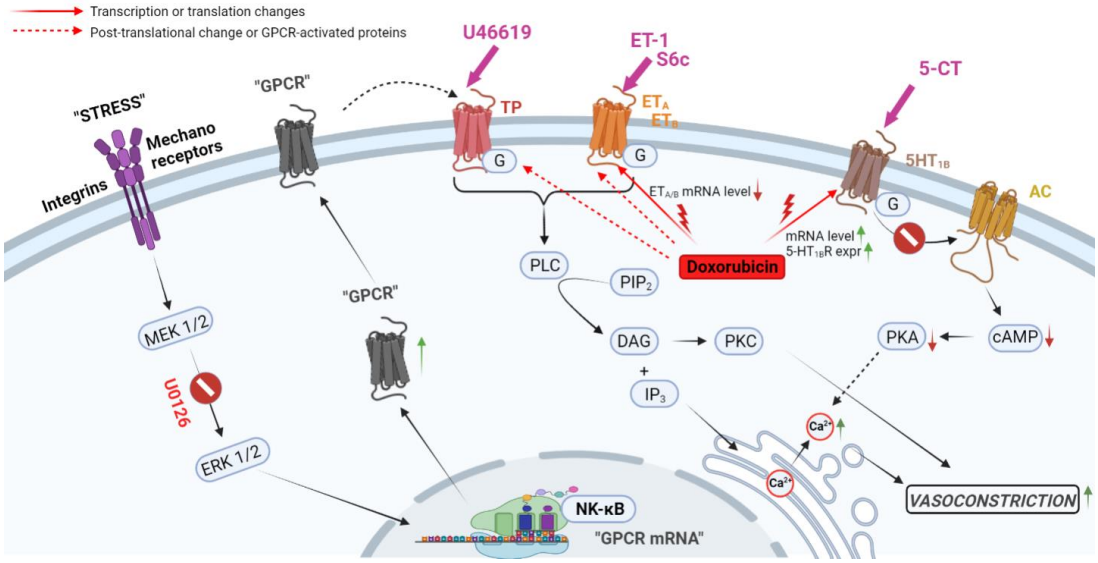

Figure 7-1: Summary of the effect of doxorubicin-induced vasotoxicity on the four studied GPCRs (i.e. ET_A, ET_B, 5-HT_{1B} and TP receptors) and the intracellular pathways leading to vasocontraction. Mechanoreceptors and integrins initiate the MEK/ERK signalling pathways in response to physiological stress and lead to the activation of growth factors, such as NK-κB and the transcription of GPCRs, and thus promote the GPCRs expression on smooth muscle cells (SMC) membrane. However, this MEK/ERK pathway is inhibited by a MEK 1/2 receptor: U0126. The activation of the endothelin A and B receptors and TP receptors in SMC initiates the same signalling pathway with the activation of the phospholipase C (PLC). PLC hydrolyses phosphatidylinositol 4,5-biphosphate (PIP2) to diacylglycerol (DAG) and inositol triphosphate (IP3) promoting the protein kinase C (PKC) activation and IP3 stimulated release of calcium from the sarcoplasmic reticulum, which leads to a strong vasocontractile response. The activation of 5-HT_{1B} receptors on the SMC membrane initiates a different signalling pathway with the inhibition of the adenylyl cyclase (AC). The AC inhibition reduces the second

messenger cAMP formation and protein kinase A (PKA) activity leading to intracellular calcium release from the sarcoplasmic reticulum, and thus a strong vasoconstriction. GPCR = G-protein coupled receptors, expr = expression

The present study also demonstrated that the expression level of five vascular injury-associated miRNAs (i.e. miR-10a, miR-126, miR-143, miR-150 and miR-320a) was down-regulated in cancer patients treated with anthracyclines at time points post-chemotherapy compared to baseline. Interestingly, the reduced miRNA expression levels of miR-126 and miR-320a were associated with the development of cardiovascular complications in the in cancer patients post-chemotherapy, which underlines the potential use of miR-126 and miR-320a as biomarkers to assess chemotherapy-induced cardiotoxicity at an early stage.

From this study, it is evident that doxorubicin has a vasotoxic effect in the coronary vasculature and increases the vascular tone through GPCRs and the MEK/ERK 1/2 pathway activation. Furthermore, doxorubicin therapy of cancer patients can result in severe cardiotoxicity and key miRNAs associated with vascular injury are altered specifically in doxorubicin treated cancer patients that are diagnosed with cardiovascular complications.

8. References

2012. Cytotoxic Antibiotics. *LiverTox: Clinical and Research Information on Drug-Induced Liver Injury.* Bethesda (MD).

ADNER, M., CANTERA, L., EHLERT, F., NILSSON, L. & EDVINSSON, L. 1996. Plasticity of contractile endothelin-B receptors in human arteries after organ culture. *Br J Pharmacol,* 119**,** 1159-66.

ALBERT, P. R. & TIBERI, M. 2001. Receptor signaling and structure: insights from serotonin-1 receptors. *Trends Endocrinol Metab,* 12**,** 453-60.

ALM, R., EDVINSSON, L. & MALMSJO, M. 2002. Organ culture: a new model for vascular endothelium dysfunction. *BMC Cardiovasc Disord,* 2**,** 8.

ANAND, I., MCMURRAY, J., COHN, J. N., KONSTAM, M. A., NOTTER, T., QUITZAU, K., RUSCHITZKA, F., LUSCHER, T. F. & INVESTIGATORS, E. 2004. Long-term effects of darusentan on left-ventricular remodelling and clinical outcomes in the EndothelinA Receptor Antagonist Trial in Heart Failure (EARTH): randomised, double-blind, placebo-controlled trial. *Lancet,* 364**,** 347-54.

ANAND, U., DEY, A., SINGH CHANDEL, A., SANYAL, R., MISHRA, A., PANDEY, D., DE FALCO, V., UPADHYAY, A., KANDIMALLA, R., CHAUDHARY, A., DHANJAL, J., DEWANJEE, S., VALLAMKONDU, J. & PÉREZ DE LA LASTRA, J. 2022. Cancer chemotherapy and beyond: Current status, drug candidates, associated risks and progress in targeted therapeutics. *Genes & Diseases*.

ANAVEKAR, N. S. & OH, J. K. 2009. Doppler echocardiography: a contemporary review. *J Cardiol,* 54**,** 347-58.

ANGUS, J. A. & WRIGHT, C. E. 2000. Techniques to study the pharmacodynamics of isolated large and small blood vessels. *Journal of Pharmacological and Toxicological Methods,* 44**,** 395-407.

ANSAR, S., EFTEKHARI, S., WALDSEE, R., NILSSON, E., NILSSON, O., SAVELAND, H. & EDVINSSON, L. 2013. MAPK signaling pathway regulates cerebrovascular receptor expression in human cerebral arteries. *BMC Neurosci,* 14**,** 12.

ARCAMONE, F., CASSINELLI, G., FANTINI, G., GREIN, A., OREZZI, P., POL, C. & SPALLA, C. 1969. Adriamycin, 14-hydroxydaunomycin, a new antitumor antibiotic from S. peucetius var. caesius. *Biotechnol Bioeng,* 11**,** 1101-10.

ARCARO, A., PIROZZI, F., ANGELINI, A., CHIMENTI, C., CROTTI, L., GIORDANO, C., MANCARDI, D., TORELLA, D. & TOCCHETTI, C. G. 2016. Novel Perspectives in Redox Biology and Pathophysiology of Failing Myocytes: Modulation of the Intramyocardial Redox Milieu for Therapeutic Interventions-A Review Article from the Working Group of Cardiac Cell Biology, Italian Society of Cardiology. *Oxid Med Cell Longev,* 2016**,** 6353469.

AUDEBRAND, A., DESAUBRY, L. & NEBIGIL, C. G. 2019. Targeting GPCRs Against Cardiotoxicity Induced by Anticancer Treatments. *Front Cardiovasc Med,* 6**,** 194.

AUNG, L. L., MOURADIAN, M. M., DHIB-JALBUT, S. & BALASHOV, K. E. 2015. MMP-9 expression is increased in B lymphocytes during multiple sclerosis exacerbation and is regulated by microRNA-320a. *J Neuroimmunol,* 278**,** 185-9.

AVILA, M. S., AYUB-FERREIRA, S. M., DE BARROS WANDERLEY, M. R., JR., DAS DORES CRUZ, F., GONCALVES BRANDAO, S. M., RIGAUD, V. O. C., HIGUCHI-DOS-SANTOS, M. H., HAJJAR, L. A., KALIL FILHO, R., HOFF, P. M., SAHADE, M., FERRARI, M. S. M., DE PAULA COSTA, R. L., MANO, M. S., BITTENCOURT VIANA CRUZ, C. B., ABDUCH, M. C., LOFRANO ALVES, M. S., GUIMARAES, G. V., ISSA, V. S., BITTENCOURT, M. S. & BOCCHI, E. A. 2018. Carvedilol for Prevention of Chemotherapy-Related Cardiotoxicity: The CECCY Trial. *J Am Coll Cardiol,* 71**,** 2281-2290.

AYDIN, S., UGUR, K., AYDIN, S., SAHIN, I. & YARDIM, M. 2019. Biomarkers in acute myocardial infarction: current perspectives. *Vasc Health Risk Manag,* 15**,** 1-10.

BACON, C. R. & DAVENPORT, A. P. 1996. Endothelin receptors in human coronary artery and aorta. *Br J Pharmacol,* 117**,** 986-92.

BARNES, N. M. & SHARP, T. 1999. A review of central 5-HT receptors and their function. *Neuropharmacology,* 38**,** 1083-152.

BARTEL, D. P. 2004. MicroRNAs: genomics, biogenesis, mechanism, and function. *Cell,* 116**,** 281-97.

BATENBURG, W. W., GARRELDS, I. M., BERNASCONI, C. C., JUILLERAT-JEANNERET, L., VAN KATS, J. P., SAXENA, P. R. & DANSER, A. H. 2004. Angiotensin II type 2 receptor-mediated vasodilation in human coronary microarteries. *Circulation,* 109**,** 2296-301.

BAXI, A. J., RESTREPO, C., MUMBOWER, A., MCCARTHY, M. & RASHMI, K. 2015. Cardiac Injuries: A Review of Multidetector Computed Tomography Findings. *Trauma Mon,* 20**,** e19086.

BEG, S. A., HANSEN-SCHWARTZ, J. A., VIKMAN, P. J., XU, C. B. & EDVINSSON, L. I. 2006. ERK1/2 inhibition attenuates cerebral blood flow reduction and abolishes ET(B) and 5-HT(1B) receptor upregulation after subarachnoid hemorrhage in rat. *J Cereb Blood Flow Metab,* 26**,** 846-56.

BENZA, R. L., BARST, R. J., GALIE, N., FROST, A., GIRGIS, R. E., HIGHLAND, K. B., STRANGE, C., BLACK, C. M., BADESCH, D. B., RUBIN, L., FLEMING, T. R. & NAEIJE, R. 2008. Sitaxsentan for the treatment of pulmonary arterial hypertension: a 1-year, prospective, open-label observation of outcome and survival. *Chest,* 134**,** 775-782.

BEREZIN, A. E. & BEREZIN, A. A. 2020. Adverse Cardiac Remodelling after Acute Myocardial Infarction: Old and New Biomarkers. *Dis Markers,* 2020**,** 1215802.

BERKEY, F. J. J. A. F. P. 2010. Managing the adverse effects of radiation therapy. 82**,** 381-388.

BERS, D. M. 2002. Cardiac excitation-contraction coupling. *Nature,* 415**,** 198-205.

BEVAN, J. A. & OSHER, J. V. 1972. A direct method for recording tension changes in the wall of small blood vessels in vitro. *Agents and Actions,* 2**,** 257–260.

BHAGAT, A. & KLEINERMAN, E. S. 2020. Anthracycline-Induced Cardiotoxicity: Causes, Mechanisms, and Prevention. *In:* KLEINERMAN, E. S. & GORLICK, R. (eds.) *Current Advances in Osteosarcoma : Clinical Perspectives: Past, Present and Future.* Cham: Springer International Publishing.

BLAZIE, S. M., GEISSEL, H. C., WILKY, H., JOSHI, R., NEWBERN, J. & MANGONE, M. 2017. Alternative Polyadenylation Directs Tissue-Specific miRNA Targeting in Caenorhabditis elegans Somatic Tissues. *Genetics,* 206**,** 757-774.

BOLLA, M., MATROUGUI, K., LOUFRANI, L., MACLOUF, J., LEVY, B., LEVY-TOLEDANO, S., HABIB, A. & HENRION, D. 2002. p38 mitogen-activated protein kinase activation is required for thromboxane- induced contraction in perfused and pressurized rat mesenteric resistance arteries. *J Vasc Res,* 39**,** 353-60.

BONVALLET, S. T., ZAMORA, M. R., HASUNUMA, K., SATO, K., HANASATO, N., ANDERSON, D., SATO, K. & STELZNER, T. J. 1994. BQ123, an ETA-receptor antagonist, attenuates hypoxic pulmonary hypertension in rats. *Am J Physiol,* 266**,** H1327-31.

BOSCH, X., ROVIRA, M., SITGES, M., DOMENECH, A., ORTIZ-PEREZ, J. T., DE CARALT, T. M., MORALES-RUIZ, M., PEREA, R. J., MONZO, M. & ESTEVE, J. 2013. Enalapril and carvedilol for preventing chemotherapy-induced left ventricular systolic dysfunction in patients with malignant hemopathies: the OVERCOME trial (preventiOn of left Ventricular dysfunction with Enalapril and caRvedilol in patients submitted to intensive ChemOtherapy for the treatment of Malignant hEmopathies). *J Am Coll Cardiol,* 61**,** 2355-62.

BOSMAN, M., FAVERE, K., NEUTEL, C. H. G., JACOBS, G., DE MEYER, G. R. Y., MARTINET, W., VAN CRAENENBROECK, E. M. & GUNS, P. D. F. 2021a. Doxorubicin induces arterial stiffness: A comprehensive in vivo and ex vivo evaluation of vascular toxicity in mice. *Toxicol Lett,* 346**,** 23-33.

BOSMAN, M., KRUGER, D. N., FAVERE, K., WESLEY, C. D., NEUTEL, C. H. G., VAN ASBROECK, B., DIEBELS, O. R., FAES, B., SCHENK, T. J., MARTINET, W., DE MEYER, G. R. Y., VAN CRAENENBROECK, E. M. & GUNS, P. D. F. 2021b. Doxorubicin Impairs Smooth Muscle Cell Contraction: Novel Insights in Vascular Toxicity. *Int J Mol Sci,* 22.

BOUCEK, R. J., JR., OLSON, R. D., BRENNER, D. E., OGUNBUNMI, E. M., INUI, M. & FLEISCHER, S. 1987. The major metabolite of doxorubicin is a potent inhibitor of membrane-associated ion pumps. A correlative study of cardiac muscle with isolated membrane fractions. *J Biol Chem,* 262**,** 15851-6.

BOULTON, T. G., NYE, S. H., ROBBINS, D. J., IP, N. Y., RADZIEJEWSKA, E., MORGENBESSER, S. D., DEPINHO, R. A., PANAYOTATOS, N., COBB, M. H. & YANCOPOULOS, G. D. 1991. ERKs: a family

of protein-serine/threonine kinases that are activated and tyrosine phosphorylated in response to insulin and NGF. *Cell,* 65**,** 663-75.
BRODIE, B. B. & SHORE, P. A. 1957. A concept for a role of serotonin and norepinephrine as chemical mediators in the brain. *Ann N Y Acad Sci,* 66**,** 631-42.
BUETOW, B. & LAFLAMME, M. 2018. *Comparative anatomy and histology : a mouse, rat and human atlas*, Elsevier.
BURRY, R. W. 2011. Controls for immunocytochemistry: an update. *J Histochem Cytochem,* 59**,** 6-12.
BUZA, V., RAJAGOPALAN, B. & CURTIS, A. B. 2017. Cancer Treatment-Induced Arrhythmias: Focus on Chemotherapy and Targeted Therapies. *Circ Arrhythm Electrophysiol,* 10.
CALDERONE, A., DE CHAMPLAIN, J. & ROULEAU, J. L. 1991. Adriamycin-induced changes to the myocardial beta-adrenergic system in the rabbit. *J Mol Cell Cardiol,* 23**,** 333-42.
CALORE, M., LORENZON, A., DE BORTOLI, M., POLONI, G. & RAMPAZZO, A. 2015. Arrhythmogenic cardiomyopathy: a disease of intercalated discs. *Cell Tissue Res,* 360**,** 491-500.
CANCERRESEARCHUK. Available: https://www.cancerresearchuk.org/health-professional/cancer-statistics/survival/all-cancers-combined [Accessed].
CAO, L., PING, N. N., CAO, Y. X., LI, W., CAI, Y., WARFVINGE, K. & EDVINSSON, L. 2016. The effects of MEK1/2 inhibition on cigarette smoke exposure-induced ET receptor upregulation in rat cerebral arteries. *Toxicol Appl Pharmacol,* 304**,** 70-8.
CAO, Z., JIA, Y. & ZHU, B. 2019. BNP and NT-proBNP as Diagnostic Biomarkers for Cardiac Dysfunction in Both Clinical and Forensic Medicine. *Int J Mol Sci,* 20.
CAPORALI, S., AMARO, A., LEVATI, L., ALVINO, E., LACAL, P. M., MASTROENI, S., RUFFINI, F., BONMASSAR, L., ANTONINI CAPPELLINI, G. C., FELLI, N., CARE, A., PFEFFER, U. & D'ATRI, S. 2019. miR-126-3p down-regulation contributes to dabrafenib acquired resistance in melanoma by up-regulating ADAM9 and VEGF-A. *J Exp Clin Cancer Res,* 38**,** 272.
CAPRA, V., BACK, M., ANGIOLILLO, D. J., CATTANEO, M. & SAKARIASSEN, K. S. 2014. Impact of vascular thromboxane prostanoid receptor activation on hemostasis, thrombosis, oxidative stress, and inflammation. *J Thromb Haemost,* 12**,** 126-37.
CHABNER, B. A. & ROBERTS, T. G., JR. 2005. Timeline: Chemotherapy and the war on cancer. *Nat Rev Cancer,* 5**,** 65-72.
CHAE, C. U., PFEFFER, M. A., GLYNN, R. J., MITCHELL, G. F., TAYLOR, J. O. & HENNEKENS, C. H. 1999. Increased pulse pressure and risk of heart failure in the elderly. *JAMA,* 281**,** 634-9.
CHANG, D., LI, H., QIAN, C. & WANG, Y. 2019. DiOHF Protects Against Doxorubicin-Induced Cardiotoxicity Through ERK1 Signaling Pathway. *Front Pharmacol,* 10**,** 1081.
CHAOSUWANNAKIT, N., D'AGOSTINO, R., JR., HAMILTON, C. A., LANE, K. S., NTIM, W. O., LAWRENCE, J., MELIN, S. A., ELLIS, L. R., TORTI, F. M., LITTLE, W. C. & HUNDLEY, W. G. 2010. Aortic stiffness increases upon receipt of anthracycline chemotherapy. *J Clin Oncol,* 28**,** 166-72.
CHAUIN, A. 2021. The Main Causes and Mechanisms of Increase in Cardiac Troponin Concentrations Other Than Acute Myocardial Infarction (Part 1): Physical Exertion, Inflammatory Heart Disease, Pulmonary Embolism, Renal Failure, Sepsis. *Vasc Health Risk Manag,* 17**,** 601-617.
CHEN, H. 2018. Role of thromboxane A2 signaling in endothelium-dependent contractions of arteries. *Prostaglandins Other Lipid Mediat,* 134**,** 32-37.
CHEN, H. H. W. & KUO, M. T. 2017. Improving radiotherapy in cancer treatment: Promises and challenges. *Oncotarget,* 8**,** 62742-62758.
CHEN, J., ZHOU, Y., LIU, S. & LI, C. 2020. Biomechanical signal communication in vascular smooth muscle cells. *J Cell Commun Signal,* 14**,** 357-376.
CHEN, Q., CHEN, S., ZHAO, J., ZHOU, Y. & XU, L. 2021. MicroRNA-126: A new and promising player in lung cancer. *Oncol Lett,* 21**,** 35.
CHEN, Q. W., EDVINSSON, L. & XU, C. B. 2009. Role of ERK/MAPK in endothelin receptor signaling in human aortic smooth muscle cells. *BMC Cell Biol,* 10**,** 52.
CHEN, T., WANG, C., LIU, Q., MENG, Q., SUN, H., HUO, X., SUN, P., PENG, J., LIU, Z., YANG, X. & LIU, K. 2015. Dasatinib reverses the multidrug resistance of breast cancer MCF-7 cells to doxorubicin

by downregulating P-gp expression via inhibiting the activation of ERK signaling pathway. *Cancer Biol Ther,* 16**,** 106-14.

CHIEN, A. J. & MOASSER, M. M. 2008. Cellular mechanisms of resistance to anthracyclines and taxanes in cancer: intrinsic and acquired. *Semin Oncol,* 35**,** S1-S14; quiz S39.

CHOI, J., YIP-SCHNEIDER, M., ALBERTIN, F., WIESENAUER, C., WANG, Y. & SCHMIDT, C. M. 2008. The effect of doxorubicin on MEK-ERK signaling predicts its efficacy in HCC. *J Surg Res,* 150**,** 219-26.

CHRISTENSEN, S. T., JOHANSSON, S. E., RADZIWON-BALICKA, A., WARFVINGE, K., HAANES, K. A. & EDVINSSON, L. 2019. MEK1/2 inhibitor U0126, but not nimodipine, reduces upregulation of cerebrovascular contractile receptors after subarachnoid haemorrhage in rats. *PLoS One,* 14**,** e0215398.

CHRISTOWITZ, C., DAVIS, T., ISAACS, A., VAN NIEKERK, G., HATTINGH, S. & ENGELBRECHT, A. M. 2019. Mechanisms of doxorubicin-induced drug resistance and drug resistant tumour growth in a murine breast tumour model. *BMC Cancer,* 19**,** 757.

CHU, C. & RUBIN, S. 2018. Basic Principles of Chemotherapy. *In:* PHILIP J. DISAIA, W. T. C., ROBERT S. MANNEL, D. SCOTT MCMEEKIN, DAVID G. MUTCH (ed.) *Clinical Gynecologic Oncology (Ninth Edition).*

CHUNG, R., MAULIK, A., HAMARNEH, A., HOCHHAUSER, D., HAUSENLOY, D. J., WALKER, J. M. & YELLON, D. M. 2016. Effect of Remote Ischaemic Conditioning in Oncology Patients Undergoing Chemotherapy: Rationale and Design of the ERIC-ONC Study--A Single-Center, Blinded, Randomized Controlled Trial. *Clin Cardiol,* 39**,** 72-82.

COLVIN, O. M. 2002. Alkylating Agents. *In:* BERTINO, J. R. (ed.) *Encyclopedia of Cancer (Second Edition).*

CORRADO, D., BASSO, C. & JUDGE, D. P. 2017. Arrhythmogenic Cardiomyopathy. *Circ Res,* 121**,** 784-802.

CORREMANS, R., ADAO, R., DE KEULENAER, G. W., LEITE-MOREIRA, A. F. & BRAS-SILVA, C. 2019. Update on pathophysiology and preventive strategies of anthracycline-induced cardiotoxicity. *Clin Exp Pharmacol Physiol,* 46**,** 204-215.

COSSA, G., GATTI, L., CASSINELLI, G., LANZI, C., ZAFFARONI, N. & PEREGO, P. 2013. Modulation of sensitivity to antitumor agents by targeting the MAPK survival pathway. *Curr Pharm Des,* 19**,** 883-94.

CRAMER, H., SCHMENGER, K., HEINRICH, K., HORSTMEYER, A., BONING, H., BREIT, A., PIIPER, A., LUNDSTROM, K., MULLER-ESTERL, W. & SCHROEDER, C. 2001. Coupling of endothelin receptors to the ERK/MAP kinase pathway. Roles of palmitoylation and G(alpha)q. *Eur J Biochem,* 268**,** 5449-59.

CURIGLIANO, G., CARDINALE, D., SUTER, T., PLATANIOTIS, G., DE AZAMBUJA, E., SANDRI, M. T., CRISCITIELLO, C., GOLDHIRSCH, A., CIPOLLA, C., ROILA, F. & GROUP, E. G. W. 2012. Cardiovascular toxicity induced by chemotherapy, targeted agents and radiotherapy: ESMO Clinical Practice Guidelines. *Ann Oncol,* 23 Suppl 7**,** vii155-66.

CURIGLIANO, G., LENIHAN, D., FRADLEY, M., GANATRA, S., BARAC, A., BLAES, A., HERRMANN, J., PORTER, C., LYON, A. R., LANCELLOTTI, P., PATEL, A., DECARA, J., MITCHELL, J., HARRISON, E., MOSLEHI, J., WITTELES, R., CALABRO, M. G., ORECCHIA, R., DE AZAMBUJA, E., ZAMORANO, J. L., KRONE, R., IAKOBISHVILI, Z., CARVER, J., ARMENIAN, S., KY, B., CARDINALE, D., CIPOLLA, C. M., DENT, S., JORDAN, K. & CLINICALGUIDELINES@ESMO.ORG, E. G. C. E. A. 2020. Management of cardiac disease in cancer patients throughout oncological treatment: ESMO consensus recommendations. *Ann Oncol,* 31**,** 171-190.

DAS, A. V. & PILLAI, R. M. 2015. Implications of miR cluster 143/145 as universal anti-oncomiRs and their dysregulation during tumorigenesis. *Cancer Cell Int,* 15**,** 92.

DAS, K. & RAO, L. V. M. 2022. The Role of microRNAs in Inflammation. *Int J Mol Sci,* 23.

DE LA FUENTE-NUNEZ, C., SILVA, O. N., LU, T. K. & FRANCO, O. L. 2017. Antimicrobial peptides: Role in human disease and potential as immunotherapies. *Pharmacol Ther,* 178**,** 132-140.

DEMBIC, Z. 2020. Antitumor Drugs and Their Targets. *Molecules,* 25.

DENG, S., KRUGER, A., KLESCHYOV, A. L., KALINOWSKI, L., DAIBER, A. & WOJNOWSKI, L. 2007. Gp91phox-containing NAD(P)H oxidase increases superoxide formation by doxorubicin and NADPH. *Free Radic Biol Med,* 42**,** 466-73.

DESAI, V. G., J, C. K., VIJAY, V., MOLAND, C. L., HERMAN, E. H., LEE, T., HAN, T., LEWIS, S. M., DAVIS, K. J., MUSKHELISHVILI, L., KERR, S. & FUSCOE, J. C. 2014. Early biomarkers of doxorubicin-induced heart injury in a mouse model. *Toxicol Appl Pharmacol,* 281**,** 221-9.

DESAI, V. G., VIJAY, V., LEE, T., HAN, T., MOLAND, C. L., PHANAVANH, B., HERMAN, E. H., STINE, K. & FUSCOE, J. C. 2022. MicroRNA-34a-5p as a promising early circulating preclinical biomarker of doxorubicin-induced chronic cardiotoxicity. *J Appl Toxicol,* 42**,** 1477-1490.

DEVAUX, Y., VAUSORT, M., MCCANN, G. P., KELLY, D., COLLIGNON, O., NG, L. L., WAGNER, D. R. & SQUIRE, I. B. 2013. A panel of 4 microRNAs facilitates the prediction of left ventricular contractility after acute myocardial infarction. *PLoS One,* 8**,** e70644.

DHALLA, N. S., SAINI-CHOHAN, H. K. & DUHAMEL, T. A. 2008. Strategies for the regulation of intracellular calcium in ischemic heart disease. *Future Cardiol,* 4**,** 339-45.

DHINGRA, R., GUBERMAN, M., RABINOVICH-NIKITIN, I., GERSTEIN, J., MARGULETS, V., GANG, H., MADDEN, N., THLIVERIS, J. & KIRSHENBAUM, L. A. 2020. Impaired NF-kappaB signalling underlies cyclophilin D-mediated mitochondrial permeability transition pore opening in doxorubicin cardiomyopathy. *Cardiovasc Res,* 116**,** 1161-1174.

DI MARTINO, S., ACIERNO, C. & LICITO, A. 2018. Experimental study on the prevention of liver cancer angiogenesis via miR-126. Promising results for targeted therapy. *Eur Rev Med Pharmacol Sci,* 22**,** 853-855.

DINH, T. K., FENDLER, W., CHALUBINSKA-FENDLER, J., ACHARYA, S. S., O'LEARY, C., DERASKA, P. V., D'ANDREA, A. D., CHOWDHURY, D. & KOZONO, D. 2016. Circulating miR-29a and miR-150 correlate with delivered dose during thoracic radiation therapy for non-small cell lung cancer. *Radiat Oncol,* 11**,** 61.

DONATO, A. J., LESNIEWSKI, L. A., STUART, D., WALKER, A. E., HENSON, G., SORENSEN, L., LI, D. & KOHAN, D. E. 2014. Smooth muscle specific disruption of the endothelin-A receptor in mice reduces arterial pressure, and vascular reactivity and affects vascular development. *Life Sci,* 118**,** 238-43.

DORN, G. W., 2ND 2011. MicroRNAs in cardiac disease. *Transl Res,* 157**,** 226-35.

DRAKE, M. T., SHENOY, S. K. & LEFKOWITZ, R. J. 2006. Trafficking of G protein-coupled receptors. *Circ Res,* 99**,** 570-82.

DUNCIA, J. V., JOSEPH B, S., HIGLEY, C. A., PITTS, W. J., WITYAK, J., FRIETZE, W. E., RANKIN, F. W., SUN, J.-H., EARL, R. A., TABAKA, A. C., TELEHA, C. A., BLOM, K. F., FAVATA, M. F., MANOS, E. J., DAULERIO, A. J., STRADLEY, D. A., HORIUCHI, K., COPELAND, R. A., SCHERLE, P. A., TRZASKOS, J. M., MAGOLDA, R. L., TRAINOR, G. L., WEXLER, R. R., HOBBS, F. W. & OLSON, R. E. 1998. MEK INHIBITORS: THE CHEMISTRY AND BIOLOGICAL ACTIVITY OF U0126, ITS ANALOGS, AND CYCLIZATION PRODUCTS. *Bioorganic & Medicinal Chemistry Letter,* 8.

EDGERTON, M. D., CHABERT, C., CHOLLET, A. & ARKINSTALL, S. 1994. Palmitoylation but not the extreme amino-terminus of Gq alpha is required for coupling to the NK2 receptor. *FEBS Lett,* 354**,** 195-9.

EFENTAKIS, P., VARELA, A., CHAVDOULA, E., SIGALA, F., SANOUDOU, D., TENTA, R., GIOTI, K., KOSTOMITSOPOULOS, N., PAPAPETROPOULOS, A., TASOULI, A., FARMAKIS, D., DAVOS, C. H., KLINAKIS, A., SUTER, T., COKKINOS, D. V., ILIODROMITIS, E. K., WENZEL, P. & ANDREADOU, I. 2020. Levosimendan prevents doxorubicin-induced cardiotoxicity in time- and dose-dependent manner: implications for inotropy. *Cardiovasc Res,* 116**,** 576-591.

ENEVOLDSEN, F. C., SAHANA, J., WEHLAND, M., GRIMM, D., INFANGER, M. & KRUGER, M. 2020. Endothelin Receptor Antagonists: Status Quo and Future Perspectives for Targeted Therapy. *J Clin Med,* 9.

ESKESEN, K. & EDVINSSON, L. 2006. Upregulation of endothelin ETB receptor-mediated vasoconstriction in rat coronary artery after organ culture. *Eur J Pharmacol,* 539**,** 192-4.

EZZATI, M., HENLEY, S. J., THUN, M. J. & LOPEZ, A. D. 2005. Role of smoking in global and regional cardiovascular mortality. *Circulation,* 112**,** 489-97.

FAN, J., UNOKI, H., IWASA, S. & WATANABE, T. 2000. Role of endothelin-1 in atherosclerosis. *Ann N Y Acad Sci,* 902**,** 84-93; discussion 93-4.

FAN, Y., GENG, Y., SHEN, L. & ZHANG, Z. 2021. Advances on immune-related adverse events associated with immune checkpoint inhibitors. *Front Med,* 15**,** 33-42.

FANG, X., ARDEHALI, H., MIN, J. & WANG, F. 2023. The molecular and metabolic landscape of iron and ferroptosis in cardiovascular disease. *Nat Rev Cardiol,* 20**,** 7-23.

FANG, Y., SHI, C., MANDUCHI, E., CIVELEK, M. & DAVIES, P. F. 2010. MicroRNA-10a regulation of proinflammatory phenotype in athero-susceptible endothelium in vivo and in vitro. *Proc Natl Acad Sci U S A,* 107**,** 13450-5.

FAREH, J., TOUYZ, R. M., SCHIFFRIN, E. L. & THIBAULT, G. 1996. Endothelin-1 and angiotensin II receptors in cells from rat hypertrophied heart. Receptor regulation and intracellular Ca2+ modulation. *Circ Res,* 78**,** 302-11.

FARKONA, S., DIAMANDIS, E. P. & BLASUTIG, I. M. 2016. Cancer immunotherapy: the beginning of the end of cancer? *BMC Med,* 14**,** 73.

FERNANDEZ-HERNANDO, C. & SUAREZ, Y. 2018. MicroRNAs in endothelial cell homeostasis and vascular disease. *Curr Opin Hematol,* 25**,** 227-236.

FILL, M. & COPELLO, J. A. 2002. Ryanodine receptor calcium release channels. *Physiol Rev,* 82**,** 893-922.

FISH, J. E., SANTORO, M. M., MORTON, S. U., YU, S., YEH, R. F., WYTHE, J. D., IVEY, K. N., BRUNEAU, B. G., STAINIER, D. Y. & SRIVASTAVA, D. 2008. miR-126 regulates angiogenic signaling and vascular integrity. *Dev Cell,* 15**,** 272-84.

FORRESTER, S. J., BOOZ, G. W., SIGMUND, C. D., COFFMAN, T. M., KAWAI, T., RIZZO, V., SCALIA, R. & EGUCHI, S. 2018. Angiotensin II Signal Transduction: An Update on Mechanisms of Physiology and Pathophysiology. *Physiol Rev,* 98**,** 1627-1738.

FRERES, P., BOUZNAD, N., SERVAIS, L., JOSSE, C., WENRIC, S., PONCIN, A., THIRY, J., MOONEN, M., OURY, C., LANCELLOTTI, P., BOURS, V. & JERUSALEM, G. 2018. Variations of circulating cardiac biomarkers during and after anthracycline-containing chemotherapy in breast cancer patients. *BMC Cancer,* 18**,** 102.

FROMMER, K. W. & MULLER-LADNER, U. 2008. Expression and function of ETA and ETB receptors in SSc. *Rheumatology (Oxford),* 47 Suppl 5**,** v27-8.

FRYE, J. N., SUTTERFIELD, S. L., CALDWELL, J. T., BEHNKE, B. J., COPP, S. W., BANISTER, H. R. & ADE, C. J. 2018. Vascular and autonomic changes in adult cancer patients receiving anticancer chemotherapy. *J Appl Physiol (1985),* 125**,** 198-204.

FU, G., BRKIC, J., HAYDER, H. & PENG, C. 2013. MicroRNAs in Human Placental Development and Pregnancy Complications. *Int J Mol Sci,* 14**,** 5519-44.

GALAN-ARRIOLA, C., VILCHEZ-TSCHISCHKE, J. P., LOBO, M., LOPEZ, G. J., DE MOLINA-IRACHETA, A., PEREZ-MARTINEZ, C., VILLENA-GUTIERREZ, R., MACIAS, A., DIAZ-RENGIFO, I. A., OLIVER, E., FUSTER, V., SANCHEZ-GONZALEZ, J. & IBANEZ, B. 2022. Coronary microcirculation damage in anthracycline cardiotoxicity. *Cardiovasc Res,* 118**,** 531-541.

GALEANO-OTERO, I., DEL TORO, R., GUISADO, A., DIAZ, I., MAYORAL-GONZALEZ, I., GUERRERO-MARQUEZ, F., GUTIERREZ-CARRETERO, E., CASQUERO-DOMINGUEZ, S., DIAZ-DE LA LLERA, L., BARON-ESQUIVIAS, G., JIMENEZ-NAVARRO, M., SMANI, T. & ORDONEZ-FERNANDEZ, A. 2020. Circulating miR-320a as a Predictive Biomarker for Left Ventricular Remodelling in STEMI Patients Undergoing Primary Percutaneous Coronary Intervention. *J Clin Med,* 9.

GAMBLIEL, H. A., BURKE, B. E., CUSACK, B. J., WALSH, G. M., ZHANG, Y. L., MUSHLIN, P. S. & OLSON, R. D. 2002. Doxorubicin and C-13 deoxydoxorubicin effects on ryanodine receptor gene expression. *Biochem Biophys Res Commun,* 291**,** 433-8.

GAO, Q., XU, L. & CAI, J. 2021. New drug targets for hypertension: A literature review. *Biochim Biophys Acta Mol Basis Dis,* 1867**,** 166037.

GAO, S., LIU, S., WEI, W., QI, Y. & MENG, F. 2023. Advances in targeting of miR-10-associated lncRNAs/circRNAs for the management of cancer (Review). *Oncol Lett,* 25**,** 89.

GAO, Y. & GALIS, Z. S. 2021. Exploring the Role of Endothelial Cell Resilience in Cardiovascular Health and Disease. *Arterioscler Thromb Vasc Biol,* 41**,** 179-185.

GAO, Y., TANG, S., ZHOU, S. & WARE, J. A. 2001. The thromboxane A2 receptor activates mitogen-activated protein kinase via protein kinase C-dependent Gi coupling and Src-dependent phosphorylation of the epidermal growth factor receptor. *J Pharmacol Exp Ther,* 296**,** 426-33.

GARCIA-REDONDO, A. B., BRIONES, A. M., MARTINEZ-REVELLES, S., PALAO, T., VILA, L., ALONSO, M. J. & SALAICES, M. 2015. c-Src, ERK1/2 and Rho kinase mediate hydrogen peroxide-induced vascular contraction in hypertension: role of TXA2, NAD(P)H oxidase and mitochondria. *J Hypertens,* 33**,** 77-87.

GASSER, A., CHEN, Y. W., AUDEBRAND, A., DAGLAYAN, A., CHARAVIN, M., ESCOUBET, B., KARPOV, P., TETKO, I., CHAN, M. W. Y., CARDINALE, D., DESAUBRY, L. & NEBIGIL, C. G. 2019. Prokineticin Receptor-1 Signaling Inhibits Dose- and Time-Dependent Anthracycline-Induced Cardiovascular Toxicity Via Myocardial and Vascular Protection. *JACC CardioOncol,* 1**,** 84-102.

GERLO, S., KOOIJMAN, R., BECK, I. M., KOLMUS, K., SPOOREN, A. & HAEGEMAN, G. 2011. Cyclic AMP: a selective modulator of NF-kappaB action. *Cell Mol Life Sci,* 68**,** 3823-41.

GHARANEI, M., HUSSAIN, A., JANNEH, O. & MADDOCK, H. 2013a. Attenuation of doxorubicin-induced cardiotoxicity by mdivi-1: a mitochondrial division/mitophagy inhibitor. *PLoS One,* 8**,** e77713.

GHARANEI, M., HUSSAIN, A., JANNEH, O. & MADDOCK, H. L. 2013b. Doxorubicin induced myocardial injury is exacerbated following ischaemic stress via opening of the mitochondrial permeability transition pore. *Toxicol Appl Pharmacol,* 268**,** 149-56.

GHIGO, A., LI, M. & HIRSCH, E. 2016. New signal transduction paradigms in anthracycline-induced cardiotoxicity. *Biochim Biophys Acta,* 1863**,** 1916-25.

GILLE, L. & NOHL, H. 1997. Analyses of the molecular mechanism of adriamycin-induced cardiotoxicity. *Free Radic Biol Med,* 23**,** 775-82.

GOHLA, A., SCHULTZ, G. & OFFERMANNS, S. 2000. Role for G(12)/G(13) in agonist-induced vascular smooth muscle cell contraction. *Circ Res,* 87**,** 221-7.

GOLDBERG, M. A., ANTIN, J. H., GUINAN, E. C. & RAPPEPORT, J. M. 1986. Cyclophosphamide Cardiotoxicity: An Analysis of Dosing as a Risk Factor. *Blood,* 68**,** 1114 - 1118.

GRANN, M., COMERMA-STEFFENSEN, S., ARCANJO, D. D. & SIMONSEN, U. 2016. Mechanisms Involved in Thromboxane A2 -induced Vasoconstriction of Rat Intracavernous Small Penile Arteries. *Basic Clin Pharmacol Toxicol,* 119 Suppl 3**,** 86-95.

GREGAN, B., JURGENSEN, J., PAPSDORF, G., FURKERT, J., SCHAEFER, M., BEYERMANN, M., ROSENTHAL, W. & OKSCHE, A. 2004. Ligand-dependent differences in the internalization of endothelin A and endothelin B receptor heterodimers. *J Biol Chem,* 279**,** 27679-87.

HADDY, F. J. 1983. Potassium effects on contraction in arterial smooth muscle mediated by Na+, K+-ATPase. *Fed Proc,* 42**,** 239-45.

HADER, S. N., ZINKEVICH, N., NORWOOD TORO, L. E., KRIEGEL, A. J., KONG, A., FREED, J. K., GUTTERMAN, D. D. & BEYER, A. M. 2019. Detrimental effects of chemotherapy on human coronary microvascular function. *Am J Physiol Heart Circ Physiol,* 317**,** H705-H710.

HALADE, G. V., JIN, Y. F. & LINDSEY, M. L. 2013. Matrix metalloproteinase (MMP)-9: a proximal biomarker for cardiac remodeling and a distal biomarker for inflammation. *Pharmacol Ther,* 139**,** 32-40.

HANDE, K. R. 1998. Clinical applications of anticancer drugs targeted to topoisomerase II. *Biochim Biophys Acta,* 1400**,** 173-84.

HANSEN-SCHWARTZ, J., HOEL, N. L., XU, C. B., SVENDGAARD, N. A. & EDVINSSON, L. 2003. Subarachnoid hemorrhage-induced upregulation of the 5-HT1B receptor in cerebral arteries in rats. *J Neurosurg,* 99**,** 115-20.

HANSEN-SCHWARTZ, J., SVENSSON, C. L., XU, C. B. & EDVINSSON, L. 2002. Protein kinase mediated upregulation of endothelin A, endothelin B and 5-hydroxytryptamine 1B/1D receptors during organ culture in rat basilar artery. *Br J Pharmacol,* 137**,** 118-26.

HARTMANN, J. T., HAAP, M., KOPP, H. G. & LIPP, H. P. 2009. Tyrosine kinase inhibitors - a review on pharmacology, metabolism and side effects. *Curr Drug Metab,* 10**,** 470-81.

HAYNES, W. G., STRACHAN, F. E. & WEBB, D. J. 1995. Endothelin ETA and ETB receptors cause vasoconstriction of human resistance and capacitance vessels in vivo. *Circulation,* 92**,** 357-63.

HAYWARD, R., HYDOCK, D., GIBSON, N., GREUFE, S., BREDAHL, E. & PARRY, T. 2013. Tissue retention of doxorubicin and its effects on cardiac, smooth, and skeletal muscle function. *J Physiol Biochem,* 69**,** 177-87.

HE, H., WANG, L., QIAO, Y., ZHOU, Q., LI, H., CHEN, S., YIN, D., HUANG, Q. & HE, M. 2019. Doxorubicin Induces Endotheliotoxicity and Mitochondrial Dysfunction via ROS/eNOS/NO Pathway. *Front Pharmacol,* 10**,** 1531.

HEEMSKERK, J. W., BEVERS, E. M. & LINDHOUT, T. 2002. Platelet activation and blood coagulation. *Thromb Haemost,* 88**,** 186-93.

HEID, C. A., STEVENS, J., LIVAK, K. J. & WILLIAMS, P. M. 1996. Real time quantitative PCR. *Genome Res,* 6**,** 986-94.

HENRIKSSON, M., STENMAN, E., VIKMAN, P. & EDVINSSON, L. 2007. MEK1/2 inhibition attenuates vascular ETA and ETB receptor alterations after cerebral ischaemia. *Exp Brain Res,* 178**,** 470-6.

HERMAN, E. H., EL-HAGE, A. N., FERRANS, V. J. & ARDALAN, B. 1985. Comparison of the severity of the chronic cardiotoxicity produced by doxorubicin in normotensive and hypertensive rats. *Toxicol Appl Pharmacol,* 78**,** 202-14.

HERMAN, E. H. & FERRANS, V. J. 1998. Preclinical animal models of cardiac protection from anthracycline-induced cardiotoxicity. *Semin Oncol,* 25**,** 15-21.

HIRATA, Y., EMORI, T., EGUCHI, S., KANNO, K., IMAI, T., OHTA, K. & MARUMO, F. 1993. Endothelin receptor subtype B mediates synthesis of nitric oxide by cultured bovine endothelial cells. *J Clin Invest,* 91**,** 1367-73.

HIRSCH, J. 2006. An anniversary for cancer chemotherapy. *JAMA,* 296**,** 1518-20.

HOFFMAN, R. K., KIM, B. J., SHAH, P. D., CARVER, J., KY, B. & RYEOM, S. 2021. Damage to cardiac vasculature may be associated with breast cancer treatment-induced cardiotoxicity. *Cardiooncology,* 7**,** 15.

HOLMBERG, S. R. & WILLIAMS, A. J. 1990. Patterns of interaction between anthraquinone drugs and the calcium-release channel from cardiac sarcoplasmic reticulum. *Circ Res,* 67**,** 272-83.

HORENSTEIN, M. S., VANDER HEIDE, R. S. & L'ECUYER, T. J. 2000. Molecular basis of anthracycline-induced cardiotoxicity and its prevention. *Mol Genet Metab,* 71**,** 436-44.

HOYER, D., CLARKE, D. E., FOZARD, J. R., HARTIG, P. R., MARTIN, G. R., MYLECHARANE, E. J., SAXENA, P. R. & HUMPHREY, P. P. 1994. International Union of Pharmacology classification of receptors for 5-hydroxytryptamine (Serotonin). *Pharmacol Rev,* 46**,** 157-203.

HSU, P. Y., MAMMADOVA, A., BENKIRANE-JESSEL, N., DESAUBRY, L. & NEBIGIL, C. G. 2021. Updates on Anticancer Therapy-Mediated Vascular Toxicity and New Horizons in Therapeutic Strategies. *Front Cardiovasc Med,* 8**,** 694711.

HUANG, W., XU, R., ZHOU, B., LIN, C., GUO, Y., XU, H. & GUO, X. 2022. Clinical Manifestations, Monitoring, and Prognosis: A Review of Cardiotoxicity After Antitumor Strategy. *Front Cardiovasc Med,* 9**,** 912329.

HUGHES, J. P., REES, S., KALINDJIAN, S. B. & PHILPOTT, K. L. 2011. Principles of early drug discovery. *Br J Pharmacol,* 162**,** 1239-49.

HUNTER, C., BARER, G. R., SHAW, J. W. & CLEGG, E. J. 1974. Growth of the heart and lungs in hypoxic rodents: a model of human hypoxic disease. *Clin Sci Mol Med,* 46**,** 375-91.

HUTCHINS, K. K., SIDDEEK, H., FRANCO, V. I. & LIPSHULTZ, S. E. 2017. Prevention of cardiotoxicity among survivors of childhood cancer. *Br J Clin Pharmacol,* 83**,** 455-465.

INNO, A., CHIAMPAN, A., LANZONI, L., VERZE, M., MOLON, G. & GORI, S. 2021. Immune Checkpoint Inhibitors and Atherosclerotic Vascular Events in Cancer Patients. *Front Cardiovasc Med,* 8**,** 652186.

ISHIDA, T., KAWASHIMA, S., HIRATA, K., SAKODA, T., SHIMOKAWA, Y., MIWA, Y., INOUE, N., UEYAMA, T., SHIOMI, M., AKITA, H. & YOKOYAMA, M. 2001. Serotonin-induced hypercontraction through 5-hydroxytryptamine 1B receptors in atherosclerotic rabbit coronary arteries. *Circulation,* 103**,** 1289-95.

ITO, H., MILLER, S. C., BILLINGHAM, M. E., AKIMOTO, H., TORTI, S. V., WADE, R., GAHLMANN, R., LYONS, G., KEDES, L. & TORTI, F. M. 1990. Doxorubicin selectively inhibits muscle gene expression in cardiac muscle cells in vivo and in vitro. *Proc Natl Acad Sci U S A,* 87**,** 4275-9.

ITOH, T., IZUMI, H. & KURIYAMA, H. 1982. Mechanisms of relaxation induced by activation of beta-adrenoceptors in smooth muscle cells of the guinea-pig mesenteric artery. *J Physiol,* 326**,** 475-93.

JAKOB, P., KACPROWSKI, T., BRIAND-SCHUMACHER, S., HEG, D., KLINGENBERG, R., STAHLI, B. E., JAGUSZEWSKI, M., RODONDI, N., NANCHEN, D., RABER, L., VOGT, P., MACH, F., WINDECKER, S., VOLKER, U., MATTER, C. M., LUSCHER, T. F. & LANDMESSER, U. 2017. Profiling and validation of circulating microRNAs for cardiovascular events in patients presenting with ST-segment elevation myocardial infarction. *Eur Heart J,* 38**,** 511-515.

JENEI, Z., BARDI, E., MAGYAR, M. T., HORVATH, A., PARAGH, G. & KISS, C. 2013. Anthracycline causes impaired vascular endothelial function and aortic stiffness in long term survivors of childhood cancer. *Pathol Oncol Res,* 19**,** 375-83.

JENSEN, B. V., SKOVSGAARD, T. & NIELSEN, S. L. 2002. Functional monitoring of anthracycline cardiotoxicity: a prospective, blinded, long-term observational study of outcome in 120 patients. *Ann Oncol,* 13**,** 699-709.

JOHNSSON, E., MADDAHI, A., WACKENFORS, A. & EDVINSSON, L. 2008. Enhanced expression of contractile endothelin ET(B) receptors in rat coronary artery after organ culture. *Eur J Pharmacol,* 582**,** 94-101.

KACIMI, R. & GERDES, A. M. 2003. Alterations in G protein and MAP kinase signaling pathways during cardiac remodeling in hypertension and heart failure. *Hypertension,* 41**,** 968-77.

KAMATO, D., THACH, L., BERNARD, R., CHAN, V., ZHENG, W., KAUR, H., BRIMBLE, M., OSMAN, N. & LITTLE, P. J. 2015. Structure, Function, Pharmacology, and Therapeutic Potential of the G Protein, Galpha/q,11. *Front Cardiovasc Med,* 2**,** 14.

KAMIYA, A. & TOGAWA, T. 1980. Adaptive regulation of wall shear stress to flow change in the canine carotid artery. *Am J Physiol,* 239**,** H14-21.

KAMPHUIS, J. A. M., LINSCHOTEN, M., CRAMER, M. J., DOEVENDANS, P. A., ASSELBERGS, F. W. & TESKE, A. J. 2020. Early- and late anthracycline-induced cardiac dysfunction: echocardiographic characterization and response to heart failure therapy. *Cardiooncology,* 6**,** 23.

KATUGAMPOLA, S. D. & DAVENPORT, A. P. 2001. Thromboxane receptor density is increased in human cardiovascular disease with evidence for inhibition at therapeutic concentrations by the AT(1) receptor antagonist losartan. *Br J Pharmacol,* 134**,** 1385-92.

KAUFMANN, S. H. & EARNSHAW, W. C. 2000. Induction of apoptosis by cancer chemotherapy. *Exp Cell Res,* 256**,** 42-9.

KAUMANN, A. J., FRENKEN, M., POSIVAL, H. & BROWN, A. M. 1994. Variable participation of 5-HT1-like receptors and 5-HT2 receptors in serotonin-induced contraction of human isolated coronary arteries. 5-HT1-like receptors resemble cloned 5-HT1D beta receptors. *Circulation,* 90**,** 1141-53.

KEEGAN, A., MORECROFT, I., SMILLIE, D., HICKS, M. N. & MACLEAN, M. R. 2001. Contribution of the 5-HT(1B) receptor to hypoxia-induced pulmonary hypertension: converging evidence using 5-HT(1B)-receptor knockout mice and the 5-HT(1B/1D)-receptor antagonist GR127935. *Circ Res,* 89**,** 1231-9.

KENAKIN, T. P. & SCIENCEDIRECT 2017. *Pharmacology in drug discovery and development : understanding drug response*.

KEYS, D. N., AU-YOUNG, J. K. & FEKETE, R. A. 2010. TaqMan Array Cards in pharmaceutical research. *Methods Mol Biol,* 632**,** 87-97.

KHANAGHAEI, M., TOURKIANVALASHANI, F., HEKMATIMOGHADDAM, S., GHASEMI, N., RAHAIE, M., KHORRAMSHAHI, V., SHEIKHPOUR, A., HEYDARI, Z. & POURRAJAB, F. 2016. Circulating miR-126 and miR-499 reflect progression of cardiovascular disease; correlations with uric acid and ejection fraction. *Heart Int,* 11**,** e1-e9.

KHANDELWAL, A., SHARMA, U., BARWAL, T. S., SEAM, R. K., GUPTA, M., RANA, M. K., VASQUEZ, K. M. & JAIN, A. 2021. Circulating miR-320a Acts as a Tumor Suppressor and Prognostic Factor in Non-small Cell Lung Cancer. *Front Oncol,* 11**,** 645475.

KIM, E. J., LIM, K. M., KIM, K. Y., BAE, O. N., NOH, J. Y., CHUNG, S. M., SHIN, S., YUN, Y. P. & CHUNG, J. H. 2009. Doxorubicin-induced platelet cytotoxicity: a new contributory factor for doxorubicin-mediated thrombocytopenia. *J Thromb Haemost,* 7**,** 1172-83.

KIM, S. H., LIM, K. M., NOH, J. Y., KIM, K., KANG, S., CHANG, Y. K., SHIN, S. & CHUNG, J. H. 2011. Doxorubicin-induced platelet procoagulant activities: an important clue for chemotherapy-associated thrombosis. *Toxicol Sci,* 124**,** 215-24.

KIM, S. Y., KIM, S. J., KIM, B. J., RAH, S. Y., CHUNG, S. M., IM, M. J. & KIM, U. H. 2006. Doxorubicin-induced reactive oxygen species generation and intracellular Ca2+ increase are reciprocally modulated in rat cardiomyocytes. *Exp Mol Med,* 38**,** 535-45.

KIN, K., MIYAGAWA, S., FUKUSHIMA, S., SHIRAKAWA, Y., TORIKAI, K., SHIMAMURA, K., DAIMON, T., KAWAHARA, Y., KURATANI, T. & SAWA, Y. 2012. Tissue- and plasma-specific MicroRNA signatures for atherosclerotic abdominal aortic aneurysm. *J Am Heart Assoc,* 1**,** e000745.

KO, F. N., YU, S. M., KANG, Y. F. & TENG, C. M. 1995. Characterization of the thromboxane (TP-) receptor subtype involved in proliferation in cultured vascular smooth muscle cells of rat. *Br J Pharmacol,* 116**,** 1801-8.

KOBILKA, B. K. 2007. G protein coupled receptor structure and activation. *Biochim Biophys Acta,* 1768**,** 794-807.

KOLETTIS, T. M. 2014. Ventricular tachyarrhythmias during acute myocardial infarction: the role of endothelin-1. *Life Sci,* 118**,** 136-40.

KONSTANTINO, Y., NGUYEN, T. T., WOLK, R., AIELLO, R. J., TERRA, S. G. & FRYBURG, D. A. 2009. Potential implications of matrix metalloproteinase-9 in assessment and treatment of coronary artery disease. *Biomarkers,* 14**,** 118-29.

KONTARAKI, J. E., MARKETOU, M. E., ZACHARIS, E. A., PARTHENAKIS, F. I. & VARDAS, P. E. 2014. Differential expression of vascular smooth muscle-modulating microRNAs in human peripheral blood mononuclear cells: novel targets in essential hypertension. *J Hum Hypertens,* 28**,** 510-6.

KOWALCZYK, A., KLENIEWSKA, P., KOLODZIEJCZYK, M., SKIBSKA, B. & GORACA, A. 2015. The role of endothelin-1 and endothelin receptor antagonists in inflammatory response and sepsis. *Arch Immunol Ther Exp (Warsz),* 63**,** 41-52.

KUBISTA, M., ANDRADE, J. M., BENGTSSON, M., FOROOTAN, A., JONAK, J., LIND, K., SINDELKA, R., SJOBACK, R., SJOGREEN, B., STROMBOM, L., STAHLBERG, A. & ZORIC, N. 2006. The real-time polymerase chain reaction. *Mol Aspects Med,* 27**,** 95-125.

KUMAR, S., KIM, C. W., SIMMONS, R. D. & JO, H. 2014. Role of flow-sensitive microRNAs in endothelial dysfunction and atherosclerosis: mechanosensitive athero-miRs. *Arterioscler Thromb Vasc Biol,* 34**,** 2206-16.

KUO, J. T., TSAI, H. E., LIN, C. T., LEE, C. I., LEE, P. L., RUAN, Y. R., CHIU, J. J. & LEE, D. Y. 2021. Low Levels of MicroRNA-10a in Cardiovascular Endothelium and Blood Serum Are Related to Human Atherosclerotic Disease. *Cardiol Res Pract,* 2021**,** 1452917.

KWOK, J. C. & RICHARDSON, D. R. 2003. Anthracyclines induce accumulation of iron in ferritin in myocardial and neoplastic cells: inhibition of the ferritin iron mobilization pathway. *Mol Pharmacol,* 63**,** 849-61.

LATERZA, O. F., LIM, L., GARRETT-ENGELE, P. W., VLASAKOVA, K., MUNIAPPA, N., TANAKA, W. K., JOHNSON, J. M., SINA, J. F., FARE, T. L., SISTARE, F. D. & GLAAB, W. E. 2009. Plasma MicroRNAs as sensitive and specific biomarkers of tissue injury. *Clin Chem,* 55**,** 1977-83.

LAURENT, S. & BOUTOUYRIE, P. 2020. Arterial Stiffness and Hypertension in the Elderly. *Front Cardiovasc Med,* 7**,** 544302.

LEENDERS, A. G. & SHENG, Z. H. 2005. Modulation of neurotransmitter release by the second messenger-activated protein kinases: implications for presynaptic plasticity. *Pharmacol Ther,* 105**,** 69-84.

LEFRAK, E. A., PITHA, J., ROSENHEIM, S. & GOTTLIEB, J. A. 1973. A clinicopathologic analysis of adriamycin cardiotoxicity. *Cancer,* 32**,** 302-14.

LEGER, K. J., LEONARD, D., NIELSON, D., DE LEMOS, J. A., MAMMEN, P. P. & WINICK, N. J. 2017. Circulating microRNAs: Potential Markers of Cardiotoxicity in Children and Young Adults Treated With Anthracycline Chemotherapy. *J Am Heart Assoc,* 6.

LI, L., ZHAO, G. D., SHI, Z., QI, L. L., ZHOU, L. Y. & FU, Z. X. 2016. The Ras/Raf/MEK/ERK signaling pathway and its role in the occurrence and development of HCC. *Oncol Lett,* 12**,** 3045-3050.

LI, N., ARTIGA, E., KALYANASUNDARAM, A., HANSEN, B. J., WEBB, A., PIETRZAK, M., BIESIADECKI, B., WHITSON, B., MOKADAM, N. A., JANSSEN, P. M. L., HUMMEL, J. D., MOHLER, P. J., DOBRZYNSKI, H. & FEDOROV, V. V. 2021. Altered microRNA and mRNA profiles during heart failure in the human sinoatrial node. *Sci Rep,* 11**,** 19328.

LIAO, J. K. & LAUFS, U. 2005. Pleiotropic effects of statins. *Annu Rev Pharmacol Toxicol,* 45**,** 89-118.

LIEBL, M. C. & HOFMANN, T. G. 2019. Identification of responders to immune checkpoint therapy: which biomarkers have the highest value? *J Eur Acad Dermatol Venereol,* 33 Suppl 8**,** 52-56.

LIM, W., KIM, J. H., GOOK, E., KIM, J., KO, Y., KIM, I., KWON, H., LIM, H., JUNG, B., YANG, K., CHOI, N., KIM, M., KIM, S., CHOI, H. & KIM, O. 2009. Inhibition of mitochondria-dependent apoptosis by 635-nm irradiation in sodium nitroprusside-treated SH-SY5Y cells. *Free Radic Biol Med,* 47**,** 850-7.

LINDER, M. E. & DESCHENES, R. J. 2007. Palmitoylation: policing protein stability and traffic. *Nat Rev Mol Cell Biol,* 8**,** 74-84.

LING, L., MAGUIRE, J. J. & DAVENPORT, A. P. 2013. Endothelin-2, the forgotten isoform: emerging role in the cardiovascular system, ovarian development, immunology and cancer. *Br J Pharmacol,* 168**,** 283-95.

LIPSHULTZ, S. E., MILLER, T. L., SCULLY, R. E., LIPSITZ, S. R., RIFAI, N., SILVERMAN, L. B., COLAN, S. D., NEUBERG, D. S., DAHLBERG, S. E., HENKEL, J. M., ASSELIN, B. L., ATHALE, U. H., CLAVELL, L. A., LAVERDIERE, C., MICHON, B., SCHORIN, M. A. & SALLAN, S. E. 2012. Changes in cardiac biomarkers during doxorubicin treatment of pediatric patients with high-risk acute lymphoblastic leukemia: associations with long-term echocardiographic outcomes. *J Clin Oncol,* 30**,** 1042-9.

LIU, J., GU, X.-H., CASLEY, D. J. & NAYLER, W. G. 1990. Reoxygenation, But Neither Hypoxia nor Intermittent Ischemia, Increases [125I]Endothelin-1 Binding to Rat Cardiac Membranes. 15**,** 436-443.

LIU, J., MAO, W., DING, B. & LIANG, C. S. 2008. ERKs/p53 signal transduction pathway is involved in doxorubicin-induced apoptosis in H9c2 cells and cardiomyocytes. *Am J Physiol Heart Circ Physiol,* 295**,** H1956-65.

LIU, K., XUEKELATI, S., ZHANG, Y., YIN, Y., LI, Y., CHAI, R., LI, X., PENG, Y., WU, J. & GUO, X. 2017. Expression levels of atherosclerosis-associated miR-143 and miR-145 in the plasma of patients with hyperhomocysteinaemia. *BMC Cardiovasc Disord,* 17**,** 163.

LIU, S., PREMONT, R. T., KONTOS, C. D., HUANG, J. & ROCKEY, D. C. 2003. Endothelin-1 activates endothelial cell nitric-oxide synthase via heterotrimeric G-protein betagamma subunit signaling to protein jinase B/Akt. *J Biol Chem,* 278**,** 49929-35.

LIU, Y., GIBSON, A. W., LEVINSTEIN, M. R., LESIAK, A. J., ONG, S. E. & NEUMAIER, J. F. 2019. 5-HT1B Receptor-Mediated Activation of ERK1/2 Requires Both Galphai/o and beta-Arrestin Proteins. *ACS Chem Neurosci,* 10**,** 3143-3153.

LONGMORE, J., MAGUIRE, J. J., MACLEOD, A., STREET, L., SCHOFIELD, W. N. & HILL, R. G. 2000. Comparison of the vasoconstrictor effects of the selective 5-HT1D-receptor agonist L-775,606 with the mixed 5-HT1B/1D-receptor agonist sumatriptan and 5-HT in human isolated coronary artery. *Br J Clin Pharmacol,* 49**,** 126-31.

LOTFINIA, M., LOTFINIA, A. A. & ASAADI, S. 2014. Effect of Sumatriptan on Learning and Memory Impairment Resulting from Repetitive Spreading Depression %J The Neuroscience Journal of Shefaye Khatam. 2**,** 37-44.

LOZAHIC, C., MADDOCK, H. & SANDHU, H. 2021. Anti-cancer Therapy Leads to Increased Cardiovascular Susceptibility to COVID-19. *Front Cardiovasc Med,* 8**,** 634291.

LUM, B. L., SVEC, J. M. & TORTI, F. M. 1985. Doxorubicin: alteration of dose scheduling as a means of reducing cardiotoxicity. *Drug Intell Clin Pharm,* 19**,** 259-64.

LUNA, C., LI, G., QIU, J., EPSTEIN, D. L. & GONZALEZ, P. 2009. Role of miR-29b on the regulation of the extracellular matrix in human trabecular meshwork cells under chronic oxidative stress. *Mol Vis,* 15**,** 2488-97.

LUO, L., CHEN, B., LI, S., WEI, X., LIU, T., HUANG, Y. & LIN, X. 2016. Plasma miR-10a: A Potential Biomarker for Coronary Artery Disease. *Dis Markers,* 2016**,** 3841927.

LUU, A. Z., CHOWDHURY, B., AL-OMRAN, M., TEOH, H., HESS, D. A. & VERMA, S. 2018. Role of Endothelium in Doxorubicin-Induced Cardiomyopathy. *JACC Basic Transl Sci,* 3**,** 861-870.

LV, H., TAN, R., LIAO, J., HAO, Z., YANG, X., LIU, Y. & XIA, Y. 2020. Doxorubicin contributes to thrombus formation and vascular injury by interfering with platelet function. *Am J Physiol Heart Circ Physiol,* 319**,** H133-H143.

MAASSEN VANDENBRINK, A., REEKERS, M., BAX, W. A. & SAXENA, P. R. 2000. Human isolated coronary artery contraction to sumatriptan characterised by the selective 5-HT1B/1D receptor antagonist GR55562. *Pharmacol Toxicol,* 86**,** 287-90.

MACFARLANE, L. A. & MURPHY, P. R. 2010. MicroRNA: Biogenesis, Function and Role in Cancer. *Curr Genomics,* 11**,** 537-61.

MACLEAN, M. R., SWEENEY, G., BAIRD, M., MCCULLOCH, K. M., HOUSLAY, M. & MORECROFT, I. 1996. 5-Hydroxytryptamine receptors mediating vasoconstriction in pulmonary arteries from control and pulmonary hypertensive rats. *Br J Pharmacol,* 119**,** 917-30.

MAGUIRE, J. J. & DAVENPORT, A. P. 2015. Endothelin receptors and their antagonists. *Semin Nephrol,* 35**,** 125-36.

MAHDI, A., WERNLY, B., PERNOW, J. & ZHOU, Z. 2021. Sunitinib and its effect in the cardiovascular system. *Drug Discov Today,* 26**,** 1773-1775.

MALLOUPPAS, M., CHUNG, R., GHOSH, A., MACKLIN, A., YELLON, D. & WALKER, M. 2023. Anthracyclines and Biomarkers of Myocardial Injury: The Effect of Remote Ischemic Conditioning (RIC). *JACC: CardioOncology*.

MARTIN, W. 1984. The combined role of atheroma, cholesterol, platelets, the endothelium and fibrin in heart attacks and strokes. *Med Hypotheses,* 15**,** 305-22.

MARTINS-TEIXEIRA, M. B. & CARVALHO, I. 2020. Antitumour Anthracyclines: Progress and Perspectives. *ChemMedChem,* 15**,** 933-948.

MARTINS, F., SOFIYA, L., SYKIOTIS, G. P., LAMINE, F., MAILLARD, M., FRAGA, M., SHABAFROUZ, K., RIBI, C., CAIROLI, A., GUEX-CROSIER, Y., KUNTZER, T., MICHIELIN, O., PETERS, S., COUKOS, G., SPERTINI, F., THOMPSON, J. A. & OBEID, M. 2019. Adverse effects of immune-checkpoint inhibitors: epidemiology, management and surveillance. *Nat Rev Clin Oncol,* 16**,** 563-580.

MASON, R. P., KALINOWSKI, L., JACOB, R. F., JACOBY, A. M. & MALINSKI, T. 2005. Nebivolol reduces nitroxidative stress and restores nitric oxide bioavailability in endothelium of black Americans. *Circulation,* 112**,** 3795-801.

MASSON, J., EMERIT, M. B., HAMON, M. & DARMON, M. 2012. Serotonergic signaling: multiple effectors and pleiotropic effects. 1**,** 685-713.

MASSOTTE, D. & KIEFFER, B. L. 2005. Structure–Function Relationships in G Protein-Coupled Receptors. *In:* DEVI, L. A. (ed.) *THE G PROTEIN-COUPLED RECEPTORS HANDBOOK.* Contemporary Clinical Neuroscience

MATOS, L. L., TRUFELLI, D. C., DE MATOS, M. G. & DA SILVA PINHAL, M. A. 2010. Immunohistochemistry as an important tool in biomarkers detection and clinical practice. *Biomark Insights,* 5**,** 9-20.

MCDONALD, R. A., HATA, A., MACLEAN, M. R., MORRELL, N. W. & BAKER, A. H. 2012. MicroRNA and vascular remodelling in acute vascular injury and pulmonary vascular remodelling. *Cardiovasc Res,* 93**,** 594-604.

MCKILLOP, J., BRISTOW, M., GORIS, M., BILLINGHAM, M. & BOCKEMUEHL, K. 1983. Sensitivity and specificity of radionuclide ejection fractions in doxorubicin cardiotoxicity. *American Heart Journal,* 106.

MEDEROS Y SCHNITZLER, M., STORCH, U., MEIBERS, S., NURWAKAGARI, P., BREIT, A., ESSIN, K., GOLLASCH, M. & GUDERMANN, T. 2008. Gq-coupled receptors as mechanosensors mediating myogenic vasoconstriction. *EMBO J,* 27**,** 3092-103.

MEHRLING, T. 2015. Chemotherapy is getting 'smarter'. *Future Oncol,* 11**,** 549-52.

MIASIRO, N., KARAKI, H., MATSUDA, Y., PAIVA, A. C. & RAE, G. A. 1999. Effects of endothelin ET(B) receptor agonists and antagonists on the biphasic response in the ileum. *Eur J Pharmacol,* 369**,** 205-13.

MIN, B. W., KIM, C. G., KO, J., LIM, Y., LEE, Y. H. & SHIN, S. Y. 2008. Transcription of the protein kinase C-delta gene is activated by JNK through c-Jun and ATF2 in response to the anticancer agent doxorubicin. *Exp Mol Med,* 40**,** 699-708.

MINOTTI, G., MENNA, P., SALVATORELLI, E., CAIRO, G. & GIANNI, L. 2004. Anthracyclines: molecular advances and pharmacologic developments in antitumor activity and cardiotoxicity. *Pharmacol Rev,* 56**,** 185-229.

MIRABITO-COLAFELLA, K. M., NEVES, K. B., MONTEZANO, A. C., GARRELDS, I. M., VAN VEGHEL, R., DE VRIES, R., UIJL, E., BAELDE, H. J., VAN DEN MEIRACKER, A. H., TOUYZ, R. M., DANSER, A. H. J. & VERSMISSEN, J. 2020. Selective ETA vs. dual ETA/B receptor blockade for the prevention of sunitinib-induced hypertension and albuminuria in WKY rats. *Cardiovasc Res,* 116**,** 1779-1790.

MITRY, M. A. & EDWARDS, J. G. 2016. Doxorubicin induced heart failure: Phenotype and molecular mechanisms. *Int J Cardiol Heart Vasc,* 10**,** 17-24.

MLINAR, B., FALSINI, C. & CORRADETTI, R. 2003. Pharmacological characterization of 5-HT(1B) receptor-mediated inhibition of local excitatory synaptic transmission in the CA1 region of rat hippocampus. *Br J Pharmacol,* 138**,** 71-80.

MOHAMMAD-ZADEH, L. F., MOSES, L. & GWALTNEY-BRANT, S. M. 2008. Serotonin: a review. *J Vet Pharmacol Ther,* 31**,** 187-99.

MONTAIGNE, D., MARECHAL, X., PREAU, S., BACCOUCH, R., MODINE, T., FAYAD, G., LANCEL, S. & NEVIERE, R. 2011. Doxorubicin induces mitochondrial permeability transition and contractile dysfunction in the human myocardium. *Mitochondrion,* 11**,** 22-6.

MORECROFT, I., HEELEY, R. P., PRENTICE, H. M., KIRK, A. & MACLEAN, M. R. 1999. 5-hydroxytryptamine receptors mediating contraction in human small muscular pulmonary arteries: importance of the 5-HT1B receptor. *Br J Pharmacol,* 128**,** 730-4.

MORINELLI, T. A., MAIS, D. E., OATIS, J. E., JR., CRUMBLEY, A. J., 3RD & HALUSHKA, P. V. 1990. Characterization of thromboxane A2/prostaglandin H2 receptors in human vascular smooth muscle cells. *Life Sci,* 46**,** 1765-72.

MORINELLI, T. A., ZHANG, L. M., NEWMAN, W. H. & MEIER, K. E. 1994. Thromboxane A2/prostaglandin H2-stimulated mitogenesis of coronary artery smooth muscle cells involves activation of mitogen-activated protein kinase and S6 kinase. *J Biol Chem,* 269**,** 5693-8.

MOTZER, R. J., ESCUDIER, B., GANNON, A. & FIGLIN, R. A. 2017. Sunitinib: Ten Years of Successful Clinical Use and Study in Advanced Renal Cell Carcinoma. *Oncologist,* 22**,** 41-52.

MOUDGIL, R. & YEH, E. T. H. 2017. Molecular Mechanisms of Anthracycline-Induced Cardiotoxicity. *Cardio-Oncology.*

MOZOS, I., BORZAK, G., CARABA, A. & MIHAESCU, R. 2017. Arterial stiffness in hematologic malignancies. *Onco Targets Ther,* 10**,** 1381-1388.

MULVANY, M. J. & HALPERN, W. 1977. Contractile Properties of Small Arterial Resistance Vessels in Spontaneously Hypertensive and Normotensive Rats. *CIRCULATION RESEARCH,* 41**,** 19-26.

MURAKOSHI, N., MIYAUCHI, T., KAKINUMA, Y., OHUCHI, T., GOTO, K., YANAGISAWA, M. & YAMAGUCHI, I. 2002. Vascular endothelin-B receptor system in vivo plays a favorable inhibitory role in vascular remodeling after injury revealed by endothelin-B receptor-knockout mice. *Circulation,* 106**,** 1991-8.

MURATA, T., YAMAWAKI, H., HORI, M., SATO, K., OZAKI, H. & KARAKI, H. 2001a. Chronic vascular toxicity of doxorubicin in an organ-cultured artery. *Br J Pharmacol,* 132**,** 1365-73.

MURATA, T., YAMAWAKI, H., YOSHIMOTO, R., HORI, M., SATO, K., OZAKI, H. & KARAKI, H. 2001b. Chronic effect of doxorubicin on vascular endothelium assessed by organ culture study. *Life Sci,* 69**,** 2685-95.

NAGATOMO, T., RASHID, M., ABUL MUNTASIR, H. & KOMIYAMA, T. 2004. Functions of 5-HT2A receptor and its antagonists in the cardiovascular system. *Pharmacol Ther,* 104**,** 59-81.

NASSER, S. A. & EL-MAS, M. M. 2014. Endothelin ETA receptor antagonism in cardiovascular disease. *Eur J Pharmacol,* 737**,** 210-3.

NEBIGIL, C. G. 2009. Prokineticin receptors in cardiovascular function: foe or friend? *Trends Cardiovasc Med,* 19**,** 55-60.

NEBIGIL, C. G. & DESAUBRY, L. 2018. Updates in Anthracycline-Mediated Cardiotoxicity. *Front Pharmacol,* 9**,** 1262.

NERI SERNERI, G. G., ABBATE, R., GENSINI, G. F., PANETTA, A., CASOLO, G. C. & CARINI, M. 1983. TxA2 production by human arteries and veins. *Prostaglandins,* 25**,** 753-66.

NGUYEN, T. L., GASSER, A. & NEBIGIL, C. G. 2013. Role of Prokineticin Receptor-1 in Epicardial Progenitor Cells. *J Dev Biol,* 1**,** 20-31.

NICE, N. I. F. H. A. C. E. *Doxorubicin hydrochloride* [Online]. Available: https://bnf.nice.org.uk/drugs/doxorubicin-hydrochloride/ [Accessed].

NILSSON, T., LONGMORE, J., SHAW, D., OLESEN, I. J. & EDVINSSON, L. 1999a. Contractile 5-HT1B receptors in human cerebral arteries: pharmacological characterization and localization with immunocytochemistry. *Br J Pharmacol,* 128**,** 1133-40.

NILSSON, T., LONGMORE, J., SHAW, D., PANTEV, E., BARD, J. A., BRANCHEK, T. & EDVINSSON, L. 1999b. Characterisation of 5-HT receptors in human coronary arteries by molecular and pharmacological techniques. *Eur J Pharmacol,* 372**,** 49-56.

NISHIYAMA, S. K., ZHAO, J., WRAY, D. W. & RICHARDSON, R. S. 2017. Vascular function and endothelin-1: tipping the balance between vasodilation and vasoconstriction. *J Appl Physiol (1985),* 122**,** 354-360.

NOREL, X. 2007. Prostanoid receptors in the human vascular wall. *ScientificWorldJournal,* 7**,** 1359-74.

NORIS, M., MORIGI, M., DONADELLI, R., AIELLO, S., FOPPOLO, M., TODESCHINI, M., ORISIO, S., REMUZZI, G. & REMUZZI, A. 1995. Nitric oxide synthesis by cultured endothelial cells is modulated by flow conditions. *Circ Res,* 76**,** 536-43.

O'BRIEN, J., HAYDER, H., ZAYED, Y. & PENG, C. 2018. Overview of MicroRNA Biogenesis, Mechanisms of Actions, and Circulation. *Front Endocrinol (Lausanne),* 9**,** 402.

O'QUINN, S., DAVIS, R. L., GUTTERMAN, D. L., PAIT, G. D. & FOX, A. W. 1999. Prospective large-scale study of the tolerability of subcutaneous sumatriptan injection for acute treatment of migraine. *Cephalalgia,* 19**,** 223-31; discussion 200.

O'ROURKE, M. 1990. Arterial stiffness, systolic blood pressure, and logical treatment of arterial hypertension. 15**,** 339-347.

OCTAVIA, Y., TOCCHETTI, C. G., GABRIELSON, K. L., JANSSENS, S., CRIJNS, H. J. & MOENS, A. L. 2012. Doxorubicin-induced cardiomyopathy: from molecular mechanisms to therapeutic strategies. *J Mol Cell Cardiol,* 52**,** 1213-25.

OESTERLE, A., LAUFS, U. & LIAO, J. K. 2017. Pleiotropic Effects of Statins on the Cardiovascular System. *Circ Res,* 120**,** 229-243.

OKONKWO, K. & OJHA, U. 2020. Vasospasm induced myocardial ischaemia secondary to sumatriptan use. *BMJ Case Rep,* 13.

OLIVEIRA, P. J., GONCALVES, L., MONTEIRO, P., PROVIDENCIA, L. A. & MORENO, A. J. 2005. Are the antioxidant properties of carvedilol important for the protection of cardiac mitochondria? *Curr Vasc Pharmacol,* 3**,** 147-58.

OLSON, R. D., GAMBLIEL, H. A., VESTAL, R. E., SHADLE, S. E., CHARLIER, H. A., JR. & CUSACK, B. J. 2005. Doxorubicin cardiac dysfunction: effects on calcium regulatory proteins, sarcoplasmic reticulum, and triiodothyronine. *Cardiovasc Toxicol,* 5**,** 269-83.

OLSON, R. D., MUSHLIN, P. S., BRENNER, D. E., FLEISCHER, S., CUSACK, B. J., CHANG, B. K. & BOUCEK, R. J., JR. 1988. Doxorubicin cardiotoxicity may be caused by its metabolite, doxorubicinol. *Proc Natl Acad Sci U S A,* 85**,** 3585-9.

OLUKMAN, M., CAN, C., EROL, A., OKTEM, G., ORAL, O. & CINAR, M. G. 2009. Reversal of doxorubicin-induced vascular dysfunction by resveratrol in rat thoracic aorta: Is there a possible role of nitric oxide synthase inhibition? *Anadolu Kardiyol Derg,* 9**,** 260-6.

ONG, Q., GUO, S., ZHANG, K. & CUI, B. 2015. U0126 protects cells against oxidative stress independent of its function as a MEK inhibitor. *ACS Chem Neurosci,* 6**,** 130-7.

ORETO, L., TODARO, M. C., UMLAND, M. M., KRAMER, C., QAMAR, R., CARERJ, S., KHANDHERIA, B. K. & PATERICK, T. E. 2012. Use of echocardiography to evaluate the cardiac effects of therapies used in cancer treatment: what do we know? *J Am Soc Echocardiogr,* 25**,** 1141-52.

OTTERVANGER, J. P., WILSON, J. H. & STRICKER, B. H. 1997. Drug-induced chest pain and myocardial infarction. Reports to a national centre and review of the literature. *Eur J Clin Pharmacol,* 53**,** 105-10.

OZAKI, H. & KARAKI, H. 2002. Organ culture as a useful method for studying the biology of blood vessels and other smooth muscle tissues. *Jpn J Pharmacol,* 89**,** 93-100.

PARK, J. B. & SCHIFFRIN, E. L. 2001. ET(A) receptor antagonist prevents blood pressure elevation and vascular remodeling in aldosterone-infused rats. *Hypertension,* 37**,** 1444-9.

PARR, S. K., LIANG, J., SCHADLER, K. L., GILCHRIST, S. C., STEELE, C. C. & ADE, C. J. 2020. Anticancer Therapy-Related Increases in Arterial Stiffness: A Systematic Review and Meta-Analysis. *J Am Heart Assoc,* 9**,** e015598.

PAZ-ARES, L., LUFT, A., VICENTE, D., TAFRESHI, A., GUMUS, M., MAZIERES, J., HERMES, B., CAY SENLER, F., CSOSZI, T., FULOP, A., RODRIGUEZ-CID, J., WILSON, J., SUGAWARA, S., KATO, T., LEE, K. H., CHENG, Y., NOVELLO, S., HALMOS, B., LI, X., LUBINIECKI, G. M., PIPERDI, B., KOWALSKI, D. M. & INVESTIGATORS, K.-. 2018. Pembrolizumab plus Chemotherapy for Squamous Non-Small-Cell Lung Cancer. *N Engl J Med,* 379**,** 2040-2051.

PEREIRA, J. D., TOSATTI, J. A. G., SIMOES, R., LUIZON, M. R., GOMES, K. B. & ALVES, M. T. 2020. microRNAs associated to anthracycline-induced cardiotoxicity in women with breast cancer: A systematic review and pathway analysis. *Biomed Pharmacother,* 131**,** 110709.

PETER, M. G. & DAVENPORT, A. P. 1996. Characterization of the endothelin receptor selective agonist, BQ3020 and antagonists BQ123, FR139317, BQ788, 50235, Ro462005 and bosentan in the heart. *Br J Pharmacol,* 117**,** 455-462.

PHAM-HUY, L. A., HE, H. & PHAM-HUY, C. 2008. Free radicals, antioxidants in disease and health. *Int J Biomed Sci,* 4**,** 89-96.

PINEDO, H. M., AND SMORENBURG, CAROLIEN H. EDITOR 2006. *Drugs Affecting Growth of Tumours*.

PING, N. N., CAO, L., XIAO, X., LI, S. & CAO, Y. X. 2014. The determination of optimal initial tension in rat coronary artery using wire myography. *Physiol Res,* 63**,** 143-6.

PISKA, K., KOCZURKIEWICZ, P., BUCKI, A., WOJCIK-PSZCZOLA, K., KOLACZKOWSKI, M. & PEKALA, E. 2017. Metabolic carbonyl reduction of anthracyclines - role in cardiotoxicity and cancer resistance. Reducing enzymes as putative targets for novel cardioprotective and chemosensitizing agents. *Invest New Drugs,* 35**,** 375-385.

PODYACHEVA, E. Y., KUSHNAREVA, E. A., KARPOV, A. A. & TOROPOVA, Y. G. 2021. Analysis of Models of Doxorubicin-Induced Cardiomyopathy in Rats and Mice. A Modern View From the Perspective of the Pathophysiologist and the Clinician. *Front Pharmacol,* 12**,** 670479.

POPHALI, P. & LITZOW, M. 2017. What Is the Best Daunorubicin Dose and Schedule for Acute Myeloid Leukemia Induction? *Curr Treat Options Oncol,* 18**,** 3.

POVLSEN, G. K. & EDVINSSON, L. 2015. MEK1/2 inhibitor U0126 but not endothelin receptor antagonist clazosentan reduces upregulation of cerebrovascular contractile receptors and delayed cerebral ischemia, and improves outcome after subarachnoid hemorrhage in rats. *J Cereb Blood Flow Metab,* 35**,** 329-37.

QIN, X., CHANG, F., WANG, Z. & JIANG, W. 2018. Correlation of circulating pro-angiogenic miRNAs with cardiotoxicity induced by epirubicin/cyclophosphamide followed by docetaxel in patients with breast cancer. *Cancer Biomark,* 23**,** 473-484.

RAHMAN, A. M., YUSUF, S. W. & EWER, M. S. 2007. Anthracycline-induced cardiotoxicity and the cardiac-sparing effect of liposomal formulation. *Int J Nanomedicine,* 2**,** 567-83.

RAICHLIN, E., PRASAD, A., MATHEW, V., KENT, B., HOLMES, D. R., JR., PUMPER, G. M., NELSON, R. E., LERMAN, L. O. & LERMAN, A. 2008. Efficacy and safety of atrasentan in patients with cardiovascular risk and early atherosclerosis. *Hypertension,* 52**,** 522-8.

RAJ, S., FRANCO, V. I. & LIPSHULTZ, S. E. 2014. Anthracycline-induced cardiotoxicity: a review of pathophysiology, diagnosis, and treatment. *Curr Treat Options Cardiovasc Med,* 16**,** 315.

RANGREZ, A. Y., MASSY, Z. A., METZINGER-LE MEUTH, V. & METZINGER, L. 2011. miR-143 and miR-145: molecular keys to switch the phenotype of vascular smooth muscle cells. *Circ Cardiovasc Genet,* 4**,** 197-205.

RAPPORT, M. M. 1997. The discovery of serotonin. *Perspect Biol Med,* 40**,** 260-73.

RASANEN, M., DEGERMAN, J., NISSINEN, T. A., MIINALAINEN, I., KERKELA, R., SILTANEN, A., BACKMAN, J. T., MERVAALA, E., HULMI, J. J., KIVELA, R. & ALITALO, K. 2016. VEGF-B gene therapy inhibits doxorubicin-induced cardiotoxicity by endothelial protection. *Proc Natl Acad Sci U S A,* 113**,** 13144-13149.

RASCHI, E., VASINA, V., URSINO, M. G., BORIANI, G., MARTONI, A. & DE PONTI, F. 2010. Anticancer drugs and cardiotoxicity: Insights and perspectives in the era of targeted therapy. *Pharmacol Ther,* 125**,** 196-218.

RAVINGEROVA, T., KINDERNAY, L., BARTEKOVA, M., FERKO, M., ADAMEOVA, A., ZOHDI, V., BERNATOVA, I., FERENCZYOVA, K. & LAZOU, A. 2020. The Molecular Mechanisms of Iron Metabolism and Its Role in Cardiac Dysfunction and Cardioprotection. *Int J Mol Sci,* 21.

RAWAT, P. S., JAISWAL, A., KHURANA, A., BHATTI, J. S. & NAVIK, U. 2021. Doxorubicin-induced cardiotoxicity: An update on the molecular mechanism and novel therapeutic strategies for effective management. *Biomed Pharmacother,* 139**,** 111708.

REAL, C., PÁRRAGA, R., PIZARRO, G., GARCÍA-LUNAR, I., GONZÁLEZ-CALVO, E., MARTÍNEZ-GÓMEZ, J., SÁNCHEZ-GONZÁLEZ, J., SAMPEDRO, P., SANMAMED, I., DE MIGUEL, M., DE COS-GANDOY, A., BODEGA, P., IBANEZ, B., SANTOS-BENEIT, G., FUSTER, V. & FERNÁNDEZ-JIMÉNEZ, R. 2023. Magnetic resonance imaging reference values for cardiac morphology, function and tissue composition in adolescents. *eClinicalMedicine,* 58.

REICHARDT, P., TABONE, M. D., MORA, J., MORLAND, B. & JONES, R. L. 2018. Risk-benefit of dexrazoxane for preventing anthracycline-related cardiotoxicity: re-evaluating the European labeling. *Future Oncol,* 14**,** 2663-2676.

REN, X. P., WU, J., WANG, X., SARTOR, M. A., JONES, K., QIAN, J., NICOLAOU, P., PRITCHARD, T. J. & FAN, G. C. 2009. MicroRNA-320 is involved in the regulation of cardiac ischemia/reperfusion injury by targeting heat-shock protein 20. *Circulation,* 119**,** 2357-2366.

REYLAND, M. E. 2007. Protein kinase Cdelta and apoptosis. *Biochem Soc Trans,* 35**,** 1001-4.

RILEY, R. S., JUNE, C. H., LANGER, R. & MITCHELL, M. J. 2019. Delivery technologies for cancer immunotherapy. *Nat Rev Drug Discov,* 18**,** 175-196.

ROBERT, J. 1993. Epirubicin. Clinical pharmacology and dose-effect relationship. *Drugs,* 45 Suppl 2**,** 20-30.

ROLIN, S., HANSON, J., VASTERSAEGHER, C., CHERDON, C., PRATICO, D., MASEREEL, B. & DOGNE, J. M. 2007. BM-520, an original TXA2 modulator, inhibits the action of thromboxane A2 and 8-iso-prostaglandin F2alphain vitro and in vivo on human and rodent platelets, and aortic vascular smooth muscles from rodents. *Prostaglandins Other Lipid Mediat,* 84**,** 14-23.

ROMAINE, S. P., TOMASZEWSKI, M., CONDORELLI, G. & SAMANI, N. J. 2015. MicroRNAs in cardiovascular disease: an introduction for clinicians. *Heart,* 101**,** 921-8.

ROSENBAUM, D. M., RASMUSSEN, S. G. & KOBILKA, B. K. 2009. The structure and function of G-protein-coupled receptors. *Nature,* 459**,** 356-63.

ROSENBERG, A. J., LANE-CORDOVA, A. D., WEE, S. O., WHITE, D. W., HILGENKAMP, T. I. M., FERNHALL, B. & BAYNARD, T. 2018. Healthy aging and carotid performance: strain measures and beta-stiffness index. *Hypertens Res,* 41**,** 748-755.

ROSENDORFF, C. 1997. Endothelin, vascular hypertrophy, and hypertension. *Cardiovasc Drugs Ther,* 10**,** 795-802.

RUDIC, R. D., SHESELY, E. G., MAEDA, N., SMITHIES, O., SEGAL, S. S. & SESSA, W. C. 1998. Direct evidence for the importance of endothelium-derived nitric oxide in vascular remodeling. *J Clin Invest,* 101**,** 731-6.

RUGGERI, B. A., CAMP, F. & MIKNYOCZKI, S. 2014. Animal models of disease: pre-clinical animal models of cancer and their applications and utility in drug discovery. *Biochem Pharmacol,* 87**,** 150-61.

RUSSELL, F. D. & DAVENPORT, A. P. 1996. Characterization of the binding of endothelin ETB selective ligands in human and rat heart. *Br J Pharmacol,* 119**,** 631-6.

SAAB, F., ROUTIER, S., MÉROUR, J.-Y., BÉNÉTEAU, V. & SCHOENTGEN, F. J. I. J. O. H. T. S. 2010. Comparison of the efficiencies of two TR-FRET methods to detect in vitro natural and synthesized inhibitors of the Raf/MEK/ERK signaling pathway. 1**,** 81-98.

SALAHUDEEN, M. S. & NISHTALA, P. S. 2017. An overview of pharmacodynamic modelling, ligand-binding approach and its application in clinical practice. *Saudi Pharm J,* 25**,** 165-175.

SALAZAR, N. C., CHEN, J. & ROCKMAN, H. A. 2007. Cardiac GPCRs: GPCR Signaling in Healthy and Failing Hearts. *Biochim Biophys Acta***,** 1006–1018.

SALLOUM-ASFAR, S., SATHEESH, N. J. & ABDULLA, S. A. 2019. Circulating miRNAs, Small but Promising Biomarkers for Autism Spectrum Disorder. *Front Mol Neurosci,* 12**,** 253.

SANDHU, H., ANSAR, S. & EDVINSSON, L. 2010. Comparison of MEK/ERK pathway inhibitors on the upregulation of vascular G-protein coupled receptors in rat cerebral arteries. *Eur J Pharmacol,* 644**,** 128-37.

SANDHU, H. & MADDOCK, H. 2014. Molecular basis of cancer-therapy-induced cardiotoxicity: introducing microRNA biomarkers for early assessment of subclinical myocardial injury. *Clin Sci (Lond),* 126**,** 377-400.

SANDHU, H., XU, C. B. & EDVINSSON, L. 2011. Alteration in contractile G-protein coupled receptor expression by moist snuff and nicotine in rat cerebral arteries. *Toxicol Appl Pharmacol,* 252**,** 138-49.

SANGWENI, N. F., DLUDLA, P. V., CHELLAN, N., MABASA, L., SHARMA, J. R. & JOHNSON, R. 2021. The Implication of Low Dose Dimethyl Sulfoxide on Mitochondrial Function and Oxidative Damage in Cultured Cardiac and Cancer Cells. *Molecules,* 26.

SANTOS, R., URSU, O., GAULTON, A., BENTO, A. P., DONADI, R. S., BOLOGA, C. G., KARLSSON, A., AL-LAZIKANI, B., HERSEY, A., OPREA, T. I. & OVERINGTON, J. P. 2017. A comprehensive map of molecular drug targets. *Nat Rev Drug Discov,* 16**,** 19-34.

SATTAR, N., PREISS, D., MURRAY, H. M., WELSH, P., BUCKLEY, B. M., DE CRAEN, A. J., SESHASAI, S. R., MCMURRAY, J. J., FREEMAN, D. J., JUKEMA, J. W., MACFARLANE, P. W., PACKARD, C. J., STOTT, D. J., WESTENDORP, R. G., SHEPHERD, J., DAVIS, B. R., PRESSEL, S. L., MARCHIOLI, R., MARFISI, R. M., MAGGIONI, A. P., TAVAZZI, L., TOGNONI, G., KJEKSHUS, J., PEDERSEN, T. R., COOK, T. J., GOTTO, A. M., CLEARFIELD, M. B., DOWNS, J. R., NAKAMURA, H., OHASHI, Y., MIZUNO, K., RAY, K. K. & FORD, I. 2010. Statins and risk of incident diabetes: a collaborative meta-analysis of randomised statin trials. *Lancet,* 375**,** 735-42.

SAYED-AHMED, M. M., KHATTAB, M. M., GAD, M. Z. & OSMAN, A. M. 2001. Increased plasma endothelin-1 and cardiac nitric oxide during doxorubicin-induced cardiomyopathy. *Pharmacol Toxicol,* 89**,** 140-4.

SCHAUE, D. & MCBRIDE, W. H. 2015. Opportunities and challenges of radiotherapy for treating cancer. *Nat Rev Clin Oncol,* 12**,** 527-40.

SCHNEIDER, M. P., BOESEN, E. I. & POLLOCK, D. M. 2007. Contrasting actions of endothelin ET(A) and ET(B) receptors in cardiovascular disease. *Annu Rev Pharmacol Toxicol,* 47**,** 731-59.

SCHOLAR, E. 2007. Alkylating Agents. *xPharm: The Comprehensive Pharmacology Reference***,** 1-4.

SEIFRIED, H. E., ANDERSON, D. E., SORKIN, B. C. & COSTELLO, R. B. 2004. Free radicals: the pros and cons of antioxidants. Executive summary report. *J Nutr,* 134**,** 3143S-3163S.

SEKOVANIC, A., DOROTIC, A., JURASOVIC, J., PASALIC, D., KOVACIC, J., STASENKO, S., MIOC, T., PIASEK, M. & ORCT, T. 2021. Pre-amplification as a method for improvement of quantitative RT-PCR analysis of circulating miRNAs. *Biochem Med (Zagreb),* 31**,** 010901.

SELVEN, H., BUSUND, L. R., ANDERSEN, S., BREMNES, R. M. & KILVAER, T. K. 2021. High expression of microRNA-126 relates to favorable prognosis for colon cancer patients. *Sci Rep,* 11**,** 9592.

SERONDE, M. F., VAUSORT, M., GAYAT, E., GORETTI, E., NG, L. L., SQUIRE, I. B., VODOVAR, N., SADOUNE, M., SAMUEL, J. L., THUM, T., SOLAL, A. C., LARIBI, S., PLAISANCE, P., WAGNER, D. R., MEBAZAA, A., DEVAUX, Y. & NETWORK, G. 2015. Circulating microRNAs and Outcome in Patients with Acute Heart Failure. *PLoS One,* 10**,** e0142237.

SHAUL, Y. D. & SEGER, R. 2007. The MEK/ERK cascade: from signaling specificity to diverse functions. *Biochim Biophys Acta,* 1773**,** 1213-26.

SHEIBANI, M., FAGHIR-GHANESEFAT, H., AZIZI, Y., MOKHTARI, T., YOUSEFI-MANESH, H., SATTARZADEH BADKOUBEH, R., EMAMI, A. & DEHPOUR, A. 2021. Anti-Inflammatory and Antioxidative Effects of Sumatriptan Against Doxorubicin-Induced Cardiotoxicity in Rat. *Acta Medica Iranica,* 59.

SHEN, B., YE, C. L., YE, K. H., ZHUANG, L. & JIANG, J. H. 2009. Doxorubicin-induced vasomotion and [Ca(2+)](i) elevation in vascular smooth muscle cells from C57BL/6 mice. *Acta Pharmacol Sin,* 30**,** 1488-95.

SHINLAPAWITTAYATORN, K., CHATTIPAKORN, S. C. & CHATTIPAKORN, N. 2022. The effects of doxorubicin on cardiac calcium homeostasis and contractile function. *J Cardiol,* 80**,** 125-132.

SHIRAVAND, Y., KHODADADI, F., KASHANI, S. M. A., HOSSEINI-FARD, S. R., HOSSEINI, S., SADEGHIRAD, H., LADWA, R., O'BYRNE, K. & KULASINGHE, A. 2022. Immune Checkpoint Inhibitors in Cancer Therapy. *Curr Oncol,* 29**,** 3044-3060.

SHUKLA, A., HILLEGASS, J. M., MACPHERSON, M. B., BEUSCHEL, S. L., VACEK, P. M., PASS, H. I., CARBONE, M., TESTA, J. R. & MOSSMAN, B. T. 2010. Blocking of ERK1 and ERK2 sensitizes human mesothelioma cells to doxorubicin. *Mol Cancer,* 9**,** 314.

SIKARWAR, A. S., HINTON, M., SANTHOSH, K. T., CHELIKANI, P. & DAKSHINAMURTI, S. 2014. Palmitoylation of Galphaq determines its association with the thromboxane receptor in hypoxic pulmonary hypertension. *Am J Respir Cell Mol Biol,* 50**,** 135-43.

SKOVSTED, G. F., KILIC, S. & EDVINSSON, L. 2015. Endothelin-1 and Endothelin-3 Regulate Endothelin Receptor Expression in Rat Coronary Arteries. *Basic Clin Pharmacol Toxicol,* 117**,** 297-305.

SKOVSTED, G. F., KRUSE, L. S., BERCHTOLD, L. A., GRELL, A. S., WARFVINGE, K. & EDVINSSON, L. 2017. Myocardial ischemia-reperfusion enhances transcriptional expression of endothelin-1 and vasoconstrictor ETB receptors via the protein kinase MEK-ERK1/2 signaling pathway in rat. *PLoS One,* 12**,** e0174119.

SKOVSTED, G. F., PEDERSEN, A. F., LARSEN, R., SHEYKHZADE, M. & EDVINSSON, L. 2012. Rapid functional upregulation of vasocontractile endothelin ETB receptors in rat coronary arteries. *Life Sci,* 91**,** 593-9.

SMYTH, E. M. 2010. Thromboxane and the thromboxane receptor in cardiovascular disease. *Clin Lipidol,* 5**,** 209-219.

SOMMARIVA, E., D'ALESSANDRA, Y., FARINA, F. M., CASELLA, M., CATTANEO, F., CATTO, V., CHIESA, M., STADIOTTI, I., BRAMBILLA, S., DELLO RUSSO, A., CARBUCICCHIO, C., VETTOR, G., RIGGIO, D., SANDRI, M. T., BARBUTI, A., VERNILLO, G., MURATORI, M., DAL FERRO, M., SINAGRA, G., MOIMAS, S., GIACCA, M., COLOMBO, G. I., POMPILIO, G. & TONDO, C. 2017. MiR-320a as a Potential Novel Circulating Biomarker of Arrhythmogenic CardioMyopathy. *Sci Rep,* 7**,** 4802.

SPIERS, A. & PADMANABHAN, N. 2005. A Guide to Wire Myography. *Hypertension, Methods and Protocols***,** 91-104.

SRITHARAN, S. & SIVALINGAM, N. 2021. A comprehensive review on time-tested anticancer drug doxorubicin. *Life Sci,* 278**,** 119527.

STAUFFER, B. L., WESTBY, C. M. & DESOUZA, C. A. 2008. Endothelin-1, aging and hypertension. *Curr Opin Cardiol,* 23**,** 350-5.

SU, H. F., SAMSAMSHARIAT, A., FU, J., SHAN, Y. X., CHEN, Y. H., PIOMELLI, D. & WANG, P. H. 2006. Oleylethanolamide activates Ras-Erk pathway and improves myocardial function in doxorubicin-induced heart failure. *Endocrinology,* 147**,** 827-34.

SUDHAKAR, A. 2009. History of Cancer, Ancient and Modern Treatment Methods. *J Cancer Sci Ther,* 1**,** 1-4.

SUDHESH DEV, S., ZAINAL ABIDIN, S. A., FARGHADANI, R., OTHMAN, I. & NAIDU, R. 2021. Receptor Tyrosine Kinases and Their Signaling Pathways as Therapeutic Targets of Curcumin in Cancer. *Front Pharmacol,* 12**,** 772510.

SUNG, H., FERLAY, J., SIEGEL, R. L., LAVERSANNE, M., SOERJOMATARAM, I., JEMAL, A. & BRAY, F. 2021. Global Cancer Statistics 2020: GLOBOCAN Estimates of Incidence and Mortality Worldwide for 36 Cancers in 185 Countries. *CA Cancer J Clin,* 71**,** 209-249.

SUTER, T. M. & EWER, M. S. 2013. Cancer drugs and the heart: importance and management. *Eur Heart J,* 34**,** 1102-11.

SUTTON-TYRRELL, K., NAJJAR, S. S., BOUDREAU, R. M., VENKITACHALAM, L., KUPELIAN, V., SIMONSICK, E. M., HAVLIK, R., LAKATTA, E. G., SPURGEON, H., KRITCHEVSKY, S., PAHOR, M., BAUER, D., NEWMAN, A. & HEALTH, A. B. C. S. 2005. Elevated aortic pulse wave velocity, a marker of arterial stiffness, predicts cardiovascular events in well-functioning older adults. *Circulation,* 111**,** 3384-90.

SZELENBERGER, R., KACPRZAK, M., SALUK-BIJAK, J., ZIELINSKA, M. & BIJAK, M. 2019. Plasma MicroRNA as a novel diagnostic. *Clin Chim Acta,* 499**,** 98-107.

TAI, K., VANDENBERG, G., HAMAIDE, M. C., WIBO, M. & MOREL, N. 2009. Effect of organ culture on noradrenaline- evoked contraction, calcium signalling and TRPC expression in rat mesenteric artery. *J Vasc Res,* 46**,** 353-64.

TARKOWSKI, R. & RZACA, M. 2014. Cryosurgery in the treatment of women with breast cancer-a review. *Gland Surg,* 3**,** 88-93.

TEERLINK, J. R., BREU, V., SPRECHER, U., CLOZEL, M. & CLOZEL, J. P. 1994. Potent vasoconstriction mediated by endothelin ETB receptors in canine coronary arteries. *Circ Res,* 74**,** 105-14.

THAVENDIRANATHAN, P., WINTERSPERGER, B. J., FLAMM, S. D. & MARWICK, T. H. 2013. Cardiac MRI in the assessment of cardiac injury and toxicity from cancer chemotherapy: a systematic review. *Circ Cardiovasc Imaging,* 6**,** 1080-91.

THOMAS, S. A., GRAMI, Z., MEHTA, S., PATEL, K. J. C. C. & MICROENVIRONMENT 2016. Adverse effects of 5-fluorouracil: Focus on rare side effects. 3.

THORN, C. F., OSHIRO, C., MARSH, S., HERNANDEZ-BOUSSARD, T., MCLEOD, H., KLEIN, T. E. & ALTMAN, R. B. 2011. Doxorubicin pathways: pharmacodynamics and adverse effects. *Pharmacogenet Genomics,* 21**,** 440-6.

TIAN, W., YANG, L., LIU, Y., HE, J., YANG, L., ZHANG, Q., LIU, F., LI, J., LIU, J., SUMI, S., SHEN, Y. & QI, Z. 2020. Resveratrol attenuates doxorubicin-induced cardiotoxicity in rats by up-regulation of vascular endothelial growth factor B. *J Nutr Biochem,* 79**,** 108132.

TIGER, M., VARNAS, K., OKUBO, Y. & LUNDBERG, J. 2018. The 5-HT1B receptor - a potential target for antidepressant treatment. *Psychopharmacology (Berl),* 235**,** 1317-1334.

TOUCHBERRY, C. D., SILSWAL, N., TCHIKRIZOV, V., ELMORE, C. J., SRINIVAS, S., AKTHAR, A. S., SWAN, H. K., WETMORE, L. A. & WACKER, M. J. 2014. Cardiac thromboxane A2 receptor activation does not directly induce cardiomyocyte hypertrophy but does cause cell death that is prevented with gentamicin and 2-APB. *BMC Pharmacol Toxicol,* 15**,** 73.

TOYO-OKA, T., AIZAWA, T., SUZUKI, N., HIRATA, Y., MIYAUCHI, T., SHIN, W. S., YANAGISAWA, M., MASAKI, T. & SUGIMOTO, T. 1991. Increased plasma level of endothelin-1 and coronary spasm induction in patients with vasospastic angina pectoris. *Circulation,* 83**,** 476-83.

TRUBACOVA, R., DRASTICHOVA, Z. & NOVOTNY, J. 2022. Biochemical and physiological insights into TRH receptor-mediated signaling. *Front Cell Dev Biol,* 10**,** 981452.

TYKOCKI, N. R., GARIEPY, C. E. & WATTS, S. W. 2009. Endothelin ET(B) receptors in arteries and veins: multiple actions in the vein. *J Pharmacol Exp Ther,* 329**,** 875-81.

VALLANCE, P. & HINGORANI, A. 1999. Endothelial nitric oxide in humans in health and disease. *Int J Exp Pathol,* 80**,** 291-303.

VAN ROOIJ, E., SUTHERLAND, L. B., LIU, N., WILLIAMS, A. H., MCANALLY, J., GERARD, R. D., RICHARDSON, J. A. & OLSON, E. N. 2006. A signature pattern of stress-responsive microRNAs that can evoke cardiac hypertrophy and heart failure. *Proc Natl Acad Sci U S A,* 103**,** 18255-60.

VANDAMME, T. F. 2014. Use of rodents as models of human diseases. *J Pharm Bioallied Sci,* 6**,** 2-9.

VASILATOU, D., PAPAGEORGIOU, S., PAPPA, V., PAPAGEORGIOU, E. & DERVENOULAS, J. 2010. The role of microRNAs in normal and malignant hematopoiesis. *Eur J Haematol,* 84**,** 1-16.

VASQUEZ-VIVAR, J., MARTASEK, P., HOGG, N., MASTERS, B. S., PRITCHARD, K. A., JR. & KALYANARAMAN, B. 1997. Endothelial nitric oxide synthase-dependent superoxide generation from adriamycin. *Biochemistry,* 36**,** 11293-7.

VILLANI, F., FAVALLI, L. & PICCININI, F. 1980. Relationship between the Effect on Calcium Turnover and Early Cardiotoxicity of Doxorubicin and 4'-EPI-Doxorubicin in Guinea Pig Heart Muscle. 66**,** 689-697.

VOLKOVA, M. & RUSSELL, R., 3RD 2011. Anthracycline cardiotoxicity: prevalence, pathogenesis and treatment. *Curr Cardiol Rev,* 7**,** 214-20.

VOLPE, M., RUBATTU, S. & BURNETT, J., JR. 2014. Natriuretic peptides in cardiovascular diseases: current use and perspectives. *Eur Heart J,* 35**,** 419-25.

WACKENFORS, A., INGEMANSSON, R. & MALMSJO, M. 2003. Endothelin receptors in endothelium-denuded human coronary artery bypass grafts and coronary arteries. *Ann Thorac Surg,* 75**,** 874-81.

WALLACE, K. B., HAUSNER, E., HERMAN, E., HOLT, G. D., MACGREGOR, J. T., METZ, A. L., MURPHY, E., ROSENBLUM, I. Y., SISTARE, F. D. & YORK, M. J. 2004. Serum troponins as biomarkers of drug-induced cardiac toxicity. *Toxicol Pathol,* 32**,** 106-21.

WALWEEL, K. & LAVER, D. R. 2015. Mechanisms of SR calcium release in healthy and failing human hearts. *Biophys Rev,* 7**,** 33-41.

WAN, Q., XU, T., DING, W., ZHANG, X., JI, X., YU, T., YU, W., LIN, Z. & WANG, J. 2018. miR-499-5p Attenuates Mitochondrial Fission and Cell Apoptosis via p21 in Doxorubicin Cardiotoxicity. *Front Genet,* 9**,** 734.

WANG, A., ZHANG, H., LIANG, Z., XU, K., QIU, W., TIAN, Y., GUO, H., JIA, J., XING, E., CHEN, R., XIANG, Z. & LIU, J. 2016. U0126 attenuates ischemia/reperfusion-induced apoptosis and autophagy in myocardium through MEK/ERK/EGR-1 pathway. *Eur J Pharmacol,* 788**,** 280-285.

WANG, B., LI, Y., HAO, X., YANG, J., HAN, X., LI, H., LI, T., WANG, D., TENG, Y., MA, L., LI, Y., ZHAO, M. & WANG, X. 2021. Comparison of the Clinical Value of miRNAs and Conventional Biomarkers in AMI: A Systematic Review. *Front Genet,* 12**,** 668324.

WANG, F., REN, X. & ZHANG, X. 2015a. Role of microRNA-150 in solid tumors. *Oncol Lett,* 10**,** 11-16.

WANG, J., GARERI, C. & ROCKMAN, H. A. 2018. G-Protein-Coupled Receptors in Heart Disease. *Circ Res,* 123**,** 716-735.

WANG, P., YANG, D., ZHANG, H., WEI, X., MA, T., CHENG, Z., HONG, Q., HU, J., ZHUO, H., SONG, Y., JIA, C., JING, F., JIN, Q., BAI, C., MAO, H. & ZHAO, J. 2015b. Early Detection of Lung Cancer in Serum by a Panel of MicroRNA Biomarkers. *Clin Lung Cancer,* 16**,** 313-9 e1.

WANG, S., AURORA, A. B., JOHNSON, B. A., QI, X., MCANALLY, J., HILL, J. A., RICHARDSON, J. A., BASSEL-DUBY, R. & OLSON, E. N. 2008. The endothelial-specific microRNA miR-126 governs vascular integrity and angiogenesis. *Dev Cell,* 15**,** 261-71.

WANG, X., LIAN, Y., WEN, X., GUO, J., WANG, Z., JIANG, S. & HU, Y. 2017. Expression of miR-126 and its potential function in coronary artery disease. *Afr Health Sci,* 17**,** 474-480.

WAYMAN, B. H., TAYLOR, W. R., RACHEV, A. & VITO, R. P. 2008. Arteries respond to independent control of circumferential and shear stress in organ culture. *Ann Biomed Eng,* 36**,** 673-84.

WEBER, J. A., BAXTER, D. H., ZHANG, S., HUANG, D. Y., HUANG, K. H., LEE, M. J., GALAS, D. J. & WANG, K. 2010. The microRNA spectrum in 12 body fluids. *Clin Chem,* 56**,** 1733-41.

WEI, C. M., LERMAN, A., RODEHEFFER, R. J., MCGREGOR, C. G., BRANDT, R. R., WRIGHT, S., HEUBLEIN, D. M., KAO, P. C., EDWARDS, W. D. & BURNETT, J. C., JR. 1994. Endothelin in human congestive heart failure. *Circulation,* 89**,** 1580-6.

WEI, S. C., DUFFY, C. R. & ALLISON, J. P. 2018. Fundamental Mechanisms of Immune Checkpoint Blockade Therapy. *Cancer Discov,* 8**,** 1069-1086.

WENCESLAU, C. F., MCCARTHY, C. G., EARLEY, S., ENGLAND, S. K., FILOSA, J. A., GOULOPOULOU, S., GUTTERMAN, D. D., ISAKSON, B. E., KANAGY, N. L., MARTINEZ-LEMUS, L. A., SONKUSARE, S. K., THAKORE, P., TRASK, A. J., WATTS, S. W. & WEBB, R. C. 2021. Guidelines for the measurement of vascular function and structure in isolated arteries and veins. *Am J Physiol Heart Circ Physiol,* 321**,** H77-H111.

WETTSCHURECK, N. & OFFERMANNS, S. 2005. Mammalian G proteins and their cell type specific functions. *Physiol Rev,* 85**,** 1159-204.

WHITMARSH, A. J. & DAVIS, R. J. 1996. Transcription factor AP-1 regulation by mitogen-activated protein kinase signal transduction pathways. *J Mol Med (Berl),* 74**,** 589-607.

WILSON, B. E., JACOB, S., YAP, M. L., FERLAY, J., BRAY, F. & BARTON, M. B. 2019. Estimates of global chemotherapy demands and corresponding physician workforce requirements for 2018 and 2040: a population-based study. *Lancet Oncol,* 20**,** 769-780.

WOUTERS, J., DURANT, F. & MASEREEL, B. 1999. Antagonism of the TXA2 receptor by seratrodast: a structural approach. *Bioorg Med Chem Lett,* 9**,** 2867-70.

WU, X., LI, Y., ZHANG, S. & ZHOU, X. 2021. Ferroptosis as a novel therapeutic target for cardiovascular disease. *Theranostics,* 11**,** 3052-3059.

WYLD, L., AUDISIO, R. A. & POSTON, G. J. 2015. The evolution of cancer surgery and future perspectives. *Nat Rev Clin Oncol,* 12**,** 115-24.

XIA, Q. G., REINECKE, A., DORENKAMP, M., DAEMEN, M. J., SIMON, R. & UNGER, T. 2006. Effects of endothelin ETA receptor blocker LU 135252 on cardiac remodeling and survival in a hypertensive rat model of chronic heart failure. *Acta Pharmacol Sin,* 27**,** 1417-22.

XU, C. B., ZHENG, J. P., ZHANG, W., ZHANG, Y. & EDVINSSON, L. 2008. Lipid-soluble smoke particles upregulate vascular smooth muscle ETB receptors via activation of mitogen-activating protein kinases and NF-kappaB pathways. *Toxicol Sci,* 106**,** 546-55.

XU, X., PERSSON, H. L. & RICHARDSON, D. R. 2005. Molecular pharmacology of the interaction of anthracyclines with iron. *Mol Pharmacol,* 68**,** 261-71.

YAMADA, H., SUZUKI, K., FUJII, R., KAWADO, M., HASHIMOTO, S., WATANABE, Y., ISO, H., FUJINO, Y., WAKAI, K. & TAMAKOSHI, A. 2021. Circulating miR-21, miR-29a, and miR-126 are associated with premature death risk due to cancer and cardiovascular disease: the JACC Study. *Sci Rep,* 11**,** 5298.

YAMASHITA, J., OGAWA, M. & SHIRAKUSA, T. 1995. Plasma endothelin-1 as a marker for doxorubicin cardiotoxicity. *Int J Cancer,* 62**,** 542-7.

YANAGISAWA, M., KURIHARA, H., KIMURA, S., TOMOBE, Y., KOBAYASHI, M., MITSUI, Y., YAZAKI, Y., GOTO, K. & MASAKI, T. 1988. A novel potent vasoconstrictor peptide produced by vascular endothelial cells. *Nature,* 332**,** 411-5.

YANG, F., TEVES, S. S., KEMP, C. J. & HENIKOFF, S. 2014. Doxorubicin, DNA torsion, and chromatin dynamics. *Biochim Biophys Acta,* 1845**,** 84-9.

YE, D., WANG, Z., XU, Y., YE, J., WANG, M., LIU, J., ZHANG, J., ZHAO, M., CHEN, J. & WAN, J. 2020. Interleukin-9 aggravates doxorubicin-induced cardiotoxicity by promoting inflammation and apoptosis in mice. *Life Sci,* 255**,** 117844.

YIN, Z., ZHAO, Y., LI, H., YAN, M., ZHOU, L., CHEN, C. & WANG, D. W. 2016. miR-320a mediates doxorubicin-induced cardiotoxicity by targeting VEGF signal pathway. *Aging (Albany NY),* 8**,** 192-207.

YOUNG, R. C., OZOLS, R. F. & MYERS, C. E. 1981. The anthracycline antineoplastic drugs. *N Engl J Med,* 305**,** 139-53.

YU, Q., LI, K., ZHAO, A., WEI, M., HUANG, Z., ZHANG, Y., CHEN, Y., LIAN, T., WANG, C., XU, L., ZHANG, Y., XU, C. & LIU, F. 2021. Sorafenib not only impairs endothelium-dependent relaxation but also promotes vasoconstriction through the upregulation of vasoconstrictive endothelin type B receptors. *Toxicol Appl Pharmacol,* 414**,** 115420.

ZAMORANO, J. L., LANCELLOTTI, P., RODRIGUEZ MUNOZ, D., ABOYANS, V., ASTEGGIANO, R., GALDERISI, M., HABIB, G., LENIHAN, D. J., LIP, G. Y. H., LYON, A. R., LOPEZ FERNANDEZ, T., MOHTY, D., PIEPOLI, M. F., TAMARGO, J., TORBICKI, A., SUTER, T. M. & GROUP, E. S. C. S. D. 2016. 2016 ESC Position Paper on cancer treatments and cardiovascular toxicity developed under the auspices of the ESC Committee for Practice Guidelines: The Task Force for cancer treatments and cardiovascular toxicity of the European Society of Cardiology (ESC). *Eur Heart J,* 37**,** 2768-2801.

ZHANG, R., OGLETREE, M. L. & MORELAND, S. 1996. Characterization of thromboxane A2/prostaglandin endoperoxide receptors in aorta. *Eur J Pharmacol,* 317**,** 91-6.

ZHANG, W., ZHANG, Y., EDVINSSON, L. & XU, C. B. 2008. Up-regulation of thromboxane A2 receptor expression by lipid soluble smoking particles through post-transcriptional mechanisms. *Atherosclerosis,* 196**,** 608-16.

ZHANG, W., ZHANG, Y., EDVINSSON, L. & XU, C. B. 2009. Transcriptional down-regulation of thromboxane A(2) receptor expression via activation of MAPK ERK1/2, p38/NF-kappaB pathways. *J Vasc Res,* 46**,** 162-74.

ZHAO, C., SUN, X. & LI, L. 2019. Biogenesis and function of extracellular miRNAs. *ExRNA,* 1.

ZHAO, W., ZHAO, S. P. & ZHAO, Y. H. 2015. MicroRNA-143/-145 in Cardiovascular Diseases. *Biomed Res Int,* 2015**,** 531740.

ZHOU, S., STARKOV, A., FROBERG, M. K., LEINO, R. L. & WALLACE, K. B. 2001. Cumulative and irreversible cardiac mitochondrial dysfunction induced by doxorubicin. *Cancer Res,* 61**,** 771-7.

ZHU, Z., LI, X., DONG, H., KE, S. & ZHENG, W. H. 2018. Let-7f and miRNA-126 correlate with reduced cardiotoxicity risk in triple-negative breast cancer patients who underwent neoadjuvant chemotherapy. *Int J Clin Exp Pathol,* 11**,** 4987-4995.

ZOU, M., HUANG, C., LI, X., HE, X., CHEN, Y., LIAO, W., LIAO, Y., SUN, J., LIU, Z., ZHONG, L. & BIN, J. 2017. Circular RNA expression profile and potential function of hsa_circRNA_101238 in human thoracic aortic dissection. *Oncotarget,* 8**,** 81825-81837.

9. Appendices

9.1. The pharmacokinetics of the GPCR specific agonists and antagonists used in chapters 4 and 5:

Table 9.1: Selectivity of the agonists used to study the GPCRs-mediated vasoconstriction. K_D = Dissociation constant, which represents the inverse of receptor's affinity to the ligand when at equilibrium, and smaller is K_D, higher is the affinity of receptor to the ligand (Salahudeen and Nishtala, 2017). pEC_{50} = negative logarithm of the agonist concentration that produces 50 % of the maximal contraction, LV = Left ventricle, ET_A = Endothelin A receptors, ET_B = Endothelin B receptors, 5-HT_{1B} = 5-hydroxytryptamine receptors 1B, 5-HT_{2A} = 5-hydroxytryptamine receptors 2A, TP = thromboxane prostanoid receptors.

Agonist	Receptors	Selectivity		Receptors localisation	Reference
Sarafotoxin 6c	ET_B	K_D	0.06 nM	Rat LV	(Russell and Davenport, 1996)
	ET_A	K_D	3.50 µM	Rat LV	
	ET_B	K_D	0.34 nM	Human LV	
	ET_A	K_D	2.00 µM	Human LV	
Endothelin-1	$ET_{A/B}$	K_D	0.093 nM	Rat Heart	(Liu *et al.*, 1990)
		K_D	12.70 pM	Human LV muscle strips	
5-carboxamido tryptamine	5-HT_{1B}	pEC_{50}	$10^{-7.9}$ M	A7r5* (Rat)	(Hoyer *et al.*, 1994)
	5-HT_{2A}	pEC_{50}	$10^{-3.5}$ M		
U46619	TP	EC_{50}	7.0 nM	Rat aorta	(Ko *et al.*, 1995)

* fibroblast-like cell isolated from the aortic thoracic smooth muscle of an embryonic rat

Table 9.2: Selectivity of the antagonists used to study the GPCRs-mediated vasoconstriction. K_D = Dissociation constant, which represents the inverse of receptor's affinity to the ligand when at equilibrium, and smaller is K_D, higher is the affinity of receptor to the ligand (Salahudeen and Nishtala, 2017). K_B = the equilibrium dissociation constant of the antagonist. pA2 = The measure of the affinity of a competitive antagonist for specific receptor, pKi = inhibition constant of the antagonist, LV = Left ventricle, ET_A = Endothelin A receptors, ET_B = Endothelin B receptors, 5-HT_{1B} = 5-hydroxytryptamine receptors 1B, 5-HT_{2A} = 5-hydroxytryptamine receptors 2A, TP = thromboxane prostanoid receptors.

Antagonist	**Receptors**	**Selectivity**		**Receptors localisation**	**Reference**
BQ788	ET_B	K_D	31 nM	Rat LV	(Russell and Davenport, 1996)
	ETA	K_D	1.39 µM	Rat LV	
	ET_B	K_D	9.8 nM	Human LV	
	ET_A	K_D	1.01 µM	Human LV	
BQ123	ET_A	K_D	1.18 nM	Rat LV	(Peter and Davenport, 1996)
	ET_B	K_D	1370 µM	Rat LV	
GR55562	5-HT_{1B}	pKi	7.4	Human cerebral arteries	(Nilsson *et al.*, 1999a)
	5-HT_{1B}	K_B	≈100 nm	Rat hippocampus	(Mlinar *et al.*, 2003)
Seratrodast	TP	pA2	8.4	Rat aorta	(Zhang *et al.*, 1996)

9.2. The difference in vasocontraction between specific groups and the statistical significance (Chapter 4):

Table 9-3: The difference of contraction between 0.25 % DMSO and 5 µM U0126 groups and the p values during the vasocontractile response to the cumulative application of sarafotoxin 6c (S6c) (ET_B receptor agonist) normalised to 60 mM K^+ KH-induced vasocontraction in rat LAD arteries. Doxo = doxorubicin, S6c = sarafotoxin 6c.

Log(S6c)			14	13.5	13	12.5	12	11.5	11	10.5	10	9.5	9	8.5	8	7.5
Vehicle group versus:	Doxo	Difference (%)	3	4	3	6	4	6	5	9	8	-11	-29	-50	-60	-50
		p value	*> 0.99*	*> 0.99*	*> 0.99*	*> 0.99*	*> 0.99*	*> 0.99*	*> 0.99*	*> 0.99*	*> 0.99*	*> 0.99*	*0.171*	*< 0.0001*	*< 0.0001*	*< 0.0001*
	Doxo + U0126	Difference (%)	0	0	0	2	2	2	2	10	6	-6	-28	-52	-72	-65
		p value	*> 0.99*	*> 0.99*	*> 0.99*	*> 0.99*	*> 0.99*	*> 0.99*	*> 0.99*	*> 0.99*	*> 0.99*	*> 0.99*	*0.076*	*< 0.0001*	*< 0.0001*	*< 0.0001*
	Vehicle + U0126	Difference (%)	0	2	4	3	5	8	10	15	14	-3	-4	-15	-5	3
		p value	*> 0.99*	*> 0.99*	*> 0.99*	*> 0.99*	*> 0.99*	*> 0.99*	*> 0.99*	*> 0.99*	*> 0.99*	*> 0.99*	*> 0.99*	*> 0.99*	*> 0.99*	*> 0.99*
Doxo group versus:	Doxo + U0126	Difference (%)	-3	-4	-3	-4	-2	-4	-3	1	-2	5	1	-2	-12	-15
		p value	*> 0.99*	*> 0.99*	*> 0.99*	*> 0.99*	*> 0.99*	*> 0.99*	*> 0.99*	*> 0.99*	*> 0.99*	*> 0.99*	*> 0.99*	*> 0.99*	*> 0.99*	*> 0.99*

Table 9-4: The difference of contraction between 0.5 % DMSO and 10 µM U0126 groups and the p values during the vasocontractile response to the cumulative application of sarafotoxin 6c (S6c) (ET_B receptor agonist) normalised to 60 mM K^+ KH-induced vasocontraction in rat LAD arteries. Doxo = doxorubicin, S6c = sarafotoxin 6c.

Log(S6c)			14	13.5	13	12.5	12	11.5	11	10.5	10	9.5	9	8.5	8	7.5
Vehicle group	Doxorubicin	Difference (%)	6	10	11	18	23	29	32	26	20	-3	-24	-59	-66	-67
		p value	*> 0.999*	*> 0.999*	*> 0.999*	*0.453*	*0.162*	*0.029*	*0.016*	*0.073*	*0.350*	*> 0.999*	*0.087*	*< 0.0001*	*< 0.0001*	*< 0.0001*
	Doxorubicin + U0126	Difference (%)	0	2	2	3	5	4	3	0	-9	-38	-79	-109	-123	-124
		p value	*> 0.999*	*> 0.999*	*> 0.999*	*> 0.999*	*> 0.999*	*> 0.999*	*> 0.999*	*> 0.999*	*> 0.999*	*0.002*	*< 0.0001*	*< 0.0001*	*< 0.0001*	*< 0.0001*
	Vehicle + U0126	Difference (%)	-1	0	0	0	-1	-3	-3	-6	-15	-41	-44	-27	-6	-4
		p value	*> 0.999*	*> 0.999*	*> 0.999*	*> 0.999*	*> 0.999*	*> 0.999*	*> 0.999*	*> 0.999*	*> 0.999*	*0.001*	*0.000*	*0.084*	*> 0.999*	*> 0.999*
Doxorubicin group	Doxorubicin + U0126	% difference	-6	-8	-9	-15	-18	-25	-29	-26	-29	-35	-55	-50	-57	-57
		p value	*> 0.999*	*> 0.999*	*> 0.999*	*0.710*	*0.363*	*0.066*	*0.025*	*0.052*	*0.031*	*0.003*	*< 0.0001*	*< 0.0001*	*< 0.0001*	*< 0.0001*

Table 9-5: The difference of contraction between 0.25 % DMSO and 5 µM U0126 groups and the p-values during the vasocontractile response to the cumulative application of endothelin-1 (ET-1) ($ET_{A/B}$ receptor agonist) normalised to 60 mM K^+ KH-induced vasocontraction in rat LAD arteries. Doxo = doxorubicin, ET-1 = Endothelin-1.

Log(ET-1)			14	13.5	13	12.5	12	11.5	11	10.5	10	9.5	9	8.5	8	7.5
Vehicle group	Doxo	Difference (%)	0	0	-1	0	1	1	4	2	4	4	10	**30**	8	10
		p value	> 0.999	> 0.999	> 0.999	> 0.999	> 0.999	> 0.999	> 0.999	> 0.999	> 0.999	> 0.999	> 0.999	**0.0001**	> 0.999	0.906
	Doxo + U0126	Difference (%)	0	1	-1	-1	0	0	0	-1	0	0	3	2	**-35**	**-33**
		p value	> 0.999	> 0.999	> 0.999	> 0.999	> 0.999	> 0.999	> 0.999	> 0.999	> 0.999	> 0.999	> 0.999	> 0.999	**< 0.0001**	**< 0 .0001**
	Vehicle + U0126	Difference (%)	0	0	0	0	0	0	0	-1	0	-1	0	2	**-29**	**-21**
		p value	> 0.999	> 0.999	> 0.999	> 0.999	> 0.999	> 0.999	> 0.999	> 0.999	> 0.999	> 0.999	> 0.999	> 0.999	**0.001**	**0.030**
Doxo group	Doxo + U0126	Difference (%)	0	1	0	-1	-1	-1	-4	-3	-4	-4	-7	**-28**	**-43**	**-43**
		p value	> 0.999	> 0.999	> 0.999	> 0.999	> 0.999	> 0.999	> 0.999	> 0.999	> 0.999	> 0.999	> 0.999	**0.0003**	**< 0.0001**	**< 0.0001**

Table 9-6: The difference of contraction between 0.5 % DMSO and 10 µM U0126 groups and the p-values during the vasocontractile response to the cumulative application of endothelin-1 (ET-1) ($ET_{A/B}$ receptor agonist) normalised to 60 mM K^+ KH-induced vasocontraction in rat LAD arteries. Doxo = doxorubicin, ET-1 = Endothelin-1.

Log(ET-1)			14	13.5	13	12.5	12	11.5	11	10.5	10	9.5	9	8.5	8	7.5
Vehicle group	Doxo	Difference (%)	4	2	2	4	4	10	12	11	16	20	0	-10	**-44**	**-32**
		p value	> 0.999	> 0.999	> 0.999	> 0.999	> 0.999	> 0.999	> 0.999	> 0.999	0.527	0.142	> 0.999	> 0.999	**< 0.0001**	**0.003**
	Doxo + U0126	Difference (%)	1	1	0	0	1	1	3	2	4	3	-22	**-50**	**-102**	**-86**
		p value	> 0.999	> 0.999	> 0.999	> 0.999	> 0.999	> 0.999	> 0.999	> 0.999	> 0.999	> 0.999	0.081	**< 0 .0001**	**< 0 .0001**	**< 0 .0001**
	Vehicle + U0126	Difference (%)	1	0	0	0	0	0	0	-1	0	-1	**-28**	**-43**	-3	**32**
		p value	> 0.999	> 0.999	> 0.999	> 0.999	> 0.999	> 0.999	> 0.999	> 0.999	> 0.999	> 0.999	**0.016**	**< 0 .0001**	> 0.999	**0.010**
Doxo group	Doxo + U0126	% difference	-3	-1	-2	-4	-3	-9	-9	-9	-12	-17	**-22**	**-40**	**-58**	**-54**
		p value	> 0.999	> 0.999	> 0.999	> 0.999	> 0.999	> 0.999	> 0.999	> 0.999	0.985	0.297	**0.049**	**< 0.0001**	**< 0.0001**	**< 0.0001**

Table 9-7: The difference of contraction between 0.25 % DMSO and 5 µM U0126 groups and the p-values during the vasocontractile response to the cumulative application of 5-carboxamidotryptamine (5-CT) (5-HT_{1B} receptor agonist) normalised to 60 mM K^+ KH-induced vasocontraction in rat LAD arteries. Doxo = doxorubicin, 5-CT = 5-carboxamidotryptamine.

Log(5-CT)			12	11.5	11	10.5	10	9.5	9	8.5	8	7.5	7	6.5	6	5.5
Vehicle group	Doxo	Difference (%)	1	2	4	3	5	6	7	10	**12**	**14**	**19**	**23**	**39**	**49**
		p value	> *0.999*	> *0.999*	> *0.999*	> *0.999*	> *0.999*	*0.944*	*0.575*	*0.286*	***0.046***	***0.016***	***0.0003***	< ***0.0001***	< ***0.0001***	< ***0.0001***
	Doxo + U0126	Difference (%)	0	0	1	1	2	3	3	6	6	7	9	13	**17**	11
		p value	> *0.999*	> *0.999*	> *0.999*	> *0.999*	> *0.999*	> *0.999*	> *0.999*	> *0.999*	> *0.999*	> *0.999*	*0.609*	*0.140*	***0.012***	*0.218*
	Vehicle + U0126	Difference (%)	0	0	-1	0	0	0	0	1	0	0	2	1	3	0
		p value	> *0.999*	> *0.999*	> *0.999*	> *0.999*	> *0.999*	> *0.999*	> *0.999*	> *0.999*	> *0.999*	> *0.999*	> *0.999*	> *0.999*	> *0.999*	> *0.999*
Doxo group	Doxo + U0126	Difference (%)	-1	-2	-3	-2	-3	-3	-4	-4	-6	-7	-10	-10	**-22**	**-38**
		p value	> *0.999*	> *0.999*	> *0.999*	> *0.999*	> *0.999*	> *0.999*	> *0.999*	> *0.999*	> *0.999*	> *0.999*	*0.226*	*0.260*	< ***0.0001***	< ***0.0001***

Table 9-8: The difference of contraction between 0.5 % DMSO and 10 µM U0126 groups and the p-values during the vasocontractile response to the cumulative application of 5-carboxamidotryptamine (5-CT) (5-HT_{1B} receptor agonist) normalised to 60 mM K^+ KH-induced vasocontraction in rat LAD arteries. Doxo = doxorubicin, 5-CT = 5-carboxamidotryptamine.

Log(5-CT)			12	11.5	11	10.5	10	9.5	9	8.5	8	7.5	7	6.5	6	5.5
Vehicle group	Doxo	Difference (%)	0	1	2	2	4	4	6	6	11	**14**	**16**	**15**	**32**	**22**
		p value	> *0.999*	> *0.999*	> *0.999*	> *0.999*	> *0.999*	> *0.999*	> *0.999*	> *0.999*	*0.130*	***0.033***	***0.007***	***0.013***	< ***0.0001***	< ***0.0001***
	Doxo + U0126	Difference (%)	-1	0	0	0	2	1	1	2	2	3	3	2	4	**-22**
		p value	> *0.999*	> *0.999*	> *0.999*	> *0.999*	> *0.999*	> *0.999*	> *0.999*	> *0.999*	> *0.999*	> *0.999*	> *0.999*	> *0.999*	> 0.999	< ***0.0001***
	Vehicle + U0126	Difference (%)	-1	0	0	-1	1	0	-1	-1	-1	0	1	-1	-3	**-37**
		p value	> *0.999*	> *0.999*	> *0.999*	> *0.999*	> *0.999*	> *0.999*	> *0.999*	> *0.999*	> *0.999*	> *0.999*	> *0.999*	> *0.999*	> 0.999	< ***0.0001***
Doxo group	Doxo + U0126	Difference (%)	-1	-1	-2	-2	-2	-3	-5	-4	-9	-11	**-13**	-13	**-28**	**-44**
		p value	> *0.999*	> *0.999*	> *0.999*	> *0.999*	> *0.999*	> *0.999*	> *0.999*	> *0.999*	*0.317*	*0.114*	***0.046***	*0.058*	< ***0.0001***	< ***0.0001***

Table 9-9: The difference of contraction between 0.25 % DMSO and 5 µM U0126 groups and the p-values during the vasocontractile response to the cumulative application of U46619 (TP receptor agonist) normalised to 60 mM K^+ KH-induced vasocontraction in rat LAD arteries. Doxo = doxorubicin.

Log(U46619)			12	11.5	11	10.5	10	9.5	9	8.5	8	7.5	7	6.5
Vehicle group	Doxo	Difference (%)	-1	-2	-1	0	0	3	1	3	**21**	**47**	**40**	**26**
		p value	*> 0.999*	*> 0.999*	*> 0.999*	*> 0.999*	*> 0.999*	*> 0.999*	*> 0.999*	*> 0.999*	***0.027***	***< 0.0001***	***< 0.0001***	***0.003***
	Doxo + U0126	Difference (%)	0	-2	0	0	-1	1	0	0	6	**27**	6	-8
		p value	*> 0.999*	*> 0.999*	*> 0.999*	*> 0.999*	*> 0.999*	*> 0.999*	*> 0.999*	*> 0.999*	*> 0.999*	***0.007***	*> 0.999*	*> 0.999*
	Vehicle + U0126	Difference (%)	0	-2	0	0	-1	0	0	-1	1	13	-1	-4
		p value	*> 0.999*	*> 0.999*	*> 0.999*	*> 0.999*	*> 0.999*	*> 0.999*	*> 0.999*	*> 0.999*	*> 0.999*	*0.620*	*> 0.999*	*> 0.999*
Doxo group	Doxo + U0126	Difference (%)	1	0	1	0	-1	-2	-1	-3	-15	-20	**-34**	**-34**
		p value	*> 0.999*	*> 0.999*	*> 0.999*	*> 0.999*	*> 0.999*	*> 0.999*	*> 0.999*	*> 0.999*	*0.392*	*0.076*	***0.0001***	***< 0.0001***

Table 9-10: The difference of contraction between 0.5 % DMSO and 10 µM U0126 groups and the p-values during the vasocontractile response to the cumulative application of U46619 (TP receptor agonist) normalised to 60 mM K^+ KH-induced vasocontraction in rat LAD arteries. Doxo = doxorubicin.

Log(U46619)			12	11.5	11	10.5	10	9.5	9	8.5	8	7.5	7	6.5
Vehicle group	Doxo	Difference (%)	-1	-1	-1	-2	1	2	3	5	16	**29**	**29**	15
		p value	*> 0.999*	*> 0.999*	*> 0.999*	*> 0.999*	*> 0.999*	*> 0.999*	*> 0.999*	*> 0.999*	*0.194*	***0.001***	***0.0004***	*0.234*
	Doxo + U0126	Difference (%)	1	0	0	-1	-2	-2	-2	-1	6	6	**-24**	**-42**
		p value	*> 0.999*	*> 0.999*	*> 0.999*	*> 0.999*	*> 0.999*	*> 0.999*	*> 0.999*	*> 0.999*	*> 0.999*	*> 0.999*	***0.007***	***< 0.0001***
	Vehicle + U0126	Difference (%)	-1	0	0	-1	-1	-1	-1	-1	1	-12	**-51**	**-44**
		p value	*> 0.999*	*> 0.999*	*> 0.999*	*> 0.999*	*> 0.999*	*> 0.999*	*> 0.999*	*> 0.999*	*> 0.999*	*0.809*	***< 0.0001***	***< 0.0001***
Doxo group	Doxo + U0126	Difference (%)	2	1	1	1	-3	-4	-5	-6	-10	**-23**	**-53**	**-57**
		p value	*> 0.999*	*> 0.999*	*> 0.999*	*> 0.999*	*> 0.999*	*> 0.999*	*> 0.999*	*> 0.999*	*> 0.999*	***0.005***	***< 0.0001***	***< 0.0001***

9.3. Results from fresh versus organ cultured-LAD artery molecular studies on transcriptional and translational levels of the four GPCRs studied in Chapter 5:

(A) (B)

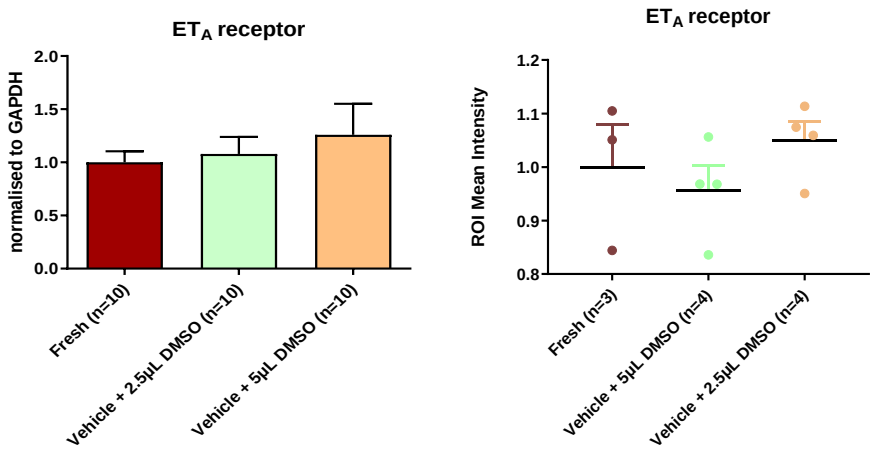

Figure 9-1: The transcriptional changes induced by organ culture on ET_A receptors of LAD arteries. (A) The ET_A receptors mRNA levels relative to the GAPDH level. Fresh LAD arteries (n=10), Vehicle + 2.5 µL of DMSO (n=10) and Vehicle + 5 µL of DMSO (n=10). (B) The ET_A receptors expression on LAD arteries normalised to the fresh group. Fresh LAD arteries (n=3), Vehicle + 2.5 µL of DMSO (n=4) and Vehicle + 5 µL of DMSO (n=4). DMSO = Dimethyl sulfoxide. The different group were compared using one-way ANOVA and Fisher's post hoc test (*=p<0.05, **=p<0.01 and ***= p<0.005).

(A) (B)

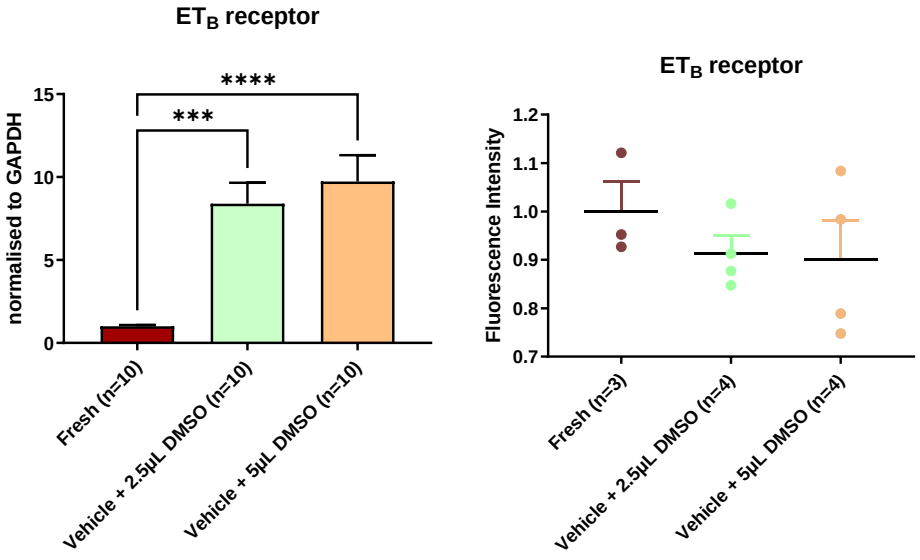

Figure 9-2: The transcriptional changes induced by organ culture on ET_B receptors of LAD arteries. (A) The ET_B receptors mRNA levels relative to the GAPDH level. Fresh LAD arteries (n=10), Vehicle + 2.5 µL of DMSO (n=10) and Vehicle + 5 µL of DMSO (n=10). (B) The ET_B receptors expression on LAD arteries normalised to the fresh group. Fresh LAD arteries (n=3), Vehicle + 2.5 µL of DMSO (n=4) and Vehicle + 5 µL of DMSO (n=4). DMSO = Dimethyl sulfoxide. The different group were compared using one-way ANOVA and Fisher's post hoc test (*=p<0.05, **=p<0.01 and ***= p<0.005).

(A) (B)

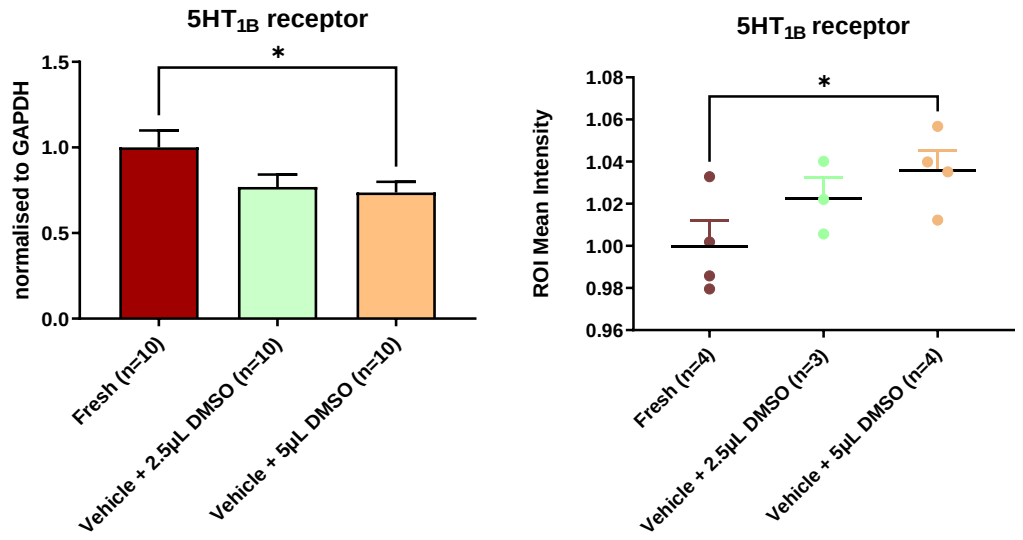

Figure 9-3: The transcriptional changes induced by organ culture on 5-HT$_{1B}$ receptors of LAD arteries. (A) The 5-HT$_{1B}$ receptors mRNA levels relative to the GAPDH level. Fresh LAD arteries (n=10), Vehicle + 2.5 µL of DMSO (n=10) and Vehicle + 5 µL of DMSO (n=10). (B) The 5-HT$_{1B}$ receptors expression on LAD arteries normalised to the fresh group. Fresh LAD arteries (n=4), Vehicle + 2.5 µL of DMSO (n=3) and Vehicle + 5 µL of DMSO (n=4). DMSO = Dimethyl sulfoxide. The different group were compared using one-way ANOVA and Fisher's post hoc test (*=p<0.05, **=p<0.01 and ***= p<0.005).

(A) (B)

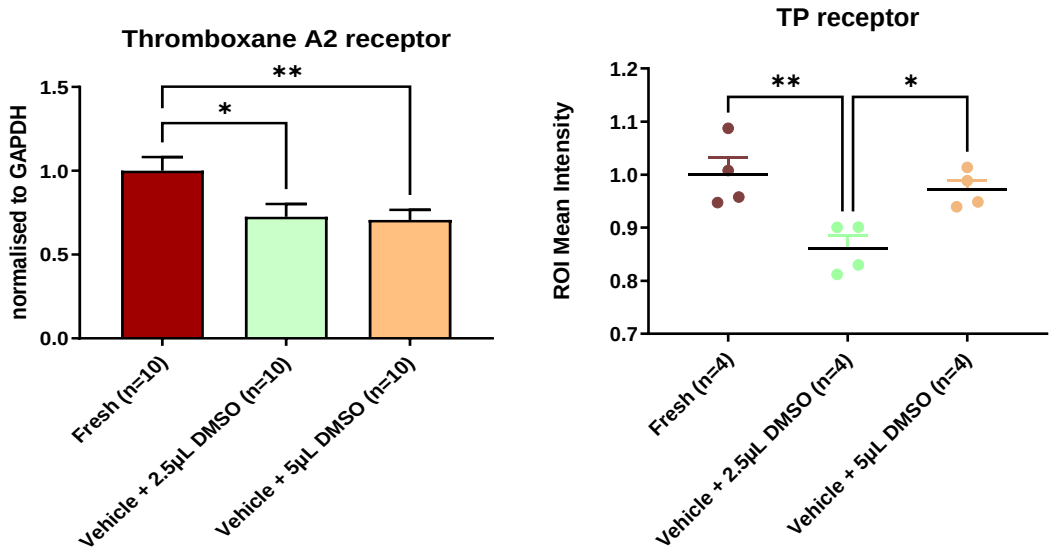

Figure 9-4: The transcriptional changes induced by organ culture on TP receptors of LAD arteries. (A) The TP receptors mRNA levels relative to the GAPDH level. Fresh LAD arteries (n=10), Vehicle + 2.5 µL of DMSO (n=10) and Vehicle + 5 µL of DMSO (n=10). (B) The TP receptors expression on LAD arteries normalised to the fresh group. Fresh LAD arteries (n=4), Vehicle + 2.5 µL of DMSO (n=3) and Vehicle + 5 µL of DMSO (n=4). DMSO = Dimethyl sulfoxide. The different group were compared using one-way ANOVA and Fisher's post hoc test (*=p<0.05, **=p<0.01 and ***= p<0.005).

10. Ethics:

10.1. Animal experiment:

Certificate of Ethical Approval

Applicant:

Caroline Lozahic

Project Title:

Cardiotoxicity assessment of chemotherapy drugs on rat hearts using the in vitro Langendorff model

This is to certify that the above named applicant has completed the Coventry University Ethical Approval process and their project has been confirmed and approved as Medium Risk

Date of approval:

28 May 2019

Project Reference Number:

P90600

10.2. Human plasma experiment:

Certificate of Ethical Approval

Applicant:

Caroline Lozahic

Project Title:

Assessment of microRNA expression in blood circulation of cancer patients treated with anthracycline chemotherapy

This is to certify that the above named applicant has completed the Coventry University Ethical Approval process and their project has been confirmed and approved as Low Risk

Date of approval:

03 June 2019

Project Reference Number:

P90761